THE JOURNAL OF

PHYSICAL CHEMISTRY

Volume 71, Number 3 February 1967

NOTES

COMMUNICATIONS TO THE EDITOR

AUTHOR INDEX

THE JOURNAL OF
PHYSICAL CHEMISTRY

VOLUME 71, NUMBER 3 FEBRUARY 15, 1967

The Infrared Spectrum of Ammonia Adsorbed on Silica–Alumina

by Michael R. Basila and Theodore R. Kantner

Gulf Research & Development Co., Pittsburgh, Pennsylvania *(Received October 28, 1966)*

An infrared spectroscopic study of ammonia adsorbed on silica–alumina has shown that physically adsorbed NH_3, coordinately bonded NH_3, and NH_4^+ are the only detectable adsorbed species. From the relative intensities of the appropriate bands, the ratio of Lewis and Brønsted acid sites was found to be 4:1. As in the case of pyridine chemisorption, the effect of H_2O was to convert a portion of the Lewis sites to Brønsted sites. Subsequent evacuation selectively removed H_2O and the original distribution of Lewis and Brønsted acid sites was recovered. The results of this study are consistent with and hence support the model proposed in which all of the primary acid sites on a silica–alumina are of the Lewis type centered on active surface aluminum atoms, and apparent Brønsted sites are produced by a second-order interaction between the molecule chemisorbed on a Lewis site and a nearby surface hydroxyl group. Direct spectroscopic evidence for the transfer of protons from a chemisorbed molecule to a physically adsorbed molecule was obtained in a study of the dual adsorption of ammonia and pyridine.

Introduction

The amount of ammonia adsorbed at a given temperature is frequently used as a measure of the number of acid sites of a given strength (defined arbitrarily by the temperature) on a catalytic surface.[1,2] A number of studies have been made of the infrared spectrum of NH_3 adsorbed on a variety of surfaces, such as synthetic silica–alumina,[3–6] alumina,[7,8] porous glass,[9,10] iron oxide,[11] natural aluminum silicates,[12] and zeolites.[13] The object of most of these studies was to distinguish between Lewis and Brønsted type acid sites by utilizing differences in the infrared spectra of coordinately bonded NH_3 (LNH_3) and NH_4^+. In all but the silica–aluminas, only LNH_3 (or its decomposition products) are observed.[7–11] In synthetic silica–alumina cracking catalysts both LNH_3 and NH_4^+ are observed with LNH_3 predominating in the highly dehydrated and NH_4^+ predominating in the hydrated form.[3–7] Both species are also observed on the zeolite, the ratio being dependent on the degree of hydration.[13] On the other

(1) A. N. Webb, *Ind. Eng. Chem.*, **49**, 261 (1957).

(2) R. T. Barth and E. V. Ballou, *Anal. Chem.*, **33**, 1080 (1961).

(3) J. E. Mapes and R. P. Eischens, *J. Phys. Chem.*, **58**, 1059 (1954).

(4) L. M. Roev, V. N. Filimonov, and A. N. Terenin, *Opt. i Spektroskopiya*, **4**, 328 (1958).

(5) D. E. Nicholson, *Nature*, **186**, 630 (1960).

(6) J. J. Fripiat, A. Leonard, and J. B. Uytterhoeven, *J. Phys. Chem.*, **69**, 3274 (1965).

(7) R. P. Eischens and W. A. Pliskin, "Advances in Catalysis," Vol. X, Academic Press, Inc., New York, N. Y., 1958, pp 1–56.

(8) (a) J. B. Peri and R. B. Hannan, *J. Phys. Chem.*, **64**, 1526 (1960); (b) J. B. Peri, *ibid.*, **69**, 231 (1965).

(9) (a) M. Folman and D. J. C. Yates, *Proc. Roy. Soc.* (London), **A246**, 32 (1958). (b) M. Folman and D. J. C. Yates, *J. Phys. Chem.*, **63**, 183 (1959).

(10) M. Folman, *Trans. Faraday Soc.*, **57**, 2000 (1961).

hand, only the adsorbed NH_4^+ species was observed on natural aluminum silicates.[12]

Recent studies of the infrared spectrum of pyridine chemisorbed on a synthetic silica–alumina cracking catalyst have indicated the presence of both Lewis and Brønsted acid sites.[14-16] Estimates[16] of the relative absorption coefficients of the bands characteristic of the protonated and coordinately bonded chemisorbed species led to the conclusion that the ratio of Lewis to Brønsted acid sites is approximately six. The present paper reports a study of the infrared spectrum of ammonia adsorbed on the same synthetic silica–alumina.

Experimental Section

Materials. The silica–alumina used in this work was the same sample of American Cyanamid Triple A that was used in our previous work.[15-17] It contains 25% Al_2O_3 by weight on a dry basis and has a surface area of 430 m^2/g.

Matheson anhydrous ammonia was distilled *in vacuo* over P_2O_5 through a glass wool–P_2O_5 drying train immediately before use. This treatment lowered the H_2O content to less than 0.1% as estimated by infrared measurements.

Techniques. The preparation of catalyst samples and spectroscopic techniques were identical with those used in our previous work.[15-17] The sample wafers were slowly heated with continuous evacuation from ambient to 500° over a 3-hr period after which they were calcined in oxygen for 4 hr or longer at 500°. Following calcination, the samples were evacuated at 500° for at least 3 hr, but generally overnight. A conventional vacuum system capable of maintaining pressures in the 10^{-6}-mm range was used. Samples prepared by this technique are referred to as SA.

A Perkin-Elmer 421 grating spectrophotomer was used to record the spectra in most of the work. For a few experiments a Perkin-Elmer 221 prism-grating instrument was used. Both instruments were frequency calibrated against known standards. The frequencies quoted are believed to be within 1 or 2 cm^{-1} of the true values. The spectral slit width of the Model 421 was approximately 2–3 cm^{-1} and that of the Model 221 was roughly 4 cm^{-1}. All spectra were recorded at room temperature using standard instrument settings. In some cases an attenuator was used in the reference beam to compensate for losses due to reflection and scattering by the sample.

A conventional quartz spiral balance having a sensitivity of 0.5 mm/mg was used for the quantitative chemisorption experiments.

Results

Ammonia Chemisorption on Silica–Alumina. In Figure 1 spectra of NH_3 adsorbed on SA under various conditions are given. The bands in spectrum (a) of SA have been previously assigned.[17] The band at 3745 cm^{-1} is due to free (nonhydrogen-bonded) surface OH groups attached to surface Si atoms; the band at 1633 cm^{-1} is an SiO overtone and is associated with the lattice rather than the surface; the band at 1394 cm^{-1}, on the other hand, is due to a surface group which has not been identified to date. In (b) the spectrum of NH_3 adsorbed on SA at 150° is given. The NH_3 was added by exposing the evacuated SA to 10 mm of NH_3 vapor for 1 hr and evacuating for 1 hr, all at 150°. Bands are observed at 3341, 3280, 3230, 3195, 1620, and 1432 cm^{-1}. A decrease in the intensity of the 3745-cm^{-1} band and the disappearance of the 1394-cm^{-1} band are also noted. In (c) the spectrum of NH_3 adsorbed at 25° is given. The NH_3 was adsorbed by the same 1-hr exposure and 1-hr evacuation technique. All bands increased in intensity except the 3745-cm^{-1} band which decreased. In (d) the spectrum of

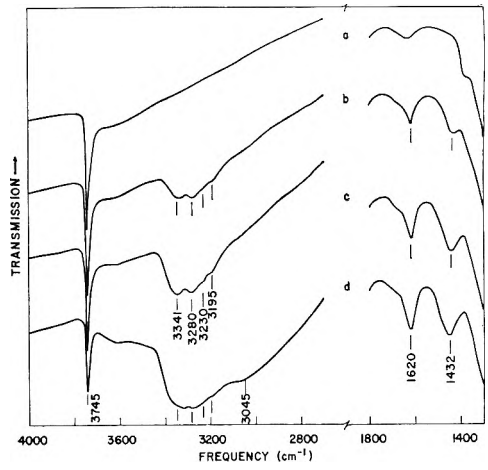

Figure 1. (a) SA calcined 16 hr in O_2 at 500°, evacuated 5 hr at 500°; (b) exposed to 10 mm of NH_3 for 1 hr at 150°, evacuated 1 hr at 150°; (c) subsequently exposed to 10 mm of NH_3 for 1 hr at 25°, evacuated for 1 hr at 25°; (d) subsequently exposed to 10 mm of NH_3 for 1 hr, no evacuation. Very weak bands due to gaseous NH_3 have been subtracted.

(11) G. Blyholder and E. A. Richardson, *J. Phys. Chem.*, **66**, 2597 (1962).

(12) M. M. Mortland, J. J. Fripiat, J. Chaussidon, and J. Uytterhoeven, *ibid.*, **67**, 248 (1963).

(13) J. B. Uytterhoeven, L. G. Christner, and W. K. Hall, *ibid.*, **69**, 2117 (1965).

(14) E. P. Parry, *J. Catalysis*, **2**, 371 (1963).

(15) M. R. Basila, T. R. Kantner, and K. H. Rhee, *J. Phys. Chem.*, **68**, 3197 (1964).

(16) M. R. Basila and T. R. Kantner, *ibid.*, **70**, 1681 (1966).

(17) M. R. Basila, *ibid.*, **66**, 2223 (1962).

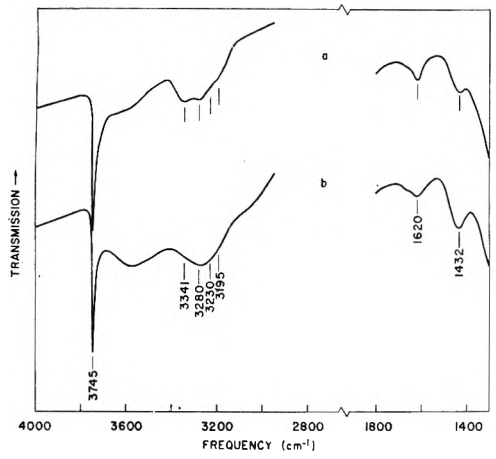

Figure 2. (a) SA calcined 16 hr in O_2 at 500°, evacuated 16 hr at 500°, exposed to 20 mm of NH_3 for 1 hr at 150°, evacuated 1 hr at 150°; (b) subsequently exposed to 15 mm of H_2O at 150°, evacuated 1 hr at 150°.

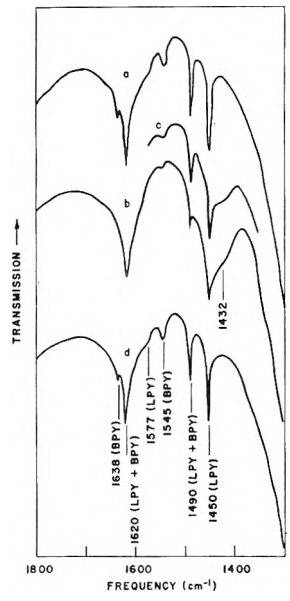

Figure 3. (a) SA calcined 16 hr in O_2 at 500°, evacuated 16 hr at 500°, exposed to 17 mm of PY for 1 hr at 150°, evacuated 16 hr at 150°; (b) subsequently exposed to 15 mm of NH_3 for 1 hr at 150° after which the NH_3 vapor was condensed in a trap cooled with liquid nitrogen for 1 hr; (c) subsequently evacuated for 1 hr at 150°; (d) further evacuation for 18 hr.

NH_3 adsorbed after 1 hr exposure to 10 mm of NH_3 vapor and subsequent condensation of the NH_3 vapor in a side arm cooled to liquid nitrogen temperature is given. Intensification of the 1620- and 1432-cm^{-1} bands, broadening and intensification of the bands near 3300 cm^{-1}, and a decrease in intensity of the 3745-cm^{-1} band were observed. In addition, a broad underlying band at 3050 cm^{-1} appeared. Similar spectral changes occurred upon further NH_3 adsorption, the most notable being a loss of structure in the 3300-cm^{-1} region giving a single broad band centered at 3320 cm^{-1} and the disappearance of the 3745-cm^{-1} band with an accompanying increase in the 3050-cm^{-1} band.

Dual Adsorption of Ammonia and Water on Silica–Alumina. The results of an experiment in which NH_3 was first chemisorbed on evacuated SA at 150° by the standard method and H_2O subsequently adsorbed at 150° are shown in Figure 2. It is evident from absorbance measurements that the addition of H_2O leads to the enhancement of the bands at 3230, 3195, and 1432 cm^{-1} and attenuation of the bands at 3745, 3341, and 3280 cm^{-1}. The behavior of the 1620-cm^{-1} band is masked by the 1633-cm^{-1} band due to the H_2O bending vibration. Upon subsequent evacuation at 150° for 16 hr the H_2O was removed, and the spectrum was identical with the original spectrum.

Dual Adsorption of Ammonia and Pyridine on Silica–Alumina. In Figure 3 the results of an experiment in which pyridine (PY) was first chemisorbed on SA at 150° and then the sample exposed to NH_3 vapor at 15 mm are given. In (a) the spectrum of PY chemisorbed on SA is given. The bands characteristic[14,15] of coordinately bonded pyridine (LPY) and pyridinium ion (BPY) are indicated in the figure. When NH_3 was subsequently added at 150° as shown in (b), the bands characteristic of LPY and BPY were attenuated and new bands appeared at 3341, 3280, 3230, 3195, and 1432 cm^{-1}. The bands characteristic of BPY at 1638 and 1545 cm^{-1} appeared to be more drastically affected than those due to LPY. A decrease in the 3745-cm^{-1} band was also observed. Surprisingly, after evacuation at 150° for several hours, the new bands essentially disappeared and the bands of LPY and BPY reappeared very close to their original intensity. Figure 3c was included to demonstrate the attenuation of the LPY band at 1450 cm^{-1}. This spectrum was taken at an intermediate stage of the evacuation. The absorbance of the 1450-cm^{-1} band is 0.06 as compared to 0.10 in the initial spectrum (Figure 3a). Two different experiments were run and in the first, the intensities of the LPY and BPY bands were completely restored and in the second, the LPY bands were completely restored and the BPY bands about 80% restored.

Discussion

NH_3 Chemisorbed on Silica–Alumina. The spectrum of NH_3 chemisorbed on SA at 150° is essentially the same as that observed by previous workers.[3–6] The

assignment of the bands is summarized in Table I. These assignments are supported by the observation that the dual adsorption of H_2O and NH_3 on SA enhances the bands at 3230, 3195, and 1432 cm^{-1} which have been assigned to LNH_3. The net effect of H_2O is to increase the protonated chemisorbed species at the expense of the coordinately bonded chemisorbed species, as has been shown in other work[14,15] on the dual adsorption of H_2O and pyridine. The H_2O is removed by extended evacuation giving the original distribution of LNH_3 and NH_4^+ as was observed in the dual adsorption of pyridine and H_2O.[15]

Table I: Assignment of the Bands of NH_3 Chemisorbed on Silica–Alumina

Frequency, cm^{-1}	Adsorbed species[a]	Assignment
3341	LNH_3, PNH_3	ν_3 (e) (NH stretch)
3280	LNH_3, PNH_3	ν_1 (a_1) (NH stretch)
3230	NH_4^+	ν_3 (t_2) (NH stretch)
3195	NH_4^+	ν_1 (a_1) (NH stretch)
1620	LNH_3, PNH_3	ν_4 (l) (HNH deformation)
1432	NH_4^+	ν_4 (t_2) (HNH deformation)

[a] See text for definitions of LNH_3 and PNH_3.

Model for Brønsted Sites on Silica–Alumina. In our earlier work[15] it was suggested that all the primary acidic sites on a highly dehydrated silica–alumina are of the Lewis type. It was also suggested that surface OH groups adjacent to Lewis acid sites can transfer protons to a molecule chemisorbed on a Lewis site provided that the interaction distance does not exceed the CID (critical interaction distance) and that the molecule is suitably activated by the Lewis site. A similar conclusion was reached by Fripiat, *et al.*,[6] in a study of ammonia chemisorption on a series of silica–aluminas in various stages of dehydration. The nature of the chemisorbed molecule is an important factor; for example, an olefin requires a proton to form a classical carbonium ion, whereas a paraffin can form a classical carbonium ion by hydride abstraction, as proposed by Leftin and Hall,[18] and hence does not require a proton.

The present experimental data offer an opportunity to examine the model further, especially the role of the surface OH group. In Figure 4 the concentration of adsorbed NH_3 (LNH_3 plus PNH_3, where PNH_3 is physically adsorbed NH_3) is plotted *vs.* that of adsorbed NH_4^+.[19] As would be expected, the slope, $\Delta[NH_4^+]/\Delta[NH_3]$, decreases as the total amount of ammonia adsorbed increases and approaches zero at highest

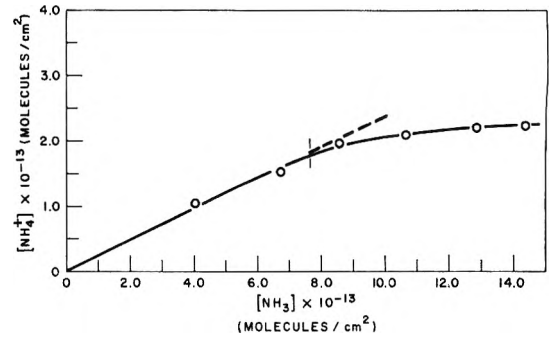

Figure 4. A comparison of the concentrations of NH_3 and NH_4^+ adsorbed on SA as the total amount of ammonia adsorbed increases. $[NH_3]$ is the sum of $[PNH_3]$ and $[LNH_3]$. The vertical line denotes the point of straight-line intersection in Figure 5.

coverage. The initial slope of the plot is 0.25; hence, one out of every five chemisorbed molecules is adsorbed as NH_4^+. In our experiments with PY[16] we found that one out of every seven molecules is adsorbed as the protonated species. In view of the experimental difficulties involved these two sets of results are in reasonable agreement.

In Figure 5 the concentration of *non*hydrogen-bonded surface OH groups is plotted against the sum of the NH_3 and NH_4^+ concentrations. It is evident that a dramatic change in slope occurs as the surface concentration of ammonia increases. It is convenient to approximate this curve as two intersecting linear segments as shown in the figure. The low-coverage segment which corresponds predominantly to the chemisorption of ammonia has an inverse slope, $(\Delta[NH_3]/\Delta[OH])_L = 5.5 \pm 0.5$, and the high-coverage segment which corresponds predominantly to physical adsorption of ammonia has an inverse slope, $(\Delta[NH_4]/\Delta[OH])_H = 0.98 \pm 0.09$. Hence, one out of every five or six chemisorbed ammonia molecules is hydrogen bonded to a surface OH group whereas essentially every physically adsorbed molecule is hydrogen bonded to a surface OH group. This latter behavior is confirmed by the appearance of the 3050-cm^{-1} band due to hydrogen-bonded surface OH and is in accord with the results of Kiselev, *et al.*,[20] which demonstrate that the predominant interaction in the physical adsorption of NH_3 on silica is hydrogen bonding.

(18) H. P. Leftin and W. K. Hall, *Actes Congr. Intern. Catalyse 2e Paris*, 1, 1353 (1961).

(19) The concentrations of the adsorbed NH_3 and NH_4^+ and the surface OH groups were estimated from the intensities of the appropriate bands. The methods used for calibration are discussed in the Appendix.

(20) A. V. Kiselev, V. I. Lygin, and T. I. Titova, *Zh. Fiz. Khim.*, 38, 2730 (1964).

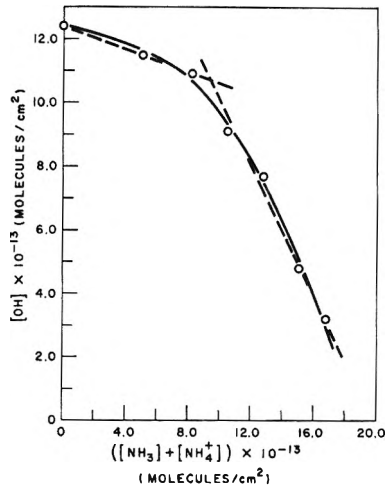

Figure 5. The concentration of nonhydrogen-bonded surface OH groups *vs.* the total amount of ammonia adsorbed on SA. $[NH_3]$ is the sum of $[PNH_3]$ and $[LNH_3]$.

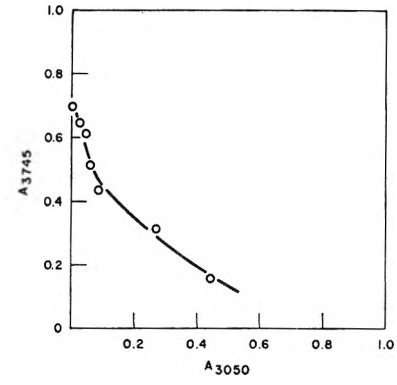

Figure 6. A comparison of the concentrations of free and hydrogen-bonded surface OH groups as the amount of ammonia adsorbed increases. The values of A are the peak absorbancies of the characteristic bands.

The values of $\Delta[NH_4^+]/\Delta[NH_3]$ and $(\Delta[NH_3]/\Delta[OH])_L$ are consistent (within experimental error) with the prediction of the model that the number of surface OH groups interacting with NH_3 molecules chemisorbed on Lewis acid sites will be equal to or greater than the number of NH_4^+ ions. The slopes indicate that most of these interacting surface OH groups are engaged in the proton-transfer interaction. This conclusion can be checked by observing the intensity of the 3050-cm^{-1} band which is due to the hydrogen-bonded surface OH groups. Those surface OH groups which are involved in a proton-transfer interaction would not exhibit an OH vibration and hence would not contribute to the 3050-cm^{-1} band. Thus taking Figure 5 into account the model would predict that at low coverage where chemisorption predominates the intensity of the 3050-cm^{-1} band should increase (with increasing coverage) at a very much lower rate than at high coverage where physical adsorption predominates. This behavior is evident in Figure 6 where the peak absorbance of the 3745-cm^{-1} band is plotted *vs.* that of the 3050-cm^{-1} band. Figure 6 cannot be taken as conclusive since the argument that the band due to surface OH groups hydrogen bonded to chemisorbed molecules may have a different peak frequency and absorption coefficient than the 3050-cm^{-1} band cannot be ruled out. However, it is consistent with the predictions of the model.

In our study of PY chemisorption on SA it was found that every chemisorbed PY was hydrogen bonded to a surface OH group, a fact which might appear inconsistent with the present results.[15] However, PY is a much larger molecule and contains a π-electron system that can hydrogen bond to surface OH groups;[21] hence, a greater amount of hydrogen bonding to the chemisorbed PY species is expected. In support of this concept, it was noted in our earlier study[17] that very little or no hydrogen bonding occurs when H_2O is chemisorbed on SA under comparable conditions. In those experiments small changes expected (in view of the results with NH_3) in the intensity of the 3745-cm^{-1} band would have been difficult to observe because of the problem of correcting for the background absorbtion of the OH stretching vibration of the chemisorbed water molecule.

It is evident from the discussion above that our present results are consistent with the model for Brønsted acidity on silica–alumina. Additional support for the model is obtained from the kinetic studies published by Hall and co-workers.[22,23] Their findings indicate that the cracking activities of silica–alumina and alumina are very similar.[22] On the other hand, the marked differences which are evident in the isomerization of butene over silica–alumina and alumina have led to the postulation of different mechanisms—carbonium ion in the case of silica–alumina and an intramolecular rearrangement over dual acid–base sites in the case of alumina.[23] These findings are exactly what would be predicted from the proposed model. As mentioned earlier, a paraffin does not need a proton to form a classical carbonium ion; hence, one would expect alumina, which has only Lewis type acid sites,[8,14,15,24] to behave essentially the same as silica–

(21) M. R. Basila, *J. Chem. Phys.*, **35**, 1151 (1961).

(22) W. K. Hall, F. E. Lutinski, and H. R. Gerberich, *J. Catalysis*, **3**, 512 (1964).

(23) H. R. Gerberich and W. K. Hall, *ibid.*, **5**, 99 (1966).

(24) J. B. Peri, *Actes Congr. Intern. Catalyse 2e Paris*, **1**, 1333 (1961).

alumina. However, since olefins need a proton to form a classical carbonium ion, it is expected that isomerization would not proceed *via* a carbonium-ion mechanism on alumina, but would on silica–alumina. These results, therefore, support the basic contention of the model, that the primary sites on a highly dehydrated silica–alumina are of the Lewis type, and that the proton necessary in some reactions is available through interaction with a nearby surface hydroxyl group.

Proton Transfer between Adsorbed Species. In the experiments in which PY and NH_3 are adsorbed consecutively (Figure 3) it was observed that the bands due to BPY almost disappear, those due to LPY were attenuated, and the bands due to LNH_3 and/or PNH_3 NH_4^+ appeared. These changes were accompanied by an increase in the number of hydrogen-bonded OH groups; however, no bands due to HPY (physically adsorbed, hydrogen-bonded pyridine[15]) were observed. Subsequent evacuation at 150° removed the NH_3 and NH_4^+ and the bands due to LPY and BPY returned to their original intensity. The implication is that part of the ammonia interacted with both a surface OH group and a chemisorbed PY molecule. The fact that the bands due to LPY and BPY were restored after the adsorbed ammonia was removed indicates that the chemisorbed PY molecules were not displaced from the acid site, otherwise they would have been removed by subsequent evacuation. Also, if the PY had been displaced, the bands of HPY would have been observed. These results suggest that proton transfer has occurred between physically adsorbed NH_3 molecules and chemisorbed BPY molecules. This is in accord with the recent results of Fripiat[26] who has obtained evidence for proton transfer between chemically and physically adsorbed species by conductivity measurements.

Appendix

Surface NH_3 and NH_4^+ Concentrations. In order to convert the band intensities to surface concentrations it is necessary to determine the relative absorption coefficients of the 1620- and 1432-cm^{-1} bands and the total amount of ammonia adsorbed. Eischens[26] has estimated the ratio $\epsilon_{1432}/\epsilon_{1620}$ to be approximately three. More recently, Fripiat, *et al.*,[6,25] have estimated this ratio to be seven by the dual adsorption of NH_3 and H_2O in which all of the NH_3 is converted to NH_4^+. We have also obtained a value of seven by contacting a sample of SA which had previously been exposed to 10 mm of NH_3 vapor at 100° for 1 hr and evacuated at 100° for 1 hr to excess HCl, which converted the LNH_3 to NH_4Cl (adsorbed).

The total amount of NH_3 adsorbed was determined gravimetrically in a quartz spiral balance for an identically treated SA sample. The measurements were made under conditions which were identical with the spectroscopic experiments corresponding to the first three points (at lowest coverage) in Figures 4 and 5. The final conversion factors derived for the 1620- and 1432-cm^{-1} bands amounted to $72 \pm 7 \times 10^{13}$ and $10 \pm 1 \times 10^{13}$ molecules/cm^2/absorbance unit, respectively. These values have no fundamental significance since they are a function of the amount of SA sample in the infrared beam. The indicated average deviation in the conversion factors produces a comparable uncertainty (approximately 10%) in the values of $(\Delta[NH_3]/\Delta[OH])_L$ and $(\Delta[NH_3]/\Delta[OH])_H$.

In Figures 4 and 5 it has been assumed that the absorption coefficients for LNH_3 and PNH_3 are identical. This is supported by the fact that the conversion factor for the third calibration point in Figures 4 and 5 is identical with those for the first two points even though appreciable physical adsorption occurs under the conditions for point three. Additional support is contributed by the value of $(\Delta[NH_3]/\Delta[OH])_H$ of one which is consistent with expectations for physical adsorption. Although these observations suggest that the assumption is reasonable, they are not conclusive. It should be recognized, therefore, that this assumption does not critically affect the conclusions of this paper.

Surface OH Concentration. The concentration of OH groups on the surface of evacuated SA which was determined by the thermogravimetric technique[15] and checked by deuterium-exchange experiments, amounted to 1.24×10^{14} OH/cm^2. Since surface SiOH groups are the only OH species,[17] the surface OH concentrations were estimated from the relative intensity of the 3745-cm^{-1} band without further calibration.

(25) J. J. Fripiat, private communication.

(26) R. P. Eischens, *Z. Elektrochem.*, 60, 782 (1956).

Molecular Association in Sodium, Potassium, and Cesium Vapors at High Temperatures

by C. T. Ewing, J. P. Stone, J. R. Spann, and R. R. Miller

U. S. Naval Research Laboratory, Washington, D. C. 20390 *(Received December 14, 1965)*

Imperfections in three alkali metal vapors at high temperatures (to 1400°) and high pressures (to 30 atm) are examined. Recently measured compressibility data are analyzed quasi-chemically by assuming that all types of imperfections may be treated ideally as an extent of the association of atoms into molecules. This analysis confirms the existence of substantial dimerization in the vapors and suggests that stable tetramer molecules may also exist. The equilibrium constants and enthalpies of dimerization and tetramerization (except for cesium) are evaluated.

Introduction

Spectroscopic and vapor-pressure[1] studies have shown that the vapors of alkali metals exhibit significant dimerization. Corroborating evidence from PVT data has been lacking and no information has been available on the type and extent of larger molecules (trimers or tetramers) which may also exist in the vapors. Compressibility data for vapor states of sodium, potassium, and cesium over substantial temperature ranges were reported by Stone, *et al.*[2] These data were reduced by the present authors[3-5] to yield consistent bodies of engineering properties, but the thermodynamic treatment of each metal was based on virial equations and no information on the molecular state of the vapors resulted. A quasi-chemical analysis of the same PVT data has been made in an effort to identify the molecular reactions occurring in the vapors and obtain quantitative information as to their extent.

Quasi-Chemical Study of PVT Data

Imperfections in Alkali Metal Vapors. An apparent equilibrium constant of dimerization, k_2', may be computed from PVT data at any given temperature and pressure by assuming that only ideal monomeric and dimeric species are present. A cursory examination of the PVT data of Stone, *et al.*,[2] based on this assumption reveals several facts. The apparent constants along any given isotherm increase substantially with increase in pressure and this increase varies systematically with temperature, becoming more pronounced at lower temperatures. This dependency of k_2' on temperature and pressure is characteristic of all three metals. It can be explained by the neglect of molecular species higher than the dimer, by failure to treat the individual species as real gases, or by any combination of higher molecular weight species and nonideality.

Theories dealing with association and gas imperfections may be reduced to two general forms. One, which is discussed by Hirschfelder, *et al.*,[6] fundamentally assumes that all imperfections may be regarded as the association of perfect-gas atoms to form perfect-gas assemblies of two or more atoms. The second theory, illustrated in the treatise by Vukalovich, *et al.*,[7] assumes that the atoms in a gas may combine to form stable molecules, but that both the interacting

(1) W. H. Evans, R. Jacobson, T. R. Munson, and D. D. Wagman, *J. Res. Natl. Bur. Std.*, 55, 83 (1955).

(2) J. P. Stone, C. T. Ewing, J. R. Spann, E. W. Steinkuller, D. D. Williams, and R. R. Miller, *J. Chem. Eng. Data*, 11, 309 (1966).

(3) C. T. Ewing, J. P. Stone, J. R. Spann, and R. R. Miller, *ibid.*, 11, 460 (1966).

(4) C. T. Ewing, J. P. Stone, J. R. Spann, and R. R. Miller, *ibid.*, 11, 468 (1966).

(5) C. T. Ewing, J. P. Stone, J. R. Spann, and R. R. Miller, *ibid.*, 11, 473 (1966).

(6) J. O. Hirschfelder, F. T. McClure, and I. F. Weeks, *J. Chem. Phys.*, 10, 201 (1942).

(7) M. P. Vukalovich, I. I. Novikov, D. V. Lebed, V. S. Siletsky, B. V. Dzampov, V. N. Zubarev, and D. S. Rasskasov, *Proc. Conf. Thermodyn. Transport Properties Fluids* (London), 91 (1958).

particles and the molecules must be treated as van der Waals (imperfect) gases.

Simple collisions among the species undoubtedly do lead to imperfections of the type described by Vukalovich, but whether or not these van der Waals imperfections may be incorporated ideally into association equilibria is debatable. In any event, since the contribution from this source to total imperfection (including association) would be expected to be small and cannot, at present, be partitioned from the total, it will be assumed for this treatment that all species behave as perfect gases.

Quasi-Chemical Method and Treatment of PVT Data. For an equilibrium mixture of ideal molecular species, the association of the vapor can be represented by a series of independent equilibria of the type

$$nX \rightleftarrows X_n \tag{1}$$

and the equilibrium constants in the series are defined by

$$k_n = \frac{N_n}{(N_1)^n p^{n-1}} \tag{2}$$

where N is mole fraction, p is pressure, and n may be 2, 3, or 4 for the dimeric, trimeric, and tetrameric reactions.

The method employed to identify species higher than the dimer is one which has been applied to the study of association in hydrogen-bonded organics.[8,9] The apparent equilibrium constant of dimerization, k_2', can be expressed as a power series[8]

$$k_2' = k_2 + 2k_3p + 3k_4p^2 + 2k_3^2p^3 - 2k_2k_4p^3 + \ldots \tag{3}$$

involving the pressure and the true equilibrium constants of the association reactions. The apparent dimerization constants at a given temperature may be computed from the PVT data, and the relationship of the apparent constants to pressure may be used to identify the higher reactions present in the vapor and to compute their equilibrium constants.

Although the possibility of the coexistence of significant amounts of trimer and tetramer was recognized, the existence of only one higher molecular weight species was believed to be more probable. If PVT data are of sufficiently high precision, a distinction between trimer and tetramer can be made with eq 3. If, in a vapor mixture, species of molecular weight higher than the trimer are not present, eq 3 (by setting $k_4 = 0$) reduces to

$$k_2' - 2k_3^2p^3 = k_2 + 2k_3p \tag{4}$$

Likewise, if the trimeric species is taken as insignificant, the same equation reduces to

$$k_2' + 2k_2k_4p^3 = k_2 + 3k_4p^2 \tag{5}$$

It follows from these equations that a linear relationship between $(k_2' - 2k_3^2p^3)$ and p implies the existence of trimer, while a linear relationship between $(k_2' + 2k_2k_4p^3)$ and p^2 implies the existence of tetramer.

Graphical plots of the apparent dimerization constants for each alkali metal vapor against p and p^2 were compared at several temperatures covering the experimental range of the data. For sodium and potassium, preliminary values of k_3 and k_4 were obtained and the dimerization constants were adjusted for the small p^3 terms. For cesium, on the other hand, these equilibrium constants were not obtained, so

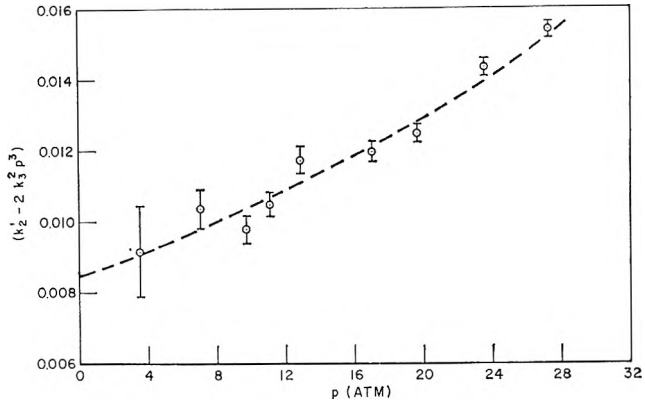

Figure 1. Plot of $(k_2' - 2k_3^2p^3)$ *vs.* p for potassium at 1344°.

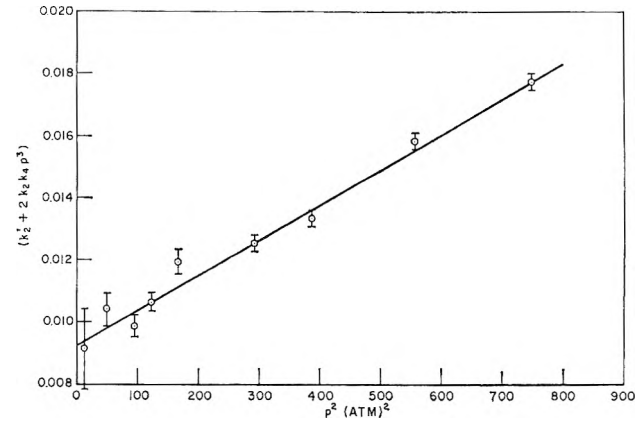

Figure 2. Plot of $(k_2' + 2k_2k_4p^3)$ *vs.* p^2 for potassium at 1344°.

(8) E. W. Johnson and L. K. Nash, *J. Am. Chem. Soc.*, **72**, 547 (1950).

(9) F. H. MacDougall, *ibid.*, **63**, 3420 (1941).

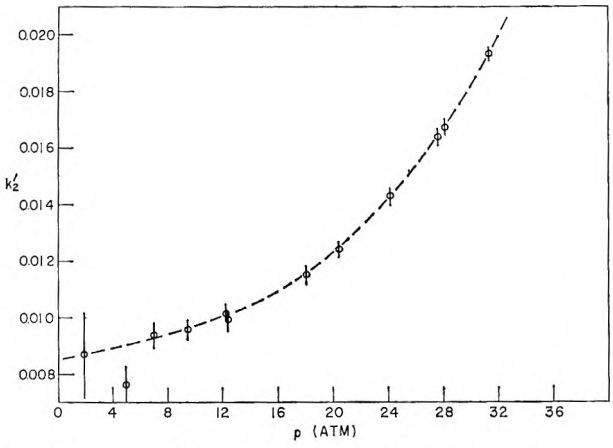

Figure 3. Plot of k_2' *vs.* p for cesium at 1316°.

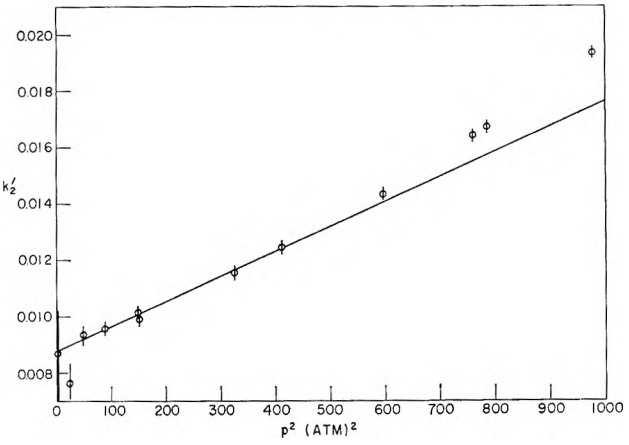

Figure 4. Plot of k_2' *vs.* p^2 for cesium at 1316°.

the higher order terms were neglected. The graphical testing of the data is illustrated with typical plots for potassium (Figures 1 and 2) and for cesium (Figures 3 and 4). Corresponding plots for sodium are not included since they are qualitatively similar to those presented for potassium. The tetramer relationship was found to provide the best correlation of the data for all three metals, but it is satisfactory for cesium only up to a pressure of 20 atm. Above this point, an even higher degree of association is required to satisfy the quasi-chemical picture. This analysis suggests that the more correct model for sodium and potassium is a near-perfect mixture of monomeric, dimeric, and tetrameric species, and that the more correct model for cesium is a similar mixture of near-perfect gases with a fourth species of molecular weight higher than the tetramer. However, the higher temperature and pressure states for cesium are much closer to the critical state than are those for potassium and sodium, and it is possible that interaction imperfections of the van der Waals type may become important for this metal.

Equilibrium Constants and Equations of State. Equilibrium constants were derived graphically by plotting functions along constant temperature lines. The functions were derived from smoothed compressibilities (at 27.8° temperature intervals) as obtained from large-scale plots of the data reported by Stone, *et al.*[2] The association constant of the dimer reaction at each temperature was obtained as the lim $k_2'_{(p^2\to 0)}$ and the association constant of the tetramer reaction as d(k_2')/d$(3p^2 - 2k_2p^3)$. The constants for each reaction for the full temperature range were effectively fitted by a single logarithmic relationship in $1/T$. The resulting equations, together with their experimental ranges and the standard deviations of the experimental points, are presented in Table I.

Equilibrium constants for the tetramer reaction are reported for two of the metals but not for cesium, since reactions of even higher order are required to satisfy the quasi-chemical picture for this metal. For sodium or potassium, the equations in Table I for the two reactions (with all species behaving as perfect gases) constitute an equation of state. The degree of fit of each equation of state to the observed PVT data may be shown mathematically. For example, all the compressibility data for either potassium or sodium as reported by Stone, *et al.*,[2] may be calculated from the appropriate equation of state with a standard deviation of less than 0.35%.

Apparent Equilibrium Composition of the Saturated Vapor of an Alkali Metal. If it is assumed that an alkali metal vapor is an ideal mixture of monomeric, dimeric, and tetrameric species, the relative amounts of dimer and tetramer in the equilibrium vapor at any pressure and temperature state may be computed with a modification of the method of Ritter and Simons.[10]

The molecular composition of sodium and potassium vapor was computed at saturation states covering the experimental temperature ranges. The two metals exhibited similar trends of composition with temperature, and the results presented for potassium in Figure 5 are typical of both metals. For a vapor system of this type, increasing temperature favors dissociation of each complex molecule while increasing pressure favors its formation. It is interesting that at saturation conditions the effect due to increasing pressure overbalances that due to increasing temperature, and both the dimer content and the apparent tetramer content increase with temperature.

(10) H. L. Ritter and J. H. Simons, *J. Am. Chem. Soc.*, 67, 757 (1945).

Table I: Equilibrium Constants of Reactions in Sodium, Potassium, and Cesium Vapors[a]

Metal	Correlation eq	Exptl temp range, °C	Std % dev (in terms of equil const)
Sodium	$\log k_2 = -4.3249 + 4002.3/T$	1135–1413	4.5
	$\log k_4 = -10.6798 + 9069.4/T$	1135–1413	4.7
Potassium	$\log k_2 = -3.8611 + 2951.4/T$	1035.4–1400	2.4
	$\log k_4 = -10.1453 + 7636.1/T$	1035.4–1400	5.5
Cesium	$\log k_2 = -3.6561 + 2538.9/T$	955.2–1400	1.7

[a] Equilibrium constants based on pressure in atmospheres. In the equations T is in °K.

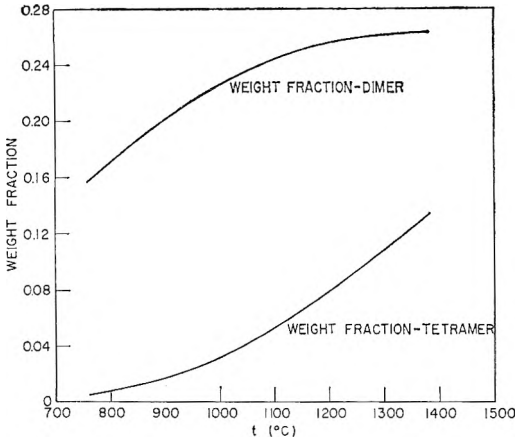

Figure 5. Apparent composition of saturated potassium vapor as a function of temperature.

Standard Heats of Reaction. These were obtained with the van't Hoff equation by substituting known differentials from the equations in Table I. The standard enthalpies[11] so obtained are

$$2Na \rightleftarrows Na_2,\ \Delta H_2^\circ = -18.30 \text{ kcal/mole}$$

$$4Na \rightleftarrows Na_4,\ \Delta H_4^\circ = -41.48 \text{ kcal/mole}$$

$$2K \rightleftarrows K_2,\ \Delta H_2^\circ = -13.50 \text{ kcal/mole}$$

$$4K \rightleftarrows K_4,\ \Delta H_4^\circ = -34.92 \text{ kcal/mole}$$

$$2Cs \rightleftarrows Cs_2,\ \Delta H_2^\circ = -11.61 \text{ kcal/mole}$$

Dimerization Enthalpies at Absolute Zero. These important thermodynamic quantities may be evaluated from PVT data using either a third-law[6] or a second-law[7] relationship. Reaction enthalpies at absolute zero

$$\frac{(\Delta H^\circ_0)_2}{T} = -R \ln k_2 - \Delta\left(\frac{F^\circ - H^\circ_0}{T}\right) \quad (6)$$

$$(\Delta H^\circ_0)_2 = \Delta H_2^\circ - \Delta(H^\circ - H^\circ_0) \quad (7)$$

were computed with both these equations and are presented in Table II along with corresponding spectroscopic values by Herzberg[12] and molecular beam values by Lewis.[13] The observed quantities, ΔH_2° and k_2, required for these calculations were evaluated from PVT data, and the enthalpy and free-energy functions were taken from the work of Evans, *et al.*[1] The enthalpy values obtained for each metal from the second- and third-law equations are in good agreement with the molecular beam values by Lewis and in reasonable agreement with the spectroscopic values selected by Herzberg.

Table II: Enthalpies of Dimerization at Absolute Zero

	NRL (eq 6)	NRL (eq 7)	Spectroscopic value	Mol beam value
Sodium	−16.8 to −16.9	−17.0	−17.53	−16.91
Potassium	−12.6 to −13.0	−12.4	−11.85	−12.67
Cesium	−10.9 to −11.1	−10.7	−10.38	

Discussion

The quasi-chemical analysis of the PVT data of the three alkali metal vapors confirms the existence of substantial dimerization at moderate temperatures and pressures and suggests that higher imperfections result principally from the formation of stable tetramer molecules. Each vapor is treated as an ideal mixture of molecular species and the identification of the tetramer when viewed from the standpoint of the association theory takes on added significance. This can be shown by considering the limiting case where

(11) The calorie used throughout this article is the mean calorie where 1 cal = 4.1860 absolute joules.

(12) G. Herzberg, "Molecular Spectra and Molecular Structure, I. Spectra of Diatomic Molecules," D. Van Nostrand Co., Inc., New York, N. Y., 1950, p 499.

(13) L. C. Lewis, *Z. Physik*, 69, 786 (1931).

the assumed ideality of the vapor species is incorrect and all the higher imperfections are simple interactions which do not lead to stable complexes. If these interactions are then analyzed as association equilibria, one would expect on a pure probability basis to find principally dimer and trimer molecules. The fact that trimers were not identified in the quasi-chemical fitting of the PVT data suggests that the higher order imperfections are due mainly to the association of particles into tetramer complexes. It must be recognized that this conclusion, in addition to its dependence upon the validity of the association theory, is further subject to the limitations imposed by the precision of the PVT data. There is an obvious need for the identification of the higher molecular weight species by an alternate technique.

Acknowledgment. This work was supported in part by the National Aeronautics and Space Administration.

Luminescence and Energy Transfer in Solutions of Rare Earth Complexes. II. Studies of the Solvation Shell in Europium(III) and Terbium(III) as a Function of Acetate Concentration

by John L. Kropp and Maurice W. Windsor

Chemical Sciences Department, Quantum Physics Laboratory, Physical Research Center, TRW Systems, Redondo Beach, California *(Received March 22, 1966)*

The fluorescence intensity and fluorescence lifetimes of Eu^{3+} and Tb^{3+} ions have been measured in H_2O solution and in D_2O solution as a function of the concentration of added acetate ion. By comparing the data for H_2O with those for D_2O solutions, it is possible to obtain (a) the radiative rate constant for fluorescence, $k_F(Ac^-)$, and (b) the fractional amount of water in the ion solvation shell m/m_s, both as a function of acetate ion concentration. The value of $k_F(Ac^-)$ increases steadily with acetate concentration, which indicates that acetate lowers the symmetry of the ion environment. This is supported by spectral absorption data. Agreement between our values of m/m_s and potentiometric measurements by Sonesson is obtained provided the ratio $m_s/n = 6$, where m_s is the hydration number in pure water and n is the number of water molecules replaced by each acetate ion. This agreement indicates the possibility of using the differential ($H_2O - D_2O$) quenching rate to assay the fractional water content of the ion solvation shell.

I. Introduction

The fluorescence yield and fluorescence lifetime of rare earth ions in solution are a function of the environment about the ion, being dependent upon the nature, number, and arrangement of the molecules present in the coordination shell of the ion. We have shown previously (part I of this series) that the dominant mode of quenching for excited rare earth ions in solution occurs *via* coupling of the electronic excitation to O–H and C–H vibrations in the solvation shell and that the rate constant for quenching is proportional to the number of bonds of each species present.[1] We showed

also that solvent deuteration greatly suppressed these nonradiative processes and led to a marked increase in the intensity and lifetime of fluorescence. In the present study, we have applied the technique of fluorescence enhancement by solvent deuteration to obtain information about the composition of the coordination shell surrounding Eu^{3+} and Tb^{3+} ions in aqueous solution, and how changes in the nature of the coordination shell affect the rate constants for fluorescence and for quenching for these ions. Data are obtained on lifetime and intensity of rare earth ion fluorescence as a function of the concentration of acetate ion. The data allow the determination of the fraction of the hydration shell not replaced by acetate and the rate constant for fluorescence emission by the excited ion as a function of acetate concentration.

II. Experimental Section

Anhydrous europium chloride and terbium chloride were prepared by heating the rare earth oxide in a 33% solution of HCl. Anhydrous Baker AR grade potassium acetate was used as received. Potassium acetate-d_3 was used as received from Merck Sharp and Dohme of Canada. H_2O was distilled water further deionized to remove heavy metals. D_2O was 99.7+% from General Dynamics Corp. (San Carlos, Calif.).

Stock solutions of europium chloride and terbium chloride in H_2O or D_2O were prepared at 0.5 M. Likewise, potassium acetate and potassium acetate-d_3 were prepared at about 10 M in either H_2O or D_2O. The experimental solutions were made by mixing and appropriately diluting portions of the above stock solutions. Solutions were not deoxygenated because previous work had shown oxygen quenching of rare earth ion fluorescence in solution to the unimportant.[1] Gravimetric analyses showed that the rare earth salts, as prepared, were not strictly anhydrous; thus the D_2O solution may have had up to 1.0% H_2O present as an impurity. Lifetime and intensity measurements were made on an apparatus previously described.[1]

III. Results and Discussion

Figure 1 shows the effect of increasing acetate ion concentration upon the total fluorescence intensity of the Eu^{3+} ion in H_2O and in D_2O and of the Tb^{3+} ion in D_2O. For Eu^{3+} in D_2O, increasing the acetate concentration from zero to 0.5 M causes an increase in fluorescence intensity by a factor of 2.2. At higher acetate concentrations, up to 3.0 M, the fluorescence intensity shows no further increase. The pattern is similar for $TbCl_3$ in D_2O except that the factor of increase is 1.9 up to 5.0 M. In H_2O the intensity of Eu^{3+} fluorescence increases eightfold between zero acetate

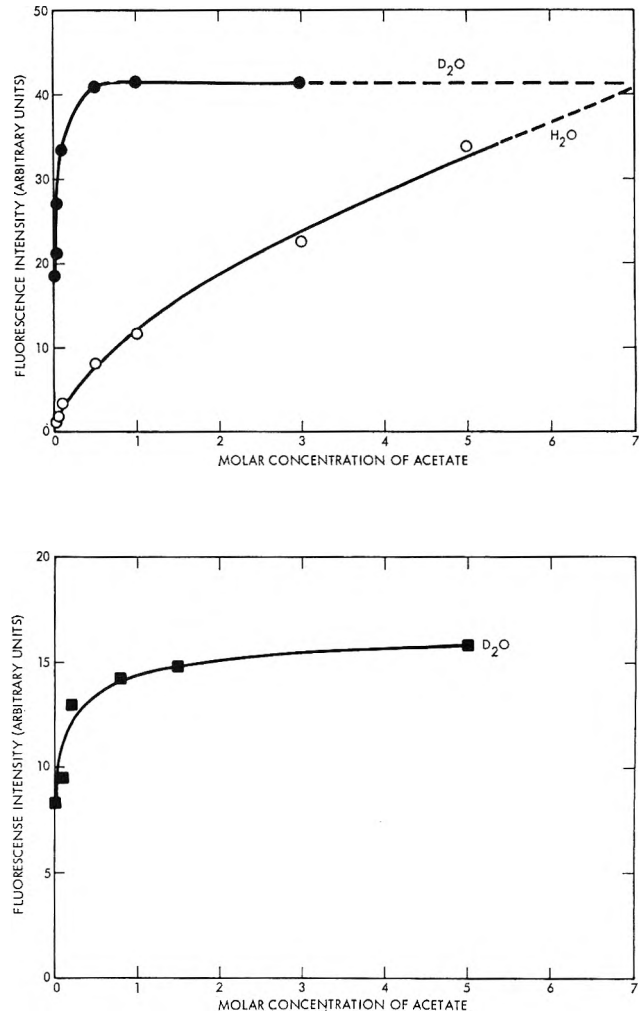

Figure 1. Fluorescence intensities of Eu^{3+} and Tb^{3+} solutions as a function of acetate concentration: (a) Eu^{3+} in H_2O (○) and in D_2O (●); (b) Tb^{3+} in D_2O (■).

concentration and 0.5 M and continues to increase in almost linear fashion to a final factor of 34 at 5.0 M.

Similar data for the fluorescence lifetimes as a function of acetate concentration are given in Figure 2. The fluorescence lifetime of $EuCl_3$ in D_2O shows a reduction by a factor of 1.5 over the 0 to 0.5 M range, and shows a gradual further drop with increasing acetate to a factor of 1.7 at 5.0 M acetate. The fluorescence lifetime of $EuCl_3$ in H_2O shows about a twofold increase between 0 and 0.5 M and has increased by a factor of 6 at 7.0 M, the highest acetate concentration studied. The lifetime of $TbCl_3$ in D_2O decreases by a factor of about 1.8 between 0 and 1.5 M acetate and then remains constant. The lifetime of $TbCl_3$ in H_2O increases by a factor of 2.5 between 0 and 5.0 M.

(1) J. L. Kropp and M. W. Windsor, *J. Chem. Phys.*, **42**, 1599 (1965).

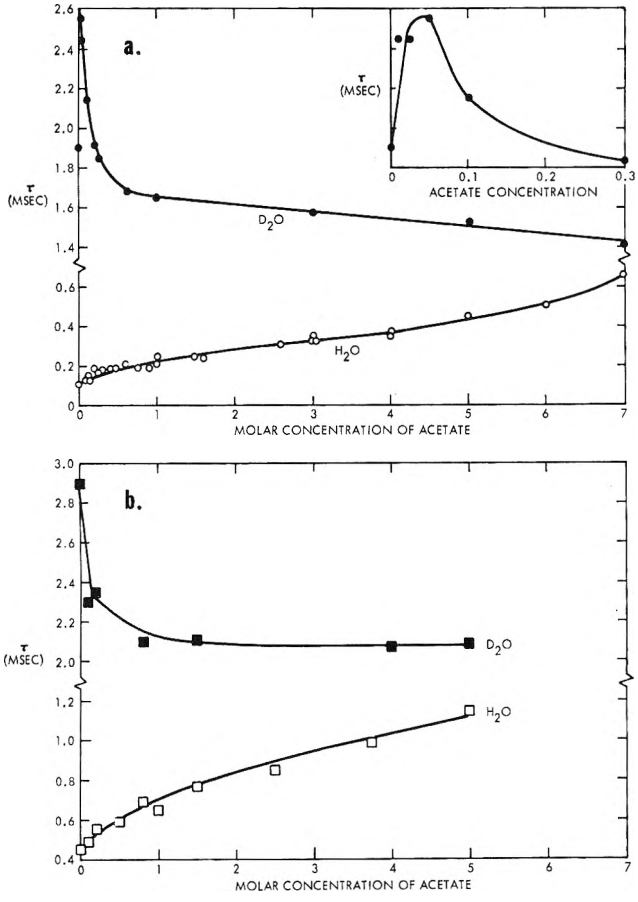

Figure 2. Fluorescence lifetimes, τ_F, of $EuCl_3$ and $TbCl_3$ solutions as a function of acetate ion concentration: (a) $EuCl_3$ in H_2O (○) and in D_2O (●). The insert shows the variation of τ_F at low acetate ion concentration. (b) $TbCl_3$ in H_2O (□) and in D_2O (■).

For all solutions, a plot of log I *vs.* t gives a linear relationship. This corresponds to a single lifetime characteristic of the solution studied. Gallagher[2] has done experiments similar to our previous work and reports two distinct lifetimes, one of 0.12 msec and one of 3.9 msec. On the basis of these lifetimes, he assumes that two fluorescing species are present: (a) a long-lived species having an hydration shell consisting entirely of D_2O, and (b) species with one or more OH groups in the hydration shell, all of which have a lifetime of 0.12 msec. We have shown elsewhere[3] that with regard to the functional way in which the fluorescence intensity of Eu^{3+} varies with per cent D_2O, Gallagher's data and ours are in agreement. However, we do not agree on the lifetime measurements. We have carefully reevaluated our previous data and those measured for the present report and find always a single decay time. In optically thin samples, there is a fast initial decay with a time constant of about 20 μsec, but this corresponds to the lifetime of the flashlamp. According to Gallagher, we should observe an initial decay time of 0.12 msec for all solutions containing less than 90% D_2O. In fact, we do not observe such behavior. We cannot explain this difference between our observations and Gallagher's.

We do not think that Gallagher's two-species model is reasonable in view of what is known about the rate of exchange of water molecules between the hydration shell and the bulk solvent. We can find no data on the exchange rates between hydrated water and solvent water specifically for Eu^{3+}. However, exchange rates of about 2×10^7 sec^{-1} have been quoted by Caldin[4] for La^{3+}. This is much faster than the rate of fluorescence of the Eu^{3+} ion. The net effect of this exchange will be to quench those Eu^{3+} ions that had a complete D_2O shell when originally excited. Thus, using Gallagher's assumption that one OH in the hydration shell is sufficient to quench the Eu^{3+} fluorescence completely to the pure H_2O value of 0.12 msec, we would expect a two-component decay. There would be an initial decay of 0.12 msec corresponding to species having at least one OH in their hydration shell at the time of excitation (static quenching). In addition, there would be a long-lived component whose lifetime varies between 0.12 msec and 3.9 msec depending on the H_2O concentration in the bulk solution. This latter corresponds to ions which have a complete D_2O shell when initially excited, but which are quenched subsequently owing to the migration of H_2O into the hydration shell (dynamic quenching).

Our observation of a single decay time which varies with H_2O concentration, together with the above arguments, leads us to conclude that exchange between bulk solvent and hydration shell is so rapid that each excited Eu^{3+} ion sees the same average environment at a given solvent composition. Our failure to observe a short-lived component strengthens our conviction that the quenching rate increases with the number of O–H bonds present in the hydration shell.

Thus, we shall interpret our present results in terms of the model we described previously.[1] We assume that the rare earth chloride in water is completely dissociated and that the Eu^{3+} or Tb^{3+} ion is surrounded by water molecules in the solvation shell. In H_2O solution, the excited rare earth ion is strongly quenched by radiationless processes which involve transfer of the electronic excitation of the ion to the high-fre-

(2) P. K. Gallagher, *J. Chem. Phys.*, **43**, 1742 (1965).

(3) J. L. Kropp and M. W. Windsor, *ibid.*, **45**, 761 (1966).

(4) E. F. Caldin, "Fast Reactions in Solution," John Wiley and Sons, Inc., New York, N. Y., 1964, p 277.

quency O–H vibrations of the solvent. By substitution of D_2O for H_2O, these radiationless processes are almost eliminated, because of the lower frequency of the O–D vibration. The effect is to increase both the fluorescence efficiency and the observed lifetime. Acetate ions displace H_2O or D_2O from the solvation shell because the rare earth ion and acetate ion form a more stable complex. Acetate affords protection against quenching similar to that provided by D_2O. This accounts in part for the enhancement of intensity and lifetime caused by acetate in the H_2O solutions. In the case of acetate, however, there is an added effect; whereas D_2O does not affect the rate constant for fluorescence emission, k_F, acetate lowers the symmetry about the rare earth ion, thereby enhancing k_F. Thus in D_2O solutions, the fluorescence intensity is increased, but the lifetime is shortened when acetate is added.

The change in symmetry with changing ion environment is known to affect the absorption spectra. Miller, Sayre, and Freed[5a] found, in comparing methanol solutions to those in 80% water–20% methanol mixtures, that the electric dipole transitions were enhanced in the methanol-rich system compared to water, while those that were magnetic dipole had the same intensity in both solutions. They attribute this to a lowering of the symmetry about the Eu^{3+} ion from D_{2h} in water[5b] to C_{2v} in methanol. We have similar data for some transitions in europium acetate solutions. The $^5D_0 \leftarrow {}^7F_0$ transition at 5800 A shows a slight decrease in integrated area with increase in acetate concentration. This transition is electric dipole in nature, and one may expect that the addition of acetate would make it more allowed. The other transitions, however, all show normal behavior. The transition at 5290 A, ($^5D_1 \leftarrow {}^7F_1$), according to previous workers, is electric dipole and increases in intensity from almost zero at low acetate ion concentration up to about 1.0 at 4 *M* acetate ion; the transition at 5240 A ($^5D_1 \leftarrow {}^7F_0$) is magnetic dipole in character and is unaffected by acetate ion from zero to 4 *M* acetate ion. The band at 4650 A ($^5D_2 \leftarrow {}^7F_0$) is electric dipole in character and increases by a factor of 30 from zero acetate to 4 *M* acetate ion. These changes are all in the direction one expects if the complexing by acetate ion lowers the symmetry about the rare earth ion. Thus, the spectral data substantiate the conclusion drawn from the fluorescence intensity and lifetime data.

Evaluation of Rate Constants. We can evaluate the various rate constants more explicitly. Previous work has shown that in solution at room temperature almost all emission occurs from the lowest excited state of the Eu^{3+} or Tb^{3+} ion. Energy is removed from this level by several processes. These, with their respective rate constants, are: fluorescence, k_F; quenching by hydrogen vibrations, k_H, or deuterium vibrations, $k_{D'}$; quenching by acetate, k_{Ac}; and quenching by unspecified residual mechanisms, k_X. In a previous paper,[1] we determined values for ($k_{D'} + k_X$). It is not possible from the data available to separate these two rate constants. In the present treatment, therefore, we use k_D to represent the sum of these two processes ($k_{D'} + k_X$). This will be shown to introduce very little error because ($k_{D'} + k_X$) is small compared to k_H.

The values of k_H, k_D, and k_{Ac} will vary with the number of water molecules or acetate ions in the coordination shell. We have shown previously that k_H is a linear function of the number of H_2O molecules in the coordination shell.[1] It is reasonable to expect a similar relationship to hold for k_{Ac}. We define k_H', k_D', and k_{Ac}' to be the rate constants for quenching *per molecule or ion present in the coordination shell.* If at zero acetate concentration, there are m_s water molecules present,[6-9] and if each acetate replaces n water molecules, the fluorescence intensity I_F and the fluorescence lifetime, τ_F, can be expressed in terms of rate constants as

$$I_F = Ck_F(Ac^-)\left[k_F(Ac^-) + mk_H' + \frac{1}{n}(m_s - m)k_{Ac}'\right]^{-1} \quad (1)$$

$$\tau_F = \left[k_F(Ac^-) + mk_H' + \frac{1}{n}(m_s - m)k_{Ac}'\right]^{-1} \quad (2)$$

where C is a proportionality constant and m is the number of H_2O molecules present in the coordination shell at any given acetate solution (*i.e.*, the ligand number). Similar expressions hold for the D_2O case with k_D' replacing k_H'. As already pointed out, the radiative rate constant, $k_F(Ac^-)$ will be a function of the acetate concentration, but, as we have defined them, k_H' and k_D' will have constant values and k_{Ac}', although it may vary with acetate concentration, will have the same value in both H_2O and D_2O solutions. Dividing eq 1 by 2 we obtain

(5) (a) D. G. Miller, E. V. Sayre, and S. Freed, *J. Chem. Phys.*, **29**, 454 (1958); (b) E. V. Sayre, D. G. Miller, and S. Freed, *ibid.*, **26**, 109 (1957).

(6) There is considerable uncertainty in the literature regarding the correct value of m_s. Morgan[7] and Ketelaar[8] show that the coordination number may be 8 or 9. However, Judd[9] shows that numbers between 6 and 9 are all possible. Thus, although 9 seems to be the favored coordination number for Eu^{3+} in water, we have chosen to leave m_s unspecified in the present discussion.

(7) L. O. Morgan, *J. Chem. Phys.*, **38**, 2786 (1963).

(8) J. A. A. Ketelaar, *Physica*, **4**, 619 (1937).

(9) B. R. Judd, *Phys. Rev.*, **127**, 750 (1962).

$$I_F/\tau_F = Ck_F(Ac^-) \quad (3)$$

Dividing this by its corresponding expression at zero acetate concentration, ($k_F(Ac^- = 0) = k_F^0$), we get

$$k_F(Ac^-) = k_F^0 \times \frac{I_F/I_F^0}{\tau_F/\tau_F^0} \quad (4)$$

The value of k_F^0 is not known for Eu^{3+} in aqueous solution. However, for Eu^{3+} in hydrated crystals, the value has been determined to be 70 sec^{-1};[10] the solution value should be similar. For $TbCl_3$ in H_2O and in D_2O, a value of 120 sec^{-1} for k_F^0 has been determined in this laboratory.[11] Using these values and data in Figures 1 and 2, we can determine $k_F(Ac^-)$ as a function of $[Ac^-]$ for the D_2O solutions.[12] The result is given in Figure 3. For Eu^{3+} the value for $k_F(Ac^-)$ shows a slight drop at low $[Ac^-]$ from the value in pure H_2O and then increases steadily to a value of 190 sec^{-1} at $[Ac^-] = 3.0\ M$. For Tb^{3+} no low concentration values are available, but $k_F(Ac^-)$ increases to 360 at $[Ac^-] = 5.0\ M$.

Change in Hydration Shell with Acetate Concentration. The difference between eq 2 and its analog for the D_2O solution at the same acetate concentration gives

$$1/\tau_F^H - 1/\tau_F^D = m[k_H' - k_D'] + [k_F^H(Ac^-) - k_F^D(Ac^-)] \quad (5)$$

Since $k_F(Ac^-)$, although dependent on acetate concentration, is independent of whether the solvent is H_2O or D_2O, the last term on the right in eq 5 is zero. Previous work in Eu^{3+} solutions[1] shows k_H is 9400 sec^{-1} and hence $k_H' = 9400/m_s$ sec^{-1}. Similarly, k_D was found to be 370 sec^{-1}, giving $k_D' = 370/m_s$ sec^{-1}. Actually, as stated earlier, k_D includes contributions from unspecified residual quenching mechanism in addition to quenching by O–D vibrations. The true value for quenching by O–D vibrations alone may, therefore, be somewhat lower.[13] However, the value of k_D does not greatly affect the determination of m since $k_D \ll k_H$ under any circumstances.[14] For Tb^{3+} solutions, the corresponding values of k_H' and k_D' are $2200/m_s$ sec^{-1} and $275/m_s$ sec^{-1}. Using these values, we can calculate values for m/m_s. The results are shown in Figure 4. The fraction m/m_s measures the fraction of the hydration shell not replaced by acetate. For both Eu^{3+} and Tb^{3+} the hydration shell is about half replaced by acetate at an acetate concentration of 0.5 M.

Sonesson has measured ligand numbers, l, for acetate ion in the acetate complexes of Gd^{3+}, Sm^{3+}, and Dy^{3+} by a potentiometric method.[15,16] Unfortunately, he studied neither Eu^{3+} nor Tb^{3+}. However, one would expect Eu^{3+} to be intermediate in behavior between Sm^{3+} and Gd^{3+}, and Tb^{3+} to be intermediate between Gd^{3+} and Dy^{3+}. We can obtain values of m/m_s from Sonesson's data using the relation $m/m_s = (1 - (n/m_s)l)$. This can be done for various values of the ratio m_s/n. The shaded area in Figure 4 embraces the results of this calculation for $m_s/n = 6$ for Gd^{3+}, Sm^{3+}, and Dy^{3+} from Sonesson's data. In addition, we have calculated values of m/m_s from Sonesson's data, using $m_s/n = 5$ and also 7. The

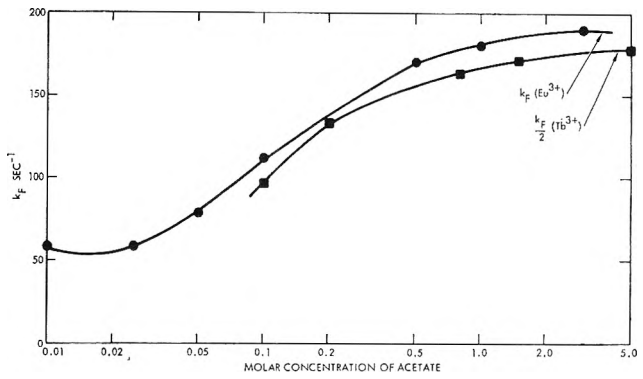

Figure 3. Variation of the radiative rate constant, $k_F(Ac^-)$, for Eu^{3+} (●) and Tb^{3+} (■) in D_2O as a function of acetate ion concentration. Values for Tb^{3+} have been divided by 2 to fit the curve.

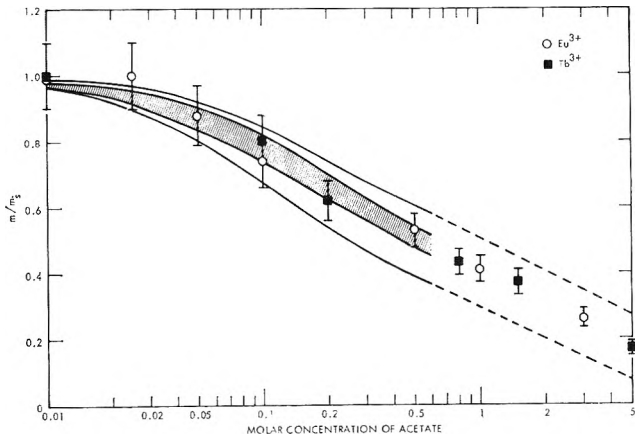

Figure 4. The fraction m/m_s as a function of acetate concentration, (○) for Eu^{3+}, and (■) for Tb^{3+}.

(10) B. Rinck, *Z. Naturforsch.*, 3a, 406 (1948).

(11) W. R. Dawson, J. L. Kropp, and M. W. Windsor, *J. Chem. Phys.*, 44, 2410 (1966).

(12) In H_2O solutions, the value of I_F^0 has too large an uncertainty to yield meaningful values of $k_F(Ac^-)$.

(13) A recent determination by Gallagher[2] sets k_D at 186 sec^{-1}.

(14) Use of Gallagher's value for k_D changes ($k_H - k_D$) by only 2%, which is not a significant change compared to the experimental error in the value of k_H itself.

(15) A. Sonesson, *Acta Chem. Scand.*, 12, 165 (1958).

(16) A. Sonesson, *ibid.*, 12, 1937 (1958).

higher solid line in Figure 4 is the locus of points for $m_s/n = 7$ for Sm^{3+}; corresponding points for Gd^{3+} and Dy^{3+} all lie below this line. The lower solid line is the locus of points for $m_s/n = 5$ for Dy^{3+}; corresponding points for Gd^{3+} and Sm^{3+} all lie above this line. Thus the two solid lines embrace all of the data points for all three rare earth ions for $m_s/n = 5, 6,$ or 7. Our experimental values of m/m_s for Eu^{3+} and Tb^{3+} lie well within the two solid lines and show good agreement with the narrower shaded band derived from Sonesson's data using $m_s/n = 6$. Five of our points at high acetate concentration lie beyond the range of Sonesson's measurements. Even so, they fall well within the extrapolations of the two solid lines. The data show best agreement for $m_s/n = 6$. This value of m_s/n embraces most of the physically reasonable combinations of m_s, the hydration number in pure water, and n, the number of water molecules replaced by each acetate ion. These are $m_s = 12$, $n = 2$; $m_s = 9$, $n = {}^3/_2$; $m_s = 6$, $n = 1$. It should be emphasized that the agreement is not dependent on a particular choice of hydration number, but only upon a particular value of the ratio, m_s/n.

What significance should be attached to the above agreement? The environment of a rare earth ion in solution at a particular acetate concentration probably varies with a time constant of the order of 10^{-6} sec. Thus, the number of acetate ions and water molecules in the coordination shell, and perhaps even the total coordination number, may fluctuate over such short periods of time. However, the fluorescence lifetime is several orders of magnitude greater than 10^{-6} sec. Thus, our observations measure the *average* environment of the ion. Sonesson's data measures the ligand number which is defined as the average number of acetate ions per rare earth ion. Sonesson's measurements were made at constant ionic strength and his data are undoubtedly more accurate than ours. The agreement with Sonesson's data, coupled with our observation of a single lifetime, strengthens our contention that the fluorescent properties of the system are dependent upon the average composition of the coordination shell about the rare earth ion in the water–acetate system.

The agreement with Sonesson's data shows also that the differential (H_2O–D_2O) quenching rate can be used to assay the fractional H_2O content, m/m_s, of the hydration shell of the ion in the presence of other ligands. Further, if the maximum hydration number m_s is known, the hydration number m can be obtained as a function of anion concentration.

IV. Summary and Conclusions

The results of this paper can be summarized as follows.

(1) Substitution of acetate for H_2O in the solvation shell of excited Eu^{3+} and Tb^{3+} ions leads to enhancement of the radiative process and reduction of nonradiative quenching. The observed net effect is a large increase in fluorescence intensity and a smaller increase in lifetime.

(2) In D_2O solutions, acetate enhances the radiative process to the same extent as in H_2O; because the order of quenching ability is $H_2O \gg Ac^- \sim D_2O$, the effect on the nonradiative process is smaller than in H_2O and in the reverse direction. The result is a small increase in intensity and a comparable decrease in lifetime.

(3) The value of the radiative rate constant, k_F, increases from 70 sec^{-1} at zero acetate concentration to 190 sec^{-1} at 3.0 M acetate for Eu^{3+}, and from 120 sec^{-1} at zero acetate to 350 sec^{-1} at 5.0 M for Tb^{3+}.

(4) By comparing the rates of quenching in H_2O with those in D_2O, the fractional amount of water in the ion solvation shell can be found as a function of acetate concentration.

The technique of solvent deuteration is useful for determining how the values of the radiative rate constant for fluorescence and the rate constants for the various nonradiative quenching processes change with the concentration of the complexing ligand. In addition, it can give useful information on the composition of the solvation shell in aqueous solutions of fluorescent cations. Whereas the potentiometric and other techniques give information on the number of anions present, the present method tells what fraction of the solvation shell is occupied by water molecules as a function of the concentration of the complexing anion. Ligand numbers for water can be obtained, provided one knows the number of water molecules initially present.

Osmotic Coefficient Data for the System Benzene–Benzoic Acid at 25°

by Kenneth R. Harris and Peter J. Dunlop

Department of Physical and Inorganic Chemistry, University of Adelaide, Adelaide, South Australia
(Received April 4, 1966)

An apparatus is described for the isopiestic measurement of the osmotic coefficients of organic solutions. Data for the system benzene–benzoic acid are reported. An exact equation relating the association constant of dimerization to the osmotic coefficient and the stoichiometric molality for a binary solution is also derived.

Introduction

The purpose of this note is to report osmotic coefficient data for the organic system, benzoic acid in benzene. The activity data of O-M. H. von Gierke[1] for the system benzene–diphenyl was used as an isopiestic reference. His results, expressed as osmotic coefficients (ϕ_R) at the various molalities (m_R), are arranged in Table I. They were transformed,[2] by the method of least squares, into a polynomial of the form

$$\phi_R = 1 + \sum_{i=1}^{6} A_i m_R^i \qquad (m_R < 18.2) \qquad (1)$$

The coefficients A_i, together with the standard deviation, are given in Table II. Although von Gierke's results were precise enough to show the temperature dependence of the solvent activity coefficient of the system benzene–diphenyl (and for this reason his data were preferred as a reference to those of other workers[3–5]), this dependence is insignificant within the molality range used in this work. Consequently the reference equation (eq 1) obtained from his results at 20 and 50° could be applied without correction at the intermediate temperature of 25°.

Theory[6]

The results in Table III were used to estimate the association constant, K_N, for benzoic acid in benzene where

$$K_N = \frac{N_2}{N_1^2} \qquad (2)$$

and N_i is the mole fraction of species i. Throughout this paper, subscripts 0, 1, and 2 are used to denote benzene, benzoic acid monomer, and benzoic acid dimer, respectively. Stoichiometric concentrations are not distinguished by subscripts. If deviations from ideality are attributed to the monomer–dimer equilibrium, a simple relation between the association constant and the experimental data may be derived. After some manipulation one obtains[9,10]

$$K_N = \frac{(1 - \psi)}{(2\psi - 1)^2}\left(\psi + \frac{1}{m\omega_0}\right) \qquad (3)$$

where

(1) O-M. H. von Gierke, Dissertation, Johannes Gutenberg University, Mainz, West Germany, 1957.

(2) The *practical* osmotic coefficient is used here and is defined for a nonelectrolyte by the relation

$$\phi = -\frac{1}{m\omega_0} \ln a_0$$

where a_0 is the solvent activity.

(3) J. H. Baxendale and B. V. Enüstün, *Phil. Trans. Roy. Soc. London, Ser. A*, **243**, 176 (1951).

(4) D. H. Everett and M. F. Penney, *Proc. Roy. Soc.* (London), **A212**, 164 (1952).

(5) H. Tompa, *J. Chem. Phys.*, **16**, 292 (1948).

(6) By assuming an ideal dilute solution, Schellman (see ref 7) obtained an equation for the association constant on the molality scale

$$K_m = \frac{m_2}{m_1^2} \frac{(1 - \phi)}{m(2\phi - 1)^2}$$

As Stokes (see ref 8) has recently indicated, the association constant must be defined on the mole fraction scale (eq 2) for an ideal solution; thus

$$K_N = \frac{(1 - \psi)}{(2\psi - 1)^2}\left(\psi + \frac{1}{m\omega_0}\right)$$

(7) J. A. Schellman, *Compt. Rend. Trav. Lab. Carlsberg, Ser. Chim.*, **29**, 223 (1955).

(8) R. H. Stokes, *J. Phys. Chem.*, **69**, 4012 (1965).

(9) Eq 3 and 4 are equivalent to eq 22, 23, and 24 in ref 10.

(10) H. D. Ellerton and P. J. Dunlop, *J. Phys. Chem.*, **70**, 1831 (1966).

$$\psi = \frac{\exp(\phi m \omega_0) - 1}{m\omega_0} \quad (4)$$

where ω_0 is one thousandth of the solvent molecular weight. It will be noted that as $m \rightarrow 0$, $\psi \rightarrow \phi \rightarrow 1$.

Experimental Section

Materials. Univar "Analytical Reagent" thiophene-free benzene was shaken with concentrated sulfuric acid several times until no further discoloration was observed, in order to remove unsaturated, nonaromatic, and heterocyclic compounds. It was then washed, dried, and crystallized. The crystallized fraction (about two-thirds) was distilled through a clean, dry, 1-m column packed with stainless steel helices 4 mm × 4 mm. The center fraction was collected and stored over sodium wire. Analysis by gas chromatography showed less than 0.05% impurity. The density, determined with Pyrex, single-stem pycnometers, was found to be $d^{25} = 0.87366 \pm 0.00001$ g/cc, which may be compared with the literature value[11,12] of 0.87368.

Diphenyl, obtained from British Drug Houses Ltd., U. K., was recrystallized from Univar AR petroleum ether (bp 60–80°). No difference was detected between the first and second recrystallized samples by the isopiestic method. It was then dried *in vacuo* and stored over silica gel.

ACS standard benzoic acid from Matheson, Coleman and Bell was similarly purified and stored. No difference between the unpurified, dried sample and the first recrystallized sample was detected by the isopiestic method.

The Isopiestic Apparatus and Its Operation. All solutions were prepared gravimetrically and the weights recorded were corrected to values *in vacuo*. They were prepared so that their molality ratio was reasonably close to its equilibrium value. The molecular weights used for benzene, benzoic acid, and diphenyl were 78.1150, 122.1247, and 154.2135, respectively; the densities of benzoic acid and diphenyl were taken to be 1.120 and 1.166 g/cc, respectively.

The apparatus (Figure 1) consisted of a large copper block mounted in a Pyrex vacuum desiccator, 8 in. in diameter, which had a brass lid. A brass plate, held in position by four rods and suspended a little above the block, contained eight holes symmetrically arranged, each for an isopiestic dish. Each dish was always placed in the same hole during each run. A

Table I: Osmotic Coefficients (ϕ_R) of Diphenyl–Benzene of Various Molalities (m_R) at 20 and 50° (Derived from the Results of von Gierke[1])

20°		50°	
m_R	ϕ_R	m_R	ϕ_R
0.3959	0.9557	0.5320	0.9653
0.8243	0.9442	0.7450	0.9496
1.166	0.9285	1.069	0.9353
1.487	0.9151	1.841	0.9010
1.775	0.8983	2.215	0.8871
1.787	0.8996	3.052	0.8559
2.129	0.8854	3.192	0.8509
2.397	0.8756	4.554	0.8095
2.517	0.8688	4.689	0.8065
2.652	0.8669	6.548	0.7597
2.689	0.8584	6.985	0.7511
2.864	0.8570	8.783	0.7148
3.577	0.8310	10.52	0.6851
3.596	0.8300	11.40	0.6714
4.447	0.8052	14.28	0.6318
4.484	0.8047	17.16	0.5973
4.500	0.8045	17.61	0.5915
6.016	0.7659	18.20	0.5849
6.243	0.7580		
6.311	0.7604		

Table II

Polynomial order, i	Coefficient
1	-0.77257×10^{-1}
2	0.14703×10^{-1}
3	-0.22935×10^{-2}
4	0.20176×10^{-3}
5	-0.88044×10^{-5}
6	0.14837×10^{-6}
Std dev	0.47×10^{-2}

Table III: Experimental Isopiestic Molalities, Osmotic Coefficients (ϕ), and Corresponding Values of the Function (ψ)

Diphenyl–benzene		Benzoic acid–benzene		
m_R	ϕ_R	m	ϕ	ψ
0.1883	0.9860	0.3643	0.5096	0.5133
0.2065	0.9847	0.4016	0.5063	0.5104
0.2264	0.9832	0.4406	0.5052	0.5196
0.3058	0.9777	0.5993	0.4989	0.5048
0.3392	0.9754	0.6699	0.4939	0.5003
0.3473	0.9748	0.6857	0.4937	0.5003
0.3874	0.9721	0.7669	0.4911	0.4983
0.4238	0.9697	0.8402	0.4891	0.4971

(11) G. Scatchard, S. E. Wood, and J. M. Mochel, *J. Am. Chem. Soc.*, 68, 1960 (1946).

(12) F. D. Rossini, *et al.*, "Selected Values of Physical and Thermodynamic Properties of Hydrocarbons and Related Compounds," Carnegie Press, Pittsburgh, Pa., 1953.

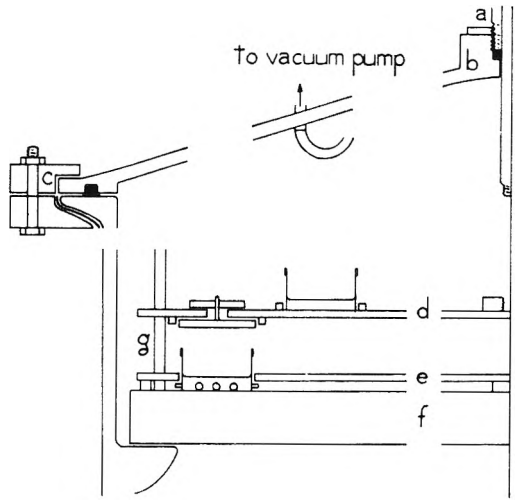

Figure 1. Section of the isopiestic apparatus. (a) Piston and sealing O ring, (b) brass lid, (c) clamping rings (with polythene padding around the glass lip), (d) movable upper plate, (e) fixed lower plate, (f) copper block, (g) guide rod. The diaphragm tap which is attached directly to the exit tube and which rests on the lid is not shown.

second plate, which could be moved up and down on the four guide rods by a piston in the lid, also had eight holes in it. The lids had small, circular handles which protruded through the holes when the plate rested on the dishes. Short pieces of nylon rod fitted loosely into the lid handles and held the lids to the top plate. Thus, when the desiccator was closed, the dish lids could be raised by screwing the piston home into the top plate and lifting it. The dishes had small brass tabs fitted to their sides which enabled them to be placed (*via* slots in the plate) so that, if the lids stuck slightly when the piston was moved upwards, the dishes pulled against the plate. The resultant pull was enough to free the lids without any splashing. The apparatus was sealed by buna rubber O rings, one around the lip of the lid and two between the piston and its cylinder. A diaphragm (Teflon) vacuum tap was used. These modifications of the more usual apparatus were made to reduce the benzene losses caused by evaporation which contribute most to the experimental error.

The apparatus was used in the following way. Four dishes were each filled with 5 cc of diphenyl solution and four with the same volume of benzoic acid solution. The dishes were weighed before and after filling. They were then placed on the copper block in the holes in the lower plate and the upper plate fixed to the lids by the nylon rods. A small crystallizing dish containing phosphorus pentoxide was placed on the upper plate to absorb any moisture present in the system. Two more isopiestic dishes without lids and containing a small amount of benzene, *i.e.*, enough to saturate the volume of the desiccator and to compensate for that lost during the pumping down process, were also included. The lid was replaced and air pumped slowly out of the apparatus until the internal pressure was a little above the vapor pressure of benzene. The presence of the pure benzene seemed to prevent the solutions from "splattering." The lid was clamped down (to prevent leaks) and the desiccator placed in a water bath and rocked gently to and fro by a special mechanical framework. Three stainless steel ball bearings (4 mm in diameter) in each dish served to stir the solutions. The dishes were removed after a week, reweighed to determine the equilibrium concentrations and the molalities were averaged. At the end of a run, the dishes were weighed as quickly as possible, having been kept on a silvered copper block in a benzene saturated atmosphere before being weighed.

The isopiestic dishes were made of cast silver and had polished flat bottoms. Some were gold or rhodium plated, but no difference was detected in the behavior of the three types of dish. The temperature of the water bath was kept constant to $\pm 0.005°$ over a period of 24 hr by a mercury–toluene regulator.

Results

The experimental equilibrium molalities, the corresponding osmotic coefficients, and the corresponding values of the function ψ are given in Table III. It is believed that the experimental molalities are precise to $\pm 0.2\%$ or better.

Since the values of the function ψ are close to a half so that $(2\psi - 1)$ has values comparable to the experimental error of ψ, *viz.*, $\pm 0.4\%$, K may not be accurately determined by use of eq 3.[13] However the results show that activity data may be readily obtained for systems in which the solvent has a much greater vapor pressure than water, provided the solute has a low enough volatility.

It is interesting to note that the densities of benzoic acid–benzene solutions, which we have also measured at 25°, show no variation with concentration in a way which might be ascribed to association of the solute. The density may be expressed by the equation

$$d = 0.87366 + 0.029824C \quad (0.044 < C < 0.65)$$

with an average deviation of $\pm 0.003\%$, where C is the

(13) F. T. Wall and P. E. Rouse, Jr., *J. Am. Chem. Soc.*, 63, 3002 (1941), have also studied this system by a volumetric isopiestic method. Their experiments were performed at lower concentrations than ours (about 0.09–0.38 *m*) and at higher temperatures (32.5, 44, and 56°); by assuming their reference solution (benzene–phenanthrene) to be ideal they obtained log K at each temperature to an accuracy of approximately $\pm 1.6\%$.

concentration in moles per 1000 cm^3. The apparent molar volume has the value 105.7_2 over the whole concentration range.

Acknowledgment. We wish to thank Professor G. V. Schultz of the Science Faculty of the Johannes Gutenberg University, Mainz, West Germany, for kindly making available to us the thesis of Dr. O-M. H. von Gierke.

Pyrolysis and High-Temperature Radiolysis of *o*-Terphenyl[1]

by J. M. Scarborough and R. B. Ingalls

Atomics International, A Division of North American Aviation, Inc., Canoga Park, California
(Received April 21, 1966)

The pyrolysis and high-temperature radiolysis (400–482°) of liquid *o*-terphenyl have been studied. The pyrolytic decomposition was found to follow simple first-order kinetics with an activation energy of 71.7 ± 1.3 kcal/mole. The radiolytically induced decomposition occurred with an apparent activation energy of about 22 kcal/mole. The ratio of biphenyl formation to terphenyl disappearance is about 0.35 for pyrolysis but increases with increasing temperature during radiolysis with 1-Mev electrons. A thermal spike model of low LET radiolysis originally derived to explain the radiolysis of toluene at low temperatures is shown to account for the major features of the data.

Introduction

In order to rationalize the occurrence of chemical reactions which require high activation energies during low temperature, low LET (linear energy transfer) radiation, regions of high-energy density called thermal spikes have been suggested.[2] In ref 2a it was estimated that radiation-induced reactions take place at "temperatures" on the order of 500° above ambient. If ambient temperature is sufficiently high, it is to be expected, then, that (radiation-induced) pyrolytic decomposition will occur in the thermal spike in addition to the decomposition induced more directly by the ionizing radiation. Thus the theory predicts a kind of synergistic effect of high temperature and ionizing radiation rather than the simple addition of the two effects. Such synergism has been observed in the high-temperature radiolysis of *o*-terphenyl which is the subject of the present paper.

Experimental Section

Samples of chromatographically pure *o*-terphenyl contained in evacuated stainless steel capsules were pyrolyzed at 419, 428, 455, and 482°. Other samples of the same *o*-terphenyl were irradiated with 1-Mev electrons at controlled temperatures in special irradiation cells which were designed to operate at high temperatures and pressures. The samples were thoroughly degassed and the cells were sealed under vacuum in a manner similar to that used for the pyrolysis capsules. A cross-sectional drawing of the irradiation cell is shown in Figure 1. The unique feature of this cell is the reinforcement of the thin window with a stainless steel honeycomb structure. The completed cell withstood a pressure of 1600 psi at 480° in air and passed virtually all of the electron beam that would be transmitted by the unsupported window.

Precautions were taken to minimize thermal degradation of the samples during heating to experimental

(1) This work was supported by the U. S. Atomic Energy Commission.

(2) (a) R. B. Ingalls, P. Spiegler, and A. Norman, *J. Chem. Phys.*, 41, 837 (1964); (b) J. M. Scarborough and J. G. Burr, *ibid.*, 37, 1890 (1962).

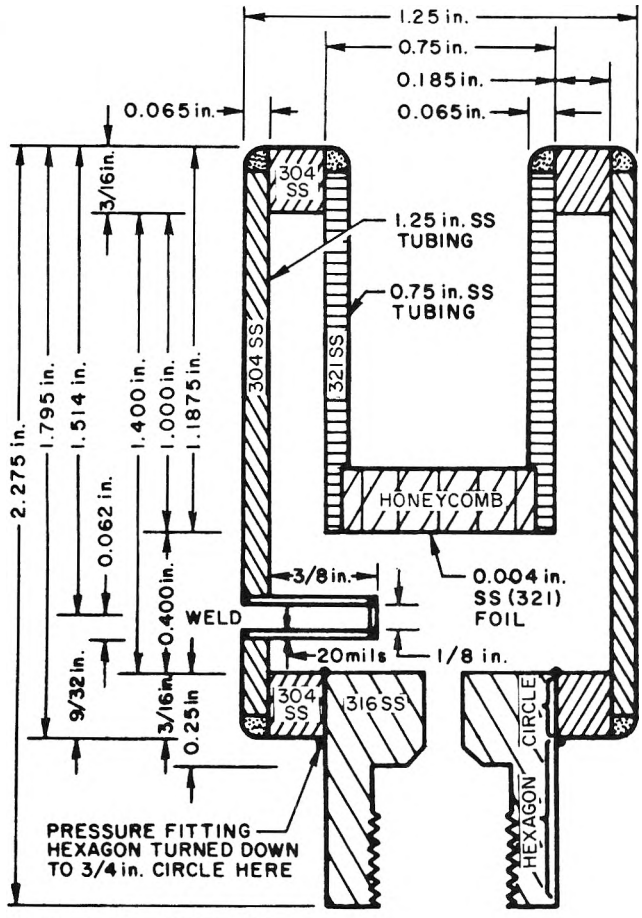

Figure 1. Irradiation cell.

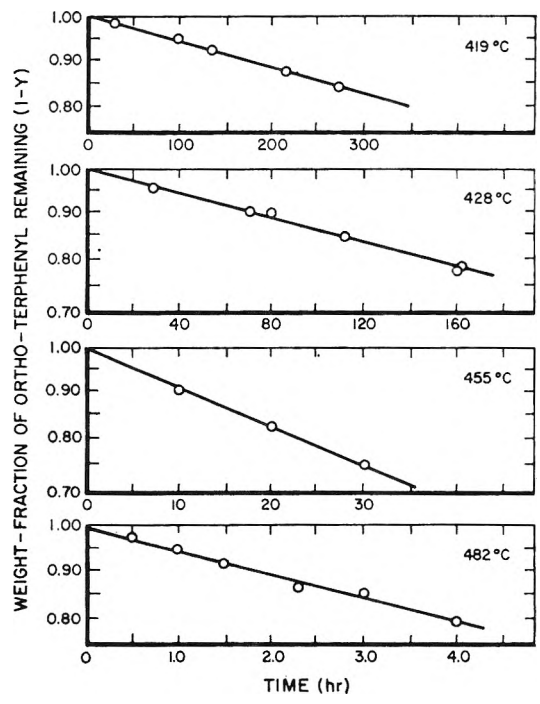

Figure 2. Weight fraction of o-terphenyl *vs.* time.

temperature, and corrections were made for the slight damage which did occur during initial heating and cooling. This correction was significant only at 482° and even at 482° it was less than 2%.

All irradiated and pyrolyzed samples were analyzed by standard methods of gas chromatography to determine the major components, o-terphenyl and biphenyl.

Dosimetry was based on the hydrogen yield (G_{H_2} = 0.038) from benzene.

Results

Pyrolysis. Experimental results for the pyrolysis experiments are shown in Figure 2. The concentration (weight fraction) of o-terphenyl remaining as a function of time at a given temperature was found to be best represented by a first-order equation of the form

$$(1 - y) = e^{-kt}$$

where $(1 - y)$ is the weight fraction of o-terphenyl remaining after t hours, and k is specific rate constant (initial decomposition rate). Figure 2 shows the semilog plots of concentration *vs.* time in hours.

Specific reaction rates, k, for each temperature were determined by the method of least squares. Thus the specific reaction rates at 419, 428, 455, and 482° were 0.00067, 0.00154, 0.0103, and 0.0588 hr^{-1}, respectively.

The initial thermal decomposition rate for o-terphenyl as a function of temperature is given by the expression

$$\ln R_{(-\phi_3)} = -(36{,}100/T) + 44.9$$

where R is in weight fraction per hour and T is temperature in degrees Kelvin. An Arrhenius plot of initial rates is shown in Figure 3; the corresponding activation energy is 71.7 ± 1.3 kcal/mole.

Owing to the scatter in the data for the formation of biphenyl, it is not possible to establish clearly whether biphenyl formation is a zero or first-order reaction. However, a somewhat better fit of the data was obtained from a first-order equation of the form

$$\phi_2 = c(1 - e^{-kt})$$

where ϕ_2 is the weight fraction of biphenyl present in the sample, t is the time in hours, k is the specific rate constant for terphenyl disappearance, and c is a constant. The initial formation rates for biphenyl at 428, 455, and 482° are thus 0.00040, 0.0028, and 0.0149 weight fraction/hr, respectively.

The temperature dependence of biphenyl formation is plotted in Figure 3 and is given by the expression

Table I: Radiolysis of *o*-Terphenyl

Temp, °C	Time, hr	Total dosage, w hr/g	Dosage rate, w/g	Composition of sample, wt fraction: *o*-terphenyl, $1 - y$	Total decompn products, y	Biphenyl, ϕ_2
400 ± 3	0.517	0.419	0.810	0.923	0.077	0.0056
	1.00	0.862	0.862	0.900	0.100	0.0075
	1.58	1.296	0.820	0.862	0.138	0.0238
	3.00	2.473	0.824	0.789	0.211	0.0372
	4.08	3.342	0.819	0.749	0.251	0.0454
	5.0	4.438	0.888	0.696	0.304	0.0557
	12.0	9.91	0.826	0.589	0.411	0.0678
	20.0	16.45	0.823	0.477	0.523	0.756
428 ± 3	0.333	0.241	0.723	0.931	0.069	0.0178
	0.750	0.541	0.721	0.866	0.134	0.0348
	1.25	0.940	0.752	0.827	0.173	0.0405
	1.50	1.071	0.714	0.823	0.177	0.0389
	3.00	2.140	0.713	0.709	0.291	0.0649
	6.75	4.766	0.706	0.568	0.432	0.0856
	10.0	7.170	0.717	0.447	0.553	0.103
454 ± 3	0.50	0.431	0.861	0.815	0.185	0.0448
	0.80	0.689	0.861	0.760	0.240	0.0585
	1.53	1.310	0.856	0.673	0.327	0.0805
481 ± 3	0.50	0.445	0.889	0.752	0.248	0.0639
	1.00	0.893	0.893	0.643	0.357	0.0904
	1.50	1.252	0.834	0.595	0.405	0.103
	2.3	1.830	0.796	0.500	0.500	0.123

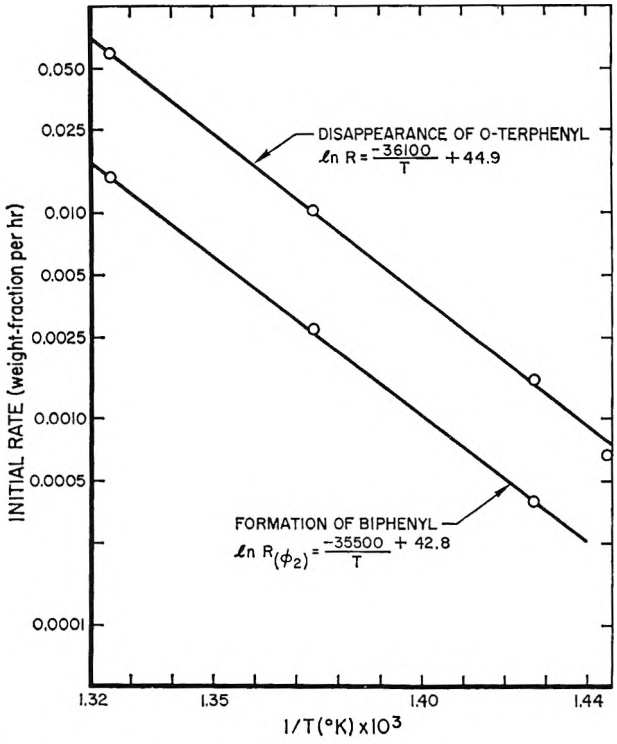

Figure 3. Initial rates *vs.* inverse of temperature.

$$\ln R_{(\phi_2)} = (-35{,}500/T) + 42.8$$

where R is in weight fraction per hour and T is in degrees Kelvin. The activation energy is therefore about 71 kcal/mole. This is, within experimental error, the same as the activation energy for terphenyl decomposition.

Radiolysis. Radiolysis data are shown in Table I. Since simple first, second, or third-order kinetic equations did not provide satisfactory representation of the data, the differential method[3] was used to determine the initial rates (specific rates) graphically.

Initial G values (molecules of *o*-terphenyl destroyed per 100 ev of energy absorbed) were calculated from initial decomposition rates. The temperature dependence of initial G values is shown in Figure 4 and is represented by the expression

$$\ln G = (-11{,}100/T) + 17.2$$

Thus the radiolytic decomposition of *o*-terphenyl occurs with an activation energy of 22 kcal/mole.

Biphenyl Formation. The differential method was

(3) K. J. Laidler, "Chemical Kinetics," McGraw-Hill Book Co., Inc., New York, N. Y., 1950, p 14.

also used to determine the initial formation rates (specific rates) for biphenyl from data in Table I. Initial G values for the formation of biphenyl were calculated from initial rates. The temperature dependence of biphenyl formation based on initial G values is shown in Figure 4. It may also be seen from Figure 4 that the Arrhenius plot for biphenyl formation is linear and corresponds to an activation energy of about 40 kcal.

Discussion

Pyrolysis. The activation energy (71.7 ± 1.3 kcal) observed for the pyrolysis of *o*-terphenyl is significantly lower than the dissociation energy of the weakest bond; *i.e.*, about 95 kcal for the C–C bond between rings. This suggests that a chain mechanism is involved in the thermal decomposition. The pyrolysis of the three isomeric terphenyls has been studied quite extensively by Juppe, Alvarenga, and Hannaert.[4] Their results indicate that the molar yields of benzene and biphenyl are approximately equal, that the moles of hydrogen formed equal roughly the number of moles of higher molecular weight products such as quater- and quinquephenyl, and that there is significant isomerization of *o*-terphenyl by a first-order reaction.

These findings suggest that displacement reactions of the type

$$\begin{aligned} \dot{\varphi}_3 + \varphi_3 &\longrightarrow H + \varphi_6 \\ &\longrightarrow \dot{\varphi} + \varphi_5 \\ &\longrightarrow \dot{\varphi}_2 + \varphi_4 \\ &\longrightarrow \dot{\varphi}_4 + \varphi_2 \\ &\longrightarrow \dot{\varphi}_5 + \varphi \end{aligned}$$

are common. Furthermore, C–H bond breaking will probably occur to an appreciable extent at these temperatures, so that the reaction mechanism is probably quite complicated. However we do not need to understand this mechanism in detail in order to use the thermal decomposition of *o*-terphenyl as a measure of local temperatures, which is what we do in effect below.

Radiolysis. The average LET of cobolt-60 γ-ray radiolysis is so low as to suggest that no track effects should be observed. However, there are δ rays produced which may deposit 1 kev or more of energy[5] in a very small volume. This energy is deposited largely as excitation and ionization of the molecules of an organic liquid. Such electronic excitation will usually lead directly to vibrational excitation since the intranuclear distance at minimum energy is in general different in an excited state than it is in a ground state. Thus, Franck–Condon transitions lead to vibrational (and rational) excitation which is quickly equilibrated with its surroundings and forms the basis for assigning a "temperature."

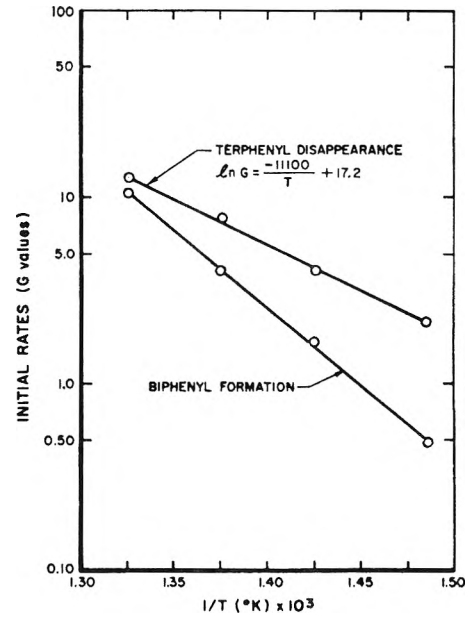

Figure 4. Temperature dependence of initial G values.

The lifetimes of ions and electronically excited states are probably quite short in an organic liquid so that most of the energy originally deposited as electronic energy is converted into the form of vibrational and rotational energy ("heat") in a short time. Magee[6] has estimated that after about 10^{-12} sec it is possible to assign temperatures with some validity. Thus, these δ rays constitute thermal spikes which are qualitatively different from the rest of the solution. The LET in the δ rays is quite high[7] even though the average LET is low. Most of the chemical reactions induced by γ or electron irradiation occur in the low LET portion of the electron path (*i.e.*, outside of the thermal spike) but the higher temperatures and higher concentrations of excited molecules in the δ-ray thermal spikes allow reactions to proceed which cannot otherwise occur at measurable rates. Thus, certain products may be formed in the thermal spikes *exclusively*.

We propose that this thermal spike model is applicable to the high-temperature electron irradiation of *o*-terphenyl, and we will compare the properties of this model with the experimental results.

(4) G. Juppe, A. Alvarenga, and H. Hannaert, *European Atomic Energy Community*, Euratom publication EUR 1647e (1964).

(5) The number of such events is small and difficult to determine but the energy deposited in these high-energy δ rays may be as high as 8% of the total absorbed from Co^{60} radiation. See A. M. Rauth and J. A. Simpson, *Radiation Res.*, **22**, 643 (1964).

(6) J. L. Magee, *Discussions Faraday Soc.*, **36**, 232 (1963).

(7) 1 kev in 6×10^{-7} cm = 17 ev/A.

The decomposition of *o*-terphenyl induced by ionizing radiation at room temperature is more than an order of magnitude lower than that induced by radiation at the temperature used in this investigation. Thus to a first approximation the decomposition induced directly by the ionizing radiation may be neglected by comparison with the decomposition which is induced by both heat and radiation. Presumably, most of the energy of the ionizing radiation is lost in processes which are quite independent of temperature.

However, temperatures in the thermal spike have been estimated[2a] to be in the order of 500° above the temperature of the bulk of the sample. Although these thermal spikes are of short duration, encompass a small number of molecules, and account for only 8% of the energy of the ionizing radiation, they may be responsible for initiating most of the decomposition observed during radiolysis at high temperatures. Thermal spikes attaining "temperatures" of several hundred degrees above the temperatures at which the irradiations reported in this paper were carried out result in the thermal dissociation of substrate molecules as well as free radicals and other intermediates. This initiation is followed by a chain and thereby enhances the decomposition markedly. Thus, we propose that the only chemically important step in the "radiation-induced pyrolysis" of *o*-terphenyl which occurs in the thermal spike is the initial dissociation of the molecules into free radicals which requires about 95 kcal/mole, since there is not time for the chain reactions involved to take place before the thermal spike cools off. Chain propagation probably requires a sufficiently low activation energy that it occurs readily outside the thermal spike in these experiments. Thus the thermal spike "temperature" referred to in this paper is "vibrational temperature," since translational and rotational degrees of freedom do not play a major role in the dissociation of molecules.

The conclusion that there is a chain reaction occurring outside the thermal spike is supported by the magnitude of the yields observed. At 481° $G(-o\text{-terphenyl})$ is 12.7, which requires that about 1500 molecules be decomposed per thermal spike. There are only about 300 molecules in a volume with a radius of 3×10^{-7} cm,[8] however, so that the spikes are simply not large enough to account for the yields if all the reaction were to take place in the spike. Furthermore, at 1200–1500°K only a fraction of the molecules in the spike are expected to decompose in 10^{-11} sec.[8] This time is long compared to the lifetime of excited states in a liquid and is long compared to the time required for a molecule to dissociate, but at 1200–1500°K only a small fraction of the molecules have sufficient energy to dissociate. Thus, it is clear that the model requires that a chain reaction continue outside the thermal spike in general agreement with the accepted interpretation of the pyrolysis of *o*-terphenyl.

Therefore, the energy required to break the weakest bond (≈95 kcal) and initiate the chain is taken as the approximate activation energy of the "radiation-induced pyrolysis" and a value of 1430°K is obtained for the temperature in the thermal spike calculated on that basis.[9] This is some 700° higher than the bulk temperature which is higher than the 500° above ambient estimated in the case of toluene. Quite obviously these estimates do not take into account all the observed decomposition such as the temperature dependence of chain length, so that 500 and 700° temperature rise for these two systems is satisfactory agreement.

The fact that pyrolytic reactions are not the only reactions involved in the high-temperature radiolysis of *o*-terphenyl is demonstrated by the fact that the ratio of biphenyl yield to *o*-terphenyl disappearance is constant in pyrolysis but varies with temperature in radiolysis (Figure 5). Thus, the model must not only account for a variation of the ratio of biphenyl formation to *o*-terphenyl disappearance, but it must account for a higher value of the ratio of biphenyl formation to terphenyl disappearance in high-temperature radiolysis than in pure pyrolysis.

These results are accounted for by the model because of the formation of a high concentration of phenyl and biphenyl radicals as a result of thermal dissociation in the thermal spike. These radicals are then available for reaction with the biphenyl–cyclohexadienyl radical produced *via* radiolysis.[10] The products of these reactions are probably benzene, biphenyl, terphenyl, and quaterphenyl. Another reaction which may occur in the thermal spike which would result in the formation of benzene and biphenyl is the direct combination of hydrogen atoms with phenyl and biphenyl radicals (produced pyrolytically). By either of these mechanisms or by a combination of the two, the relative yield of biphenyl will increase with increasing temperature, and can exceed the yields, relative to terphenyl disappearance, which occur in pure pyrolysis.

However, it should be pointed out that this is by no

(8) The dimensions of the thermal spike were estimated theoretically in ref 2a.

(9) The estimate of the local temperature in the thermal spike is made as in ref 2a by solving for the temperature T at which a reaction with an activation energy E = 95 kcal will change its rate by the observed factor ρ = 12.7/2.14 = 5.94 in a change of temperature ΔT = 400° − 481° = −81°, as observed. This temperature is 1430°K.

(10) Hydrogen atoms, a major intermediate in the radiolysis of aromatic systems, add to the aromatic substrate to produce cyclohexadienyl radicals.

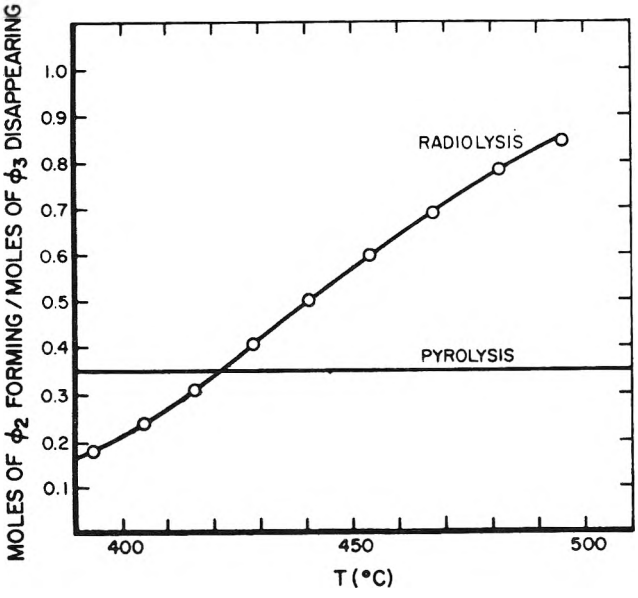

Figure 5. Ratio of biphenyl formation to terphenyl disappearance *vs.* temperature.

means the only possible kind of explanation for our results. Other workers[11] have suggested that the thermal decomposition of free radicals produced by the ionizing radiation leads to a chain reaction and is responsible for the small variations of yield with temperature. Such a mechanism is possible in saturated hydrocarbon systems. However, aromatic radicals in the *o*-terphenyl will not dissociate with an activation energy near 20 kcal/mole. Therefore, this explanation is not applicable to the *o*-terphenyl system. "Hot" atoms or radicals may provide the basis for still another explanation.[12] Radiolytic instability of some pyrolytic decomposition products[13] or pyrolysis of radiation-induced products[14] have also been suggested for aromatic systems. However, the success of the thermal spike model in accounting qualitatively for the variation of yields of products formed by high activation energy processes (those products produced mostly in the thermal spike) in at least two systems makes it attractive even if other explanations exist for each system separately.

Thus the thermal spike model provides the basis for explanation of the large yields observed and temperature dependence of the data presented, and this same model has been used to explain the low-temperature dependence and low yields of hydrogen observed in the low-temperature radiolysis of toluene.[2a] In the earlier example of its application the bulk temperature was so low and the LET so small that no significant pyrolysis occurred. In the experiments reported here, the bulk temperature is apparently high enough so that the energy density in the thermal spike is sufficient to induce significant thermal dissociation. This initiation is followed by a chain reaction which leads to the high yields of products observed.

If the combined pyrolytic and radiolytic decomposition yields are compared to the pyrolytic yields and low-temperature radiolysis yields (assuming that radiolysis and pyrolysis are additive), it is found that, separately, they each contribute only slightly to the total decomposition rate. Even at 482° pyrolysis alone accounts for less than 6% of the combined radiolytic and pyrolytic rate, at a dosage rate of 0.8 w/g and the low-temperature radiation yield is lower by more than an order of magnitude. Thus high temperatures and ionizing radiation are synergistic, as predicted by the thermal spike model.

The thermal spike model is admittedly crude and in need of refinement. It is inherently approximate so long as it uses the concept of "temperature" to describe a region which is obviously not in thermodynamic equilibrium. Also, an exact description of the shape of the spike (*i.e.*, energy density as a function of time and space) is not easily determinable. However such limitations may not impair the usefulness of the model in correlating observations and predicting results.

Summary and Conclusions

The pyrolytic decomposition of *o*-terphenyl follows simple first-order kinetics. Specific reaction rates were established at 419, 455, and 482° and the activation energy for the thermal decomposition of *o*-terphenyl was found to be 71.7 ± 1.3 kcal/mole.

Biphenyl formation in pyrolysis also follows apparent first-order kinetics and may occur with the same rate-determining step as the decomposition of *o*-terphenyl; the activation energy for biphenyl formation is equal within experimental error to that for *o*-terphenyl disappearance.

This work establishes a temperature dependence for the radiolysis of *o*-terphenyl not clearly indicated in previous work. An activation energy of 22 kcal/mole was observed in the temperature range studied which is significantly lower than that expected for free-radical dissociations in aromatic systems. Thus, this

(11) A. V. Topchiev, "Radiolysis of Hydrocarbons," English ed, R. A. Holroyd, Ed., Elsevier Publishing Co., Amsterdam, 1964, p 204; and P. L. Lucchesi, B. L. Tarmy, R. B. Long, D. L. Baeder, and J. P. Longwell, *Ind. Eng. Chem.*, **50**, 879 (1958).

(12) J. Y. Yang and J. G. Burr, *J. Chem. Phys.*, **44**, 1307 (1966); R. B. Ingalls, *ibid.*, **44**, 1308 (1966).

(13) J. Weiss, C. H. Collins, J. Sacher, and N. Carciello, *Ind. Eng. Chem.*, **3**, 73 (1964).

(14) P. Leveque, F. Franzetti, M. Van der Venne, and M. Guilani, *U. N. Intern. Conf. Peaceful Uses At. Energy, 3rd*, **A**, 28/P/53, May 1964.

result suggests that one or more of the rate-controlling steps in the high-temperature radiolytic decomposition involves thermal dissociation in a thermal spike.

Acknowledgment. The authors wish to thank Dr. Richard Holroyd of our laboratory for extremely helpful discussions and criticism of this work. We wish to acknowledge the help of Dr. Trent Tiedeman, also of this laboratory, for his assistance in calculating the activation energies of certain free-radical processes which may occur during pyrolysis of *o*-terphenyl.

Rates and Solvent Participation in Acid–Base Reactions of Substituted Phenols and Phenoxides in Methanol[1a]

by Ernest Grunwald,[1b] Charles F. Jumper, and Mohindar S. Puar[1b]

Bell Telephone Laboratories, Inc., Murray Hill, New Jersey, and Lecks Chemical Laboratories, Brandeis University, Waltham, Massachusetts *(Received May 31, 1966)*

The kinetics of proton exchange between methanol (the solvent) and *p*-nitrophenol or *p*-bromophenol has been investigated by the nmr method in buffered solutions containing phenol and phenoxide and in acid solutions containing phenol and HCl at −80°. Rates of proton exchange are derived from measurements of the CH_3– and OH–proton resonances of methanol and of the OH–proton resonance of the phenol. The following processes involving the given numbers of solvent molecules have been identified: (1) base dissociation of ArO^-, which involves two solvent molecules, $ArO^- + HO(CH_3) + HOCH_3 \rightleftarrows ArOH + (CH_3)OH + {}^-OCH_3$; (2) a symmetrical process that involves one solvent molecule, $ArO^- + HO(CH_3) + HOAr \rightarrow ArOH + (CH_3)OH + {}^-OAr$; and (3) a process that involves one methyloxonium ion, one ArOH, and an unknown number of solvent molecules. Rate constants for these processes and base dissociation constants K_B for reaction 1 are reported. Substituent effects on K_B at −80° are nearly equal to those at 25° and are largely entropy effects. Reversal of reaction 1 is fast enough so that this rate could be diffusion controlled even at −80°. The self-association of *p*-nitrophenol was measured at −80° by means of nmr chemical shifts and was substantially that to be expected on the basis of volume fraction statistics. A noteworthy and unsolved problem in the interpretation of the CH_3–proton resonance of methanol is that plausible rate laws can be obtained only if values of $1/\tau$ based on the Bloch equations are first corrected by means of an empirical function, $\phi(\tau)$, as described in the paper.

In previous papers from these laboratories, nuclear magnetic resonance (nmr) was used to measure rates and solvent participation in acid–base reactions in water and other hydroxylic solvents.[2] We now apply the nmr method to the proton exchange reactions of phenols and their conjugate bases in methanol. Our substrates are *p*-bromophenol and *p*-nitrophenol, the reaction temperature is −80°, and the pH of the reac-

(1) (a) Work supported in part by the Petroleum Research Fund of the American Chemical Society. Grateful acknowledgment is made to the donors of that fund. (b) Brandeis University Waltham, Mass.

tion mixtures ranges from about +2 (0.01 *M* HCl) to that of buffers containing both phenol and phenoxide. Under these conditions, we find the following reactions to be kinetically significant.

1. Reaction of ArOH with Methanol and Methoxide Ion

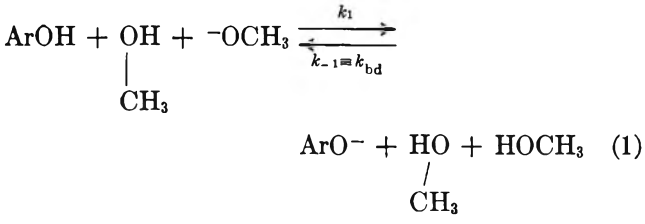

(1)

Note that the reverse of reaction 1 is the base dissociation of ArO^- as a Brønsted base (rate constant k_{bd}).

2. Reaction of ArOH with Methanol and ArO^-

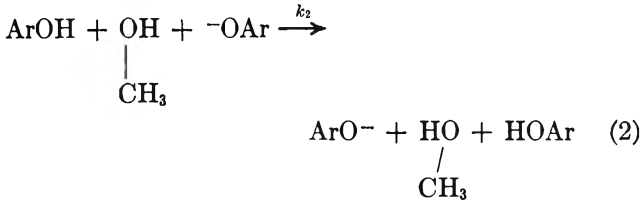

(2)

3. Reaction of ArOH with Methyloxonium Ion. The number of methanol molecules participating here could not be determined. Some plausible reaction mechanisms are shown below.

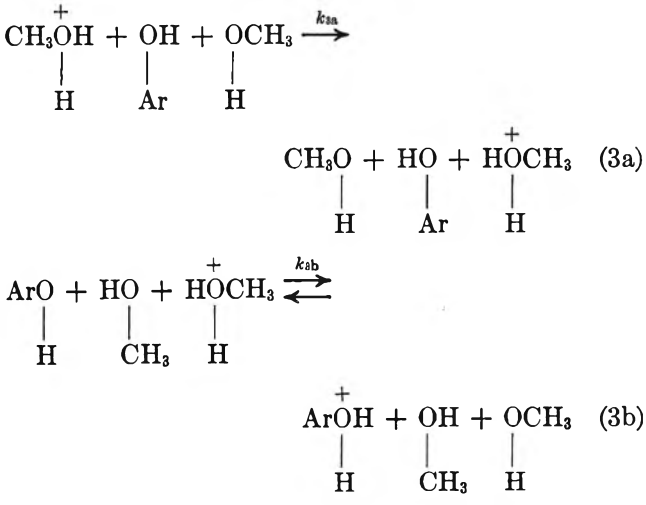

(3a)

(3b)

Reaction 3a represents a symmetrical proton exchange process analogous to reaction 2; reaction 3b is the conjugate of reaction 1 in the sense that the protons move toward rather than away from ArOH.

4. Proton Exchange between CH_3O^- and Methanol. In addition, in the buffered solutions there is proton exchange between CH_3O^- and methanol,[3] and in the presence of HCl there is proton exchange between $CH_3OH_2^+$ and methanol.[3]

Since some of the measurements were made at moderate solute concentrations (up to 0.7 *M* ArOH), we also measured chemical shifts of solvent and solute protons as a function of concentration in order to elucidate the intermolecular interactions. We found that the self-association of *p*-nitrophenol, *i.e.*, the probability of formation of adjacent pairs of ArOH·ArOH, is substantially that expected for an ideal mixture of ArOH and methanol. Moreover, there was no significant interaction chemical shift when the two solutes, ArOH and NaOAr, were both present in solution.

Rate constants have been reported in water at 25° for analogous proton transfer reactions between ArOH and the hydroxide ion, between ArO^- and the hydrogen ion, and between phenol, water, and the phenoxide ion.[4-7] Lifetimes for proton transfer between ArOH and methanol have been reported for *o*-ClC_6H_4OH in very concentrated solutions.[8] If these lifetimes may be extrapolated to dilute solution, they probably describe the acid dissociation of ArOH in methanol.

Experimental Section

Materials. Solvent methanol for most experiments was first dried with magnesium and then doubly distilled, as described previously.[3] Since the interpretation of nmr spectra in this solvent ran into an unexplained complication (see below) we wished to rule out the possible presence of kinetically active impurities. We therefore repeated some measurements using a sample of methanol that had been supplied to us by Dr. Calvin D. Ritchie, whose cooperation we acknowledge gratefully. This sample had been dried by Dr. Ritchie with molecular sieves, and acidic or basic impurities had been removed by treatment with ion-exchange resins. The sample was then redistilled by us just before use, the middle fraction being used. Nmr spectra for solutions in this solvent were indistinguishable from those for formally identical solutions in the magnesium-dried solvent.

Eastman White Label *p*-bromophenol was twice recrystallized from chloroform and dried *in vacuo*.

(2) See, for example, (a) E. Grunwald, C. F. Jumper, and S. Meiboom, *J. Am. Chem. Soc.*, **85**, 522 (1963); (b) Z. Luz and S. Meiboom, *J. Chem. Phys.*, **39**, 366 (1963); (c) E. Grunwald and M. Cocivera, *Discussions Faraday Soc.*, **39**, 105 (1965).

(3) E. Grunwald, C. F. Jumper, and S. Meiboom, *J. Am. Chem. Soc.*, **84**, 4664 (1962).

(4) M. Eigen and K. Kustin, *ibid.*, **82**, 5952 (1960).

(5) Z. Luz and S. Meiboom, *ibid.*, **86**, 4766 (1964).

(6) For a recent review see M. Eigen, W. Kruse, G. Maas, and L. De Maeyer, *Progr. Reaction Kinetics*, **2**, 285 (1964).

(7) Protolysis kinetics of electronically excited ArOH has been reviewed by A. Weller, *ibid.*, **1**, 187 (1961).

(8) E. Krakower and L. W. Reeves, *Trans. Faraday Soc.*, **59**, 2528 (1963).

For experiments involving very high acid–base ratios, this recrystallized material was further zone refined on a Fisher zone refiner.

Fisher White Label *p*-nitrophenol was twice recrystallized from toluene, air dried, and finally dried *in vacuo* over $Mg(ClO_4)_2$.

Solutions. Solutions were made up from freshly prepared reagents by quantitative methods. Standard solutions of sodium methoxide (for HOAr–NaOAr solutions) or of HCl were prepared from pure methanol and pure sodium metal or HCl gas in all-glass apparatus. Since some of the phenoxide or HCl concentrations were very low (10^{-4}–10^{-3} *M*), these concentrations were checked by potentiometric titration of the actual reaction mixtures (which of course also contained HOAr) using methanolic HCl or NaOMe titrants. Furthermore, for the *p*-nitrophenyl reagents concentrations were also confirmed by spectrophotometry of the reaction mixtures. As a result, we are confident that we know concentrations with an accuracy of at least 2% in even the most weakly buffered of the reaction mixtures.

In order to minimize errors from ion exchange of the sodium or hydrogen ion between weakly buffered reaction mixtures and their glass containers, we prepared all such mixtures twice. The first preparation was used only to establish ionic quasi-equilibrium between the solution and the required containers, including the nmr sample tube. The containers were then rinsed with pure methanol, dried, and used to receive a second, duplicate preparation on which the actual measurements were made.

Water content of the reaction mixtures was monitored by Karl Fischer titration after the conclusion of each series of experiments (usually 1 or 2 days after preparation) and was usually less than 0.01 *M* and always less than 0.015 *M*.

Nmr Measurements. All measurements were made at a frequency of 60 Mc/sec. Most of the measurements were made on Dr. S. Meiboom's nmr spectrometer at Bell Telephone Laboratories;[3] the rest were made at Brandeis University on a Varian Model HR60 nmr spectrometer equipped with Meiboom's temperature-controlled probe.[9]

Experimental techniques followed previous practice.[2a,3] All measurements were made on air-saturated solutions at a nominal temperature of −80°.

Interpretation of Nmr Spectra

In measuring kinetic order with respect to methanol in the proton transfer reactions of *p*-bromo- and *p*-nitrophenol we used a method reported by Grunwald, Jumper, and Meiboom.[2a] Briefly, we used the CH_3–proton resonance of methanol to evaluate proton exchange rates in the spin-coupled OH group of methanol; and we used the OH–proton resonance of the $ArOH$–CH_3OH proton system (which collapses into a single line at fast exchange rates) to evaluate proton exchange rates in the OH group of ArOH.

OH–Proton Exchange Rate of Methanol. The calculation of proton exchange rates in the OH group of methanol from slow passage nmr spectra of the spin-coupled CH_3 group has already been described in detail.[3] We now wish to report a complication that had not been envisaged in the previous work. We cannot give a theoretical explanation of the complicating phenomenon, but we shall try to characterize it empirically. In the following report we shall use the notation of ref 3.

The slow passage nmr spectrum of the CH_3 protons of methanol is regarded as a function of two characteristic times: the transverse relaxation time, T_2, of the CH_3 protons and the time, τ, between proton spin inversions in the OH group. OH–proton spin inversion is assumed to occur by two parallel mechanisms, T_1 relaxation and chemical exchange (which proceeds at a rate of R g-atom/l. sec^{-1}). On the basis of a large

$$1/\tau = 2(\text{rate of OH–proton spin inversion}/[\text{MeOH}]) \quad (4)$$

body of data for proton exchange in methanol at −80° we find, however, that we cannot derive plausible rate laws unless we add an empirical correction, ϕ, as in

$$1/\tau = (1/T_1)_{OH} + R/[\text{MeOH}] \quad (5)$$

eq 6.[10] This correction is a function either of τ or R—we cannot decide empirically because $(T_1)_{OH}$, on the basis of spin–echo measurements, varies relatively little in the experimental range. All our evidence indicates, however, that ϕ does *not* depend on the nature of the solutes or the rate law for R. For convenience we shall write $\phi(\tau)$ and values of ϕ at −80° are plotted *vs.* $1/\tau$ in Figure 1. As shown below, these values were obtained from slow passage CH_3–proton spectra for a single system, *p*-nitrophenol–*p*-nitrophenoxide ion in methanol, under conditions where the rate law

$$1/\tau = (1/T_1)_{OH} + \phi(\tau) + R/[\text{MeOH}] \quad (6)$$

(9) We gratefully acknowledge the help of Dr. S. Meiboom with construction and installation.

(10) After completion of this manuscript A. Allerhand, H. S. Gutowsky, J. Jonas, and R. A. Meinzer have published a critical analysis of errors in nmr measurements of chemical exchange rates [*J. Am. Chem. Soc.*, 88, 3185 (1966)]. However none of the errors described by them could have been large enough in our experiments to account for $\phi(\tau)$. In particular, the theoretical line shapes used for evaluating τ were based on density-matrix line shape equations, see ref 3.

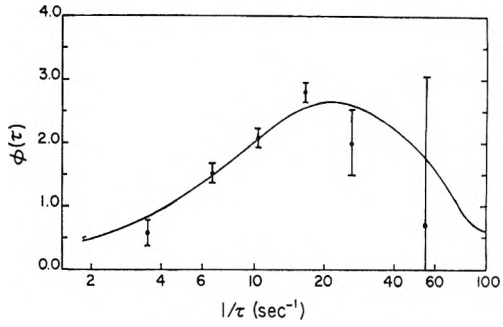

Figure 1. Plot of the empirical function $\phi(\tau)$ in eq 6 for CH_3–proton resonance of methanol at −80°. The smooth curve is a plot of $117\tau/(1 + 478\tau^2)$.

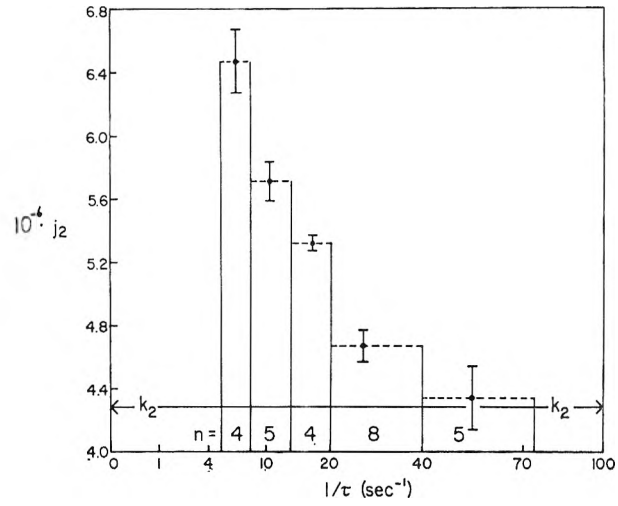

Figure 2. Histogram showing j_2 (eq 7) as a function of $1/\tau$ for *p*-nitrophenol–*p*-nitrophenoxide solutions in methanol at −80°. The ratio [ArOH]/[NaOAr] ranges from 90 to 1000 in these experiments.

for R is simple. Although our method of evaluating ϕ involves an arbitrary assumption, it accomplishes the following result. Without the $\phi(\tau)$ correction, slow passage CH_3–proton spectra of methanol at −80° lead to implausible rate laws for solutions of the following acids and their conjugate bases: benzoic acid, acetic acid, *p*-bromophenol, *p*-nitrophenol, and trimethylammonium ion. On applying the $\phi(\tau)$ correction shown in Figure 1 the kinetic behavior of all of these substrates becomes entirely rational.

Let us give an example. In previous work[2a] on benzoic acid–benzoate buffers in methanol at −80°, we calculated R on the basis of eq 5 and obtained the rate law

$$R = k_1[\mathrm{HBz}] + k_2[\mathrm{HBz}][\mathrm{NaBz}] + k_3[\mathrm{HBz}]^{1/2}[\mathrm{NaBz}]^{1/2}$$

The third (square root) kinetic term seemed implausible because we could not make it consistent with any theory that conformed to (i) the mass law of chemical reaction rate, (ii) microscopic reversibility in chemical systems at dynamic equilibrium, and (iii) stability principles of molecular structure. However, when the same data are recalculated on the basis of eq 6, taking $\phi(\tau)$ from Figure 1, the implausible (square root) kinetic term becomes insignificant and can be dropped from the rate law.

$\phi(\tau)$ in eq 6 for the CH_3–proton resonance of methanol at −80° was evaluated using our extensive slow passage nmr data for *p*-nitrophenol–*p*-nitrophenoxide buffers in methanol. Experimental results for $1/\tau$ at [ArOH]/[NaOAr] ratios ranging from 90 to 1000 depend accurately on a single variable, the concentration product [ArOH][NaOAr]. This suggests that reaction 2 is the only reaction that is kinetically significant under these conditions. If in first approximation we calculate R on the basis of eq 5 and if we then calculate an apparent rate constant j_2 according to eq 7, we obtain the result shown in Figure 2. It

$$j_2 = [\tau^{-1} - (T_1)_{\mathrm{OH}}^{-1}][\mathrm{MeOH}]/[\mathrm{ArOH}][\mathrm{NaOAr}] \quad (7)$$

is seen that j_2 is constant within experimental error when $1/\tau > 40$ and that j_2 increases significantly as $1/\tau$ goes to lower values. We have been unable to reconcile this variation of j_2 with any plausible reaction mechanism.

To calculate $\phi/(\tau)$ we assume that j_2 approaches k_2 in the limit as $1/\tau$ becomes large. In Figure 2, we have taken this limit to be 4.28×10^6 sec^{-1} M^{-1}. We then calculate $\phi(\tau)$ from eq 8. The resulting values and estimated standard errors are plotted in Figure 1.

$$\phi(\tau) = \tau^{-1} - (T_1)_{\mathrm{OH}}^{-1} - k_2[\mathrm{ArOH}][\mathrm{NaOAr}]/[\mathrm{MeOH}] \quad (8)$$

The smooth curve in Figure 1 is a graph of the empirical eq 9, which fits the values satisfactorily. Accordingly,

$$\phi(\tau)_{-80°} = 117\tau/(1 + 478\tau^2) \quad (9)$$

$\phi(\tau)$ at −80° approaches zero at both large and small values of τ and goes through a maximum at $1/\tau =$ 21.9 sec^{-1}. This maximum very nearly coincides with that value of $1/\tau$ at which the CH_3 resonance of methanol just fails to be a resolved doublet. As $1/\tau$ increases above 21.9 sec^{-1} $\phi(\tau)$ rapidly becomes of the order of the experimental error in $1/\tau$, amounting to 10% of $1/\tau$ at 26 sec^{-1} and to 5% at 43 sec^{-1}. On the other hand, as $1/\tau$ decreases below 21.9 sec^{-1} $\phi(\tau)$ gains progressively in relative importance, amounting to 25% of $1/\tau$ at 4 sec^{-1}.

The physical significance of $\phi(\tau)$ is obscure to us. The effect cannot be ascribed to an impurity in the methanol solvent because of its high reproducibility, considering that the solvent was prepared by two different methods and in many independent batches. For a given value of τ, the effect is independent of pH and, apparently, of the nature of the solutes. Thus everything indicates that $\phi(\tau)$ is a characteristic property of the solvent, methanol. Perhaps $\phi(\tau)$ represents a mechanism of OH–proton spin inversion that is triggered by proton exchange in a nonspecific way so that the effect depends only on the total rate of exchange. (In that case we should write $\phi(R)$ rather than $\phi(\tau)$.) It is more likely that there is a flaw in the equations that were used to calculate theoretical nmr spectra for methanol as a function of τ.[11] This explanation is suggested by the fact that $\phi(\tau)$ goes through a maximum near the "coalescence point" of the CH_3 doublet. Cocivera, in spin–echo measurements of T_1, has obtained evidence for cross relaxation of magnetization between CH_3 and OH protons of the sort described by Solomon and Bloembergen.[12] His work is relevant because a term for cross relaxation was not included explicitly in the theoretical equations.[11] However, that sort of cross relaxation is at a maximum when $1/\tau = \delta$, whereas our effect is at a maximum when $1/\tau \approx J/\sqrt{2}$. ($J$ = spin coupling constant, δ = difference in chemical shift.) Note that for methanol at $-80°$ $\delta/J \approx 30$. Note also that in the present as in previous work, spin–echo measurements on a representative number of solutions indicate that $(1/T_1)_{OH}$ varies only slightly, and approximately linearly with solute concentration, in the experimental range of $1/\tau < 100\ \text{sec}^{-1}$.

OH–Proton Exchange Rate of ArOH. In some experiments we measured the OH–proton resonance of ArOH under conditions of lifetime broadening; in others we measured the coalesced OH resonance of ArOH and methanol. The interpretation of these nmr spectra was analogous to that of CO_2H–OH proton spectra for benzoic acid solutions in methanol.[2a] $1/T_1$ for the phenolic OH protons was measured by rf saturation of slow passage spectra and was found to be 6.0 sec^{-1} for *p*-bromophenol and 6.7 sec^{-1} for *p*-nitrophenol at $-80°$. The chemical shift between the two kinds of OH protons was 4.07 ppm for *p*-bromophenol and 5.27 ppm for *p*-nitrophenol at ~0.1 *M* [ArOH] and $-80°$.

Results

Rate Constants. We shall use the symbol k with a superscript to denote a phenomenological rate constant in an empirical rate law and k with a subscript to denote an actual rate constant for a particular reaction.

The OH–proton exchange rate of methanol, R, was measured in the near-neutral to alkaline pH range. The data for *p*-bromophenol are consistent with the rate law, eq 10. The data for *p*-nitrophenol are consistent with the same rate law except that the term $k^*[\text{ArO}^-]$ is insignificantly small. Rate constants are listed in Table I.

$$R = k^{\text{I}}[\text{ArO}^-]/[\text{ArOH}] + k^*[\text{ArO}^-] + k^{**}[\text{ArOH}][\text{ArO}^-] \quad (10)$$

Table I: Rate Constants for Proton Exchange of *p*-Bromophenol and *p*-Nitrophenol in Methanol[a]

Kinetic constant	Value and std dev for *p*-Bromophenol, −81.6°	Value and std dev for *p*-Nitrophenol, −80.0°
$k^{\text{I}} = k_{\text{MeO}}\text{-}K_{\text{B}}$	$(1.08 \pm 0.1) \times 10^4$	42 ± 2
$k^* = 3k_{\text{bd}}$	$(9 \pm 2) \times 10^4$	[b]
$k^{**} = k_2$	$(1.43 \pm 0.15) \times 10^6$	4.28×10^6
$k^{*\prime} = k_{\text{bd}}$	$(3 \pm 1) \times 10^4$	[c]
$k^{**\prime} = k_2$	$(1.52 \pm 0.10) \times 10^6$	[c]
$k'' = k_3$	$(21 \pm 4) \times 10^4$	$(0.94 \pm 0.1) \times 10^4$

[a] All kinetic constants are based on the second as the unit of time and the mole per liter (at the reaction temperature) as the unit of concentration. [b] Too small to measure ($< 2 \times 10^4$). [c] Not measured.

The OH–proton exchange rate of ArOH, R', was measured for *p*-bromophenol both in the near-neutral and in the distinctly acid pH range. The data are consistent with the rate law eq 11. For *p*-nitrophenol R' was measured only in the distinctly acid pH range where only the last term of eq 11 is significant. Rate constants are given in Table I.

$$R' = k^{*\prime}[\text{ArO}^-] + k^{**\prime}[\text{ArOH}][\text{ArO}^-] + k''[\text{ArOH}][\text{MeOH}_2^+] \quad (11)$$

Because of their concentration dependence and for reasons stated below, we believe that kinetic terms can be identified with chemical reactions as follows: (a) $k^{\text{I}}[\text{ArO}^-]/[\text{ArOH}] = k_{\text{MeO}}\text{-}[\text{MeO}^-]$, proton exchange between methoxide ion and methanol. Hence, $k^{\text{I}} = k_{\text{MeO}}\text{-}K_{\text{B}}$, where $K_{\text{B}} = [\text{ArOH}][\text{MeO}^-]/[\text{ArO}^-]$; (b) k^* and $k^{*\prime}$ with reaction 1; (c) k^{**} and $k^{**\prime}$ with reaction 2; and (d) k'' with reaction 3.

(11) See ref 3 and literature references cited therein.

(12) (a) M. Cocivera, Bell Telephone Laboratories, private communication; (b) I. Solomon, *Phys. Rev.*, 99, 559 (1955); (c) I. Solomon and N. Bloembergen, *J. Chem. Phys.*, 25, 261 (1956).

The rate laws, eq 10 and 11, were established with high statistical probability on the basis of an extensive series of measurements covering a wide range of all relevant concentrations. All told, the measurements of R involved 41 separate solutions for p-bromophenol and 35 for p-nitrophenol; those of R' involved 15 separate solutions for p-bromophenol and 7 for p-nitrophenol. The complete data are made available elsewhere.[13]

Solvent Participation. The number of methanol molecules participating in a given kinetic process can be deduced from the ratio of rate constants for corresponding kinetic terms in the rate laws for R and R' (eq 10 and 11).[2a] Thus, for the kinetic term proportional to $[ArO^-]$, $k^* = 3k^{*\prime}$ within experimental error. Since the rates are measured at dynamic equilibrium, the corresponding reaction must be such that in each reversible cycle three methanol molecules exchange an OH proton for every ArOH molecule that exchanges an OH proton. Furthermore, the forward reaction of the reversible cycle must be formulated so as to be kinetically of the first order in $[ArO^-]$. A reversible cycle consisting of reaction 1, first from right to left, then from left to right, will fit these requirements. To predict the three-to-one ratio, we count the protons that enter a given state in one cycle, regardless of where they come from.[14] In reaction 1 from right to left, one proton enters the state "methanol" and one proton enters the state "ArOH." In the reverse of this reaction, two protons enter the state "methanol" and zero protons enter the state "ArOH." If this interpretation be granted, then $k^{*\prime}$ must be identified with k_{bd}.

For the kinetic term proportional to $[ArOH][ArO^-]$, $k^{**} = k^{**\prime}$ within experimental error. Hence, the two kinds of OH protons exchange in a 1:1 ratio. This result is consistent with reaction 2.

Reactions 1 and 2 share with many other proton-transfer processes the feature that they are termolecular[15] and that they probably involve a concerted push–pull mechanism.[15,16]

Acid and Base Dissociation Constants. pK_A has been measured in methanol at 25° for phenol (14.2) and p-nitrophenol (11.2).[17] Upon applying Hammett's ρ–σ equation with appropriate σ^- values[18] we calculate that $\rho = 2.36$ and predict that $K_A(p\text{-}NO_2)/K_A(p\text{-}Br) = 280$.

The above substituent effects at 25° may be compared with substituent effects on the kinetic parameter k^I at −80°. If $k^I = k_{MeO^-}K_B$, then $k^I(p\text{-}Br)/k^I(p\text{-}NO_2) = K_A(p\text{-}NO_2)/K_A(p\text{-}Br) = 260$ using the data in Table I. Similarly, $\rho = -(\delta_R \log k_1/\delta_R\sigma^-) = 2.3_2$ at −80°. The close agreement between these values and those obtained at 25° from the thermodynamic pK_A values suggests that k^I is indeed equal to $k_{MeO^-}K_B$ as assumed. If this be granted, then it follows that substituent effects on pK_A of phenols in methanol are quite independent of the temperature; hence, $\delta_R\Delta H^\circ \approx 0$ and the substituent effect is largely an entropy effect. From a long extrapolation of data at 25 and 0°[3,19] we estimate that $k_{MeO^-} \approx 5 \times 10^8$ sec^{-1} at −80°. This in turn enables us to estimate pK_B because $K_B = k^I/k_{MeO^-}$. The result is $pK_B = 4.7$ for p-bromophenol and 7.1 for p-nitrophenol at −80°. For p-nitrophenol we can also estimate ΔH_B° and ΔS_B° since $pK_B = 5.7$ at 25° on the basis of pK_A and the autoprotolysis constant of methanol.[20] Thus $\Delta H_B^\circ = 3.5$ kcal and $\Delta S_B^\circ = -14$ eu at about −30°. By comparison, an independent and quite different kinetic determination of K_B in methanol leads to $\Delta H_B^\circ = 0.7$ kcal for phenol at about 50°.[21]

The absence of a kinetic term due to acid dissociation in eq 10 and 11 establishes a lower limit of 14.4 to pK_A of p-nitrophenol, and hence of 14.4 + 7.1, or 21.5, to $pK_{autoprotolysis}$ of methanol at −80°. From an extrapolation of the data of Koskikallio[20] we estimate a $pK_{autoprotolysis}$ of 22.2 at −80°, well above the lower limit based on the kinetic data.

Given the estimates of pK_B, we are able to test whether the previous identification of $k^{*\prime} = k^*/3$ with k_{bd} in eq 1 is physically reasonable. In water, reaction of the hydroxide ion with phenols appears to be diffusion controlled.[4,6] If the reaction of methoxide ion with p-bromophenol at −80° were similarly diffusion controlled, the rate constant, k_1 (eq 1), for this reaction should be about 8×10^8 M^{-1} sec^{-1} at −80°.[22]

(13) Document No. 9223 with the A. D. I. Auxiliary Publication Project, Photoduplication Service, Library of Congress, Washington, D. C. 20540. A copy may be obtained by citing document number and advance payment of $1.25 for photocopy or $1.25 for microfilm. Make checks payable to Chief, Photoduplication Service.

(14) Alternatively we could count the number of protons that leave a given state in one cycle and obtain the identical result.

(15) (a) E. Grunwald and M. Cocivera, *Discussions Faraday Soc.*, 39, 105 (1965); (b) E. Grunwald and S. Meiboom, *J. Am. Chem. Soc.*, 85, 2047 (1963).

(16) (a) C. G. Swain and M. M. Labes, *ibid.*, 79, 1084 (1957); (b) C. G. Swain, J. T. McKnight, and V. P. Kreiter, *ibid.*, 79, 1088 (1957).

(17) C. W. Clare, D. Cook, E. C. F. Ko, Y. C. Mac, and A. J. Parker, *ibid.*, 88, 1911 (1966). This paper reviews the previous literature and also lists pK_A values for several *ortho*-substituted phenols.

(18) (a) L. P. Hammett, "Physical Organic Chemistry," McGraw-Hill Book Co., New York, N. Y., 1940, Chapter 7; (b) J. E. Leffler and E. Grunwald, "Rates and Equilibria of Organic Reactions," John Wiley and Sons, Inc., New York, N. Y., 1963, pp 211, 235.

(19) E. Grunwald, to be submitted.

(20) J. Koskikallio, *Suomen Kemistilehti*, B30, 111, 155 (1957).

(21) B. D. England and D. A. House, *J. Chem. Soc.*, 4421 (1962).

We therefore predict that $K_B = k_{bd}/k_1 = 4 \times 10^{-5}$ and that $pK_B = 4.4$ for *p*-bromophenol, in adequate agreement with the previous estimate of 4.7.

Brønsted Slopes. Reactions 2 and 3 can be regarded as examples of general acid or base catalysis. Although we have data for only two phenols, it is of interest to estimate the Brønsted catalytic slopes, α, for comparison with other systems.[18] We shall calculate α from eq 12, where k is k_2 or k_3. Thus $\alpha = 0.19$ for reaction 2 and -0.56 for reaction 3. The α value for reaction 2 is very similar to that obtained for the analogous reaction of substituted benzoic acids in methanol at 25°.[15b] The absolute value of α for reaction 3 is very similar to that obtained for other proton-transfer reactions in which either the forward or the reverse reaction in the cycle of reactions leading to proton exchange is ultrafast.[23]

$$\alpha = -\delta \log k/\delta \log k^I \qquad (12)$$

Solute–Solute Interaction. The existence of aromatic molecules on adjacent sites can be detected easily by the nmr chemical shifts that result from the interaction of magnetic nuclei with nearby circuits of aromatic ring current.[24] We have therefore measured some proton chemical shifts of solutions of *p*-nitrophenol and *p*-nitrophenoxide in methanol at −80°. The analysis of phenyl proton nmr spectra of *para*-disubstituted benzenes has been discussed exhaustively by Martin and Dailey.[25] Our spectra were of the A_2X_2 type (Figure 3 of ref 25) and were closely analogous[25] to those of *p*-nitroanisole and *p*-nitroaniline in two respects: (1) the dominant spin–spin interaction between protons on adjacent carbon atoms was identical with that reported for *p*-nitroaniline and *p*-nitroanisole and amounted to 9.0 ± 0.1 cps for both *p*-nitrophenol and *p*-nitrophenoxide; and (2) spin–spin interaction of protons on *meta* or *para* sites is relatively small. In our case, in methanol at −80°, the 9.0-cps spin–spin interaction was the only one that could be resolved. We have therefore calculated the chemical shifts of the phenyl protons on the assumption that the small, unresolved couplings are zero. If the couplings were actually the same as for *p*-nitroaniline or *p*-nitroanisole, assuming them to be zero would introduce a constant error of 0.006 ppm at all concentrations.

Our results for *p*-nitrophenol solutions are listed in Table II. In that table and throughout this section, chemical shifts are expressed relative to the CH_3–proton resonance of methanol, which is used as an internal standard. We have estimated the self-association constant of *p*-nitrophenol as follows.

Assuming a monomer–dimer equilibrium we let c, c_M, and c_D denote the formal, monomer, and dimer concentration, respectively. Thus we write eq 13 and 14, where K is the self-association constant. For $2c_D/c < 1$, the quantity $(1 - 2c_D/c)^2$ may be expressed as a convergent power series of Kc as in eq 15. Since

$$c = c_M + 2c_D \qquad (13)$$

$$c_D = K(c - 2c_D)^2$$

$$c_D = Kc^2(1 - 2c_D/c)^2 \qquad (14)$$

$$c_D = Kc^2[1 - 4Kc(1 - 5Kc + 12K^2c^2 - \ldots)] \qquad (15)$$

the self-association takes place very rapidly, the formal chemical shift[8] of any solute proton species is the weighted mean of the chemical shifts of monomer (δ_M) and dimer (δ_D) as in eq 16. Finally, combining eq 13, 15, and 16 we obtain eq 17. Equation 17 contains the quantities δ_M, $(\delta_E - \delta_M)$, and K. δ_M is obtained by a short extrapolation of δ to $c = 0$. The other quantities were calculated by a method of successive approximations. In the first approximation the term in

$$\delta = (c_M\delta_M + 2c_D\delta_D)/c \qquad (16)$$

$$(\delta - \delta_M)/c = 2(\delta_D - \delta_M)K \times [1 - 4Kc(1 - 5Kc + 12K^2c^2 - \ldots)] \qquad (17)$$

Table II: Proton Chemical Shifts[a] in Solutions of *p*-Nitrophenol in Methanol at −80°

[ArOH], *M*	Chemical shift (ppm) MeO*H*	Phenyl-A	Phenyl-B	ArO*H*
0.824	2.485	3.494	4.774	...
0.740	2.476	3.494	4.779	7.683
0.577	2.465	3.501	4.790	7.683
0.449	2.456	3.512	4.802	...
0.330	2.448	3.515	4.808	7.680
0.208	2.437	3.524	4.819	7.683
0.082	2.426	3.531	4.830	...
0.000[b]	2.420	3.5375	4.838	7.680

[a] Relative to CH_3–proton resonance of methanol. [b] Extrapolated.

(22) We use the equation, $k_1 = a4\pi N_0(D_A + D_B)/1000$, where N_0 is Avogadro's number, a the collision diameter, and D the diffusion coefficient. In methanol at −80° $10^6D \approx 1.86$ cm²/sec for *p*-bromophenol and 0.59 cm²/sec for methoxide ion on the basis of D at 15° and the viscosity ratio (−80°/15°) of methanol. For a we use 4.3 A, consistent with the termolecular mechanism shown in eq 1. See "International Critical Tables," Vol. V, McGraw-Hill Book Co., New York, N. Y., pp 11, 72; A. G. Ogsten, *Trans. Faraday Soc.*, **32**, 1679 (1936).

(23) E. Grunwald, *Progr. Phys. Org. Chem.*, **3**, 317 (1965).

(24) J. A. Pople, W. G. Schneider, and H. J. Bernstein, "High-Resolution Nuclear Magnetic Resonance," McGraw-Hill Book Co., New York, N. Y., 1959, p 180.

(25) J. Martin and B. P. Dailey, *J. Chem. Phys.*, **37**, 2594 (1962).

brackets equals $(1 - 4Kc)$; hence, the plot of $(\delta - \delta_M)/c$ *vs.* c should be nearly linear and yield first estimates of $(\delta_D - \delta_M)$ and K. In second and higher approximations the variables yielding a linear plot are $(\delta - \delta_M)/c$ and $c(1 - 5Kc + 12K^2c^2)$, where K is taken from the next lower approximation. Convergence is rapid; final linear plots for phenyl-A and phenyl-B proton chemical shifts are shown in Figure 3. The "best value" for K is 0.11 M^{-1} at $-80°$.

It should be noted that the value, $K = 0.11$, is of the magnitude to be expected for a random distribution of molecules. Following Fuoss,[26] we express K in the form of eq 18, where the preexponential factor $4\pi\sigma^3 \cdot N_0/3000$ has been derived by the method of excluded volume.[26] In eq 18 σ is the "distance of closest approach"; N_0 is Avogadro's number; g (a symmetry factor) is one-half for the association of like molecules (as in the present case) and unity for that of unlike ones; and u is the net change in interaction energy that attends the formation of 1 mole of association complex from an equivalent quantity of separated, solvated solute molecules. In the present case, $4\pi\sigma^3N_0/3000$ is estimated conveniently from the partial molar volume of *p*-nitrophenol in methanol (102 ml at 25°) and a packing factor (0.58 at 25°) based on the model of random packing of spheres (eq 19).[27] On

$$K = (4\pi\sigma^3N_0/3000)(ge^{-u/RT}) \qquad (18)$$

$$^4/_3\pi N_0(\sigma/2)^3 = 0.58[102 \text{ (ml/mole)}] \qquad (19)$$

substituting eq 19 in eq 18 we obtain $K = 0.24 \exp(-u/RT)$. Using the experimental value, $K = 0.11$ at 193°K, we then obtain $u = 300$ cal/mole. Although this estimate of u is uncertain by perhaps 500 cal/mole because of approximations in the model, it is clear that u is small and that the distribution of adjacent molecular pairs is nearly random.

Table III lists phenyl-B chemical shifts at $-80°$ (relative to the CH_3 protons of methanol) for methanol solutions of (i) *p*-nitrophenol, (ii) sodium *p*-nitrophenoxide, and (iii) both of these solutes in a roughly 1:1 molar ratio. It is seen (in the two columns on the right) that chemical shifts observed in (iii) are very close to values predicted from (i) and (ii) on the assumption that any interaction chemical shift is negligible.

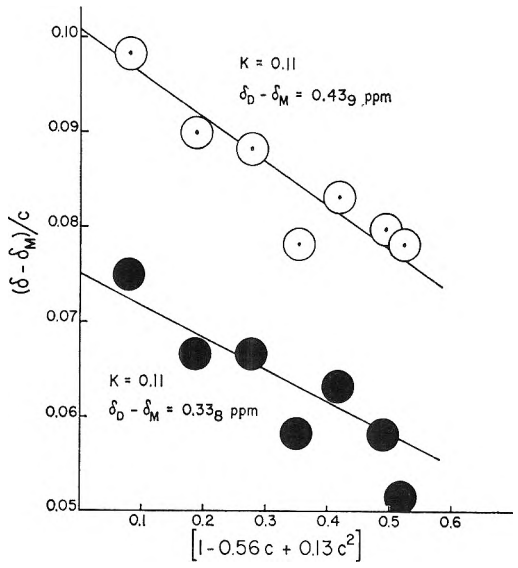

Figure 3. Final approximation in the calculation of K for the self-association of *p*-nitrophenol in methanol at $-80°$: ●, phenyl-A proton chemical shifts; ○, phenyl-B proton chemical shifts; δ in ppm, c in moles/l.

Table III: Phenyl-B Proton Chemical Shifts[a] of *p*-Nitrophenol–*p*-Nitrophenoxide Solutions in Methanol at $-80°$

(i) ArOH, M	ArOH alone δ, ppm	(ii) NaOAr, M	NaOAr alone δ, ppm	(iii) Both solutes δ, obsd	(iii) Both solutes δ, calcd[b]
0.275	4.813	0.282	4.678	4.743	4.745
0.220	4.818	0.226	4.672	4.743	4.743
0.165	4.822	0.170	4.677	4.743	4.748
0.110	4.827	0.113	4.672	4.747	4.748
0.055	4.832	0.057	4.672	4.752	4.750
0.033	4.835	0.034	4.672	4.752	4.752
0.016	4.837	0.017	4.672	4.752	4.753

[a] Relative to CH_3–proton resonance of methanol. [b] δ, calcd = 0.5066δ (ArOH alone) + 0.4934δ (NaOAr alone). The coefficients 0.5066 add 0.4934 represent the molar ratio of the solutes in these experiments.

(26) R. M. Fuoss, *J. Am. Chem. Soc.*, **80**, 5059 (1958).

(27) R. H. Stokes and R. A. Robinson, *Trans. Faraday Soc.*, **53**, 301 (1957).

Nitrogen Isotope Effects in Nickel–Ammonia Complex and Ammonia System

by A. R. Gupta and S. K. Sarpal

Atomic Energy Establishment Trombay, Chemistry Division, Bombay 28, India (Received June 8, 1966)

The nitrogen isotope effect in nickel–ammonia complexes/ammonia equilibrium has been determined, using an ion-exchange breakthrough operation, as a function of resin cross-linking and ammonia concentration. The experimental (over-all) single-stage factors have been calculated from the data using the material balance equation as well as Glueckauf's theory of ion-exchange columns. The good agreement between the calculated and observed breakthrough curves provides an experimental proof of the validity of Glueckauf's theory. The effect of cross-linking on the height equivalent of a theoretical plate and over-all efficiency of the column has been discussed in terms of various parameters like the diffusion coefficients and the effective single-stage factors. The single-stage separation factors for $Ni(NH_3)_4^{2+}$, $Ni(NH_3)_5^{2+}$, and $Ni(NH_3)_6^{2+}$ *vs.* ammonia equilibria in the aqueous phase have been obtained from an analysis of the data, taking into consideration the equilibrium concentrations of various nickel–ammonia complexes at different ammonia concentrations; the values are 1.0062, 1.0079, and 1.010, respectively. The single-stage factor for the hexaammine nickel–ammonia system has been calculated from the available vibrational data for this complex. There is good agreement between the calculated and experimentally determined values for the single-stage factor of the $Ni(NH_3)_6^{2+}$–NH_3(aq) system.

In the chemical equilibrium between transition metal ammines and ammonia in aqueous solutions, a considerable nitrogen isotope effect has been observed[1] because of the very different chemical environment of the nitrogen atom in the two compounds. The isotope-exchange reaction involved can be written as

$$[M(^{14}NH_3)_{n-1}(^{14}NH_3)]^{z+}(aq) + {}^{15}NH_3(aq) \rightleftharpoons [M(^{14}NH_3)_{n-1}(^{15}NH_3)]^{z+}(aq) + {}^{14}NH_3(aq) \quad (A)$$

This reaction has an isotope separation factor defined by[2]

$$\alpha_A = (N^{15}/N^{14})_{complex}/(N^{15}/N^{14})_{ammonia} = (1/n)K_A$$

where K_A is the equilibrium constant of the reaction A as written, *i.e.*

$$K_A = \frac{\{M(^{14}NH_3)_{n-1}(^{15}NH_3)\}^{z+}(aq)}{\{M(^{14}NH_3)_{n-1}(^{14}NH_3)\}^{z+}(aq)} \Big/ \frac{^{15}NH_3(aq)}{^{14}NH_3(aq)}$$

The magnitude of this isotope effect varies with the nature of the transition metal ion which determines the strength of the metal–nitrogen bond formed. On the one hand, for very strong complexes, it may be comparable to the effect observed in NH_4^+–NH_3 system and on the other side, for very weak complexes, it will approach unity. For this effect to be experimentally observed, a further requirement is that the above exchange reaction should be rapid. Thus besides a strong interaction between metal cation and ammonia, the complex formed should also be labile. Many of the very stable transition metal ammines, *e.g.*, $Co(NH_3)_6^{3+}$ and $Cr(NH_3)_6^{3+}$, also happen to be inert. Out of the labile ammonia complexes of transition metal cations, nickel, copper, and zinc complexes are quite stable. Nickel–ammonia complexes have special features, *e.g.*, more pronounced dependence of the equilibrium distribution of various species (complexes with different n values) on ammonia concentration. For these reasons, we have first selected nickel–ammonia complex for a detailed investigation, so that we can have a better understanding of the theoretical implications of these isotope effects as well

(1) T. Ishimori, *Bull. Chem. Soc. Japan*, **33**, 520 (1960).

(2) J. Bigeleisen in "Separation of Isotopes," H. London, Ed., George Newnes Ltd., London, 1961, pp 100–123.

as of the special features one encounters in the experimental determination of the same.

In principle, the isotope effect for reaction A can be calculated if the normal vibrational frequencies of the various species involved are known. From a survey of the literature on the vibrational spectra of transition metal ammines, it appeared that frequencies corresponding to some of the vibrational modes either have not been observed at all or have not been assigned unequivocally. The existing data, therefore, are not sufficient to calculate these isotope effects exactly. With the help of the available data, however, one can calculate these effects, though not to a very high degree of accuracy. These results for the hexaammine nickel–ammonia system are reported here. Whereas Ishimori[1] depended upon a salting-out technique for the experimental determination of the equilibrium isotope effects in this complex, an ion-exchange column technique has been successfully used here. The ion-exchange method is based on the property of transition metal ions that they form stable complexes in the exchanger phase.[3] In general, it has been observed that, if the situation is not complicated by any specific interactions between the ligand and the resin matrix or between the metal ion and the resin, the stability of the variety of such complexes formed by the transition metal ions is almost the same as in the solution phase.[4-6] As similar data on the nickel–ammonia complexes are not available, the stability of these complexes in different ion exchangers *vis a vis* their stability in aqueous solutions was first investigated. Having confirmed the nature of the nickel–ammonia complex in the resin phase, the isotope effect was determined by a breakthrough operation on ion-exchange columns. The use of the column technique, besides permitting a clean separation between the complex and ammonia, also multiplies the isotope effect. The latter can be of great advantage in those cases where the separation factor is small. The isotope effects have been calculated from the data in two independent ways: (i) the usual application of material balance equation, and (ii) Glueckauf's[7] theory of ion-exchange columns. The effective separation factors have been measured using ion exchangers of 4, 8, and 12% DVB content. In the presence of the ion exchanger, instead of reaction A, the following isotopic exchange reaction takes place

$$[Ni(^{14}NH_3)_{n-1}(^{14}NH_3)]_R^{z+} + {}^{15}NH_3(aq) \rightleftharpoons [Ni(^{14}NH_3)_{n-1}(^{15}NH_3)]_R^{z+} + {}^{14}NH_3(aq) \quad (B)$$

This reaction is related to the reaction A through the additional equilibrium

$$[Ni(^{14}NH_3)_{n-1}(^{14}NH_3)]_R^{z+} + [Ni(^{14}NH_3)_{n-1}(^{15}NH_3)]^{z+}(aq) \rightleftharpoons [Ni(^{14}NH_3)_{n-1}(^{15}NH_3)]_R^{z+} + [Ni(^{14}NH_3)_{n-1}(^{14}NH_3)]^{z+}(aq) \quad (C)$$

The relation between the three equilibria is $K_A = K_B/K_C$ and the separation factor for reaction A is given by

$$\alpha_B/\alpha_C = \alpha_A$$

There is no way of directly observing α_C, as the nickel–ammonia complexes are stable only in an excess of ammonia. The importance of equilibrium C is shown by the varying values of α_B obtained from experiments on ion exchangers of different cross linking. In the absence of directly measured values of α_C they have been estimated from a consideration of similar equilibria on these resins. The single-stage factor for reaction A thus obtained has been discussed in the light of the theoretically calculated value and the previously observed value for the same reaction.

Experimental Section

Chemicals. Resins used were of sulfonic acid type, *viz.*, Dowex 50 W of different cross-linking (4, 8, and 12% DVB) and different mesh size (20–50 and 100–200) supplied by J. T. Baker Chemicals Co., Phillipsburg, N. J. Nickel chloride was BDH(LR) grade and was purified by filtering its ~1 *M* solution and then passing it through an ion-exchange column. Ammonia used was E. Merck GR grade.

Stability of Nickel–Ammonia Complexes in the Ion Exchanger. The stability of nickel–ammonia complexes in the ion-exchanger phase was determined as follows. A stock of Ni form of the resin (20–50 mesh) was prepared in the usual manner in a column and air-dried at room temperature (~30°). Its capacity was determined by volumetric estimation of Ni by the KCN method.[8] The value was verified by converting the resin into H form and then estimating the H^+ ions. The values of the capacity obtained by the two methods were in very good agreement. The capacities and the moisture contents of the different resins were as follows: Dowex 50 W-X4, 2.224 mequiv, 40.97%; Dowex

(3) R. Nelson and H. F. Walton, *J. Phys. Chem.*, **48**, 406 (1944).

(4) R. H. Stoke and H. F. Walton, *J. Am. Chem. Soc.*, **76**, 3327 (1954).

(5) L. Cockerell and H. F. Walton, *J. Phys. Chem.*, **66**, 75 (1962).

(6) M. G. Suryaraman and H. F. Walton, *ibid.*, **66**, 78 (1962).

(7) E. Glueckauf in "Separation of Isotopes," H. London, Ed., George Newnes Ltd., London, 1961, pp 209–248.

(8) A. I. Vogel, "A Textbook of Quantitative Inorganic Analysis," Longmans Green & Co., London, 1958, p 264.

50 W-X8, 2.665 mequiv, 37.58%; and Dowex 50 W-X-12, 2.828 mequiv., 26.69% (all referred to the Ni form of the resin).

Weighed quantities of the Ni form of resin, usually 1.0 g, were taken in 100-ml conical flasks and equilibrated by overnight shaking with 50 ml of ammonia solutions of different concentrations. The outside ammonia solution, in equilibrium with the nickel complex in the resin, was titrated volumetrically using a mixed indicator.[9] The average number of ammonia molecules coordinated to nickel ion ($\bar{n}$) was calculated from the difference in the concentrations of ammonia solutions before and after equilibration. The amount of free ammonia in the resin was neglected as the resin volume is much less compared with the total solution volume.

Column Experiments for the Nitrogen Isotope Effects. Columns of about 55-cm length and 19-mm i.d. were used for these experiments. Resin of the desired cross linking (100–200 mesh) was packed in the columns. Smaller size particles were removed from the column by repeated back washing. The columns were subjected to sodium–hydrogen cycle in the usual manner to ensure uniform packing. Total exchange capacity of the column in the hydrogen as well as the nickel form was determined by estimating the eluted H^+ and Ni^{2+} ions as described earlier. The column was thoroughly washed with distilled water after converting it into Ni form. Ammonia solution of ~0.15 *N* strength was taken in a reservoir kept at a height and connected to the column with a tygon tube. The flow rate of ammonia solution was controlled by the stopcock at the bottom of the column. The front boundary of the band moved down fairly sharply and no channeling was usually observed. When the whole of the column was converted into the nickel complex form and ammonia appeared in the effluent, a number of 10-ml fractions were collected and their ammonia content determined by titrating against standard HCl using the mixed indicator. The acidified samples were concentrated to a convenient volume for isotopic analysis. The amount of ammonia coordinated to Ni was estimated by eluting the complex with dilute HCl and determining the ammonia in the effluent by Kjeldahl distillation technique. However, a correction was made for the excess of ammonia which was not present in the complex form in the column. This amount of ammonia was determined by repeating the experiment with Na form of the resin instead of the nickel form and keeping all other parameters constant.

Preparation and Isotopic Analysis of the Samples. The ammonia samples from the column, in the ammonium chloride form, were decomposed by sodium hypobromite solution to get gaseous nitrogen as described by Rittenberg.[10a] Isotopic analysis was carried out with the CEC mass spectrometer type 21-103C (180° and single collector), using 28 and 29 peaks.

Results and Discussion

A. Calculation of the Isotope Effect. A general analysis of the various vibrational modes of an octahedral hexaammine like $M(NH_3)_6^{2+}$ has been discussed by Cotton.[10b] For an exact calculation of the isotope effect, one should know the frequencies of all the normal vibrational modes of the molecule. In the case of $Ni(NH_3)_6^{2+}$ many of the normal modes have not been observed. Thus an exact calculation of this isotope effect cannot be performed. However, the magnitude of the primary isotope effect is essentially determined by changes in the force constants of bonds made directly with the isotopically substituted atom.[11] On this basis it has been pointed out by Kresge, *et al.*,[12] that to a good approximation primary isotope effects can be understood by considering only the isotopically substituted atom and those atoms which are bound directly to it. Accordingly, in the present problem the $NiNH_3$ model for the complex has been chosen. This model is consistent with the assumption generally made in the interpretation of vibrational spectra of complexes that the interaction of vibrations in one NH_3 ligand with those in another is small or negligible. Further, the only vibrational modes this particular model excludes from consideration, *e.g.*, N–Ni–N bending modes, are those which lie in the low-frequency range. Their contribution to the isotope effect, in any case, will be negligible. Thus no serious error is introduced by their exclusion from the isotope effect calculations.

Assuming a tetrahedral orientation of $NiNH_3$ and an over-all symmetry of C_{3v} for this part, the observed vibrational frequencies of the nickel hexaammine perchlorate have been assigned to different modes of vibration.[13] The frequencies and their assignments are given in Table I.

(9) This indicator was prepared by mixing five parts of 0.1% solution of bromocresol green and one part of 0.1% solution of methyl red in methyl alcohol. Fresh indicator was prepared after every 2 weeks. The end point was detected by change in color from blue to red.

(10) (a) D. Rittenberg, "Preparation and Measurement of Isotopic Tracers," J. W. Edwards, Ann Arbor, Mich., 1948, p 34; (b) F. A. Cotton in "Modern Coordination Chemistry," J. Lewis and R. G. Wilkins, Ed., Interscience Publishers, Inc., New York, N. Y., 1960, p 361.

(11) M. Wolfsberg and M. J. Stern, *Pure Appl. Chem.*, 8, 225 (1964).

(12) A. J. Kresge, N. N. Lichtin, K. N. Rao, and R. E. Weston, Jr., *J. Am. Chem. Soc.*, 87, 437 (1965).

(13) K. Nakamoto, "Infrared Spectra of Inorganic Coordination Compounds," John Wiley and Sons, Inc., New York, N. Y., 1963.

Table I: Vibrational Frequencies of Nickel Hexaammine Perchlorate (cm^{-1})

	Vibrational modes	N^{14} complex	N^{15} complex
$\nu_1(A_1)$	Sym NH_3 stretching	3312	3310
$\nu_2(A_1)$	Sym NH_3 deformation	1236	1230
$\nu_3(A_1)$	M–N stretching	334	324
$\nu_4(E)$	Antisym NH_3 stretching	3397	3387
$\nu_5(E)$	Degenerate NH_3 deformation	1618	1613
$\nu_6(E)$	NH_3 rocking	620	619

Vibrational frequencies for the N^{15}-substituted complex were evaluated by the usual kind of normal coordinate analysis based on Wilson's G and F matrix method. As some of the frequencies listed in Table I are in doubt a precise calculation based on the solution of the eigenvalue equation

$$|GF - E\lambda| = 0$$

was not attempted. Instead a simplification of the problem was affected by considering only the diagonal elements of the G and F matrices. Nakagawa and Mizushima[14] have demonstrated in their calculations of the hydrogen deformation vibrations of ammonia in the $Co(NH_3)_6^{3+}$ complex based on the same model that this approximation leads essentially to correct values of the frequencies. The calculated values of the frequencies for the N^{15}-substituted complex are given in Table I.

The isotope effect can then be calculated employing Bigeleisen and Mayer's reduced partition function ratio method[15] using

$$\ln s/s'f = \Sigma_i G(u_i)\Delta u_i$$

The vibrational data needed for the calculation of the reduced partition function ratio for ammonia were taken from Herzberg's compilation.[16] The value of the isotope effect comes out to be 1.016. A study of the vibrational spectra of this complex is under progress, and when more definite values of the vibrational frequencies are available, a more accurate calculation of the isotope effect will be carried out. All the same, the value reported here is believed to be accurate within 0.001. However, this calculated value for the separation factor is for the equilibrium between the solid nickel complex and gaseous ammonia and needs corrections for the isotope effects which might arise because in reaction A these molecules are in different phases. As far as the nickel complex is concerned, the vibrational frequencies of the solid complex and aqueous solutions of the complex are not likely to be very different and the isotope effect arising out of these differences can be safely neglected. The equilibrium between ammonia gas and aqueous solutions of ammonia, *i.e.*

$$^{14}NH_3(aq) + {}^{15}NH_3(g) \rightleftharpoons {}^{15}NH_3(aq) + {}^{14}NH_3(g)$$

has been studied and a value of 1.005 for its separation factor has been reported.[17]

The theoretical value for the isotope separation factor in reaction A then becomes 1.011 ± 0.001.

B. Stability of Nickel–Ammonia Complexes in the Ion Exchanger-Phase. Plots of $\bar{n}$ *vs.* equilibrium ammonia concentration obtained from the equilibrium experiments for resins of 4, 8, and 12% DVB content are given in Figure 1. Bjerrum's[18] values in the aqueous solution have also been plotted for comparison. It is evident from the figure that $\bar{n}$ values in the resin phase are slightly lower than those in the aqueous phase as reported by Bjerrum. This difference can arise owing to the equilibrium concentration of ammonia in the outside solution being different from the actual concentration of ammonia inside the resin, with which the complex is in equilibrium. In general, the equilibrium concentration of ammonia in the resin will decrease with increasing cross linking, thus decreasing $\bar{n}$ values with cross linking of the resin, as observed experi-

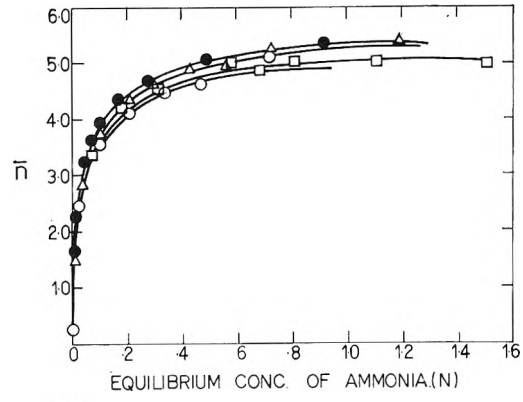

Figure 1. $\bar{n}$ *vs.* equilibrium concentration of ammonia for nickel–ammonia complex on Dowex 50 W of different DVB contents: ●——●, Bjerrum's value for aqueous solutions; △——△, 4% DVB; □——□, 8% DVB; ○——○, 12% DVB.

(14) I. Nakagawa and S. Mizushima, *Bull. Chem. Soc. Japan*, 28, 589 (1955).

(15) J. Bigeleisen and M. Goeppert-Mayer, *J. Chem. Phys.*, 15, 261 (1947).

(16) G. Herzberg, "Infrared and Raman Spectra of Poly-atomic Molecules," D. Van Nostrand Co., Inc., New York, N. Y., 1960, p 295.

(17) I. Kirshenbaum and H. Baumgartel, *Z. Naturforsch.*, 1, 514 (1946).

(18) J. Bjerrum, "Metal Ammine Formation in Aqueous Solutions," P. Haase and Sons, Copenhagen, 1957, p 183.

Table II: Apparent Separation Factors on Resins of Different Cross-Linking

Expt no.	Resin, %	Ammonia concn, N	Capacity, mequiv	Bed height, cm	Flow rate, ml/min	α	α_{av}
1	4	0.150	213.4	40.0	1.43	1.0042	1.0043
2	4	0.146	213.4	39.0	1.43	1.0045	
3	8	0.147	225.0	33.1	1.84	1.0062	
4[a]	8	0.149	154.9	23.7	1.56	1.0056	1.0063
5	8	0.147	154.9	23.3	2.06	1.0063	
6	12	0.150	231.9	31.6	1.47	1.0072	1.0070
7	12	0.149	231.9	31.2	1.59	1.0068	
8	4	0.400	160.0	28.5	1.90	1.0051	1.0051
9	12	0.397	231.9	31.1	0.89	1.0081	1.0081

[a] Some channeling was observed in this experiment.

mentally. Thus from the data in Figure 1 it is concluded that the nickel–ammonia complexes in the resin phase are almost as stable as they are in the aqueous solution.

C. Experimental Separation Factors. (1) From the Material Balance Equation. From the information obtained from chemical and isotopic analyses of effluent samples, the isotopic composition of the ion-exchange column can be calculated. The isotopic enrichment factor *vs.* the amount of ammonia in the effluent samples has been plotted for some typical runs in Figure 2. Curves A, B, and C have been obtained on 4, 8, and 12% DBV resins, respectively. In general, it was observed in these experiments that the ammonia concentration in the effluent reached the initial value very rapidly, indicating a sharp front. On the other hand, the isotopic composition of the samples reached the natural value much more slowly (Figure 2), implying that isotopic equilibrium is attained more slowly than chemical equilibrium. The area under the curves in Figure 2 directly gives the amount of N^{15} transferred to the column. Knowing the total capacity of the column for ammonia at the concentration used, one can calculate the effective separation factor in a straightforward way. The effective separation factor is related to the apparent or experimental separation factor for the isotope-exchange reaction taking place in the column by the following relation[7]

$$\epsilon_{eff} = \frac{\alpha_{app} - 1}{1 + (\sigma C/F)}$$

where σ is the void fraction, C the concentration in millimoles/milliliter in the solution phase, and F the concentration in millimoles/milliliter in the resin phase. As we are using resins of different cross linking, σ and F are expected to be different in each case. To determine α_{app}, σ and F were measured for each resin sample and $\sigma C/F$ calculated. Its value in all the three cases was of the order of 0.0001 and for all practical purposes can be neglected. The results of the experiments on Dowex 50 W-X4, Dowex 50 W-X8, and Dowex 50 W-X12 with different ammonia concentrations are summarized in Table II. The estimated error in the value of the separation factors is less than 0.001.

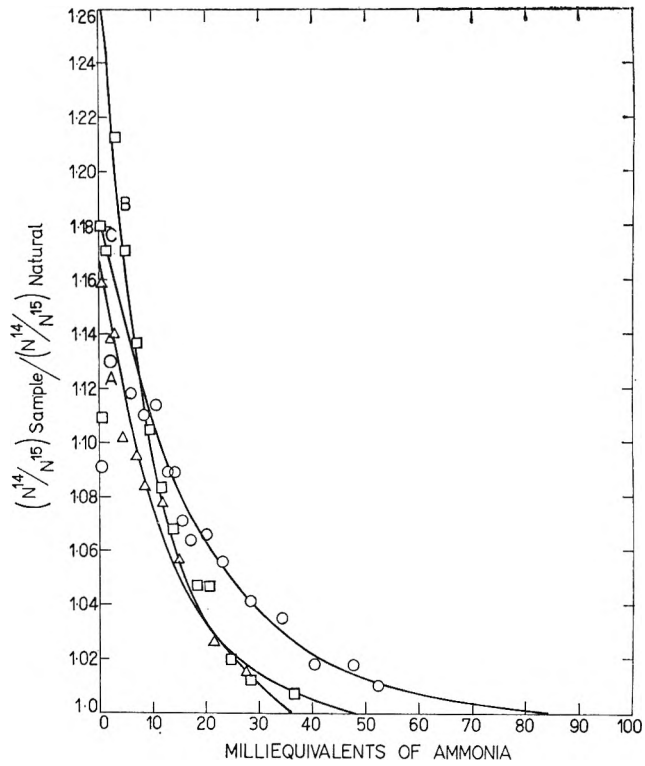

Figure 2. Breakthrough curves for the system nickel–ammonia complex/ammonia at ~0.15 N ammonia concentration on Dowex 50 W of different cross linking: A, 4% DVB; B, 8% DVB; C, 12% DVB.

(2) Using Glueckauf's Theory of Ion-Exchange Columns. The general solution of the problem of nonlinear breakthrough operation for isotope separation on ion-exchange columns obtained by Glueckauf[19] can be written as

$$c_2/c_2^0 = \left[\frac{1}{2} - A_\epsilon\{p(1-b)\}\right] - \frac{p\sqrt{2}}{\sqrt{\pi}} \times \exp\left\{-\frac{p^2(1-b)^2}{2}\right\} + \left[\frac{1}{2} - A_\epsilon\{p(1+b)\}\right] \times [1 + 2p^2(1+b)] \exp(2p^2b) \quad (1)$$

where $p = \epsilon\sqrt{N}$, $b = (v - \bar{v})/\epsilon\bar{v}$, $\bar{v}$ = elution volume at the front, c_2 = concentration at elution volume, v, and c_2^0 = initial concentration.

For the special case of small values of p, *i.e.*, small enrichments, and in the vicinity of the front, the equation reduces to

$$c_2/c_2^0 \simeq 1 - (2p\sqrt{2})/\sqrt{\pi} + p^2 + 2p^2b \quad (2)$$

Under the same conditions, at the front where b is zero, one gets

$$c_2(\text{front})/c_2^0 \simeq 1 - (2p\sqrt{2})/\sqrt{\pi} + p^2 \quad (3)$$

Substituting eq 3 into eq 2 we get

$$\frac{c_2}{c_2^0} - \frac{c_2(\text{front})}{c_2^0} = 2p^2b = 2\epsilon N\frac{(v-\bar{v})}{\bar{v}} \quad (4)$$

Solving eq 3 for p, *i.e.*, $\epsilon\sqrt{N}$, and eq 4 for ϵN, one can get both ϵ and N. In this approach, a further advantage is that a reliable value of c_2(front) can be obtained by using many values of v and making the results self-consistent among themselves. The values of apparent separation factors for different resins are given in Table III along with the other details involved in the calculation. There is very good agreement between the α values calculated by the two methods. The breakthrough curves, using the exact eq 1, and the values of α and N obtained by the approximate equation have also been computed. Two of these curves calculated for the exchange on Dowex 50 W-X4 (0.15 N ammonia) and Dowex 50 W-X8 (0.15 N ammonia) along with the corresponding experimental curves are given in Figure 3. A very satisfactory agreement between the theoretical and the experimental breakthrough curves has been obtained, confirming the validity of using the approximate equation for the evaluation of α and N. This also provides an experimental proof of the validity of Glueckauf's theory of ion-exchange columns.

D. Effect of Cross-Linking of the Resins on the Separation Factors. The increase in the separation factor with an increase in cross linking of the resin is attributed to varying contributions from reaction C. In the absence of directly determined values of α_c on different resins, its contribution has been estimated on the basis of observed changes in the equilibrium constant of the following similar isotopic exchange reaction on resins of different cross linking

$$^{14}NH_4R + {}^{15}NH_4^+(aq) \rightleftharpoons {}^{15}NH_4R + {}^{14}NH_4^+(aq)$$

The α value for this reaction is 0.9996 for 8%[20] and nearly 1.000 for 12%[21] DVB resins. As reaction C is very similar to the above reaction, one would expect it to have almost the same α values. Therefore, as a very good approximation, we have taken α_c on 8% DVB resin to be identical with α of the above reaction on 8% DVB resin. α_C for other resins can then be calculated using the data in Table II. The reliability of these values of α_C can be tested by using them for calculating α_A for 0.4 N NH_4OH solution. The value

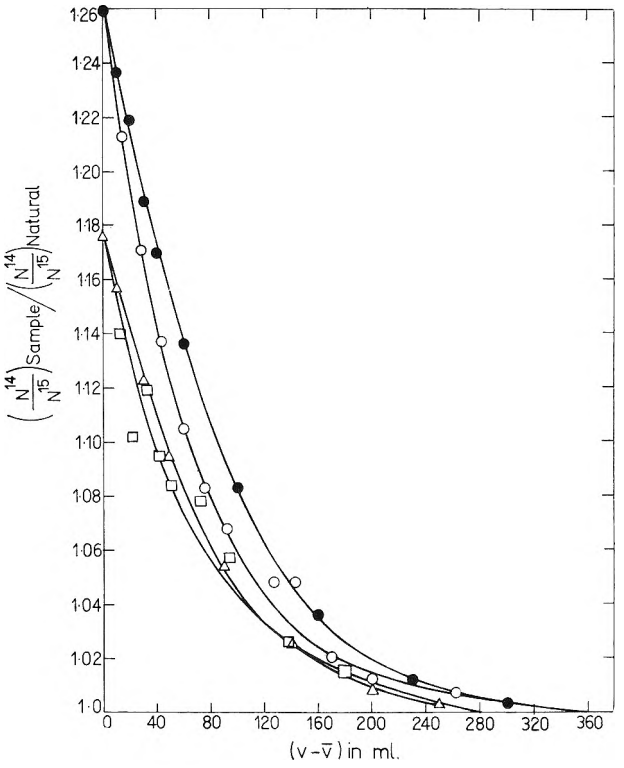

Figure 3. Theoretical and experimental breakthrough curves for nickel–ammonia complex/ammonia system: ●——●, calculated from eq 1, ϵ = 0.0063, N = 503; ○——○, experimental ammonia concentration, 0.15 N, 8% DVB; △——△, calculated from eq 1, ϵ = 0.0041, N = 595; □——□, experimental ammonia concentration 0.15 N, 4% DVB.

(19) Reference 7, p 238.

(20) T. Ishimori, *Bull. Chem. Soc. Japan*, **33**, 516 (1960).

(21) F. H. Spedding, *J. Chim. Phys.*, **60**, 89 (1962).

Table III: Calculation of ϵ and N Using $c_2/c_2^0 = 1 - [(2p\sqrt{2})/\sqrt{\pi}] + p^2 + 2p^2b$

v	$\frac{2(v-\bar{v})}{\bar{v}}$	c_2/c_2^0	ϵN	ϵ	N	HETP, mm
		A. 4% DVB resin				
		$\bar{v} = 2850$; $c_2/c_2^0(\bar{v}) = 0.850$; $\epsilon^2 N = 0.01$				
2860	0.00703	0.8673	2.46	0.00407	603	
2865	0.01051	0.8757	2.44	0.00410	595	
2870	0.01402	0.8840	2.43	0.00413	587	
				Av 0.0041	Av 595	0.66
		B. 8% DVB resin				
		$\bar{v} = 2990$; $c_2/c_2^0(\bar{v}) = 0.794$; $\epsilon^2 N = 0.02017$				
3000	0.0067	0.8150	3.13	0.00645	485	
3010	0.0134	0.8380	3.28	0.00615	533	
3020	0.0201	0.8569	3.14	0.00640	490	
				Av 0.0063	Av 503	0.68
		C. 12% DVB resin				
		$\bar{v} = 2926$; $c_2/c_2^0(\bar{v}) = 0.848$; $\epsilon^2 N = 0.01$				
2940	0.00952	0.863	1.575	0.00635	248	
2950	0.01640	0.874	1.585	0.00632	251	
2960	0.02320	0.884	1.550	0.00645	240	
				Av 0.0064	Av 246	1.28

of α_C for different cross-linked resins and α_A for different ammonia concentrations are given in Table IV. The close agreement between the values of α_A obtained from data on resins of different cross-linking shows that this approach to the problem as well as the values of α_C are essentially correct.

Table IV: Separation Factors for Reactions A and C

Resin, %	α_C	α_A: 0.15 N NH_4OH	α_A: 0.40 N NH_4OH
4	0.997	1.0068	1.0080
8	0.9996	1.0067	...
12	1.0003	1.0067	1.0078
		Av 1.0067	1.0079

Besides the effective separation factor, the difference in the cross linking of the resin also influences the over-all separation in a column, or in other words, the efficiency of the column. The best way to discuss this is in terms of the total number of theoretical plates of HETP (height equivalent of theoretical plate) obtained in a particular column. HETP in an ion-exchange column depends upon the diffusion coefficient, particle size, flow rate, and distribution coefficient. For the experiments described in Table III the linear flow rates (1.0–1.2 cm/hr), the particle size (100–200 mesh), and the distribution coefficients were quite comparable. The diffusion coefficients in resins of different cross linking are expected to be different and vary in the following order: D(4% DVB) > D(8% DVB) > D(12% DVB). As isotopic equilibrium in the column is achieved by the diffusion of ammonia molecules into and out of the resin particles, one would expect the largest number of plates (or the smallest HETP) in 4% DVB resin column and the least number (or the largest HETP) in 12% DVB resin column, the particle size and flow rate being the same. The data in Table III confirm the above expectation. The separation, *i.e.*, the depletion in the front of the band, however, depends on both the number of plates in a column and the effective separation factor. As these two factors vary in opposite directions with an increase in cross linking of the resin, the frontal depletion does not follow a definite pattern. The largest separation has been achieved on resin of 8% DVB content, which shows the importance of considering both the factors, *i.e.*, HETP and ϵ_{eff}, simultaneously if the aim is to obtain maximum separation.

E. Effect of Ammonia Concentration on Separation Factors. The interpretation of the experimental values of the separation factors is complicated by the presence of many different species in the system. In fact, all the nickel complexes having one to six ammonia molecules coordinated to the nickel ion are present in equilibrium with one another at a particular ammonia concentration. Thus α_{app} or α_{exp} represents the weighted average of the six independent separation

factors of the equilibria represented by reaction A having n values from one to six. The equilibrium concentrations of the various species change with ammonia concentration and thus their contribution to α_{exp} also varies. The data in Table IV clearly show that α_{exp} increases with ammonia concentration. Ishimori's value of 1.0076 for α of this system at ~0.3 N ammonia concentration is intermediate between the values at 0.15 and 0.40 N reported here and confirms the above trend. This dependence of the separation factor on ammonia concentration, *i.e.*, concentration of various complex species present in the system, implies that the separation factors for equilibria involving individual complexes are different. These will be denoted by α_1, α_2, etc., and $(\alpha_1 - 1)$ and $(\alpha_2 - 1)$ by ϵ_1, ϵ_2, etc. To evaluate the individual contributions of the equilibria with the nickel complexes having specific values of n, one needs to know the equilibrium distribution of the various species at different ammonia concentrations. Using the stability constants for the nickel–ammonia complexes given by Bjerrum, *et al.*,[22] the equilibrium distribution of the various stepwise complexes was calculated for the three different ammonia concentrations and is given in Table V. It is obvious that the major contribution to α_{exp} comes from equilibria where complexes with three, four, five and six ammonia molecules are involved.

Table V: Equilibrium Composition[a] of Nickel–Ammonia Complexes at Various Concentrations

Concn of ammonia	No. of ammonia molecules					
	1	2	3	4	5	6
0.15	0.83	2.16	17.27	40.3	33.13	5.5
0.3	0.07	0.39	6.2	28.9	48.7	15.7
0.40	0.025	0.18	0.32	23.7	53.0	22.7

[a] In mole per cent.

The concentration of the complex having three ammonia molecules is significant only at 0.15 N ammonia. As a first approximation, α_3 is taken to be equal to α_4. Then α_{exp} can be written as

$$(\alpha_{exp} - 1) = (x_3 + x_4)(\alpha_4 - 1) + x_5(\alpha_5 - 1) + x_6(\alpha_6 - 1)$$

or

$$\epsilon_{exp} = x_4'\epsilon_4 + x_5\epsilon_5 + x_6\epsilon_6$$

where x_3, x_4, etc., represent the mole fractions of the corresponding nickel–ammonia complexes. Using the three different values of α_{exp} for different x_4', x_5, and x_6, a set of three simultaneous equations is obtained which can be solved for the three unknowns, ϵ_4, ϵ_5, and ϵ_6. The results are given in Table VI.

Table VI: Separation Factors for Different Nickel–Ammonia Complexes

No. of ammonia molecules	α
4	1.00615
5	1.0079
6	1.010

The theoretically calculated value of the separation factor is for the hexaammine nickel–ammonia system and compares very favorably with the experimentally observed value for the isotopic exchange reaction involving hexaammine nickel ion.

Conclusions

The above agreement shows that the various approximations made in the theoretical calculations of the isotope effects—particularly the one proposed by Kresge, *et al.*,[12] that only those atoms which are directly bonded to the isotopic atom need be considered in such calculations—are quite valid. The success of the simple ion-exchange breakthrough technique in the isotope effect determination demonstrates the power of this technique in solving such problems. A much needed experimental proof of the validity of Glueckauf's theory of ion-exchange columns, especially for the breakthrough operations, is provided for the first time by the good agreement between the values of the single-stage factor obtained from this theory and the material balance equation. A simple way of calculating single-stage factors and the number of theoretical plates from the experimental data based on this theory has been found and successfully applied. A more convincing proof of Glueckauf's theory is provided by the good agreement between the calculated and observed breakthrough curves. This new application of Glueckauf's theory can be of great importance for the industrial chemist interested in large-scale separations on ion-exchange columns. However, the most significant result which emerges out of this investigation is that the isotope effects, in a series of stepwise complexes of a metal cation with the same ligand, are different. This implies that the funda-

(22) J. Bjerrum, G. Schwarzenbach, and L. G. Sillen, "Stability Constants," Vol. II, The Chemical Society, London, 1958, p 47.

mental vibrational frequencies or the force constants are different in these stepwise complexes. It will be interesting to see whether one can experimentally observe such differences in the vibrational spectra of the different nickel–ammonia complexes.

Acknowledgment. The authors wish to express their sincere thanks to Dr. J. Shankar for his interest and encouragement during the course of this investigation. They also wish to acknowledge the help of Mr. K. N. Bhide in the isotopic analysis of the samples.

The Influence of 1,4-Dioxane and Tetrahydrofuran as Solvents upon the Stability and the Solvation of Negative Ions of the Potassium Compounds of Naphthalene and Anthracene

by Karlheinz K. Brandes and R. J. Gerdes[1]

Contribution from the Department of Chemistry, Newberry College, Newberry, South Carolina, and the Georgia Institute of Technology, Atlanta, Georgia 30332 *(Received June 10, 1966)*

Potassium compounds of naphthalene and anthracene were prepared under high-vacuum conditions (10^{-7} to 10^{-8} torr). Electronic spectra of the solutions of the compounds indicate that dipotassium anthracene is stable in tetrahydrofuran but partly splits into monopotassium anthracene and potassium metal if dissolved in 1,4-dioxane. Dipotassium naphthalene is not soluble in 1,4-dioxane. In tetrahydrofuran as solvent it is completely decomposed into monopotassium naphthalene. The electric conductivities of the potassium compounds of naphthalene and anthracene dissolved in tetrahydrofuran and 1,4-dioxane were determined to be about 10^6 times higher than the corresponding conductivities of the solutions in 1,4-dioxane as solvent. The dissociation energies of the potassium compounds of naphthalene and anthracene in the two solvents used were found to be 2 to 3 kcal/mole in 1,4-dioxane and -5 to -7 kcal/mole in tetrahydrofuran, at room temperature.

Introduction

Compounds of aromatic hydrocarbons and alkali metals are now generally agreed to consist of ion-pair complexes with the hydrocarbon as the negative ion. This assumption is mainly based on electronic spectra[2–10] and on esr spectra[11–14] of the dissolved compounds. In some cases, however, the published results differed. This was, for instance, the case for a wide absorption band at 23,000 cm^{-1} in the spectrum of potassium naphthalene and several maxima in the spectrum of dipotassium anthracene.[15] There is already some evidence from conductivity measurements[15,16] that these differences may be due to the

(1) To whom all correspondence should be addressed at Georgia Institute of Technology, Atlanta, Ga.

(2) G. J. Hoijtink and J. van Schooten, *Rec. Trav. Chim.*, **71**, 1089 (1958).

(3) G. J. Hoijtink and J. van Schooten, *ibid.*, **73**, 355 (1954).

(4) P. Balk, G. J. Hoijtink, and J. W. H. Schreuers, *ibid.*, **76**, 813 (1957).

(5) P. Balk, S. de Bruijn, and G. J. Hoijtink, *ibid.*, **76**, 907 (1957).

(6) G. J. Hoijtink and H. van de Meij, *Z. Physik. Chem.* (Frankfurt), **20**, 1 (1959).

nature of the solvents used. It is also possible that different preparation methods are of some influence because of the extreme sensitivity of the alkali metal compounds to water and other impurities. Potassium compounds of naphthalene and anthracene were, therefore, prepared in a high-vacuum apparatus at 10^{-7} to 10^{-8} torr (gas pressure of residual gases other than the reactants). The behavior of the compounds in two solvents of different polarities was studied through electronic spectra and electric conductivities.

Experimental Section

Purification. The alkali metal used was potassium. It is more volatile than sodium and therefore more suitable for high-vacuum distillation. The metal was prepared from potassium dichromate and zirconium.[17] It was degassed several times through distillation in a high-vacuum apparatus. Finally the metal was distilled into sample tubes which were sealed off under a pressure of 10^{-7} torr.

Naphthalene and anthracene, after column chromatography and recrystallization, were sublimed several times and collected under a pressure of 10^{-7} torr in sample tubes with break-seal valves.

It was most important to dry and to degas the solvents, 1,4-dioxane and tetrahydrofuran. After the chemical prepurification according to the method by Pestemer[18,19] the solvents were refluxed over sodium wire while dry nitrogen was passing through. Then a rectification was carried out. By alternate solidification and melting under 10^{-8} torr a great part of the dissolved gases were liberated and could be pumped off. In order to remove last traces of water and air, the solvents were distilled over potassium films in a high-vacuum apparatus which previously had been evacuated by means of a mercury diffusion pump to a pressure of 10^{-7} to 10^{-8} torr at a bake-out temperature of about 350° for at least 10 hr. Liberated gases, mainly hydrogen, were pumped off, and the solvents were distributed among sample tubes which were sealed off at 10^{-6} torr. The purified solvents did not show any absorbancy of light beyond 234 mμ. The specific electric conductance of 1,4-dioxane was 10^{-14} ohm^{-1} cm^{-1} and of tetrahydrofuran 2×10^{-10} ohm^{-1} cm^{-1}.

Preparation of the Solutions. The solutions of the alkali metal compounds were prepared by forming the compounds in the solid state and dissolving them at 10^{-8} torr residual gas pressure. First a potassium film was formed by distilling the metal out of a sample tube into a glass bulb which had been evacuated at about 350° bake-out temperature for at least 10 hr. Then, after the bulb was sealed off from the high-vacuum apparatus, another sample tube containing the hydrocarbon was opened. The hydrocarbon was sublimed onto the potassium and allowed to react with the alkali metal for 1 week. The sample tube which contained the hydrocarbon was then cooled with liquid nitrogen so that all of the excess hydrocarbon could sublime back and was then sealed off. A thin metal film (about 10^{-5} cm thick) and an excess of the hydrocarbon (20–30 mg) was used if a monopotassium compound was to be formed. For the preparation of a dicompound the potassium film was about 0.05–0.1 cm thick and only a small amount (about 1 mg) of the hydrocarbon was allowed to react with the alkali metal.

The solid potassium compounds of naphthalene and anthracene were dissolved in a glass apparatus with three quartz cells, used for spectrometric measurements, in one conductivity cell, and in two pycnometer bulbs. A sample tube filled with a solvent and a glass bulb containing a solid potassium compound, both equipped with break-seal valves, were sealed to the apparatus. The glass apparatus was evacuated by means of a nitrogen-trapped mercury diffusion pump at a temperature of about 400° until a pressure of 10^{-8} torr was maintained for 2 hr. Then the glass apparatus was sealed off from the high-vacuum pump system, the break-seal valves were opened, and the solvent was poured into the bulb containing the solid alkali metal compound. A small amount was dissolved in order to obtain a solution of about 10^{-4} mole/l. The solution was poured back through a frit which retained small bits of potassium. Then the measurement cells were filled and sealed off.

Measurements. The concentrations of the solutions were determined through potentiometric titration of

(7) P. Balk, S. de Bruijn, and G. F. Hoijtink, *Mol. Phys.*, **1**, 151 (1958).

(8) G. J. Hoijtink, *ibid.*, **2**, 85 (1959).

(9) G. J. Hoijtink and P. J. Zandstra, *ibid.*, **3**, 371 (1960).

(10) G. J. Hoijtink, N. H. Velthorts, and P. J. Zandstra, *ibid.*, **3**, 533 (1960).

(11) D. Lipkin, D. E. Paul, J. Townsend, and S. I. Weissman, *Science*, **117**, 534 (1953).

(12) T. R. Tuttle, R. L. Ward, and S. I. Weissman, *J. Chem. Phys.*, **21**, 2227 (1953).

(13) E. de Boer, *ibid.*, **25**, 190 (1956).

(14) E. de Boer and S. I. Weissman, *J. Am. Chem. Soc.*, **80**, 4549 (1958).

(15) R. Suhrmann and R. Matejec, *Z. Physik. Chem.* (Frankfurt), **14**, 246 (1958).

(16) D. F. Paul, D. Lipkin, and S. I. Weissman, *J. Am. Chem. Soc.*, **78**, 116 (1956).

(17) J. H. de Boer, J. Broos, and H. Emmens, *Z. Anorg. Allgem. Chem.*, **191**, 113 (1930).

(18) M. Pestemer, *Angew. Chem.*, **63**, 118 (1951).

(19) M. Pestemer, *ibid.*, **67**, 740 (1955).

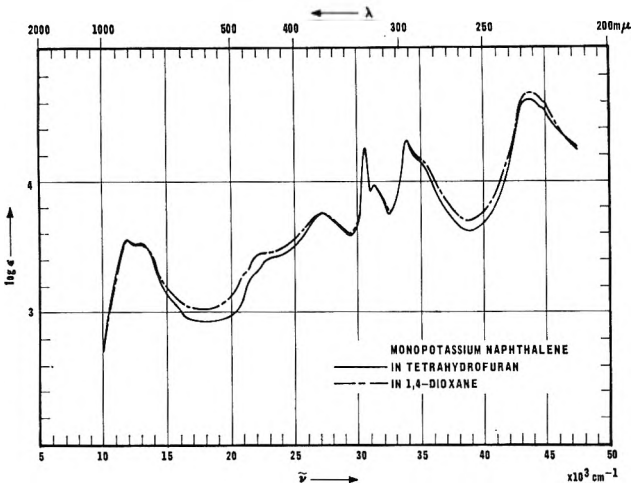

Figure 1. Spectra of the solutions of monopotassium naphthalene in tetrahydrofuran ($c = 3.55 \times 10^{-4}$ mole/l.) and in 1,4-dioxane ($c = 2.1 \times 10^{-4}$ mole/l.).

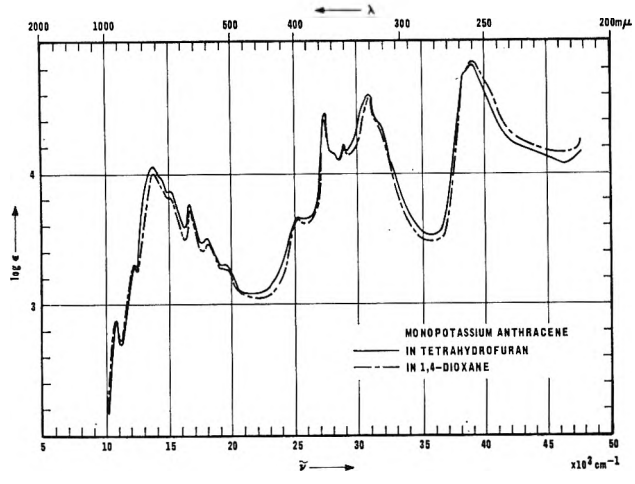

Figure 2. Spectra of the solutions of monopotassium anthracene in tetrahydrofuran ($c = 3.05 \times 10^{-4}$ mole/l.) and in 1,4-dioxane ($c = 1.4 \times 10^{-4}$ mole/l.).

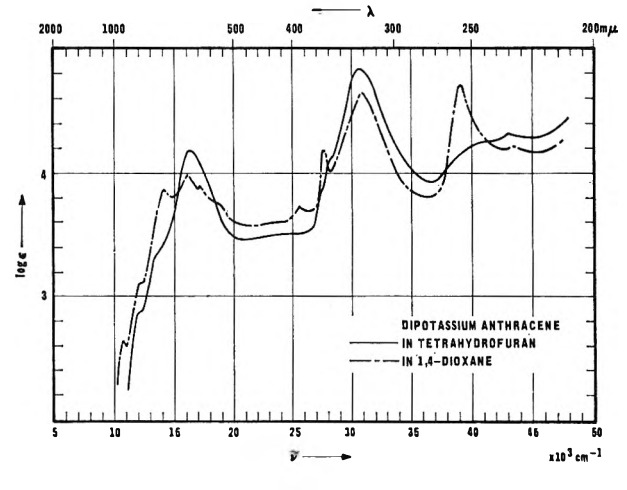

Figure 3. Spectra of the solutions of dipotassium anthracene in tetrahydrofuran ($c = 1.0 \times 10^{-4}$ mole/l.) and in 1,4-dioxane ($c = 1.8 \times 10^{-5}$ mole/l.).

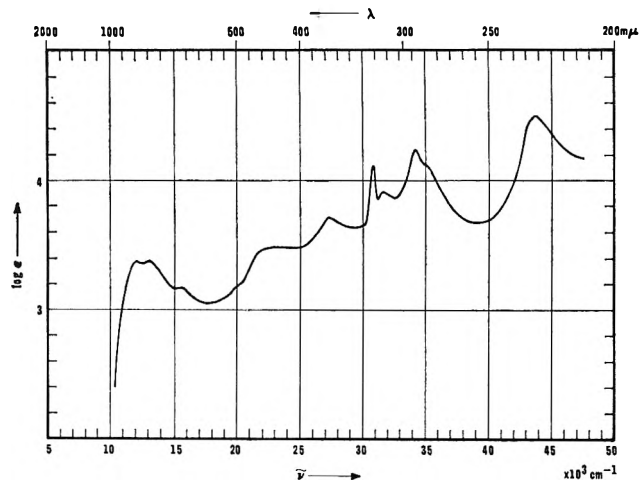

Figure 4. Spectrum of the solution of monopotassium naphthalene, obtained by dissolving solid dipotassium naphthalene in tetrahydrofuran ($c = 2.1 \times 10^{-4}$ mole/l.).

the potassium hydroxide formed by hydrolyzing the solutions. The concentrations were in the range of 10^{-4} mole/l. The electronic spectra were measured by means of a Hilger and Watts (London) spectrophotometer H 700 308. A Knick (Berlin) picoamperemeter P 27 equipped with a 120-v dc source was used for the determination of the low-electric conductivity of the solutions in 1,4-dioxane. The higher conductivity data of the corresponding solutions in tetrahydrofuran were measured by means of a Wheatstone bridge and a Heathkit voltmeter as null indicator. The voltage was 12 v, 50 cps ac.

Results and Discussion

Electronic Spectra. The spectra of the solutions of the green monopotassium naphthalene (Figure 1) and of the blue monopotassium anthracene (Figure 2) in both solvents, 1,4-dioxane and tetrahydrofuran, are actually identical. Although 1,4-dioxane and tetrahydrofuran have different dielectric constants (2.2 and 7.6), the polarity of the solvent apparently has no appreciable influence upon the energy of π-electron transitions in the mononegative ions of naphthalene and anthracene. The results agree also with data of the monosodium compounds of naphthalene and anthracene which have been published previously.[4-10]

The blue dipotassium anthracene, dissolved in tetrahydrofuran (Figure 3), has its main absorption bands at 30.2×10^3 and 16.2×10^3 cm^{-1}. The

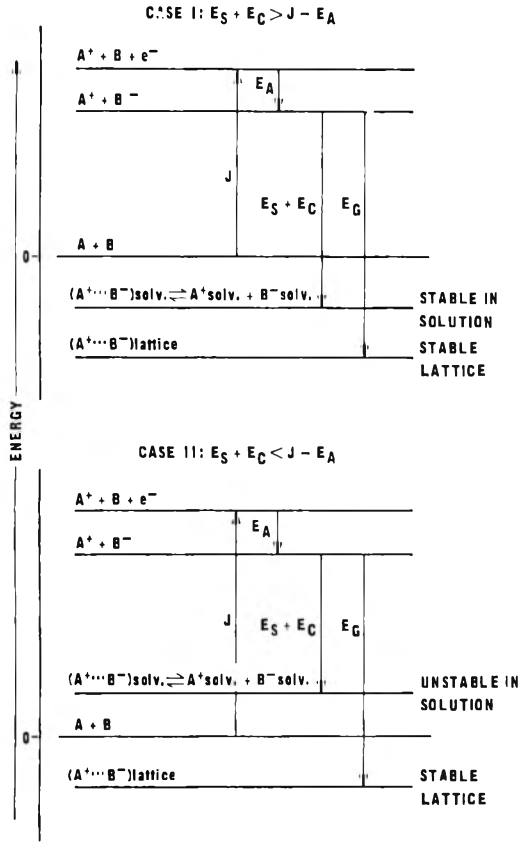

Figure 5. Energy diagram indicating the behavior of the monopotassium and dipotassium compounds in solid state and in solution: J, ionization of the energy of the alkali metal; E_A, electron affinity of the electron acceptor; E_C, ion-pair bonding energy; E_G, lattice energy; and E_S, solvation energy of the ion-pair complex.

corresponding solution in 1,4-dioxane shows, in addition to these two peaks, the main absorption maxima of the mononegative ion of anthracene to some extent. According to this result, the dipotassium anthracene is partly split into the monocompound and free alkali metal. A further peculiarity of the solution of dipotassium anthracene in 1,4-dioxane is the low-saturation concentration of 1.8×10^{-5} mole/l.

The dipotassium naphthalene, which is purple in the solid state,[20] is not soluble in 1,4-dioxane. In tetrahydrofuran the compound could be dissolved. However, the color of the solution obtained was not purple but green, and the spectrum of this solution (Figure 4) was actually identical with the spectrum of monopotassium naphthalene. This result indicates that a complete cleavage of the dipotassium naphthalene into the monopotassium naphthalene and free alkali metal had occurred.

The more or less complete cleavage of the dissolved dipotassium compounds of naphthalene and anthracene may be interpreted by means of the energy diagram in Figure 5.

An ion-pair complex, AB, is formed in the solid state if $E_G > J - E_A$. It is also stable in solution if $E_C + E_S > J - E_A$ (case 1). Examples are the monopotassium compounds of naphthalene and anthracene. On the other hand, a compound containing positive and negative ions will decompose in solution, more or less completely, into its initial components if $E_C + E_S < J - E_A$ (case 2), for instance, as does dipotassium naphthalene in tetrahydrofuran. The dissolved dipotassium anthracene shows both kinds of behavior: it is stable in tetrahydrofuran (case 1) but partly unstable in 1,4-dioxane (case 2). Apparently this is due to a small solvation energy, E_S, of the dissolving process in 1,4-dioxane, a fact that might also explain the insolubility of the dipotassium compound of naphthalene in this solvent. This concept appears reasonable in view of the difference of the dielectric constants of the solvents, 1,4-dioxane ($d = 2.2$) and tetrahydrofuran ($d = 7.6$).

The spectra of the alkali metal compounds of naphthalene and anthracene show changes with time. However, these alterations caused a change of the color only in one case: the color of the solution obtained by dissolving the dipotassium naphthalene in tetrahydrofuran changed from green to orange within 1 hr. But in all spectra a broad absorption band at 22,500–23,000 cm^{-1} appeared after about 2 days. In the spectra of the mononegative ions this band was a mere shoulder, but it became very pronounced in the spectrum of the dinegative ion of anthracene. These changes are very probably caused by the formation of the protonated negative ion of naphthalene and anthracene.[6,9,10]

Electrical Conductance. The electric conductances of solutions of the potassium compounds of naphthalene and anthracene dissolved in 1,4-dioxane and tetrahydrofuran at 20° are listed in Table I.

The electric conductance of the solutions in tetrahydrofuran is about 10^6 times higher than the conductance of the solutions in 1,4-dioxane. These extremely great differences can be interpreted only by assuming a much higher degree of dissociation of the ion-pair complexes if dissolved in the more polar tetrahydrofuran rather than in 1,4-dioxane.

The molar conductivities of alkali metal compounds of naphthalene and anthracene in 1,4-dioxane agree with earlier results determined by Suhrmann and

(20) Solid dipotassium naphthalene could be identified by its spectrum; M. M. Gloger, Ph.D. Thesis, Technische Hochschule, Hannover, Germany, 1964.

Table I: Specific and Molar Electric Conductances

Solvent	Compound	χ, ohm^{-1} cm^{-1}	c, mole/l.	Λ_c, ohm^{-1} cm^2 mole^{-1}
Tetrahydrofuran	Monopotassium naphthalene	6.4×10^{-7}	3.55×10^{-4}	1.8×10^{-3}
	Monopotassium anthracene	20.7×10^{-7}	3.05×10^{-4}	6.8×10^{-3}
	Dipotassium anthracene	6.1×10^{-7}	1.00×10^{-4}	6.1×10^{-3}
1,4-Dioxane	Monopotassium naphthalene	2.9×10^{-13}	2.1×10^{-4}	1.4×10^{-9}
	Monopotassium anthracene	5.05×10^{-13}	1.2×10^{-4}	4.2×10^{-9}

Matejec.[15] The corresponding data of the solutions in tetrahydrofuran, however, turned out to be much lower than those found by other investigators[16] who did not work under comparable high-vacuum conditions.

The electric conductance of the potassium compounds in 1,4-dioxane increases with the temperature in the range of 11°, the melting point of the solvent, up to 35°. In the case of the solutions in tetrahydrofuran, which solidifies at a much lower temperature, the conductance also increases with the temperature, but after passing a maximum in the range of -20 to $-10°$, an inverse effect was observed. Plotting the logarithm of the molar conductivities of the solutions in 1,4-dioxane *vs.* $1/T$ yields straight lines (Figure 6). From the corresponding data for the solutions in tetrahydrofuran, curves with maxima have been obtained. The sloping and ascending branches of these curves can be approximated by straight lines (Figure 7).

The electrolytic dissociation and the viscosity of the solvent are the main influences in the temperature dependence of the electric conductance of a dissolved ionic compound. The Debye–Hückel interionic attraction can be neglected if the solution is as dilute as the investigated solutions of the potassium compounds of naphthalene and anthracene (1–4 $\times$ 10^{-4} mole/l.). With

$$\Lambda_c = \text{constant} \times 1/\eta \times (c_{A^+} + c_{B^-}) = \text{constant}' \times 1/\eta \times c_{A^+} \quad (1)$$

where Λ_c is molar conductance, η viscosity coefficient, and c_{A^+} and c_{B^-} concentrations of the ions formed from 1 mole of the compound, AB, and with

$$k_d = c_{A^+}c_{B^-}/c_{AB} \quad (2)$$

where k_d is the dissociation constant, one obtains

$$\Lambda_c = \text{constant}' \times 1/\eta \times \sqrt{k_d} \quad (3)$$

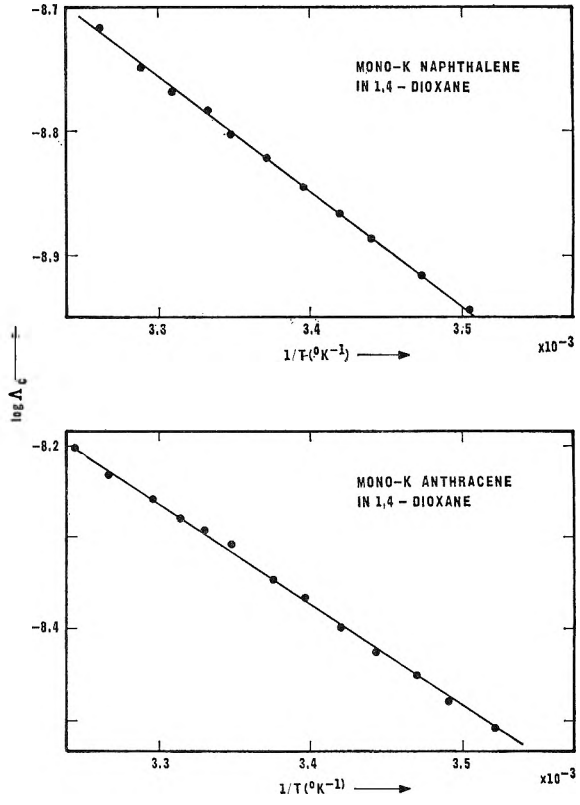

Figure 6. Logarithm of the molar conductance as a function of $1/T$ of the compounds dissolved in 1,4-dioxane: top, monopotassium naphthalene (c = 2.1 $\times$ 10^{-4} mole/l.); bottom, monopotassium anthracene (c = 1.2 $\times$ 10^{-4} mole/l.).

if k_d is small, and $c_{A^+} = c_{B^-}$, and if c_{AB} is unity. Writing eq 3 in logarithmic form and substituting for k_d from the van't Hoff law, $\ln k_d = -\Delta H_d/RT +$ const, will lead to the expression

$$\log \Lambda_c + \log \eta = \text{const}'' - \log e/2R \times \Delta H_d \times 1/T \quad (4)$$

The dissociation enthalpies of the potassium compounds of naphthalene and anthracene in the two sol-

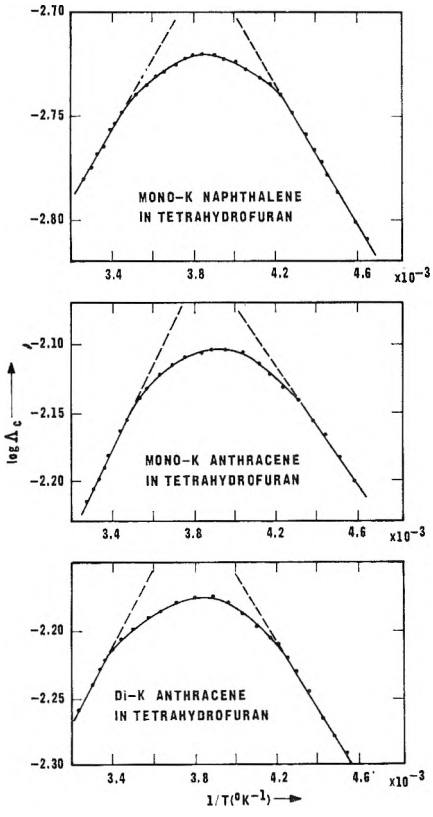

Figure 7. Logarithm of the molar conductance as a function of $1/T$ of the compounds dissolved in tetrahydrofuran: top, monopotassium naphthalene ($c = 3.55 \times 10^{-4}$ mole/l); center, monopotassium anthracene ($c = 3.05 \times 10^{-4}$ mole/l.); bottom, dipotassium anthracene ($c = 1.0 \times 10^{-4}$ mole/l.).

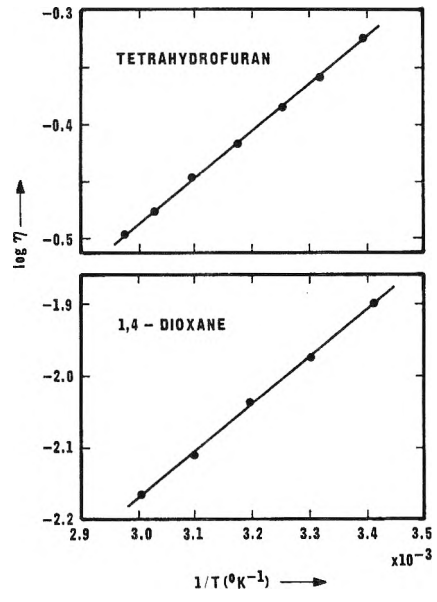

Figure 8. Logarithm of the viscosity coefficient as a function of $1/T$ for tetrahydrofuran (top) and 1,4-dioxane (bottom). (Prof. Dr. Kuss, Technische Hochschule, Hannover, Germany, private communication, 1963).

vents used have been calculated from the gradients of the straight lines in Figures 6 and 7 and by plotting the logarithm of the viscosity coefficients of the solvents *vs.* $1/T$ (Figure 8). The data, listed in Table II, indicate that the dissociation of all investigated potassium compounds requires energy if 1,4-dioxane is used as the solvent, but occurs with liberation of energy in tetrahydrofuran.

The enthalpy of dissociation can be considered as composed of the positive ion-pair bonding energy and the negative enthalpy of solvation. The ion-pair bonding energy depends only upon the nature of the ion-pair compound. Therefore the enthalpies of dissociation (Table II) signify that the enthalpy of solvation is approximately 9 kcal/mole more negative if the dissociation of the potassium compounds of naphthalene and anthracene occurs in tetrahydrofuran rather than in 1,4-dioxane, in the range of 11–35°. Table II furthermore shows that the enthalpies of solvation of the potassium compounds dissolved in tetrahydrofuran increase with the temperature, indicating a higher degree of solvation.

Table II: Molar Enthalpies of Dissociation

Compound	Solvent	Temp, °C	ΔH_d, kcal/mole
Monopotassium naphthalene	1,4-Dioxane	11 to 35	2.67
Monopotassium anthracene	1,4-Dioxane	11 to 35	3.09
Monopotassium naphthalene	Tetrahydrofuran	11 to 35	−5.28
Monopotassium anthracene	Tetrahydrofuran	11 to 35	−6.61
Dipotassium anthracene	Tetrahydrofuran	11 to 35	−6.40
Monopotassium naphthalene	Tetrahydrofuran	−55 to −35	−2.20
Monopotassium anthracene	Tetrahydrofuran	−55 to −35	−1.73
Dipotassium anthracene	Tetrahydrofuran	−55 to −35	−1.50

Acknowledgment. The authors wish to thank Professor Emeritus Dr., Dr. h.c.R. Suhrmann of the Technische Hochschule, Hannover, Germany, for his helpful discussions and suggestions during this work.

Aerosol Studies by Light Scattering.[1] V. Preparation and Particle Size Distribution of Aerosols Consisting of Particles Exhibiting High Optical Absorption

by R. T. Jacobsen,[2] M. Kerker, and E. Matijević

Department of Chemistry and Institute of Colloid and Surface Science, Clarkson College of Technology, Potsdam, New York 13676 *(Received June 13, 1966)*

Aerosols consisting of solid spheres have been prepared in a newly designed generator by two-stage evaporation–condensation of vanadium pentoxide in a furnace capable of operating up to 1500°. Nuclei were prepared by evaporation of aluminum at 1000°, condensation to an aluminum aerosol, and subsequent burning in oxygen to Al_2O_3. The particle size distribution of the aerosols was determined by analysis of the angular distribution of the polarization of the scattered light. The special feature of this work resides in the high optical absorption of aerosol particles at the blue end of the visible spectrum (comparable to that of metals) and the low absorption at the red end (comparable to dielectrics). By considering several wavelengths, the very different scattering data on the same physical system led to size distributions which agreed with each other. The uniqueness of these results was explored with the aid of error contour maps.

Introduction

This paper describes the preparation of aerosols consisting of submicronic spheres obtained by evaporation–condensation of vanadium pentoxide and the determination of their particle size distribution by light scattering. The special feature of this aerosol, which motivated the research, is its high optical absorption in the lower wavelength part of the visible spectrum, comparable to that of metals. On the other hand, the dispersion of the optical constants is such that at the higher visible wavelengths there is very little absorption, so that in this range it behaves as a dielectric. Thus the same physical system scatters light as a metal-like highly absorbing material or as a moderately absorbing "colored" material, depending upon which part of the visible spectrum is selected for the incident radiation.

Interestingly, in his development of the theory of scattering by spheres, Mie[3] was primarily concerned with metal sols, and in Born's book[4] the subject of light scattering is still classified under the "optics of metals." However, although there has been some recent work on aerosols[5] and hydrosols[6–8] consisting of metallic or highly absorbing particles, the overwhelming bulk of experimental work today deals with dielectric spheres.

In earlier studies, we developed a light-scattering technique, designated as the polarization ratio method,[9] in order to determine the particle size distribution of hydrosols,[10] of aerosols consisting of liquid droplets,[11]

(1) This investigation was supported by Grant DA-SIG-36-039-61-G-15, U. S. Army Material Agency, Ft. Monmouth, N. J.

(2) The work presented in this paper is based on the Ph.D. Thesis of R. T. Jacobsen.

(3) G. Mie, *Ann. Phys.*, (4) 25, 377 (1908).

(4) M. Born and E. Wolf, "Principles of Optics," Pergamon Press, London, 1959.

(5) M. Kerker, A. L. Cox, and M. D. Schoenberg, *J. Colloid Sci.*, 10, 413 (1955).

(6) M. Kerker, G. L. Jones, Jr., J. B. Reed, C. N. P. Yang, and M. D. Schoenberg, *J. Phys. Chem.*, 58, 1147 (1954).

(7) R. H. Doremus, *J. Chem. Phys.*, 42, 414 (1965).

(8) R. H. Morriss and L. F. Collins, *ibid.*, 41, 3357 (1964).

(9) M. Kerker, E. Matijević, W. F. Espenscheid, W. A. Farone, and S. Kitani, *J. Colloid Sci.*, 19, 213 (1964).

(10) M. Kerker, E. Daby, G. Cohen, J. P. Kratohvil, and E. Matijević, *J. Phys. Chem.*, 67, 2105 (1963).

(11) E. Matijević, S. Kitani, and M. Kerker, *J. Colloid Sci.*, 19, 223 (1964); E. Matijević, M. Kerker, and K. F. Schulz, *ibid.*, 17, 26 (1962).

of aerosols consisting of solid spheres,[12] and of aerosols consisting of solid spheres encased in a liquid spherical shell.[13] Recently, the technique has been applied to cylindrical fibers having submicronic radii.[14] In all cases these were dielectric materials. The method consists in comparing experimental values of the angular variation of the polarization ratio of the scattered light with a catalog of values calculated for various size distributions and the appropriate refractive index. The solution of the problem is obtained by selection of that size distribution for which there is an optimum match between the experimental and calculated values.

Use of Polarization Rather Than Polarization Ratio for Analysis of Light-Scattering Data

The polarization ratio at any particular angle is the ratio of the intensity of the parallel-polarized component of the scattered light to that of the perpendicularly polarized component

$$\rho = \frac{I_2(\theta)}{I_1(\theta)} = \frac{\int i_2(\theta) f(\alpha) \mathrm{d}\alpha}{\int i_1(\theta) f(\alpha) \mathrm{d}\alpha} \qquad (1)$$

The angular distribution functions i_1 and i_2, which depend on the particle-size parameter, α, and the refractive index, are defined elsewhere.[15] The frequency function, $f(\alpha)\mathrm{d}\alpha$, gives the number of particles with size parameter between α and $\alpha + \mathrm{d}\alpha$ where

$$\alpha = 2\pi a/\lambda \qquad (2)$$

in which a is the particle radius and λ is the wavelength in the medium. A two-parameter logarithmic distribution involving the modal value of the size parameter, α_M, and a breadth parameter, σ_0, was used,[16] such that

$$f(\alpha) = \frac{\exp\dfrac{-(\ln \alpha - \ln \alpha_M)}{2\sigma_0^2}}{\sqrt{2\pi}\sigma_0 \alpha_M \exp(\sigma_0^2/2)} \qquad (3)$$

The procedure for analyzing the light-scattering data was altered in this work by utilizing the angular variation of the polarization defined by

$$P = \frac{I_2 - I_1}{I_2 + I_1} = \frac{\rho - 1}{\rho + 1} \qquad (4)$$

rather than the polarization ratio (see eq 1). There are two advantages in using P rather than ρ.

Firstly, the value of ρ extends from zero to infinity, with $\rho = 1$ representing unpolarized light. For $I_2 > I_1$, the value of ρ extends from unity to infinity, whereas for $I_2 < I_1$, it is restricted to the range from zero to unity. This leads to a misleading impression concerning the structure in a scattering curve. The effect is illustrated in Figure 1. The two polarization ratio

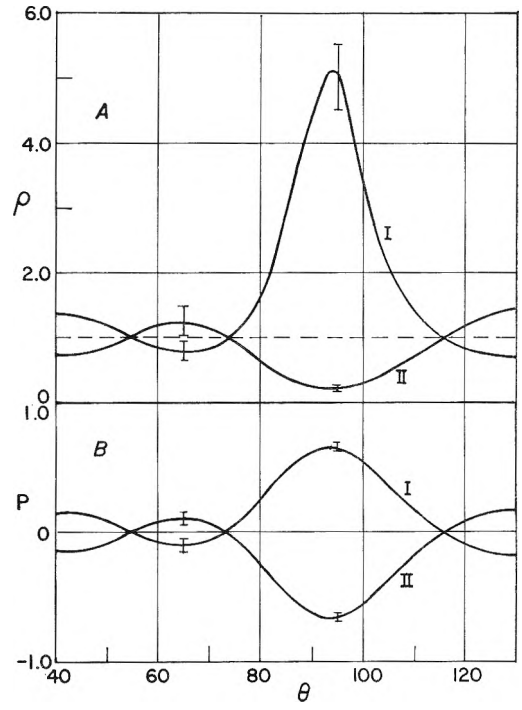

Figure 1. Comparison of polarization (P) *vs.* θ with polarization ratio (ρ) *vs.* θ for the same intensity data. A, ρ *vs.* θ; B, P *vs.* θ.

curves, as shown in part A, appear quite different. Curve I appears more "structured" than curve II and yet these curves actually differ only in that the values of I_2 and I_1 are interchanged. When the data are plotted as P *vs.* the angle θ as in part B of Figure 1, the similarity of the results is apparent and the advantage of P in depicting these "structural" effects is clearly demonstrated.

A second advantage is related to the criterion used for determining which of the calculated particle size distributions best fits the experimental results for a particular aerosol. The criterion used here was a minimum in the deviation parameter

$$\Delta = \left\{ \sum_{\theta=40^\circ (5^\circ)}^{130^\circ} [P_E(\theta) - P_T(\theta)]^2 \right\}^{1/2} \qquad (5)$$

where $P_E(\theta)$ is the measured value of the polarization at angle θ and $P_T(\theta)$ is the theoretical value calculated for a particular size distribution (α_M and σ_0) and the

(12) W. F. Espenscheid, E. Matijević, and M. Kerker, *J. Phys. Chem.*, **68**, 2831 (1964).

(13) W. F. Espenscheid, E. Willis, E. Matijević, and M. Kerker, *J. Colloid Sci.*, **20**, 501 (1965).

(14) W. A. Farone and M. Kerker, *J. Opt. Soc. Am.*, 56, 481 (1966).

(15) H. C. van de Hulst, "Light Scattering by Small Particles," John Wiley and Sons, Inc., New York, N. Y., 1957.

(16) W. F. Espenscheid, M. Kerker, and E. Matijević, *J. Phys. Chem.*, **68**, 3093 (1964).

complex refractive index at the particular wavelength.

In the earlier work in which the polarization ratio had been used, the corresponding criterion utilized the residuals of the fractional deviations of the experimental and calculated values of ρ. Actually, it was not quite correct to assume a constant fractional error in ρ as had been done because values of ρ close to zero or very large values of ρ correspond to one of the polarized components being very weakly scattered. Under such circumstances, the systematic errors (spurious reflection, dark current noise, etc.) become significant compared to those errors which are proportional to the signal. Accordingly, there is a higher fractional error. However, for the polarization P, this effect is at least partially compensated for when only the residual of P is used, as in eq 5. This follows because, for a constant fractional error in the intensity (which, in turn, leads to a constant fractional error in ρ), the residual in P is smaller for values of P closer to unity. It is just these values of P that correspond to values of ρ which are either close to zero or are large. Accordingly, using the unweighted residuals in P corresponds to using weighted residuals of the fractional deviations in ρ. This effect is shown in Figure 1, where the vertical lines depict the error corresponding to a 10% error in ρ. The corresponding error in P is less as P approaches unity.

Theoretical values of P were calculated from I_2 and I_1 which, in turn, were computed for an array of α_M, θ, σ_0, and m combinations. In computing I_2 and I_1, the numerical integration was cut off at limits $e^{\pm 3\sigma_0}$.

Vanadium Pentoxide Aerosol Generator

The technique for producing aerosols, consisting of solid submicronic spheres, by evaporation of vanadium pentoxide differs somewhat from that used earlier to prepare aerosols of NaCl[12,17] and AgCl.[13] A carrier gas, upon passage through a furnace, picks up vapor of the material from which the aerosol is to be formed. The gas mixture cools after leaving the furnace, and condensation takes place upon foreign nuclei, if these have been introduced into the system, or, in their absence, upon fluctuation embryos. The first case will be referred to as heterogeneous nucleation, the second as homogeneous nucleation.

Earlier experience in generating solid aerosols of NaCl and AgCl indicated the following general rules.

(1) Particle size increases with furnace temperature.

(2) If the aerosol is formed in two successive stages, this results in a narrower size distribution, but addition of a third stage does not continue to narrow the distribution significantly.

(3) For a given set of operating conditions, larger particles are formed in the presence of foreign nuclei. Up to a certain point, decreasing the concentration of foreign nuclei results in still larger particles.

(4) Under conditions of self-nucleation, larger particles are formed at higher flow rates of carrier gas. With foreign nuclei present, smaller particles are formed at higher flow rates.

Even with these guidelines, we were unable, by exhaustive trial and error experimentation with the previously existing apparatus, to obtain the aerosols required for this work. These should consist of particles with radii in the tenths of a micron range and of narrow size distribution. The particle concentration should be sufficiently high to give appreciable light scattering and yet not so high that extensive coagulation or multiple scattering occurs.

It seemed reasonable to expect that the crucial parameter might be the vapor pressure generated in the furnace. The temperature ranges over which various aerosols (NaCl, AgCl, octanoic acid) had previously been obtained indicated that optimum conditions for homogeneous nucleation were reached when the vapor pressure was approximately 1 torr. On this basis, it appeared that a temperature of 1000°, or even considerably higher, would be needed for vanadium pentoxide.[18-21]

A high-temperature furnace, capable of operating up to 1500°, was designed and built. The refractory material was Harbison and Walker H-W 28 insulating brick. The heating elements were carborundum Delta Globars, Type AT. Temperature was monitored by measurement of power dissipation after calibration by a chromel–alumel thermocouple. Detailed drawings of the high-temperature furnace and its operating conditions are described elsewhere.[22]

A schematic diagram of the new aerosol generator is shown in Figure 2. The upper section of the diagram is the nucleator where the small, nonvolatile foreign nuclei are produced and dispersed into the gas stream. The lower section depicts the main part of the generator where either heterogeneously or homogeneously nu-

(17) W. F. Espenscheid, E. Matijević, and M. Kerker, *J. Colloid Sci.*, **18**, 91 (1963).

(18) "International Critical Tables," Vol. III, National Research Council, 1928, p 213.

(19) C. G. Maier, U. S. Bureau of Mines Technical Paper 360, 1925.

(20) Yu. Polyakov, *J. Phys. Chem. USSR*, **20**, 1021 (1946).

(21) J. Berkowitz, W. A. Chupka, and M. G. Inghram, *J. Chem. Phys.*, **27**, 87 (1957).

(22) R. T. Jacobsen, Ph.D. Thesis, Clarkson College of Technology, 1966, University Microfilm.

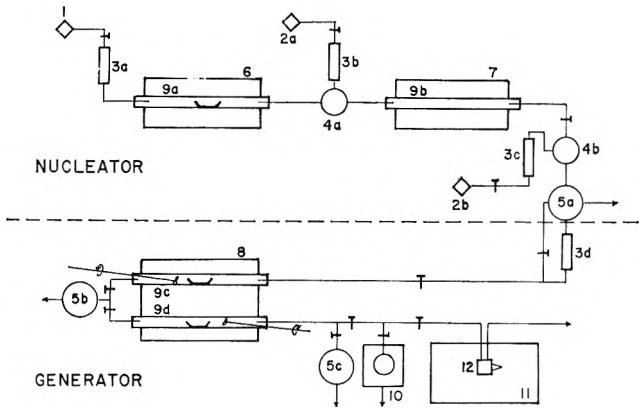

Figure 2. Schematic diagram of the aerosol generator: (1) argon source; (2a, b) oxygen sources; (3a, b, c, d) flow meters; (4a, b) mixing chambers; (5a, b, c) viewing chambers; (6) nucleator furnace; (7) burner furnace; (8) boiler furnace; (9a, b, c, d) combustion tubes; (10) thermopositor; (11) light-scattering photometer; (12) light-scattering cell.

cleated aerosols are formed. The lower section will be described first.

A stream of metered carrier gas enters a viewing chamber (5a) from either the nucleator or from an external source and is then directed through combustion tubes (9c) and (9d) located in the high-temperature furnace (8). In (9c) the carrier gas picks up the vapor supplied from a glazed porcelain boat containing vanadium pentoxide. Condensation to an aerosol occurs when the vapor stream reaches the cold zone near the exit of the furnace. A second stage of growth occurs in the second combustion tube (9d), and the aerosol may then be directed to a chamber (5c) for visual inspection, a thermal precipitator (10) for collection on electron microscope grids, or a cell for light-scattering measurements (11, 12). All exhausts were led into a fume hood. The reader is cautioned that vanadium oxide vapors have been reported to be highly toxic.[23]

Despite the expectation that a furnace temperature of 1000° or slightly higher might generate sufficient vapor to form aerosols of sufficiently large particle size, this did not turn out to be the case.

In the molten phase, V_2O_5 begins to polymerize at temperatures above 900°, as evidenced by a marked increase in the apparent viscosity of the melt and also by a complete change in appearance upon cooling. Whereas the material cooled from 750° was quite lustrous and decidedly crystalline in appearance with a definite melting point, the material cooled from temperatures above 900° slowly thickened into a dull mass.

In addition, the V_2O_5 began to decompose at the high temperatures, probably into oxygen and a lower oxide, as has been reported in the literature.[24,25] This was evidenced by the formation of a precipitate in the hot melt. In order to inhibit this decomposition, the carrier gas was changed from helium to oxygen, and this did result in the aerosol particles becoming somewhat larger. The enhanced stability of vanadium pentoxide in an oxygen atmosphere is in accordance with thermodynamic data as reported by Mah and Kelley.[26]

Further improvement was obtained by installing quartz stirrers in each combustion tube in order to mix the heavy vapors with the carrier gas. With these improvements, self-nucleated aerosols, having a modal radius ranging from 0.075 to 0.200 μ, could be produced over the temperature range 1000–1400° at a flow rate of 0.6 l./min. Useful aerosols were not obtained at substantially higher temperatures, probably due to the decomposition even in pure oxygen.

We now consider the problem of selection of a substance from which to form foreign nuclei. The conditions are rather stringent. The material should be sufficiently volatile to vaporize and then condense to nuclei, and yet it may not evaporate in the high-temperature furnace of the generator where it must serve as a condensation nucleus.

The technique finally evolved utilizes aluminum in a two-step process. This will be described with reference to the nucleator section of the schematic diagram in Figure 2. Filtered and metered argon (1) passes through a combustion tube which contains molten aluminum in a glazed porcelain boat (9a). Both furnaces in this section of the generator were standard hinged-type single-tube combustion furnaces controlled by auto-transformers. The combustion tubes were fused quartz, since it was found that the aluminum vapor attacks ceramic tubes, causing rupture after 2 or 3 hr of operation. In the nucleator furnace the inert carrier stream picks up aluminum vapor which presumably condenses into nuclei upon leaving the hot zone. From here, the aluminum–argon stream enters flask (4a) where it is mixed with oxygen entering through flow meter (3b), and the mixture passes into furnace (7) where the aluminum burns to Al_2O_3. The carrier gas with the Al_2O_3 nuclei then passes into mixing chamber (4b) where it is diluted further with oxygen, then into viewing chamber (5a) where visual inspection in a light beam can be performed to ensure that the

(23) E. A. Mel'nikova, *Gigiena i Sanit.*, 22, 25 (1957).

(24) K. Iwase and N. Nasu, *Sci. Rept. Tohoku Univ.*, Series 1, K. Honda Anniversary Vol., 476 (1936).

(25) F. Vratny and F. Micale, *Trans. Faraday Soc.*, 59, 2739 (1963).

(26) A. D. Mah and K. K. Kelley, U. S. Bureau of Mines Report Investigation 5858, 1961.

particles are not too large. From here, part of the stream can be exhausted to adjust the final flow rate before entering the generator section.

The temperature at which to operate furnace (6) was determined in the same manner used to predict the necessary furnace temperatures for the V_2O_5. Previous experimental experience indicated that successful nucleation resulted when the vapor pressure of the nucleating material (*e.g.*, NaCl, NaF) was approximately 0.1 torr. In this work, the nucleator furnace was kept at 1000°, at which temperature the vapor pressure of aluminum is ~0.1 torr.

Other Experimental Arrangements

The other experimental arrangements were, for the most part, the same as used in our earlier work. Collection for electron micrographic observation was made by means of thermal precipitation in a Model B thermopositor produced by the American Instrument Co. The deposition was on collodion-coated, 200-mesh, $^1/_8$-in. copper screens. Observations were made directly on the samples as collected with a Philips Model 75B electron microscope. No shadowing or replication techniques were used. The particles appeared spherical, and any aggregation in the electron micrographs appeared to be an artifact of the collection procedure. This was shown to be the case by varying the collection time. As this is shortened, the fraction of apparently aggregated particles decreases, indicating that the aggregates actually form by collision on the collection grid.

No attempt was made to determine the composition of the aerosol particles obtained by the condensation of the vaporized V_2O_5. Electron diffraction patterns were taken of especially dense collections of particles. These showed none of the sharp lines characteristic of crystalline material, but only a single diffuse diffraction maximum which was due in a large part to the collodion substrate. The lack of a sharp diffraction pattern apparently was not due to line broadening caused by the small particle size, since the electron diffraction pattern for particles from a V_2O_5 hydrosol, which are even smaller but which are crystalline, did give a sharp diffraction pattern. It is quite possible that the aerosol particles consisted of a mixture of vanadium oxides.[27] This, however, has no effect upon the particle size distribution analysis by light scattering, because the measurements were taken on the *same* aerosol using different wavelengths, and the refractive index was obtained by a fitting procedure.

Particle size analyses of the electron micrographs were made on a Zeiss Model TGZ-3 particle size analyzer.[28] Calibration to absolute size was accomplished by means of a carbon replica grating with 28,800 lines/in. This was photographed with each aerosol at the same electron microscope settings.

For the light-scattering measurements, the aerosol was directed into a specially designed cell mounted on the cell table of a modified Brice-Phoenix Series 2000 light-scattering photometer, as described elsewhere.[13] Glan-Thompson prisms were used in place of the standard polaroid filters, and the wiring to the lamp house of the instrument was modified to accept either the standard power supply for an AH-3 mercury arc or a 6-v, 18-amp projector lamp which was used with interference filters for wavelengths of 489 and 659 mμ. The 406, 436, 546, and 578-mμ mercury lines were also isolated with interference filters. A 2-mm circular nose piece was mounted in front of the photomultiplier, producing a 5° angle of acceptance.

Refractive Index of Vanadium Pentoxide

The complex refractive index necessary for the calculation of i_1 and i_2 was not known for vanadium pentoxide. This was determined ellipsometrically by reflectance measurements from a single crystal of vanadium pentoxide approximately 2 × 8 × 25 mm, grown by Servi-Elements, Inc., and cut and polished by Harshaw Chemical, Crystal and Solid State Division. Because crystalline vanadium pentoxide is anisotropic, this led to three principal refractive indices corresponding to the three symmetry axes. Since the composition of the aerosol particles was not known, an average of the three refractive indices for the crystal was used as a *preliminary trial* value in the light-scattering work. The final result was a set of values for α_M, σ_0, and the complex refractive index which gave the best fit between the calculated and experimental values of the polarization over the angular range 40°(5°)130°. The values for the complex refractive index of the aerosol particles which were finally used are given in Table I. The ellipsometric work is described in detail elsewhere.[22]

Results and Discussion

Although the technique for producing aerosols using solid V_2O_5 as starting material, which was finally evolved as described above, did produce aerosols which were amenable to light-scattering analysis, these were not as stable nor as reproducible nor could they be prepared over as wide a range of sizes as the NaCl and AgCl aerosols obtained earlier. For this reason, there will be no attempt here to correlate the aerosol proper-

(27) L. Brewer, *Chem. Rev.*, **52**, 1 (1953).

(28) F. Endter and H. Gebauer, *Optik*, **13**, 97 (1965).

Table I: Complex Refractive Index of Amorphous V_2O_5 Aerosol Particle

Wavelength, mμ	406	436	490	546	578	659
Refractive index	$2.1-0.55i$	$2.5-0.30i$	$2.3-0.15i$	2.25	2.25	2.25

ties with the generator conditions in a systematic way. By stability we refer to a constant output by the generator over an extended period of time. In this case, where light-scattering data were being collected at six different wavelengths (λ = 406, 436, 489, 546, 578, and 659 mμ) and 19 scattering angles [40°(5°) to 130°], it was desirable to have a stable output for several hours. This degree of stability could be achieved only over a narrow range of furnace temperatures and flow rates. The aerosols prepared by condensation upon foreign nuclei were generally more stable than the homogeneously nucleated systems. By reproducibility, we refer to production of a similar aerosol on different days when the same generating conditions are used.

The general features obtained earlier with other solid aerosols, as described above, were also apparent for vanadium pentoxide aerosols, except that both homogeneously and heterogeneously nucleated aerosols increased in particle size with increasing flow rate up to a maximum value which depended upon temperature. Upon further increase in flow rate, the particle size decreased.

A large number of both homogeneously and heterogeneously nucleated aerosols were prepared and the particle size distribution of each of these was determined at several wavelengths by the light-scattering procedure which has just been described. For aerosols which remained stable over the period of the experiment, the light-scattering data at various wavelengths led to particle size distributions which were in excellent agreement with each other.

Here only one case will be considered. It is presented primarily in order to demonstrate the use of an error contour chart for considering whether or not a particular size distribution *uniquely* fits the light-scattering data. We consider the result of the analysis of a heterogeneously nucleated aerosol as shown in Table II and Figure 3. As expected, the experimental curves of polarization *vs.* scattering angle differ at each wavelength, since both the "optical size," α, and the refractive index vary with wavelength. The calculated size distributions (α_M, σ_0), for which the deviation parameter, Δ, was a minimum, are given in the second and third columns of Table II. The modal value of the radius is in the fourth column of the table, and the corresponding size distributions are plotted in the inset of Figure 3. The internal consistency of these size

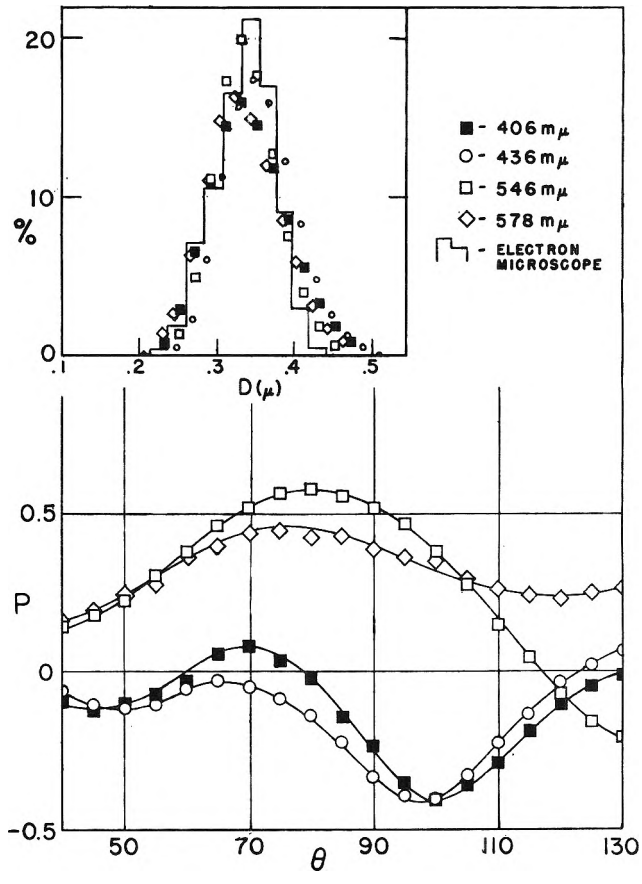

Figure 3. Variation of polarization, P, with angle, θ, for a vanadium pentoxide aerosol at four different wavelengths: ■, 406 mμ; ○, 436 mμ; □, 546 mμ; and ◇, 578 mμ. The inset shows the distributions as calculated from the P *vs.* θ curves (points). The histogram is obtained from electron microscopy.

Table II: Size Distribution of a Heterogeneously Nucleated Aerosol (Furnace Temperatures, (9c) 1356°, (9d) 1400°; Flow Rate, 0.5 l./min)

Wavelength, mμ	α_M	σ_0	a_M, μ
406	2.5	0.15	0.16
436	2.4	0.15	0.17
546	2.0	0.13	0.17
578	1.8	0.12	0.17

distributions determined at four different wavelengths is excellent, and these results are in agreement with the

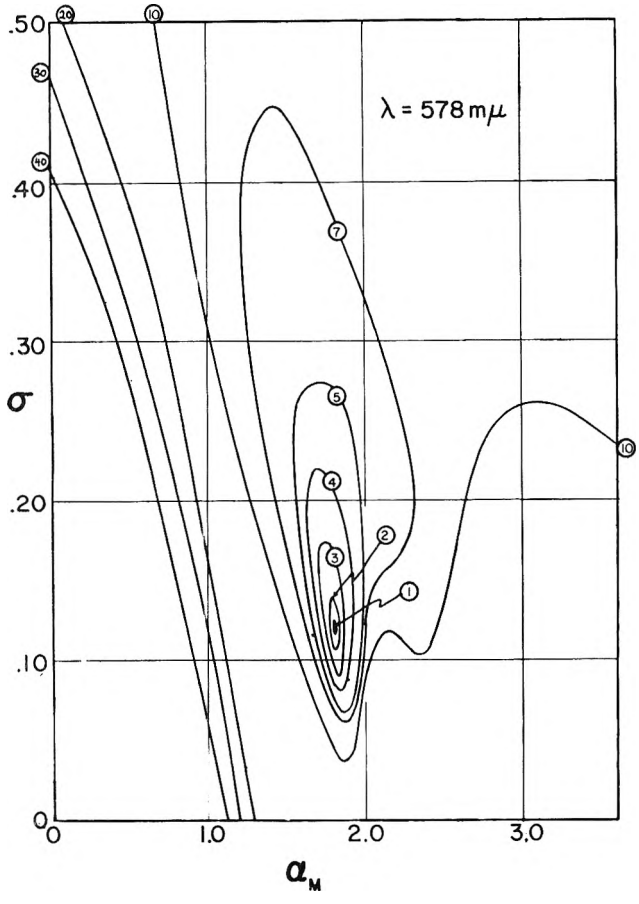

Figure 4. Error contour map for the same run as in Figure 3 at λ = 578 mμ. Contours are labeled as $\Delta \times 10$.

particle size histogram obtained by electron microscopy. This is also shown in the inset.

Any iterative matching technique, such as used here, raises the question of the uniqueness of the solution. Granted that although there is excellent concordance between experimental and calculated results, and also that there is internal consistency among results obtained at four different wavelengths, might there not be other size distributions that would fit these data equally well?

An error contour map for the aerosol corresponding to Table II and Figure 3 is shown in Figure 4 in order to illuminate this point. This map is for λ = 578 mμ. The contour lines in the $\alpha_M - \sigma_0$ domain represent loci of equal error between experiment and calculations as measured by the deviation parameter, Δ. The lines designated 1, 2, 3, etc., correspond to Δ = 0.1, 0.2, 0.3, etc. The topography over the terrain in Figure 4 is a deep well with steep sides. The precision of the solution at the bottom of the well is depicted by the shaded area within the lowest contour line. Since this is the only well or valley, this solution is unique over the domain shown.

The error contour maps for λ = 406 and 546 mμ showed the same features, although the precision was not as great as for λ = 578 mμ, as indicated by a larger area for the inner contour. For λ = 436 mμ, there were two separate valleys in the error contour map, one with a deviation Δ = 0.4 and another with Δ = 0.5, leading to two distinct values of α_M and a broad range of uncertainty in σ_0. However it was observed that this aerosol was unstable and was changing in the course of the measurements at λ = 436 mμ, so that the poor precision can be attributed to this instability. Had only the data at 436 mμ been available, it would not have been possible to assign a size distribution to the aerosol. Thus this method, when coupled with such an error contour map, has the particular virtue that such a multivalued result can be spotted. Agreement between theory and calculations at just one particular point in the $\alpha_M - \sigma_0$ domain provides only a necessary, but not a sufficient, condition for a satisfactory fit. In addition, there must be an absence of a fit over the remainder of the domain. However, even if there should be a multivalued result at a particular wavelength for a stable aerosol, it may still be possible to determine the correct size distribution if data at other wavelengths are also obtained. Indeed, for a material such as this where the refractive index as well as the optical size varies markedly with wavelength, internal agreement at several wavelengths provides a particularly stringent test of the validity of these particular results and, in a general way, of the analytical method.

Ultrasonic Vibration Potentials and Their Use in the Determination of Ionic Partial Molal Volumes[1a]

by Raoul Zana[1b] and Ernest Yeager

Condensed State Center and Department of Chemistry, Western Reserve University, Cleveland, Ohio *(Received June 27, 1966)*

The propagation of ultrasonic waves through an ionic solution gives rise to alternating potential differences (ionic vibration potentials) within the solution as a result of differences in the dynamic reactions of the cations and anions to the acoustical waves. The amplitude of the effect is a function of the masses of the solvated ions minus the mass of the free solvent displaced by each ion. Experimental studies have been carried out with many electrolytes with particular attention to the elimination of possible false effects. The observed dependence of the ionic vibration potentials on various parameters is in good agreement with theory. From ionic vibration potentials and density data, the absolute values for the ionic partial molal volumes have been determined for a number of simple monovalent ions without any assumption as to the value for a given ion or the ratio of values for any pair of ions.

I. Introduction

In an electrolytic solution, ultrasonic waves produce alternating potentials between points separated by a phase distance other than an integral multiple of the wavelength. These alternating potentials were first predicted by Debye[2a] in 1933 and were suggested by him as a means for studying ion–solvent interactions.

The effect occurs because of differences in the amplitudes and phases of the displacements of the cations and anions as a consequence of differences in the effective masses and fractional coefficients of the solvated cations and anions. The mechanism is represented in Figure 1 with displacements at a particular instant represented on the ordinate and distance in the direction of propagation on the abscissa. The lengths of the arrows are intended to indicate the relative displacements of the cations (+) and anions (−) at any instant with the former assumed smaller (for purposes of illustration). For the conditions represented in Figure 1, region A will be charged positively relative to region B. If inert metal probes are placed at positions A and B, an alternating potential difference will be observed since the curve representing displacement may be considered as traveling in the positive direction at the speed of sound in a progressive sound field. The frequency of the alternating potentials corresponds to that of the sound field. Ionic vibration potentials can be measured in terms of either the potential difference between two points or the potential variations at any one point relative to the average potential of the solution.

II. Theory

The dynamic reaction of a particular ion (jth ion) in the sound field must be equal to the various forces acting on the ion[2b]

$$e_jX - \rho_j(\nu_j - \nu_0) - e_j\left[\frac{|e_1e_2|q\kappa X}{(3DkT)[1 + q^{1/2}(1 + i\omega\theta)^{1/2}]}\right] - \frac{e_jX\kappa\rho_j}{6\pi\eta_0} - \frac{kT}{n_j}\frac{\partial n_j}{\partial x} + v_j s_0\frac{d\nu_0}{dt} = m_j\frac{d\nu_j}{dt} \quad (1)$$

electric field; frictional force; relaxation force; electrophoretic force; diffusion gradient; pressure gradient; reaction

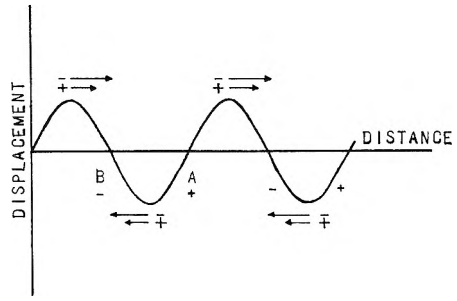

Figure 1. Mechanism for ionic vibration potentials.

where e_j is the charge of jth ion, ρ_j the fractional coefficient, v_j the velocity, m_j the mass, v_j the volume, n_j the number of ions of the jth type per unit volume, k the Boltzmann constant, D the dielectric constant, T the absolute temperature, v_0 the velocity of the solvent, s_0 the solvent density, η_0 the solvent viscosity, X the electric field intensity, x the distance in the direction of propagation of the sound wave, and t the time. The third and fourth terms in eq 1 include the usual parameters of the ionic atmosphere: θ is the relaxation time, $1/\kappa$ is the effective thickness of the ionic atmosphere, and q is defined by the equation

$$q = \left(\frac{e_1}{\rho_1} - \frac{e_2}{\rho_2}\right)\left[(e_1 - e_2)\left(\frac{1}{\rho_1} + \frac{1}{\rho_2}\right)\right]^{-1} \quad (1a)$$

for a solution consisting of the two types of ions 1 and 2.

In his original treatment,[2a] Debye included only the first and second terms on the left-hand side of eq 1. Later workers added the relaxational and electrophoretic forces[3] associated with the ionic atmosphere, the diffusion corrections,[4] and the forces associated with the pressure gradient[4] in the sound field. The last correction pointed out by Hermans[4] is the most important.

The final equation[2b] obtained for the alternating potentials (Φ) at any one point in the solution is

$$\Phi = \Phi_0 \exp[i(\omega\tau - \sigma x - \Delta)] \quad (2)$$

where

$$\Phi_0 = ca_0\left[\frac{\Sigma \bar{n}_j e_j (w_j - d)/\rho_j}{\Sigma \bar{n}_j e_j^2/\rho_j}\right]\left[\frac{(4\pi L_\infty)^2}{(4\pi L_\omega)^2 + (\omega D_\omega)^2}\right]^{1/2} \quad (2a)$$

$$\Delta = \arctan \frac{\omega D_\omega}{4\pi L_\omega} \quad (2b)$$

$$w_j = m_j - v_j s_0 \quad (2c)$$

and

$$d = kT/c^2 \quad (2d)$$

σ is the propagation constant ($2\pi/\Lambda$), a_0 the velocity amplitude, c the velocity of sound, D_ω and L_ω the dielectric constant and the specific conductance of the solution at the angular frequency ω, L_∞ the specific conductance in the absence of ionic interactions, $\bar{n}_j$ the time-average number of ions of the jth type per unit volume, w_j the mass of the solvated ion of the jth type less the mass of free displaced solvent, and the other symbols have their usual meaning.

For a moderately dilute solution of $C_m^{z+}A_n^{z-}$ electrolyte, eq 2a–d reduce to the approximate form

$$\Phi_0 = \frac{ca_0}{f}\left[\frac{(W_+/\rho_+) - (W_-/\rho_-)}{(z_+/\rho_+) + (z_-/\rho_-)}\right] = 1.55 \times 10^{-7} a_0\left[\frac{t_+}{z_+}W_+ - \frac{t_-}{z_-}W_-\right] \quad (3)$$

where W_+ and W_- are the apparent molar masses of the solvated cations and anions, z_+ and z_- are the number of charges, t_+ and t_- are the transport numbers at infinite dilution, and ρ_+ and ρ_- are the fractional coefficients. Equation 3 is applicable only if the diffusion term is neglected, $\lambda_\infty = \lambda_\omega$, and the term $4\pi L_\omega/(\omega D_\omega)$ is large compared to unity, as appears to be true when the ratio of ionic strength to angular frequency is greater than 10^{-11}. The quantities W_+ and W_- in eq 3 are defined by

$$W_+ = Aw_+ = (M_+)_h - (V_+)_h s_0 \quad (4a)$$

and

$$W_- = Aw_- = (M_-)_h - (V_-)_h s_0 \quad (4b)$$

where $(M_+)_h$ and $(M_-)_h$ are the molecular weights of the solvated cations and anions, $(V_+)_h$, and $(V_-)_h$ are the corresponding molar volumes, and A is Avogadro's number. The terms W_+ and W_- include contributions from only those surrounding solvent molecules which are appreciably compressed due to electrostriction effects of the ions. Solvent molecules which are bound to an ion without appreciable electrostriction will contribute equally to the two terms in eq 4a and b, and their contributions will cancel out. Consequently the definition of what constitutes the extent of the solvated ion is not critical in the present consideration, provided all significantly electrostricted solvent molecules are included.

Only relative values for either W_+ or W_- can be ob-

(1)(a) Research supported by the U. S. Office of Naval Research. (b) On leave from CRM-CRNS, Strasbourg, France.

(2) (a) P. Debye, *J. Chem. Phys.*, **1**, 13 (1933); (b) J. Bugosh, E. Yeager, and F. Hovorka, *ibid.*, **15**, 592 (1947).

(3) S. Oka, *Proc. Phys.-Math. Soc. Japan*, **15**, 413 (1933).

(4) J. Hermans, *Phil. Mag.*, [7] **25**, 426 (1938); [7] **26**, 674 (1938).

tained from measurements of ionic vibration potentials alone. Any attempt to determine absolute values for W_+ and W_- from measurements in several electrolytes with common cations and/or anions is unsuccessful because the various equations of the form of eq 3 for the series of electrolytes are linearly dependent and cannot be solved for unique solutions.

The apparent masses of the solvated ions can be related to the ionic partial molal volumes. In eq 4a and b, the mass of the jth solvated ions is given by the equation

$$(M_j)_h = M_j + (M_j)_w \quad (5)$$

where M_j is the intrinsic molar mass of the ion and $(M_j)_w$ is the mass of bound water per mole of ion. The precise definition of what constitutes bound water is unnecessary since $(M_j)_w$ will cancel out of the calculations. In dilute solutions, the ionic partial molal volume, $\bar{V}_j$, is

$$\bar{V}_j = (V_j)_h - (M_j)_w/s_0 \quad (6)$$

where $(V_j)_h$ is the molar volume of the solvated jth ion. The term $(M_j)_w/s_0$ corresponds to the volume which the bound water would have occupied if it were free. From eq 4–6, the apparent mass of the jth ion is

$$W_j = M_j - \bar{V}_j s_0 \quad (7)$$

While the values for $\bar{V}_+$ and $\bar{V}_-$ are unknown, the sum $m_+\bar{V}_+ + n_-\bar{V}_-$ corresponds to the over-all partial molal volume, $\bar{V}_2$, of the electrolyte and can be obtained from density data. From a knowledge of $\bar{V}_2$ and ionic vibration potentials, with eq 3 and 7 it is possible to determine the individual values for $\bar{V}_+$ and $\bar{V}_-$ as well as W_+ and W_- without the usual assumption concerning the partial molal volume of some reference ion or the ratio of the values for some electrolyte.

A theoretical treatment of ionic vibration potentials which takes into account fast physical and chemical processes occurring within the solution has not yet been developed. Of possible interest is the situation where the mean times for exchange of solvent molecules between the hydration sheaths of the ions and the bulk of the solvent are comparable to the period of the sound waves. One might expect the frequency dependence of the vibration potentials to deviate substantially from that predicted by eq 2a under such circumstances and furthermore that the frequency dependence might be used to study the kinetics of such exchange processes. Unfortunately preliminary considerations indicate that ionic vibration potentials cannot be used for this purpose. The reasoning is as follows: when a water molecule associated with an ion exchanges with a bulk water molecule, the velocity of the ion momentarily increases or decreases, depending on its velocity relative to the solvent, because of the need for the newly bound water molecule to acquire the same velocity as the ion. The time required for steady-state velocity to be reached relative to the bulk solvent, however, is only 10^{-12} to 10^{-13} sec, depending on the mass and drag coefficient of the ion. For a significant deviation in the frequency dependence of the ionic vibration potentials to be observed, the exchange rates for either the cations or anions or both would need to be sufficient for the velocity of the ions relative to the solvent to be perturbed substantially (10^{11} to 10^{12} exchanges/sec) and, in addition, the frequency of the sound waves would need to approach within one order of magnitude of the exchange rates (10^{10} to 10^{11} cycles). While the exchange rates for water molecules associated with simple univalent ions such as Na^+, K^+, Cl^-, and Br^- are probably sufficient to affect substantially the velocity of these ions, measurements of ionic vibration potentials at sufficiently high frequencies are quite impossible.

III. Previous Experimental Work

Experimental evidence for the existence of ionic vibration potentials was first reported[5] in 1949, some 16 years after Debye's original prediction. This delay reflects in part difficulties associated with the measurement of an acoustically produced electrical signal of the order of 10^{-6} v when many watts of electrical energy of the same frequency are used in close proximity for the generation of sound waves. The detection of the effect in 1949 was accomplished at 265 kc with a standing wave technique which permitted the acoustically produced effect to be distinguished from the false electromagnetically induced signals in terms of the spatial dependence of the observed signals on the node–antinode structure of the standing wave field. Only relative values for the amplitude of the observed effect were determined, however, because of complications associated with accurate velocity–amplitude measurement in the complex standing wave field. An estimate of 3 μv per unit velocity amplitude (1 cm/sec) was made for the amplitude of the effect in a 0.005 N KCl solution on the basis of acoustical intensities as evaluated from radiation-pressure measurements. The effect was found to depend on the type of electrolyte but to be substantially independent of electrolyte concentration in the range 5×10^{-4} to 5×10^{-3} N for uni-univalent electrolytes. In 1951, Dèrouet and Denizot[6] reported that they had detected the effect in 0.005 N

(5) E. Yeager, J. Bugosh, F. Hovorka, and J. McCarthy, *J. Chem. Phys.*, **17**, 411 (1949).

(6) B. Dèrouet and F. Denizot, *Compt. Rend.*, **233**, 368 (1951).

KCl at 80 kc, also with a standing wave technique. These workers found a value of 10^{-5} v per unit velocity amplitude.

In 1953, ionic vibration potentials were measured[7] at Western Reserve with pulse-modulated ultrasonic waves which permitted differentiation between the acoustically produced effect and false electromagnetically induced effects on the basis of the difference in the time of propagation of the acoustical waves and the electromagnetic waves. In addition, more reliable measurements of velocity amplitude were possible with pulse-modulated sound waves, since reflected waves and waves scattered from the walls of the confining vessel could be distinguished from the directly received waves. In further studies with pulse-modulated ultrasonic waves in 1959,[8] an effect of 3 μv per unit velocity amplitude was found in 0.01 N KCl at both 200 and 840 kc. This value corresponds to a difference of approximately 40 apparent mass units between the cations and anions.

In 1958, Hunter[9] called attention to the existence of acoustically produced alternating potentials observed with glass-mounted platinum probes in conductivity water. With pulse-modulated waves at a frequency of 465 kc, Hunter found an effect for pure water of approximately 50 μv per unit velocity amplitude, a value an order of magnitude greater than that for alkali halide solutions such as 0.01 N KCl. Even more alarming were the results of Rutgers and Rigole[10] who, using standing waves at 1 Mc, observed an apparent effect not only in distilled water, but also in pure organic liquids such as methanol, ethanol, 2-propanol, nitrobenzene, and even n-heptane. While a satisfactory explanation for these potentials in nonionic solutions was not advanced by either Hunter or Rutgers and Rigole, both suggested that such effects might cause serious complications in the quantitative interpretation of ultrasonic vibration potentials in electrolyte solutions. Weinmann[11] has considered, as a possible explanation for the effects observed by Hunter[9] and also Rutgers and Rigole[10] in pure liquids, the interaction of the sound waves with solvent dipoles, but Weinmann's treatment does not establish the absolute magnitude of such an effect.

Millner[12] has measured ionic vibration potentials with pulse-modulated ultrasonic waves at 200 kc in various alkali halide solutions. Millner also reported a residual effect in distilled water, but with a single probe consisting of platinum sealed in glass capillary tubing, the residual effect in distilled water was only approximately 2 μv per unit velocity amplitude. At concentrations of the alkali halides above 10^{-3} N, Millner's data show very little variation with concentration in accord with the theory of ionic vibration potentials.

Work in the authors' laboratory[13] has demonstrated that one possible source for the effect observed in distilled water and nonionic liquids is the glass tubing in which the platinum probes are sealed. Measurements have been carried out with probe assemblies in which only the platinum probes entered the liquid under examination. Under these conditions, ac signals were observed only in ionic solutions. When glass-mounted platinum probes were slowly lowered into a pure liquid with ultrasonic waves at a frequency of 200 kc, no effect was observed ($<10^{-6}$ v per unit velocity amplitude), even with high-input impedance amplifiers, until the glass mounting contacted the liquid, at which instant a large signal abruptly appeared. Millner[14] has confirmed this finding. Thus the experimental evidence indicates that any effect associated with the interaction of the sound waves with solvent dipoles in pure liquids is well below 10^{-6} v per unit velocity amplitude.

The abnormal acoustical response associated with the glass probe mounting may be caused by pseudo-piezoelectric properties of the strained glass, some type of streaming potential, or a condenser microphone effect in which the capacity between the platinum wire and the glass–liquid interface is modulated by the sound waves. In any event, the ac response associated with the mounting for the probe wires should be characterized by a high internal impedence. At reasonable ionic concentrations (*e.g.*, greater than 0.001 N) in aqueous solutions, the internal impedance associated with the ionic vibration potentials is quite low. As a result, the observed response in ionic solutions should be predominantly the ionic vibration potentials and not any false microphonic effects associated with the probe mounting. If solutions of ionic strength much less than 10^{-3} are used, however, serious complications may arise unless precautions are taken to prevent such false effects (see part V).

(7) E. Yeager, H. Dietrick, and F. Hovorka, *J. Acoust. Soc. Am.*, **25**, 456 (1953).

(8) E. Yeager, J. Booker, and F. Hovorka in "The Structure of Electrolytic Solutions," W. Hamer, Ed., John Wiley and Sons, Inc., New York, N. Y., 1959, pp 86–96.

(9) A. Hunter, *Proc. Phys. Soc.* (London), **71**, 847 (1958); A. Hunter and T. Jones, *ibid.*, **79**, 795 (1962).

(10) A. Rutgers and R. Rigole, *Trans. Faraday Soc.*, **54**, 139 (1958).

(11) A. Weinmann, *Proc. Phys. Soc.* (London), **73**, 345 (1959); **75**, 102 (1960).

(12) R. Millner, *Z. Elektrochem.*, **65**, 639 (1961).

(13) E. Yeager, J. Booker, and F. Hovorka, *Proc. Phys. Soc.* (London), **73**, 690 (1959).

(14) R. Millner, private communication, 1965; R. Millner and H. D. Muller, *Ann. Physik*, **17**, 160 (1966).

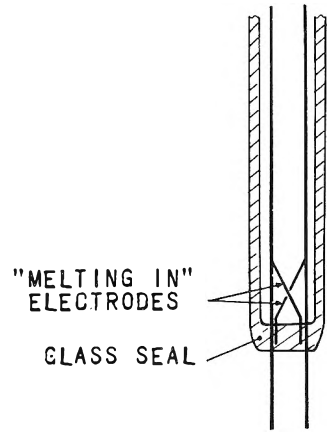

Figure 2. Millner's[14] double-probe assembly.

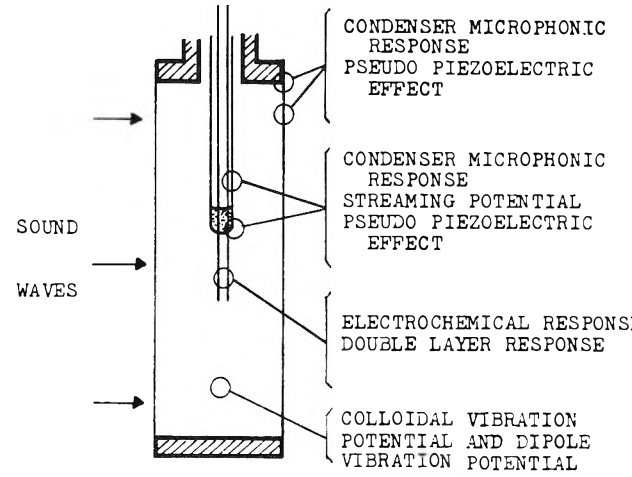

Figure 3. Possible mechanism for false effects.

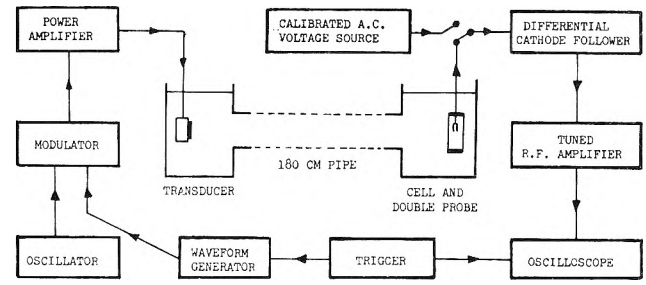

Figure 4. Block diagram of the apparatus.

Millner[14] has constructed a probe assembly designed to cancel out microphonic effects. This assembly consists of four platinum wires sealed in glass with two wires extending into the solution and two buried within the glass (Figure 2). This assembly has been used by Millner[14] to study a number of electrolytes.

Other possible sources of false acoustically produced effects must also be considered before the potentials observed in electrolytic solutions at concentrations even above 10^{-3} N can be attributed entirely to ionic vibration potentials. These include (1) alternating potentials originating at the surface of the probe electrodes because of the interaction of the sound waves with the ionic double layer and/or electrochemical processes at the probe surfaces, (2) effects originating from the modulation of the size of micro gas bubbles possibly present on the surface of the probes, (3) effects associated with residual colloidal particles in the liquid, (4) microphonic effects associated with the walls of the vessel in which the liquid is confined, and (5) an intrinsic effect associated with interaction of the sound waves with the solvent dipoles. An attempt has been made to classify the possible false effects in Figure 3 according to the site of the effect. The results of the investigations concerning those possible false effects are given in part V of this paper.

IV. Equipment and Procedures

A block diagram of the apparatus used in the present work is shown in Figure 4. Pulse-modulated ultrasonic waves at frequencies of 220 and 500 kc with a pulse length of 1.2 msec and a repetition period of 25 msec were produced by barium titanate plates of 7.5-cm diameter and transmitted between two large tanks (70 × 60 × 60 cm) through a 180-cm long pipe with an internal diameter of 20 cm. This system was filled with distilled water maintained at 22 ± 0.5° and provided a delay time of approximately 2 msec, permitting the use of the relatively long pulse lengths necessary to achieve essentially steady-state response in the tuned radiofrequency amplifier of the detection system. The ultrasonic waves entered the acoustical cell (Figure 5) containing the electrolyte and impinged on a double-probe assembly used to detect the ionic vibration potentials. The ac signals were fed into a differential cathode follower, amplified by a tuned radiofrequency amplifier, and then displayed on the oscilloscope. The comparison of the acoustically produced signals with a signal of the same frequency from a calibrated ac voltage source (General Radio signal generator, Model 805C) permitted the measurement of the observed effects with an accuracy of ±5% (±1 μv).

The acoustical cell (Figure 5) containing the electrolyte consisted of a plastic tube with an internal diameter of 15 cm, a length of 4 cm, and a wall thickness of 0.5 cm. The sound waves were transmitted into and out of this cell through Mylar film windows stretched over the ends of the cylinder. Immediately behind the cell were placed several 1-cm sheets of a butyl rubber (supplied by the B. G. Goodrich Co.) which has

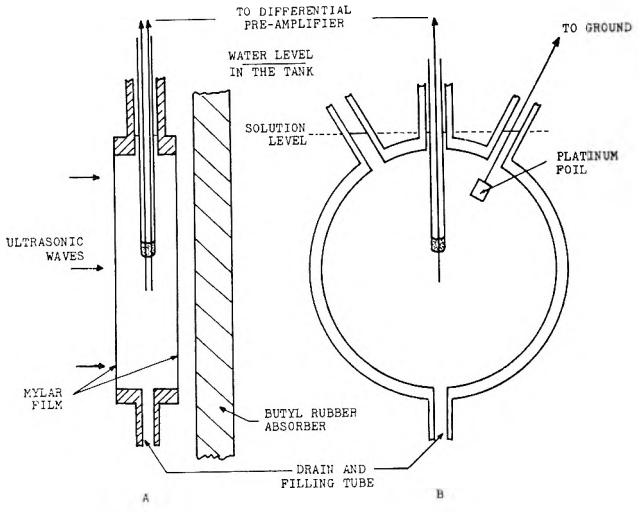

Figure 5. Cell arrangement for the measurement of ionic vibration potentials. A, side view perpendicular to ultrasonic beam; B, front view parallel to ultrasonic beam.

substantially the same acoustical impedance of water and which served as an absorber for the sound waves transmitted through the cell. All measurements were made at 22 ± 0.5°.

A double-probe assembly was used in the present work rather than a single probe as in some of the earlier studies for the following reasons: (a) the observed signal is twice as great with the double probe and noise problems are reduced; (b) electromagnetically induced signals are reduced to a very low level through cancellation, and hence there is no tendency for the amplifier to be overloaded by a large electromagnetically induced signal; and (c) the orientation sensitivity of the double probe provides a way to check that the observed effects are produced within the solution and not on or at the walls of the acoustic cell as a result of some microphonic effect (see part V-A).

The probe assembly used for the majority of the measurements is represented in Figure 6. It consisted of two platinum wires, each 0.025 cm in diameter and 2 cm in length, sealed in a glass tubing. The purity of the platinum was at least 99.9%, but purity is not believed to be critical in the present experiments. The measurements were carried out with both blunt ends and semispherical ends; no differences were observed.

Unless otherwise indicated, the measurements were made with the inner shields surrounding the leads from the probes in the glass tubing (Figure 6) driven by connecting them to the two cathodes of the input differential cathode follower. This arrangement reduced substantially the ground capacitance of the probe assembly and thus increased the input impedance of the

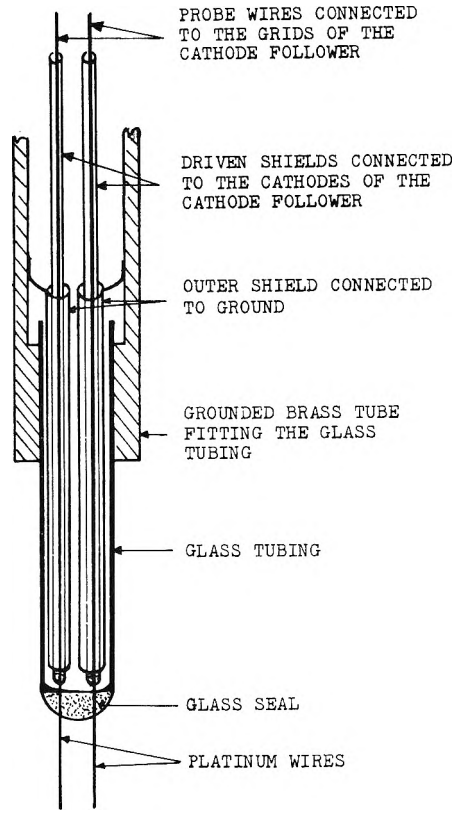

Figure 6. Exploded view of a double-probe assembly.

detection system. At 220 kc, measurements showed the input impedance of the assembly differential cathode follower–double probe to be equivalent to a 1.5-megohm resistance (minimum value) shunted by a 10-pf capacitor.

The two platinum wires of the probe assembly were positioned parallel to each other at a distance of approximately 0.5 cm (unless otherwise stated); which is slightly greater than the half-wavelength ($\lambda/2$ = 0.34 cm) at 220 kc. In the measurements at both 220 and 500 kc, the probe assembly was rotated about the vertical axis until a maximum ac potential was observed, corresponding to the adjustment of the probes to a phase distance of a half-wavelength.

The two electrodes of the double probe were placed in the approximate center of the cell. A mechanical positioning device was used to move the cell and the probe assembly together in a plane perpendicular to the direction of propagation until the observed effect was a maximum for a concentrated electrolytic solution, *e.g.*, 0.03 *N* RbCl. This permitted the electrodes to be placed at a position corresponding to a maximum of velocity amplitude in the acoustic field.

The velocity amplitudes were determined through radiation-pressure measurements with a radiation gauge

similar to that of Herrey[15] employing a highly absorbing rubber disk of 50-cm² area (approximately 8-cm diameter) perpendicular to the direction of propagation of sound waves. In these measurements the nonhomogeneity of the acoustic field in the cell over the area subtended by the radiation disk was taken into account. The profile of the pressure amplitude over the dimensions of the disk was determined with an uncalibrated hydrophone consisting of a 2-mm diameter barium titanate cylinder.[7] The response of the hydrophone along two diameters of the cell, one vertical and the other horizontal and both perpendicular to the direction of propagation of the sound waves, is shown in Figure 7. Those curves have been obtained by placing the hydrophone in the cell after removing the probe electrodes. The maximum corresponds to the position occupied by the center of the probe electrode. A calibration factor was then derived relating the response of the hydrophone to the integrated radiation pressure over the area subtended by the disk. The maximum response to the hydrophone within the cell was then used with the calibration factor to calculate the velocity amplitude over the central section, 2.5-cm diameter of the disk. The response of the hydrophone was found to vary by only 10% over this central section of the disk. Since the probe wires used to obtain the final data were only 1.5–2 cm long and positioned centrally, the velocity amplitude was practically uniform between and over the length of the dual probes. The estimated accuracy of the radiation-pressure measurements was 10%.

The sound level was sufficient to produce velocity amplitudes of at least 6 cm/sec within the acoustical cell containing the liquid under study. As the noise level was about 2 μv, with the double-probe assembly the sensitivity of the measuring apparatus expressed in terms of Φ/a_0 was about 0.15 μv cm^{-1}/sec.

The electrolytes were all of reagent grade purity. The water used for the preparation of the solutions was singly distilled water. No difference was observed with two solutions of a given electrolyte at a given concentration prepared with singly and triply distilled water.

V. Experimental Studies of False Effects and Electrical Loading

In view of the questions raised by other authors[9,10] as to possible interference from false effects, this aspect of the research will be presented in some detail.

A. Response Associated with the Cell Structure. Conclusive evidence that the signal observed with the double-probe assembly is not associated to any appreciable extent with some type of response of the overall cell structure (*e.g.*, capacitance modulation or pseudo-piezoelectric effects arising at the walls or Mylar windows) to the acoustical waves is provided by the following observations: (1) the observed signal disappears completely when an absorbing material is placed in the ultrasonic beam just in front of the platinum probes, leaving the cell walls exposed to the sound field; (2) the introduction of a grounded lead into the solution within the cell produces no detectable change in the observed signals; and (3) the observed response shows the expected dependence on polar orientation of the double-probe assembly (see Figure 8) with no observed signal when the two wires are positioned in a plane parallel to the wave front.

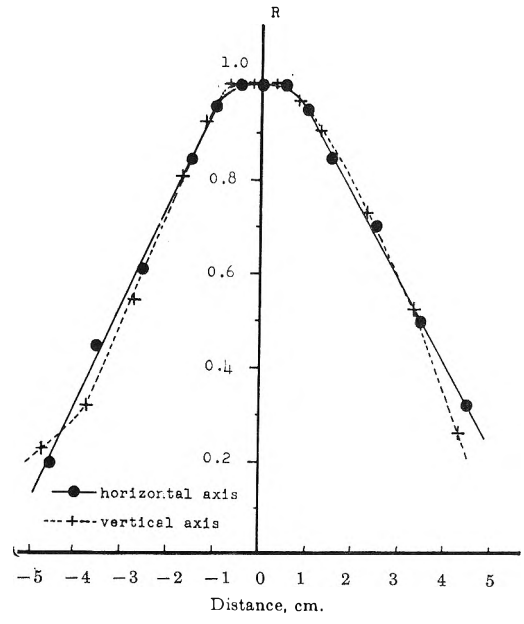

Figure 7. Relative response, R, of the hydrophone placed within the cell along the horizontal axis, —●—, and the vertical axis, – – + – –.

The curves in Figure 8 represent the polar responses of two double-probe assemblies in a 0.03 N RbCl solution at 220 kc as functions of the angle between the wave front and the plane defined by the two probe electrodes. The two probe assemblies used in obtaining the data shown in this figure differed in interelectrode distance, with one 0.35 cm (close to $\lambda/2$ = 0.34 cm at 220 kc) and the other 0.45 cm. The response of the first assembly exhibited two maxima corresponding to the plane defined by the two electrodes perpendicular to the wave front. The response of the second assembly involved four maxima, each of which corresponded to the projection of the interelectrode distance in the direction of propagation of the sound waves equal to

(15) E. Herrey, *J. Acoust. Soc. Am.*, **27**, 891 (1955).

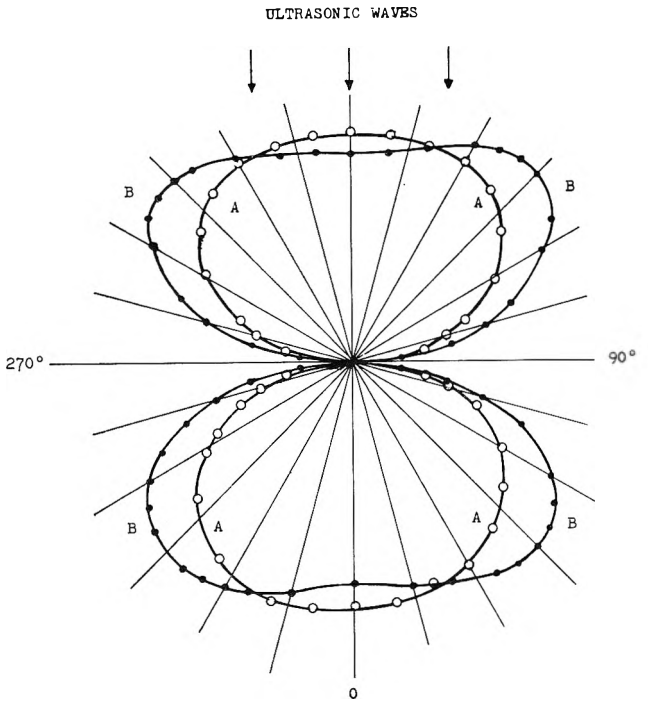

Figure 8. Polar responses of two different double-probe assemblies at 220 kc. Curve A, interelectrode distance 3.4 mm; curve B, interelectrode distance 4.5 mm.

$\lambda/2$. For both assemblies there was no response when the plane of the two probe electrodes was coincident with the acoustic wave front since the signals from each were equal and in phase and hence canceled out in the differential cathode follower input stage. The graphs in Figure 8 provide rather strong evidence that the acoustically produced ac signals originated in the solution between the probe wires or at the surfaces of the probe wires.

In earlier work with a glass acoustical cell,[7] the ac signals observed with a single-probe electrode relative to ground were just one-half of those found between the two electrodes of the double-probe assembly at an orientation corresponding to a phase difference of 180° between the two electrodes. This has been shown in the present work to be true only in relatively concentrated electrolytic solutions ($>10^{-2}$ N). In more dilute solutions the single-probe response was usually greater than one-half of that found with the double-probe assembly. Furthermore, a substantial residual effect was observed with the single probe when an acoustically opaque material was placed in the ultrasonic field just in front of the single probe but not blocking the cylindrical walls of the cell. In addition, the introduction of a grounded platinum wire or foil into the cell (see Figure 5) produced a significant change in the observed effect with the single probe, even with the grounded conductor located in a remote position relative to the detection probe. These difficulties with the single-probe assembly in dilute solutions can be explained on the basis of ac potential differences produced by the sound waves between the inside and outside surfaces of the cell walls and Mylar windows.

B. The Junction Effect. No detectable effect (<0.15 μv cm^{-1} sec) was observed at 220 kc with the double-probe assembly with or without the driven shield in singly or triply distilled water or in polar organic liquids such as methanol or acetone, provided the liquid was in contact with only the platinum electrodes. If the liquid level was raised relative to the probe assembly so as to place the liquid in contact with the glass seal, an observed effect of 10–20 μv cm^{-1} sec abruptly appeared. This phenomenon has also been observed at 1000 kc in earlier work[13] with a single-probe assembly and a similar observation has been reported by Millner.[14] With the double-probe assembly in 2×10^{-5} N KCl, the ac signal increase from less than 0.3 to 15 μv cm^{-1} sec as the liquid contacted the junction. The same experiment in 0.2 N KCl, however, yielded an increase from only 1.6 to 1.7 μv cm^{-1} sec. The change in the more concentrated electrolyte is much smaller than in the very dilute solution or distilled water because the effective internal ac impedance associated with the junction effect is very high and loaded out internally when the ac impedance of the solution is low.

The nature of the junction effect has not yet been established. Possible mechanisms include streaming potentials, a pseudo-piezoelectric effect, and the modulation of the capacity between the wire as it enters within the mounting and the solution surrounding the mounting.

Two procedures are possible for minimizing or eliminating the junction effect in dilute solutions: (1) the use of additional metal leads completely buried in the glass or plastic seal, as employed by Millner[14] (see Figure 2), and (2) the positioning of the junction outside of the sound field by either having the junction completely out of contact with the liquid (see Figure 9b) or having such long probe wires that the junction can be located at a position where the sound pressure is virtually zero. The first procedure suffers from uncertainty as to whether the buried metal probes fully cancel out the junction effect, particularly over a range of frequencies, orientations, and electrolyte concentrations. Since the junction effect can be large, partial cancellation can still lead to substantial errors. Even with his presumedly best probe assembly, Millner[14] still observed a residual effect of 1.6 μv cm^{-1} sec in pure water, not taking into account the large

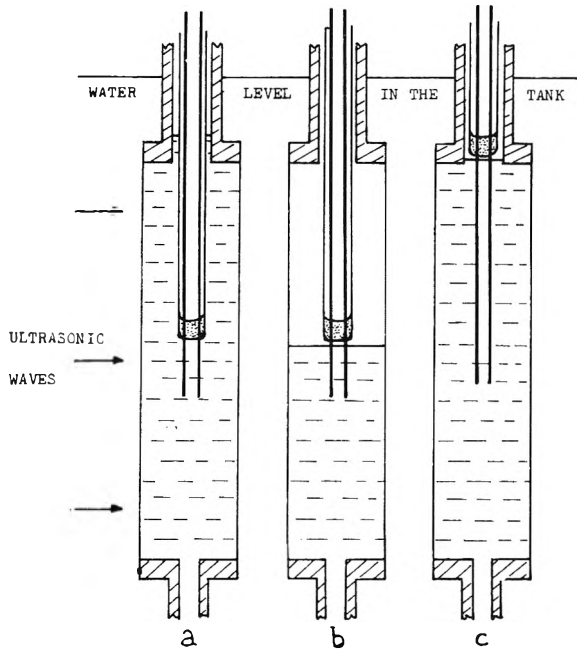

Figure 9. Cell arrangements used in the present work: a, standard arrangement leading to large "junction effects" for dilute electrolyte solutions; b, arrangement with the cell half-filled; c, arrangement with long-wire, double-probe assembly and cell completely filled.

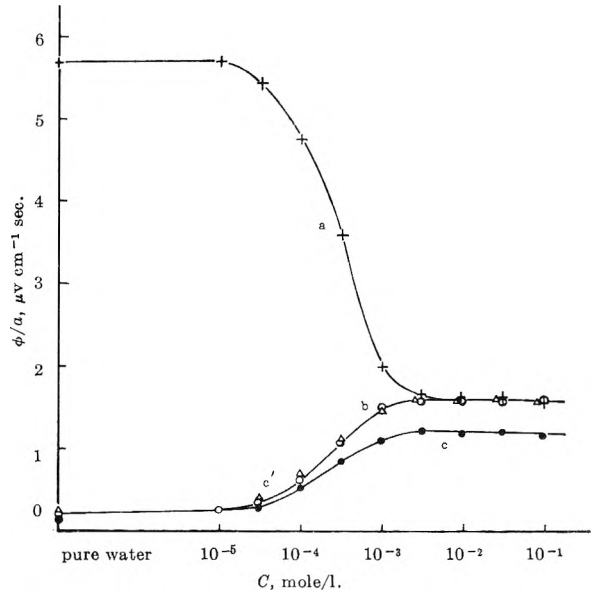

Figure 10. Terminal responses in KCl solutions at 220 kc with cell arrangements shown in Figure 9. Curves a, b, and c correspond to cell arrangements a, b, and c, respectively. Curve c′ was obtained from curve c by multiplying the ordinates by the factor 1.35.

loading effect. Such large residual response implies that a serious error may occur with Millner's probe assembly in dilute solutions. Consequently, we have chosen the second procedure with the junction located just above the liquid surface (Figure 9b).

The cell arrangement in Figure 9b eliminates scattering of the sound off the probe mounting, but the free liquid surface (a pressure-release surface) might seriously perturb the sound field along the submerged length of the probes. To gain further insight, the responses associated with the three cell arrangements shown in Figure 9a, b, and c have been examined at various electrolyte concentrations. The probe assemblies used in arrangements a and b were identical, and the length of each probe wire was 1.5 cm. The probe assembly in arrangement c differed in that each probe wire was 7.5 cm long. In both arrangements b and c the glass seal was located approximately 1 mm above the surface of the liquid. In arrangements a and b, the sound pressure was a maximum on the axis of the cell. In work with arrangement c, the entire cell assembly was positioned such that the sound pressure was a maximum somewhere near the center of the probe wires. The observed response with arrangement c was relatively insensitive to vertical position.

The terminal responses for these three arrangements are shown in Figure 10. Both arrangements a and b gave virtually the same results in more concentrated solution ($>3 \times 10^{-2}$ N). This provides evidence that the close proximity of the free surface does not perturb significantly the sound field along the immersed portion of the probe wire. The large observed response with arrangement a in dilute solutions and distilled water corresponds to the junction effect. The signal with arrangements b and c in very dilute solutions and pure water is almost the same as the noise level. The response plotted for arrangement c in Figure 10 is based on the maximum value of the velocity amplitude at the center of the long probe wires. To obtain a true response for this arrangement, account must be taken of the variation of the velocity amplitude along the length of the probe wires. The correction factor has been obtained by finding the ratio of maximum-to-average velocity amplitude along the length of the wires using the relative hydrophone response shown in Figure 7. The correction factor calculated in this manner is 1.35 and has been used to obtain curve c′ in Figure 7 from curve c. For a number of electrolytes at concentrations greater than 10^{-4} N, the ratio of the response for arrangements c and b has been found to be within a few per cent of this value.

For all of the subsequently reported measurements in this paper, the probe arrangement shown in Figure 9b has been used. For future work at higher frequencies, it will be necessary to use much thinner

wires and to meet much more rigid requirements with respect to parallelism. This can be realized only by anchoring the wires in some type of frame under tension. Furthermore, the junctions of the wires with the frame must be shielded acoustically in order that the sound pressure at the junctions is essentially zero. Studies involving such more sophisticated probe assemblies are in progress.

C. False Effects Arising in the Liquid Phase. The measurements in pure liquids cited in part V-B as well as earlier publications[13,14] have failed to indicate any intrinsic effect associated with nonionic species and provide evidence that earlier reports of the existence of such effects by other workers[9,10] are the result of the junction effect and possibly other artifacts. Hunter,[9] however, has raised the question of whether our failure to observe an intrinsic effect in pure nonionic solvents is associated with a large loading effect as a result of a high ratio of internal to external impedance. This explanation does not appear valid. In the present work with, for example, distilled water, the measured internal impedance between the two probes corresponded to 20 pf shunted by 300 kilohm, while the load impedance of the detection system including the probe assembly (without the driven shield) corresponded to 20 pf shunted by 1.5 megohm. Thus the ratio of the terminated to open-circuit response would be expected to be approximately 1:2, and the present experiment should have been capable of detecting an effect with an open-circuit response of 0.4 μv cm^{-1} sec. On the basis of these observations the authors concluded that measurements in ionic solutions of substantial concentration ($>10^{-3}$ N) have not been perturbed by any appreciable intrinsic effect associated with the solvent, *e.g.*, dipole vibration potentials.[9-11] The lack of a detectable effect in pure liquids also provides evidence that residual colloidal particles are insufficient, at least in pure liquids, to provide any appreciable response.

D. Electrochemical Response of the Probe Surfaces. Theoretical considerations[16] indicate that temperature and pressure variations in a sound field can give rise to an alternating component in the potential of an electrode whose potential is determined by one or more temperature and/or pressure-sensitive faradaic processes, *e.g.*, $H^+ + e^- \rightleftharpoons H_{(adsorbed)}$. The effect should decrease rapidly with increasing frequency, however, because of the internal loading effect associated with the large nonfaradaic capacitive component associated with the electrode interface. At a frequency as high as that involved in the present work (220 kc), very few faradaic processes could be sufficiently reversible to exhibit detectable ac response.

A means for experimentally demonstrating that such electrochemical response does not interfere appreciably with ionic vibration potential measurements is to compare the observed signals with probes consisting of different metals. The nature and reversibility of any possible potential-determining faradaic process should be strongly dependent on the particular metal as well as its prior treatment. In Table I are reported the results for dual probes consisting of platinum and gold wires sealed in glass and tantalum and nickel wires sealed in Kel-F with neither mounting material in contact with the solution. All four probe assemblies were geometrically identical. The small deviations evident in this table are within experimental error, particularly considering the difficulty of aligning the two wire electrodes exactly parallel to each other. Consequently, electrochemical response is not a significant factor in the present study.

Table I: Observed Values[a] of Φ/a (μv cm^{-1} sec) at 220 Kc and 22°

Electrolyte	Tantalum in Kel-F	Nickel in Kel-F	Platinum in glass	Gold in glass
3×10^{-2} N CsCl	8.6	8.0	8.6	8.2
3×10^{-2} N RbCl	5.0	5.1	5.3	4.8
3×10^{-2} N $BaCl_2$	4.7	4.1	5.0	4.4

[a] Double-probe assembly with cell arrangement shown in Figure 9b.

E. Modulation of the Double-Layer Capacity. Acoustically produced periodic variations in the dielectric constant and thickness of the ionic double layer can lead to periodic variations in both the Helmholtz and diffuse-layer components of the double-layer capacity. Such variations in turn can result in alternating components[16] in the electrode potential with the amplitude dependent on the potential drop across the double layer and, hence, the electrical potential relative to the point of zero charge. The dc potential of the electrode can be controlled by biasing the electrode with an external dc voltage source of such high impedance that the alternating component is not appreciably loaded. The biasing of the two platinum probes in a 0.01 N KCl solution from -0.5 to $+0.7$ v (reference electrode Ag|AgCl(s)), 0.01 N KCl resulted in a change in the observed response from 1.7 to 1.6 μv cm^{-1} sec, or an almost negligible change of -0.1 μv cm^{-1} sec. Within this range of dc voltages the potential drop across the

(16) E. Yeager and F. Hovorka, *J. Electrochem. Soc.*, 98, 14 (1951).

double layer should have gone to zero and changed sign.[17] These results indicate that any error associated with the modulation of the double-layer capacity is probably not more than ± 0.1 μv cm^{-1} sec, which is about the precision of the experiments from run to run.

F. Loading Effects of the Measurement Circuit. In dilute solutions, the effective internal impedance associated with the vibration potentials becomes comparable with the input impedance of the measurement system and corrections for loading effects are necessary in quantitative studies. The internal impedance associated with the vibration potentials has been determined by placing various additional resistive loads across the probes and then solving the simultaneous equations for the real and imaginary components of the internal impedance. This approach assumes that the concept of lumped internal impedance is valid for the vibration potentials as measured with the double-probe assembly. These studies indicate that loading effects are negligible at concentrations greater than 10^{-3} N. For example, a 3×10^{-3} N RbCl solution was found to have an internal impedance equivalent to 3.5 kilohms shunted by 200 pf at 200 kc. This is to be compared with an impedance of 1.5 megohm shunted by 10 pf to ground for either side of the input circuit of the measurement system including the probe mounting with the driven shield.[18] Under these circumstances the terminated response is just a few per cent lower than the open-circuit response. With the exception of the data represented in Figure 10, all of the values for ionic vibration potential herein reported are for concentrations of 10^{-3} N or higher and hence, corrections for loading effects have been considered unimportant.

The rapid decrease of the response with decreasing concentration of KCl below 10^{-3} N, shown by curves b and c in Figure 10, is not believed to be caused principally by either loading effects or a decrease in the second term on the right side of eq 2a, but rather by the presence of carbonic acid in the solutions. The ionic vibration potential for this electrolyte would be expected to be very small on the basis of the ionic partial molal volumes reported later in this paper (part VI-A). As a component in a mixture, it would be expected to depress the observed effect (see part VI-B).

VI. Experimental Results

A. Ionic Vibration Potentials in Single Electrolytes. Table II contains the values measured at 220 kc and 22° for the ionic vibration potentials expressed as Φ/a in μv cm^{-1} sec for a series of 1–1, 2–1, 1–2, and 2–2 electrolytes at various concentrations in the range 10^{-3} to 1 N. The precision of the measurements listed in Table II has been found to be $\pm 5\%$ (± 0.3 μv cm^{-1} sec), depending on whichever is larger, for a sound level corresponding to a velocity amplitude of 6 cm/sec. A major portion of the 1–1 electrolytes has also been studied at 500 kc and found to yield the same results within the precision of the measurements. In most instances the effect appears to be independent of concentration above 3×10^{-3} N, as is to be expected from eq 3. Some variation of the effect with concentration above this value was found for electrolytes with vibration potentials smaller than 1 μv cm^{-1} sec, *i.e.*, NaOH, KOH, HCl, $CuSO_4$, NaF, and NaCl. For the first four of these electrolytes, these variations are within the over-all precision but were found consistently in each of three independent runs. For NaOH and KOH the changes with concentration are probably associated with the formation of carbonates. The abnormal behavior of NaF and NaCl at low concentrations remains unexplained.

The values for Φ/a in Table III have been obtained from the data in Table II and similar data for other electrolytes at various concentrations by assuming that the most meaningful values for Φ/a are those corresponding to the plateaus in the plots of Φ/a *vs.* concentration. In most instances, the variation of Φ/a with concentration has been found to be of the same order as the precision of the measurements and a mean value weighted somewhat towards higher concentrations has been chosen. The signs indicated for Φ/a in Table III have been assigned in such a way as to render the data self-consistent. For electrolytes with small values of Φ/a, possible confusion concerning sign has been avoided by studying mixtures of the electrolyte in question with a second electrolyte for which no ambiguity exists as to the sign of the effect. This procedure will be more evident to the reader after he has examined the results in part VI-C.

In Table III are also listed values for the ionic partial molal volumes, $\bar{V}_+$ and $\bar{V}_-$, calculated from the transference numbers, t_- and t_-, at low concentrations or infinite dilution as compiled by Parsons[19] and the over-all partial molal volumes of the electrolytes at low concentrations or infinite dilutions as listed in various

(17) *E.g.*, P. Delahay in "Double Layer and Electrode Kinetics," Interscience Publishers, Inc., John Wiley and Sons, Inc., New York, N. Y., 1965, p 133.

(18) The input capacitance of the measurement circuit was this high despite the use of a driven shield principally because the input circuit contained a switch assembly which was not surrounded by a driven shield. In newly designed equipment for future work this shortcoming has been remedied.

(19) R. Parsons, "Handbook of Electrochemical Constants," Butterworth and Co. Ltd., London, 1959, pp 60, 85.

Table II: Dependence of Ionic Vibration Potentials[a] Φ/a (μv cm^{-1} sec) on Electrolyte Concentration at 220 Kc and 22°

Electrolytes	Concentrations, N						
	10^{-3}	3×10^{-3}	10^{-2}	3×10^{-2}	10^{-1}	3×10^{-1}	1
NaF	2.1	1.5	1.0	0.9	0.8	...	...
KF	2.2	2.0	1.9	1.9	1.9	2.0	2.0
RbF	6.6	5.9	5.9	5.9	5.8	...	...
CsF	9.4	9.4	9.4	9.4	9.4	...	...
HCl	0.2	0.3	0.5	0.6	0.6	0.5	...
LiCl	0.3	0.1	0.05	0.1	0.05	0.05	0.05
NaCl	1.15	1.0	0.8	0.7	0.6	0.6	0.5
KCl	1.9	1.8	1.7	1.7	1.7	1.7	...
RbCl	5.2	5.2	5.2	5.2	5.2	5.2	...
CsCl	8.1	8.1	8.1	8.1	8.1	8.1	...
$LiIO_3$	8.7	9.2	9.7	9.7	9.7	9.7	...
$NaIO_3$	7.7	6.8	6.9	6.8	6.7	...	...
KIO_3	4.5	4.4	4.5	4.4	4.2	...	...
HNO_3	0.3	0.1	0.1	0.1	0.1	...	...
KNO_3	0.6	0.7	0.7	0.7	0.7	0.8	...
NaOH	0.2	0.1	0.4	0.5	0.5	0.3	...
KOH	0.2	0.2	0.2	0.2	0.3	0.4	...
$MgCl_2$	1.1	1.1	1.1	1.1	1.1	1.1	1.0
$CaCl_2$	1.2	1.2	1.2	1.2	1.2	1.1	1.0
$SrCl_2$	2.5	2.4	2.4	2.4	2.3	2.1	...
$BaCl_2$	4.0	4.1	4.1	4.0	4.0	3.9	3.5
$Be(NO_3)_2$	0.7	0.7	0.7	0.7	0.8	1.0	...
$Mg(NO_3)_2$	0.2	0.2	0.2	0.2	0.1	0.1	...
$Ca(NO_3)_2$	0.2	0.1	0.1	0.1	0.1	0.1	...
$Sr(NO_3)_2$	1.3	1.3	1.3	1.3	1.2	1.2	...
$Ba(NO_3)_2$	2.6	2.6	2.6	2.6	2.6	2.6	...
Li_2SO_4	2.4	2.4	2.4	2.4	2.4	...	...
Na_2SO_4	1.7	1.7	1.7	1.7	1.7	...	...
K_2SO_4	0.3	0.3	0.3	0.3	0.2	...	...
$ZnSO_4$	0.5	0.4	0.3	0.3	0.3	...	...
$CuSO_4$	0.5	0.4	0.3	0.3	0.2	...	...
$CoSO_4$	0.4	0.4	0.5	0.5	0.4	...	...

[a] Measured with double-probe assembly with cell arrangement in Figure 9b and driven inner shields.

compilations.[19-22] A test for the self-consistency of the results is to compare the values for $\bar{V}_j$ for a given ion obtained by measurements in various salts. From the precision of ± 0.3 μv cm^{-1} sec in the measurements of vibration potentials, deviations from the mean values of ionic partial molal volumes are expected to be not more than approximately ± 2 cm^3/mole for monovalent ions and ± 4 cm^3/mole for divalent ions. This is confirmed by the data compiled in Table III with the exception of salts of Li^+, Al^{3+}, Be^{2+}, Mg^{2+}, Ba^{2+}, and Pb^{2+}. Hydrolysis, incomplete dissociation, and/or ion pairing occur extensively in general with the higher valency electrolytes. Such effects cause difficulties in the calculation of ionic partial molal volumes from vibration potential data and in the determination of true partial molal volumes, $\bar{V}_2$, from density data. For the electrolytes with polyvalent cations the lack of additivity for $\bar{V}_+$ and $\bar{V}_-$ is quite evident from the inconsistency of the differences in $\bar{V}_2$ between various pairs of electrolytes containing a common divalent cation.

The mean values for the ionic partial molal volumes have been calculated from the data in Table IIIa and b. These values for univalent cations and anions plus CO_2^{2-} and SO_4^{2-} are listed in Table IV together

(20) B. Owens and S. Brinkley, *Chem. Rev.*, 29, 461 (1942).

(21) A. Couture and K. Laidler, *Can. J. Chem.*, 34, 1209 (1956).

(22) A. Bodansky and W. Kauzmann, *J. Phys. Chem.*, 66, 179 (1962).

with the root-mean square deviations. The latter have been calculated from the deviations of the values for a given ion in various electrolytes from the mean in instances where measurements have been made in two or more electrolytes containing the ion. In calculating the partial molal volumes of the anions, the ionic vibration potentials for lithium salts have not been used because of the abnormalities described earlier.

In Table III the values for the partial molal volumes of the anions ($\bar{V}_-$) obtained from measurements in lithium salts show more than the expected deviations (± 2 cm^3/mole) from the mean values for these same anions obtained from measurements in electrolytes with other cations. In each instance the value for $\bar{V}_-$ is high by 3–5 cm^3/mole. The authors would not expect the ion-pair formation in lithium salt solutions to be sufficient at concentrations below 10^{-2} N to account for these somewhat high results, but abnormality of lithium salt solutions is evident in many types of measurements.

B. Comparison of Ionic Partial Molal Volumes Determined from Vibration Potentials with Values by Other Methods. In Table V the values for the ionic partial molal volumes determined from the ionic vibration potentials are compared with values obtained by other authors using the following procedures to obtain absolute values. (1) Bernal and Fowler[23] assume that the ratio of the ionic partial molal volumes for a given electrolyte is equal to the ratio of the cubes of the crystallographic radii (see also ref 24 and 25). (2) Fajans and Johnson[26] assume that the ionic partial molal volumes of NH_4^+ and Cl^- ions are equal on the basis of certain theoretical and experimental evidences. (3) Stokes and Robinson[27] assume that the electrostriction of solvent surrounding a large ion, for example I^-, is negligible and that the partial molal volume of such an ion is that anticipated for "close random packing" of water molecules around a hard sphere with a radius corresponding to the crystallographic value (see also ref 28). (4) Mukerjee[29] adjusts the ionic partial molal volumes of one ion (H^+) so as to give a linear relation between ionic partial molal volumes of univalent cations and anions and the cube of the crystallographic radii, as predicted by Hepler.[30] With the exception of the lithium ion, all of the present results are between the values of Stokes and Robinson and of Mukerjee.

C. Ionic Vibration Potentials in Mixtures of 1–1 Electrolytes. For a mixture of two 1–1 electrolytes, A^+B^- and C^+D^-, at concentrations C_{AB} and C_{CD}, respectively, eq 2a becomes (with the same assumptions leading to eq 3)

$$\Phi_M = \frac{\Phi_{AB}}{1 + \dfrac{u_C + u_D}{u_A + u_B}\dfrac{C_{CD}}{C_{AB}}} + \frac{\Phi_{CD}}{1 + \dfrac{u_A + u_B}{u_C + u_D}\dfrac{C_{AB}}{C_{CD}}} \quad (8)$$

where Φ_{AB} and Φ_{CD} are the vibration potentials for a solution of AB alone and of CD alone. The quantities u_i are the mobilities of the ionic species indicated by the subscripts. In applying this equation to mixtures we shall assume that Φ_{AB} and Φ_{CD} are independent of concentration over the range 10^{-3} to 10^{-1} N on the basis of the experimental results listed in Table II as well as theoretical considerations.

Equation 8 has been verified for a number of mixtures of CsCl with various salts over a large range of concentrations. The points in Figure 11 represent the experimental results, while the curves have been calcu-

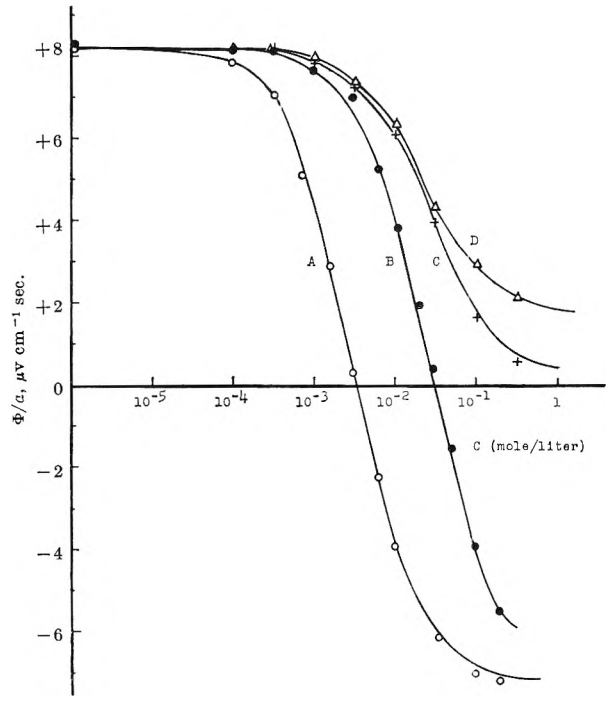

Figure 11. Vibration potentials for mixtures of 1–1 electrolytes at 220 kc. ○, 2×10^{-3} N CsCl + LiI; ●, 2×10^{-2} N CsCl + LiI; +, 2×10^{-2} N CsCl + LiCl, and △, 2×10^{-2} N CsCl + KCl.

(23) J. Bernal and R. Fowler, *J. Chem. Phys.*, **1**, 515 (1933).

(24) Y. Kobayazi, *J. Sci. Hirosnima Univ.*, A9, 241 (1939).

(25) O. Rice, "Electronic Structure and Chemical Binding," McGraw-Hill Book Co., Inc., New York, N. Y., 1940.

(26) K. Fajans and O. Johnson, *J. Am. Chem. Soc.*, **64**, 668 (1942).

(27) R. Stokes and R. Robinson, *Trans. Faraday Soc.*, **53**, 301 (1957).

(28) B. J. Alder, *J. Chem. Phys.*, **23**, 263 (1955).

(29) P. Mukerjee, *J. Phys. Chem.*, **65**, 740 (1961); **65**, 744 (1961).

(30) L. Hepler, *ibid.*, **61**, 1426 (1957).

Table III: Ionic Vibration Potentials[a] at 220 Kc and 22° and Calculated Partial Molal Volumes

Electrolytes	Φ/a, μv cm^{-1} sec	t_+	t_-	$\bar{V}_2$, cm^3/mole	$\bar{V}_+$, cm^3/mole	$\bar{V}_-$, cm^3/mole
		a. 1-1 Electrolytes				
NaF	0.8	0.476	0.524	−3.5	−6.1	2.6
KF	2.0	0.570	0.430	6.6	4.0	2.6
RbF	5.8	0.585	0.415	12.8	9.7	3.1
CsF	9.4	0.580	0.420	20.1	15.1	5.0
HCl	0.4	0.820	0.180	17.8	−5.6	23.4
LiCl	0	0.336	0.664	17.0	−9.5	26.5
NaCl	0.6	0.396	0.604	16.4	−6.4	22.8
NH_4Cl	−0.1	0.490	0.510	36.0	9.6	26.4
KCl	1.7	0.490	0.510	26.5	3.7	22.8
RbCl	5.2	0.511	0.489	31.9	8.4	23.5
CsCl	8.1	0.500	0.500	39.2	15.7	23.5
NaBr	−3.1	0.392	0.608	23.5	−6.5	30.0
KBr	−1.3	0.485	0.515	33.7	3.4	30.3
LiI	−7.2	0.344	0.656	35.5	−12.0	47.5
NaI	−6.4	0.395	0.605	35.1	−5.4	40.5
KI	−4.0	0.488	0.512	45.4	3.1	42.3
LiOH	−0.5	0.164	0.836	−4.0	−12.6	8.6
NaOH	−0.4	0.202	0.798	−4.6	−9.5	4.9
KOH	−0.2	0.271	0.729	5.4	3.6	1.8
$LiIO_3$	−9.7	0.487	0.513	24.8	−11.2	36.0
$NaIO_3$	−6.8	0.554	0.446	24.2	−10.4	34.6
KIO_3	−4.4	0.644	0.356	34.3	3.1	31.2
HNO_3	0	0.830	0.170	29.8	−5.2	35.0
KNO_3	0.7	0.507	0.493	38.3	3.6	34.6
$KClO_3$	0	0.533	0.467	45.2	2.1	43.1
$KClO_4$	−0.9	0.522	0.478	52.2	3.7	48.5
Na acetate	1.7	0.478	0.522	40.1	−10.1	50.2
$NaHCO_3$	0	0.530	0.470	22.6	−5.9	28.5
		b. 1-2 Electrolytes				
Li_2SO_4	−2.4	0.325	0.675	11.6	−10.5	32.6
Na_2SO_4	−1.7	0.386	0.614	11.5	−5.9	23.6
K_2SO_4	−0.3	0.480	0.520	32.3	4.3	23.6
$(NH_4)_2SO_4$	−2.3	0.480	0.520	51.3	11.4	28.4
Na_2CO_3	−0.6	0.420	0.580	−6.7	−6.1	5.5
		c. 2-1 and 3-1 Electrolytes				
$MgCl_2$	1.1	0.410	0.590	15.3	−36.7	26
$CaCl_2$	1.2	0.438	0.562	18.3	−25.5	21.9
$SrCl_2$	2.4	0.438	0.562	17.9	−22.1	20.0
$BaCl_2$	4.1	0.454	0.546	23.6	−15.6	19.6
$CdCl_2$	4.0	0.414	0.586	23.2	−32.4	27.8
$Be(NO_3)_2$	−0.7	0.386	0.614	52.7	−30.7	41.7
$Mg(NO_3)_2$	−0.2	0.427	0.573	37.5	−35.6	36.8
$Ca(NO_3)_2$	0.2	0.455	0.545	40.6	−28.6	34.6
$Sr(NO_3)_2$	1.3	0.455	0.545	40.2	−24.6	32.4
$Ba(NO_3)_2$	2.6	0.471	0.529	45.7	−9.5	27.6
$Cd(NO_3)_2$	1.7	0.430	0.570	38.0	−22.2	30.1
$Ni(NO_3)_2$	0.6	0.430	0.570	34.0	−33.6	34.2
$Co(NO_3)_2$	0.7	0.407	0.593	30.6	−38.4	34.5
$Pb(NO_3)_2$	5.5	0.495	0.505	42.5	−6.9	24.7
$Al(NO_3)_3$	−0.8	0.470	0.530	43	−46.7	29.9

Table III (*Continued*)

Electrolytes	Φ/a, μv cm^{-1} sec	t_+	t_-	$\bar{V}_2$, cm^3/mole	$\bar{V}_+$, cm^3/mole	$\bar{V}_-$, cm^3/mole
			d. 2-2 Electrolytes			
$MgSO_4$	−1.3	0.400	0.600	−6.0	−34.6	28.6
$ZnSO_4$	−0.4	0.400	0.600	−7.6	−32.4	24.8
$CoSO_4$	−0.4	0.380	0.620	−4.2	−34.0	29.8
$CuSO_4$	−0.3	0.415	0.585	−11.2	−32.4	21.2
$NiSO_4$	−0.3	0.400	0.600	−10.2	−36.2	26

[a] See Table II, footnote *a*.

Table IV: Mean Values for Ionic Partial Molal Volumes ($\bar{V}_j$) and Root-Mean-Square Deviations (σ) between Values in Various Electrolytes (cm^3/mole)

Ion	$\bar{V}_j$	σ
H^+	−5.4	0.2
Li^+	−11.2	1.2
Na^+	−7.4	1.9
K^+	3.4	0.6
Rb^+	9.0	0.7
Cs^+	15.5	0.3
NH_4^+	10.5	1.5
F^-	3.3	1.0
Cl^-	23.7	1.2
Br^-	30.2	0.2
I^-	41.4	0.9
NO_3^-	34.8	0.2
ClO_3^-	43.2	...
IO_3	32.9	1.7
ClO_4^-	48.5	...
Acetate$^-$	50.2	...
HCO_3^-	28.5	...
CO_3^{2-}	5.5	...
SO_4^{2-}	27.0	3.5

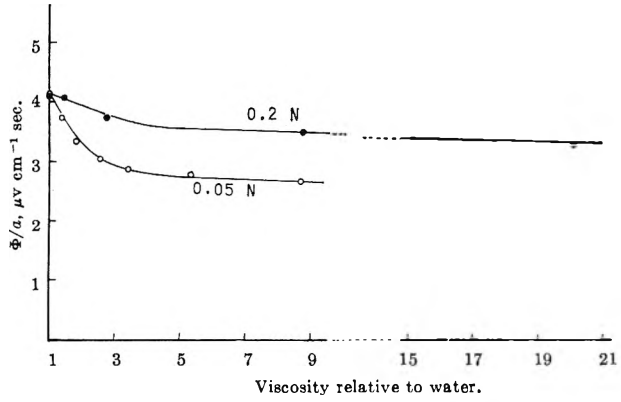

Figure 12. Dependence of ionic vibration potential on viscosity at 220 kc and 22°.

lated with eq 8 using for Φ_{AB} and Φ_{CD} the values listed in Table II. In all instances the agreement is well within the precision of the measurements. An inversion in the phase of the observed effect is evident for the mixtures of CsCl and LiI.

Table V: Comparison of Values for Ionic Partial Molal Volumes (cm^3/mole) Determined by Various Methods

Ion	Present values	B-F[23]	F-J[26]	S-R[27]	M[29]
Li^+	−11.2	−8.0	−0.9	−8.2	−5.2
Na^+	−7.4	−8.5	−1.7	−8.7	−5.7
K^+	3.4	8	8.4	1.5	4.5
Rb^+	9.0	15.5	13.7	6.4	9.5
Cs^+	15.5	27	21.1	13.9	16.9
NH_4^+	10.5	12	18	10.6	...
H^+	−5.4	−8	0.1	−7.2	−4.5
F^-	3.3	6	−1.8	5.1	2.1
Cl^-	23.7	37	18	25.3	22.3
Br^-	30.2	47.5	25.1	32.2	29.2
I^-	41.4	66	36.7	43.8	40.8
ClO_3^-	43.2	61	35.1	...	...
ClO_4^-	48.5	...	44.5	51.1	50.6
IO_3^-	32.9	42	...	...	...
NO_3^-	34.8	38	29.4	36.6	33.6
Ac^-	50.2	...	40.5	...	...
HCO_3^-	28.5	45	22.3	29.1	...
CO_3^{2-}	5.5	7	−2.8	10.7	...
SO_4^{2-}	27.0	39	15.4	...	24.8

D. Viscosity Dependence of Ionic Vibration Potentials. In eq 2a, the frictional coefficient of the jth ion (ρ_j) includes the viscosity of the solvent. Since ρ_j appears in both numerator and denominator of the right term in eq 2a, the vibration potentials, Φ, should be independent of solvent viscosity. To establish the validity of this prediction experimentally, the effective viscosity of the solvent has been modified through the introduction of a water-soluble, nonionic, complex, synthetic polyacrylamide, Polyhall-27.[31] Figure 12 shows the effect on the observed ionic vibration poten-

(31) Provided by Stein, Hall, and Co., Inc., New York, N. Y.

tials of adding Polyhall-27 to 0.05 and 0.2 N KI solutions. A small intrinsic potential of 0.5–1 μv cm^{-1} sec was observed in pure water containing Polyhall-27 with the magnitude of the intrinsic effect dependent on the polymer concentration. This intrinsic effect is to be compared with the value of 0.3 μv cm^{-1} sec observed with just pure water. Although a significant decrease in the ionic vibration potentials is produced with the addition of the polymer to the solution, this decrease is quite small in view of the extremely large increment (up to 21-fold) in the viscosity produced by the addition of the polymer. Furthermore, some change in the magnitude of the effect is to be anticipated even though eq 2a does not explicitly indicate a dependence on viscosity because of the direct electrostatic interaction of the ions with the polymer and the attendant changes in the apparent masses (W_j). All things considered, the behavior in Figure 12 appears quite reasonable.

VII. Conclusions

On the basis of the present experimental study of ionic vibration potentials, the following conclusions have been reached. (1) Measurements of ionic vibration potentials are subject to several false effects, but these can be eliminated or reduced to a magnitude where they have very little effect on the measurements. (2) Experimentally measured values for the ionic vibration potentials are in good agreement with presently available theoretical treatments. (3) Ionic vibration potentials in conjunction with density data provide an attractive approach to the determination of the absolute values of ionic partial molal volumes.

Acknowledgment. The authors are pleased to acknowledge the support of this research by the Office of Naval Research.

Reaction of AlCl(g) with MgO(c) and the Heat of Formation of $MgAl_2O_4$(c)

by D. Bhogeswara Rao and V. V. Dadape

Communication No. 939 from the National Chemical Laboratory, Poona, India *(Received June 28, 1966)*

The reaction of aluminum monochloride with magnesium oxide was investigated between 1298 and 1465°K employing a flow method. The products of the reaction and the weight-loss measurements suggest that the equilibrium reaction was $4MgO(c) + 3AlCl(g) \rightleftharpoons MgAl_2O_4(c) + AlCl_3(g) + 3Mg(g)$. The reaction yielded a third-law heat, $\Delta H_{298} = 21.85 \pm 0.84$ kcal mole^{-1}, which compared favorably with the second-law value of 24.03 ± 2.49 kcal mole^{-1}. These values gave -553.36 ± 1.89 and -551.18 ± 3.55 kcal mole^{-1}, respectively, for the heat of formation of magnesium aluminate from the elements. The heat of formation of $MgAl_2O_4$(c) from the oxides at 298°K was found to be -9.26 ± 1.89 kcal mole^{-1} from the third law and -7.08 ± 3.55 kcal mole^{-1} from the second law.

Introduction

Although the vapor-phase existence of aluminum monochloride and its highly reducing nature has been realized long ago,[1] very little is known about its action on refractory oxides. Semenkovitch[2] has reported that aluminum monochloride reacted with refractory oxides, *viz.*, MgO, BeO, ZrO_2, and SiO_2, but not with alumina. His experiments were purely qualitative. He has suggested the following mechanism for the reaction of aluminum monohalide with MgO(c) at 1100°

$$3MgO(c) + 6AlCl(g) = 3MgCl_2(g) + Al_2O_3(c) + 4Al(l) \quad (1)$$

but the possibility of the aluminum metal reacting with MgO(c) was not taken into consideration. Altman[3,4] and Grjotheim, Herstad, and Toguri[5] have measured the vapor pressures of Mg metal at about the same temperatures by studying the reaction

$$MgO(c) + 2Al(l) \rightleftharpoons MgAl_2O_4(c) + 3Mg(g) \quad (2)$$

This suggests the formation of the spinel, $MgAl_2O_4$(c), in the reaction of AlCl(g) with MgO(c) at these temperatures, which was overlooked by Semenkovitch.[2] The presence of aluminum metal also reduces the magnesium chloride with the formation of $AlCl_3$ at these temperatures, as was indicated in the work of Balduni.[6] From the above information it appears that the course of reaction between AlCl(g) and MgO(c) is not according to that indicated by Semenkovitch[2] (see reaction 1) and hence the necessity for the present investigation.

In continuation of the study of the equilibrium reaction[7]

$$2Al(l) + AlCl_3(g) \rightleftharpoons 3AlCl(g) \quad (3)$$

the gaseous monochloride was allowed to react with solid MgO. In order to establish the reaction scheme, equilibrium measurements were carried out together with the identification of the products.

Experimental Section

Materials. The magnesium oxide used in this investigation was of E. Merck grade and was dried at 1200° for 20 hr. The powder was pressed into briquettes at 1000 kg/cm^2. The briquettes were broken into small pieces to give rise to a large sample surface area to make the conditions favorable for ensuring equilibrium with the carrier gas. Aluminum chloride was also of E. Merck grade and was resublimed in an inert atmosphere before use. The material was always handled in a drybox. Aluminum metal used in the production of monochloride was of spectrographi-

(1) L. Frommer and M. Polayni, *Z. Physik. Chem.*, **B6**, 380 (1930).
(2) S. A. Semenkovitch, *J. Appl. Chem. USSR*, **33**, 557 (1960).
(3) R. L. Altman, *J. Phys. Chem.*, **67**, 366 (1963).
(4) R. L. Altman, *ibid.*, **68**, 3425 (1964).
(5) K. Grjotheim, O. Herstad, and J. M. Toguri, *Can. J. Chem.*, **39**, 443 (1961).
(6) H. Balduni, *Monatsh. Chem.*, **88**, 1038 (1957).
(7) D. B. Rao and V. V. Dadape, *J. Phys. Chem.*, **70**, 1349 (1966).

cally standard grade and was supplied by Johnson Mathey and Co. Ltd., London.

Apparatus and General Procedure. The apparatus and the method adopted to study the reaction between the gaseous monochloride and magnesium oxide was similar to that described previously.[7] This method proved successful for the purpose. The general principles involved in the chemical transportation have been extensively discussed by Margrave,[8] Schäfer,[9] Merten,[10] and Bell, *et al.*[11] In this method the carrier gas (argon) saturated with aluminum monochloride was allowed to react with MgO(c) under equilibrium conditions. The products were identified by X-ray and spectrographic methods. The amount of MgO(c) taking part in the reaction was determined by the analysis of the residue in the boat. The gaseous products of the reaction carried away by the argon gas were also analyzed. The boats used in these reactions were passivated Kyanite as described previously.[7] The reaction tube was either of alumina or passivated Kyanite which was surrounded by a platinum wire-wound tube furnace. The furnace, wound in three circuits, gave a constant zone of about 10–11 in. within ±7°. The zone was sufficient to accommodate two 5-in. long boats containing aluminum metal and magnesium oxide, respectively. The temperatures were measured with a calibrated chromel–alumel thermocouple. At higher temperatures, a Pt—Pt10–% Rh thermocouple was used.

Transpiration runs were carried out using argon as the carrier gas at flow rates of 100–180 ml/min. The previous study of the equilibrium reaction[7] showed that the effects of self-diffusion and thermal diffusion were negligible at these flow rates. After the experimental run of 1 or 2 hr, the heating of aluminum chloride was stopped and the boats were moved to the colder part of the furnace and cooled in the gas flow. The boats were finally pushed to a chamber containing dry nitrogen and weighed. The residue in the second boat was powdered in the drybox and analyzed for $MgAl_2O_4$(c).

Treatment of the Data. The X-ray examination of the powder pattern of the residue in the boat showed the formation of spinel $MgAl_2O_4$(c). Search for MgO(c) and Al_2O_3(c) revealed the fact that excess MgO(c) (unreacted) was present, and the lines did not disclose the presence of Al_2O_3 (c) even if the reaction is carried out at lower temperatures. The identification of the spinel was possible by comparing the powder pattern of the residue with that given in the ASTM index.[12] The incorporation of excess Al_2O_3 in the spinel lattice reduces the lattice parameters[13,14] while a similar incorporation of MgO increases it.[15] Considering the presence of magnesium aluminate as one of the products of the reaction, the experimental data were examined to determine the possibility of one of the following reactions

$$4MgO(c) + 3AlCl(g) = MgAl_2O_4(c) + AlCl_3(g) + 3Mg(g) \quad (4)$$

$$4MgO(c) + 2AlCl(g) = MgAl_2O_4(c) + MgCl_2(g) + 2Mg(g) \quad (5)$$

$$4MgO(c) + 3AlCl(g) = MgAl_2O_4(c) + 3MgCl(g) + Al(l) \quad (6)$$

Reaction 6 can be rejected on two facts: the MgCl(g) is not important at these temperatures and also the highly reducing nature of the aluminum metal yields the reaction

$$3MgCl(g) + Al(l) = AlCl_3(g) + 3Mg(g) \quad (7)$$

It may be stated here that the dimer, Al_2Cl_6(g) is not an important species above 1000°K. The free energies of reaction 7 also indicate that reaction 6 can be neglected under conditions of these experiments. Identification of the products and the equilibrium measurements are helpful in the examination of reactions 4 and 5.

The products collected were resublimed in dry nitrogen atmosphere at 200°. The sublimate was found to be $AlCl_3$. The absence of chloride in the residue showed that $MgCl_2$(g) was not the product of reaction. Consequently, reaction 4 may be the only possible equilibrium reaction.

The vapor pressures of AlCl(g), $AlCl_3$(g), and Mg(g) were calculated from the experimentally determined weight losses of Al(l) and MgO(c). Assuming that the ideal gas law holds good, in the equilibrium zone, the partial pressures of the various components are calculated as follows.

(8) J. L. Margrave in "Physico-Chemical Measurements at High Temperatures," J. O'M. Bockris, J. L. White, and J. D. Mackenzie, Ed., Butterworth and Co. Ltd., London, 1959, Chapter 10.

(9) H. Schäfer, "Chemical Transport Reactions," Academic Press, London, 1964.

(10) U. Merten, *J. Phys. Chem.*, **63**, 443 (1959).

(11) W. E. Bell, U. Merten, and M. Tagami, *ibid.*, **65**, 510 (1961).

(12) ASTM X-Ray Powder Data File 5.0672.

(13) G. L. Clark, E. E. Howe, and A. E. Badger, *J. Am. Ceram. Soc.*, **17**, 7 (1934).

(14) D. M. Roy, R. Roy, and E. F. Osborn, *Am. J. Sci.*, **251**, 337 (1953).

(15) A. M. Alper, R. N. McNally, P. H. Ribbe, and R. C. Doman, *J. Am. Ceram. Soc.*, **45**, 263 (1962).

Table I: Experimental Data for the Reaction $4MgO(c) + 3AlCl(g) \rightleftharpoons MgAl_2O_4(c) + AlCl_3(g) + 3Mg(g)$

T, °K	t, min	ΔW Al, g	ΔW MgO, g	P_{AlCl_3}, atm	P_{AlCl_3}', atm	P_{Mg}, atm	P_{AlCl}, atm	K_p, atm
1298	100	0.8187	1.4460	1.4053×10^{-2}	1.9069×10^{-2}	4.2159×10^{-2}	2.9184×10^{-2}	5.7487×10^{-2}
1321	100	1.1535	2.0100	1.9530×10^{-2}	2.3402×10^{-2}	5.8590×10^{-2}	4.1913×10^{-2}	6.3926×10^{-2}
1336	80	1.2813	2.2550	2.3742×10^{-2}	2.7342×10^{-2}	7.1226×10^{-2}	4.9728×10^{-2}	8.0342×10^{-2}
1372	90	1.6092	2.8060	3.2238×10^{-2}	3.6165×10^{-2}	9.6714×10^{-2}	6.9058×10^{-2}	9.9338×10^{-2}
1398	120	2.3092	3.8660	4.6526×10^{-2}	4.9922×10^{-2}	1.3958×10^{-1}	1.0957×10^{-1}	1.0320×10^{-1}
1428	80	1.9850	3.2650	6.1877×10^{-2}	6.5178×10^{-2}	1.8563×10^{-1}	1.5150×10^{-1}	1.1990×10^{-1}
1465	60	2.1180	3.6540	7.8916×10^{-2}	8.4558×10^{-2}	2.3675×10^{-1}	1.7335×10^{-1}	2.1541×10^{-1}

P_{AlCl} = pressure of AlCl generated

$$= \frac{{}^3/_2 n_{Al} RT_r}{Vr} \quad (8)$$

$$P_{AlCl_3} = \frac{{}^1/_4 n_{MgO} RT_r}{Vr} \quad (9)$$

$$P_{Mg} = \frac{{}^3/_4 n_{MgO} RT_r}{Vr} \quad (10)$$

$$P_{AlCl(unreacted)} = (n_{AlCl} - {}^3/_4 n_{MgO}) \frac{RT_r}{Vr} \quad (11)$$

The equilibrium constant

$$K_p = \frac{(P_{Mg}{}^3)(P_{AlCl_3}')}{P_{AlCl}{}^3} \quad (12)$$

The pressure of the unreacted $AlCl_3$ in reaction 3 was taken account of while calculating the equilibrium constant of reaction 4. This was necessary because $AlCl_3$ was one of the products of the reaction between $AlCl_3$(g) and MgO(c). The results are given in Table I. The reaction between $AlCl_3$(g) and MgO(c) was negligible in comparison to that of AlCl(g).

The free-energy and third-law heats were calculated employing the relations

$$\Delta F_T = -RT \ln K_p \quad (13)$$

$$\Delta H_{298} = T\left[-\Delta\frac{F_T - H_{298}}{T} - R \ln K_p\right] \quad (14)$$

The free-energy functions for AlCl(g), $AlCl_3$(g), and Mg(g) were taken from the "JANAF Tables."[16] The thermal functions for $MgAl_2O_4$(c) crystal were taken from Bonnickson.[17] The third-law calculations for reaction 4 are given in Table II, and they yielded an average heat of $\Delta H_{298} = 21.85 \pm 0.84$ kcal/mole. To vercome the wide scattering of the points in the second-law plot of log K *vs.* $1/T$, a Σ-plot treatment[18] was employed (Figure 1). The heat capacities for Mg(g), AlCl(g), MgO(c), $AlCl_3$(g), and $MgAl_2O_4$(c) are taken from Stull and Sinke,[19] Kelley,[20] Dingmann,[21]

Table II: Thermodynamic Properties of the Reaction, $4MgO(c) + 3AlCl(c) \rightleftharpoons MgAl_2O_4(c) + AlCl_3(g) + 3Mg(g)$

T, °K	Log K_p	ΔF, kcal mole^{-1}	$-\frac{\Delta F° T - H°_{298}}{T}$	ΔH_{298}, kcal mole^{-1}
1298	−1.2404	7.37	11.28	22.01
1321	−1.1943	7.22	11.28	22.12
1336	−1.0951	6.69	11.28	21.78
1372	−1.0029	6.30	11.29	21.79
1398	−0.9864	6.31	11.29	22.09
1428	−0.9212	6.02	11.29	22.14
1465	−0.6668	4.47	11.29	21.01
				Av = 21.85 ± 0.84 kcal

and Bonnickson,[17] respectively. The Σ plot of this data gives an equation

$$\log K = \left[-\frac{4615.5 + 545}{T} + 2.18 \log T - 0.87 \times 10^{-4} T - 0.54 \times 10^{5} T^{-2} - 4.3636 \pm 0.39\right] \quad (15)$$

The heat of reaction from Σ plot is given by

$$\Delta H°_T(\text{kcal/mole}) = [21.12 + 4.33 \times 10^{-3} T - 0.40 \times 10^{-6} T^2 + 4.94 \times 10^{2} T^{-1}] \quad (16)$$

(16) "JANAF Thermochemical Tables," The Dow Chemical Co., Midland, Mich., 1964.

(17) K. R. Bonnickson, *J. Phys. Chem.*, **59**, 220 (1955).

(18) K. K. Kelley, U. S. Bureau of Mines. Bulletin 601, U. S. Government Printing Office, Washington, D. C., 1962; or G. N. Lewis and R. Randall, "Thermodynamics," revised by K. S. Pitzer and L. Brewer, McGraw-Hill Book Co., Inc., New York, N. Y., 1961, p 175.

(19) D. R. Stull and G. C. Sinke, "Thermodynamic Properties of the Elements," American Chemical Society, Washington, D. C., 1956.

(20) K. K. Kelley, U. S. Bureau of Mines Bulletin 584, U. S. Government Printing Office, Washington, D. C., 1960.

(21) T. Dingmann, *Z. Anorg. Chem.*, **166**, 133 (1927). See also O. Kubaschewski and E. L. Evans, "Metallurgical Thermochemistry," Pergamon Press, Inc., New York, N. Y., 1965.

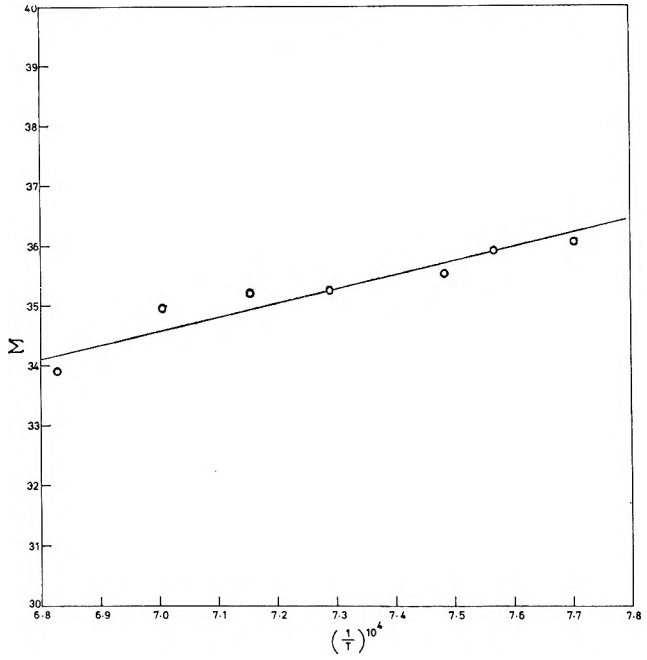

Figure 1. Σ plot for the reaction, $4MgO_{(c)} + 3AlCl(g) = MgAl_2O_4(c) + AlCl_3(g) + 3Mg(g)$.

The constants from eq 16 lead to a value of $\Delta H°_{298} = 24.03 \pm 2.49$ kcal mole^{-1}. The second-law value is in satisfactory agreement with that of the third law (21.85 ± 0.84 kcal). The difference of 2.18 kcal may be due to the errors dependent on temperatures. The variation of ±7° will cause a discrepancy of 2.65 kcal in the second law and 0.1 kcal in the third law.

Combining the heat of reaction with the heats of formation of $AlCl_3(g)$, MgO(c), AlCl(g), and Mg(g) from "JANAF" tables, one obtains a value of $\Delta Hf_{298} = -553.36 \pm 1.89$ kcal mole^{-1} from the third-law value and -551.18 ± 3.55 kcal mole^{-1} from the second-law value for the heat of formation of magnesium aluminate from its elements. These give $\Delta H_{298} = -9.26 \pm 1.89$ and -7.08 ± 3.55 kcal mole^{-1}, respectively, for the formation of $MgAl_2O_4(c)$ from the oxides

$$MgO(c) + Al_2O_3(c) \rightleftharpoons MgAl_2O_4(c) \qquad (17)$$

The values are in excellent agreement with the values obtained by Altman,[3] Grjotheim, Herstad, and Toguri,[5] and Navrotsky and Kleppa.[22] The pressures of magnesium are slightly less than those reported by Grjotheim,[5] *et al.*

It is difficult to assess the correctness of the third-law value because of the errors in the free-energy functions of $AlCl_3(g)$. These were discussed at length[7,23] previously. Therefore the heat of formation of $MgAl_2O_4(c)$ from the oxides may be about -6 to -8 kcal mole^{-1} at 298°K.

Although free-energy considerations suggest more feasibility for reaction 5, reaction 4 is more important because of the following reasons. Because of the nearly similar value of bond energies in AlCl(g) and $AlCl_3(g)$ and the tendency of binding aluminum into more stable halides,[24] the process as indicated by reaction 5 might have reduced to reaction 4.

Acknowledgment. One of the authors (D. B. R.) thanks the Council of Scientific and Industrial Research (India) for the award of the Research Fellowship. The authors are thankful to the NBS authorities for the permission to utilize the equipment in the PL-480 scheme at the National Chemical Laboratory, Poona, India, on "The Chemical and Thermodynamic Properties of Refractory Materials at High Temperatures." The authors are also thankful to Professor J. L. Margrave of Rice University and Dr. W. S. Horton, Chief of the High Temperature Chemistry Section, National Bureau of Standards, Washington, for making available the necessary data from the "JANAF" tables.

(22) A. Navrotsky and O. J. Kleppa, *Inorg. Chem.*, **5**, 192 (1966).
(23) M. A. Frisch, M. A. Greenbaum, and F. Farber, *J. Phys. Chem.*, **69**, 3001 (1965).
(24) F. Irman, *Helv. Chim. Acta*, **33**, 1449 (1950).

Reversible Photochemical Dimerization of Acenaphthylene. I. The Reaction in Liquid Solutions[1]

by Robert Livingston and Kei Sin Wei

Division of Physical Chemistry, University of Minnesota, Minneapolis, Minnesota *(Received July 5, 1966)*

Acenaphthylene is photodimerized by visible and near-ultraviolet light. In solution, the quantum yield increases with increasing concentration and is depressed by dissolved O_2. Only the *cis* dimer is formed in O_2-saturated solutions. In O_2-free solutions, both dimers are formed; the *trans* dimer is the dominant species in dilute solutions and the *cis* dimer in concentrated solutions. The effects of the nature of the solvent and of temperature were studied. The results are compatible with a relatively simple mechanism. The dimers are efficiently photodissociated, re-forming acenaphthylene. The quantum yield of photodissociation does not depend on the concentrations of dimer or of O_2.

Introduction

The photodimerization of acenaphthylene was first reported in 1912 by Dziewonski and Rapalski[2] and was studied quantitatively by Bowen and Marsh in 1947.[3a] Our present study of this reaction is in general agreement with these published results; however, being more extensive and differing quantitatively in some respects from earlier studies, it demands a somewhat more complex mechanism than that outlined by Bowen.[3a] Unlike acenaphthene and alkyl-substituted naphthalenes, acenaphthylene is weakly, if at all, fluorescent[3b] and has an absorption tail which extends far into the visible. The dimer, cyclobuta(1,2-*a*:3,4-*a'*)diacenaphthylene, exists in two stereoisomeric forms. In O_2-saturated solutions, the product of photodimerization is exclusively the *cis* form, but in the absence of O_2 a mixture of the isomers is formed, low concentration favoring the *trans* isomer. The dimers are efficiently photodissociated, reforming acenaphthylene. If light of wavelength longer than 350 mμ is used, dimerization only is observed, since the dimers do not absorb in this region. By the use of shorter wavelengths (*e.g.*, 254 mμ) and dilute solutions of a dimer, the dimerization may be neglected relative to photodissociation, since the quantum yield of dimerization is small for dilute solutions (less than 0.01 for concentrations smaller than 0.05 *M*) and the yield for photodissociation is about one and independent of concentration. The use of ultraviolet light and of moderately concentrated solutions results in a steady state, in which the concentrations of dimer and monomer are comparable.

Methods and Materials

Materials. The acenaphthylene was a K and K product. Before use, it was thrice recrystallized from methanol and then passed through a silica gel column using hexane as the elutant. This material has a melting point of 92–93°. In an alternative method of purification, the *cis* dimer was prepared photochemically, recrystallized, and then converted to acenaphthylene photochemically.

The solvents were either of analytical reagent or spectrograde and were used without further purification.

The samples of the dimers which were prepared photochemically were freed from unchanged acenaphthylene by washing with hexane on an alumina column. They were separated by recrystallization from methanol, in which the *trans* is much less soluble than the *cis* dimer. The melting points of these samples of *trans* and *cis* dimers were 305 and 234°,[2] respectively.

Determination of Quantum Yields. The number of

(1) This work was sponsored by the U. S. Army Research Office (Durham). K. S. W. wishes also to express his gratitude for a fellowship from E. I. du Pont de Nemours Co.

(2) K. Dziewonski and G. Rapalski, *Chem. Ber.*, **45**, 2491 (1912); **46**, 1986 (1913); **47**, 1679 (1914).

(3) (a) E. J. Bowen and J. Marsh, *J. Chem. Soc.*, 109 (1947); (b) E. J. Bowen, *Advan. Photochem.*, **1**, 36 (1963).

photons absorbed was determined by the use of a ferrioxalate actinometer, following the procedure outlined by Parker.[4] Except for a few experiments made with especially dilute solutions, the absorption of the incident light was practically complete. For dilute solutions, the percent absorption was calculated from the known extinction coefficients, making allowance[5] for the relatively small decrease (less than 10%) in absorption due to the disappearance of the reactant. The correction was somewhat greater for measurements of photodissociation of the dimers, where the product also absorbs the incident light, but even in these cases, the uncertainty introduced by the correction was probably small compared to random errors.

The reaction vessels were quartz or Pyrex cells, 10 mm in diameter and either 10.0 or 1.00 mm in length. Mercury-in-quartz arcs, either GE AH6 or Hanovia S-100, were used as light sources. Wavelengths were isolated by suitable combinations of glass, solution, and Cl_2-gas filters. The temperature of the reaction vessel was controlled with a water bath provided with plane, transparent windows. During the photolyses of dimers and of some concentrated solutions of the monomer, the reaction mixtures were stirred continuously with a fine stream of gas bubbles. The solutions were deoxygenated by several cycles of the freeze–pump–thaw routine. To introduce definite concentrations of O_2, the evacuated vessel was opened to a side tube which contained air at a definite volume and pressure.

The concentration of the acenaphthylene monomer was measured spectrophotometrically before and after illumination using light of 335 mμ, which is not appreciably absorbed by the dimers. When the product of dimerization consisted of a mixture of the dimers, their relative amounts were determined spectrophotometrically after removing the unchanged monomer on an alumina column.

The absorption spectra were measured with a Cary 15 spectrophotometer. Fluorescence spectra were determined using either 365- or 313-mμ exciting light isolated from a mercury arc. The fluorescent light, emitted at right angles to the exciting beam, passed through a Bausch and Lomb Model 33-86-45 grating monochromator and was measured with a photomultiplier and a micro-microammeter. The variation of sensitivity with wavelength of the apparatus was estimated approximately using the fluorescence of anthracene[6] as a standard.

Results and Conclusions

The Quantum Yield of Dimerization. The quantum yield of dimerization increases with increasing acenaphthylene concentration and is decreased by dissolved O_2, as is shown by Figure 1 and Table I. The

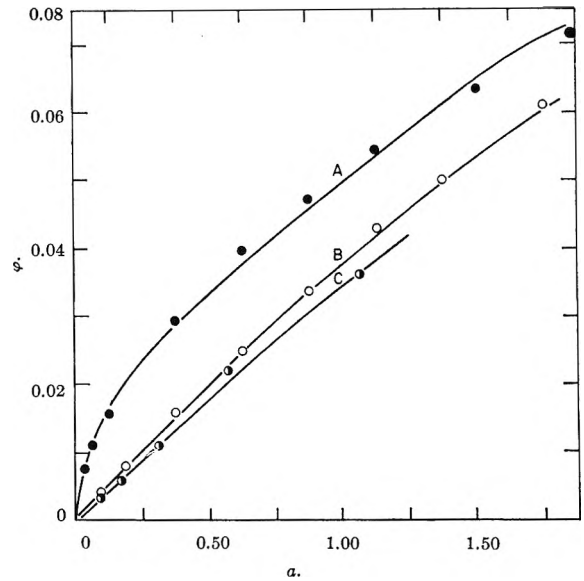

Figure 1. Quantum yield of dimerization as a function of the concentration of acenaphthylene: A, deoxygenated solution; B, air-saturated solution; C, O_2-saturated solution.

Table I: Quantum Yield of Dimerization of 0.075 *M* Acenaphthylene in Benzene at 25°

$[O_2] \times 10^3$	10.0	2.00	0.265	0.143	0.070	0
$\phi \times 10^2$	0.30	0.38	0.61	0.81	1.06	1.35

curves of Figure 1 are referred to in the Discussion. These data conform approximately to the following empirical equation

$$\frac{\phi}{[A]} = \alpha + \frac{1}{\beta + \gamma[A] + \delta[O_2]} \qquad (1)$$

Empirical values of the coefficients for several solvents are listed in Table II.

Table II: Values of the Coefficients Which Fit the Data Obtained in Different Solvents

Solvent	α	β	γ	δ
Benzene	0.042	2.5	62	3×10^4
Hexane	0.046	2.3	64	3×10^4
Methanol	0.085	1.9	125	5.5×10^4

(4) C. Parker, *Proc. Roy. Soc.* (London), **A220**, 104 (1953).
(5) K. S. Wei, Doctoral Thesis, University of Minnesota, 1966.
(6) C. Parker and W. Rees, *Analyst*, **85**, 587 (1960).

A few measurements of the quantum yield which were made in other solvents, at 25° in air-saturated solutions, are summarized in Table III.

Table III: Quantum Yields of Dimerization in Other Solvents

[A], moles/l.	Solvent: Toluene	Ethyl ether	Ethanol	CCl_4
0.10	0.006	0.005	0.011	0.006
0.40	0.021	0.017	0.042	0.022
0.80	0.053	0.042	...	0.054

The addition of water to methanol increases the quantum yield, as is shown in the following table. The measurements were made at 25° with air-saturated solutions, using 0.025 *M* acenaphthylene.

Table IV: Effect of Added Water on the Quantum Yield in Methanol

Mole %	0	11.0	20.0	28.5	35.5	42.5
$\phi \times 10^3$	2.00	2.33	2.65	3.10	4.05	5.25

The effect of temperature on the quantum yield is relatively small and depends upon the concentration of O_2 and, in deoxygenated solutions, to a lesser extent on the concentration of acenaphthylene. For reasons of experimental convenience, toluene rather than benzene was the solvent in these experiments. In the air-free solutions, the concentration of acenaphthylene was 0.020 *M;* in the air-saturated solutions, it was 0.20 *M*. These data conform closely to the Arrhenius relation. The energy of activation is 1200 ± 75 cal/mole for air-free solutions, and has the negative value, −600 ± 50 cal/mole, for air-saturated solutions.

Table V: Quantum Yields as a Function of Temperature in Air-Free and Air-Saturated Solutions in Toluene

	0°	42°	90°
Air saturated	1.10×10^{-2}	9.6×10^{-3}	8.3×10^{-3}
Deoxygenated	6.5×10^{-3}	8.5×10^{-3}	1.12×10^{-2}

To test for a possible effect of solvent viscosity on the quantum yield, comparable measurements were made in *n*-hexane (η = 0.374 cp at 17°) and in cyclohexane (η = 1.02 cp at 17°). In 0.20 *M* air-saturated solutions, the yields were 0.0125 and 0.0120—identical within the limits of uncertainty. In air-free solutions, the yields in normal and cyclohexane were, respectively, 0.0235 and 0.0156 at 0.20 *M* and 0.075 and 0.0048 at 0.020 *M*.

The quantum yield of dimerization was measured (in a 0.20 *M* air-saturated solution in benzene) using light intensities ranging from 2×10^{-7} to 3×10^{-6} einstein/cm² sec. Within the limit of uncertainty, which was about ±4%, the measured values were independent of the intensity.

From 4360 to 2537 A the quantum yield of dimerization appears to be independent of the wavelength of the actinic light. These experiments were made using 0.05 *M* acenaphthylene dissolved in air-free cyclohexane at 25°. The yields using separately 4360 and 3660 A were determined by direct comparison to the ferrioxalate actinometer. Direct measurements of the yields were not practicable when light of 3130 or 2537 A was used, since both monomer and dimer absorb strongly in this region. The yields in this range were determined from measurements of the steady-state concentrations, utilizing the directly measured value of the yield of photodissociation and the extinction coefficients of monomer and dimer. The values obtained, in order of decreasing wavelength, are 0.0032, 0.0030, 0.0033, and 0.0033; the average errors of single values, based upon eight measurements at each wavelength, ranged from 3% at 4300 A to 6% at 2537 A. In some cases (*e.g.*, the data of Table I), relative quantum yields were determined using the radiation from a GE AH6 mercury arc after it passed through a glass filter which absorbed wavelengths shorter than 3400 A.

Spectroscopic and Related Data. The absorption spectrum of acenaphthylene in solution has a relatively sharp peak at 322 mμ (log ε 4.0) and a stronger absorption on the short-wavelength side of 230 mμ. Unlike acenaphthene and alkyl-substituted naphthalenes, its absorption extends weakly to long wavelengths, at least to 500 mμ (see Figure 2). This long-wavelength tail was not affected by careful purification (including preparation by photodissociation of a purified sample of the dimer). This fact and the persistence of the vibrational structure to about 470 mμ indicate that the weak tail is an intrinsic property of acenaphthylene rather than being due to a persistent impurity. The use of methanol rather than hexane as the solvent has little effect on the absorption spectra; the maxima are not appreciably shifted, although the vibrational structure appears to be somewhat less sharp in methanol. In benzene, the extinction coefficients of acenaphthylene appeared to be independent of concentra-

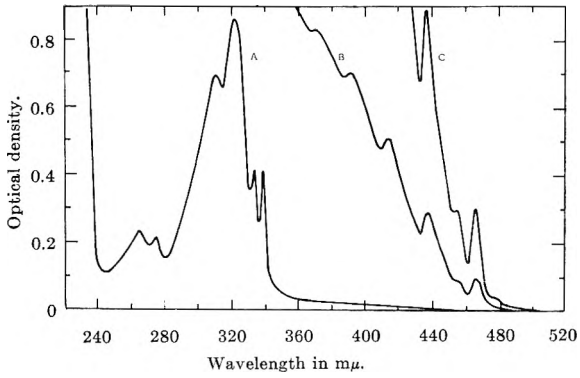

Figure 2. Absorption spectrum of acenaphthylene in *n*-hexane: A, 8.5×10^{-5} *M*; B, 2.35×10^{-3} *M*; C, 7.0×10^{-3} *M*.

tion, in the range 10^{-3} to 1.5 *M*. A quartz cell with adjustable optical path (1.00–0.010 mm) was employed in these measurements. In an attempt to learn whether the weak tail corresponded to a singlet–triplet transition, the absorption spectrum was measured in CH_2Br_2. There was no marked enhancement of the weak absorption.

It has been reported[3b] that acenaphthylene is nonfluorescent. Our samples of the purified material exhibited a weak fluorescence, extending from about 420 to 580 mμ, with a maximum at 500 mμ. A crude comparison of the intensity of the fluorescence of 10^{-4} *M* acenaphthylene in hexane to a dilute alkaline solution of fluorescein indicated that the quantum yield of fluorescence is about 0.001. It is difficult to establish that such weak fluorescence is not due to a trace of a strongly fluorescent impurity. However, the fluorescence could not be due to the most likely contaminant, acenaphthene, since its fluorescence maximum is at about 335 mμ. Measurements[7] with a phase-shift apparatus on a deaerated hexane solution, about 10^{-5} *M* solution of acenaphthylene, indicated a mean lifetime of about 5×10^{-9} sec.

Since acenaphthylene is practically photochemically stable in dilute solution ($<10^{-3}$ *M*) and is almost nonfluorescent,[3b] it was anticipated that it would exhibit a transient (triplet–triplet?) absorption when studied with flash photolytic apparatus. Using carefully deoxygenated solutions in hexane at concentrations from 10^{-5} to 10^{-4} *M*, no absorption transients were observed in the range between 380 and 600 mμ. Our apparatus[8] should have detected transients with mean lifetimes equal to or greater than 20 μsec.

The absorption spectrum of purified samples of the *cis* and *trans* dimers were measured in *n*-hexane and are plotted on Figure 3. It is noteworthy that the area under the long-wavelength band is much less for the *cis* than for the *trans* dimer.

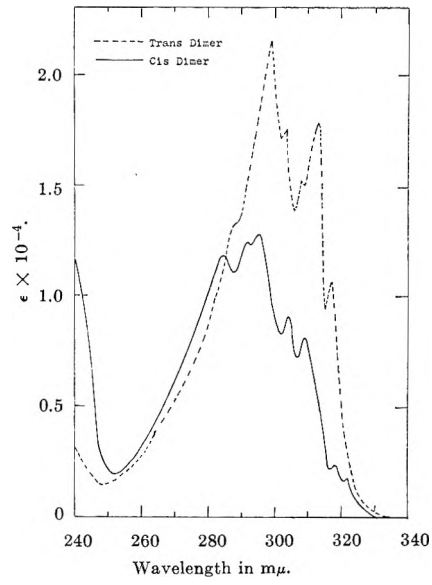

Figure 3. Absorption spectra of *trans* and *cis* dimers of acenaphthylene in *n*-hexane.

Relative Yields of cis and trans Dimers. The relative amounts of *cis* and *trans* forms in a mixture can be determined spectrophotometrically, conveniently, by measuring the optical densities at 312.5 and 298 mμ. However, most experiments were terminated when about 10% of the monomer had reacted and the absorption of the remaining monomer masked that of the dimers. To eliminate this difficulty, the monomer was separated from the mixture of dimers on an alumina column. The dimers were then eluted with acetone and their relative amounts determined spectrophotometrically. This analytical method was checked using solutions containing known amounts of the pure compounds.

In air-saturated solutions, the photochemical product is practically the pure *cis* dimer, but in air-free solutions, it is a mixture of the two dimers, their relative amounts being determined by the solvent and by the concentration of the monomer. The mole per cent of *cis* dimer formed in deoxygenated solutions is shown on Figure 4. Curve C of this figure is referred to in the Discussion.

Photodissociation of the Dimers. The dimers are efficiently photodissociated into monomeric acenaphthylene when they are illuminated with ultraviolet light. By using dilute solutions (10^{-3} to 2×10^{-5} *M*),

(7) We are indebted to R. Lumry and M. Walker, Biophysical Laboratory, School of Chemistry, University of Minnesota, for these measurements.

(8) K.-H. Grellmann, R. Memming, and R. Livingston, *J. Am. Chem. Soc.*, **84**, 546 (1962).

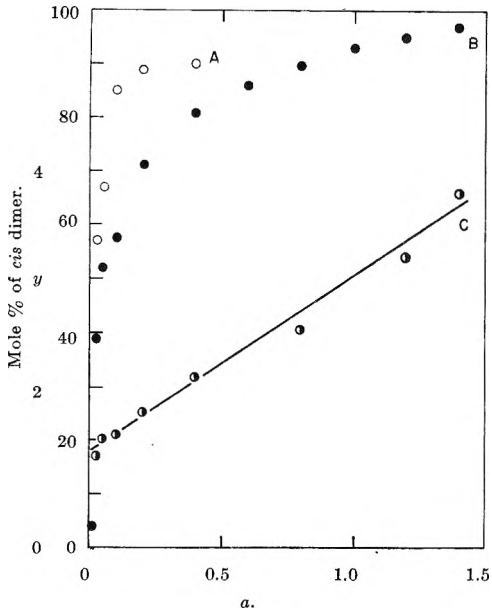

Figure 4. A and B, mole % of *cis* dimer formed in deoxygenated solutions (A, solvent, methanol; B, solvent, benzene); C, plot of $y = \frac{1}{P_{trans}}(1 + \frac{k_5 K p_1}{k_4} a)$ *vs.* *a*.

irradiating with either 310 or 253.7 mμ, and limiting the reaction to 10% conversion, the effect of the back reaction may be neglected. The quantum yields of dissociation of the *cis* and the *trans* dimers were measured under a variety of conditions. Within the range of a maximum scatter of 10%, the yields were the same in air-saturated and air-free solutions—in benzene, methanol, *n*-hexane, cyclohexane, and ether—at temperatures ranging from 0 to 75°, at concentrations ranging from 1.0×10^{-3} to 2.0×10^{-5} *M*, and when irradiated with either 310 or 253.7 mμ. The average values for the yields of the *cis* and *trans* isomers were 0.91 and 0.85, respectively. This difference is probably significant.

Discussion

Nearly 20 years ago, Bowen[3a] suggested two alternative explanations of the photodimerization of acenaphthylene. He concluded from the data which were then available that the reaction resulted from the absorption of light by weak, van der Waals type dimers, followed by a unimolecular reaction of the excited complex, leading to the formation of the stable dimer containing a cyclobutane ring. There is no direct spectroscopic evidence for the existence of these postulated weak dimers; solutions of acenaphthylene conform to Beer's law over a wide range of concentrations (see Results and Calculations). However, determination of the apparent molecular weight[9] in a 0.10 *M* acenaphthylene solution in *n*-hexane at 25° indicated a value (154) slightly but probably significantly, higher than the formula weight (152). The corresponding equilibrium constant, $K = [A_2]/[A]^2$, is 0.09 l./mole. Although this value is little better than a crude estimate, it is probably of the correct order of magnitude.

The results of our first measurements of the quantum yield of dimerization, which were made with air-saturated solutions, are in satisfactory (although not exact) agreement with the simple mechanism postulated by Bowen.[3a] However, subsequent measurements with deoxygenated solutions and determinations of the relative amounts of *cis* and *trans* isomers under various circumstances demonstrated that the photodimerization proceeds by more than one path. The following mechanism is consistent with our data. The symbols A, A_2, D, and *a* refer to acenaphthylene monomer, its van der Waals type dimer, its stable dimer, and its initial stoichiometric concentration, respectively. In

$2A = A_2$	$K = [A_2]/[A]^2$, $[A_2] \cong \frac{Ka^2}{1 + 2Ka}$
$h\nu + A_2 \longrightarrow A_2^*$	$2I_{abs}[A_2]/a$
$A_2^* \xrightarrow{1} D\ (cis)$	$k_1 p_1 [A_2^*]$
$A_2^* \xrightarrow{1} 2A$	$k_1(1 - p_1)[A_2^*]$
$h\nu + A \longrightarrow A^*$	$I_{abs}(1 - 2[A_2]/a)$
$A^* \xrightarrow{2} A$	$k_2[A^*]$
$A + A^* \xrightarrow{3} 2A$	$k_3[A][A^*]$
$A + A^* \xrightarrow{4} D\ (trans)$	$k_4 p_{trans}[A][A^*]$
$A + A^* \xrightarrow{4} D\ (cis)$	$k_4(1 - p_{trans})[A][A^*]$
$A_2 + A^* \xrightarrow{5} A + A_2^*$	$k_5[A_2][A^*]$
$O_2 + A^* \xrightarrow{6} A + O_2$	$k_6[O_2][A^*]$

evaluating $[A_2]$ it was assumed that for all concentrations investigated, $[A_2]^2 << a^2$. Consistent with the Beer's law study, it was assumed that the molar extinction coefficient of A_2 is twice that of A. Several possible reaction steps have been omitted. For example, the analysis of the kinetic data strongly suggests

(9) These measurements were made by T. Unterechter using a differential vapor pressure method.[10] We are indebted to him and to S. Bruckenstein for their cooperation and assistance.

(10) S. Bruckenstein and A. Saito, *J. Am. Chem. Soc.*, 87, 698 (1965).

that the quenching of A_2^* by O_2 is negligible, even in O_2-saturated solutions, presumably because the mean lifetime of A_2^* is very short ($<10^{-10}$ sec). Making the usual steady-state approximation and tentatively neglecting step 5 (the transfer of energy of excitation), it follows that

$$\phi_D = \frac{a}{1 + 2Ka}\left(2Kp_1 + \frac{k_4}{k_2 + k_6[O_2] + (2k_2K + k_3 + k_4 + 2Kk_6[O_2])a}\right) \quad (2)$$

Comparison of this equation with the data indicates that in O_2-saturated solutions (and approximately in air-saturated solutions) the second term is of negligible importance and

$$\phi_D(O_2 \text{ satd}) \cong \frac{2Kp_1a}{1 + 2Ka} \quad (3)$$

The three curves of Figure 1 are plots of the relation

$$\phi_D = \frac{a}{1 + 0.17a}\left(0.0495 + \frac{0.018}{0.0486 + a + 1.7 \times 10^3[O_2]}\right) \quad (4)$$

which is consistent with eq 2. The factor $0.17 = 2K$ corresponds to $K = 0.085$, in fortuitous agreement with the value obtained from the vapor pressure measurements. The corresponding value of p_1, the probability that the excitation of A_2 will lead to the formation of D, is 0.29. Comparing eq 2 and 4, it follows that $k_6/k_2 \cong 4 \times 10^4\ M^{-1}$ and $k_6/k_4 \cong 10^5$. Since $k_6 \leqslant 10^{10}\ M^{-1}$ sec^{-1}, it follows that $k_2 \leqslant 2.5 \times 10^5\ \text{sec}^{-1}$. This value is incompatible with the measured mean life, 5×10^{-9} sec, of fluorescence, indicating either that the photochemically active state is a relatively short-lived triplet or that the observed fluorescence is due to a persistent impurity. The observation reported by Schenck and Wolgast,[11] that Rosebengal sensitizes the dimerization of acenaphthylene in air-free methanol to light of 590 mμ, yielding 65% of the *trans* isomer, appears to be consistent with the postulate that the excited monomer is a triplet state. A similar step in the mechanism of the photodimerization of coumarin was suggested by Hammond, *et al.*[12]

Additional important information on the reaction mechanism can be obtained from a study of the effects of O_2 and acenaphthylene concentrations upon the relative amounts of *cis* and *trans* dimers formed. In O_2 or air-saturated solutions, the product appears to be exclusively the *cis* isomer, indicating that step 1 yields only this product. In air-free solutions, a mixture of the isomers is formed, high concentrations favoring the production of the *cis* compound (Figure 4). It seems very probable that the relative amount of *cis* isomer formed by step 4 will be independent of the monomer concentration. Setting p_{trans} equal to the molar proportion of the *trans* compound formed in this way and introducing step 5 into the mechanism, the following expressions are obtained for the total quantum yield and for the quantum yield of the *trans* dimer, both in the absence of O_2.

$$\phi_D = \frac{a}{1 + 2Ka} \times \left(2Kp_1 + \frac{k_5Kp_1a + k_4}{k_2 + (2k_2K + k_3 + k_4)a + k_5Ka^2}\right) \quad (5)$$

$$\phi_{D,trans} = \frac{a}{1 + 2Ka} \times \frac{p_{trans}k_4}{k_2 + (2k_2K + k_3 + k_4)a + k_1Ka^2} \quad (6)$$

It follows that

$$y = \frac{\phi_D - \dfrac{2Kp_1a}{1 + 2Ka}}{\phi_{D,trans}} = \frac{1}{p_{trans}}\left(1 + \frac{k_1Kp_1}{k_4}a\right) \quad (7)$$

A plot of the function y against a (Figure 4) is a straight line with a slope of 2.6 l./mole and an intercept of 1.40; *i.e.*, $p_{trans} = 0.71$. Combining these data with the value $Kp_1 = 0.0248$, we obtain $k_5/k_4 = 7.5$. To be consistent, an equation corresponding to eq 5 but containing the O_2 terms, rather than eq 2, should have been fitted to the data of Figure 1. However, it is apparent that such an equation, which is similar to eq 2 but contains an additional adjustable constant, would be consistent with the data. For high concentrations of O_2, both equations reduce to eq 3 and therefore yield the same values of K and p_1. Substitution of the complete equation for eq 2 would change the values of k_6/k_4 and k_6/k_2. However, these changes should not be great, since k_6Kp_1a does not exceed $k_4/5$ even for high values of a.

The effects of temperature (Table V) are consistent with the mechanism. For air-saturated solutions where dimerization is due chiefly to step 1, temperature can affect only Kp_1. The observed small negative "energy of activation" suggests that p_1 is not noticeably affected by temperature, since the molar enthalpy of formation of A_2 should have a small negative value.[3a] For dilute

(11) G. Schenck and R. Wolgast, *Naturwissenschaften*, 49, 36 (1962).
(12) G. Hammond, C. Stout, and A. Lamola, *J. Am. Chem. Soc.*, 86, 3103 (1964).

air-free solutions, the principal effect of changing temperature should be on k_4/k_2. It is postulated in the mechanism that step 4 (like steps 3, 5, and 6) is an efficient bimolecular reaction whose rate is probably limited by diffusion. Step 2 is chiefly a nonradiative transition; as such, it may be temperature dependent. Accordingly, the energy of activation of k_4/k_2 should be equal to or less than the value calculated from the variation of viscosity with temperature. The experimental values are ΔH_η (for toluene) = 2.1 kcal/mole and $\Delta H^{\pm}_{k_4/k_2}$ = 1.2 kcal/mole.

The mechanism also implies that the quantum yield of the reaction in O_2-saturated solutions should be independent of viscosity, but for the reaction in O_2-free solutions it should decrease with increasing viscosity. The results of measurements in *n*-hexane and cyclohexane are consistent with these predictions.

Substitution of an alcohol for a hydrocarbon solvent (Table III) or addition of water to methanol[13] (Table IV) increases the quantum yield for an air-saturated solution and therefore Kp_1. This change is probably due to an increase in K.

The two acenaphthylene molecules which constitute the weak complex, A_2, are presumably held together by the dispersion forces between the π electrons of the naphthalene rings. If the two external double bonds occur at the same end of the complex, electronic excitation could lead directly to the formation of the *cis* but not the *trans* dimer. If the external double bonds are at opposite ends of the complex, photodimerization would not be expected to occur. This crude analysis is consistent with the observation that step 1 leads exclusively to the formation of the *cis* dimer with a probability $p_1 = 0.29$. It is not obvious what fraction of the reactions involving the excited monomer, step 4, should result in the formation of the *cis* dimer. The corresponding experimental quantity, $1 - p_{trans}$, is 0.29.

Step 5 was introduced into the mechanism to render it consistent with the observed *cis–trans* ratio of the dimers in air-free solutions. This is by no means the only possible interpretation of the data. Indeed, the equation derived from this mechanism is not compatible with a few results obtained in very dilute solutions (4% *cis* dimer formed in 0.0018 *M* solution). An alternative explanation[5] could be based on the postulate that two different excited states, A* and A′, are intermediates in the reaction. If it be further assumed that the intrinsic lifetime of A′ is greater than that of A* and that A′ leads exclusively to the *trans* dimer, the amended mechanism is consistent with all of the available data. A systematic study of the photosensitized reaction may be of help to distinguish between these alternative mechanisms.

No direct *cis–trans* isomerization of the dimers was observed. However, ultraviolet radiation of moderately concentrated solutions should lead to stereoisomerization by way of photodissociation followed by photodimerization. This indirect isomerization should be most efficient if *trans* dimers were illuminated in an air-saturated solution.

(13) K. Uberreiter and K. Jonder, *Makromol. Chem.*, **40**, 97 (1960).

Reversible Photochemical Dimerization of Acenaphthylene. II. The Reaction in the Molten and Crystalline Phase[1]

by Kei Sin Wei and Robert Livingston

Division of Physical Chemistry, University of Minnesota, Minneapolis, Minnesota *(Received July 5, 1966)*

Between 0 and 25° the photodimerization of crystalline acenaphthylene is inefficient ($\varphi < 0.005$) and the only product is the *trans* isomer. Above 60°, the *cis* isomer is the dominant product, and the yield increases rapidly with increasing temperature, reaching 0.04 at 70°. Illumination of molten acenaphthylene produces both the *cis* dimer and a polymer. The quantum yield of dimerization is 0.20 at 90°.

Photochemical reactions of both crystalline[2a] and molten[2b] acenaphthylene have been reported. In the present study we have confirmed the published qualitative results and have determined the quantum yields under several different conditions.

Materials and Methods

The methods and materials were similar to those described in part I of this study.[3] A few special techniques are described in the following sections.

Dimerization and Polymerization in the Molten State. Illumination of the melt produces the *cis* dimer, a polymer, and traces of a yellow substance which was not identified. No *trans* dimer was detected in the products.

The melt, contained in Pyrex cylinders about 1.0 mm thick, was exposed to light of 436 mμ, which was isolated from the radiation of an AH6 mercury arc. The measurements were made at 90°. This is 2° below the melting point of acenaphthylene, but at this temperature the supercooled melt did not crystallize spontaneously. In comparing this photochemical reaction to the actinometer,[4] it was assumed that the melt absorbed all of the light incident upon it.

The polymer was separated from the dimer and unchanged monomer by treating the mixture with an excess of methanol. The polymer is insoluble in methanol; it was filtered out of the solution, washed, dried, and weighed. The remaining mixture was transferred to *n*-hexane, and the dimer was washed free from the monomer with *n*-hexane on an alumina column.[3]

The average of eight determinations of the quantum yield of dimerization is 0.20 ± 0.02. A comparison of these results with those obtained in solution indicates that this dimerization is due to excitation of the van der Waals dimers, step 1 of the proposed mechanism.[3]

The corresponding quantum yield of polymerization, expressed in terms of disappearance of the monomer, is 0.14 ± 0.01. The average molecular weight of the polymer formed by a thermal, induced reaction is reported[2b] to be about 2×10^4. If the molecular weight of the photopolymer is of the same order of magnitude, the photoinitiation of polymerization is very inefficient at 90°. Presumably, radicals are formed by a side reaction of the excited monomer molecules—an inefficient and temperature-dependent process.

The ultraviolet spectrum (Figure 1) of the photopolymer, dissolved in CCl_4, was compared to that of a sample of polymer which was prepared by a thermal reaction initiated by benzoyl peroxide.[2b] The spectra, normalized at 300 mμ, were identical.

Dimerization of Crystalline Acenaphthylene. Crystalline acenaphthylene was photolyzed in the form of thin layers of fine crystals. These layers were deposited on the inner surface of a window of a Pyrex cell by evaporating the hexane from a solution of acenaphthy-

(1) This work was sponsored by the U. S. Army Research Office (Durham). K. S. W. wishes also to express his gratitude for a fellowship from the E. I. du Pont de Nemours Co.

(2) (a) K. Dziewonski and G. Rapalski, *Chem. Ber.*, **45**, 2491 (1912); **46**, 1986 (1913); **47**, 1679 (1914); (b) K. Überreiter and K. Jonder, *Makromol. Chem.*, **40**, 97 (1960).

(3) R. Livingston and K. S. Wei, *J. Phys. Chem.*, 71, 541 (1967).

(4) C. Parker, *Proc. Roy. Soc.* (London), **A220**, 104 (1953).

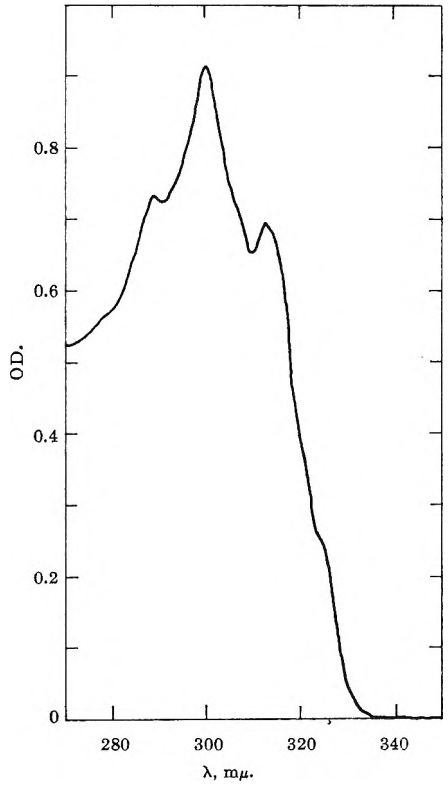

Figure 1. Absorption spectrum of the photopolymer of acenaphthylene. 1.00-cm cell; 0.21 g/l.; solvent, CCl_4.

lene. The cell was placed in a water bath, the temperature of which was controlled manually to about ±0.5°. The exciting light was 436 mμ, isolated from an AH6 mercury arc. The photochemical transformation was limited to less than 1% of the monomer present. In estimating the quantum yield, it was assumed that all of the incident light was absorbed by the acenaphthylene.

The product, a mixture of *cis* and *trans* dimers, was analyzed by the method described in part I of this study.[3] Below 25° only the *trans* dimer is detectable, but above 60° the principal product is the *cis* dimer. The results are summarized in Table I.

Table I: Photodimerization of Crystalline Acenaphthylene

Temp, °C	φ_{cis}	φ_{trans}	Mole % of *trans* dimer
0	0.0000	0.0029	100
20	0.0000	0.0041	100
40	0.0002	0.0052	98
50	0.0006	0.0061	92
60	0.0078	0.0055	42
65	0.0231	0.0025	10
70	0.0405	0.0041	9

Griffin and Veber[5] state that "acenaphthylene affords only *trans*-dimer in the solid state in sharp contrast to irradiation in solution." Presumably, these experiments were made at room temperature.

In the range from 0 to 50°, log φ_{trans} is a linear function of T^{-1}, which corresponds to an Arrhenius energy of activation of 2.4 kcal/mole. Similarly, the variation of φ_{cis} with temperature corresponds to an energy of activation of 40 kcal. The decrease of the quantum yield of *trans* dimerization at high temperatures suggests that this reaction competes with *cis* dimerization for the energy of activation. The formation of the *trans* dimer, which is inefficient at all temperatures studied, may be the result of migration of energy of excitation to certain crystal imperfections. For *cis* dimerization, the energy of activation and the corresponding preexponential factor are surprisingly high. Any attempt to explain these results in detail is scarcely justified by the available data.

Recently Schmidt predicted[6] that the photochemical dimerization of crystalline acenaphthylene could lead to the formation of both *cis* and *trans* dimers. This prediction is based upon the supposition that the crystal structure of acenaphthylene is closely related to that of acenaphthene.

(5) G. Griffin and D. Veber, *J. Am. Chem. Soc.*, 82, 6417 (1960).

(6) G. Schmidt, Institut International de Physique Solvay, Conseil de Physique, 13th, Brussels, Oct 1965, Vol. IX, p 4.

Adsorption of Potential-Determining Ions at the Ferric Oxide–Aqueous Electrolyte Interface

by R. J. Atkinson, A. M. Posner, and J. P. Quirk

Department of Soil Science and Plant Nutrition, Institute of Agriculture, University of Western Australia, Nedlands, Western Australia *(Received July 6, 1966)*

Potentiometric titrations in indifferent aqueous electrolyte were used to measure the surface charge characteristics of microcrystalline particles of ferric oxides. The net adsorption density ($\Gamma_{H^+} - \Gamma_{OH^-}$ microequivalents per gram) is described by equations for the surface excesses of H^+ and OH^-, derived by equating the electrochemical potentials of potential-determining ions and indifferent counterions in solution and surface phases, and neglecting counterions in the diffuse layer. The equations contain interaction constants arising from the small but finite distances of separation between planes of adsorbed potential-determining ions and indifferent counterions under conditions of ferric ion solvation at the interface. The BET nitrogen area does not satisfactorily represent the dependence of parameters and interaction constants on particle surface area, for different preparations. The equations were interpreted as showing that adsorbed counterions remain solvated, forming electrostatically bound ion pairs with only a small proportion dissociating into the diffuse layer.

Solid oxide particles immersed in aqueous electrolyte solutions develop surface electrical charges by adsorption or desorption of potential-determining ions. For ferric oxide,[1-5] these ions are H^+ and OH^-, and ferric hydroxo complex ions derived from the solid phase by dissolution, when any ions which are specifically adsorbed at the oxide surface are absent. The contribution made to surface charge by transfer of metal hydroxo complex ions across the interface is usually considered to be very small in relation to H^+ and OH^- ion transfer, since solubility data[3-5] show that either H^+ or OH^- ions always greatly exceed ferric hydroxo complex ion in solution concentration for the pH range 3.5 to 11. Surface charge measurement thus requires only adsorption–desorption measurements for H^+, which are readily carried out by the direct method of potentiometric titration of microcrystalline particles of oxide in dilute aqueous suspension using various ionic strengths of an indifferent electrolyte.[3,4] From such measurements, it is known that ferric oxide–aqueous electrolyte interfaces have important differences in double-layer structure and the magnitude of electrical properties when compared with AgI, Ag_2S, or liquid mercury in contact with aqueous electrolyte.[3-5] Quantitative interpretation has not been attempted, and in previous publications the ferric oxide system has been characterized only by measurements of the pH at the zero point of charge.

In this paper, equations to describe potential-determining ion binding are derived for ferric oxides in aqueous suspension under conditions of high ionic strength of indifferent electrolyte. The form of analysis was suggested by the ideas of Gilbert and Rideal[6] on the titration of fibrous proteins. Two simple methods of eliminating electrical potential terms from ion-binding equations are examined, and it is found that the more satisfactory method does not require one to

(1) G. A. Parks, *Chem. Rev.*, **65**, 177 (1965).

(2) P. G. Johansen and A. S. Buchanan, *Australian J. Chem.*, **10**, 392 (1957).

(3) G. A. Parks and P. L. de Bruyn, *J. Phys. Chem.*, **66**, 967 (1962).

(4) A. E. Albrethson, Ph.D. Thesis, Massachusetts Institute of Technology, 1963.

(5) G. Y. Onoda and P. L. de Bruyn, *Surface Sci.*, **4**, 48 (1966).

(6) G. A. Gilbert and E. K. Rideal, *Proc. Roy. Soc.* (London), **A182**, 335 (1944).

Table I

	Ferric oxide						
	Goethite (27.7.65)	Hematite ((1)22.7.64)	Hematite (24.3.65)	Hematite (2)	Hematite (10.2.65)	Hematite (Albrethson)	Hematite (Parks and de Bruyn)
BET N_2 area, $cm^2\ g^{-1}$	70.9×10^4	43.5×10^4	44.6×10^4	34.1×10^4	36.4×10^4	23×10^4	22×10^4
Temp of measurement, °C	20.3 ± 0.4	...	19.5 ± 0.6	...	20 ± 2	25	21
Test. concn. of oxide, g in 25 ml	0.1376	0.2728	0.1576	0.1375	0.0949	...	...
Washing method	Dialysis	KOH	Dialysis	KOH	Dialysis	KOH	KOH
Initial charge before titration, μequiv g^{-1}	4 ± 1.0	7 ± 2	85 ± 2	12 ± 3	72 ± 4	...	...
pH, zpc	7.55 ± 0.15	8.60 ± 0.2	9.27 ± 0.10	8.45 ± 0.2	8.90 ± 0.15	8.70	8.5
Surface density of charge at pH 4 in 1 *M* KCl, μequiv cm^{-2}	1.41×10^{-4}	1.63×10^{-4}	3.68×10^{-4}	4.22×10^{-4}	4.89×10^{-4}	7.25×10^{-2}	...
$k_{H^+}V_{H^+}$	0.527×10^6	0.37×10^6	3.40×10^6	0.889×10^6	1.17×10^6	2.26×10^6	1.32×10^6
$k_{H^+}V_{H^+}/A$	0.74	0.85	7.62	2.61	3.21	9.83	6.00
K_1, μequiv^{-1} g	0.03647	0.05387	0.03089	0.02596	0.02081	0.02765	0.02405
K_1A	2.59×10^4	2.34×10^4	1.38×10^4	0.89×10^4	0.76×10^4	0.64×10^4	0.53×10^4
K_2, μequiv^{-1} g	0.047	...	0.0165	...	0.011	...	0.043
K_2A	3×10^4	...	0.9×10^4	...	0.4×10^4	...	0.9×10^4
Indifferent electrolyte used	KCl	KNO_3	KCl	KNO_3	KCl	NaCl	KNO_3

account for the small proportion of counterions which dissociate from the surface as free ions.

Experimental Materials and Methods

(*i*) *Preparation of Ferric Oxides.* Microcrystalline precipitates of hematite α-Fe_2O_3 and goethite α-FeOOH were prepared from ferric nitrate of at least 98% purity manufactured by May and Baker Ltd., Dagenham, England. Solutions containing 100 g of $Fe(NO_3)_3 \cdot 9H_2O$/l. were prepared at room temperature and boiled at 100° for 18 days under reflux conditions.[3] Final pH values were between 0 and 1. Goethite was prepared by the addition of 200 ml of 2.5 *N* KOH to 50 g of $Fe(NO_3)_3 \cdot 9H_2O$ in 825 ml of double-distilled water to give a final pH near 12, followed by aging for 24 hr in a 60° oven. Pyrex glass vessels were used, and no precautions were taken to prevent silicate contamination, which is possible at high pH. Goethite and hematite precipitates were dialyzed in cellulose tubing using double-distilled water changed twice daily until NO_3^- concentrations were $<10^{-4}$ *M*. Some hematite precipitates were washed by repeated centrifugation and decantation using KOH to raise the pH to 9 for the initial washes (Table I); at this pH the oxide was flocculated. Suspensions contained 0.02 to 0.03 g of ferric oxide/ml and were stored in polythene bottles from which 5-ml samples were pipetted as required for titrations or weight delivery determinations after 24 hr drying at 110°. X-Ray powder diffractometer traces for hematites generally showed a slight goethite peak at 4.18-A spacing. This is the most intense goethite peak,[7] and its presence could be due to a goethite-like surface remaining on hematite when dried at 110°. Hematite was not detected in goethite preparations. Surface area measurements were made by application of the BET equation to conventional volumetric data for nitrogen adsorption on compressed cores of ferric oxide at −195° after 100° outgassing. Preliminary measurements showed that K^+, Cl^-, or NO_3^- were not adsorbed at the zero point of charge (zpc), and that KCl and KNO_3 were equally indifferent.

(*ii*) *Surface Charges in the Absence of Specific Adsorption.* The method used was essentially that of Parks and de Bruyn.[3] Titration data were obtained using recording potentiometric titration apparatus (Radiometer, Copenhagen) with Radiometer G202B and K401 glass and calomel electrodes. Polythene titration cells were used containing 0.1 to 0.15 g of ferric oxide in 25.0 ml of potassium chloride solution mixed with a Teflon stirrer and flushed with wet CO_2-free N_2 gas. Blank titrations were similarly carried out using 25.0 ml of the appropriate KCl solution. Uptake of H^+ or OH^- by the oxide was found by taking differences between test suspension and blank

(7) H. P. Rooksby in "The X-Ray Identification and Crystal Structures of Clay Minerals," G. Brown, Ed., Mineralogical Society, London, 1961, Chapter 10.

titration volumes at particular pH values. Adsorption densities ($\Gamma_{H^+} - \Gamma_{OH^-}$) microequivalents per gram of oxide (110° dry weight) were calculated relative to the zpc located by the common point of intersection of titration curves at different ionic strengths. The temperature for titrations was 20 ± 1.5°. The titrants used were 0.1 *N* HCl and 0.1 *N* KOH which were standardized against 0.005 *M* potassium hydrogen phthalate and 0.001 *M* borax $Na_2B_4O_7 \cdot 10H_2O$; all solutions were prepared with double-distilled water. Additions of titrant did not exceed 0.25 ml in the pH range 3.5 to 10.5, so that ionic strengths were kept essentially constant except at the lowest ionic strength, 0.002 *M*. Each titration was carried out twice using two different speeds which corresponded approximately to 2.5 and 5 pH units/hr. Good agreement (±3%) was found between these replicate titrations. The uncertainty in pH measurements was ±0.05, although absolute errors were greater at pH extremes. Preliminary experiments showed that suspension effects were not significant and liquid junction potentials were taken as being close to zero. The ferric oxides used in the adsorption experiments reported here were not subjected to any drying treatments.

Results and Discussion

Criteria for attainment of equilibria in reactions at hydrated solid surfaces are often difficult to establish. After the initially rapid adsorption or desorption of H^+ occurring with pH change, ferric oxide surfaces continue to adsorb or desorb protons very slowly. The slow H^+ transfer has been attributed to the extension of the proton-excess charge (or proton-deficit charge) into hydrated surface layers of the oxide,[5] or may arise from structural rearrangement of ferric hydroxo complex ions existing at the surface, to expose effectively a greater number of proton acceptor or proton donor sites at the interface. The slow H^+ transfer in any event involves reactions different in form to the initial rapid H^+ transfer occurring when solution pH is changed, and accordingly only the initial fast reaction at the phase boundary is considered here. Other experiments are being conducted in these laboratories to gain information on the structural bases for differences in ferric oxide adsorption capacities for H^+, which cannot be simply related to BET nitrogen surface area or known differences in preparation methods.

Preliminary experiments on the adsorption behavior of dried (110°) finely ground hematite indicated that H^+ adsorption or desorption from solution was greatly reduced with respect to quantity and rate, while phosphate adsorption was only slightly depressed. This suggested that the degree of crystal dispersion was not the important factor, and instead the possibility that slow insertion of water molecules into surface crystalline layers is a rate-determining step for dried ferric oxides is being investigated.

The quantity obtained from potentiometric titration measurements is the net adsorption, $\Gamma_{H^+} - \Gamma_{OH^-}$, in microequivalents per gram. Thus

$$\sigma = \frac{1}{A}(\Gamma_{H^+} - \Gamma_{OH^-}) \ \mu\text{equiv cm}^{-2} \qquad (1)$$

where σ is the surface density of charge, Γ_{H^+} and Γ_{OH^-} are the surface excesses, in microequivalents per gram, and A is the surface area in square centimeters per gram. In the presence of an excess of indifferent electrolyte, the adsorbed potential-determining ions are assigned to the solid side of the interface;[3] that is, the only counterions present in the solution phase are solvated Cl^- (or K^+ if the surface is negatively charged).

Two features of the ferric oxide titration curves (Figures 1 and 2) suggest a form for theoretical analyses.

(i) The titration curves may be regarded as adsorption isotherms for H^+ or OH^- by use of the approximations

$$\sigma A = (\Gamma_{H^+} - \Gamma_{OH^-}) \simeq \Gamma_{H^+}$$
on the acid side of the zpc (2)

$$\sigma A = (\Gamma_{H^+} - \Gamma_{OH^-}) \simeq -\Gamma_{OH^-}$$
on the alkaline side of the zpc (3)

Positive charges on the surface are thus considered to be due entirely to excess adsorbed H^+ with respect to the zpc. Negative charges are considered to arise entirely from a surface excess of OH^-.

(ii) The uptake of HCl or KOH does not appear to reach any maximum value as pH is decreased or increased, respectively. Dissolution of the solid is not thought to be appreciable until pH <3.5, when the curves became steeper and time dependence for HCl uptake became important, so that no reliable equilibrium pH was established below 3.5. Plots of ($\Gamma_{H^+} - \Gamma_{OH^-}$) as a function of hydrogen ion concentration suggest the same conclusions. There was no evidence for appreciable dissolution at pH 11. The lack of any defined HCl or KOH adsorption maxima suggest that in the pH range 4 to 11 only a small proportion of available adsorption sites became charged, and that fractional coverages of the surface with positively or negatively charged sites remain small. An example of the highest recorded charge densities is 4.9×10^{-4} μequiv cm^{-2} (47 μcoulombs cm^{-2}) for hematite no. 10.2.65 (Table I) at pH 4 in 1 *M* KCl, corresponding to one

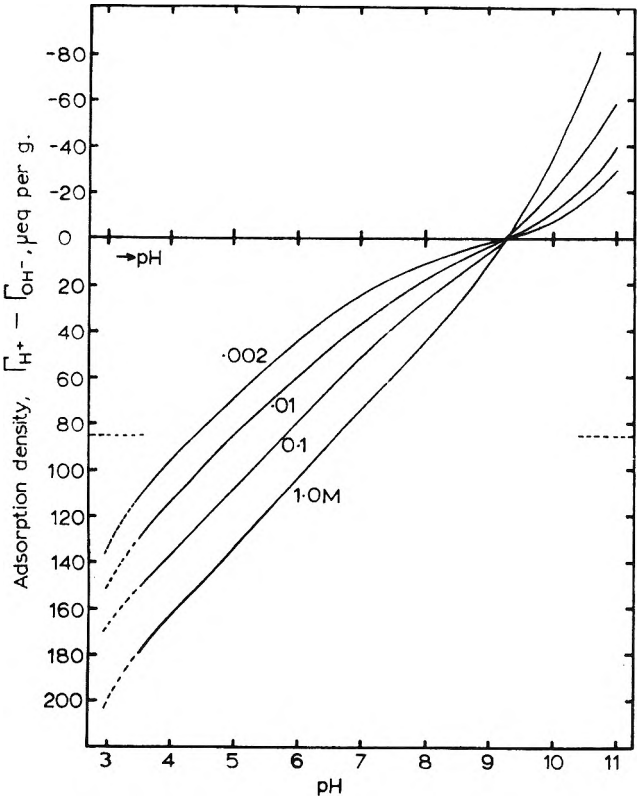

Figure 1. Hematite no. 24.3.65. Adsorption of potential-determining ions as a function of pH and molar concentrations of KCl indifferent electrolyte.

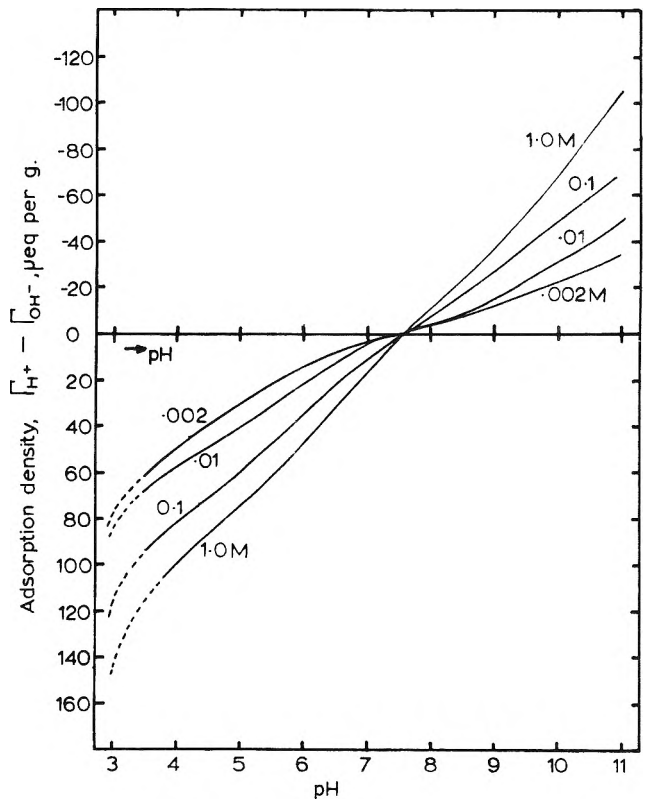

Figure 2. Goethite no. 27.7.65. Adsorption of potential-determining ions as a function of pH and molar concentrations of KCl indifferent electrolyte.

excess proton per 34 A^2 if uniformly distributed over the BET area. The ion-binding equations considered are simplified by use of these approximations which enable evaluation of the constants which appear. The binding of excess H^+ on the surface of the solid phase is first considered. The treatment for binding of excess OH^- is analogous.

The chemical potential μ_H of H^+ ions distributed at random among a limited number of sites on the solid surface, occupying a fraction θ_H of them, and in a region of electrostatic potential ψ_H with respect to the bulk solution, is given by[6]

$$\mu_H = \mu_H^\circ(T,P)_{solid} + RT \ln \frac{\theta_H}{1 - \theta_H} + \psi_H F \quad (4)$$

$\mu_H^0(T,P)_{solid}$ is defined as the chemical potential at pressure P and temperature T when $\theta_H = 0.5$ and $\psi_H = 0$. The corresponding equation for H^+ ions in the bulk of the solution at equilibrium with the solid surface is

$$\mu_H^\circ = \mu_H(T,P)_{soln} + RT \ln y_H(H^+) \quad (5)$$

where $\mu_H^0(T,P)_{soln}$ is the chemical potential at unit activity, y_H is the molar ionic activity coefficient, and (H^+) is the molar concentration. The equation obtained by equating μ_H in bulk solution and solid surface phases at equilibrium is

$$RT \ln \frac{\theta_H}{1 - \theta_H} = -\Delta\mu_H + RT \ln y_H(H^+) - \psi_H F \quad (6)$$

where $\Delta\mu_H = \mu_H^0(T,P)_{solid} - \mu_H^0(T,P)_{soln}$ is the change in standard chemical potential of H^+ during adsorption. $\Delta\mu_H$ is regarded here as a constant by assuming that the properties of a site, such as its effective volume, are constant.

Eliminating Electrical Potential Terms Using Diffuse Double-Layer Theory. Equation 6 may be rewritten in a Langmuir form

$$\theta_H = \frac{k_H y_H(H^+) \exp\frac{-e\psi_H}{kT}}{1 + k_H y_H(H^+) \exp\frac{-e\psi_H}{kT}} \quad (7)$$

where $k_H = \exp(-\Delta\mu_H/RT)$, e is the protonic charge, and k is the Boltzmann constant. Equation 7 is of the same form as that used to account for H^+ adsorption by thorium oxide,[8] and is also of the same form as an

equation used for adsorption of long-chain alkyl ions at air–water and oil–water interfaces.[9]

If Γ_{H^+} is small relative to V_{H^+}, the maximum number of sites available for H^+, the denominator in eq 7 may be approximated to one, and since $\theta_H = \Gamma_{H^+}/V_{H^+}$ then

$$\log \Gamma_{H^+} + \mathrm{pH} = \log k_H V_{H^+} - \frac{1}{2.303}\frac{e\psi_H}{kT} \quad (8)$$

A simple approximation with which ψ may be eliminated from eq 8 is obtained from diffuse double-layer theory for colloidal particles when ψ is small.[10]

$$\frac{e\psi_0}{kT} = \sigma\sqrt{\frac{2\pi}{\epsilon nkT}} \quad (9)$$

ψ_0 is the potential at the surface identified with ψ_H, ϵ is the dielectric constant, and n = concentration of ions in the bulk solution. Therefore, from eq 8

$$\log \Gamma_{H^+} + \mathrm{pH} = \log k_H V_{H^+} - \frac{\Gamma_{H^+}}{2.303A}\sqrt{\frac{2\pi}{nkT\epsilon}} \quad (10)$$

since σ has been approximated to Γ_{H^+}/A μequiv cm^{-2}. This suggests that plots of log Γ_{H^+} + pH as a function of Γ_{H^+} should approximate to straight lines having

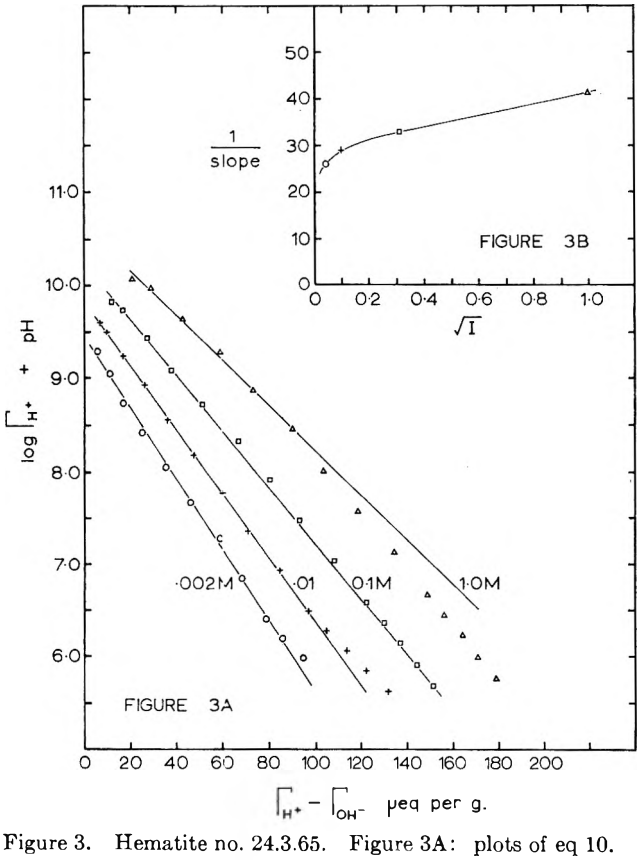

Figure 3. Hematite no. 24.3.65. Figure 3A: plots of eq 10. Figure 3B: the reciprocal slopes of the straight lines in 3A plotted as a function of $\sqrt{I}$ (omitting activity coefficients).

intercept log $k_H V_{H^+}$ and slopes which vary inversely with the square root of ionic strength, $\sqrt{I}$. Although linear plots were obtained (Figure 3A), the slopes were relatively insensitive to changes of KCl concentration from 0.002 to 1.0 M (Figure 3B). It was concluded that the use of simple diffuse double-layer theory to eliminate electrical potential terms could not satisfactorily account for the effect of varying ionic strength on H^+ or OH^- binding by ferric oxides.

Elimination of Electrical Potential Terms Using Equations for the Electrochemical Potential of Counterions. The positive charge on the acid side of the zpc is considered first. The equation for chloride counterions at the surface,[6] corresponding to eq 4 for H^+ ions, is

$$\mu_{Cl} = \mu_{Cl}^\circ(T,P)_{solid} + RT \ln \frac{\theta_{Cl}}{1 - \theta_{Cl}} - \psi_{Cl}F \quad (11)$$

where definitions of terms are analogous to those given for H^+ and the chloride ions are in a region of electrostatic potential ψ_{Cl}. For chloride ions in solution, the equation corresponding to eq 5 for H^+ ions (with analogous definitions of terms) is

$$\mu_{Cl} = \mu^\circ(T,P)_{soln} + RT \ln y_{Cl}(Cl^-) \quad (12)$$

Equating the chemical potential of Cl^- in solution and surface phases at equilibrium leads to

$$RT \ln \frac{\theta_{Cl}}{1 - \theta_{Cl}} = -\Delta\mu_{Cl} + RT \ln y_{Cl}(Cl^-) + \psi_{Cl}F \quad (13)$$

where $\Delta\mu_{Cl}$ is the change in standard chemical potential of Cl^- during adsorption.

If eq 6 and 13 are added and it is assumed that the number of sites for H^+ and Cl^- are equal, *i.e.*, $\theta_H = \theta_{Cl}$, then the equation obtained is

$$2RT \ln \frac{\theta_H}{1 - \theta_H} = -(\Delta\mu_H + \Delta\mu_{Cl}) + RT \ln (H^+)(Cl^-) - F(\psi_H - \psi_{Cl}) \quad (14)$$

Activity coefficients have been omitted in view of the approximation made in relation to use of the potential difference $(\psi_H - \psi_{Cl})$.[11] Equation 14 may be rewritten in the form

$$\frac{\theta_H}{1 - \theta_H} = k_{H^+}\sqrt{(H^+)(Cl^-)}\exp\left[-\frac{F}{2RT}(\psi_H - \psi_{Cl})\right] \quad (15)$$

(8) P. J. Anderson, *Trans. Faraday Soc.*, **54**, 130 (1958).

(9) J. T. Davies, *Proc. Roy. Soc.* (London), **A245**, 417 (1958).

(10) J. Th. G. Overbeek in "Colloid Science," Vol. I, H. R. Kruyt, Ed., Amsterdam, 1952, Chapter IV.

(11) E. A. Guggenheim, "Thermodynamics," North-Holland Publishing Co., Amsterdam, 1959, Chapter 9.

in which

$$k_{H^+} = \exp\left[\frac{-(\Delta\mu_H + \Delta\mu_{Cl})}{2RT}\right]$$

Two further approximations are then made. If V_{H^+}, the maximum number of sites available for H^+, is large compared with Γ_{H^+}, then $\theta_H/1 - \theta_H \simeq \Gamma_{H^+}/V_{H^+}$. Secondly, it is assumed that Γ_{H^+}, the surface excess of H^+, is a linear function of the potential difference $(\psi_H - \psi_{Cl})$. The simplest approximation that $\psi_H = \psi_{Cl}$, which was used by Gilbert and Rideal,[6] does not prove useful in this case.

The equation to be tested is

$$\Gamma_{H^+} = k_{H^+}V_{H^+}\sqrt{(H^+)(Cl^-)}\exp(-K_1\Gamma_{H^+}) \quad (16)$$

in which K_1 is an interaction constant which is inversely proportional to surface area A. Dimensions are microequivalents^{-1} gram for K_1, and moles liter^{-1} for k_{H^+}. The linear form for eq 16 is

$$\log \Gamma_{H^+} + {}^1/_2\text{pH} = \log k_{H^+}V_{H^+} + {}^1/_2 \log (Cl^-) - \frac{K_1\Gamma_{H^+}}{2.303} \quad (17)$$

which is tested in Figures 4 and 5 for hematite no. 24.3.65 and goethite no. 27.7.65, having approximately obtained Γ_{H^+} from $\Gamma_{H^+} - \Gamma_{OH^-}$ data (Figures 1 and 2). The intercepts $\log k_{H^+}V_{H^+} + {}^1/_2 \log (Cl^-)$ should form a straight line of unit slope when plotted as a function of ${}^1/_2 \log (Cl^-)$ (see Figure 6). Both requirements appear to be satisfied. Some values of the constants K_1 and $k_{H^+}V_{H^+}$ are given in Table I.

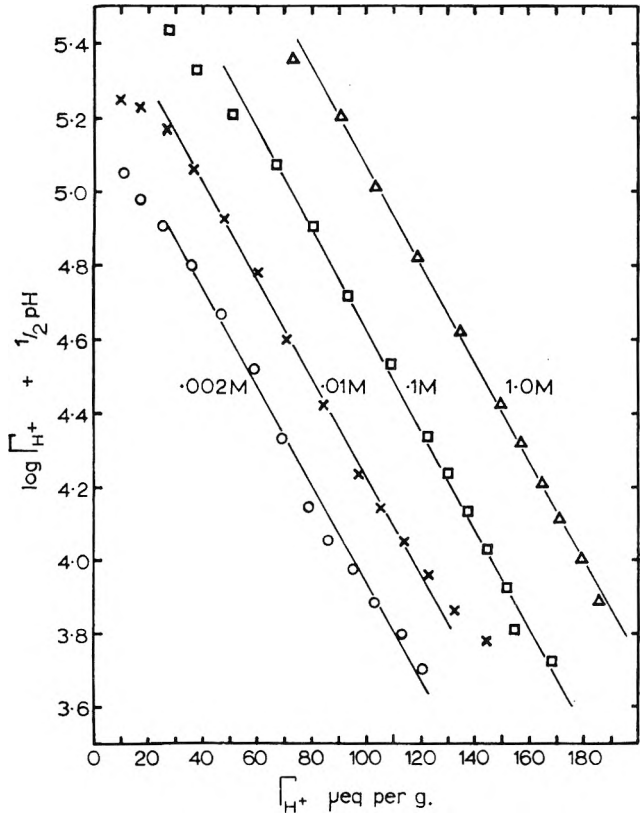

Figure 4. Hematite no. 24.3.65. Plots of eq 17 on the acid side of the zpc.

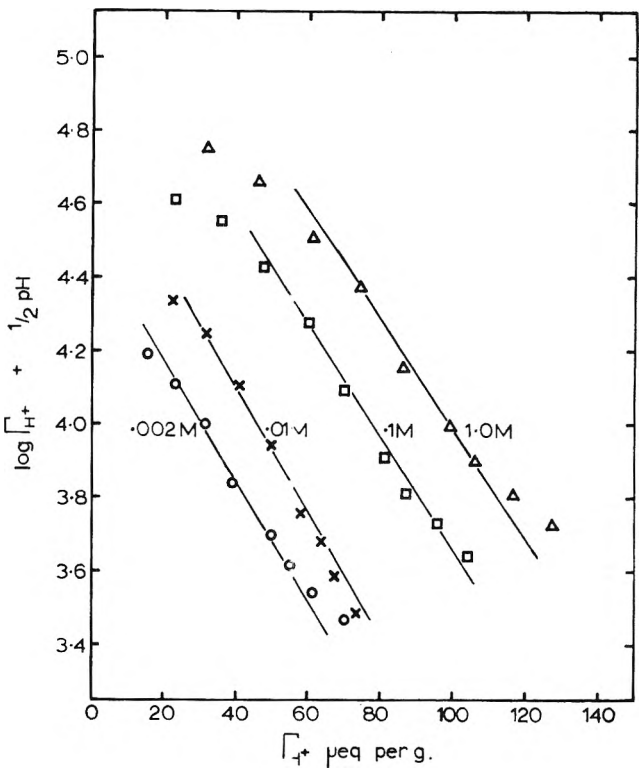

Figure 5. Goethite no. 27.7.65. Plots of eq 17 on the acid side of the zpc

Recalculation of isotherms requires constants for the corresponding equation on the alkaline side of the zpc, *viz.*

$$\Gamma_{OH^-} = k_{OH^-}V_{OH^-}\sqrt{(K^+)(OH^-)}\exp(-K_2\Gamma_{OH^-}) \quad (18)$$

in which Γ_{OH^-}, the magnitude of the surface excess of OH^-, is small compared with V_{OH^-}, the maximum number of sites for OH^-. Other symbols are analogous to those in eq 16. The linear form is

$$\log \Gamma_{OH^-} - {}^1/_2\text{pH} = {}^1/_2 \log K_w + \log k_{OH^-}V_{OH^-} + {}^1/_2 \log (K^+) - \frac{K_2\Gamma_{OH^-}}{2.303} \quad (19)$$

in which K_w is the appropriate dissociation constant for water.

However, the approximations made to evaluate constants on the acid side of the zpc are not suitable for the restricted range of Γ_{OH^-} values on the alkaline side

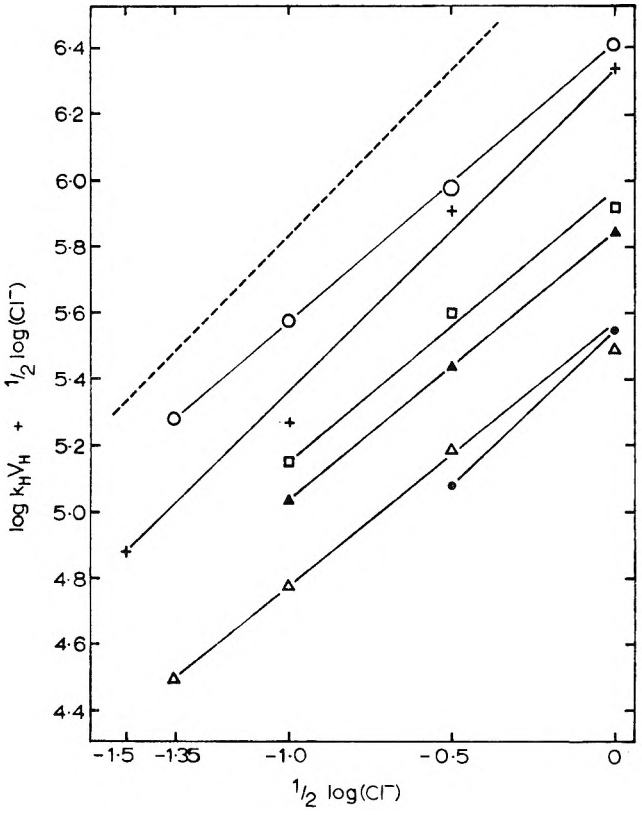

Figure 6. Plots of the intercepts log $k_H V_H$ + $^1/_2$ log (Cl$^-$) as a function of $^1/_2$ log (Cl$^-$) (see eq 17): ○, hematite no. 24.3.65; +, hematite, Albrethsen, ref 4; □, hematite no. 10.2.65; ▲, hematite no. 2; △, goethite no. 27.7.65; ●, hematite no. 22.7.64. The dashed line gives the theoretical slope.

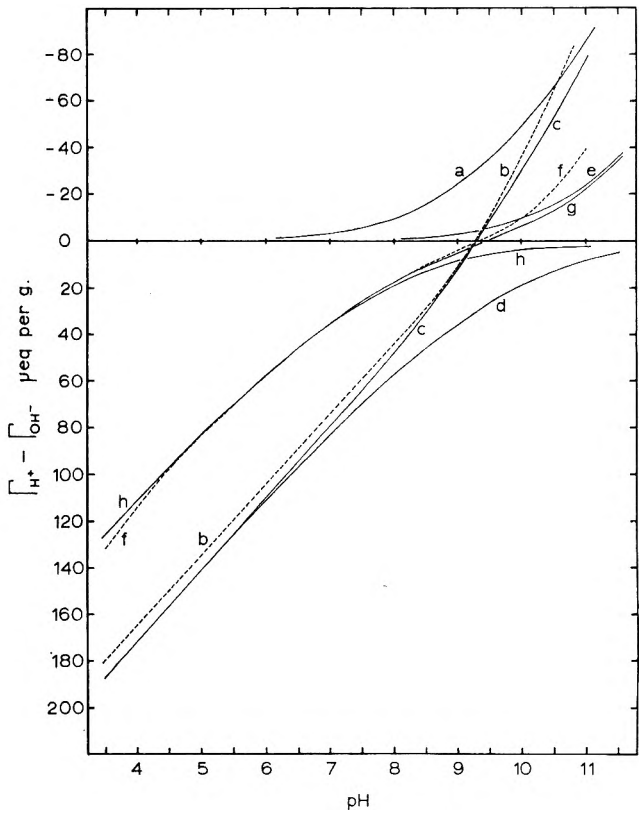

Figure 7. Recalculation of adsorption density as a function of pH and molar concentration of KCl, for hematite no. 24.3.65. Dashed curves are the original experimental data. Solid curves have been calculated from eq 17 and 19 using the parameters: K_1 = 0.0309; K_2 = 0.0165; log $k_H V_H$ = 6.53; $^1/_2$ log K_w + log $k_{OH} V_{OH}$ = −2.95. a, Γ_{OH^-}, 1.0 *M* KCl (calcd); b, $\Gamma_{H^+} - \Gamma_{OH^-}$, 1.0 *M* KCl (exptl); c, $\Gamma_{H^+} - \Gamma_{OH^-}$, 1.0 *M* KCl (calcd); d, Γ_{H^+}, 1.0 *M* KCl (calcd); e, Γ_{OH^-}, 0.01 *M* KCl (calcd); f, $\Gamma_{H^+} - \Gamma_{OH^-}$, 0.01 *M* KCl (exptl); g, $\Gamma_{H^+} - \Gamma_{OH^-}$, 0.01 *M* KCl (calcd); h, Γ_{H^+}, 0.01 *M* KCl (calcd).

of the zpc. Γ_{OH^-} could not be satisfactorily approximated by the measured ($\Gamma_{H^+} - \Gamma_{OH^-}$). The method chosen to obtain approximations for $k_{OH^-}V_{OH^-}$ and K_2 was to plot log $|\Gamma_{H^+} - \Gamma_{OH^-}| - {}^1/_2$pH as a function of $|\Gamma_{H^+} - \Gamma_{OH^-}|$ and fit straight lines having the intercepts predicted from the empirical equation for the acid side and the zero point of charge pH. Some values for K_2 are given in Table I.

The form of calculated isotherms is shown in Figure 7. These were obtained by solving the equations for pH, using the appropriate constants, at various values of Γ_{H^+} or Γ_{OH^-}, and then obtaining the ($\Gamma_{H^+} - \Gamma_{OH^-}$) curve by graphical interpolation.

Agreement between calculated isotherms and experiment (Figure 7) may be improved by introducing mean ionic activity coefficients for KCl[12] when evaluating the constant $k_{H^+}V_{H^+}$ from the intercepts log $k_{H^+}V_{H^+}$ + $^1/_2$ log (Cl$^-$). For the present purposes, isotherms have been recalculated using arithmetic mean values of $k_{H^+}V_{H^+}$ obtained without applying an activity coefficient to $^1/_2$ log (Cl$^-$). Under these circumstances, the agreement between recalculated isotherms and experiment is considered to be satisfactory.

Model of the Ferric Oxide–Aqueous Electrolyte Interface. The assumption that Γ_{H^+} is a linear function of a potential difference ($\psi_H - \psi_{Cl}$) made in obtaining eq 16 implies that the capacity of the double layer is a constant. Use of the relationship between σ and δ the thickness of a Stern layer[13]

$$\sigma = \frac{\epsilon'}{4\pi} \frac{(\psi_0 - \psi_\delta)}{\delta} \qquad (20)$$

where ϵ' is the dielectric constant within the Stern layer, should enable approximate calculation of the

(12) R. A. Robinson and R. H. Stokes, "Electrolyte Solutions," 2nd ed, Butterworth and Co. Ltd., London, 1959.

(13) J. T. Davies and E. K. Rideal, "Interfacial Phenomena," Academic Press, London, 1961, p 89.

interaction constants K_1 and K_2. ψ_0 is identified with ψ_H, ψ_δ with ψ_{Cl}, and Γ_{H^+}/A with σ. The expression obtained on evaluating constants at 293°K is

$$K = \frac{4\pi F\delta}{2RT\epsilon' A} = \frac{2.16 \times 10^5 \delta}{\epsilon' A}\ \mu\text{equiv}^{-1}\ \text{g} \qquad (21)$$

A is expressed in square centimeters per gram and δ is expressed in Angstrom units. δ is the average distance, in the direction normal to the surface plane, between the plane of surface charge and the plane of average approach of the centers of solvated counterions. Values for δ and ϵ' are not known; however, the correct magnitude for K is obtained on taking reasonable assumed values. For example, calculation using $\delta = 0.5$ A and a value[14] of $\epsilon' = 6$ for water at dielectric saturation, leads to $K_1 \simeq 0.04$ for hematite no. 24.3.65 of BET nitrogen area 44.5×10^4 cm^2 g^{-1}, compared with the experimental value $K_1 = 0.03$.

It is possible that both ϵ' and δ decrease with increasing surface charge while their ratio remains approximately constant. The hydrated ferric oxide surface is likely to have a sufficiently irregular configuration to permit small values of δ, of the order of 0.2 to 2 A, by "embedding" of the solvated counterions. The variation in values of the interaction constants K (Table I) for different hematite preparations may be understood qualitatively by consideration of the structural nature of the surface.

In the bulk of hematite crystals, each ferric ion is surrounded by a distorted octahedral arrangement of oxygen ions, but in the surface phase of crystals in aqueous suspension the coordinated species may be oxygen ions, hydroxyl ions, or water molecules. Ferric ions at the surface are partially solvated and the surface phase consists of polymerized derivatives of ferric hydroxo complex ions with coordinated water molecules and hydroxyl ions behaving as proton donors and acceptors. Although protons are probably relatively mobile within the surface phase, extension of the proton-excess (or proton-deficit) charge into the crystal lattice proper probably involves only a small fraction of the excess protons and would be limited to small distances of the order of 2 to 5 A. Little information is available on the effect of drying,[15] but the surface phase found on precipitated hematite crystals is probably lost by mild drying to $p/p_0 = 0.95$.

In the preparation methods used here for hematite, the final stage of crystal growth occurs when the pH of the refluxed suspension is increased during washing to remove HNO_3, causing precipitation of the high solution content of ferric ions which exists at very acid pH. Washing by dialysis is thought to complete crystal growth under conditions of high surface charge with slow attachment of ferric ions of the form $Fe(OH)(H_2O)_5^{2+}$ or $Fe(OH)_2(H_2O)_4^+$, resulting in a well-ordered surface. Poorly ordered surfaces with relatively greater inclusion of water molecules result from KOH washing which completes crystal growth by rapid attachment of polymerized derivatives of ferric ions under conditions of slight surface charge. These considerations suggest the average distance of closest approach of counterions is likely to vary for different ferric oxide preparations. This factor is proposed as the cause of differences in values of the interaction constant K which remain after multiplication by surface area A. That is, $\epsilon' AK$ is proportional to δ considering ϵ' to be a characteristic constant for all systems and considering relative values of A to be represented by the BET nitrogen area. Hematite preparations washed by KOH would thus be expected to have smaller values for AK_1 than hematites washed by distilled water dialysis only, as closer penetration of Cl^- counterions could occur into a more disordered surface structure compared with surface structures in dialyzed preparations. However, in Table I the relationship between the interaction constant K and the washing method is not clear. This suggests that the suitability of the BET nitrogen area for representing relative surface areas should be examined.

The similarity of the interaction constants K_1 and K_2 for positive and negative charges is considered to reflect similar distances of approach for Cl^- and K^+ counterions. Under the pH conditions of these experiments, chloride ions or nitrate ions do not enter the first coordination shells of ferric ions, although it is possible that water molecules are shared between Fe^{3+} coordination shells and Cl^- hydration spheres. The binding of solvated K^+, Cl^-, or NO_3^- counterions is largely electrostatic in origin and arises from the requirements for electroneutrality in the surface phase. Anions such as phosphate which are desolvated and specifically adsorbed by ferric oxides are considered to form a new potential determining layer by ligand exchange reactions with OH^- or H_2O in the ferric first coordination shell.

In view of the approximations necessary to evaluate the constants of eq 14 and 16, the agreement of these equations with experiment is considered satisfactory. The approximations made to eliminate the electrical potential terms appear to be suitable for the ferric oxide–aqueous electrolyte interface. Since the equations neglect the presence of counterions in the diffuse

(14) J. O'M. Bockris, M. A. V. Devanathan, and K. Müller, *Proc. Roy. Soc.* (London), **A274**, 55 (1963).

(15) J. J. Jurinak, *J. Colloid Sci.*, **19**, 447 (1964).

layer or Gouy layer by equating θ_H and θ_{Cl}, it is suggested that under these conditions the proportion of counterions in the diffuse layer is small, and surface potentials are reduced as a result of ion binding between counterions and the surface.[16] Electrokinetic phenomena, determined by the small proportion of counterions in the diffuse layer, are not expected to give reliable calculations of amounts of adsorbed ions under the conditions of ionic strength used here.

The considerable extent of ion-pair binding[16] of counterions is suggested to be primarily related to the closeness of counterion approach which is possible under the conditions of ferric ion solvation at the interface. The electrostatic interaction is then large compared with the thermal energy of ions. An alternative suggestion[6] is that for large particles, of "microscopic" rather than "atomic" dimensions, only a very small fractional dissociation of counterions is required to give large electrostatic interactions relative to the thermal energies of the particle and counterions, when surface densities of charge are not low.

Acknowledgments. Scholarship assistance received by R. J. Atkinson from the Australian Agricultural Council and the Commonwealth Scientific and Industrial Research Organization is gratefully acknowledged.

(16) D. G. Edwards, A. M. Posner, and J. P. Quirk, *Trans. Faraday Soc.*, **61**, 2808 (1965).

Reaction of $NO(A^2\Sigma^+)$ with Carbon Dioxide

by Norman Cohen and Julian Heicklen

Aerospace Corporation, El Segundo, California *(Received July 21, 1966)*

In the presence of CO_2, $NO(A^2\Sigma^+)$ was produced by irradiation of NO–CO_2 mixtures with a cadmium arc. The products monitored were N_2, whose yield dropped as the $(CO_2):(NO)$ ratio was enhanced, and CO, whose yield rose with the $(CO_2):(NO)$ ratio to a constant upper limit. Product formation was unaffected by temperature changes (23–300°) or by the addition of xenon or NO_2. The results are explained by the simple competition $NO(A^2\Sigma^+) + NO \rightarrow N_2 +$ other products and $NO(A^2\Sigma^+) + CO_2 \rightarrow NO_2 + CO$. Carbon dioxide is about 3.4 times more efficient than NO in the competition.

I. Introduction

As part of a continuing program in our laboratory on the reactions of $NO(A^2\Sigma^+)$, we have examined its reaction with CO_2. Fluorescence quenching of the $A^2\Sigma^+$ state of NO by CO_2 has been studied in a number of laboratories,[1-5] and the quenching constant is reasonably well known. It is very large ($\sim 10^{11}$ M^{-1} sec^{-1}), and it has been suggested that chemical reaction may occur.[1] However, as far as we know, no detailed study of product formation has been made prior to our work.

II. Experimental Details

The quartz reaction vessel was 10 cm long and 5 cm in diameter. It was jacketed in a wire-wound furnace

(1) A. V. Kleinberg and A. N. Terenin, *Dokl. Akad. Nauk SSSR*, **101**, 1031 (1955).

(2) N. Basco, A. B. Callear, and R. G. W. Norrish, *Proc. Roy. Soc.* (London), **A260**, 459 (1961).

(3) R. Young and R. Sharpless, *Discussions Faraday Soc.*, **33**, 228 (1962).

(4) A. B. Callear and I. W. M. Smith, *Trans. Faraday Soc.*, **59**, 1720 (1963).

(5) H. Broida and T. Carrington, *J. Chem. Phys.*, **38**, 136 (1963)

that overlapped each end by 2.5 cm. Temperature measurements were taken by a thermocouple; the temperature remained constant throughout a run to within a few degrees. Both ends of the furnace were covered with quartz plates to minimize heat loss by convection. The optical source was a quartz-jacketed, cadmium spectral lamp from the Philips Co., Type 93107. The effective radiation was at 2144 and 2265 A. Before entering the reaction cell, the radiation passed through a sodium chloride filter sandwiched between quartz plates. This effectively removed radiation below 2050 A.

The gases used were from the Matheson Co. The xenon and oxygen were used directly from the cylinder without further purification. The CO_2 was degassed twice at $-196°$ before use. The nitric oxide was degassed twice at $-196°$; it was then warmed to $-186°$ by liquid argon. The fraction not retained by liquid argon was collected and used. In this way, NO_2 and most of the N_2O, both of which were impurities in the NO, were excluded from the reaction mixture. The N_2O was reduced to about 0.01% of the NO.

After irradiation of pure nitric oxide, the cell gases were expanded into the vacuum line through a trap frozen in solid nitrogen. On the far side of the trap was a McLeod gauge that read the pressure of the noncondensable gases—nitrogen plus carbon monoxide. The gases were then collected by a Toepler pump for analysis on a Loe Engineering Co. gas chromatograph employing a 4-ft column of 30–60-mesh, 5-A molecular sieves. Some oxygen appeared in the chromatograms because of air in our sampling system. Appropriate corrections, based on the oxygen, were made to the nitrogen peak.

The absorption of the 2144-A line of the cadmium lamp was measured by monitoring the light passing through the reaction cell. A Bausch and Lomb ultraviolet monochromator, Model No. 33-86-01, with a 2700-groove/mm grating, in conjunction with an RCA 6903 photomultiplier tube, was placed at the exit window of the cell. The monochromator slit width was 24 A. The light from the lamp was attenuated with an iris diaphragm to ensure that the photomultiplier was operating in the linear region.

III. Results

Periodically throughout the study, pure NO was photolyzed and the rate of N_2 production, $R_0(N_2)$ (the subscript 0 means that CO_2 was absent), was measured. The results are shown in Figure 1. For low NO pressures, $R_0(N_2)$ rises with (NO), but then becomes constant as (NO) exceeds 150 mm. For NO pressures in excess of a few millimeters, first-order

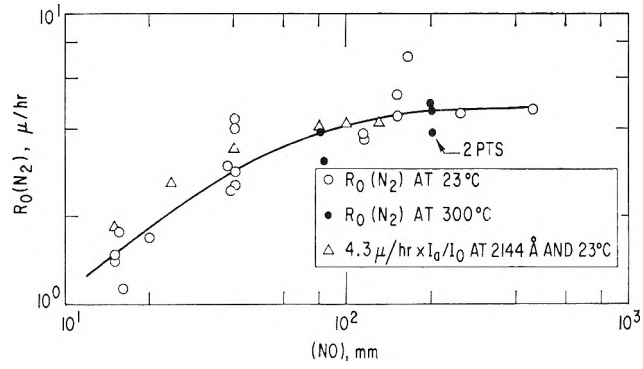

Figure 1. Plot of $R_0(N_2)$ *vs.* (NO).

processes (*i.e.*, fluorescence) removing NO($A^2\Sigma^+$) are unimportant; NO($A^2\Sigma^+$) is quenched by collision, resulting in N_2 production (as well as other products).[4,6] Furthermore, the N_2 yield is independent of pressure.[6] Consequently, the falloff in $R_0(N_2)$ at lower NO pressures reflects the fact that all the incident radiation was not absorbed, in agreement with earlier work.[6] $R_0(N_2)$ is proportional to the absorbed intensity, I_a.

To check this conclusion, the ratio of absorbed intensity to incident intensity, I_0, at 2144 A was directly measured. The data, normalized to fit $R_0(N_2)$, are shown in Figure 1, and they nearly fit the data for R_0 (N_2). That the fit is not exact is not surprising, as the radiation at both 2265 and 2144 A is responsible for $R_0(N_2)$. We were unable to measure the absorption characteristics at 2265 A because the intense cadmium line at 2288 A interfered. However, previous results[6] indicated that the absorption coefficients at both lines were similar.

The agreement for $R_0(N_2)$ at different temperatures is strictly fortuitous, but does agree with earlier unpublished work in our laboratory. There is no reason why the results at elevated temperature should coincide with those at lower temperatures; in fact, on a molar basis, they do not. Apparently, the concentration variation at different temperature is balanced by the temperature broadening of the absorption lines. Nevertheless, the fortuitous agreement facilitates calibration.

When irradiated with the cadmium arc, N_2 and CO were found in the fraction noncondensable at solid-nitrogen temperature ($-212°$). Mixtures of CO_2 and NO, or pure NO, gave a small amount of N_2 (*i.e.*, $\sim$0.2 μ/hr) with no irradiation. This must have been the result of a leak (the O_2 would react with the NO). All the reported N_2 values (with irradiation) have been corrected for this leak. Except when the (CO_2):(NO)

(6) J. J. McGee and J. Heicklen, *J. Chem. Phys.*, **41**, 2974 (1964).

Table I: Photolysis of NO–CO_2 Mixtures at 23°

$(CO_2)/(NO)$	(NO), mm	(CO_2), mm	Exposure time, hr	$R(N_2)/R_0(N_2)$	$R(CO)/R_0(N_2)$	$R(CO)/R(N_2)$
0.0105	777	8.15	15.50	0.92	0.29	0.31
0.0144	597	8.6	16.00	0.92	0.38	0.40
0.0177	482	8.5	15.50	0.91	0.40	0.44
0.023	405	9.37	15.20	0.60	0.72	1.24
0.026	528	14	6.33	0.80	0.84	1.05
0.030	466	14	6.00	0.91	0.86	0.94
0.031	298	9.25	5.50	0.97	0.74	0.76
0.036	280	10.2	5.50	0.90	0.81	0.90
0.044	480	21	5.25	0.44	0.47	1.07
0.084	111	9.35	15.5	0.63	1.15	1.83
0.103	261	27	5.16	...	...	1.86
0.139	144	20	5.00	0.91	3.0	3.3
0.26	20.7	5.3	15.00	0.44	2.6	5.9
0.26	70	18	20.75	0.53	2.7	5.1
0.26	556	147	14.50	0.82	4.0	5.0
0.28	113	31.5	...	...	...	5.6
0.28	476	135	5.00	0.69	4.0	5.8
0.30	163	49	15.75	0.67	3.6	5.3
0.30	16.5	5.0	15.50	0.45	2.8	6.3
0.305	468	143	5.83	0.89	5.2	5.8
0.31	486	149	6.00	0.72	4.5	6.0
0.31	60	18.5	5.50	0.41	4.2	10.2
0.31	154	48	15.00	0.56	3.4	6.0
0.32	500	159	6.00	1.13	4.1	3.6
0.32	14.4	4.65	6.00	0.59	3.1	5.2
0.33	15.5	5.05	14.25	0.60	3.9	6.6
0.37	407	150	4.50	1.30	4.8	3.7
0.42	47	20	15.00	...	...	7.8
0.62	243	152	8.00	0.49	5.5	11.3
1.25	40	50	20.00	0.56	6.3	11.1
1.47	38	56	16.75	0.39	7.4	19.1
3.9	114	443	5.33	0.23	8.8	36
5.2	44	231	5.50	...	9.6	...
5.5[a]	40	220	14.50	0.046	9.4	204
6.0	40	240	16.16	0.26	12.8	50
7.1	15.0	108	7.75	0.114	16.5	144
9.2	81	743	4.00	...	9.2	...
9.3	82	758	16.00	...	8.2	...
9.7	80	774	16.00	...	8.5	...
12.0	40	480	4.00	0.145	12.3	85
19.7	15	296	5.50	...	11.7	...
34	15	509	5.00	...	13.4	...
41	15	607	14.50	...	12.0	...
44	15.5	692	16.00	...	13.3	...

[a] Also 0.24 mm of NO_2 present.

ratio was greater than 1, the correction was negligible. Pure CO_2 was irradiated and no products were found other than those caused by air leakage.

The room-temperature results are listed in Table I. Below about 15 mm of NO, pressure broadening of the absorption is pronounced (see ref 6 and the references quoted therein). Therefore, below 15 mm of NO, measurements were not made. For higher pressures of NO, $R(N_2):R_0(N_2)$, as well as $R(CO):R_0(N_2)$, is tabulated. The values used for $R_0(N_2)$ are from the curve in Figure 1. The results are a function of the $(CO_2):(NO)$ ratio only. As the ratio increases from zero to infinity, $R(N_2):R_0(N_2)$ drops from unity to zero, $R(CO):R_0(N_2)$ rises from 0 to about 12, and $R(CO):R(N_2)$ increases from zero toward infinity. One run was performed wherein 0.12 mm of O_2 was mixed with the reactants to yield 0.24 mm of NO_2. The results were not noticeably altered.

Table II lists $R(CO):R(N_2)$ for runs in which a large excess of xenon was present. This ratio is essentially unaffected by the presence of xenon. $R(N_2):R_0(N_2)$ and $R(CO):R_0(N_2)$ are not tabulated for two reasons. First, some xenon is present in the noncondensable fraction at −212°, thus complicating the analysis. Second, the xenon pressure broadens the absorption spectrum.

In Table III are listed results at elevated temperatures. They are the same as those at room temperature.

Table II: Photolysis of NO–CO_2 Mixtures at 23° in the Presence of Xenon

$(CO_2)/(NO)$	(NO), mm	(CO_2), mm	(Xe), mm	Exposure time, hr	$R(CO)/R(N_2)$
0.135	36.1	4.9	568	21.00	3.0
0.190	25.2	4.8	770	17.50	3.6
0.218	43.5	9.5	728	19.00	4.6
2.81	6.95	19.05	489	16.00	52
2.94	7.1	20.9	777	20.00	74
2.96	22	65	605	...	32
3.23	6.74	21.3	601	16.25	56
3.44	8.8	30.2	615	15.00	24
4.83	8.5	41	660	...	32
6.6	20	132	558	17.50	52

IV. Discussion

In the absence of CO_2 the mechanism is[6,7]

$$NO + h\nu\begin{pmatrix}2265\ A\\2144\ A\end{pmatrix} \longrightarrow NO^* \quad (1)$$

$$NO^* + NO \xrightarrow{2NO} N_2 + 2NO_2 \quad (2a)$$

$$NO^* + NO \longrightarrow N_2O + O \xrightarrow{NO} NO_2 \quad (2b)$$

$$NO^* + NO \longrightarrow 2NO \quad (2c)$$

where NO* is the $A^2\Sigma^+$ state of NO in either its ground vibrational level (2265 A) or its first vibrational level (2144 A). Reaction 2a may proceed through two kinetically indistinguishable routes

$$NO^* + NO \longrightarrow N_2 + O_2 \xrightarrow{2NO} 2NO_2$$

$$NO^* + NO \longrightarrow NO_2 + N \xrightarrow{NO} N_2 + O \xrightarrow{NO} NO_2$$

If the second route is important, then nitrogen atoms as well as oxygen atoms will be present.

In the presence of CO_2, additional quenching reactions must be considered

$$NO^* + CO_2 \longrightarrow NO + CO_2 \quad (3a)$$

$$NO^* + CO_2 \longrightarrow NO_2 + CO \quad (3b)$$

Table III: Photolysis of NO–CO_2 Mixtures at Elevated Temperature

$(CO_2)/(NO)$	(NO), mm	(CO_2), mm	Exposure time, hr	$R(N_2)/R_0(N_2)$	$R(CO)/R_0(N_2)$	$R(CO)/R(N_2)$
			$T = 200 \pm 5°$			
0.027	382	10.3	6.50	0.81	0.64	0.79
0.029	350	10.1	15.5	...	...	0.58
0.044	350	15.5	5.25	1.19	0.81	0.68
0.088	113	10	16.25	0.75	1.02	1.36
0.155	100	15.5	15.50	0.58	1.63	2.83
6.45	62	400	4.50	0.069	8.3	120
			$T = 300 \pm 5°$			
0.087	116	10.15	15.30	0.51	0.93	1.82
5.20	106	544	6.50	0.104	8.0	77
5.34	120	640	16.50	0.063	6.7	116
9.47	70	663	15.16	0.030	7.5	250
10.42	70	730	5.50	...	7.9	...

The pressure broadening of the NO absorption at 2144 A induced by CO_2 and Xe is shown in Table IV. The effect is marked, and about 200 mm of either CO_2 or Xe doubles the light absorbed by 15 mm of NO. Data at 2265 A could not be obtained because of the interference of the intense 2288-A line of cadmium. Presumably the effect would be similar.

Also to be considered are possible atom reactions with CO_2

$$O + CO_2 \longrightarrow O_2 + CO$$

$$N + CO_2 \longrightarrow NO + CO$$

(7) J. Heicklen, *J. Phys. Chem.*, **70**, 2456 (1966).

Table IV: Pressure Broadening of NO Absorption at 2144 A and 23°; (NO) = 15 mm

(M), mm	I_a/I_0
M = CO_2	
0	0.43
28	0.65
44	0.72
65	0.76
110	0.83
130	0.85
153	0.87
215	0.91
360	0.95
580	0.98
M = Xe	
0	0.49
31	0.69
53	0.78
100	0.84

The oxygen atom reaction with CO_2 is endothermic by 9 kcal/mole and cannot be important. However, to check the possibility, we performed one run with 0.24 mm of NO_2 present. This is more NO_2 than was present at the termination of any of the other runs. The NO_2 absorbs radiation above 3000 A to produce oxygen atoms. Furthermore, NO_2 is a product of the photolysis of NO. The results with the NO_2 present were not significantly different from those without it. The reaction of nitrogen atoms with CO_2 is very slow ($k < 10^3\ M^{-1}\ \text{sec}^{-1}$ at 25°) and proceeds with an activation energy in excess of 8 kcal/mole.[8] Consequently it should not be important, especially since the N + NO reaction is fast ($k = 10^{10}\ M^{-1}\ \text{sec}^{-1}$).

On the other hand, the atoms produced from reaction 2 may have excess energy. The nitrogen atoms could have up to 42 kcal/mole and the oxygen atoms up to 72 kcal/mole. To check the possibility of hot-atom reactions, we performed runs with excess xenon present. The results were unaffected, and we conclude that hot-atom reactions are not significant.

We have measured two independent quantities: $R(\text{CO})$ and $R(\text{N}_2)$. However, the ratio of these quantities will be more reliable than either quantity alone, since any variation in absorbed intensity (because of either pressure broadening or change in incident intensity) has the same effect on both rates. Therefore, we use the ratio as one of our measured parameters. For the other, we prefer $R(\text{CO}):R_0(\text{N}_2)$ instead of $R(\text{N}_2):R_0(\text{N}_2)$ for three reasons. First, the CO analysis is more reliable than the N_2 analysis because the air

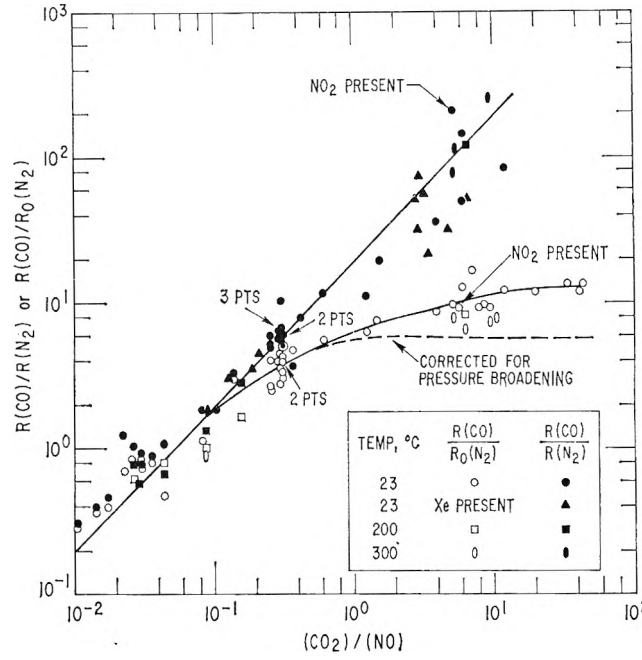

Figure 2. Plots of $R(\text{CO}):R(\text{N}_2)$ and $R(\text{CO}):R_0(\text{N}_2)$ *vs.* $(\text{CO}_2):(\text{NO})$.

leakage necessitated corrections for the N_2 analysis. Second, it is $R_0(\text{N}_2) - R(\text{N}_2)$ that is significant. For large $R(\text{N}_2)$, the difference in two comparable numbers introduces large errors, whereas for small $R(\text{N}_2)$, the experimental analysis has a large uncertainty. Third, $R(\text{CO}):R_0(\text{N}_2)$ varies with conditions from 0 to 12, whereas $R(\text{N}_2):R_0(\text{N}_2)$ only varies from 0 to 1.

The mechanism predicts that

$$\frac{R(\text{CO})}{R(\text{N}_2)} = \frac{k_{3b}(\text{CO}_2)}{k_{2a}(\text{NO})} \tag{4}$$

$$\frac{R(\text{CO})}{R_0(\text{N}_2)} = \frac{k_2}{k_{2a}} \frac{k_{3b}(\text{CO}_2)}{k_2(\text{NO}) + k_3(\text{CO}_2)} \tag{5}$$

where $k_2 = k_{2a} + k_{2b} + k_{2c}$ and $k_3 = k_{3a} + k_{3b}$. The quantities on the left-hand side of eq 4 and 5 are plotted *vs.* $(\text{CO}_2):(\text{NO})$ in Figure 2. The quantities are dependent only on the $(\text{CO}_2):(\text{NO})$ ratio, as predicted. They are independent of the individual reactant pressures, temperature, or the presence of NO_2 or xenon. For the $R(\text{CO}):R(\text{N}_2)$ data, the best straight line of slope unity is drawn on the log–log plot. The fit is quite good. The scatter at high $(\text{CO}_2):(\text{NO})$ reflects the uncertainty in the N_2 analysis for these conditions

Equation 5 predicts that $R(\text{CO}):R_0(\text{N}_2)$ should be similar to $R(\text{CO}):R(\text{N}_2)$ at small $(\text{CO}_2):(\text{NO})$ ratios. The data in Figure 2 verify this prediction. At high

(8) P. Harteck and R. Reeves, private communication, 1966.

$(CO_2):(NO)$, $R(CO):R_0(N_2)$ should be constant and equal to $k_2k_{3b}/k_{2a}k_3$. The data points in Figure 2 approach a constant upper limit of about 12. However, at high $(CO_2):(NO)$, pressure broadening is important and the absorbed intensity is enlarged. From the data in Table IV, the extent of pressure broadening can be estimated if we assume that the results at 2265 and 2144 A are comparable. The dotted line in Figure 2 shows the values of $R(CO):R_0(N_2)$ corrected for the pressure broadening. The constant upper limit is reduced from 12 to 5.8.

The rate-constant ratios are summarized in Table V. The values for k_{3b}/k_{2a} and $k_2k_{3b}/k_{2a}k_3$ are about 20 and 5.8, respectively. Now k_3 has been found[1-5] to be about 10^{11} M^{-1} sec^{-1}, which is a very large rate constant. Consequently one would expect, in accordance with Kleinberg and Terenin's suggestion,[1] that quenching is mainly by chemical reaction and that k_{3a} is negligible compared to k_{3b}. If so, then k_2/k_{2a} is about 5.8. This value is in excellent agreement with the value of 5.3 found in another study.[7] Combining the two ratios obtained from eq 5 gives a value of 0.29 for k_2/k_3. This value is in good agreement with the most reliable value[4] of 0.34 found by fluorescence quenching.

Table V: Summary of Rate-Constant Data

Ratio	Value	Source
k_{3b}/k_{2a}	20	Eq 4 and 5; Figure 2
$k_2k_{3b}/k_{2a}k_3$	5.8	Eq 5; Figure 2
k_2/k_{2a}	5.8	Assumes $k_3 = k_{3b}$
	5.3	Ref 7
k_2/k_3	0.29	Combination of first two ratios
	0.34	Ref 4
	0.93	Ref 5
	0.50	Ref 1

Acknowledgment. The authors wish to thank Mr. Richard Frey for assistance with the experiments, Dr. Sidney Benson for useful discussions, and Mrs. Barbara Peer for assistance with the manuscript. This work was supported by the U. S. Air Force under Contract No. AF 04(695)-669.

Calorimetric Study of Self-Association of 6-Methylpurine in Water[1]

by P. R. Stoesser and S. J. Gill

Department of Chemistry, University of Colorado, Boulder, Colorado *(Received July 22, 1966)*

A determination of the thermodynamics of self-association of 6-methylpurine in water has been made from heat of dilution measurements. Theoretical equations which relate the concentration dependence of the relative molal enthalpy are used to obtain one estimate of both the self-association constant, K, and the enthalpy of self-association, $\Delta H°$, from calorimetric data. The respective values are 8.6 ± 1.1 m^{-1} and −5.6 ± 0.2 kcal/mole. A second estimate of the enthalpy of self-association is made by a combination of heat of dilution data and osmotic coefficient data (Ts'o) to give a value of −6.3 ± 0.1 kcal/mole. An average value of $\Delta H°$ = −6.0 ± 0.4 kcal/mole is suggested from these values. With Ts'o's value of $\Delta G°$ = −1.1 kcal/mole a value of $\Delta S°$ = −16 ± 1 eu is obtained at 25°.

Introduction

The work of Ts'o and colleagues[2,3] has demonstrated that aqueous solutions of 6-methylpurine form complexes of various degrees of polymerization depending upon the total concentration. A stacked configuration is indicated from nuclear resonance data.[3,4] The forces which govern the formation of such complexes are of considerable interest both from a theoretical viewpoint[4,5] as well as their likely presence in stabilizing polynucleotide structures[6,7] and polynucleotide–nucleotide complexes.[7,8]

Determination of the vapor pressures as a function of temperature for a series of purine and pyrimidine compounds has provided a measure of the interaction forces in the crystal from the heats of sublimation.[9] Several recent spectroscopic studies on adenylic acid oligomers[10−12] in water have given estimates of the interaction enthalpy between purine rings of the order of −9 kcal mole^{-1}. In all of these studies a variety of effects may be present so that it is difficult to sort out the importance of various types of interactions.

The system of 6-methylpurine avoids some of these problems. It is uncharged. The equilibrium between various species can be considered to be characterized by a single equilibrium constant.[2] The mode of complexation has been indicated to be that of stacking.[3,4] It was felt that a direct calorimetric measurement of the enthalpy of association of the complex could provide relevant information on the particular interaction forces of this complex. Furthermore with the availability of enthalpy data the entropy of formation could be calculated by use of the equilibrium constant. In this way a complete thermodynamic description of the purine ring interaction for 6-methylpurine could be obtained.

Theory

The enthalpy of self-association for a dissolved compound can be determined from an analysis of heats of dilution using either additional equilibrium information[13] or assuming particularly simple reaction param-

(1) (a) Presented in part by P. R. Stoesser in a Ph.D. thesis, University of Colorado, 1966; (b) presented at the 40th National Colloid Symposium, University of Wisconsin, June 16, 1966.

(2) P. O. P. Ts'o and S. I. Chan, *J. Am. Chem. Soc.*, 86, 4176 (1964).

(3) S. I. Chan, M. P. Schweiger, P. O. P. Ts'o, and G. K. Helmkamp, *ibid.*, 86, 4182 (1964).

(4) O. Jardetzky, *Biopolymers Symp.*, 1, 501 (1964).

(5) B. Pullman, *J. Chem. Phys.*, 43, S233 (1965).

(6) D. M. Crothers and Bruno H. Zimin, *J. Mol. Biol.*, 9, 1 (1964).

(7) D. N. Holcomb and I. Tinoco, Jr., *Biopolymers*, 3, 121 (1965).

(8) M. N. Lipsett, L. A. Heppel, and D. F. Bradley, *J. Biol. Chem.*, 236, 857 (1961).

(9) L. B. Clark, G. G. Peschel, and I. Tinoco, Jr., *J. Phys. Chem.*, 69, 3615 (1965).

(10) J. Brahms, A. M. Michelson, and K. E. VanHolde, *J. Mol. Biol.*, 15, 467 (1966).

(11) K. E. VanHolde, J. Brahms, and A. M. Michelson, *ibid.*, 12, 726 (1965).

(12) M. Leng and G. Felsenfeld, *ibid.*, 15, 220 (1966).

eters. In either case one starts with the assumption that all heat effects upon dilution are due to dissociation of complex species. Furthermore, every complex is assumed to obey dilute solution laws. Both of these conditions are met at increasing dilution. Uncharged molecular species also obey dilute solution laws over a wider range of concentration than do ionic materials.

The various reaction equilibria are characterized by equations of the form

$$A + A_{n-1} = A_n \qquad (1)$$

with equilibrium constants K_n and enthalpies of reaction ΔH_n°. If the reaction stops with dimerization then n equals 2. If an unlimited number of reaction species is permitted then n can have all integer values from 2 on. The heat of infinite dilution, $-m\varphi_L$, is defined as the heat obtained when an m molal solution (1 kg of solvent) is diluted with an infinite amount of solvent. With the above assumptions we may write

$$m\varphi_L = (A_2)\Delta H_2^\circ + (A_3)(\Delta H_2^\circ + \Delta H_3^\circ) + \ldots \qquad (2)$$

where (A_n) is the molality of species A_n and the plus sign arises because the dilution process reverses the direction of the reaction of eq 1. With knowledge of the equilibrium constants K_n, $m\varphi_L$ can be expressed as

$$m\varphi_L = K_2(A)^2\Delta H_2^\circ + K_2K_3(A)^3(\Delta H_2^\circ + \Delta H_3^\circ) + \ldots \qquad (3)$$

The molality of the solution is given by

$$m = (A) + 2(A_2) + 3(A_3) + \ldots = (A) + 2K_2(A)^2 + 3K_2K_3(A)^3 + \ldots \qquad (4)$$

If the equilibrium constants are known then in principle these equations provide the means for obtaining ΔH_n° values from a set of φ_L measurements at various values of m. The practical difficulty of obtaining several equilibrium constants forces consideration of simpler cases.

We are particularly interested in the case of unlimited values on n where all equilibrium constants have the same value ($K_n = K$) and all enthalpies have the same value ($\Delta H_n^\circ = \Delta H^\circ$). The combination of eq 3 and 4 subject to these conditions yields the following result

$$\varphi_L = \Delta H^\circ - (\Delta H^\circ/K)^{1/2}(\varphi_L/m)^{1/2} \qquad (5)$$

The arrangement of this equation shows that upon plotting φ_L *vs.* $(\varphi_L/m)^{1/2}$ a straight line should result. From the value of the slope and intercept both K and ΔH° can be determined. It is of some interest to note that a straight-line plot of the parameters of eq 5 does not necessarily mean that a polymerization reaction occurs. For if one considers the case of simple dimerization, then one finds the following result

$$\varphi_L = (\Delta H^\circ/2) - {}^1/_2(\Delta H^\circ/K)^{1/2}(\varphi_L/m)^{1/2} \qquad (6)$$

where the only difference is the appearance of the factor of $^1/_2$ in the slope and intercept. Thus it is necessary to have auxillary information, such as that given by the osmotic coefficient, to assess whether a particular equation is applicable. To avoid sign problems in eq 5 or 6 it is simplest to use the absolute magnitude of φ_L and ΔH° and then recognize that the signs of φ_L and ΔH° are the same.

When osmotic coefficient data (φ) are available, as in the case of 6-methylpurine,[2] an alternate procedure is available.[14] For either of the two special cases of the preceding paragraph the value of ΔH° is given by

$$\Delta H^\circ = \varphi_L/(1 - \varphi) \qquad (7)$$

This result has been obtained before by Schellman[13] for the limiting case of polymer formation.

With the availability of two procedures for evaluating ΔH° values it should be possible to apply a test of the consistency of the assumptions upon which the equations are based, provided experimental data for heats of dilution and osmotic coefficients is available. In general one would expect the application of eq 7 to be more valid, particularly if an extrapolation can be made to very low concentrations, where dimerization becomes predominant.

Experimental Section

(*a*) *Materials.* Grade I 6-methylpurine was obtained from Cyclo Chemical Corp., Los Angeles, Calif. Tests by D. Lorusso on this material have shown that its spectroscopic properties remained unchanged upon sublimation. Solutions were prepared with distilled water in a series of dilutions of equal volumes of a given solution and water. These solutions correspond to the way in which dilutions within the calorimeter are performed.

(*b*) *Density Determinations.* In order to convert molarity to molality for the prepared solutions, density measurements were made using a 2-ml pycnometer with precision-bore (1-mm) side arms. Table I shows the solution densities along with concentrations of molality (m) and molarity (M).

(*c*) *Calorimetric Determinations.* Dilution measurements were made mixing equal volumes (0.1000 ml) of solution with water at 25° within a flow microcalo-

(13) J. A. Schellman, *Compt. Rend. Trav. Lab. Carlsberg*, **29**, No. 14 (1955).

(14) S. J. Gill, G. F. Sheats, and M. Downing, in preparation.

Table I: Concentrations 25°

Density, g/cc	M, moles/l.	m, moles/kg of solvent
1.0155	0.4758	0.5000
1.0072	0.2381	0.2442
1.0028	0.1194	0.1210
1.0007	0.0597	0.0602
1.0004	0.0299	0.0300
0.9994	0.01495	0.01500
0.9980	0.00748	0.00750
0.9979	0.00374	0.00375
0.9978	0.00187	0.00188

rimeter.[15] The endothermic heat of dilution was measured by electrical heating through calibrated resistors by means of a digital readout electronic controller.[16] The calibration of the electronic controller by both standard electrical calibration and calorimetric comparison with a direct current standard was accurate to 0.01%.

Mechanical heats of mixing pure water (0.1000 ml) with itself were found to average 15 ± 2 μcal. This value was subtracted from actual dilution runs to give a corrected heat of dilution. At least 30 runs were made for each solution. The reason for making so many runs on a given solution was to eliminate heat conduction errors by extrapolation to infinite loop gain of the servo system controller used.[16]

Results

The average heats, q_i, of equal volume dilution per number of moles of solute, n_i, are shown with the range of variation in Table II.

Table II: Heats of Dilution of 6-Methylpurine Solution with Water at 25°

Dilution, i	Initial concn, m	Final concn, m	q_i/n_i, cal/mole
1	0.5000	0.2442	617 ± 1
2	0.2442	0.1210	671 ± 2
3	0.1210	0.0602	653 ± 3
4	0.0602	0.0300	553 ± 6
5	0.0300	0.01500	402 ± 3
7	0.01500	0.00750	257 ± 7
8	0.00750	0.00375	158 ± 3
9	0.00375	0.00186	80 ± 14
10	0.00186	0.00093	48 ± 16

Since the values of q_i/n_i decrease linearly with concentration at the highest dilutions, the correction to infinite dilution is given by the last reliable dilution value. If we base this value on the ninth dilution step, then a heat of 80 ± 14 cal/mole would be expected for the process of going from 0.00186 to 0.00000 m.

The relative molal enthalpy, φ_L, is given by summing the terms q_i/n_i from the infinite dilution step to the step of the concentration that is applicable for φ_L. These values along with the factor $(\varphi_L/m)^{1/2}$ are tabulated at various concentrations in Table III.

Table III: Relative Molal Enthalpies of 6-Methylpurine in Water at 25°

m	$-\varphi_L$, cal/mole	$(\varphi_L/m)^{1/2}$	$1 - \varphi$ (Ts'o)[2]	$\Delta H°$ (eq 7), kcal/mole
0.5000	3471 ± 52	83 ± 1	0.543	−6.4 ± 0.1
0.2442	2854 ± 51	108 ± 1	0.452	−6.3 ± 0.1
0.1212	2183 ± 49	135 ± 2	0.346	−6.3 ± 0.1
0.0602	1530 ± 46	159 ± 3	0.242	−6.3 ± 0.2
0.0300	977 ± 41	180 ± 4		
0.01500	575 ± 38	196 ± 7		
0.00750	318 ± 31	205 ± 10		
0.00375	160 ± 28	207 ± 18		

A plot of the values given in Table III is shown in Figure 1. Within the range of errors indicated values of $\Delta H° = -5.6 \pm 0.2$ kcal/mole and $K = 8.6 \pm 1.1\ m^{-1}$ are found.

Discussion

The linear behavior shown in Figure 1 indicates that the assumptions used in deriving eq 5 or 6 are consistent with experimental findings. The use of the polymerization equation, eq 5, is based on the findings of Ts'o.[2] It might be noted that the determination of $\Delta H°$ by eq 5 is not as sensitive to error as is the value of K.

The range of error which we have assigned to our determination of K (8.6 ± 1.1) does not quite reach the value of 6.7 m^{-1} for K found by Ts'o. A range of error is not assigned by Ts'o. It is possible that if osmotic coefficients could be determined over a range comparable to the range of heats of dilution data, a higher value of K might be found. From the nature of the experimental technique Ts'o's measurements were limited to approximately 0.05 m concentration. In view of these considerations the K values seem quite plausible.

A calculation of $\Delta H°$ by the second approach, combining osmotic coefficient with heats of solution

(15) P. R. Stoesser and S. J. Gill, *Rev. Sci. Instr.*, in press.
(16) H. B. Albert and S. J. Gill, in preparation.

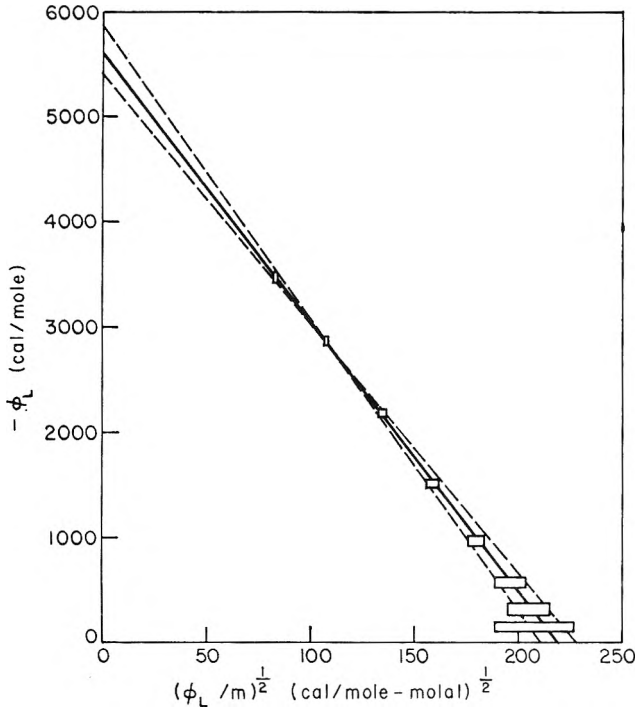

Figure 1.

data, can be made using eq 7. Ts'o has fitted his osmotic coefficient data to a sixth-degree polynomial which can be employed to calculate values of φ or $1 - \varphi$ at concentrations given in Table III. Since the osmotic coefficient data were taken on solutions above 0.05 m we shall apply Ts'o's equation only to concentrations above this range. The values of $1 - \varphi$ (Ts'o) are given in Table III along with the calculation of ΔH° by eq 7.

Whereas the application of eq 5 yields a value of $\Delta H^\circ = -5.6 \pm 0.2$ kcal/mole, the application of eq 7 in conjunction with osmotic and calorimetric data yields a value of -6.3 ± 0.1 kcal/mole. This difference appears to be beyond experimental error and more likely reflects the different weight that each of the methods places upon the assumption of ideal solution behavior. The application of eq 7 should become increasingly accurate for more and more dilute solutions where ideal solution behavior always occurs. Unfortunately osmotic coefficient data are most difficult to obtain at these low concentrations and so it seems the best that can be done at present is to assign a value for the heat of self-association of 6-methylpurine in water at 25° as -6.0 ± 0.4 kcal/mole. With this value and Ts'o's value[2] of -1.1 kcal/mole for ΔG°, the value of ΔS° is -16 ± 1 eu.

A value of ΔH° in the range of -6 kcal/mole indicates that the strength of the stacking interaction between these bases is relatively large. This is in at least qualitative agreement with studies on adenylic acid oligomers[11-12] which provide an estimate in the range of -8 to -10 kcal/mole. A variety of factors such as steric effects and differences in electronic distribution are undoubtedly the cause of these differences. A number of theoretical calculations have been made of the interaction energies between purine and pyrimidine molecules using different basic assumptions.[5,17] A calculation by Vande Vorst and A. Pullman[18] on 6-methylpurine assuming vertical overlap of the π-electron clouds has given a value of 0.37–0.43 in terms of $\beta^{\pi\pi}$ Hückel units.[18] With a conversion factor of 16.5 kcal/$\beta^{\pi\pi}$ unit[19] the stabilization energy is between -6.1 and -7.1 kcal/mole. It is difficult to assess the precise effect of solvent on these values. The theoretically calculated interaction energies are of a similar magnitude as those observed experimentally and the stacking picture offers a satisfactory explanation of the experimental observations.

Acknowledgments. We wish to acknowledge the assistance from the National Institutes of Health in the form both of research grant support and of fellowship support for one of us (P. R. S.). We also wish to acknowledge the many helpful discussions about this work with H. B. Albert and M. Downing.

(17) B. Pullman, P. Claverie, and J. Caillet, *Compt. Rend.*, 260, 5387 (1965).

(18) A. Vande Vorst and A. Pullman, *ibid.*, 261, 827 (1965).

(19) R. Daudel, R. Lefevore, and C. Moser, "Quantum Chemistry—Methods and Applications," Interscience Publishers, Inc., New York, N. Y., 1961, p 177.

Proton Chemical Shifts and Hydrogen Bonding in the Ternary System Carbon Tetrachloride–Dioxane–Water

by Norbert Muller and Paul Simon

Department of Chemistry, Purdue University, Lafayette, Indiana *(Received July 25, 1966)*

Proton chemical shifts were determined for dilute solutions of water in mixtures of dioxane and carbon tetrachloride in the range 11–70°. When the mole fraction of water is below 1.5×10^{-3}, self-association of water is negligible, and the data were interpreted assuming that there are three solute species, free water, a 1:1 water–dioxane complex, and a 1:2 complex. Thermodynamic parameters were evaluated for the two processes: water + dioxane = 1:1 complex and 1:1 complex + dioxane = 1:2 complex. Slightly different methods of treating the data yielded K_1 values between 10.5 and 12.1 mf^{-1} at 30°, K_2 values between 0.73 and 0.82 mf^{-1}, ΔH_1 between −3.3 and −3.7 kcal/mole, and ΔH_2 between −1.6 and −2.8 kcal/mole. The hydrogen-bond shift could not be determined very accurately, but it appears to be independent of the temperature.

Introduction

Quantitative interpretation of the results of nuclear magnetic resonance (nmr) studies of hydrogen bonding in liquids is often hampered by the fact that the species in solution participate in several simultaneous equilibria. This is illustrated in a number of investigations of the interactions between water and organic bases which had been reported when this work was begun.[1-5] Since the hydrogen-bonding properties of water are particularly interesting to both chemists and biologists, we undertook to investigate water–base interactions under conditions chosen to facilitate the derivation of meaningful thermochemical quantities, *i.e.*, by using a three-component system consisting of an inert solvent, a basic solvent, and water, the latter being at such low concentrations as to eliminate the complications caused by its self-association. Two papers likewise concerned with nmr studies of water–base interactions in ternary solutions appeared while this work was in progress.[6,7] Our results on carbon tetrachloride–dioxane–water reported here represent the first attempt to allow explicitly for the presence of all three of the water-containing species expected when self-association of water is negligible[8] and to study the equilibria through which they are related.

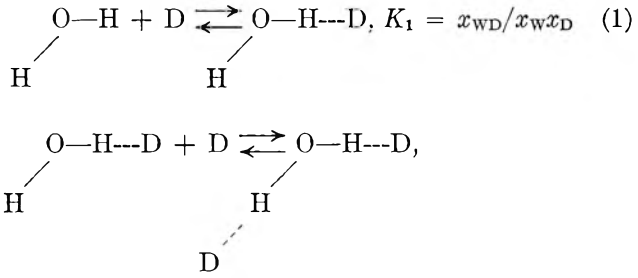

Here x_i represents the mole fraction of the ith species, W and D stand for water and dioxane, and WD and WD_2 represent the 1:1 and 1:2 complexes.

(1) W. Drinkard and D. Kivelson, *J. Phys. Chem.*, **62**, 1494 (1958).
(2) G. Mavel, *Compt. Rend.*, **248**, 1505 (1959).
(3) G. Mavel, *J. Phys. Radium*, **20**, 834 (1959).
(4) J. R. Holmes, D. Kivelson, and W. C. Drinkard, *J. Am. Chem. Soc.*, **84**, 4677 (1962).
(5) A. Fratiello and D. C.D ouglass, *J. Mol. Spectry.*, **11**, 465 (1963).
(6) T. F. Lin, S. D. Christian, and H. A. Affsprung, *J. Phys. Chem.*, **69**, 2980 (1965).
(7) F. Takahashi and N. Li, *J. Am. Chem. Soc.*, **88**, 1117 (1966).
(8) S. C. Mohr, W. D. Wilk, and G. M. Barrow, *ibid.*, **87**, 3048 (1965).

Experimental Procedures and Results[9]

Mallinckrodt SpectrAR grade carbon tetrachloride was dried with phosphorus pentoxide and transferred to a storage bulb containing Linde 5A Molecular Sieve pellets. Technical grade dioxane was purified by standard methods,[10] the product from the final distillation being collected under nitrogen and immediately transferred to a storage bulb, painted black to exclude light, attached to the vacuum line. Water from the laboratory distilled water supply was vacuum transferred into a third storage bulb.

Nmr samples were made on a vacuum manifold equipped with several calibrated reservoirs so that desired amounts of material could be measured by volume, assuming ideal-gas behavior. To determine pressures, the vapor in the measuring bulb was equilibrated with the appropriate liquid in the storage bulb maintained at a known temperature by an external cooling bath. Each tube was sealed under vacuum and stored when not in use in a lightproof container kept at about −15°. This precaution was adopted after preliminary observations had shown that storage of samples under ordinary laboratory illumination resulted in a progressive displacement of the water peak to lower fields, presumably a consequence of photolysis of the mixture.[11] Such samples also showed an impurity peak, apparently chloroform, which was absent otherwise.

Chemical-shift determinations were made with a Varian V-4311 spectrometer operated at 56.4 MHz and equipped with a VK-3529 high-sensitivity kit and V-4340 variable-temperature probe assembly. Shifts were measured by the side-band technique and represent averages of four or more sweeps in each direction, with mean deviations of about 0.3 Hz. Temperatures were maintained constant to within about ±1° of the reported values. Dioxane was used as an internal reference except for the solutions of water in "pure" carbon tetrachloride, where a trace of added cyclohexane was used instead. To allow conversion of the data to a scale based on tetramethylsilane (TMS) we examined a mixture of dioxane, cyclohexane, and TMS dissolved in a large excess of carbon tetrachloride and found the dioxane peak at −3.57 ppm and the cyclohexane peak at −1.44. The shift difference between dioxane and cyclohexane changes considerably if a major change is made in the solvent,[9] but we found that for cyclohexane dissolved in a mixture of dioxane and carbon tetrachloride it is essentially independent of the dioxane : carbon tetrachloride ratio.

Results at four temperatures are reported in Table I for several sets of samples, each with varying water concentrations at a fixed solvent composition specified by the parameter

$$S = \text{(moles of dioxane)}/\text{(moles of dioxane + moles of } CCl_4) \quad (3)$$

Since the mole fraction of water never exceeded 1.5×10^{-3} except when $S = 1$, S is for all practical purposes equal to the mole fraction of dioxane. Some of the more dilute samples were not examined at all temperatures because the spectrometer sensitivity was reduced during operation at other than room temperature.

Table I: Chemical Shift[c] as a Function of Composition and Temperature for Dilute Solutions of Water in Dioxane–Carbon Tetrachloride Mixtures

Solvent compn, S	Water concn, mf × 10^4	11°	30°	50°	70°
0	1.96	...	140.4[a]	...	...
	3.99	...	140.3[a]	...	...
	6.43	139.1[a]	140.6[a]	142.3[a]	143.8[a]
	10.5	139.3[a]	140.4[a]	142.2[a]	...
0.0567	4.18	...	116.0	...	...
	7.26	109.3	117.1	123.2	128.1
	8.20	109.9	116.9	123.0	127.6
	13.8	109.3	115.7	122.0	128.0
0.13	3.41	...	104.4	...	...
	4.04	97.4	103.8	...	...
	5.65	97.6	104.5	111.1	117.7
	8.01	...	103.8	110.0	116.2
	10.4	94.2	103.4	109.9	116.3
0.16	2.89	93.5	100.8	...	...
	3[b]	90.4	100.0	105.9	112.5
	3.64	94.0	100.9	...	...
	6[b]	92.4	100.0	106.7	113.0
	6.40	93.1	100.2	...	...
	9.87	90.5	98.7	106.2	112.4
0.36	4.46	78.8	84.4	...	...
	4.88	78.2	85.5	...	...
	7.35	...	84.6	91.3	...
	14.1	78.7	85.8	91.9	98.2
1.00	5.79	61.7	...	...	76.6
	13.8	62.1	...	...	76.6
	115	59.2	64.3	70.5	75.9

[a] Measured from cyclohexane and converted to the dioxane scale by adding 120.0 Hz. [b] Samples in which the water concentration was known only to within about ±20%. [c] Values are in Hz at 56.4 MHz from dioxane, internal reference.

(9) For additional details, see P. Simon, Ph.D. Thesis, Purdue University, 1966.

(10) A. I. Vogel, "Practical Organic Chemistry," Longmans, Green and Co., Ltd., London, 1951, p 175.

(11) S. Forsén, *Acta Chem. Scand.*, 14, 231 (1960).

Obtaining data for very dilute samples at $S = 1$ proved difficult because the water peak lies in the same region as the multiplet C^{13} satellite signal of the dioxane.[12] At 70° the water peak is upfield of these interfering peaks if the spectrometer is operated at 60 MHz, and the data reported at this temperature were obtained on a Varian A-60 and corrected to 56.4 MHz.

Discussion

The data in Table I show no systematic variation of the chemical shift with changing water concentration below 1.5×10^{-3} mole fraction. This supports the conclusion (also implied by Figure 1 of ref 6) that self-association of water is negligible in this concentration range. Hence the average of the observed shifts at any particular value of S may be equated with the limiting value approached at zero water concentration. (The results for $S = 1$ include one sample with a much higher water concentration, which must be left out in taking the average.) The resulting values are presented in Table II. In this table, the origin of the chemical-shift scale has been changed for convenience in the subsequent analysis, the shifts at each temperature being referred to the observed shift at $S = 0$ at that temperature. It should be noted that the signal from water in "pure" carbon tetrachloride moves linearly to somewhat higher fields as the temperature is raised. This must be ascribed to a temperature dependence of the solvent effect of carbon tetrachloride on the water and not to water self-association effects.

Table II: Values of $\delta - \delta_W$ as a Function of Solvent Composition and Temperature

Solvent compn, S	$(\delta - \delta_W)$ in Hz at 56.4 MHz			
	11°	30°	50°	70°
0	(0)	(0)	(0)	(0)
0.0567	−29.7	−24.0	−19.6	−15.9
0.13	−42.8	−36.4	−32.0	−27.1
0.16	−47.1	−40.3	−36.0	−31.2
0.36	−60.6	−55.3	−50.7	−45.6
1.00	−77.3	−73.9[a]	−70.5[a]	−67.2

[a] Obtained by linear interpolation between the measured values at 11 and 70°.

For the three water-containing species participating in reactions 1 and 2 the exchange-averaged hydroxyl chemical shift will be given by

$$\delta = (x_W\delta_W + x_{WD}\delta_{WD} + x_{WD_2}\delta_{WD_2})/(x_W + x_{WD} + x_{WD_2}) \quad (4)$$

or, introducing the equilibrium constants and the parameter S

$$\delta = (\delta_W + K_1S\delta_{WD} + K_1K_2S^2\delta_{WD_2})/(1 + K_1S + K_1K_2S^2) \quad (5)$$

The dependence of δ on S at each temperature is then governed by the five parameters, δ_W, δ_{WD}, δ_{WD_2}, K_1, and K_2. Complete analysis of the data also requires the evaluation of the temperature coefficient of each δ and of the two reaction enthalpies. The available information, however, does not suffice for the accurate determination of ten unknowns, and one is forced to adopt, at least provisionally, some simplifying assumptions.

We assumed that at each temperature the shifts of the free-water monomer and of the free-OH proton in the 1:1 complex are the same and equal to the measured shift at $S = 0$. We further assumed that the bridging protons have the same shift in WD as in WD_2. It then follows that

$$\delta_{WD} = 0.5(\delta_W + \delta_{WD_2}) \quad (6)$$

One set of calculations made with the alternative assumption $\delta_{WD} = 0.45\delta_W + 0.55\delta_{WD_2}$ is discussed below. Equation 5 then yields

$$\delta - \delta_W = (\delta_{WD_2} - \delta_W)K_1S(1 + 2K_2S)/2(1 + K_1S + K_1K_2S^2) \quad (7)$$

The left member of eq 7 is the observed shift referred to the shift at $S = 0$, displayed in Table II. The parameters remaining to be determined at each temperature are the two equilibrium constants and the "total hydrogen-bond shift" defined as $\delta_b = \delta_{WD_2} - \delta_W$.

To obtain a preliminary value of K_1 one may use an estimated value of δ_b and the datum at $S = 0.0567$, noting that for small values of S eq 7 reduces to

$$\delta - \delta_W \cong \delta_bK_1S/2(1 + K_1S) \quad (8)$$

The result is that K_1 lies between 10 and 20, which suggests that K_2 may be approximated using the datum at $S = 1$ and

$$(\delta - \delta_W)_{S=1} \cong \delta_b(1 + 2K_2)/2(1 + K_2) \quad (9)$$

This gives K_2 values of the order of unity, much smaller than the values of K_1. Indeed, all attempts to fit the data with the restriction $K_1 = K_2$ give very poor results.

Best values of K_1, K_2, and δ_b were obtained by a least-squares method using an IBM 7094 digital computer.[13]

(12) N. Sheppard and J. J. Turner, *Proc. Roy. Soc.* (London), **A252**, 506 (1959).

Table III: Least-Squares Parameters Obtained with Several Alternative Assumptions

		11°	30°	50°	70°
A. Best fit with $\delta_{WD} = 0.5(\delta_W + \delta_{WD_2})$	K_1 (mf^{-1})	19.5	12.1	8.8	6.3
	K_2 (mf^{-1})	1.2	0.82	0.63	0.52
	δ_b (Hz)	−102.3	−106.2	−108.4	−109.9
	Std dev (Hz)	0.31	0.55	0.359	0.59
B. Best fit with $\delta_{WD} = 0.5(\delta_W + \delta_{WD_2})$ and $\delta_b = -106.2$	K_1	18.7	12.1	9.0	6.6
	K_2	0.99	0.82	0.69	0.60
	Std dev	0.33	0.55	0.363	0.60
C. Best fit with $\delta_{WD} = 0.45\delta_W + 0.55\delta_{WD_2}$	K_1	15.9	10.5	7.9	5.8
	K_2	0.89	0.73	0.60	0.50
	δ_b	−104.4	−104.7	−105.2	−106.3
	Std dev	0.50	0.79	0.58	0.75

For a series of trial values of K_2, K_1, and δ_b were each adjusted until the standard deviation between the observed shifts and values calculated by eq 7 was minimized. The best K_2 was considered to be the value which gave the smallest minimal standard deviation. The results are shown in part A of Table III, and the agreement between calculated and observed shifts at 30° is illustrated in Figure 1. The room-temperature values, $K_1 = 12.1$ and $K_2 = 0.82$ mf^{-1}, from Table III were used to calculate the fraction of the total water present in each of the three forms, W, WD, and WD_2, as a function of solvent composition. The results, presented graphically in Figure 2, show that even at high S values a substantial amount of the 1:1 complex is present and the concentration of unbonded water monomers remains appreciable.

Obviously the δ_b values at different temperatures do not agree well with one another. Indeed, one of the objectives of the present study was to find whether or not δ_b would become smaller with increasing temperature, as suggested by observations on carboxylic acids.[14,15] Table III shows a trend in the opposite direction. This could be rationalized if δ_{WD_2} were to have a fixed value relative to TMS or cyclohexane, since δ_{WD} does not, but it seems doubtful that the trend is significant. To test this, two additional calculations were made[9] in which δ_b was assigned the temperature-independent value of −106.2 or −108.0 Hz and the K values were adjusted to fit the data. Results of one of these calculations are given in part B of Table III. The agreement with the experimental values is very nearly as good as it is for the "best" fit, and one must conclude that the measurements do not allow δ_b to be evaluated with an uncertainty less than perhaps ±5 Hz.

Fortunately the equilibrium constants obtained with δ_b fixed are not very different from the best-fit values,

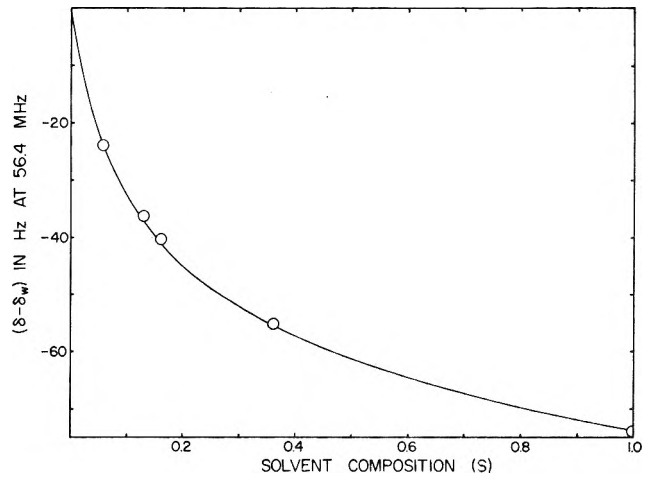

Figure 1. Chemical shift ($\delta - \delta_w$) as a function of solvent composition at 30°. The solid curve represents calculated values using parameters from part A of Table III.

and the same applies for ΔH_1, obtained from a plot of ln K_1 against $1/T$ (see Figure 3). ΔH_2, similarly evaluated, is somewhat more sensitive to changes in δ_b. These enthalpies are given in Table IV with the corresponding entropy changes. The latter were calculated first with the K values referred to concentrations in mf units and again with K values reexpressed in atm^{-1} to facilitate comparison with the tabulated values.[16] The results are in good general agreement with values for somewhat similar systems reported in ref 6 and 7.

(13) We are indebted to Professor M. Laskowski, Jr., and Mr. W. R. Finkenstadt for the loan of a computer program and assistance in using it.

(14) N. Muller and R. C. Reiter, *J. Chem. Phys.*, **42**, 3265 (1965), and references given there.

(15) N. Muller and O. R. Hughes, *J. Phys. Chem.*, in press.

(16) G. C. Pimentel and A. L. McClellan, "The Hydrogen Bond," W. H. Freeman and Co., San Francisco, Calif., 1960, Appendix B.

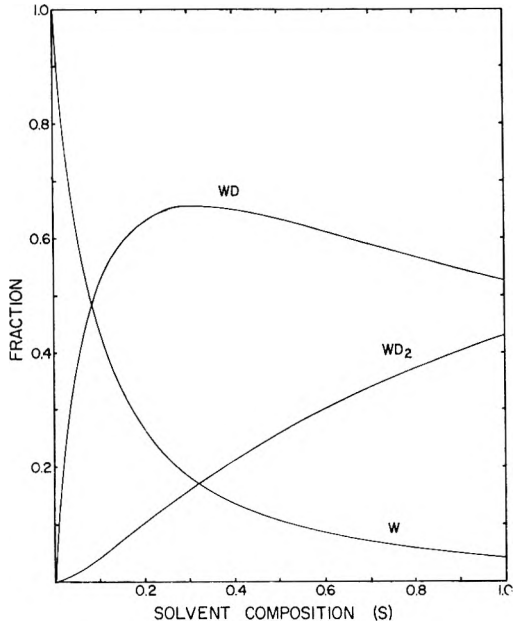

Figure 2. Fraction of water present as free monomer (W), 1:1 complex (WD), and 1:2 complex (WD_2) in dilute solutions of water in dioxane–carbon tetrachloride mixtures, as a function of solvent composition, with $K_1 = 12.1$ and $K_2 = 0.82$ mf^{-1}.

Table IV: Thermodynamic Parameters Obtained with Several Alternative Assumptions (Letters A, B, and C Refer to the Three Parts of Table III)

	A	B	C
ΔH_1 (kcal/mole)	−3.67	−3.39	−3.30
ΔH_2 (kcal/mole)	−2.75	−1.63	−1.90
ΔS_1 (eu, based on K in mf^{-1})	−7.1	−6.2	−6.2
ΔS_2 (eu, based on K in mf^{-1})	−9.5	−5.8	−6.9
ΔS_1 (eu, based on K in atm^{-1})	−18.3	−17.4	−17.4
ΔS_2 (eu, based on K in atm^{-1})	−20.7	−17.0	−18.1

It seems well established that the ratio of K_1 to K_2 is about 15:1 at room temperature, mainly as a result of a difference of about 1 kcal/mole between ΔH_1 and ΔH_2. This calls into question the validity of the assumption which led to eq 6. The O—H---O bond in WD is apparently stronger, and hence probably shorter, than that in WD_2, perhaps because of electrostatic or steric repulsion between the two dioxane molecules in the 1:2 complex, and this suggests replacing eq 6 by

$$\delta_{WD} = (1 - f)\delta_W + f\delta_{WD_2} \qquad (10)$$

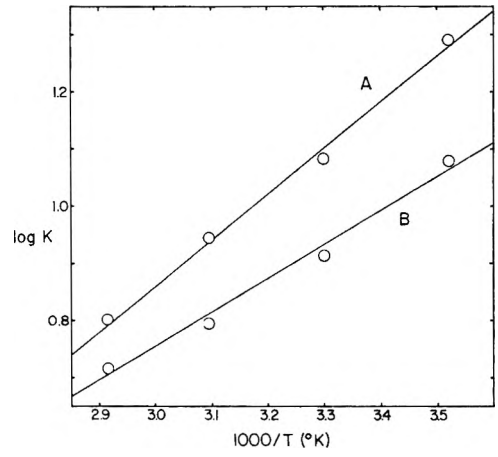

Figure 3. Plots of log K_1 (curve A) and 1 + log K_2 (curve B) against reciprocal temperature, using data from part A of Table III.

with f somewhat larger than 0.5.[17] Part C of Tables III and IV gives results of a least-squares calculation made with $f = 0.55$. They are not very different from the values found with $f = 0.5$, and the quality of the fit, judged by the standard deviations, is somewhat poorer.

Conclusions

The nmr method has been applied to the determination of the thermodynamic parameters for the formation of the 1:1 and 1:2 water–dioxane complexes. The accuracy of the results is limited by the fact that not all of the theoretically required parameters can be evaluated using nmr data alone. Slightly different methods of treating the data yielded values of ΔH_1 lying between −3.3 and −3.7 kcal/mole and ΔH_2 between −1.6 and −2.8 kcal/mole. The difference in the enthalpies causes K_1 to be about 15 times as large as K_2 at 30°. The results do not provide rigorous justification either for the assumption[4] that WD_2 is the only aqueous species present when water is dissolved in a large excess of basic solvent or for the neglect of the presence of uncomplexed water[7] in the composition range $0.5 \leq S \leq 1$. The possible variation of the hydrogen-bond shift with temperature could not be accurately determined, but any such variation appears to be much smaller than $\Delta\delta/\Delta T$ for carboxylic acid dimers. This perhaps reflects the fact that δ_b itself is much smaller than the total hydrogen bond shifts found with carboxylic acids.

(17) It is puzzling that results in ref 7 would appear to require f values near 0.3 even though these authors also conclude that the hydrogen bond is stronger in WB than in WB_2 (B = organic base).

Structural Effects on the Enthalpy and Entropy of Dilution of Aqueous Solutions of the Quaternary Ammonium Halides at 25°[1]

by G. E. Boyd, J. W. Chase, and F. Vaslow

Oak Ridge National Laboratory, Oak Ridge, Tennessee 37830 *(Received July 29, 1966)*

Heats of dilution and solution measurements at 25° were performed on the quaternary ammonium halides derived from tetramethylammonium chloride and bromide by substituting either a β-hydroxyethyl or a benzyl group, or both, for methyl groups. Heat was absorbed on dilution of all the salts except with (β-hydroxyethyl)benzyldimethylammonium fluoride whose solutions evolved heat. Values of the relative partial molal entropy, $\bar{S}_1 - S_1°$, of water in these solutions were derived by combining the measured apparent molal heat contents, ϕ_L, with free energies computed from osmotic and activity coefficient determinations. The replacement of a methyl group in the tetramethylammonium cation by either a β-hydroxyethyl or a benzyl group lowered $\bar{S}_1 - S_1°$ at all concentrations. These changes were interpreted in terms of the relative "water-structure-breaking" efficiencies of the quaternary ammonium cations or of the direct interaction of the cation with individual water molecules. Comparisons between the standard heats of halide ion exchange, $\Delta H°$, for cross-linked polystyrene type strong-base exchangers containing structurally bound (β-hydroxyethyl)benzyldimethylammonium groups and values of $\Delta\phi_L°$ for the corresponding "model compound" halides indicated that the anion exchangers became more like concentrated aqueous electrolyte mixtures as their cross-linking increased.

This paper will report findings made in additional studies on the thermodynamics of aqueous solutions of a series of quaternary ammonium halides derived by substitution of one or more of the methyl groups in the tetramethylammonium cation. Osmotic and mean molal activity coefficient measurements have been published recently on the resultant compounds.[2] Substitution of a β-hydroxyethyl for a methyl group in tetramethylammonium (TMA) chloride or bromide produced a salt whose osmotic and activity coefficients were lower than those for TMA at all concentrations up to near saturation. It was suggested that the increased "water-structure-breaking" action of a β-hydroxyethyl compared with a methyl group was the cause for the smaller coefficients of the choline halides relative to the TMA salts. Structure breaking should be reflected in other thermodynamic properties of these solutions, such as in the entropy of dilution, for example, and, therefore, determinations of the apparent molal heat contents (*i.e.*, heats of dilution to infinite dilution) of aqueous choline chloride and bromide solutions were undertaken. These measurements were combined with the osmotic and activity coefficient values for these salts to give dilution entropies.

Additional thermochemical measurements were made on solutions of benzyltrimethylammonium chloride and bromide and on (β-hydroxyethyl)benzyldimethylammonium fluoride, chloride, bromide, and iodide. These compounds were of interest in addition to the fact that they are derived from tetramethylammonium halide because they are "model compounds" for two important types of strong-base anion exchangers of which Dowex-1 and Dowex-2, respectively, are examples. Derived free energy and heat of dilution

(1) Presented before the Division of Physical Chemistry, 152nd National Meeting of the American Chemical Society, New York, N. Y., Sept 1966. Research sponsored by the U. S. Atomic Energy Commission under contract with the Union Carbide Corp.

(2) G. E. Boyd, A. Schwarz, and S. Lindenbaum, *J. Phys. Chem.*, **70**, 821 (1966).

values determined in this research for the (β-hydroxyethyl)benzyldimethylammonium halides will be employed in a comparison with the heats and free energies of anion exchange measured[3] with variously cross-linked Dowex-2. Heats of solution of a number of the crystalline substituted quaternary ammonium halides also were measured.

Experimental Section

Materials. The purified quaternary ammonium halide preparations were those used in earlier work from this laboratory[2] with the exception of the choline bromide, which was prepared from a new lot of choline chloride by treatment of the latter with silver oxide and neutralization of the filtrate with HBr followed by recrystallization. Concentrated aqueous "stock" solutions were made up by weight from the crystalline salts and pure water.

Calorimetric Measurements. The heat of dilution measurements were performed over a period during which the calorimeter and its auxiliary measuring circuits were progressively improved. The measurements on the benzyltrimethylammonium and (β-hydroxyethyl)benzyldimethylammonium halides were conducted with the calorimeter employed in heat of solution determinations on the alkali metal bromates,[4] whereas the heats of dilution of the choline halides were measured with the calorimeter recently used with the tetra-*n*-alkylammonium halides.[5] Both calorimeter systems gave consistent results as was demonstrated by the agreement observed between heats of dilution on choline chloride measured earlier and those reported below. All solutions were weighed into the calorimeter pipet from weight burets. The capacity of the pipet was *ca.* 3 ml and the volume of water in the calorimeter dewar at the beginning of the experiment was about 500 ml, accurately measured by weight. A correction for the heat of opening of the pipet of 0.010 cal was applied. A check on the accuracy of the calorimeter system was made by determining the heat of solution of KCl(c). Agreement was obtained with the recently recommended[6] "best" value of 4115 ± 10 cal mole^{-1}.

The corrections of the observed heats of dilution to infinite dilution were computed with the formula proposed by Guggenheim and Prue[7] for uni-univalent electrolytes at 25°

$$\phi_L = S_H I^{1/2}[(1 + I^{1/2})^{-1} - \sigma(I^{1/2})/3] - 2.3RT^2(dB/dT)m \quad (1)$$

where $S_H = 708$ is the theoretical limiting Debye–Hückel slope, I is the ionic strength, $\sigma(I^{1/2})$ is a tabulated special function,[8] B is a constant for the specific electrolyte, and the other symbols have their customary meaning. The quantity (dB/dT) appearing in eq 1 was estimated from the correlation between (dB/dT) and $B_{MX} - B_{KCl}$ demonstrated by Pitzer and Brewer.[9] The required values of B_{MX} for choline chloride and bromide were found by substituting the osmotic coefficients[2] for solutions more dilute than $m = 0.1$ into the formula of Guggenheim and Turgeon;[10] the values of (dB/dT) employed for these compounds in eq 1 were +0.005 and +0.006, respectively. Estimates of (dB/dT) for the benzyltrimethylammonium and (β-hydroxyethyl)benzyldimethylammonium halides could not be made, as osmotic coefficients for their dilute aqueous solutions are not available. Other considerations have suggested that (dB/dT) for these compounds will be positive and large relative to the choline salts. In this circumstance (dB/dT) arbitrarily was taken as +0.012 except for the fluoride where $(dB/dT) = 0.001$ was employed.

The ϕ_L values in Table I are believed to be reliable to ±10 cal mole^{-1} or to ±2%, whichever is the larger. The initial and final concentrations in moles per kilogram of water are indicated as m_i and m_f, respectively, and Q is the heat absorbed in calories per mole of solute on diluting from m_i to m_f. The reaction temperature was 25.2°, and all results are given in defined calories (1 cal = 4.1840 absolute joules). Heats of solution to infinite dilution, $\Delta H_\infty°$, for the crystalline compounds are summarized in Table II. Tabulations of graphically smoothed ϕ_L values for interpolated molalities, m, and of calculated relative partial molal heat contents, $\bar{L}_1$ and $\bar{L}_2$, of solvent and solute, respectively, are given in Tables III and IV. The calculations of $\bar{L}_1$ and $\bar{L}_2$ employed the smoothed ϕ_L values listed and the defining equations for these quantities given elsewhere.[11]

(3) F. Vaslow and G. E. Boyd, *J. Phys. Chem.*, **70**, 2507 (1966).

(4) G. E. Boyd and F. Vaslow, *J. Chem. Eng. Data*, **7**, 237 (1962).

(5) S. Lindenbaum, *J. Phys. Chem.*, **70**, 814 (1966).

(6) V. B. Parker, "Thermal Properties of Aqueous Uni-univalent Electrolytes," National Standard Reference Data Series, NSRDS-NBS 2, National Bureau of Standards, U. S. Government Printing Office, Washington, D. C., 1965.

(7) E. A. Guggenheim and J. E. Prue, *Trans. Faraday Soc.*, **50**, 710 (1954).

(8) H. S. Harned and B. B. Owen, "The Physical Chemistry of Electrolytic Solutions," 3rd ed, Reinhold Publishing Corp., New York, N. Y., 1958, p 176.

(9) K. S. Pitzer and L. Brewer, "Thermodynamics," G. N. Lewis and M. Randall, Ed., 2nd ed, McGraw-Hill Book Co., Inc., New York, N. Y., 1961, Figure 25-9, p 396.

(10) E. A. Guggenheim and J. C. Turgeon, *Trans. Faraday Soc.*, **51**, 747 (1955).

(11) See ref 8, p 341.

Table I: Experimental Heats of Dilution for Substituted Quaternary Ammonium Halide Solutions at 25°

m_i	$\sqrt{m_f}$	Q	ϕ_L
(β-Hydroxyethyl)trimethylammonium Chloride			
0.372	0.0440	143	−127
0.481	0.0495	204	−187
0.679	0.0570	277	−258
0.992	0.0624	371	−351
1.357	0.0708	468	−446
2.263	0.0791	628	−605
2.305	0.0762	637	−615
3.868	0.0900	801	−777
4.685	0.0971	866	−842
6.408	0.128	908	−885
6.680	0.142	903	−880
8.029	0.0891	891	−867
9.868	0.130	872	−849
12.04	0.151	805	−782
16.02	0.103	681	−657
(β-Hydroxyethyl)trimethylammonium Bromide			
0.298	0.0397	188	−174
0.466	0.0501	299	−283
0.811	0.0464	504	−489
1.302	0.0657	675	−656
1.736	0.0631	807	−789
2.115	0.0643	911	−893
2.775	0.0747	1045	−1025
4.036	0.0811	1264	−1244
6.068	0.130	1471	−1454
7.958	0.0624	1601	−1583
13.99	0.0677	1745	−1727
13.99	0.0634	1760	−1742
Benzyltrimethylammonium Chloride			
0.229	0.0456	136	−125
1.274	0.0482	510	−499
1.997	0.0416	654	−643
3.025	0.0399	812	−801
5.05	0.0427	1040	−1029
6.88	0.0405	1178	−1167
7.49	0.0471	1186	−1175
8.72	0.0391	1227	−1216
12.35	0.0425	1224	−1213
15.50	0.0405	1183	−1172
18.48	0.0448	1136	−1125
Benzyltrimethylammonium Bromide			
0.969	0.0443	714	−703
1.91	0.0411	1031	−1020
2.085	0.0432	1115	−1104
3.025	0.0422	1376	−1365
4.61	0.0392	1759	−1748
8.88	0.0358	2246	−2236
12.28	0.0411	2445	−2434
(β-Hydroxyethyl)benzyldimethylammonium Fluoride			
0.448	0.0377	−144	181
1.054	0.0694	−326	355
2.705	0.0704	−634	664
4.86	0.0675	−971	1000
9.96	0.0678	−1575	1604
17.02	0.0518	−2035	2058
(β-Hydroxyethyl)benzyldimethylammonium Chloride			
0.258	0.0994	145	−137
0.489	0.0975	242	−234
1.324	0.0959	518	−510
1.353	0.0686	512	−502
2.59	0.0956	758	−750
4.93	0.0683	1048	−1038
8.81	0.0677	1260	−1250
11.95	0.0680	1321	−1311
12.86	0.0684	1295	−1285
15.70	0.0670	1299	−1289
18.17	0.0669	1254	−1244
(β-Hydroxyethyl)benzyldimethylammonium Bromide			
0.0644	0.0620	57	−47
0.407	0.0602	375	−365
0.478	0.120	450	−445
1.120	0.0815	832	−823
2.02	0.0385	1229	−1218
3.33	0.0604	1589	−1579
3.57	0.0727	1621	−1612
5.33	0.0539	1872	−1862
8.13	0.0779	2205	−2196
8.90	0.0533	2283	−2273
10.94	0.0600	2428	−2418
12.95	0.0576	2508	−2498
13.18	0.0597	2527	−2517
(β-Hydroxyethyl)benzyldimethylammonium Iodide			
0.079	0.0537	116	−106
0.154	0.0781	245	−236
0.220	0.0550	336	−326
0.345	0.0819	512	−503

Discussion

Selected portions of the apparent molal heat content data (Table I) have been plotted to illustrate the general features of the thermal behavior of aqueous solutions of the substituted quaternary ammonium halides. It is of interest to note (Figure 1) that the apparent molal heat contents for choline chloride were larger than for tetramethylammonium chloride. However, the substitution of a benzyl for a methyl group in choline chloride or for a methyl group in $(CH_3)_4NCl$ gave quaternary ammonium chlorides with lower ϕ_L values, respectively. This behavior contrasts with that for the tetra-*n*-alkylammonium chlorides[5] where an increase in the cation size caused the heat of dilu-

Table II: Heat of Solution to Infinite Dilution in Water of Variously Substituted Crystalline Quaternary Ammonium Halides at 25°

Compound	Q, cal mole^{-1}	$\sqrt{m_f}$	$\Delta H_{\infty}°$, cal mole^{-1}
$(CH_3)_4NCl$	...	...	975 ± 75[a]
$(CH_3)_4NBr$	...	...	5,800 ± 100[a]
$(CH_3)_4NI$	...	...	10,055 ± 20[a]
$(CH_3)_3(HOC_2H_4)NCl$	3,285	0.0558	3,260 ± 100
$(CH_3)_3(C_6H_5CH_2)NCl$	2,250	0.0335	2,230 ± 100
$(CH_3)_3(C_6H_5CH_2)NBr$	5,799	...	5,700 ± 100
$(CH_3)_2(HOC_2H_4)$- $(C_6H_5CH_2)NF$	−3,905 −3,934	0.0360 0.0600	−3,900 ± 20
$(CH_3)_2(HOC_2H_4)$- $(C_6H_5CH_2)NCl$	4,420	...	4,400 ± 100
$(CH_3)_2(HOC_2H_4)$- $(C_6H_5CH_2)NBr$	8,320 8,349	0.0831 0.0628	8,305 ± 30
$(CH_3)_2(HOC_2H_4)$- $(C_6H_5CH_2)NI$	11,420	...	11,400 ± 100

[a] Reference 6.

tion to become strongly exothermic. All of the salts measured in this research, excepting (β-hydroxyethyl)-benzyldimethylammonium fluoride, absorbed heat on dilution within the concentration ranges studied.

When the structure of the cation was held constant, as in Figure 2 where it was the (β-hydroxyethyl)benzyl-dimethylammonium group, the dilution at constant initial concentration became more endothermic the heavier the anion. Thus the order of decreasing ϕ_L was $F^- > Cl^- > Br^- > I^-$. Aqueous solutions of the tetra-*n*-alkylammonium halides showed an identical sequence,[5] so that the differences between the thermal properties of the latter compounds and those of the substituted quaternary ammonium halides measured in this research must be assigned to the differences in cation structure. The differing cation structures may interact differently with the solvent water, and if this is the case, comparisons of the *excess* relative partial molal entropy given by

$$\bar{S}_1 - S_1° = (\bar{L}_1/T) - R \ln (a_1/N_1) \qquad (2)$$

for the solvent in the various solutions will be of interest.[12] The concentration dependence of $\bar{S}_1 - S_1°$ is exhibited in Figure 3, where values for the compounds measured in this research may be compared with those computed from published ϕ_L values[5] for tetramethyl-, tetraethyl-, and tetra-*n*-propylammonium chloride solutions. The upturn in the $\bar{S}_1 - S_1°$ curves with increasing concentration presumably is caused by a breaking down of the water structure by the increasing number of ions present; therefore, the

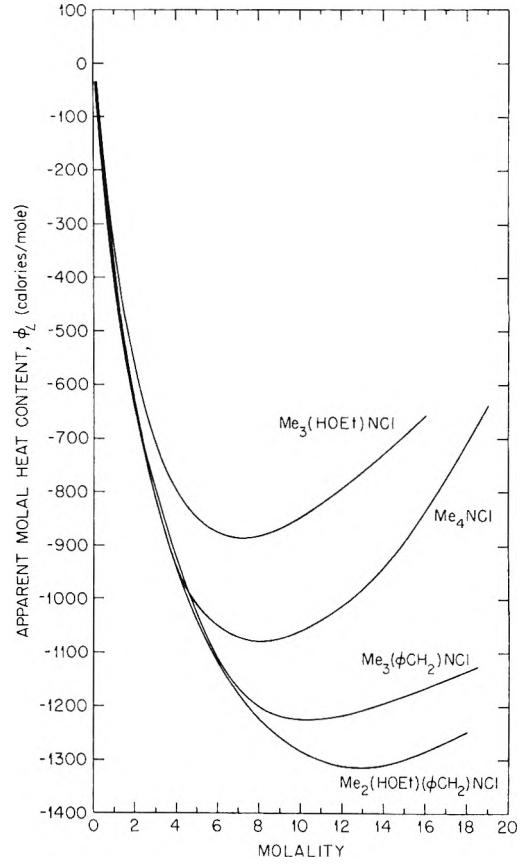

Figure 1. Apparent molal heat contents, ϕ_L, of aqueous solutions of several quaternary ammonium chlorides at 25°. (Data for Me_4NCl taken from ref 5; $Me_3(C_6H_5CH_2)NCl$ and $Me_2(HOEt)(C_6H_5CH_2)NCl$ are "model compounds" for strong-base anion exchangers of the Dowex-1 and Dowex-2 types, respectively.)

greater the disturbance of structure by an ion, the earlier and more pronounced the increase in the relative partial molal entropy of the solvent. The curve for ammonium chloride solutions is of interest because of the relatively quite small values of $\bar{S}_1 - S_1°$ it shows over a wide concentration range. The ammonium ion is believed to fit quite well into the tetrahedral structure of liquid water and may, in fact, exert a stabilizing influence on the water structure by virtue of its tetrahedral shape and its ability to form hydrogen bonds.[12] Chloride ion, which possesses a partial molal volume almost the same as that for water, appears to increase the relative partial molal entropy of water only slightly. "Water-structure-enhancing" ions are expected to show large negative $\bar{S}_1 - S_1°$ values. Judged by these criteria, tetramethylammonium appears to be a "structure-breaking" ion or, at best, the

(12) H. S. Frank and A. L. Robinson, *J. Chem. Phys.*, 8, 933 (1940).

Table III: Apparent Molal and Relative Partial Molal Heat Contents of Choline and Benzyltrimethylammonium Halides

	$(CH_3)_3(HOC_2H_4)NCl$			$(CH_3)_3(HOC_2H_4)NBr$			$(CH_3)_3(C_6H_5CH_2)NCl$			$(CH_3)_3(C_6H_5CH_2)NBr$		
m	ϕ_L	$\bar{L}_1$	$10^{-2}\bar{L}_2$	ϕ_L	$\bar{L}_1$	$10^{-2}\bar{L}_2$	ϕ_L	$\bar{L}_1$	$10^{-2}\bar{L}_2$	ϕ_L	$\bar{L}_1$	$10^{-2}\bar{L}_2$
0.1	(−5)	...	...	(−34)	...	...	(−49)	...	...	(−71)	...	...
0.2	(−53)	...	...	(−106)	...	...	(−107)	...	...	(−164)	...	...
0.3	(−102)	...	...	−178	1.1	−3.8	−158	0.8	−3.0	(−256)	...	...
0.4	−148	1.2	−3.2	−242	1.8	−4.9	−203	1.3	−3.8	(−340)	...	...
0.5	−188	1.8	−3.8	−302	2.6	−5.9	−245	1.8	−4.5	(−414)	...	...
0.6	−226	2.4	−4.5	−358	3.5	−6.8	−284	2.5	−5.2	(−480)	...	...
0.7	−262	3.1	−5.1	−410	4.6	−7.7	−322	3.3	−5.8	(−542)	...	...
0.8	−296	3.7	−5.6	−462	5.6	−8.5	−358	4.0	−6.4	(−600)	...	...
0.9	−327	4.4	−6.0	−507	6.2	−8.9	−392	4.8	−6.9	(−652)	...	...
1.0	−356	5.0	−6.4	−547	7.0	−9.4	−424	5.5	−7.3	−702	8.6	−12
1.2	−408	6.3	−7.0	−620	9.1	−10	−480	6.7	−7.9	−788	11	−13
1.4	−453	7.5	−7.5	−687	11	−11	−528	7.9	−8.4	−866	13	−14
1.6	−493	8.9	−8.0	−749	14	−12	−570	9.2	−8.9	−940	17	−15
1.8	−530	10	−8.5	−806	16	−13	−608	11	−9.4	−1010	20	−16
2.0	−564	12	−9.0	−860	19	−14	−643	12	−9.9	−1080	23	−17
2.5	−647	17	−10	−981	25	−15	−724	17	−11	−1230	34	−20
3.0	−713	19	−11	−1080	30	−16	−797	22	−12	−1380	45	−22
3.5	−763	19	−11	−1170	35	−17	−861	27	−13	−1510	55	−24
4.0	−799	19	−11	−1240	39	−18	−921	33	−14	−1630	63	−25
4.5	−827	18	−10	−1300	42	−18	−977	39	−15	−1730	68	−26
5.0	−849	17	−10	−1350	46	−19	−1030	44	−15	−1820	73	−26
5.5	−864	14	−10	−1400	51	−19	−1070	45	−15	−1890	78	−27
6	−875	12	−9.8	−1450	54	−20	−1110	44	−15	−1960	82	−27
7	−885	1.8	−9.0	−1520	60	−20	−1170	38	−15	−2070	90	−28
8	−881	−9.8	−8.1	−1590	63	−20	−1200	31	−14	−2170	98	−28
9	−868	−26	−7.1	−1630	60	−20	−1220	18	−13	−2240	100	−29
10	−846	−43	−6.1	−1670	56	−20	−1230	2.7	−12	−2310	110	−29
12	−791	−78	−4.3	−1720	47	−19	−1220	−23	−11	−2420	120	−30
14	−727	−120	−2.6	−1740	32	−19	−1190	−46	−10	...	...	...
16	−657	−170	−0.8	...	...	...	−1160	−69	−9.2	...	...	...
18	...	...	...	...	...	...	−1130	−96	−8.4	...	...	...

least strongly "structure-forming" quaternary ammonium ion. Choline chloride appears to be a better "structure-former" than $(CH_3)_4NCl$; therefore, the cause for the lower activity coefficients of the former compared with the latter compound cannot be attributed only to the effect of the cation on water structure as was assumed earlier. The curves for benzyltrimethylammonium and (β-hydroxyethyl)benzyldimethylammonium chlorides indicate increased structure formation, and, therefore, their relatively quite small mean molal activity coefficients in concentrated solutions likewise cannot be understood on the basis of water structure. The possibility that extensive ion-pair formation occurs, particularly with bromide and iodide ion, deserves to be investigated.

Comparisons with Standard Free Energies and Heats of Anion Exchange. As was pointed out in the introductory paragraphs of this paper, the benzyltrimethylammonium and the (β-hydroxyethyl)benzyldimethylammonium halides are "model compounds" for the strong-base anion exchangers of the Dowex-1 and Dowex-2 types, respectively. The standard-state anion-exchange reaction conceptually may thus be written

$$R_4NX_1(m_i) + X_2^- \rightleftharpoons R_4NX_2(m_f) + X_1^- \quad (A)$$

where X_1^- and X_2^- are differing halide ions, respectively, and the reactants and products are in their standard states. Reaction A may be regarded as the sum of two partial processes: (a) the dilution of R_4NX_1 at initial concentration, m_i, to infinite dilution

Table IV: Apparent Molal and Relative Partial Molal Heat Contents of (β-Hydroxyethyl)benzyldimethylammonium Halides

	$(CH_3)_2(HOC_2H_4)(C_6H_5CH_2)NF$			$(CH_3)_2(HOC_2H_4)(C_6H_5CH_2)NCl$			$(CH_3)_2(HOC_2H_4)(C_6H_5CH_2)NBr$			$(CH_3)_2(HOC_2H_4)(C_6H_5CH_2)NI$		
m	ϕ_L	$\bar{L}_1$	$10^{-2}\bar{L}_2$	ϕ_L	$\bar{L}_1$	$10^{-2}\bar{L}_2$	ϕ_L	$\bar{L}_1$	$10^{-2}\bar{L}_2$	ϕ_L	$\bar{L}_1$	$10^{-2}\bar{L}_2$
0.1	(50)	...	...	(−42)	...	...	−70	0.2	−1.6	−140	0.3	−3.0
0.2	(94)	...	...	(−102)	...	...	−176	0.7	−3.8	−294	1.1	−5.9
0.3	(134)	...	...	−153	0.8	−2.9	−278	1.6	−5.7	−440	2.4	−8.8
0.4	(170)	...	...	−196	1.2	−3.7	−368	2.4	−7.1			
0.5	202	−1.4	3.6	−238	1.8	−4.4	−447	3.2	−8.1			
0.6	233	−1.9	4.1	−275	2.4	−5.0	−512	4.2	−9.0			
0.7	262	−2.4	4.5	−312	3.2	−5.7	−575	5.5	−10			
0.8	288	−2.9	4.9	−348	4.0	−6.3	−636	6.9	−11			
0.9	313	−3.7	5.4	−382	4.8	−6.8	−695	8.5	−12			
1.0	339	−4.5	5.9	−414	5.5	−7.2	−752	10	−13			
1.2	385	−5.8	6.5	−470	6.8	−7.9	−858	13	−15			
1.4	428	−7.5	7.3	−519	8.3	−8.5	−956	17	−16			
1.6	470	−9.2	7.9	−565	10	−9.1	−1050	20	−17			
1.8	508	−11	8.5	−607	12	−9.7	−1130	24	−19			
2.0	545	−13	9.1	−646	14	−10	−1210	26	−19			
2.5	634	−19	11	−735	19	−12	−1370	33	−21			
3.0	718	−27	12	−813	24	−13	−1500	37	−22			
3.5	798	−34	13	−883	29	−13	−1600	41	−23			
4.0	874	−43	15	−945	33	−14	−1680	46	−23			
4.5	946	−53	16	−998	36	−14	−1760	53	−24			
5.0	1020	−63	17	−1040	39	−15	−1830	62	−25			
5.5	1090	−74	18	−1080	41	−15	−1900	72	−26			
6	1150	−86	20	−1120	42	−15	−1960	81	−27			
7	1280	−110	21	−1180	45	−15	−2080	100	−29			
8	1400	−130	23	−1220	47	−15	−2190	120	−30			
9	1510	−150	24	−1260	46	−15	−2280	120	−30			
10	1610	−170	25	−1280	41	−15	−2360	130	−31			
12	1780	−200	27	−1310	14	−14	−2470	110	−30			
14	1910	−210	27	−1310	−26	−12	...	...	...			
16	2010	−210	27	−1280	−71	−10	...	...	...			
18	...	...	...	−1250	−120	−8.7	...	...	...			

Table V: Comparison of Standard Free Energies, $\Delta G°$, and Heats, $\Delta H°$, of Anion Exchange with Free Energy and Heat of Dilution Differences for Aqueous Solutions of Model Compounds (kcal mole^{-1})[a]

Cross-linking	m_i	m_f	$-\Delta H°$	$-\Delta\phi_L°$	$-\Delta G°$	$(-\Delta G° - \int \pi dV_0)$	$-\Delta(\Delta G)$
			Br^-–Cl^- Exchange				
0.5	0.70	1.2	1.18	0.58	0.33	0.33	−0.21
4	3.1	4.3	1.33	0.89	0.57	0.50	0.28
10	7.1	9.3	1.36	1.13	0.70	0.62	0.48
24	7.2	9.7	1.31	1.16	0.81	0.71	0.47
			Br^-–F^- Exchange				
0.5	0.48	1.2	2.79	1.06	...	...	...
2	1.3	3.1	3.26	1.90	...	...	...
4	2.0	4.3	3.30	2.25	...	...	...
10	4.1	9.3	3.58	3.17	...	...	...

[a] $\Delta H°$ and $\Delta G°$ values from ref 3.

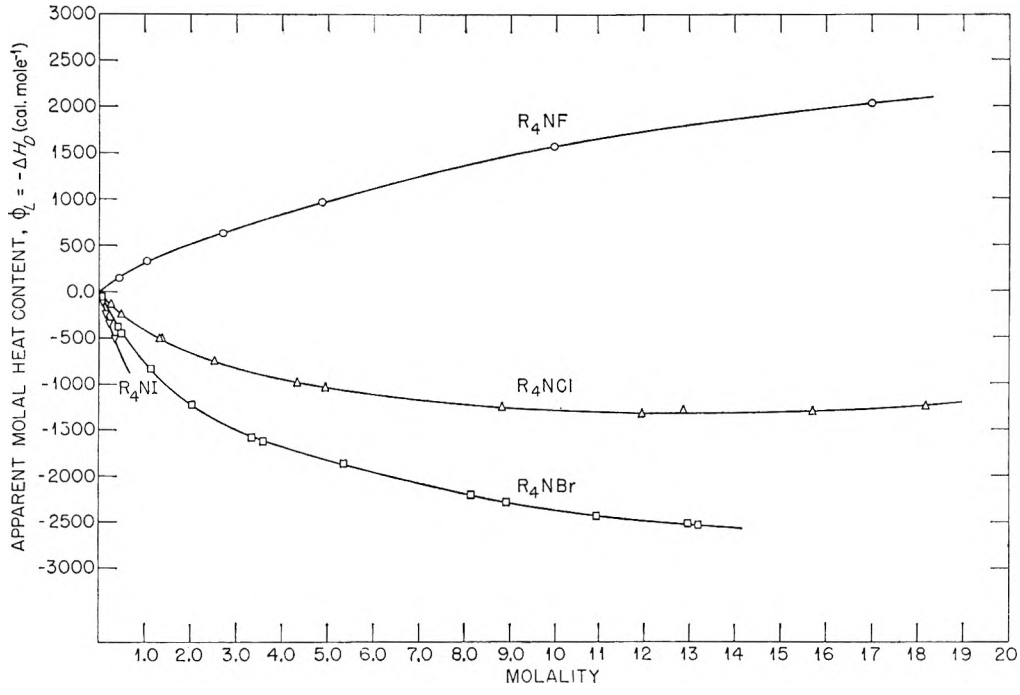

Figure 2. Concentration dependence of the apparent molal heat contents of aqueous (β-hydroxyethyl)benzyldimethylammonium halide solutions at 25°. (Note limited solubility of the iodide.)

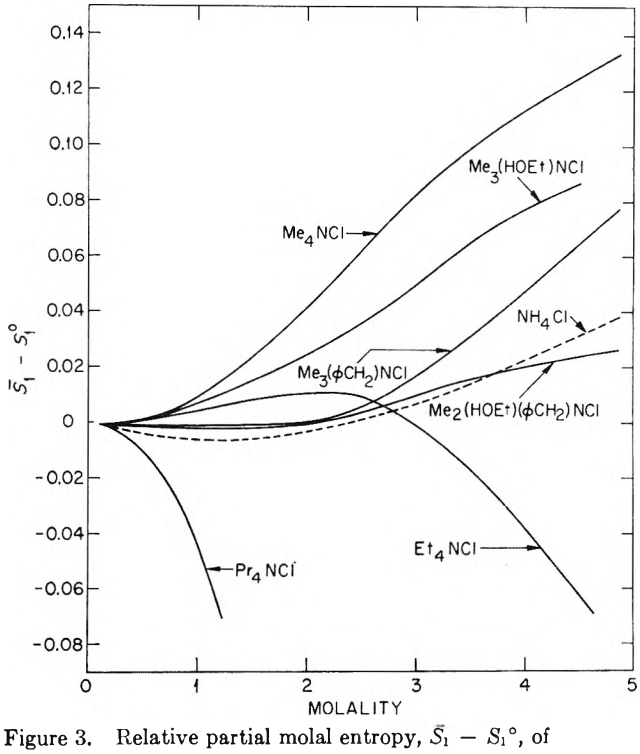

Figure 3. Relative partial molal entropy, $\bar{S}_1 - S_1^\circ$, of water in 1:1 valence type salt solutions at 25°.

$$R_4NX_1(m_i) \rightleftharpoons R_4N^+(m = 0) + X_1^-(m = 0) \quad (B)$$

and (b) the concentration of R_4N^+ and X_2^- initially at infinite dilution to a final concentration of m_f

$$R_4N^+(m = 0) + X_2^-(m = 0) \rightleftharpoons R_4NX_2(m_f) \quad (C)$$

The enthalpy change in reaction B will be $-\phi_L^\circ(m_i)$ and that in reaction C will be $+\phi_L^\circ(m_f)$, and it is proposed that their sum may be compared with the standard heat of anion exchange, ΔH°, for a cross-linked polymeric exchanger

$$\Delta H^\circ = \phi_L^\circ(m_f) - \phi_L^\circ(m_i) = \Delta\phi_L^\circ \quad (3)$$

Similarly, the standard free energy of anion exchange, ΔG°, for the cross-linked exchanger corrected for the decrease in the free energy of its molecular network, $\int \pi dV_e$, accompanying the standard-state reaction may be compared with the difference in the free energy of dilution, $\Delta(\Delta G)$, of the "model compound" solutions

$$\Delta G^\circ - \int_{V_i}^{V_f} \pi dV_e = \Delta G(m_i) - \Delta G(m_f) = \Delta(\Delta G) \quad (4)$$

The dilution free energies per mole of solute were computed with eq 5[13]

$$\Delta G = 2RT[\phi - \ln(m\gamma_\pm)] \quad (5)$$

where ϕ is the molal osmotic coefficient, m the molality, and $\gamma_\pm$ the solute mean molal activity coefficient, respectively. The integral, $\int_{V_i}^{V_f} \pi dV_e$, was evaluated from an equation of state[14] relating the swelling pres-

(13) See ref 9, p 642.

(14) G. E. Boyd and B. A. Soldano, *Z. Elektrochem.*, 57, 162 (1953).

sure, π, of the exchanger to its equivalent volume, V_e

$$\pi = k(V_e - V_0) \quad (6)$$

where k is dependent on the cross-linking of the exchanger network and V_0, its "strain-free" equivalent volume.

Values of $\Delta\phi_L^\circ$ computed with the data in Table IV and of $\Delta(\Delta G)$ computed from previously published data[2] are compared in Table V with ΔH° and $\Delta G^\circ - \int \pi dV_e$ values for the bromide–chloride and bromide–fluoride anion-exchange reactions in variously cross-linked Dowex-2. The molalities, m_i, of the fluoride- and chloride-salt forms, R_4NX_1, and m_f of the bromide salt-forms, R_4NX_2, each in their standard states given in Table V, were taken from an earlier publication.[15] The agreement between $\Delta\phi_L^\circ$ and ΔH° is seen to become progressively better as the cross-linking of the exchanger increases above a nominal 4% DVB content. The large differences for the most weakly cross-linked preparations suggest that the *average* concentrations m_i and m_f in the cross-linked gel are not relevant to the localized ionic concentrations in the vicinity of the charged polymeric chains which make up the open molecular network of these exchangers. Effectively, the exchange groups in the weakly cross-linked anion exchangers are at much higher concentrations than the "average" gel concentration obtained by dividing the moles of exchange groups per unit mass by the total water content per unit mass. This interpretation suggests that the halide ions are constrained to the vicinity of the charged polymeric chains rather than distributed throughout a diffuse double layer. When the cross-linking increases sufficiently that the counter-ion atmospheres overlap extensively, the "homogeneous gel solution" picture of the exchanger becomes more valid.

(15) G. E. Boyd, S. Lindenbaum, and G. E. Myers, *J. Phys. Chem.*, 65, 577 (1961).

Ionic Interactions in Organic Ion Exchangers. Comparisons with Model Electrolyte Mixtures[1]

by S. Lindenbaum and G. E. Boyd

Oak Ridge National Laboratory, Oak Ridge, Tennessee 37830 *(Received August 15, 1966)*

The molalities of aqueous mixtures of "model electrolyte compounds" for strong-acid cation and strong-base anion exchangers, respectively, in vapor phase equilibrium with reference solutions were determined at 25° using the gravimetric isopiestic comparison method. The activity coefficients of both components were evaluated, and the logarithm of their ratio was compared with the ratio computed from isopiestic vapor pressure measurements taken on chemically analogous lightly cross-linked ion exchangers. Satisfactory agreement was obtained between the model compound mixtures and the ion exchangers for concentrations above 5 m; below this concentration, however, the activity coefficient ratio for the electrolyte mixture became progressively smaller than for the ion exchanger and extrapolated to unity at infinite dilution. The analogy between ion exchangers and concentrated electrolyte mixtures thus appears valid for relatively high concentrations. At lower concentrations the exchanger exhibited a polyelectrolyte behavior in that activity coefficient ratios appreciably different from unity were observed even at high dilution.

A long-standing,[2] generally fruitful approach to the interpretation of the equilibrium behavior of organic ion exchangers has been based on their analogy with concentrated aqueous electrolyte mixtures. Osmotic coefficient measurements on cation exchangers containing singly charged ions,[3,4] for example, have shown that the concentration dependence of this property is quite similar to that for strong, 1–1 electrolytes in aqueous solution. The application of Harned's rule for electrolyte mixtures to the evaluation of the thermodynamic activity coefficients of ions in exchangers has been proposed,[5] and cation-exchange equilibrium constants have been estimated[3] using this rule and the assumption that the interaction coefficients, α_{12} and α_{21}, obeyed Brønsted's relation, $\alpha_{12} = -\alpha_{21}$. Thermodynamic calculations[6,7] of equilibrium constants which do not assume empirical relations such as the Harned rule have shown that the predominant contribution was given by the logarithm of the activity coefficient ratio for the ions in the exchanger. The changes in the free energy of the cross-linked molecular network of the copolymer could be neglected for these systems. The logarithm of the activity coefficient ratio for a very lightly cross-linked exchanger was found to be a nearly linear function of the weight normality, N_m, of its ion-exchange sites (N_m is expressed in equivalents per kilogram of absorbed water).

A direct test of the analogy between ion exchangers and concentrated electrolytes will be made in this paper by comparing activity coefficient ratios derived from isopiestic vapor pressure measurements on mixed aqueous solutions of "model compounds" with the ratios derived from measurements on lightly cross-linked polyelectrolytes. *p*-Ethylbenzenesulfonic acid and its alkali metal salts were taken as the model compounds for polystyrenesulfonate-type cation exchangers,

(1) Presented before the Division of Colloid and Surface Chemistry, 148th National Meeting of the American Chemical Society, Chicago, Ill., Sept 1964 (see Abstracts of Papers, p 21, No. 3); research sponsored by the U. S. Atomic Energy Commission under contract with Union Carbide Corp.

(2) W. C. Bauman and J. Eichorn, *J. Am. Chem. Soc.*, 69, 2830 (1947).

(3) E. Glueckauf, *Proc. Roy. Soc.* (London), A214, 207 (1952).

(4) G. E. Boyd and B. A. Soldano, *Z. Elektrochem.*, 57, 162 (1953).

(5) S. W. Mayer, *J. Am. Chem. Soc.*, 72, 2292 (1950).

(6) G. E. Myers and G. E. Boyd, *J. Phys. Chem.*, 60, 521 (1956).

(7) G. E. Boyd, S. Lindenbaum, and G. E. Myers, *ibid.*, 65, 577 (1961).

while the quaternary ammonium salts, benzyltrimethylammonium and (β-hydroxyethyl)benzyldimethylammonium halides, were employed as "models" for two important strong-base anion exchangers. Justification for the use of low molecular weight aromatic sulfonic acids in the interpretation of cation-exchange equilibria has been given by Bonner,[8] who demonstrated that sulfonates of differing degrees of polymerization but with the same recurring monomer unit have similar osmotic properties.

Agreement at low stoichiometric molalities between activity coefficient ratios for aqueous model electrolyte mixtures and for lightly cross-linked polyelectrolytes cannot be expected; the ionogenic groups on the polyelectrolyte cannot be separated indefinitely by dilution as can the ions in ordinary electrolyte solutions. The local concentration of counterions near a polyelectrolyte chain is much higher than the average concentration, N_m, defined above. Comparisons with concentrated aqueous electrolyte solutions may be valid, however, when N_m is large and the polyelectrolyte chains are sufficiently close together that their ion atmospheres overlap extensively.

Experimental Section

Materials. Syntheses of the strong-acid cation-exchanger "model compound," *p*-ethylbenzenesulfonic acid, were conducted following the methods of Wiley and Davis[9] and of Sempotowski,[10] respectively. Purification was accomplished by recrystallization of the barium salt of the acid; this compound was converted to the lithium and sodium salts by treatment with a small excess of Li_2SO_4 or Na_2CO_3, respectively. Further purification and isolation was effected by two recrystallizations from methanol and "freeze-drying." The melting points of the *o*- and *p*-toluidine derivatives of the acid were in agreement with literature values. Molecular weights of the salts computed from C, H, and metal analyses were in fair agreement with theory. Equivalent weights were determined by titration of the acid released when solutions containing known weights of salt were passed through a deep bed of H-form cation exchanger. Values of 185.4 and 210.3, compared with theory values of 192.2 and 208.2, were found for the Li and Na *p*-ethylbenzenesulfonates, respectively.

The anion-exchanger model compounds were benzyltrimethylammonium chloride and bromide and (β-hydroxyethyl)benzyldimethylammonium chloride and bromide, respectively. The sources, methods of purification, and analysis of these compounds have been given in a recent publication.[11]

Isopiestic Vapor Pressure Comparisons. The apparatus and techniques employed in measuring the molalities of the solutions of the model compound mixtures of known composition in vapor pressure equilibrium have been described.[12] Concentrated stock solutions of lithium and sodium *p*-ethylbenzenesulfonate were made up, and weight burets were employed in the analysis of their concentrations by cation-exchange and precision acidimetric titrations. Mixtures with varying fractions of lithium and sodium salt were prepared by weighing known amounts of these solutions into the dishes used in the gravimetric isopiestic vapor pressure comparison apparatus. Mixtures of the anion-exchanger model compounds and of tetramethylammonium chloride and bromide were made up in a similar manner.

Equilibrium isopiestic concentrations for four sets of mixtures are presented in Tables IA–D, inclusive. Concentrations of the reference sodium chloride solutions in isopiestic equilibrium also are given for the *p*-ethylbenzenesulfonate mixtures. The reference solutions for the calculations performed later in this paper with the data in Tables IB–D, inclusive, were those for which $x_{Br^-} = 0.000$ and $x_{Br^-} = 1.000$, respectively. The data (Table IA) for the pure sodium salt solutions (*i.e.*, $x_{Na} = 1.00$) extend to concentrations higher than the equilibrium solubility because of supersaturation effects. The osmotic coefficients for the pure and mixed lithium and sodium *p*-ethylbenzenesulfonates were computed with the equation

$$\nu_x m_x \phi_x = \nu_r m_r \phi_r \qquad (1)$$

where the number of ions, ν, is 2, m_x is the molality of the sulfonate solution, ϕ_x is its osmotic coefficient, and m_r and ϕ_r are the molality and osmotic coefficient of the reference electrolyte (NaCl), respectively. The osmotic coefficients for the pure sodium salt agree with previously published values;[13] however, there was a small, systematic disagreement with the lithium salt. The concentration range for the tetramethylammonium chloride–bromide mixtures was limited by the solubility of the pure bromide salt which recently has been determined[14] as 6.353 *m* at 25°.

(8) O. D. Bonner and J. R. Overton, *J. Phys. Chem.*, **67**, 1035 (1963).
(9) R. H. Wiley and R. P. Davis, *J. Am. Chem. Soc.*, **74**, 6142 (1952).
(10) L. Sempotowski, *Chem. Ber.*, **22**, 2662 (1889).
(11) G. E. Boyd, A. Schwarz, and S. Lindenbaum, *J. Phys. Chem.*, **70**, 821 (1966).
(12) S. Lindenbaum and G. E. Boyd, *ibid.*, **68**, 911 (1964).
(13) O. D. Bonner and O. C. Rogers, *ibid.*, **64**, 1499 (1960).
(14) B. J. Levien, *Australian J. Chem.*, **18**, 1161 (1965).

Table I: Molalities of Isopiestic Solutions at 25°

A. Lithium + Sodium *p*-Ethylbenzenesulfonate Mixtures

	x_{Na^+}						
m_{NaCl}	0.000	0.187	0.350	0.444	0.571	0.796	1.000
0.4886	0.5128	0.5147	0.5156	0.5168	0.5189	0.5221	0.5274
0.5947	0.6375	0.6403	0.6435	0.6460	0.6494	0.6604	0.6641
0.6674	0.7270	0.7336	0.7359	0.7388	0.7446	0.7600	0.7678
0.8732	1.005	1.022	1.031	1.045	1.061	1.100	1.135
1.208	1.548	1.593	1.637	1.669	1.717	1.841	1.939
1.221	1.562	1.619	1.659	1.690	1.741	1.870	1.974
1.537	2.091	2.175	2.238	2.288	2.367	2.567	2.723
1.764	2.441	2.561	2.639	2.701	2.799	3.054	3.218
2.164	3.006	3.164	3.274	3.352	3.471	3.717	...
2.211	3.085	3.207	3.318	3.402	3.523	3.818	4.026
2.741	3.751	3.917	4.050	4.140	4.294	4.658	...
2.792	3.785	3.995	4.149	4.258	4.403	4.863	...
3.385	4.520	4.720	4.869	4.999	5.197	...	...
4.155	5.410	5.682	5.837	6.018	...	...	...

B. Tetramethylammonium Chloride + Bromide Mixtures

		x_{Br^-}		
0.000	0.253	0.495	0.743	1.000
0.2446	0.2428	0.2506	0.2505	0.2498
0.2556	0.2576	0.2628	0.2635	0.2645
1.107	1.136	1.167	1.188	1.219
1.125	1.152	1.188	1.209	1.243
2.311	2.392	2.482	2.573	2.694
2.970	3.078	3.186	3.324	3.498
4.562	4.766	4.981	5.260	5.585
5.392	5.651	5.867	6.188	satd
6.788	7.118	7.436	satd	satd

C. Benzyltrimethylammonium Chloride + Bromide Mixtures

		x_{Br^-}		
0.000	0.246	0.499	0.732	1.000
0.2547	0.2555	0.2634	0.2684	0.2726
0.2679	0.2734	0.2776	0.2826	0.2877
1.370	1.451	1.556	1.685	1.850
1.401	1.486	1.599	1.734	1.906
3.133	3.390	3.752	4.130	4.647
4.020	4.352	4.828	5.377	6.092
6.069	6.523	7.213	7.885	8.914
6.995	7.541	8.398	9.266	10.457
8.451	9.037	10.080	11.070	12.662

D. (β-Hydroxyethyl)benzyldimethylammonium Chloride + Bromide Mixtures

			x_{Br^-}		
0.000	0.168	0.345	0.546	0.772	1.000
0.7900	0.8148	0.8434	0.8839	0.9296	0.9906
0.9105	0.9421	0.9786	1.030	1.092	1.175
1.581	1.657	1.753	1.890	2.069	2.306
2.514	2.664	2.864	3.094	3.418	3.812
2.898	3.063	3.267	3.560	3.931	4.391
4.416	4.691	4.978	5.395	5.908	6.589
5.058	5.367	5.719	6.227	6.788	7.407
6.780	7.175	7.622	8.190	8.910	9.862
9.268	9.830	10.45	11.18	12.09	13.42
9.314	9.758	10.37	11.15	12.19	13.67

Treatment of Experimental Data

Method for Activity Coefficient Calculations. Mean molal activity coefficients for each salt in the mixed aqueous solutions were computed following the method outlined by Robinson,[15] who has expressed the basic equation of McKay and Perring[16] as

$$\ln \gamma_C = \ln \gamma_C^0 + \ln R + \int_0^{M\phi} \left[\frac{1}{m^2} \left(\frac{dm}{d \ln x} \right)_{M\phi} + \frac{R-1}{M} \right] d(M\phi) \quad (2)$$

where γ_C and γ_C^0 are the activity coefficients of electrolyte C in the mixture with electrolyte B and in its own pure solution at the same ionic strength, respectively; $R = M/m$ is the isopiestic ratio where $m = m_B + m_C$ is the total molality and M is the molality of the solution of pure C isopiestic with m; ϕ is the molal osmotic coefficient, and x is defined by $m_B = xm$ where m_B is the molality of electrolyte B.

If R can be expressed as a quadratic function in x

$$R = 1 - ax - bx^2 \quad (3)$$

then eq 2 takes the form

$$\ln \gamma_C = \ln \gamma_C^0 + \ln R + x^2 \int_0^{M\phi} (b/M) d(M\phi) \quad (4)$$

for each value of M. Additionally, when (b/M) can be described by a quadratic in $M\phi$

$$-(b/M) = j + 2k(M\phi) + 3l(M\phi)^2 \quad (5)$$

eq 4 becomes

$$\ln \gamma_C = \ln \gamma_C^0 + \ln R + x^2(M\phi)[j + k(M\phi) + l(M\phi)^2] \quad (6)$$

When the isopiestic ratio is a linear function of x for each M value, eq 2 simplifies to

$$\ln \gamma_C = \ln \gamma_C^0 + \ln R \quad (7)$$

Analogous equations may be written for the calculation of the activity coefficient, γ_B, of electrolyte B in the mixture.

Tetramethylammonium Chloride–Bromide Mixtures. Within the experimental accuracy, R for this system was a linear function of x; eq 7 therefore was used for the calculation of γ_B and γ_C, where B and C refer to the bromide and chloride salts, respectively. The required values of γ_B^0 and γ_C^0 were interpolated from smooth curves constructed with the activity coefficients listed in published tables.[12]

Benzyltrimethylammonium Chloride–Bromide Mixtures. Equation 7 also was applicable to this system, and the activity coefficient values, γ_B^0 and γ_C^0, for the pure electrolyte solutions were interpolated.[11]

(β-Hydroxyethyl)benzyldimethylammonium Chloride–Bromide Mixtures. Equation 3 was required to describe the variation of R with x for each value of m, and eq 5 was needed to reproduce the dependence of (b/M) on $(M\phi)$. Least-squares methods were employed to fit the data of Table ID to eq 3 and 5, respectively, and values of γ_B^0 and γ_C^0 were interpolated.[11]

Lithium–Sodium p-Ethylbenzenesulfonate Mixtures. The dependence of R on x and x^2 for all M values in this system also required the use of eq 3 and 5. The osmotic and activity coefficients for the pure lithium and sodium salt solutions (Table II) were calculated following the procedure described earlier.[12] The required γ_B^0 and γ_C^0 values (B = sodium; C = lithium) were found by interpolation from smooth curves constructed with Table II.

Table II: Osmotic and Activity Coefficients for Lithium and Sodium *p*-Ethylbenzenesulfonate Solutions at 25°

	Li-*p*-EBS		Na-*p*-EBS	
m	ϕ	γ	ϕ	γ
0.1	(0.931)	(0.773)	(0.925)	(0.759)
0.2	(0.920)	(0.730)	(0.912)	(0.715)
0.3	(0.906)	(0.702)	(0.898)	(0.678)
0.4	(0.895)	(0.672)	0.882	0.647
0.5	(0.880)	(0.646)	0.862	0.616
0.6	0.866	0.622	0.840	0.587
0.7	0.853	0.601	0.819	0.559
0.8	0.838	0.580	0.795	0.532
0.9	0.822	0.560	0.770	0.506
1.0	0.807	0.541	0.747	0.482
1.2	0.778	0.506	0.704	0.439
1.4	0.753	0.476	0.667	0.403
1.6	0.733	0.451	0.634	0.372
1.8	0.718	0.430	0.606	0.346
2.0	0.710	0.414	0.585	0.325
2.5	0.706	0.386	0.552	0.285
3.0	0.716	0.370	0.537	0.258
3.5	0.738	0.362	0.537	0.241
4.0	0.769	0.361	0.547	0.229
4.5	0.799	0.363	0.564	0.221
5.0	0.832	0.368	0.583	0.215
5.5	0.873	0.378	...	...

Calculation of the Interaction Coefficients. The calculated γ_B and γ_C values for the mixed electrolyte

(15) R. A. Robinson, *J. Phys. Chem.*, **65**, 662 (1961).

(16) H. A. McKay and J. K. Perring, *Trans. Faraday Soc.*, **49**, 163 (1953).

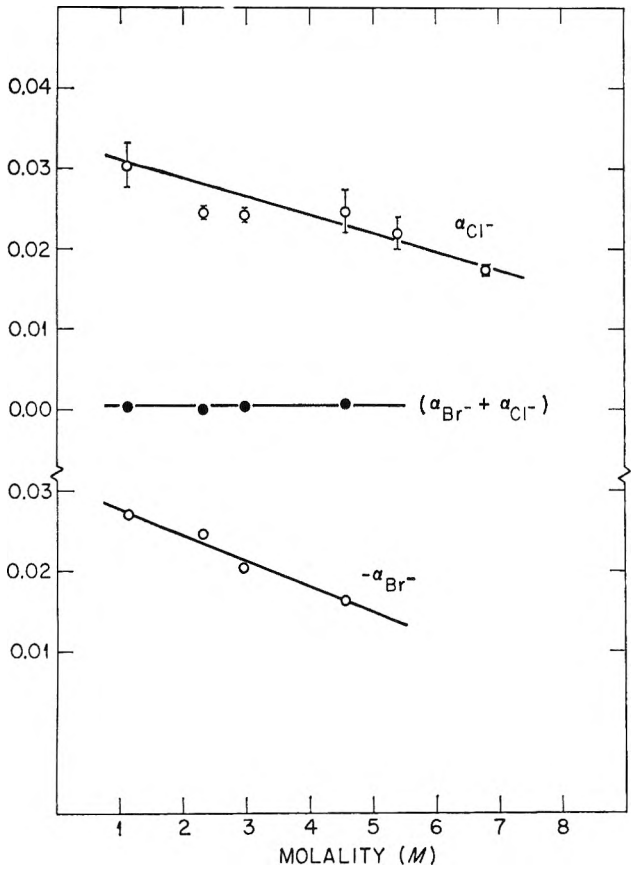

Figure 1. Variation of interaction parameters for aqueous tetramethylammonium chloride + bromide mixtures with concentration.

solutions were employed to obtain values for the coefficients, α_B and α_C, respectively, by means of the equations[17]

$$\alpha_B = -(1/m_C) \log (\gamma_B/\gamma_B^0) \quad (8a)$$

$$\alpha_C = -(1/m_B) \log (\gamma_C/\gamma_C^0) \quad (8b)$$

The variation of these coefficients and their sum $(\alpha_B + \alpha_C)$ with the total molality, $m = M$, is given in Figures 1–4. There was evidence that α_B and/or α_C also were dependent on $x = m_B/m$, although in several instances the accuracy of the data was low. An illustration of this dependence is shown in Figure 4 for the (β-hydroxyethyl)benzyldimethylammonium chloride–bromide mixtures. A dependence of α_B and/or α_C on x implies a quadratic rather than a linear dependence of the activity coefficients on molality.

$$\log \gamma_B = \log \gamma_B^0 - \alpha_B m_C - \beta_B m_C^2 \quad (9a)$$

$$\log \gamma_C = \log \gamma_C^0 - \alpha_C m_B - \beta_C m_B^2 \quad (9b)$$

A necessary consequence[18] of eq 9 is that

$$\alpha_B + \alpha_C = \text{constant} - 2m(\beta_B + \beta_C) \quad (10)$$

If $\alpha_B + \alpha_C$ is independent of m, then $\beta_B + \beta_C = 0$; however, from the slope of the α_B (or α_C) *vs.* x plots, estimates of β_B (or β_C) may be derived. The numerical values of β_B and β_C were expected to be quite small, as generally $\alpha_B + \alpha_C$ was close to zero.

Results and Discussion

Tetramethylammonium Chloride–Bromide Mixtures. In this system (Figure 1) $\alpha_B + \alpha_C = 0.0038 \pm 0.0017$, and the sum was independent of the molality within experimental error indicating that $\beta_B + \beta_C \approx 0$. However, α_B (*i.e.*, α_{Br^-}) was slightly dependent on x; hence $\beta_B = -\beta_C \approx 0.0005$. The nearly "Brønsted behavior" observed with these mixtures may be compared with that for aqueous mixtures of KCl and KBr

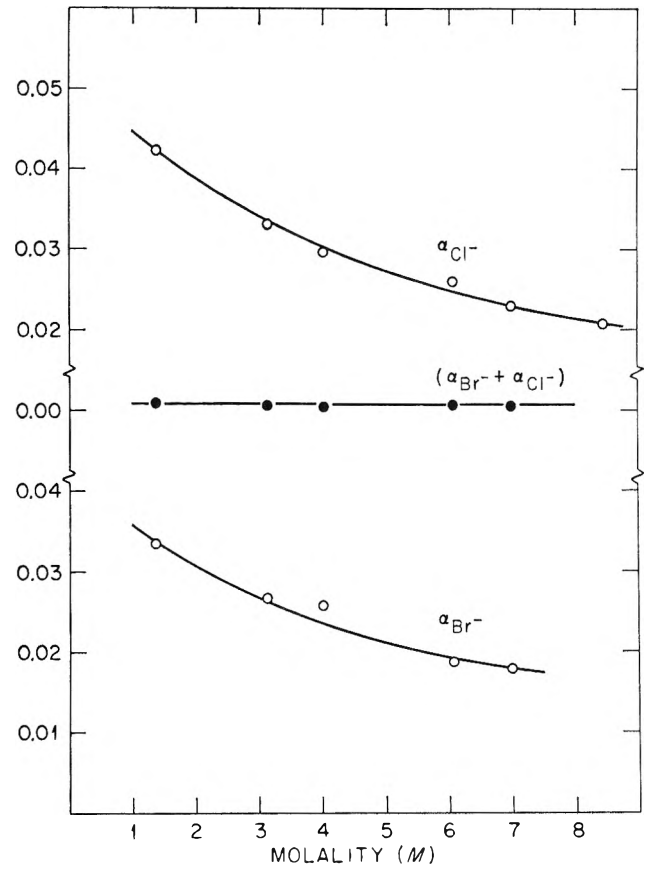

Figure 2. Concentration dependence of interaction parameters for aqueous benzyltrimethylammonium chloride + bromide mixtures.

(17) H. S. Harned and B. B. Owen, "The Physical Chemistry of Electrolytic Solutions," 3rd ed, Reinhold Publishing Corp., New York, N. Y., 1958, p 616.

(18) E. Glueckauf, H. A. C. McKay, and A. R. Mathieson, *J. Chem. Soc.*, S299 (1949).

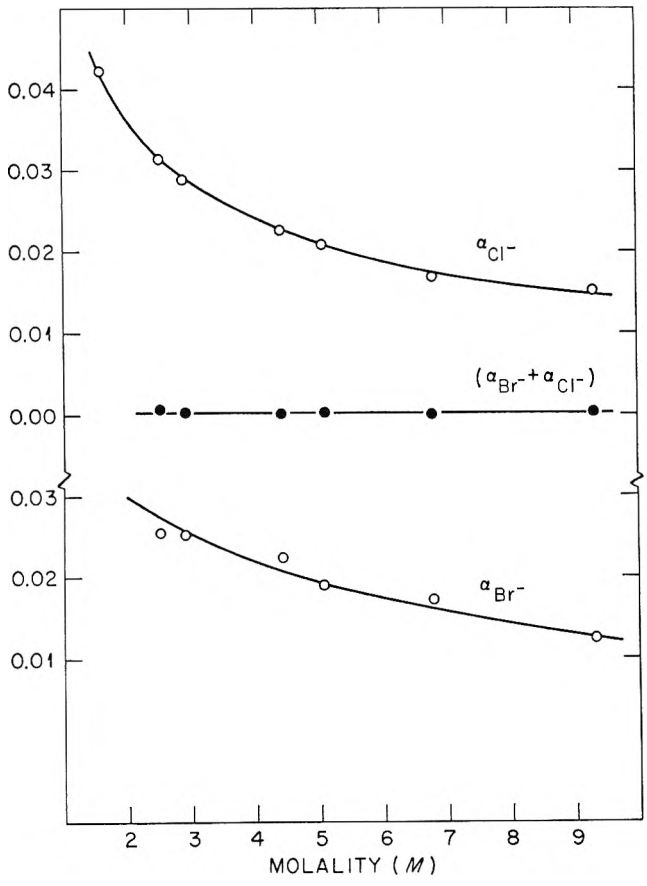

Figure 3. Concentration dependence of "first-order" interaction coefficients for aqueous (β-hydroxyethyl)benzyldimethylammonium chloride + bromide mixtures.

where, within experimental error, $\alpha_B = -\alpha_C$ was observed[19] for total molalities from 2.0 to 5.5. The values of α_B and α_C for the tetramethylammonium halide mixtures were an order of magnitude larger than for the K(Cl + Br) mixtures, however.

Benzyltrimethylammonium Chloride–Bromide Mixtures. The values of α_B and α_C for these mixtures were larger than for the tetramethylammonium chloride + bromide mixtures over the same concentration range, but, like the latter, they decreased with increasing concentration (Figure 2). The quantity $(\alpha_B + \alpha_C)$ appeared to be independent of the molality within experimental error and showed an average value of 0.0063 ± 0.0014 for total molalities of 1.4–7.0 *m*. Both α_B and α_C were slightly dependent on x, indicating that $\beta_B = -\beta_C \approx 0.0005$.

(β-Hydroxyethyl)benzyldimethylammonium Chloride–Bromide Mixtures. The interaction coefficients for this system (Figure 3) appeared to be smaller than for the benzyltrimethylammonium chloride–bromide mixtures, but they also decreased with increasing concentration. The quantity $(\alpha_B + \alpha_C)$ was quite small (*i.e.*, ≈ 0.0015) and almost independent of the total molality. However, α_B was dependent on x (Figure 4), while α_C was almost independent. These observations require $\beta_C \approx -0.002$ and $\beta_B \approx 0.0$.

Lithium–Sodium p-Ethylbenzenesulfonate Mixtures. The interaction coefficients for these mixtures (Figure 5) exhibited appreciable individuality compared with the quaternary ammonium chloride–bromide solutions discussed above. The values of α_{Li^+} appeared to be virtually constant and independent of the molality, while α_{Na^+} decreased so that $\alpha_{Li^+} + \alpha_{Na^+}$ was concentration dependent. Moreover, the magnitudes of α_{Na^+} were significantly larger than those for α_{Li^+}, and Brønsted's relationship was far from being obeyed. A value of $\beta_{Li^+} + \beta_{Na^+} = -0.0034$ was obtained from the slope of the plot of $\alpha_{Li^+} + \alpha_{Na^+}$ with m in accordance with eq 10. It is possible that either β_{Li^+} or β_{Na^+} is zero, but both coefficients cannot be zero. Unfortunately, the errors in the values of α_{Li^+} and α_{Na^+} were such as to obscure a dependence of these quantities on x and, hence, estimates of β_{Li^+} and β_{Na^+} could not be made.

Applications to Ion-Exchange Systems. A consideration will now be given to the use of the foregoing values of α_B, α_C, β_B, and β_C in an interpretation of the phenomenon of ion-exchange selectivity. The basic Gibbs–Donnan equation for the equilibrium mass law concentration product ratio or selectivity coefficient, D_C^B, for the exchange of like, singly charged cations or anions may be written[6,7]

$$\log D_C^B = P(\bar{v}_C - \bar{v}_B)/2.3RT - \log (\gamma_C/\gamma_B)_r - 2 \log (\gamma_C/\gamma_B)_w \quad (11)$$

where the first term on the right-hand side measures the contribution of the "strain energy" for the ion-exchange copolymer molecular network, and the second and third terms, which contain single-ion activity coefficient ratios, measure the "interaction free energies" in the exchanger and in the dilute, external aqueous electrolyte mixture, respectively. The second term on the right-hand side of eq 11 is dominant for the exchange of bromide with chloride ion on cross-linked Dowex-2 preparations[7] and for the exchange of sodium with lithium ions on Dowex-50,[6] respectively, so that $\log D_C^B \approx \log (\gamma_C/\gamma_B)_r$ to a fair approximation. The quantity $\log (\gamma_C/\gamma_B)_r$ may be estimated from this approximation or computed from weight-swelling measurements taken on lightly cross-linked preparations of Dowex-2[7] and on Dowex-50[6] as a function of water

(19) W. H. McCoy and W. E. Wallace, *J. Am. Chem. Soc.*, **78**, 183 (1956).

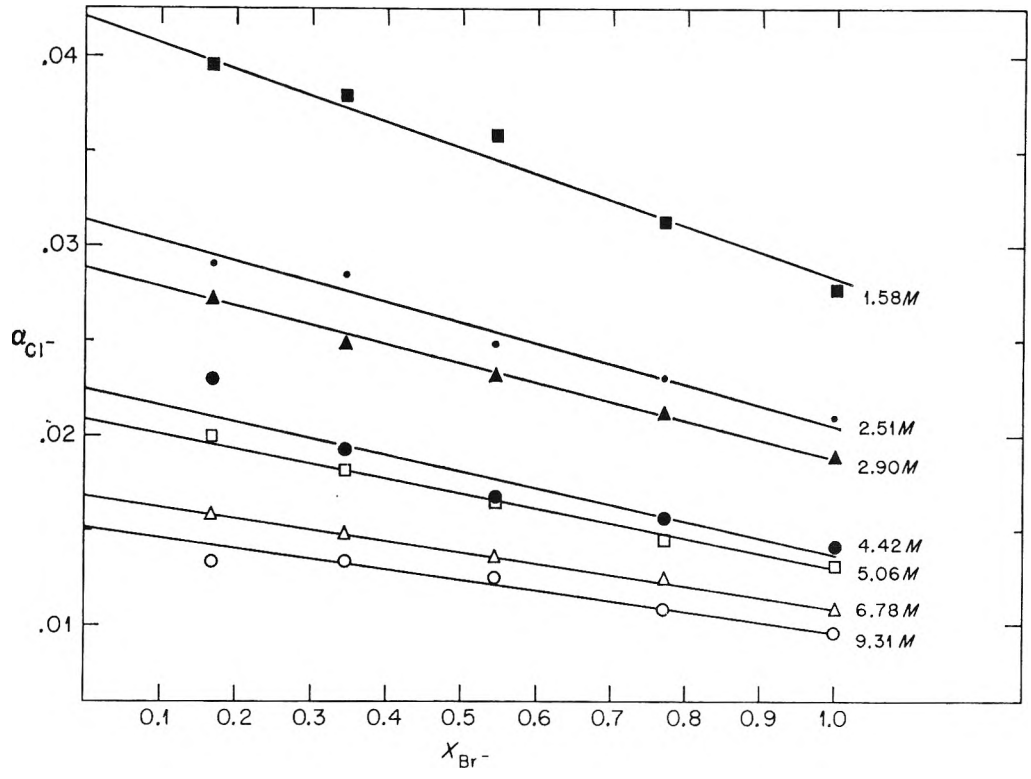

Figure 4. Dependence of chloride ion interaction coefficient for aqueous (β-hydroxyethyl)benzyldimethylammonium chloride + bromide mixtures on the bromide ion fraction, x_{Br^-}, at constant concentration.

activity. Comparisons will be made between the values obtained by the latter procedure and those found by combining eq 9a and 9b

$$\log (\gamma_C/\gamma_B) = \log (\gamma_C^0/\gamma_B^0) + \alpha_B m + \beta_B m^2 - (\alpha_B + \alpha_C)xm - 2\beta_B xm^2 - (\beta_B + \beta_C)x^2m^2 \quad (12)$$

and substituting the values of α_B, α_C, β_B, and β_C for the (β-hydroxyethyl)benzyldimethylammonium chloride–bromide and the lithium–sodium *p*-ethylbenzenesulfonate mixtures, respectively.[20]

Equation 12 simplifies to the form

$$\log (\gamma_C/\gamma_B) = \log (\gamma_C^0/\gamma_B^0) + (\alpha_B - \alpha_C)m/2 \quad (13)$$

for the aqueous "anion-exchanger model electrolyte" mixtures when $\beta_B + \beta_C = 0$ and $x = 0.5$. The calculations plotted as curve 2 in Figure 6A were made with eq 13 and values of α_B and α_C taken from Figures 3 and 4, respectively, while curve 1 for the lightly cross-linked anion exchanger was constructed from the data in Table IV of ref 7. The agreement between curves 1 and 2 falls within experimental error for concentrations above 5 *m*; at low concentrations log ($\gamma_{Cl^-}/\gamma_{Br^-}$) for the model compound mixtures approaches zero, whereas its value remains high for the anion exchanger because of the polyelectrolyte character of this material.

The equation for log (γ_C/γ_B) for the aqueous "cation-exchange model electrolyte" mixture is somewhat more complex because $\beta_B + \beta_C$ is not zero. Thus eq 12 becomes

$$\log (\gamma_C/\gamma_B) = \log (\gamma_C^0/\gamma_B^0) + [(\alpha_B - \alpha_C)m/2] - [(\beta_B + \beta_C)m^2/4] \quad (14)$$

for $x = 0.5$. The calculations plotted (curve 2) in Figure 6B were made with eq 14 and values of α_{Na^+} and α_{Li^+} taken from Figure 5 and with $\beta_{Na^+} + \beta_{Li^+} = -0.0034$. Curve 1 for log $(\gamma_{Li^+}/\gamma_{Na^+})_r$ for the cation exchanger was constructed from the data of Table III of ref 6. The agreement between curves 1 and 2 lies within the experimental errors for concentrations exceeding 5 *m*, and the discrepancy at lower concentrations may be attributed to the polyelectrolyte property of the cross-linked cation-exchange system.

Comparisons of the values of log ($\gamma_{Cl^-}/\gamma_{Br^-}$) for the tetramethylammonium chloride–bromide mixtures and for the benzyltrimethylammonium chloride–bromide mixtures with the (β-hydroxyethyl)benzyldimethylammonium chloride–bromide mixtures also are of interest. The first two systems may be described by eq 13, and

(20) The logarithm of the ionic activity coefficient ratio, of course, will be given by 2 log (γ_C/γ_B) as γ_C and γ_B are mean molal activity coefficients for 1–1 valence type electrolytes.

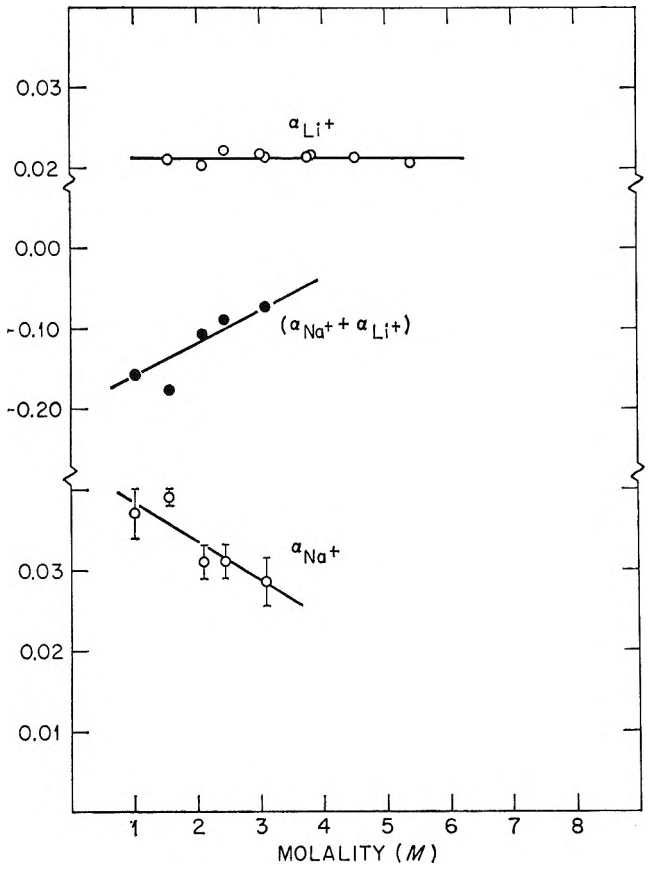

Figure 5. Concentration dependence of interaction coefficients for aqueous lithium + sodium *p*-ethylbenzenesulfonate mixtures.

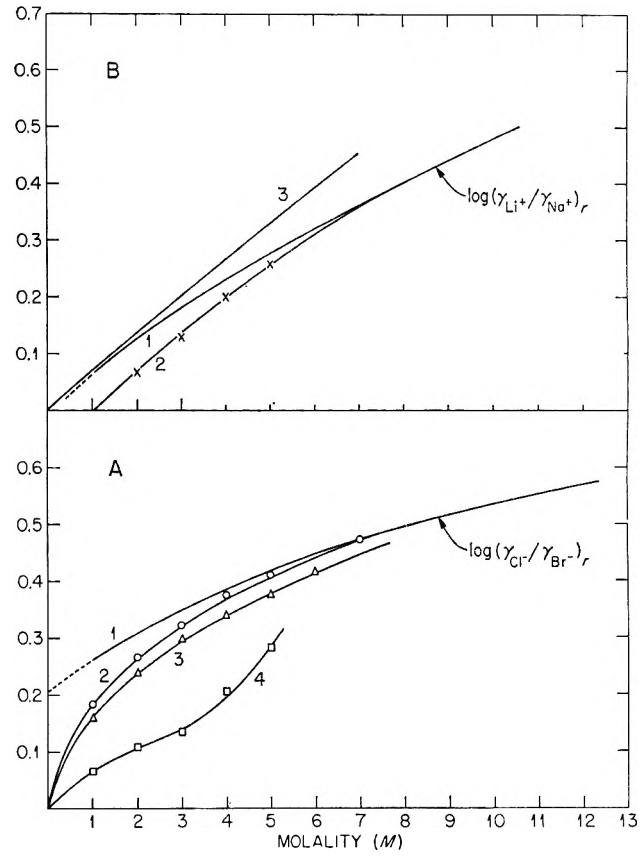

Figure 6. A. Concentration dependence of chloride–bromide ion activity coefficient ratios for an anion exchanger and several quaternary ammonium salt mixtures when x_{Br^-} = 0.5: curve 1, nominal 0.5% DVB cross-linked Dowex-2; curve 2, Dowex-2 "model compound"; curve 3, Dowex-1 "model compound"; curve 4, tetramethylammonium chloride + bromide mixture. B. Concentration dependence of lithium–sodium ion activity coefficient ratios for a cation exchanger and two salt mixtures when x_{Na^+} = 0.5: curve 1, nominal 0.5% DVB cross-linked Dowex-50: curve 2, (Li^+ + Na^+) *p*-ethylbenzenesulfonates; curve 3, (Li^+ + Na^+) chlorides.

(as may be observed in Figure 6A, curves 3 and 4) at a given molality their mean molal activity coefficient ratios are less than for the Dowex-2 model compound. This result allows the conclusion that the selectivity for bromide over chloride ion will be slightly less for Dowex-1-type exchangers where the exchange group is the benzyltrimethylammonium cation and significantly less for exchangers where tetramethylammonium cations are the exchange groups than for Dowex-2-type exchangers. The substitution of a benzyl group into the tetramethylammonium cation increases the binding of chloride and bromide ions and thus increases the selectivity for bromide ion. Replacement of a second methyl with a β-hydroxyethyl group produces an additional slight increase in bromide ion selectivity.

A comparison of the values of log $(\gamma_{Li^+}/\gamma_{Na^+})$ for mixtures of aqueous (Li^+ + Na^+)Cl solutions with those for the (Li^+ + Na^+)-*p*-EBS mixtures and for cross-linked polystyrenesulfonate cation exchangers can be made using the values of α_{Na^+} and β_{Na^+} reported by Robinson and Lim.[21] For these mixtures, $\beta_{Li^+} + \beta_{Na^+} = 0$, so that eq 13 applies for $x_{Na^+} = 0.5$. Surprisingly, as is shown in Figure 6B, curve 3, the values of log $(\gamma_{Li^+}/\gamma_{Na^+})$ for the ion exchanger and for the *p*-ethylbenzenesulfonate mixtures are both significantly lower than for the alkali chloride mixtures. This observation suggests that if chloride ion were structurally bound into a high molecular weight polymer the selectivity of the resulting "cation exchanger" would appreciably exceed that of cross-linked polystyrenesulfonates.

Acknowledgment. It is a pleasure to acknowledge

(21) R. A. Robinson and C. K. Lim, *Trans. Faraday Soc.*, 49, 1144 (1953).

with thanks the assistance of Q. V. Larson in the measurements with the lithium–sodium *p*-ethylbenzenesulfonate mixtures and of H. L. Holsopple in the preparation of several of the compounds used in this research.

Excited-State Reactivities. II. Basicities of Some Polymethylbenzenes in Their Excited Singlet States

by R. L. Flurry, Jr., and R. Keith Wilson

Department of Chemistry, Louisiana State University in New Orleans, New Orleans, Louisiana 70122
(Received July 29, 1966)

The absorption and fluorescence spectra of all of the polymethylbenzenes having three or more methyl groups have been measured in the trifluoroacetic acid–boron trifluoride solvent system. The fluorescence spectra of benzene and all of the methylbenzenes have also been measured in hydrocarbon solvents. The values for the polymethylbenzenes have been used with a Förster cycle to determine the basicities of these compounds in their excited singlet states. The compounds are found to be from 17 to 28 powers of ten more basic in their excited states than in their ground states.

Introduction

The weakly basic properties of aromatic hydrocarbons toward strong Brønsted acids have been recognized for some time.[1] Many of the ground-state properties of these protonated aromatic systems have been extensively studied.[2,3] All of these studies have dealt with the ground electronic states of the systems. Flurry and Lykos[4] have presented a quantum chemical prediction of the excited triplet-state basicities of the methyl-substituted benzenes. Unfortunately, there have, as yet, been no experimental data to compare with these predictions. One of the present authors has also recently presented a quantum chemical treatment of the excited singlet-state basicities of the series.[5]

Ratios of excited-state equilibria to ground-state equilibria may be obtained spectroscopically from the Förster cycle[6] by comparing the spectra of the reactants and products. The absorption spectra[7] and ground-state equilibrium constants[4,8] for the methylbenzenes in liquid hydrogen fluoride are known. From these, estimates of the excited-state basicity constants could be made. For most accurate results, however, the energies of the O–O transitions should be used in the Förster cycle. These O–O transitions are difficult to obtain directly. Levshin, however, discovered that there is an approximate mirror-image relationship between absorption and fluorescence spectra of complex molecules,[9] implying that a good estimate of the O–O

(1) See, for example, L. P. Hammet, "Physical Organic Chemistry," McGraw-Hill Book Co., Inc., New York, N. Y., 1940.

(2) For recent reviews, see H. H. Perkampus and E. Baumgarten, *Angew. Chem. Intern. Ed. Engl.*, **3**, 776 (1964).

(3) G. A. Olah and N. W. Meyer in "Friedel-Crafts and Related Reactions," Vol. I, G. A. Olah, Ed., Interscience Publishers, Inc., New York, N. Y., 1963, p 623.

(4) R. L. Flurry, Jr., and P. G. Lykos, *J. Am. Chem. Soc.*, **85**, 1033 (1963), paper I of this series.

(5) R. L. Flurry, Jr., *ibid.*, **88**, 5393 (1966).

(6) T. Förster, *Z. Elektrochem.*, **54**, 42 (1950).

(7) R. L. Flurry, Jr., and J. G. Jones, *J. Phys. Chem.*, in press.

(8) M. Kilpatrick and F. E. Luborsky, *J. Am. Chem. Soc.*, **75**, 577 (1953); E. L. Mackor, A. Hofstra, and J. H. van der Waals, *Trans. Faraday Soc.*, **54**, 186 (1958).

(9) W. L. Levshin, *Z. Physik*, **43**, 230 (1931).

transition for a given species can be obtained by averaging the energies of the absorption and fluorescence maxima. This, of course, will only be valid if the absorbing and fluorescing species are the same.

The present work presents an attempt to determine spectroscopically the excited-state basicity constants for all of the polymethylbenzenes having three or more methyl substituents based on the absorption spectra, the fluorescence spectra, and their average for the protonated species present in a trifluoroacetic acid–boron trifluoride system.

Experimental Section

Reagents. The methylbenzenes employed were commerically available reagent grade compounds. The liquids were fractionally distilled and the solids sublimed before using. When necessary, sulfuric acid washing was used to remove oxygen containing impurities. Owing to the extreme sensitivity of fluorescence techniques to impurities, the fluorescence spectra in both cyclohexane and the CF_3COOH–BF_3 system were taken as the final criteria for purity. In particular, the fluorescence spectra were examined for spurious peaks due to fluorescing impurities and for anomalous intensities which might be caused by the presence of fluorescence quenchers or photosensitizers. It was found that the fluorescence measurements were more sensitive to trace impurities than was gas chromatography, nmr, or the more common measurements of refractive index, melting point, or boiling point. With these precautions, the only probable impurities are very small amounts of positional isomers of the polymethyl compounds.

The fluorescence measurements of the uncomplexed aromatic were made in three solvents—ethanol, cyclohexane, and *n*-heptane. The ethanol was absolute ethanol from U. S. Industrial Chemicals Co. and the cyclohexane was fluorometric grade from Hartman-Leddon Co. Both of these were used without further purification. The heptane was Analytical reagent grade from Mallinckrodt. This was subjected to the usual hydrocarbon purification process of concentrated sulfuric acid wash, base wash, water wash, drying, and fractional distillation. It was found that the position of the fluorescence maximum was essentially insensitive to the solvent used.

The trifluoroacetic acid was Eastman White Label grade. It was distilled before use and redistilled into the absorption cells *via* a vacuum line. The boron trifluoride was from the Matheson Co. and was used without further purification.

Spectral Measurements. A vacuum line was used for preparing all of the samples in the CF_3COOH–BF_3 medium. Approximately 0.1 g of the methylbenzene was placed in a 1-cm quartz fluorescence cell with a ground-glass joint on it. This was attached to the vacuum line and approximately 3 ml of CF_3COOH was distilled in under reduced pressure. Boron trifluoride was then bubbled through the CF_3COOH solution until the entire system was at atmospheric pressure. The cell was removed and quickly stoppered with a glass stopper. The spectra were recorded immediately after the sample was prepared. Before each sample preparation, the vacuum line was dismantled, cleaned, oven dried, and reassembled.

Reproducible results were somewhat difficult to obtain in the fluorescence measurements on the acid solutions. For this reason, at least three successive samples of a given compound were measured. The standard deviations calculated for the fluorescence results reported are no greater than 1%. Fluorescence results when using cyclohexane, heptane, or ethanol as the solvent were completely reproducible.

The fluorescence measurements were made on an Aminco-Bowman Model SPF spectrophotofluorimeter, with a slit arrangement corresponding to the Aminco arrangement no. 1. The wavelength calibration on the present instrument is good to an accuracy of approximately ±1%. This, coupled with the experimental standard deviations, gives an over-all accuracy to the fluorescence energy measurements of approximately ±2%. The absorption spectra were obtained on a Perkin-Elmer Model 450 spectrophotometer. The absorption spectra of the complexes were more easily reproducible than the fluorescence spectra.

Results and Discussion

Table I presents the absorption and fluorescence maxima for the uncomplexed aromatics and their proton complexes in CF_3COOH–BF_3. For completeness, the uncomplexed values for benzene, toluene, and the xylenes are included. The complexes of these were apparently too unstable for their fluorescence to be observed under our conditions; consequently their absorption spectra in the acid media were not measured either. Also included for comparison are the absorption maxima of the entire series of complexes in liquid hydrogen fluoride.[7]

Thermodynamically, equilibrium constants are related to the difference in the standard free energy (ΔG°) between the reactant and product. Two equilibria

$$\ln K = -\frac{\Delta G^\circ}{RT} \qquad (1)$$

can be compared by comparing the ΔG° values of the reactions involved (eq 2). From the Förster cycle[6]

$$\ln \frac{K_A}{K_B} = \frac{-(\Delta G_A^\circ - \Delta G_B^\circ)}{RT} \quad (2)$$

(Figure 1) the changes in internal energy (ΔE) for the ground and excited states of the proton complexes may be related to the transition energies of the uncomplexed and complexed aromatic. In Figure 1, Ar and Ar* $$\Delta E_{Ar} + \Delta E_{ST} = \Delta E_{ArH^+} + \Delta E_{ST^*} \quad (3)$$ represent the ground and excited states of the aromatic, and ArH^+ and ArH^{+*} represent the ground and excited states of the proton complex. In Figure 1 and eq 3, ΔE_{Ar} is the energy of the first electronic transition of the aromatic, ΔE_{ArH^+} is that of the complex, and ΔE_{ST} and ΔE_{ST^*} are the stabilization energies of the ground and excited states of the complex, respectively.

Table I: Absorption and Fluorescence Spectra of the Methylbenzenes and Their Proton Complexes

Compound	λ_{max} (absorption), mμ: Hydrocarbon[a]	Liquid HF[b]	CF_3COOH–BF_3	λ_{max} (fluorescence), mμ: Hydrocarbon	CF_3COOH–BF_3
Benzene	255	320	...	285	...
Toluene	262	330	...	289	...
o-Xylene	263	335	...	...	...
m-Xylene	265	336	...	292	...
p-Xylene	274	350	...	291	...
Hemimellitene	262	345	350	294	484
Pseudocumene	267	351	344	315	461
Mesitylene	246	355	355	295	433
Prehnitene	268	339	372	298	483
Isodurene	268	365	370	298	493
Durene	278	362	364	300	482
Pentamethylbenzene	270	375	375	303	432
Hexamethylbenzene	272	385	384	310	445

[a] American Petroleum Institute Research Project 44, "Catalogue of Ultraviolet Spectrograms," National Bureau of Standards, 1945–1950. [b] Reference 7.

The ΔG° values of eq 2 contain both enthalpy and entropy terms. If, however, there is no pressure–volume work done by the system, internal energy change is equal to enthalpy change. If, furthermore, the entropy change is the same for the equilibrium in the ground-state and the excited state,[10] the ratios of the ground to excited-state basicities of the aromatics may be expressed as in eq 4. This relation also implies

$$\log \frac{K^*}{K} = \frac{(\Delta E_{Ar} - \Delta E_{ArH^+})}{2.303RT} \quad (4)$$

that there is no shift in ΔE_{Ar} in going from the hydrocarbon to the acid as the solvent. This is obviously an incorrect assumption; however, for lack of a method of estimating this shift, it was ignored. The first three columns of numbers in Table II present the logarithms of the ratios of excited-state to ground-state basicities for the molecules under consideration as calculated from the absorption spectra, the emission spectra, and the average of the two (presumably the energy difference for the O–O transition). These values are for a temperature of 27°.

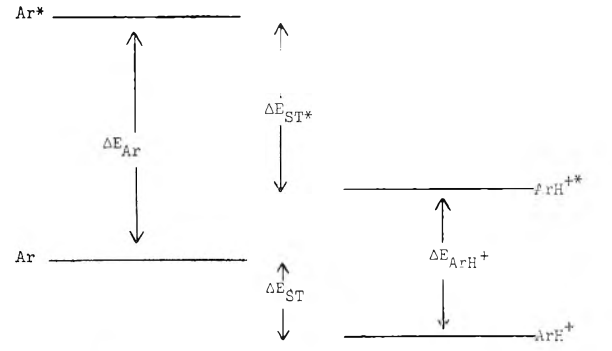

Figure 1. Förster cycle[6] for proton aromatic complexes. Ar and Ar* refer to the energies of the ground and excited states of the uncomplexed aromatic. ArH^{+*} and ArH^+ refer to those of the proton complexes. The ΔE_{ST} values are the stabilization energies.

Column four of Table II presents the ground-state basicities of these compounds in liquid hydrogen fluoride referred to hexamethylbenzene as a standard.[4,8] If the arguments of Hammett concerning relative basicities in various solvents are accepted,[11] this same scale of relative basicities should carry over into other solvent systems, including the trifluoroacetic acid–boron trifluoride system under consideration here. The relative basicities of the excited state can then be compared to a common standard by using these values.

$$\log (K^*/K_0^*) = \log (K^*/K) + \log (K/K_0) - \log (K_0^*/K_0) \quad (5)$$

Columns five, six, and seven of Table II present the excited-state basicities relative to the excited-state basicity of hexamethylbenzene.

A number of interesting facts are evident from Table II. The first and most obvious consideration is that the excited-state equilibrium constants obtained from

(10) It has been shown experimentally that the entropy change is nearly constant for protonic equilibria involving the ground and excited states of 3-hydroxyquinoline: J. C. Haylock, S. F. Mason, and B. E. Smith, *J. Chem. Soc.*, 4897 (1963).

(11) L. P. Hammett, "Physical Organic Chemistry," McGraw-Hill Book Co., Inc., New York, N. Y., 1940, Chapter 9.

Table II: Excited-State Basicities

Compound	Log (K^*/K)[b] Abs	Log (K^*/K)[b] Fl	Log (K^*/K)[b] Av	Log (K/K_0)[c]	Log (K^*/K_0^*)[d] Abs	Log (K^*/K_0^*)[d] Fl	Log (K^*/K_0^*)[d] Av	Excited singlet-state[e] localization energies, ev
Hemimellitene (1,2,3)	20.0	27.9	23.9	−3.6	−6.2	+3.8	−1.2	0.295
Pseudocumene (1,2,5)	17.5	21.4	19.4	−3.6	−8.7	−2.7	−5.7	0.403
Mesitylene (1,3,5)	26.1	22.7	24.4	−1.5	+2.0	+0.7	+1.4	0.589
Prehnitene (1,2,3,4)	20.3	26.9	23.6	−3.2	−5.5	+3.2	−1.1	0.293
Isodurene (1,2,3,5)	21.7	27.7	24.7	−1.1	−2.0	+6.1	+2.1	0.055
Durene (1,2,4,5)	17.8	26.4	22.1	−2.8	−7.6	+3.1	−2.2	0.292
Pentamethylbenzene	21.8	20.5	21.2	−1.0	−1.8	−1.0	−1.4	0.116
Hexamethylbenzene	22.6	20.5	21.5	0	0	0	0	0

[a] Position of methyl substitution in parentheses. [b] Excited-state basicities relative to ground-state basicities. Abs, fl, and av refer to absorption, fluorescence, and average, respectively. [c] Ground-state basicities relative to hexamethylbenzene.[4,8] [d] Excited-state basicities relative to hexamethylbenzene excited state. See eq 5. [e] Referred to hexamethylbenzene. From ref 5.

either the absorption or fluorescence spectra are all 17–28 powers of ten greater than the ground-state equilibrium constants. This is in qualitative agreement with the results of paper I where it was predicted that the excited triplet-state basicities should be more than 30 powers of ten greater than the ground-state basicities. The results from ref 5 permit a direct comparison of excited singlet-state calculations, as done by a configuration interaction method, with the experimental results. Table II also contains the excited singlet-state localization energies from ref 5 for comparison with the observed excited-state basicities. It is seen that there is a good agreement between the localization energies and the relative basicities as obtained from absorption measurements for all molecules except mesitylene. (The ground-state results for mesitylene in ref 5 did not agree with experiment, either.) The lack of a comparable agreement for the emission-determined basicities can be attributed in part to the use of ground-state geometries in the calculations.

Reference 5 showed that the excited singlets should be less reactive than the excited triplets. The slopes of a log (K/K_0) *vs.* localization energy plot were different for ground and excited singlet-state basicities; consequently the numerical factor of greater than 30 powers of ten for the enhancement of the triplet-state basicities reported in paper I is probably incorrect. If, however, the slope of the excited singlet-state basicities correlation were to hold for the triplets, the triplets should be from 4 (durene) to 12 (mesitylene) powers of ten more basic than the excited singlets. This, coupled with the experimental excited singlet-state basicities, should make the triplets some 22–37 powers of ten more basic than the ground states.

The rather large differences in log (K^*/K) as obtained from absorption and fluorescence measurements in certain cases is somewhat surprising (for example, a difference of 8.6 in the case of durene). There are a number of factors which could account for this. Among these are the possibility of a shift in position of protonation during the lifetime of the excited state, giving emission from a species different from that which is absorbing light radiation. A second possibility is the formation of valence isomers of the aromatic ring, similar to those produced photochemically by various workers,[12] which were the actual emitting species. It is also possible that there might have been some remaining impurities leading to spurious results. Perhaps the most likely possibility is that the geometric reorganization of the excited state is great enough that the mirror-image relationship of absorption to fluorescence no longer holds and that consequently the average of the two is no longer a good approximation for the O–O transition. To the extent that any of these processes occurs, the average absorption and fluorescence values would not represent the O–O transition and the corresponding relative basicities would not be the values desired. On the other hand, the basicities as calculated from the absorption and fluorescence probably do bracket the actual basicities of the excited singlet electronic states in their ground vibrational states.

Acknowledgments. The authors are indebted to Mr. E. W. Stout (N.S.F. Undergraduate Research Participant, academic year 1965–1966) for the spectra of hemimellitene. Financial support for this work was partially provided by an N.S.F. Undergraduate Research Participation grant (No. GE-6911).

(12) See, for example, H. J. F. Angus, J. M. Blair, and D. Bryce-Smith, *J. Chem. Soc.*, 2003 (1960); E. E. van Tamlen and S. P. Pappas, *J. Am. Chem. Soc.*, **84**, 3789 (1962); L. Kaplan, K. E. Wilzback, W. G. Brown, and S. S. Yang, *ibid.*, **87**, 675 (1965).

Oxidation of Soot by Hydroxyl Radicals

by C. P. Fenimore and G. W. Jones

General Electric Research and Development Center, Schenectady, New York *(Received August 12, 1966)*

In flame gases of temperatures from 1530 to 1890°K and $P_{O_2} \sim 10^{-4}$ to 0.3 atm, the rate of oxidation of soot does not depend very strongly on P_{O_2}. The observations are consistent with the assumption that about 0.1 of the collisions of OH with the soot remove a carbon atom, the number of collisions being calculated from P_{OH} by kinetic theory.

Millikan[1] inferred that tiny soot particles in fuel-rich hydrocarbon flames at 1700 to 1800°K were oxidized by OH radicals rather than by the much larger concentrations of CO_2 or H_2O. Graham and co-workers[2] also considered OH to be a very reactive oxidant. They proposed that the gasification of massive pieces of carbon in a very hot stream of fuel-rich combustion products was due to the removal of a carbon atom in about 0.03 of the collisions of OH with pyrolytic carbon, or in about 0.1 of those with commercial graphites.

When O_2 is present, OH might be less important. Lee and co-workers[3] reported a rate of soot oxidation of

$$1.085 \times 10^4 P_{O_2} T^{-1/2} e^{-39.3 \text{ kcal}/RT} \text{ g cm}^{-2} \text{ sec}^{-1} \quad (1)$$

in flame gases, with P_{O_2} = 0.05–0.10 atm and T = 1350–1650°K, as if O_2 were the only important reactant when P_{O_2} was considerable. Neither P_{O_2} nor T was constant in any experiment, however, and it is uncertain how well the separate effect of each variable was untangled from the observations.

We have measured soot oxidation in flame gases of constant P_{O_2} and T during each run, so that the variables were separated experimentally. In the ranges P_{O_2} = 0.04–0.30 atm and T = 1530–1890°K, we find little dependence on P_{O_2}. Even in slightly fuel-rich gas where P_{O_2} is very small, soot oxidation remains considerable. Our rates are about five times faster than those reported by Lee and co-workers at the same temperature and P_{O_2}.

One way of explaining our weak dependence on P_{O_2} is to suppose that soot is mainly oxidized by OH in our flames. We measured the partial pressure of this radical in some of our runs and found that the observed oxidation rates could be accounted for by a collision efficiency of OH on soot of about 0.1.

If OH was important, the fact should be revealed by comparing the rate of oxidation in flames with the rate of a suspension of soot in dry gas where OH was absent. We could not make this comparison at the same temperature as we would have liked to. However, soot suspended in dry gas at 1200°K oxidized more slowly than would be expected from an extrapolation of our flame results. Furthermore, the rate of oxidation in dry gas depended on P_{O_2}. We think an additional mechanism besides oxidation by O_2 is important in our flames, and we favor an oxidation by OH.

The slower rates observed by Lee and co-workers may reflect differences in the flames used; P_{OH} was doubtlessly smaller in their gases than in ours at the same P_{O_2} and T. It is possible that when P_{OH} is smaller, a reaction with O_2 became more important, as is implied by their reported dependence on P_{O_2}.

Experimental Section

Experimental Flames. Figure 1 is a sketch of the apparatus used to obtain fuel-lean sooty flames. A rich mixture of molecular proportions of $C_2H_4 + 1.2O_2 + 2.0Ar$ was burnt on a porous burner[4] to give a gas containing soot equal to about 1% of the carbon fed as ethylene. Sixteen per cent of the fuel remained in the products as hydrocarbons, mostly as acetylene and the rest as carbon oxides, steam, and hydrogen. The products were cooled, mixed with additional constituents, and finally burnt on a second burner. The

(1) R. C. Millikan, *J. Phys. Chem.*, 66, 794 (1962).

(2) J. A. Graham, A. R. G. Brown, A. R. Hall, and W. Watt, *Soc. Chem. Ind.* (London), 1958.

(3) K. B. Lee, M. W. Thring, and J. M. Beer, *Combust. Flame*, 6, 137 (1962).

(4) W. E. Kaskan, *Symp. Combustion, 6th*, 134 (1957).

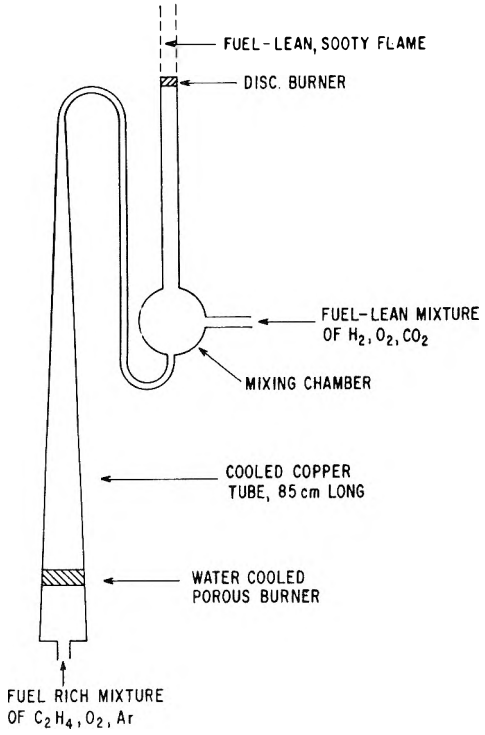

Figure 1. Arrangement of apparatus to get a fuel-lean sooty flame.

soot gasified in an environment of constant P_{O_2} and T above the second burner.

The second burner was a copper disk 2 cm in diameter by 0.6 cm thick with 220 0.1-cm holes running through it and a copper cooling coil soldered around it. Its flame consisted of a series of small cones, one per hole, whose flows merged into an approximately one-dimensional stream of burnt gas 0.1 cm above the surface. The disks were made by W. E. Kaskan when he worked in our laboratory several years ago.

The second flame usually became unstable if its temperature fell below 1600°K, although one acceptable run was obtained at 1530°. Temperature was measured by a fine quartz-coated thermocouple.[4]

The extent of reaction was determined by sucking a measured volume of gas through a quartz probe held at various distances above the disk and catching the soot on a plug of Vycor wool in the cool leg of the probe. The probe was evacuated at room temperature and then heated with a flame while oxygen was passed through it. The stream of oxygen and carbon oxides was run through hot copper oxide and the carbon dioxide trapped at 113°K (isopentane slush). The trap was cooled further in liquid nitrogen and evacuated, then warmed, and its contents expanded into a mass spectrometer where the carbon dioxide was measured.

A correction was established by analyzing over-all fuel-lean runs in which the first burner was not ignited, so that all the reactants burnt at once on the disk in a soot-free flame. The correction was 8% of the soot measured close to the disk, but a larger percentage further downstream. Measurements were not attempted after the correction had grown to 30%, which means that the region of study rarely extended farther than 1 cm downstream of the disk.

Soot samples were also caught on carbon substrates in a similar probe and submitted to E. F. Koch of our laboratory for electron micrographs. These samples were strings of uniform spheres about 200 A in diameter before burning in the second flame and about 100 A in diameter after the soot content had fallen by oxidation to 0.22% of the carbon in the ethylene.

Arrangement for Oxidation in Dry Gas. Soot, collected from the same flame used to generate it for the flame oxidations, was evacuated overnight at 500°K, then cooled and loaded into a closed vessel equipped with a sealed stirrer to disperse it. A small flow of N_2 through the stirred vessel carried entrained soot to mix with a large volume of dry preheated gas.

The large volume of preheated gas was N_2 or N_2–O_2 mixtures piped through a quartz tube of 1.3 cm inside diameter. The tube was heated by two electric furnaces each 30 cm long. The gas was preheated in the first furnace, then mixed without much drop in temperature with about 0.1% of its volume of the soot suspension from the stirred vessel. The hot dilute suspension passed through the second furnace, and the surviving soot was caught on a plug of Vycor wool and measured as before.

The soot added to the preheated gas was taken to be that which was measured when N_2 containing less than 0.2% O_2 was used in the quartz tube. This amount was a constant ±10%, independent of the gas temperature in the second furnace, 1000 to 1200°K when a constant flow was passed through the dispersing vessel. The extent of reaction was measured by the decrease in soot recovered when the hot dry gas contained oxygen. However, the uncertainty of ±10% in the soot added meant that the minimum reaction rate observable was about 0.7×10^{-6} g of carbon cm^{-2} sec^{-1}. At 1140°K or less, the rate was certainly not larger than this when $P_{O_2} = 0.21$. At 1200°K, measurable rates were obtained for $P_{O_2} = 0.12$ and 0.21 but not for $P_{O_2} = 0.05$.

Other Experiments. A few measurements were made of the rate of oxidation of soot containing 1% manganese by weight. This was made by saturating the argon flow to the soot-forming burner with volatile manganese–methylcyclopentadienyl–tricarbonyl. The

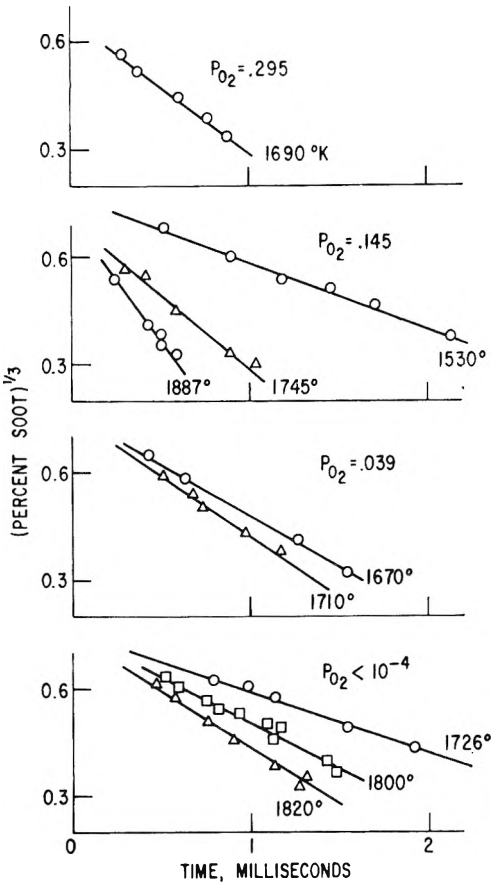

Figure 2. Cube root of the soot content *vs.* time. Soot is expressed as a percentage of the carbon fed in the ethylene; time is inferred from the known gas velocity.

yield of soot was approximately the same whether it contained manganese or not.

Results

We assume that the soot consists of uniform spheres which react, at a constant rate per unit of area, with a surrounding gas of fixed temperature and composition. From geometrical considerations, the gasification can be expressed

$$(d/d_0) = \left(\frac{\text{per cent soot}}{\text{per cent soot}_0}\right)^{1/3} = 1 - \frac{2R(t - t_0)}{\rho d_0} \quad (2)$$

where d is the diameter of a particle, per cent soot equals the carbon present as soot, expressed as a percentage of the carbon fed in the ethylene, R the reaction rate in g of carbon cm^{-2} sec^{-1}, t the time, and ρ the density of a particle. The zero subscript refers to some arbitrary point at which $d = d_0$.

Figure 2 gives the flame data in plots of (per cent soot)$^{1/3}$ *vs.* time. From each curve, a value of $(2R/\rho d_0)_{0.6}$ appropriate to eq 2 was computed and listed in Table I. In these values d_0 is the d when (per cent soot)$^{1/3}$ = 0.6; it is about 1×10^{-6} cm and unchanged from run to run; therefore, the values of $(2R/\rho d_0)_{0.6}$ are about 10^6 times R itself.

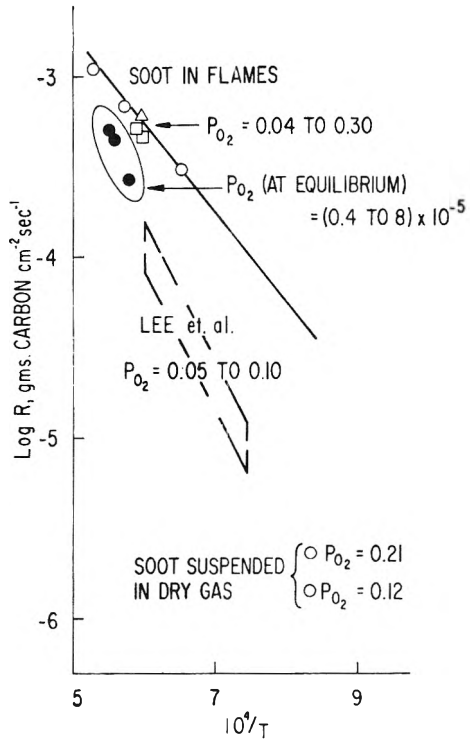

Figure 3. Reaction rate *vs.* $1/T$. Flame data from Table I. The range of observations by Lee and co-workers in the soot cloud above a hydrocarbon diffusion flame is indicated. The lower two points give measurements of oxidation rate in dry N_2–O_2 mixtures.

Values of $10^{-6}(2R/\rho d_0)_{0.6} \simeq R$ are plotted against the reciprocal of temperature in Figure 3. The six runs with appreciable P_{C_2} establish a line with activation energy of about 22 kcal mole.$^{-1}$ The three slightly fuel-rich runs lie below this line, but surprisingly close if the oxidation is truly by O_2. The slower, more oxygen-dependent rates reported by Lee and co-workers are indicated.

Figure 3 also contains two points for the oxidation of soot in dry gas at lower temperatures. These rates are less than the values expected from a long extrapolation of the flame data. Furthermore, the oxidation in dry gas depends more strongly on P_{O_2} than does our flame oxidation. It is probable that our flames possess an additional mechanism besides oxidation by O_2.

Figure 4 shows a plot of $(2R/\rho d_0)_{0.6}$ against the calculated equilibrium P_{OH}. Since P_{OH} was doubtlessly larger than the equilibrium pressure,[5] we determined

(5) W. E. Kaskan, *Combust. Flame*, 2, 229, 286 (1958).

Table I: Rate of Gasification of Soot in Flame Gases

T, °K	Gas composition, mole fraction O_2	CO_2	H_2O	Ar	CO	$\left(\frac{2R}{\rho d_0}\right)_{0.6}$, sec^{-1}
1690	0.295	0.437	0.166	0.102	...	620
1530	0.149	0.608	0.132	0.149	...	310
1745	0.143	0.561	0.161	0.135	...	700
1887	0.145	0.510	0.187	0.158	...	1090
1670	0.039	0.676	0.158	0.127	...	460
1710	0.038	0.658	0.168	0.136	...	520
1726[a]	0.04×10^{-4}	0.574	0.213	0.155	0.026	270
1800[a]	0.12×10^{-4}	0.586	0.232	0.145	0.034	450
1820[a]	0.83×10^{-4}	0.591	0.210	0.182	0.016	510

[a] P_{O_2} is the calculated equilibrium pressure for the three slightly rich runs.

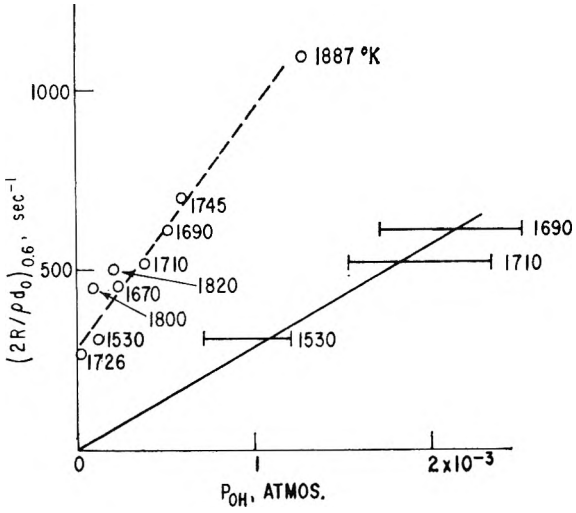

Figure 4. Upper curve is a quantity proportional to R plotted against the calculated equilibrium P_{OH}. Lower curve is the same quantity *vs.* the measured P_{OH} for three of the runs.

the actual P_{OH} in three lean runs by substituting N_2O for part of the CO_2 added in the mixing chamber and observing the rate of reaction 3 in the region of interest

$$O + N_2O \longrightarrow 2NO \qquad (3)$$

The [O] was determined from the measured [N_2O], d[NO]/dt, and T, the rate constant being known,[6] and P_{OH} was then inferred from equilibrium (reaction 4) which was certainly balanced.[5]

$$O + H_2O = 2OH \qquad (4)$$

The results of the measurements are given in Table II and a curve for these data is also drawn in Figure 4 passing through the origin with a slope of $(2R/\rho d_0)_{0.6} = 300 \pm 100$ per 10^{-3} atm of P_{OH}. A displacement of the other points so that they too fall on the corrected curve would be consistent with what is known about excess OH;[5] *i.e.*, the ratio of actual P_{OH} to the equilibrium pressure would be larger, the lower the temperature or the smaller P_{O_2}.

Table II: Ratio of Actual P_{OH} to the Calculated Equilibrium Pressure in Three Runs

T, °K	P_{O_2}	P_{OH}, equil	$\frac{P_{OH}, \text{actual}}{P_{OH}, \text{equil}}$
1690	0.295	5.3×10^{-4}	4 ± 0.8
1530	0.149	1.2	8 ± 2
1710	0.038	3.8	5 ± 1

The number of collisions of OH radicals with the soot is calculable from P_{OH} by kinetic theory. If a fraction, α, of these abstracts a carbon atom, $R = 3 \times 10^{-3}\alpha$ g of carbon cm^{-2} sec^{-1} when $P_{OH} = 10^{-3}$. Inserting this R into

$$(2R/\rho d_0)_{0.6} \simeq 300$$

and putting $\rho = 2$, $d_0 = 1 \times 10^{-6}$, we get a collision efficiency of $\alpha \simeq 0.1$.

Comparison with Lee and Co-workers. P_{OH} was doubtlessly smaller in Lee's gases than in ours even for the same final P_{O_2} and T. We added H_2 to help stabilize our flames on the second burner; its combustion generated many radicals, but Lee, *et al.*, did not have a similar source of radicals in their experiment. Furthermore, their observation times were 10 to 25 times longer than ours, so any excess radicals should have decayed farther toward equilibrium. Their linear dependence of the rate on P_{O_2}, expression 1 in

(6) C. P. Fenimore and G. W. Jones, Eighth Symposium on Combustion, Williams and Wilkins, Baltimore, Md., 1962, p 127.

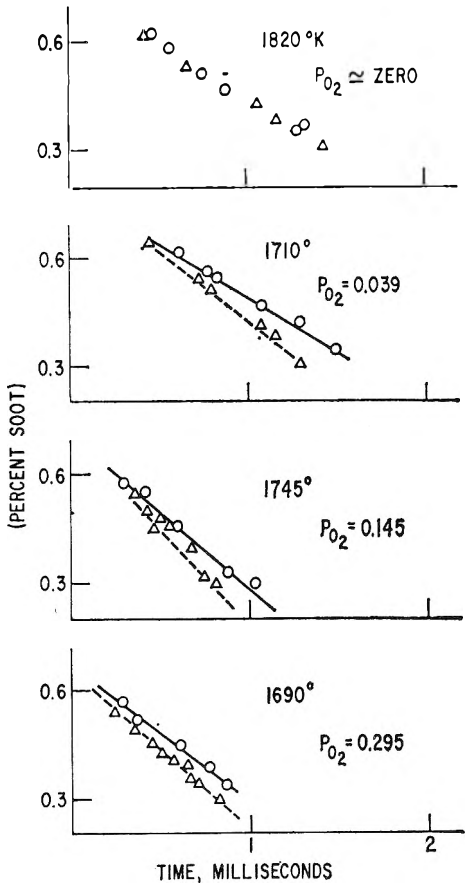

Figure 5. Circles represent data already shown in Figure 2; triangles represent similar measurements in the same flames for soot containing 1% Mn.

the introduction, suggests that when P_{OH} is only the equilibrium pressure and when $P_{O_2} = 0.075 \pm 0.025$, the oxidation by O_2 is important.

Only a small range of P_{O_2} was examined by them, however, and perhaps the dependence on this variable was not established beyond question. We want to add that if their rates did not really depend much on P_{O_2}, it is possible that an oxidation by OH was important for them too. To show this, we write out the expected rate of reaction if OH, equilibrated according to reaction 5

$$^1/_4O_2 + {}^1/_2H_2O = OH \quad \Delta H = 37.8 \text{ kcal} \qquad (5)$$

oxidized their soot with a collision efficiency, α. The expected rate under these assumptions is

$$1.63 \times 10^4 \alpha P_{O_2}{}^{1/4} P_{H_2O}{}^{1/2} T^{-1/2} e^{-37.8/RT} \qquad (6)$$

which has values of the same order as expression 1. When $\alpha = 0.1$, $P_{O_2} = 0.075$, and $P_{H_2O} = 0.2$, expression 6 predicts rates 60% as large as expression 1 in the range 1350–1650°K.

We have no reason to doubt that an oxidation by O_2 was important in Lee's work, but an oxidation by OH was probably important too.

Catalysis by Manganese. Soot containing 1% manganese by weight oxidized at a lower temperature than soot free of manganese. When heated in a stream of oxygen, initially at room temperature, and the temperature raised 6° min^{-1}, the maximum rate occurred at 680°K for the catalyzed and at 800°K for the uncatalyzed soot.

Figure 5 shows that manganese also increased the rate of reaction in flame gases having appreciable P_{O_2}, but by only about 20%. Although the catalysis may not look very clear-cut in Figure 5, it was easy to see in the flames themselves that the addition of manganese in the soot contracted the yellow carbon zone. In the slightly rich gases, the appearance of the carbon zone was unaffected by manganese in the soot, and no catalysis is seen in Figure 5 for the rich gas.

Since the catalysis only occurred in lean gas, the catalytic reaction was probably an oxidation by O_2. Perhaps it is reasonable to add that the oxidation in slightly fuel-rich gas was probably not a reaction with O_2 because it was not catalyzed. Since the rate in slightly fuel-rich flame gases was of the same order as the rate when P_{O_2} was appreciable, this may be an additional reason for believing that most of the reaction of soot occurred with some other oxidant than O_2 even when P_{O_2} was appreciable.

Acknowledgment. We are grateful to G. E. Moore for helpful discussions.

Cobalt-60 γ Radiolysis of Solutions of Potassium Bromide in 0.8 N Sulfuric Acid

by Farhataziz[1]

Radiation Laboratory,[2] University of Notre Dame, Notre Dame, Indiana 46556 *(Received August 15, 1966)*

The ^{60}Co γ radiolysis of potassium bromide in 0.8 N H_2SO_4 has been studied in detail. A new mechanism is suggested for deaerated solutions in which O_2 is produced with G = 0.008 and Br^- disappears with $G \sim 0.01$. It is concluded that $g(HO_2)$ is 0.008 in ^{60}Co γ radiolysis of 0.8 N H_2SO_4 solutions. $G(H_2) = g(H_2) = 0.38$ for bromide solutions in 0.8 N H_2SO_4. The H_2O_2 yields in bromide solutions containing $O_2 \sim 300$ μM are higher by a few per cent than in the case of aerated solutions. This difference is due to micromolar quantities of CO_2 present in aerated solutions. The k_{H+Br_2} has been estimated to be $(12 \pm 50\%) \times 10^{10}$ M^{-1} sec^{-1}.

The radiolysis of potassium bromide solutions has been studied by numerous workers with changing emphasis on the different aspects of the subject.[3-17] Recent studies[15-17] have exposed inadequacies in the previously accepted mechanism for radiolysis of aqueous bromide solutions at pH 2. In this paper, results of a detailed investigation of ^{60}Co γ radiolysis of bromide solutions in 0.8 N H_2SO_4 are presented. Such results indicate a need for revision of the mechanism applicable to 0.8 N H_2SO_4 solutions as well.

Experimental Section

The potassium bromide and sulfuric acid used in this work were Baker AR grade.

Distilled water from a Barnstead still was distilled under a stream of O_2 in a two-stage Pyrex system. The first stage contained alkaline $KMnO_4$. The second stage contained no additives and was included to trap any Mn salt which under certain conditions comes over with the water. After every distillation stage, the mixture of O_2 and steam passed through Pyrex tubing (2-cm o.d. and 25 cm long) heated to 350°. The triply distilled water was finally distilled in an Engelhard all-quartz bidistillation apparatus, Model B3. The condensed water was stored in Pyrex vessels.

The glassware used for preparation of solutions and irradiation was cleaned with chromic acid, rinsed with tap water, rinsed with the high-purity water, dried in an oven, and then heated to 450° for about 1.5 hr. The syringe techniques for irradiation, degassing, and gas solution were essentially those of Hart, *et al.*,[18] and are described in detail by Farhataziz and Dyne.[19] The commercially available all-glass 100-ml syringes were modified by sealing 5/20 $\overline{\mathbf{f}}$ joints of N51 Kimble glass to their outlets. A Hochanadel–Ghormley type 2-kc

(1) On leave from Pakistan Atomic Energy Commission.

(2) The Radiation Laboratory of the University of Notre Dame is operated under contract with the U. S. Atomic Energy Commission. This is AEC Document No. COO-38-461.

(3) H. Fricke and E. J. Hart, *J. Chem. Phys.*, **3**, 596 (1935).

(4) C. J. Hochanadel, *J. Phys. Chem.*, **56**, 587 (1952).

(5) E. R. Johnson and A. O. Allen, *J. Am. Chem. Soc.*, **74**, 4147 (1952).

(6) T. J. Sworski, *ibid.*, **76**, 4867 (1954).

(7) A. O. Allen and R. A. Holroyd, *ibid.*, **77**, 5852 (1955).

(8) J. A. Ghormley and C. J. Hochanadel, *Radiation Res.*, **3**, 227 (1955).

(9) H. A. Mahlman and J. W. Boyle, *J. Am. Chem. Soc.*, **80**, 773 (1958).

(10) H. A. Schwarz, J. M. Caffrey, and G. Scholes, *ibid.*, **81**, 1801 (1959).

(11) M. Burton and K. C. Kurien, *J. Phys. Chem.*, **63**, 899 (1959).

(12) E. Hayon, *ibid.*, **65**, 1502 (1961).

(13) C. Ferradini and A. M. Koulkes-Pujo, *J. Chim. Phys.*, **104**, 1310 (1963).

(14) B. Cercek, M. Ebert, J. P. Keene, and A. J. Swallow, *Science*, **145**, 919 (1964).

(15) A. Rafi and H. C. Sutton, *Trans. Faraday Soc.*, **61**, 877 (1965).

(16) B. Cercek, M. Ebert, C. W. Gilbert, and A. J. Swallow, Proceedings of the International Symposium on Pulse Radiolysis, Manchester, England, April 1965, Academic Press, London, 1965, p 83.

(17) H. C. Sutton, G. E. Adams, T. W. Boag, and B. O. Michael, Proceedings of the International Symposium on Pulse Radiolysis, Manchester, England, April 1965, Academic Press, London, 1965, p 61.

(18) E. J. Hart, S. Gordon, and D. A. Hutchison, *J. Am. Chem. Soc.*, **75**, 6165 (1953); E. J. Hart, *ibid.*, **76**, 4312 (1954).

(19) Farhataziz and P. J. Dyne, CRC-1205 or AECL-2113, 12, 1964.

^{60}Co source was used. The dose rate was about 1.7×10^{20} ev $l.^{-1}$ min^{-1} in 0.8 N H_2SO_4 as determined by Fricke dosimetry with $G(Fe^{3+}) = 15.6$.

Hydrogen peroxide was determined by mixing the irradiated solutions with a definite volume of ~2 mM $FeSO_4$ in 0.8 N H_2SO_4 and measuring Fe^{3+} extinction at 304 or 275 mμ. Values of the extinction coefficient used are 2240 M^{-1} cm^{-1} at 25° with a 0.7% per degree increase at 304 mμ and 1830 M^{-1} cm^{-1} at 275 mμ. If bromine is produced during radiolysis, it also will react with Fe^{2+} to give Fe^{3+}, and this method will measure both H_2O_2 and bromine.

Bromide was measured by the spectrophotometric method based on complex formation between bromide and palladous salts.[20] A stock solution of palladous sulfate of $\sim 1.5 \times 10^{-2}$ M strength in 1.5 N H_2SO_4 was prepared directly from $PdSO_4 \cdot 2H_2O$. The 1:10 dilution of stock solution with water should give an optical density from 0.15 to 0.17 at 390 mμ when compared against water in 1-cm cells. A slight precipitation of palladium occurs in the stock solution after several days. The filtered solution should be tested by the 1:10 dilution test; if needed, more $PdSO_4$ should be dissolved. For analysis, the desired volume of KBr solution in 0.8 N H_2SO_4 is taken and diluted with 0.8 N H_2SO_4 to give a total volume of 5 ml. This solution is diluted to 10 ml by adding water and 0.25 ml of palladous sulfate stock solution. The absorbance is measured at 230 mμ against a blank prepared from 5 ml of 0.8 N H_2SO_4. The extinction coefficient is 10,020 M^{-1} cm^{-1}. Hydrogen peroxide does not interfere in the estimation of bromide. However, at concentrations of ~200 μM a correction for its absorption at 230 mμ must be applied.

The gases were extracted in a modified Van-Slyke apparatus and directly injected into an F and M 700 gas chromatograph for analysis. A Molecular Sieve 5A column of 3.5-ft length was used with a thermal conductivity detector at 150°. Argon was used as flow gas for H_2 estimation and helium for O_2 estimation with a flow rate of about 55 ml/min.

Results

Deaerated Solutions. Measured 100-ev yields are denoted by G and primary yields by g. All solutions were in 0.8 N H_2SO_4. Oxygen is produced with a $G = 0.008$ that is constant over the bromide concentration range 3×10^{-5} to 3×10^{-3} M and for doses up to 450×10^{20} ev $l.^{-1}$. For the same dose range and for the bromide concentration range 1×10^{-5} to 3×10^{-3} M, $G(H_2O_2 + Br_2) = 0.38$, where Br_2 includes Br_3^-.

In 3×10^{-5} M KBr solutions, which provided the best conditions for KBr analysis, G for the disappearance of Br^- is estimated to be about 0.01 from Br^- measurements before and after a dose of $\sim 450 \times 10^{20}$ ev $l.^{-1}$. Because all other yields were independent of dose over this range, it is assumed that disappearance of Br^- behaves similarly. It is further assumed that Br^- changes to Br_2. Bromine is a stable product in the irradiation of aerated solutions at pH 2.[15]

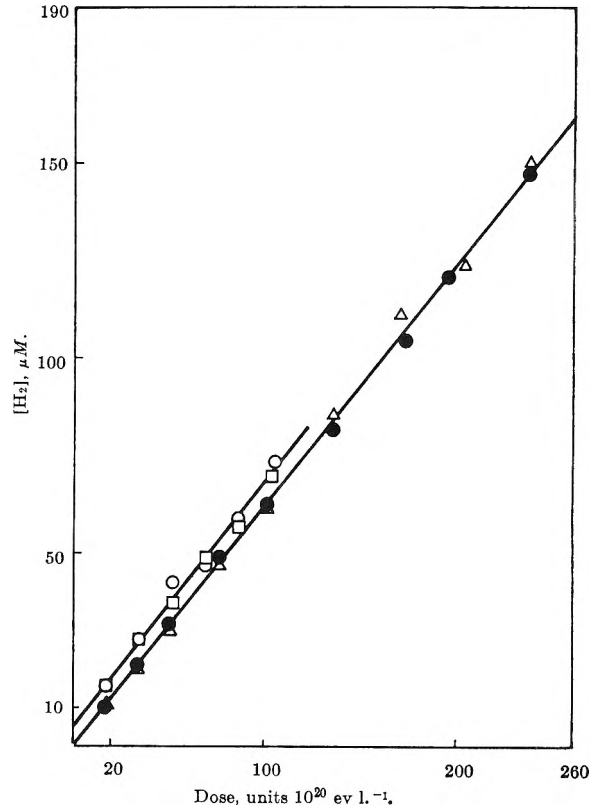

Figure 1. Hydrogen formation by ^{60}Co γ irradiation of potassium bromide solutions in 0.8 N H_2SO_4 with following initial concentrations of bromide: ○, 3.23×10^{-5} M, deaerated; □, 3.19×10^{-3} M, deaerated; ●, 3.41×10^{-5} M, $[O_2]_0 = 282$ μM, △, 3.19×10^{-3} M, $[O_2]_0 = 262$ μM.

Hydrogen yields are shown in Figure 1. The straight line has a small positive intercept on the ordinate; the slope gives $G(H_2) = 0.38$, independent of bromide concentration from 1×10^{-5} to 3×10^{-3} M.

Oxygenated Solutions. No disappearance of Br^- was detectable in KBr solutions of 1×10^{-5} to 3×10^{-3} M containing O_2 from 50 μM to saturation for doses up to 300×10^{20} ev $l.^{-1}$.

Dose dependence of the hydrogen peroxide yield in solutions of different KBr concentration containing about 300 μM O_2 is shown in Figure 2. A slight non-

(20) F. W. Chapman, Jr., and R. M. Sherwood, *Anal. Chem.*, **29**, 172 (1957).

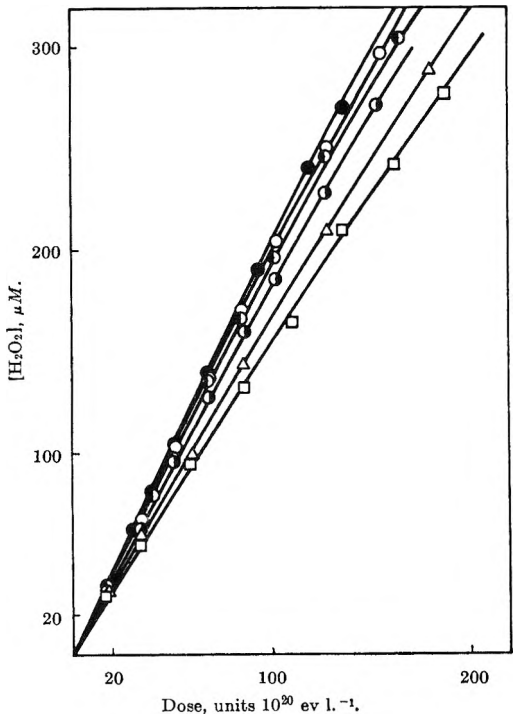

Figure 2. H_2O_2 formation by ^{60}Co γ irradiation of oxygenated ($[O_2]_0$ = 237 to 297 μM; see Table I) potassium bromide solutions in 0.8 N H_2SO_4 with following initial concentrations of bromide: □, 3.23 × 10^{-3} M; △, 1.13 × 10^{-3} M; ◑, 3.29 × 10^{-4} M; ◐, 0.99 × 10^{-4} M; ○, 3.08 × 10^{-5} M; ●, 1.30 × 10^{-5} M.

linearity is observed. Formation of H_2O_2 in 3.39 × 10^{-4} M KBr solutions was found to increase slightly with increase in O_2 concentration. The yield of H_2O_2 decreases with increase in KBr concentration of solutions containing $O_2 \sim 300$ μM. The results are summarized in Table I.

The hydrogen yield is linear with dose absorbed for all solutions containing KBr from 1 × 10^{-5} to 3 × 10^{-3} M and O_2 from 50 μM to saturation. Some results for solutions containing about 300 μM O_2 are shown in Figure 1. $G(H_2)$ increases slightly with decrease in O_2 concentration. For 3.3 × 10^{-4} M KBr solutions, $G(H_2)$ is 0.36, 0.37, and 0.38 for O_2 concentrations of 750, 260, and 55 μM, respectively. (The value for 55 μM O_2 concentration is the initial yield.) The $G(H_2)$ for zero O_2 concentration is taken to be 0.38.

Table I: Initial Yields for Different Initial Concentrations of Bromide and O_2

[KBr], M	[O_2], μM	$G(H_2O_2)$	$G(H_2)$[a]
3.23 × 10^{-3}	284	0.965	
1.13 × 10^{-3}	278	1.07	
3.39 × 10^{-4}	54.9	1.10	0.38
3.39 × 10^{-4}	295	1.11	0.37
3.39 × 10^{-4}	781	1.13	0.36
0.99 × 10^{-4}	276	1.18	
3.08 × 10^{-5}	237	1.22	
1.30 × 10^{-5}	297	1.23	

[a] These values are for 3.3 × 10^{-4} M KBr solution containing O_2 = 55, 260, and 750 μM, respectively. $G(H_2)$ for zero O_2 concentration is taken as 0.38.

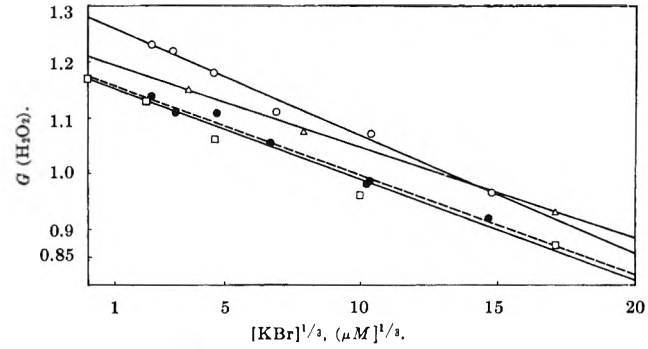

Figure 3. Initial $G(H_2O_2)$ as a function of cube root of potassium bromide concentration: ○, present work, $[O_2]_0$ = 237–297 μM (see Table I); △, Burton and Kurien,[11] aerated; □, Sworski,[6] aerated; ●, – – – –, present work, aerated.

Aerated Solutions. The yield of hydrogen peroxide in aerated solutions (~250 μM O_2) is slightly nonlinear with dose absorbed. The initial $G(H_2O_2)$ is lower by a few per cent than in solutions to which pure O_2 was added to give a concentration of about 300 μM, as shown in Figure 3. The aerated solutions contained about 12 μM CO_2. For ~3.2 × 10^{-4} M KBr solutions, the initial $G(H_2O_2)$ was suppressed from 1.06 to 0.92 when the CO_2 concentration was increased to ~200 μM in aerated solutions.

Discussion

Rafi and Sutton[15] have shown that the classical mechanism for ardiolysis of bromide solutions is inadequate in aerated solutions. Their conclusion that Br_2^- plays an important role has been supported by recent pulse radiolysis studies.[16,17] A similar conclusion is necessary to explain the results in deaerated solutions. In such solutions, the $G(O_2)$ = 0.008, independent of dose and KBr concentration, must be attributable to a spur reaction. Hart[21] has shown that a small $G(O_2)$ in the Fe^{2+}–Cu^{2+} system results from HO_2 production in spurs by the reaction OH + H_2O_2 → HO_2 + H_2O. Considering the magnitude of values, $G(O_2)$ = 0.008 measured in deaerated KBr system is in fairly good agreement with the value of 0.016 measured by Hart.

(21) E. J. Hart, *Radiation Res.*, 2, 33 (1955).

Because Br_2 is assumed to be produced (corresponding to measured Br^- loss) in radiolysis of the deaerated solutions, there are two possible reactions for O_2 formation from HO_2.

$$Br_2 + HO_2 \longrightarrow Br_2^- + H^+ + O_2 \quad (1)$$

and

$$HO_2 + HO_2 \longrightarrow H_2O_2 + O_2 \quad (2)$$

Sutton, *et al.*,[17] give $k_1 \sim 1 - 2 \times 10^8\ M^{-1}\ sec^{-1}$ while k_2 is $2.2 \times 10^6\ M^{-1}\ sec^{-1}$.[22,23] Consequently, reaction 1 must be responsible for O_2 formation. This model of O_2 formation requires that HO_2 not be an intermediate in the reaction scheme. A new reaction scheme is suggested for deaerated solutions in 0.8 N H_2SO_4 that includes reaction 1 and the following reactions

$$H_2O \longrightarrow H, OH, H_2, H_2O_2, HO_2 \quad (3)$$

$$OH + Br^- \longrightarrow Br + OH^- \quad (4)$$

$$Br + Br^- \rightleftharpoons Br_2^- \quad (5)$$

$$Br_2^- + Br_2^- \longrightarrow Br_3^- + Br^- \quad (6)$$

$$Br_3^- \rightleftharpoons Br_2 + Br^- \quad (7)$$

$$Br + Br \longrightarrow Br_2 \quad (8)$$

$$H + Br_2 \longrightarrow H^+ + Br^- + Br \quad (9)$$

$$H + H_2O_2 \longrightarrow OH + H_2O \quad (10)$$

Reactions 4 and 9 can be written alternatively as[17]

$$\left.\begin{aligned} Br^-(aq) + H^+(aq) &\rightleftharpoons (Br^-\text{----}H^+)(aq) \\ (Br^-\text{----}H^+)(aq) + OH &\longrightarrow Br + H_2O \end{aligned}\right\} \quad (4a)$$

$$H + Br_2 \longrightarrow H^+ + Br_2^- \quad (9a)$$

From the above reaction scheme, the following relations can be derived, where $G(Br_2)$ includes Br_2 and Br_3^-.

$$2G(Br_2) = G(-Br^-) = g(OH) - g(HO_2) + g(H)\frac{\frac{k_{10}[H_2O_2]}{k_9[Br_2]} - 1}{\frac{k_{10}[H_2O_2]}{k_9[Br_2]} + 1} \quad (A)$$

$$G(O_2) = g(HO_2) \quad (B)$$

$$G(H_2O_2) + G(Br_2) = g(H_2O_2) - {}^1/_2[g(H) - g(OH)] - {}^1/_2 g(HO_2) \quad (C)$$

$$G(H_2) = g(H_2) = G(H_2O_2) + G(Br_2) + 2G(O_2) \quad (D)$$

Substitution into eq D of the measured values of $G(H_2O_2) + G(Br_2)$ and $G(O_2)$ gives $G(H_2) = 0.396$, which is in good agreement with the value of 0.38 measured. Substituting $g(OH) = 2.95$,[24] $g(H) = 3.65$,[24] $k_{10} = 1.7 \times 10^8\ M^{-1}\ sec^{-1}$,[25] $G(-Br^-) = 0.01$, and for $[H_2O_2]/[Br_2]$ the value of $[G(H_2O_2) + G(Br_2) - {}^1/_2G(-Br^-)]/[{}^1/_2G(-Br^-)]$ in eq A, gives $k_9 \sim 12 \times 10^{10}\ M^{-1}\ sec^{-1}$. Sutton, *et al.*,[17] give an estimate of $k_9 \sim 10^{10}\ M^{-1}\ sec^{-1}$ in 0.1 N acid. However, they claim a fivefold uncertainty in their results. Considering the possibility of a rather large error in the measurement of $G(-Br^-) \sim 0.01$, agreement between the two values of k_9 is satisfactory.

The small positive intercept obtained for hydrogen formation at zero dose in deaerated solutions (*cf.* Figure 1) is attributed to the presence of organic impurities which can yield H_2 by H-abstraction reactions. This assumption is confirmed by the results in oxygenated solutions, where H_2 formation is linear over the whole dose range. Because H is present as HO_2 in such solutions, an H-abstraction reaction is not possible. The value of $G(H_2) = 0.38$ is in good agreement with the value of 0.384–0.404 given by Hayon[12] and 0.38 given by Ferradini and Koulkes-Pujo.[13] However, higher values have been reported.[8,9] The lower value satisfies the stoichiometric relation between H_2O_2 and H_2 (see eq D); various studies agree well with $G(H_2O_2) + G(Br_2) = 0.38$.[6,13] Because other investigators do not estimate $G(-Br^-)$, their values for $G(H_2O_2)$ are equivalent to $G(H_2O_2) + G(Br_2)$ as measured in the present study. Thus the lower value cannot be attributed to a failure to determine accurately all oxidizing and reducing species produced.

The mechanism presented differs from the old mechanism in the introduction of Br_2^- reactions and rejection of reactions such as 11 and 12. The HO_2 could conceivably become an intermediate through the following reactions.

$$Br_2^- + H_2O_2 \longrightarrow H^+ + 2Br^- + HO_2 \quad (11)$$

$$Br + H_2O_2 \longrightarrow H^+ + HO_2 + Br^- \quad (12)$$

The studies of Rafi and Sutton[15] and Sutton, *et al.*,[17] indicate that reaction 11 is too slow to play an important role; however, the results of Cercek, *et al.*,[16] are not in agreement with such a conclusion. If reaction 12 is to make a negligible contribution, it is necessary that $k_{5f}[Br^-] \geq 10\ k_{12}[H_2O_2]$. For $3 \times 10^{-5}\ M$ KBr solutions (which is the lowest KBr concentration used for O_2 measurement) with accumulation of 250

(22) J. H. Baxendale, *Radiation Res.*, **17**, 312 (1962).

(23) G. Czapski and B. H. J. Bielski, *J. Phys. Chem.*, **67**, 2180 (1963).

(24) A. O. Allen, *Radiation Res. Suppl.*, **4**, 54 (1964).

(25) M. S. Matheson, *ibid.*, **4**, 1 (1964).

μM H_2O_2 and using a value of $k_{5f} = 5.4 \times 10^9$,[16,17] a value of $k_{12} \leqq 7 \times 10^7$ M^{-1} sec^{-1} is required. Such a value differs significantly from the value of $k_{12} \approx 2.5 \times 10^9$ M^{-1} sec^{-1} for neutral solutions.[17] However, the mechanism of reaction 12 in neutral solution may be

$$H_2O_2 \rightleftharpoons HO_2^- + H^+$$

$$HO_2^- + Br \longrightarrow HO_2 + Br^-$$

which could not occur at an appreciable rate in 0.8 N H_2SO_4.

Oxygenated Solutions. In oxygenated solutions, H atoms are converted to HO_2 by

$$H + O_2 \longrightarrow HO_2 \qquad (13)$$

The results can be explained in terms of reactions 1–8 and 13. The stoichiometric relations are

$$G(H_2O_2) = g(H_2O_2) + {}^1/_2[g(H) - g(OH)] + {}^1/_2 g(HO_2) \qquad (14)$$

$$G(H_2) = g(H_2)$$

$$G(H_2O_2) + G(H_2) = 2[g(H_2O_2) + g(HO_2)] \qquad (15)$$

$G(H_2)$ decreases slightly as the concentration of O_2 is increased. Such an effect would be expected as O_2 scavenges H in spurs. The decrease in $G(H_2)$ must be accompanied by an equivalent increase in $G(H_2O_2)$ as is observed in the results of Table I. The decrease in $G(H_2O_2)$ with increased dose is attributable to H_2O_2 competition for H atoms by reaction 10; k_{13} and k_{10} are 2.6×10^{10} and 1.7×10^8 M^{-1} sec^{-1}, respectively.[25] $G(H_2O_2)$ decreases with increasing concentration of KBr and conforms to a cube-root plot[6] as shown in Figure 3. Such behavior has been interpreted in terms of scavenging by Br^- of OH in spurs.[6,26] The initial $G(H_2O_2)$ for $[Br^-] = 0$ and $\sim$300 μM O_2 is 1.28 (*cf.* Figure 3), which becomes 1.27 when corrected for H scavenging in spurs by O_2 (see Table I). Substituting $G(H_2O_2) = 1.27$, $g(HO_2) = 0.008$ and $G(H_2) = 0.38$ in eq 15 gives $g(H_2O_2) = 0.82$, which is in good agreement with the value of 0.80 given by Allen.[24] However, using $g(H) = 3.65$,[24] $g(OH) = 2.95$,[24] $g(HO_2) = 0.008$ in eq 14 and C give $g(H_2O_2) = 0.916$ and 0.734, respectively. This apparent discrepancy can be understood by addition of eq 14 and C, which gives $2g(H_2O_2)$ as the sum of measured peroxide yields in oxygenated and deaerated solutions. The $g(H_2O_2)$ so calculated is 0.825 which is in excellent agreement with the value of 0.82 calculated from eq 15. It would seem, therefore, that $[g(H) - g(OH)]$ must be 0.89 in the case of Br^- radiolysis, rather than 0.70 as calculated from $g(H) = 3.65$ and $g(OH) = 2.95$. Whether such a difference can be attributed to a change in either or both $g(H)$ and $g(OH)$ is not clear.

Effect of CO_2 on H_2O_2 Yields in Aerated Solutions. The aerated solutions have $\sim$250 μM O_2. $G(H_2O_2)$ in aerated solutions of KBr is consistently lower by a few per cent than in oxygenated solutions containing $O_2 \sim 300$ μM (*cf.* Figure 3.) The results shown in Figure 3 are in good agreement with those of Sworski[6] but not those of Burton and Kurien,[11] which may be an effect of different impurity levels in the water used.

$G(H_2O_2)$ was suppressed from 1.06 to 0.92 in aerated solutions of $\sim 3.2 \times 10^{-4}$ M KBr by the addition of $\sim$200 μM CO_2. Such a result strongly suggests that the lower $G(H_2O_2)$ in aerated, as compared to oxygenated, solutions is attributable to the presence of $\sim$12 μM CO_2. Although the effect has not been thoroughly investigated, the following reactions present a plausible interpretation.

$$CO_2 + Br_2^- \longrightarrow CO_2^- + Br_2$$

$$CO_2 + HO_2 \longrightarrow CO_2^- + H^+ + O_2$$

$$CO_2^- + H^+ \longrightarrow COOH$$

The radical COOH may dimerize to $(COOH)_2$ or react with H_2O_2.[27]

$$COOH + H_2O_2 \longrightarrow CO_2 + H_2O + OH$$

Acknowledgments. The author is grateful to Dr. E. J. Hart for a critical discussion of the results. It is a pleasure to acknowledge the encouragement received from Dr. R. R. Hentz.

(26) T. Rigg, *Discussions Faraday Soc.*, **12**, 119 (1952).

(27) E. J. Hart, J. K. Thomas, and S. Gordon, *Radiation Res. Suppl.*, **4**, 74 (1964).

The Conformational Transition of Poly(methacrylic acid) in Solution

by M. Mandel, J. C. Leyte, and M. G. Stadhouder

Laboratory of Physical Chemistry (III), The University of Leyden, Leyden, The Netherlands
(Received August 15, 1966)

New potentiometric and spectroscopic results are given in connection with the conformational transition between a compact and an extended state of poly(methacrylic acid) (PMA) in solution. Potentiometric titrations of PMA in aqueous solutions at 5 and 50° show that the temperature has a definite influence on the properties of the two mean conformations and on the region of the degree of dissociation α wherein the transition takes place. The stability of the compact state with respect to the extended state, at zero degree of ionization, is found to decrease with an increasing temperature. Spectrophotometric titrations of PMA and poly(acrylic acid) (PAA) at different concentrations in water and water–methanol (40%) mixtures are compared. It is concluded that in this mixed solvent the conformational transition of PMA still occurs in about the same region of α as in water. From Beer's law the extinction coefficients for the undissociated carboxylic groups in the compact state are found to be only slightly affected by the change in solvent composition in water–methanol mixtures up to 40% methanol. The difference between the extinction coefficient of –COOH in both states (for the extended state as derived from the titration curves) in water and in water–methanol (40%) is much more important. This difference seems to be only a matter of difference in the intensity and not due to a spectral shift. Infrared measurements in solutions of deuterated PMA in D_2O–CD_3OD mixtures up to a 40% volume fraction of alcohol show no influence of the solvent composition on the position of the C=O stretching frequency of the –COOH group in the compact state. From the experimental results it is concluded that the stabilization of the compact state of PMA is not *primarily* due to hydrophobic bonding but should be ascribed to a direct stabilization of certain chain conformations by van der Waals interactions between the methyl side chains.

I. Introduction

For some years it has been known that the solution properties of poly(methacrylic acid) (PMA) exhibit deviations from the expected behavior of synthetic polyelectrolytes as found with other polyvinylic compounds.[1–7] Recently, Leyte and Mandel[8] have shown that the peculiar titration curve of PMA can be explained by assuming that the PMA molecule undergoes a cooperative transition between two mean conformations or states. In agreement with the viscosimetric behavior of PMA, it was concluded that the undissociated or slightly charged PMA molecule is characterized by a compact mean conformation which unfolds by the charging process in a narrow region of the degree of dissociation α corresponding roughly to $0.10 < \alpha < 0.30$.

From the titration behavior of partially esterified PMA, Mandel and Stadhouder[9] concluded that the stabilization of the mean conformation at low α values (the "a state") is not due to hydrogen bonding between

(1) R. Arnold and J. T. G. Overbeek, *Rec. Trav. Chim.*, **69**, 162 (1950).

(2) A. Katchalsky and H. Eisenberg, *J. Polymer Sci.*, **6**, 145 (1951).

(3) A. Katchalsky, *ibid.*, **7**, 393 (1951).

(4) R. Arnold, *J. Colloid Sci.*, **12**, 549 (1957).

(5) A. Silberberg, J. Eliassaf and A. Katchalsky, *J. Polymer Sci.*, **23**, 259 (1957).

(6) H. P. Gregor, D. H. Gold, and M. Frederick, *ibid.*, **23**, 467 (1957).

(7) M. Mandel and J. C. Leyte, *ibid.*, **56**, S25 (1962).

(8) J. C. Leyte and M. Mandel, *ibid.*, **A2**, 1879 (1964).

(9) M. Mandel and M. G. Stadhouder, *J. Makromol. Chem.*, **80**, 141 (1964).

the carboxylic groups and should be ascribed to van der Waals interactions between the methyl side groups. They also found that the transition only depends on the *mean charge density* along the chain, as for different degrees of esterification the same transition curve was obtained as a function of the fraction of ionized groups with respect to the total number of monomers.

At the 1965 IUPAC Symposium of Macromolecular Chemistry in Prague, the compact a state of PMA was simultaneously discussed in two papers which both concluded that the uncharged molecules in water are essentially stabilized by *hydrophobic interactions* in analogy with some theories about the structure of globular proteins. Liquori and co-workers[10] showed that many properties of PMA in aqueous solutions are explainable in terms of the already proposed conformational transition between two different states. They concluded that the compact a state could be stabilized by hydrophobic interactions without obtaining any contradictions with the discussed properties. Anufrieva and co-workers[11] gave more direct evidence for this kind of stabilization. They studied the influence of different alcohols on some properties of aqueous PMA solutions, especially the binding of fluorescent dyes by this polyelectrolyte. This binding was shown to decrease with an increasing volume fraction of the alcohol and to disappear above about 40%. Starting from the assumption that only the compact state binds the dyes, these authors reached the conclusion that alcohol tends to destroy the normal compact state. They showed this to be in agreement with viscosimetric data and to advocate hydrophobic binding as the stabilizing factor for the low-pH mean conformation.

In both papers the experimental evidence for the hydrophobic bonding as defined by Kauzmann[12] and Scheraga and co-workers[13,14] for globular proteins was either qualitative or indirect. As PMA, a very simple synthetic polyelectrolyte, may serve as a model for the understanding of the behavior of more complicated macromolecules, it seemed worthwhile to gather more experimental information about its conformational transition.

Some new potentiometric and spectroscopic (ultraviolet and infrared) results are presented here which do not seem to indicate that hydrophobic interactions are the important factor for the stabilization of the compact state of PMA.

II. Experimental Section

A. Materials. Conventional poly(methacrylic acid) was obtained by the method described previously.[8] The fraction used in this work was characterized by its molecular weight, $\bar{M}_\eta$ = 185,000, determined according to Arnold and Overbeek.[1]

Poly(acrylic acid) was prepared by polymerization of acrylic acid in water in the presence of H_2O_2.[15] The fraction used here had a molecular weight, $\bar{M}_\eta$ = 136,000, determined according to Newman, *et al.*[16] Aqueous solutions were prepared with conductance water obtained from a mixed-bed exchange column mostly by dilution of a more concentrated stock solution which was stored frozen in a polyethylene flask. The concentration of the polyelectrolyte solutions was determined by potentiometric titration.

NaOH (0.1 *M*) was obtained by dilution from a Merck's Titrisol ampulla; methanol p.a. (Analar, BDH) was used without further purification; D_2O of 99.8% purity was obtained from the Dutch Reactor Center, RCN, Petten; CD_3OD was of commercial origin (Merck); and deuterated PMA was obtained by repeatedly dissolving PMA in D_2O and evaporating under reduced pressure.

B. Potentiometric Titrations. They were performed with a Radiometer automatic titration apparatus (TTT1, in conjunction with a SBR2 titrigraph and a SBU1 syringe buret) in a thermostated titration vessel under nitrogen atmosphere. Radiometer glass (G202C) and calomel (K4312) electrodes were used. All titrations were performed with 0.1 *M* NaOH.

C. Spectroscopic Measurements. Ultraviolet spectra were determined with a Zeiss nonrecording single-beam PMQ II. Ordinary cells of 1- or 0.5-cm optical path length, with Suprasil windows and a Teflon stopper, were used in testing Beer's law. Spectrophotometric titrations were performed in a specially designed titration cell (Suprasil windows) of variable path length (0.2–0.4 cm) to which NaOH could be added, under vigorous agitation, by a microburet (agitation was stopped during the measurement of the absorbance). Compensation was obtained by a variable path length reference cell, also with Suprasil windows. The operations were carried out under a nitrogen atmosphere. All of the cells were thermostated at 20°.

Infrared spectra were recorded with a Unicam re-

(10) A. M. Liquori, G. Barone, V. Crescenzi, F. Quadrifoglio, and V. Vitagliano, IUPAC Symposium of Macromolecular Chemistry, Prague, 1965, Preprint, p 588.

(11) E. V. Anufrieva, T. M. Birshtein, T. N. Nekrasova, O. B. Ptitsyn, and T. V. Sheveleva, ref 10, Preprint, p 468.

(12) W. Kauzmann, *Advan. Protein Chem.*, **14**, 1 (1959).

(13) G. Némethy and H. A. Scheraga, *J. Phys. Chem.*, **66**, 1773 (1962).

(14) H. A. Scheraga, *Ann. N. Y. Acad. Sci.*, **125**, 253 (1965).

(15) P. Selier, Thesis, Leiden, 1965.

(16) S. Newman, W. R. Krigbaum, C. Laugier, and P. J. Flory, *J. Polymer Sci.*, **14**, 451 (1954).

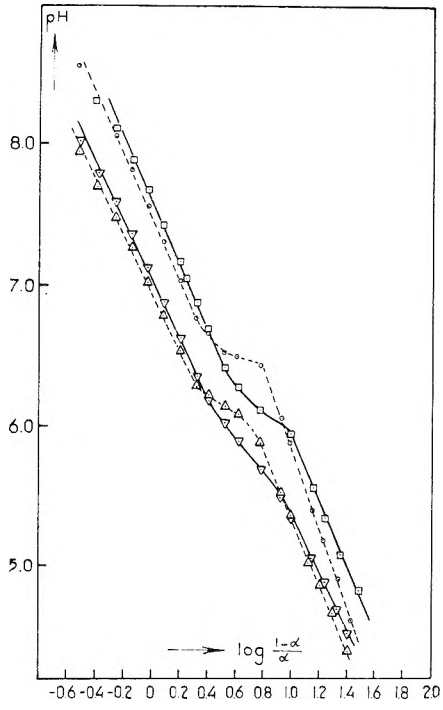

Figure 1. Henderson–Hasselbalch plots for PMA in an aqueous solution (2.60×10^{-3} equiv/l.) at different temperatures with and without added salt: ⊙, 5°; ⊡, 50°; △, 2.80×10^{-3} *M* $NaNO_3$, 5°; ▽, 2.80×10^{-3} *M* $NaNO_3$, 50°.

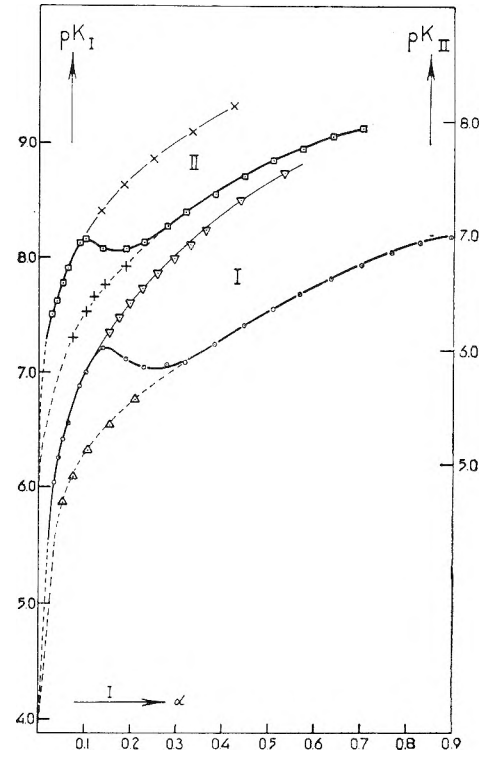

Figure 2. The apparent p*K* as a function of α for PMA in an aqueous solution (2.60×10^{-3} equiv/l.) in the absence of added salt. Curve I, 5°: ⊙, calculated from the experimental titration curve; ▽, points for PMA[a] and △, points for PMA[b], as extrapolated from the Henderson–Hasselbalch plot. Curve II, 50°: ⊡, calculated from the experimental titration curve; ×, points for PMA[a] and +, points for PMA,[b] as extrapolated from the Henderson–Hasselbalch plot (curve II is shifted upward with respect to curve I).

cording double-beam SP100. Sample solutions were measured between CaF_2 plates with Teflon spacers. D_2O and CD_3OD absorption was compensated for with a variable path length cell set at 1600 cm^{-1}. All solutions for the infrared measurements were prepared in a drybox.

III. Results

A. Potentiometric Titrations. The potentiometric titration of PMA in aqueous solutions has been performed at 5 and 50° both in the absence and in the presence of added salt ($NaNO_3$). These titrations are represented in Figure 1 as Henderson–Hasselbalch plots. It has been shown previously[8] that from a plot against α of the apparent p*K* as derived from the titration curve and the extrapolation of the p*K* of both states through the transition region (Figure 2), the difference in the Gibbs free energy, *G*, between the two states at $\alpha = 0$ can be derived. In Table I thermodynamic quantities derived from such plots are given. Index a stands for the compact, low-pH state and index b for the state of unfolded conformations; *Z* is the number of monomers per macromolecule. Thus $(G_b - G_a)_{\alpha=0}/ZkT$ is the difference in the Gibbs free energy per monomeric unit, with respect to *kT*, between states a and b, at the degree of ionization 0. Obviously this must be a positive quantity. Furthermore, $(H_b - H_a)_{\alpha=0}/ZkT$ and $(S_b - S_a)_{\alpha=0}/ZkT$ are the analogous enthalpy and entropy terms. The latter has been obtained using the relation

$$\frac{[(S_b - S_a)_{\alpha=0}]}{Zk} = \frac{[(G_b - G_a)_{\alpha=0,T''} - (G_b - G_a)_{\alpha=0,T'}]}{Zk(T'' - T')} \quad (1)$$

which implies that within the small temperature interval $(T'' - T')$ considered, the enthalpy and the entropy differences should remain constant. Both quantities are positive.

Potentiometric titrations of PMA in water–methanol (40%) mixtures at room temperature, not shown here, do not exhibit any irregularities which would indicate the presence of a conformational transition, as found

in water. Therefore, either no transition occurs at all or the difference in pK between the two states is too small to lead to such irregularities.

B. Spectroscopic Results. In aqueous solutions spectrophotometric titrations in the ultraviolet region have been carried out using four concentrations ranging from 2 to 7 $\times$ 10^{-3} equiv $l.^{-1}$ for PMA and 2 to 8.7 $\times$ 10^{-3} for PAA. The carboxylic group and its dissociated form absorb from the far-ultraviolet region down to about 40,000 cm^{-1}. The maximum for the undissociated –COOH lies at about 47,000 cm^{-1} and for the carboxylate $-COO^-$ above 52,000 cm^{-1}. In the present work all titrations have been performed at fixed frequencies ranging from 45,000 to 50,000 cm^{-1}. At each frequency a plot of the measured absorbance A of PMA against α yields the same over-all picture: for values of $\alpha \geqq 0.40$, A changes linearly with α; for $\alpha < 0.40$, the experimental points deviate from the former straight line. These deviations are greatest at the wavenumbers (σ) 46,000 and 47,000 cm^{-1} and tend to disappear at $\sigma > 48{,}000$ cm^{-1}. In Figure 3 the experimental points have been plotted as $A' = A/bC_t$ against α, where b is the optical path length in the titration cell and C_t the analytical concentration of the polyelectrolyte. Analogous curves obtained with PAA (Figure 4) are linear over the whole α range, which suggests that the deviations of linearity observed for $\alpha < 0.40$ in PMA solutions are connected to the conformational transition.

Table I: Thermodynamic Quantities for the Conformational Transition of PMA as Derived from Potentiometric Titrations[a]

	278°K		323°K
$(G_b - G_a)_{\alpha=0}/ZkT$	0.32		0.24
$(H_b - H_a)_{\alpha=0}/ZkT$	0.54		0.46
$(S_b - S_a)_{\alpha=0}/Zk$		0.22	

[a] Symbols explained in the text.

In the case of PAA, the reduced absorbance A' of the solution can be written as

$$A' = A/bC_t = \epsilon_{AH} + (\epsilon_{A^-} - \epsilon_{AH})\alpha \qquad (2)$$

Here ϵ_{AH} and ϵ_{A^-} are the extinction coefficients (expressed in 1000 cm^2 $equiv^{-1}$) of the undissociated carboxylic group and its dissociated form, respectively. Extrapolation of A' to $\alpha = 0$ yields ϵ_{AH}. This quantity can also be obtained from a check of Beer's law for unneutralized PAA solutions in the presence of an excess of $HClO_4$ (not absorbing under the experimental conditions) (Figure 5). The agreement between values of ϵ_{AH} obtained by both methods is good (see Table II).

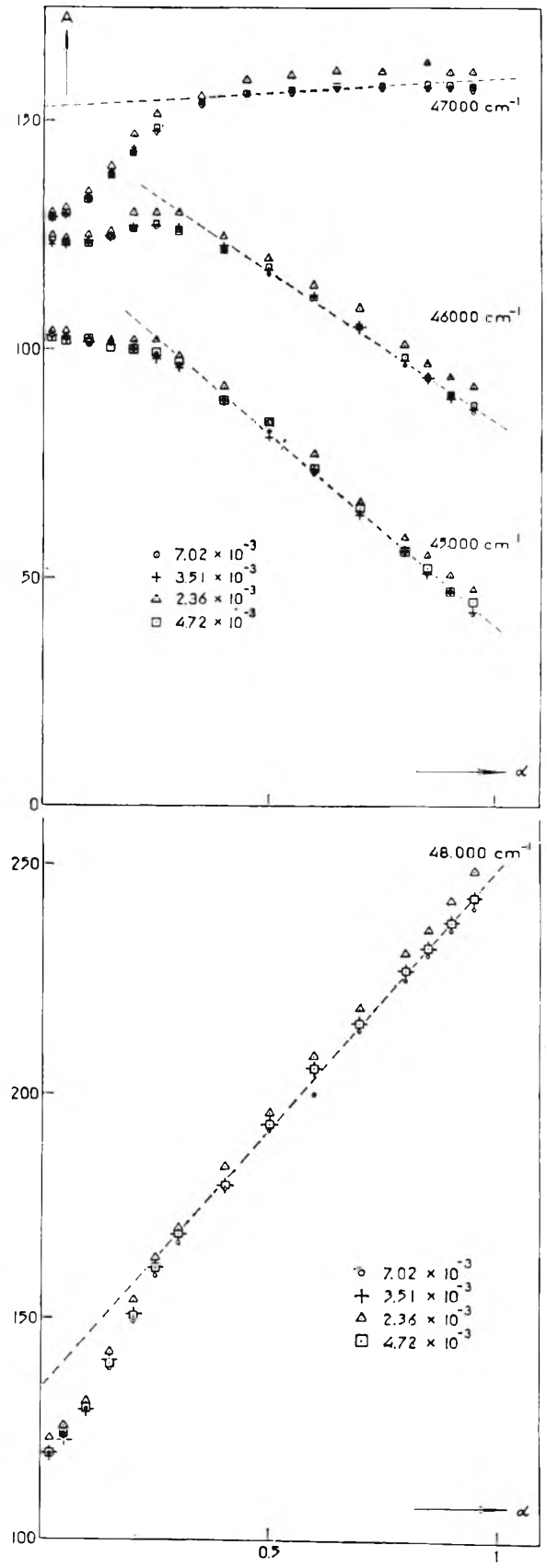

Figure 3. Spectrophotometric titration curves, $A' = A/bC_t$ *vs.* α, for PMA in (aq soln), four different concentrations (equiv/l.).

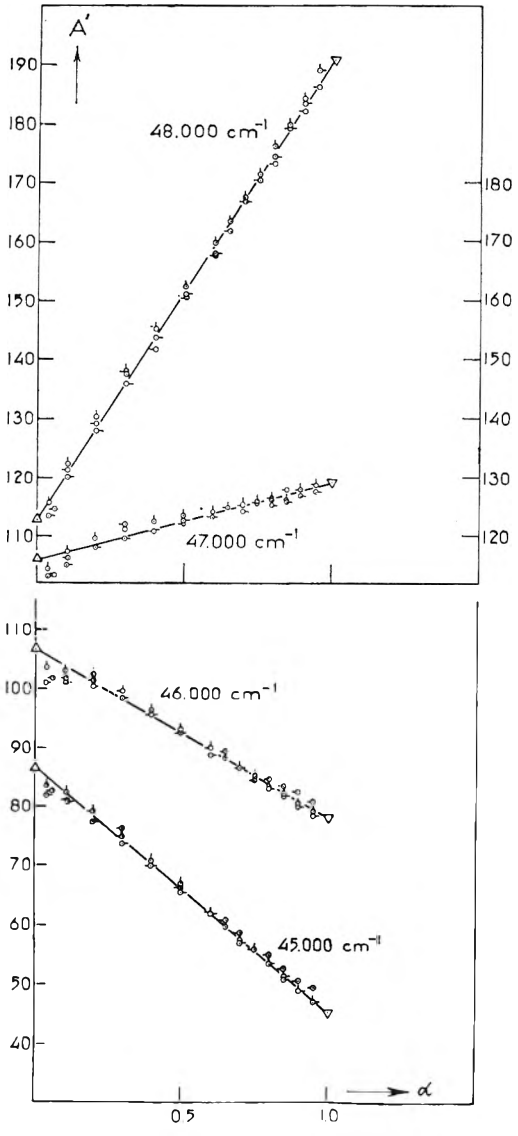

Figure 4. Spectrophotometric titration curves, A' *vs.* α, for PAA in an aqueous solution: ⊙, 8.70×10^{-3}; ⊙-, 4.43×10^{-3}; -⊙, 2.23×10^{-3} equiv/l.). The A' scale on the right-hand side is for the 47,000-cm^{-1} curve.

In the region where PMA exists in the b form only, eq 2 is also satisfied. The extinction coefficients $\epsilon_{AH}{}^{b}$ and $\epsilon_{A^-}{}^{b}$ (Table III) may therefore be determined (the least-squares method was applied to at least seven points of each titration). Assuming the exclusive existence of the a state at $\alpha = 0$, Beer's law for PMA solutions in the presence of $HClO_4$ (Figure 6) yields $\epsilon_{AH}{}^{a}$. It is impossible to obtain $\epsilon_{A^-}{}^{a}$ within the same order of accuracy although Michaeli[17] has indicated a method to estimate it. In order to obtain information about the conformational transition, it is not necessary to know both quantities, however (see Discussion).

Beer's law was found to be valid for undissociated

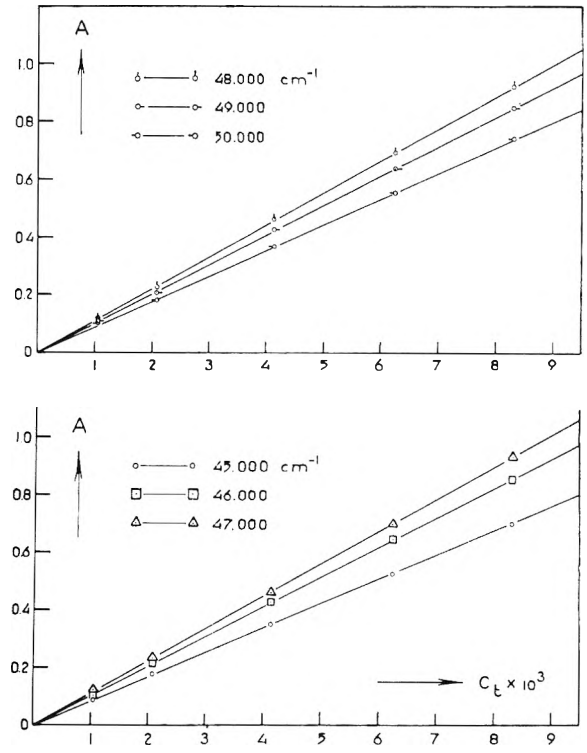

Figure 5. Absorption *vs.* concentration (Beer's law) for aqueous PAA solutions (with 2×10^{-2} *M* $HClO_4$) measured against $HClO_4$ of the same molarity.

Table II: Extinction Coefficients (1000 cm^2 $equiv^{-1}$) for -COOH of PAA in Aqueous Solutions

σ, cm^{-1}	ϵ_{AH} Beer's law	ϵ_{AH} Titration[a]
50,000	89.4	85
49,000	102.7	100
48,000	111.5	113
47,000	112.9	116
46,000	103.2	106
45,000	84.2	86

[a] Mean value derived from titration at four different concentrations.

PMA in 20, 30, and 40% methanol–water mixtures. The influence of methanol on $\epsilon_{AH}{}^{a}$ does not seem to be significant (Figure 7 and Table III). Spectrophotometric titration of PMA and PAA in water–methanol mixtures (Figures 8 and 9) reveals the same trend as in aqueous solutions; *i.e.*, the validity of eq 2 for PAA and deviations for PMA below $\alpha \simeq 0.40$.

The a → b transition is accompanied by a significant

(17) I. Michaeli, ref 10, Preprint, p 627.

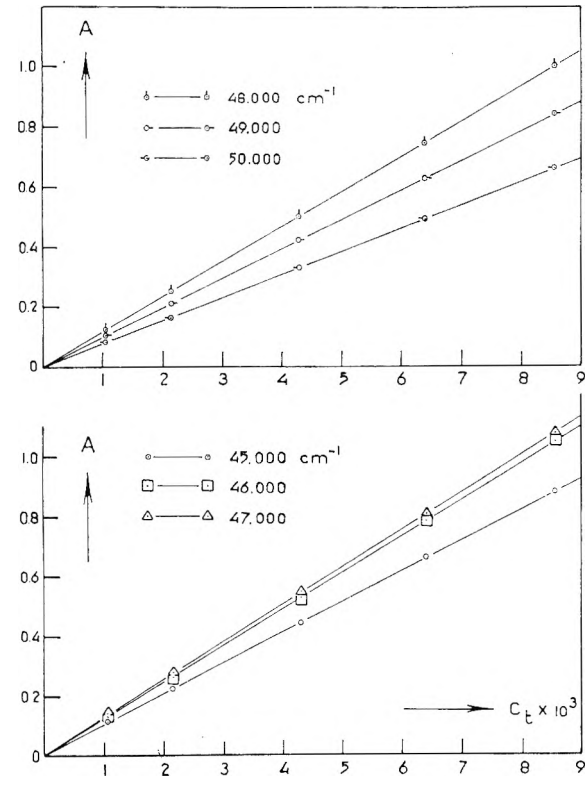

Figure 6. Beer's law for aqueous PMA solutions (with 2×10^{-2} *M* $HClO_4$).

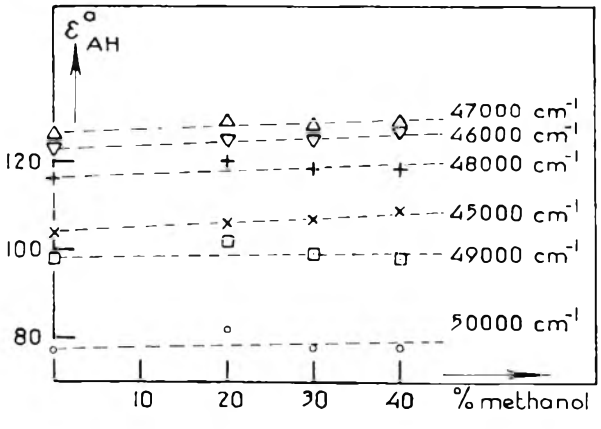

Figure 7. Values of $\epsilon_{AH}{}^{a}$ of PMA for different volume fractions of methanol.

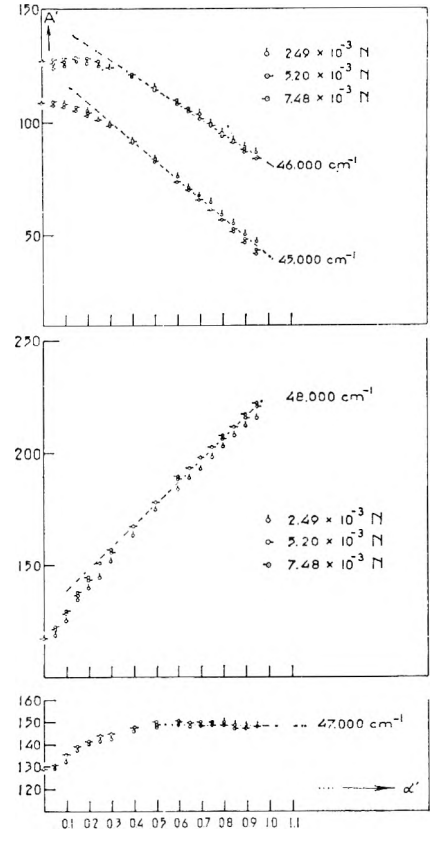

Figure 8. Spectrophotometric titration curves for solutions of PMA in 40% methanol.

Table III: Extinction Coefficients (1000 cm² equiv⁻¹) for -COOH of PMA

σ, cm⁻¹	H_2O $\epsilon_{AH}{}^{a}$	H_2O $\epsilon_{AH}{}^{b\ a}$	60% H_2O + 40% CH_3OH $\epsilon_{AH}{}^{a}$	60% H_2O + 40% CH_3OH $\epsilon_{AH}{}^{b\ b}$	CH_3OH $\epsilon_{AH}{}^{a}$
50,000	77.6	82	77.1	78	...
49,000	98.1	107	98.3	101	87.5
48,000	116.3	135	117.6	129	108.3
47,000	126.4	152	129.3	148	122.7
46,000	123.0	150	127.2	148	125.3
45,000	103.6	125	108.9	126	112.9

[a] Mean value determined from titrations at four different concentrations. [b] Mean value determined from titrations at three different concentrations.

change in the extinction coefficients (Table III) both in H_2O and the H_2O–CH_3OH mixture; no corresponding frequency shift is observed (Figure 10). (In pure methanol the -COOH absorption curve is slightly shifted to lower frequencies in agreement with current theories about medium effects).[18] The values of ϵ_{AH} for PAA and PMA are nearly four times as large as the extinction coefficients for acetic acid (as derived from Beer's law in excess $HClO_4$)[19] and butyric acid.[20] These results suggest that the absorption of the -COOH group is strongly influenced by the accumulation of such

(18) H. H. Jaffé and M. Orchin, "Theory and Applications of U.V. Spectroscopy," John Wiley and Sons, Inc., New York, N. Y., 1962.

(19) Unpublished results of this laboratory.

(20) H. Ley and B. Arends, *Z. Physik. Chem.* (Leipzig), **B17**, 177 (1932).

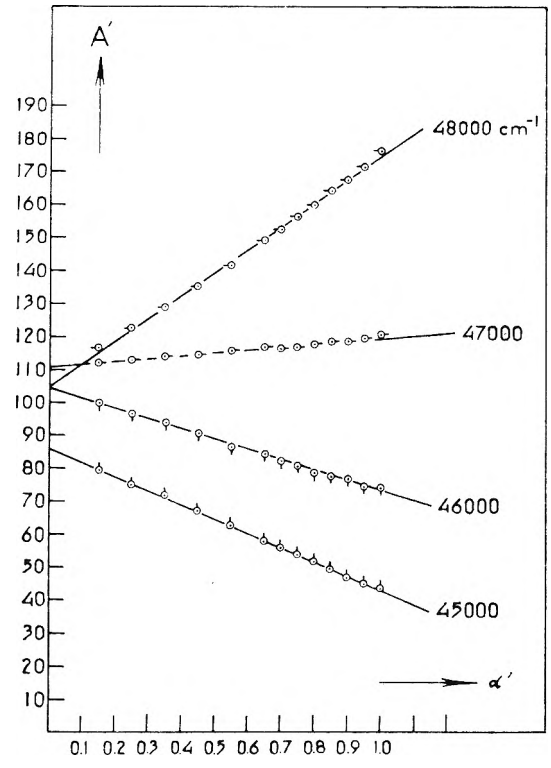

Figure 9. Spectrophotometric titration curves for solutions of PAA in 40% methanol at three different concentrations.

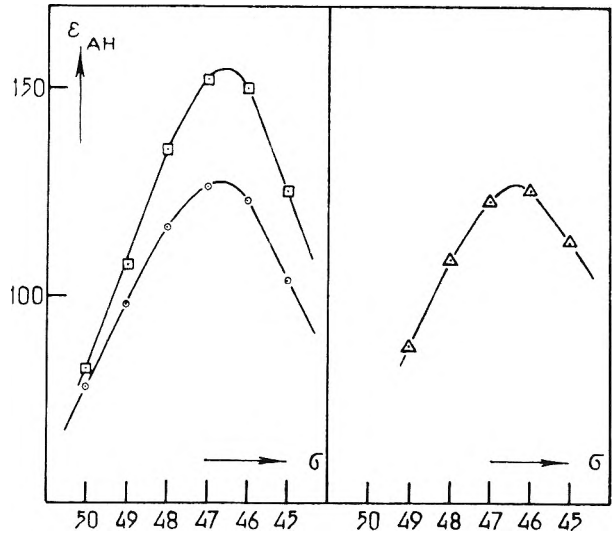

Figure 10. Absorption spectra for the carboxylic acid group of PMA: ⊙, $\epsilon_{AH}{}^{a}$ in aqueous solutions; ⊡, $\epsilon_{AH}{}^{b}$ in aqueous solutions; ⧋, $\epsilon_{AH}{}^{a}$ in 100% methanol solutions (σ, 10^3 cm^{-1}).

groups on a polymeric chain and the conformation of this chain.

Finally, infrared measurements have been performed on unneutralized deuterated PMA in D_2O–CH_3OD mixtures with CH_3OD volume fractions of 10, 20, 30, and 40%. Spectra have been recorded in the region where D_2O transmits for the path lengths used, *viz.*, between 1300 and 2150 cm^{-1}. For all the solutions examined the spectra were identical and no shift was observed with increasing CH_3OD concentration (up to 40%) for the position of the C=O stretching frequency at 1700 cm^{-1}. As an example, the spectra obtained for 0 and 30% methanol are shown in Figure 11.

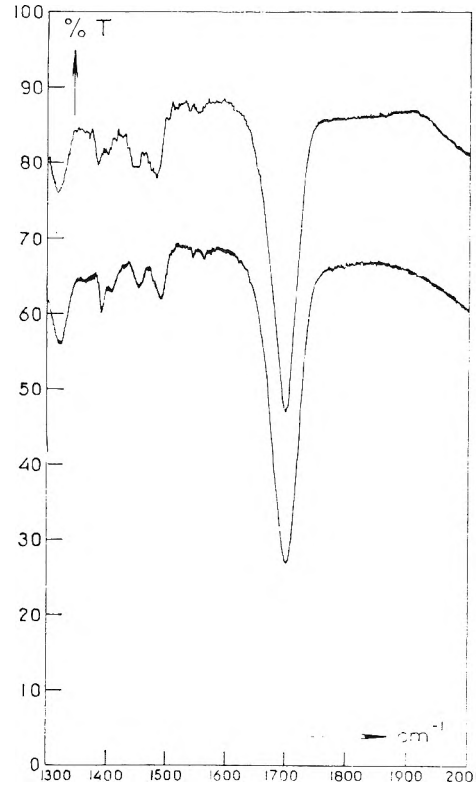

Figure 11. Infrared spectra of PMA in D_2O–CD_3OD mixtures: I, PMA in D_2O; II, PMA in 30% CD_3OD (curve I shifted 20% downward on the transmission scale.)

IV. Discussion

The validity of Beer's law for undissociated PMA shows that no concentration-dependent interactions between carboxylic groups exist in the explored concentration range.

The spectrophotometric titration of aqueous PMA reveals the conformational transition as reported already by Michaeli[17] and Barone, *et al.*[21] From the results presented here it is seen that this transition may also be observed by the spectrophotometric titration of PMA in water–methanol (40%) mixtures.

The spectrophotometric results may be analyzed in

(21) G. Barone, V. Crescenzi, and F. Quadrifoglio, *Ric. Sci.*, 8, 393 (1965).

the following way (which differs from the approach used by Michaeli[17]). Starting from the assumption that in the α region below 0.40, four different species can absorb the ultraviolet energy, the total absorbance in this region will be given by

$$A = b[\epsilon_{AH}{}^{a}C_{AH}{}^{a} + \epsilon_{AH}{}^{b}C_{AH}{}^{b} + \epsilon_{A^-}{}^{a}C_{A^-}{}^{a} + \epsilon_{A^-}{}^{b}C_{A^-}{}^{b}] \quad (3)$$

where C_j^i stands for the concentration (in equiv $l.^{-1}$) of the group j in the state i. Now using the obvious relations

$$C_{AH}{}^{a} + C_{AH}{}^{b} = (1 - \alpha)C_t \quad (4)$$

$$C_{A^-}{}^{a} + C_{A^-}{}^{b} = \alpha C_t \quad (5)$$

expression 3 can be transformed into

$$A = b[(\epsilon_{AH}{}^{a} - \epsilon_{AH}{}^{b})C_{AH}{}^{a} + (\epsilon_{A^-}{}^{a} - \epsilon_{A^-}{}^{b})C_{A^-}{}^{a} + \epsilon_{AH}{}^{b}(1 - \alpha)C_t + \epsilon_{A^-}{}^{b}\alpha C_t] \quad (6)$$

Using as a further assumption that for $\alpha \geqq 0.40$, $C^a = C_{AH}{}^{a} + C_{A^-}{}^{a} = C_{AH}{}^{a} = C_{A^-}{}^{a} = 0$, *viz.*, that the molecule is completely in the b state, only the two last terms of the right-hand side of eq 6 exist in that α region. The difference between the extrapolation of the straight part of the curve, *viz.*, $A_{ex} = b[\epsilon_{AH}{}^{b}(1 - \alpha)C_t + \epsilon_{A^-}{}^{b}\alpha C_t]$, down to values below $\alpha = 0.40$ and the measured values of A is given by

$$\Delta A = A_{ex} - A = b[(\epsilon_{AH}{}^{b} - \epsilon_{AH}{}^{a})C^a - (\epsilon_{AH}{}^{b} - \epsilon_{AH}{}^{a} - \epsilon_{A^-}{}^{b} + \epsilon_{A^-}{}^{a})C_{A^-}{}^{a}] \quad (7)$$

or

$$\Delta A = b(\epsilon_{AH}{}^{b} - \epsilon_{AH}{}^{a})C^a\left[1 - \frac{\Delta\epsilon}{(\epsilon_{AH}{}^{a} - \epsilon_{AH}{}^{b})}\frac{C_{A^-}{}^{a}}{C^a}\right] \quad (8)$$

where $\Delta\epsilon = \epsilon_{AH}{}^{b} - \epsilon_{AH}{}^{a} - \epsilon_{A^-}{}^{b} + \epsilon_{A^-}{}^{a}$. Now for $\alpha < 0.40$, $C_{A^-}{}^{a} < C^a$. It can be expected that in the frequency range between 45,000 and 48,000 cm^{-1}, $\epsilon_{AH}{}^{a} - \epsilon_{AH}{}^{b}$ is of the same order of magnitude as $\epsilon_{A^-}{}^{a} - \epsilon_{A^-}{}^{b}$, as it was found that $\epsilon_{AH}{}^{b}$ and $\epsilon_{A^-}{}^{b}$ do not differ considerably. Assuming therefore that $\Delta\epsilon/\epsilon_{AH}{}^{b} - \epsilon_{AH}{}^{a} < 1$, we have *in a first approximation*

$$\Delta A' = \Delta A/bC_t \simeq (\epsilon_{AH}{}^{b} - \epsilon_{AH}{}^{a})(C^a/C_t) \quad (9)$$

Thus from $\Delta A'$ and $\epsilon_{AH}{}^{b} - \epsilon_{AH}{}^{a}$ the value of C^a/C_t can be deduced at any degree of dissociation between $\alpha = 0$ and $\alpha = 0.40$. In Figure 12, calculated values of C^a/C_t for aqueous PMA are represented at constant concentration and four frequencies and at constant frequency and four concentrations. It may be seen that in each case the calculated points confine reasonably well to a common curve characterized by the fact that 50% of state a has disappeared at about $\alpha = 0.17$. These curves visualize the conformational transition as derived from the spectroscopic data. Values of C^a/C_t obtained for PMA in aqueous solutions and the water–methanol mixture (40%) are compared in Table IV.

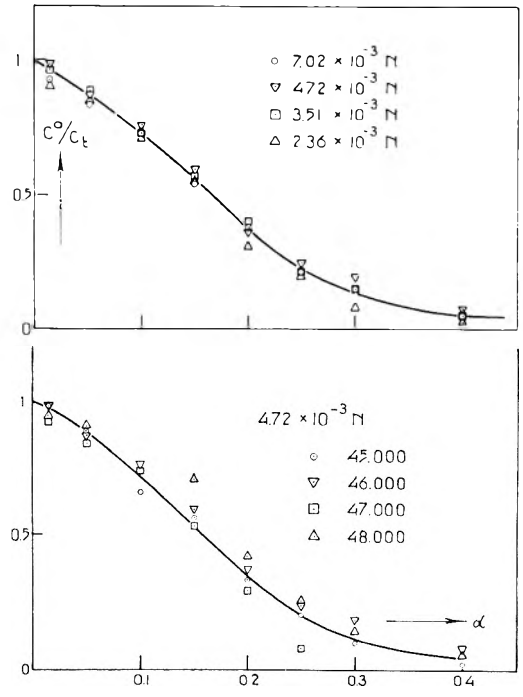

Figure 12. Plots of C^a/C_t *vs.* α, derived from the spectrophotometric titration of aqueous PMA: bottom, 4.72×10^{-3} *N* PMA at four frequencies; top, values derived at 46,000 cm^{-1} for four concentrations of PMA.

Table IV: C^a/C_t Determined from Spectrophotometric Titrations at 46,000 cm^{-1} and Different Concentrations of PMA (mequiv/l.)

	H_2O			60% H_2O + 40% methanol		
α	2.36	4.72	7.02	2.49	5.20	7.48
0.05	0.86	0.86	0.84	0.98	0.85	0.91
0.10	0.71	0.74	0.73	0.77	0.64	0.68
0.15	0.55	0.59	0.55	0.50	0.46	0.50
0.20	0.31	0.37	0.38	0.38	0.33	0.36
0.25	0.20	0.23	0.24	0.27	...	0.25
0.30	0.08	0.18	0.15	0.16	0.17	0.18

The transition curve can also be calculated from potentiometric results.[8] Values of C^a/C_t derived from potentiometric titrations carried out on two aqueous PMA solutions used in the spectroscopic measurements are plotted in Figure 13. Here again 50% of state a has disappeared at about $\alpha = 0.17$. The difference in the shape between this curve and those of Figure 12 is

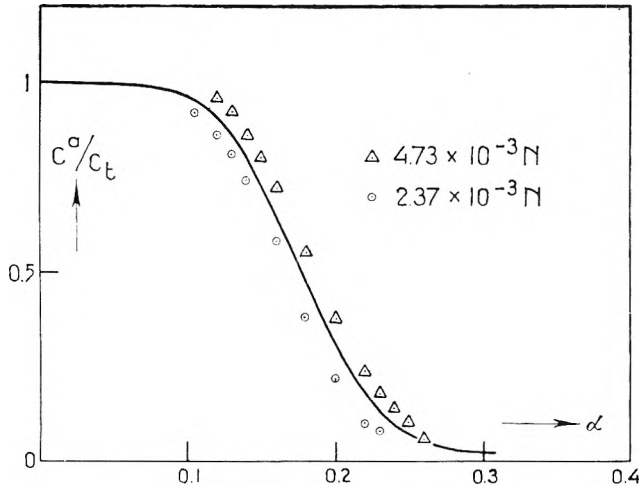

Figure 13. C^a/C_t *vs.* α, derived from the potentiometric titration at two concentrations of aqueous PMA.

caused by the unequal sensitivity of the two methods in differentiating between the a and b forms of PMA. The potentiometric behavior of the a form of PMA is markedly different from that of the b form of PMA (Figure 1). As apparently $\epsilon_{A^-} - \epsilon_{AH}$ is nearly equal for the two mean conformations, it is not even possible to observe at what degree of ionization the a → b transition starts. Furthermore, the error in C^a/C_t determined spectrophotometrically is large because ΔA is small everywhere.

From this analysis and the spectrophotometric titration curves themselves, it may be concluded that in the water–methanol mixtures as well as in pure water the transition occurs, and the stability of the a state is not significantly affected by the addition of methanol (up to 40%) (see Table IV). This view is supported by the absence of any change in the infrared spectrum of PMA on the addition of methyl alcohol, in contrast with the behavior of ν(C=O) in the transition region for aqueous solutions.[22]

In water–methanol (40%), the transition has no visible effect on the potentiometric titration curve. It should be pointed out that in water the transition region may be observed because of the magnitude of the difference in the dissociation constants of the carboxylic acid groups of the two forms (0.3 pK unit). Now it is well known that the dissociation constant of a weak acid is very sensitive to solvent effects and that influence of the solvent on the dissociation equilibrium even for ordinary acids is very intricate. Nevertheless, it may be expected from qualitative considerations involving long-range medium effects, as represented by the dielectric constant, that the difference between the pK values of the two states must be smaller in the given mixed solvent than in water (short-range effects will probably be less important as shown hereafter). This may explain the absence of a visible effect due to the transition on the titration curve of PMA in water–methanol (40%). In the case of aqueous PMA solutions the addition of salt also weakens the effect of the transition on the potentiometric titration curve.[8]

The observation that the conformational transition occurs in water–methanol (40%) is in contradiction with the results of Anufrieva, *et al.*[11] The evidence of these authors was based on the change of the fluorescent properties when methanol was added to aqueous solutions containing PMA and certain dyes. This change occurs in the same region where these authors also observed a decrease in the intrinsic viscosity of PMA solutions on the addition of methyl alcohol. It is not clear why the postulated breakdown of the a form of PMA, known as compact, should result in a *decrease* of the intrinsic viscosity. Neither has it been shown that the change in the fluorescent properties of the dyes in the presence of PMA by the addition of methanol may not be due to other effects instead of a conformational transition, *i.e.*, to the change of the solvent itself. We suggest that these fluorescence phenomena and the viscosimetric behavior in the mixed water–methanol solvent are too complex to be interpreted simply in terms of the a → b transition of PMA.

From the spectroscopic evidence, it seems that the conformational transition occurs in the 40% methanol–water mixture upon charging the polymer. Furthermore, the methanol in this mixture does not have an observable influence on the stability of the a form. This does not point to hydrophobic bonding as the determing factor for this stability.

The difference between the thermodynamic quantities of the a and b states of undissociated PMA (Table I) as derived from the potentiometric measurements shows that the transition to the compact state of PMA is accompanied by a *decrease* in enthalpy and a *somewhat smaller decrease* in entropy. This is exactly the opposite of what is to be expected if this transition were determined essentially by hydrophobic bonding.[13] The results obtained with partially esterified PMA[9] are also inconsistent with hydrophobic bonding as the main stabilizing factor for the a state, as has already been pointed out;[23] replacement of –COOH by the more hydrophobic –$COOCH_3$ does not affect the stability of the a state.

This does not mean that hydrophobic interactions

(22) J. C. Leyte, L. H. Zuiderweg, and H. J. Vledder, to be published.

(23) J. C. Leyte, *Polymer Letters*, **4**, 245 (1966).

should be totally excluded from the effects that tend to stabilize the low-pH state in PMA. The stability of this compact form seems, however, to be due *primarily* to a direct stabilization of certain conformations of the chain by interactions between its nearest neighbors rather than through the intermediary of a change in the structure of the surrounding solvent. This conclusion, of course, does not exclude the possibility of establishing important hydrophobic interactions between different PMA molecules as suggested recently by Eliassaf.[24] These should, however, become important at polyelectrolyte concentrations higher than those used in the present investigation.

Finally, it may be pointed out that the spectroscopic results give some additional information about the a state of PMA. In the previous work of this laboratory[21] it has been shown that the infrared C=O stretching frequency of the -COOH group in PMA shifts gradually *without splitting* during the conformational transition in D_2O. Thus it is not likely that the *vibrational states* of the carboxylic acid group differ in the a and b forms of PMA. As in the latter case solvation of -COOH by water certainly occurs, the same solvation for most of the carboxylic groups in the a state may be expected. The absence of any influence on ν(C=O) on the addition of methanol (up to 40%) shows that there is no infrared evidence for the replacement of water by methanol molecules at least in the first solvation layer of the -COOH group. The small changes observed for $\epsilon_{AH}{}^{a}$ in the ultraviolet region on the addition of methanol may be attributed to long-range effects involving further solvation layers.

Acknowledgment. The authors wish to thank Miss M. van Reisen for her help with the infrared measurements.

(24) J. Eliassaf, *Polymer Letters.*, **3**, 767 (1965).

The Pyridine-Sensitized Isomerization of *cis*-2-Butene

by Jacques Lemaire[1]

Department of Chemistry, University of Texas, Austin, Texas *(Received August 19, 1966)*

The yields of isomerization of *cis*-2-butene sensitized by pyridine have been measured. The yield is higher in the n → π^* than in the $\pi \rightarrow \pi^*$ region, but both yields are low. Neither fluorescence nor phosphorescence of pyridine vapor is observed. The possible methods of energy degradation are discussed.

Introduction

The electronic structure of the pyridine molecule has been extensively investigated. In the near-ultraviolet absorption spectrum of pyridine there occurs an n–π^* transition as well as a π–π^* transition.[2]

The most successful treatment of n–π^* transition uses simple molecular orbital theory in the one-electron approximation. The various singlet and triplet levels are predicted in reasonably good agreement with the data.[3] Transition energies and intensities of the π–π^* bands of pyridine have been calculated.[4,5]

Evans[6] observed an S → T absorption band of pyridine in the presence of high pressures of oxygen. He con-

(1) To whom all correspondence should be addressed at Laboratoire de Chimie Generale, University of Nancy, France.

(2) (a) M. Kasha, *Discussions Faraday Soc.*, **9**, 14 (1950); (b) H. P. Stephenson, *J. Chem. Phys.*, **22**, 1077 (1954).

(3) L. Goodman and R. W. Harrell, *ibid.*, **30**, 1131 (1959).

(4) R. Pariser and R. G. Parr, *ibid.*, **21**, 466, 767 (1953).

(5) G. Favini, I. Vandoni, and M. Simonetta, *Theoret. Chim. Acta*, **3**, 45, 418 (1965).

(6) D. F. Evans, *J. Chem. Soc.*, 3885 (1957).

cluded that the S → T transition was $\pi-\pi^*$ since it showed a very small solvent shift. The enhancement of the S → T transition has been discussed theoretically by several authors.[7-10] No fluorescence and no phosphorescence of pyridine has been observed either in the gas phase or in a solid matrix at low temperatures.[11,12]

The sensitized isomerizations of the 2-butenes have been used to determine singlet–triplet crossover yields for certain molecules.[13] The general validity of this method has never been fully proven even when energy relationships seem to be satisfactory. The reported identity of crossover yields in benzene and in pyridine seemed surprising. First results cast doubt on this identity, and after the completion of this work and personal communication of our results to Cundall,[14] a reinvestigation by him gave results in agreement with those reported below.

Experimental Section

Materials. Two samples of pyridine were used: Mallinckrodt, analytical grade, and United States Testing Co., spectrophotometric grade.

A very careful search for impurities was made in view of effects reported by Cundall, *et al.*[13] Both mass spectrometry and gas chromatography were used and the following impurities were found:

(a) Mallinckrodt pyridine: 0.025% benzene (not detectable by mass spectrometry since less than 0.1% benzene in a mixture of pyridine–benzene could not be determined); 0.1% H_2O.

(b) United States Testing Co. pyridine: no benzene; far less than 0.1% of an impurity X, not detectable by mass spectrometry and absent in pyridine Mallinckrodt; 0.001% H_2O.

Both pyridines were subjected to bulb-to-bulb distillation and different fractions behaved similarly.

The benzene was Matheson Coleman and Bell fluorometric or chromatographic grade. *cis*-2-Butene (Phillips Petroleum Co., research grade) had as its only impurity 0.06% *trans*-2-butene.

A conventional high-vacuum, grease-free line was employed.[15] All experiments were carried out in a 50-ml T-shaped cell. The cell was encased in an aluminum block which reduced stray light and could be used as a furnace. The light sources were a Hanovia S-100 medium-pressure mercury arc and an Osram HBO 500W super-pressure mercury arc. The grating monochromator (Bausch and Lomb, Model 33-86-45) has 16 A/mm as reciprocal linear dispersion. Since quantum yields were low, relatively large slit widths were used, 10 and 4 mm, respectively, for the entrance slit and 4 mm for the exit slit in most of the experiments. Thus the wavelength range under the most favorable conditions exceeded 100 A although most of the intensity was in a 60-A range.

The light transmitted through the cell was measured with an RCA 935 phototube connected to a Keithley micro-microammeter Model 410. The emission intensity was measured by an RCA 1P28 photomultiplier placed opposite the side arm of the cell.

cis- and *trans*-2-butene were analyzed on a Wilkens Hy-Fi Aerograph chromatograph, Model 600C, equipped with a 7.6-m dibenzyl ether (20% on firebrick 60–80 mesh) column followed by a 3.05-m silicone gum rubber column acting as a scrubber. At room temperature, the two peaks of *cis*- and *trans*-2-butene, respectively, were well separated. Reproducibility was improved by heating the sample to about 50° in the injector.

Results

Emission of Pyridine. Emission by pyridine, either fluorescence or phosphorescence, in the gas phase could not be observed either by use of the 1P28 tube or by use of an Aminco–Bowman spectrofluorimeter. Attempts to excite emission by wavelengths of 2400–3000 A failed. Experiments with the 1P28 tube equipped either with a Corning filter 754 (no. 9863) or with a filter 053 (no. 7740) were unsuccessful.

Photochemistry of Pyridine. Long irradiation of pure pyridine in the gas phase by either $\pi-\pi^*$ (2480 ± 128 A) or $n-\pi^*$ excitation (2650 ± 64 A), did not produce gaseous products which could be detected either by the mass spectrograph or by gas chromatography. Long irradiations at 2480 ± 128 A and at 2650 ± 64 A with 6 and 3×10^{13} photons absorbed per second gave negative results. For example, pyridine at a pressure of 10 torr was irradiated in a cell 6 cm in length as follows: (a) $\lambda = 2480 \pm 128$ A; 6×10^{13} photons sec^{-1} absorbed in the entire cell of 50-ml volume; time = 4 hr; $T = 90°$; (b) $\lambda = 2650 \pm 64$ A; 3×10^{13} photons sec^{-1} absorbed in the entire cell of 50-ml volume; time = 23 hr; room temperature.

Pyridine-Sensitized Isomerization of cis-2-Butene.

(7) M. Tsubomura and R. S. Mulliken, *J. Am. Chem. Soc.*, 82, 5966 (1960).

(8) G. W. King and E. H. Pinnington, *J. Mol. Spectry.*, 15, 394 (1965).

(9) G. J. Hoijtink, *Mol. Phys.*, 3, 67 (1960).

(10) F. A. Matsen, *J. Phys. Chem.*, 68, 3282 (1964).

(11) C. Reid, *J. Chem. Phys.*, 18, 1673 (1950).

(12) G. J. Brealey, *ibid.*, 24, 571 (1956).

(13) R. B. Cundall, F. J. Fletcher, and D. G. Milne, *Trans. Faraday Soc.*, 60, 1146 (1964).

(14) R. B. Cundall, private communication.

(15) *Cf.* I. Unger, *J. Phys. Chem.*, 69, 4284 (1965).

Table I: Pyridine-Sensitized Isomerization of *cis*-2-Butene

λ, A	Entrance slit, mm	Exit slit, mm	Light absorbed, [photon sec^{-1} (50 ml)$^{-1}$]	Irradiation time, hr	% *trans*-2-butene formed	*trans*-2-Butene quantum yields
2400	10	4	8.96×10^{13}	15.60	0.08	0.005
2480	10	4	8.37×10^{13}	22.75	0.14	0.006
2537	10	4	11.1×10^{13}	12.80	0.10	0.006
2537	4	4	3.27×10^{13}	25.67	0.05	0.006
2650	10	10	28×10^{13}	8.75	0.41	0.014
2650	10	4	15.7×10^{13}	10.79	0.34	0.018
2650	4	4	4.60×10^{13}	18	0.18	0.020
2750	10	4	2.71×10^{13}	14.43	0.35	0.081
2780	4	4	1.65×10^{13}	14.58	0.21	0.078

Table I presents the data on numbers of molecules of *trans*-2-butene formed per photon absorbed. It should be noted that neither *cis*-2-butene nor *trans*-2-butene absorbs in the spectral ranges studied.

Photochemical reaction between benzene and the 2-butenes to give an adduct has been reported by Srinivasan[16] and confirmed by Wilzbach and Kaplan.[17] The adduct is really one involving a benzene isomer formed photochemically. Evidence for at least a trace of such reaction in the gas phase has been found. In the case of pyridine no evidence for a similar adduct was found.

Possible Influence of Impurities. An efficient quenching impurity might be responsible for these low-quantum yields of sensitized isomerization.

The amount of "quenching" impurity cannot exceed 0.1% of the pyridine. From experimental values of the oscillator strengths[2b] observed in the liquid phase

$$f_{n-\pi^*} = 0.003; \qquad f_{\pi-\pi^*} = 0.04$$

we can estimate the mean lifetimes of both the singlet states

$$\tau_{n-\pi^*} \cong 10^{-7} \text{ sec}; \qquad \tau_{\pi-\pi^*} \cong 10^{-8} \text{ sec}$$

If these values have the same magnitude in the vapor phase, we may calculate the quenching cross section an impurity must have to produce the observed effect and compare it to the cross section of the *cis*-2-butene. For example, in a mixture of 12 mm of pyridine, 20 mm of *cis*-2-butene, and 0.01 mm of an impurity X, the number of collisions of one molecule of pyridine with the impurity and with the *cis*-2-butene are, respectively

$$Z_X = 2.3 \times 10^{19} \sigma_X^2$$

where σ_X is the collision diameter in centimeters, and

$$Z_{cis\text{-butene}} = 5.0 \times 10^{22} \sigma^2_{cis\text{-butene}}$$

(we assume the same molecular mass for the impurity as for pyridine). From the mean life of the singlet state of 10^{-7} sec, we may calculate $\sigma_X^2 = 4300$ A^2 and $\sigma^2_{cis\text{-butene}} = 2$ A^2. Quenching of the singlet state of pyridine by an impurity may be excluded.

Unfortunately, we cannot estimate the lifetime of pyridine triplet. If we assume a mean lifetime of 10^{-4} to 10^{-5} sec, then $\sigma_X^2 = 4.3$–43 A^2 and $\sigma^2_{cis\text{-butene}} = 0.002$–$0.02$ A^2.

In the presence of *cis*-2-butene, we must assume a high stereospecificity of the interaction between pyridine and an impurity to give high quenching of the triplet state.

We may add that two samples of pyridine of different origins containing different impurities (benzene and X) gave the same experimental results. Moreover, the effect of small quantities of benzene was checked by addition of increasing quantities of benzene in the pyridine (0.025–0.5%). The results were not altered by these additions. Therefore, we feel that a quenching by impurities will not explain the low yields of triplet formation.

Discussion

The quantum yields of the pyridine-sensitized isomerization of *cis*-2-butene as given in Table I are very low, although they are somewhat higher in the n → π* region than in the π → π* region.

Cundall and his co-workers have used the isomerization of the butenes as a means of determining triplet state yields.[13,18] The preferential excitation of triplet emission from biacetyl has also been used for certain molecules.[19] For benzene,[13,18–20] fluorobenzene,[15,21]

(16) R. Srinivasan and K. A. Hill, *J. Am. Chem. Soc.*, **87**, 4653 (1965).

(17) K. E. Wilzbach and L. Kaplan, *ibid.*, **88**, 2066 (1966).

(18) R. B. Cundall and A. S. Davies, *Trans. Faraday Soc.*, **62**, 1151 (1966).

(19) H. Ishikawa and W. A. Noyes, Jr., *J. Am. Chem. Soc.*, **84**, 1502 (1962); H. Ishikawa and W. A. Noyes, Jr., *J. Chem. Phys.*, **37**, 583 (1962).

and perfluorobenzene,[22] agreement is good within a rather large experimental error between the two methods.

In the case of pyridine, the biacetyl method gave no positive results and the Cundall method as described above shows very little triplet formation. The question now arises as to whether triplet yields are in fact very small or whether the methods themselves are fallacious.

The triplet-state yields based on the assumptions made by Cundall, *et al.*, are given below. These are obtained by dividing the yields of *trans*-2-butene by 0.578, the fraction of excited *cis*-2-butene which becomes *trans*.[13]

Quantum Yield of Triplet-State Formation: (2400–2537 A, 0.010 ± 0.001; 2650 A, 0.030 ± 0.003; and 2750–2780 A, 0.14 ± 0.01). Quite evidently, the yield is higher in the $n \rightarrow \pi^*$ than in the $\pi \rightarrow \pi^*$ region. Nevertheless, the yields in both cases are very low and there is no emission. Thus if one accepts these values for the triplet-state yields, either products are formed which have so far escaped detection or there are means of energy degradation which account for nearly all of the energy.

There are reasons based on analogy with related molecules for believing that triplet yields should be small for pyridine. The pyridazine (1,2-diazine) does not phosphoresce, even in hydrogen and rare-gas matrices, at 4.2°K, and the intersystem crossover was shown[23,24] to be 10^3 to 10^5 slower at low temperatures than in pyrazine or pyrimidine, which strongly phosphoresce.

The survey of the three diazines may allow us to point out that a lack of phosphorescence in azines at low temperatures seems to be more a consequence of an inefficient crossover than a consequence of rapid, radiationless deactivation processes from the lowest triplet state. It seems reasonable to assume that radiationless deactivation from the lowest triplet state has a similar importance for all these mono- and diazines. Therefore, the lack of phosphorescence of pyridine at low temperatures may reflect the inefficient crossovers our results show.

Nevertheless, the formation of an adduct with benzene under certain experimental conditions raises a reasonable doubt about the universal validity of the isomerization technique for triplet-state measurement.

An excited singlet state of pyridine in the spectral region used could not transfer electronic energy directly to *cis*-2-butene (unless spin conservation were violated). Nevertheless, an intermediate complex between excited pyridine and the double bond of an olefin is possible. This complex could dissociate to give two normal molecules.

It is wise not to pursue a discussion of these possibilities further. There may be methods for identifying such complexes.

Isomerization of benzene and of benzene derivatives at wavelengths around 2500 A is firmly established. The possibility of similar isomerizations with pyridine certainly exists, but no evidence for them has been reported. Such isomerizations might provide a pathway for energy degradations since the isomers would be formed endothermically from normal molecules to the extent of 2 or 3 ev. Attempts by others to find pyridine isomers have failed.

Acknowledgments. The author is greatly indebted to Professor W. A. Noyes, Jr., for his help and encouragement throughout the course of this work. He also wishes to thank colleagues for many helpful discussions. Financial support from the Robert A. Welch Foundation is also gratefully acknowledged.

(20) W. A. Noyes, Jr., W. A. Mulac, and D. A. Harter, *J. Chem. Phys.*, **44**, 2100 (1966).

(21) D. Phillips, private communication.

(22) D. Phillips, in press.

(23) M. A. El Sayed, *J. Chem. Phys.*, **36**, 573 (1962).

(24) M. A. El Sayed, *ibid.*, **38**, 2834 (1963).

Application of Irreversible Thermodynamics to Electrolyte Solutions. II. Ionic Coefficients l_{ij} for Isothermal Vector Transport Processes in Ternary Systems[1,2]

by Donald G. Miller

Lawrence Radiation Laboratory, University of California, Livermore, California *(Received August 22, 1966)*

Irreversible thermodynamics is applied to ternary electrolyte solutions undergoing isothermal vector transport processes. Rigorous expressions for the conductance Λ, Hittorf transference numbers t_i, and solvent-fixed thermodynamic diffusion coefficients $(L_{ij})_0$ are derived systematically in terms of the six solvent-fixed ionic Onsager transport coefficients l_{ij}. Conversely, expressions for the l_{ij} are given in terms of the six experimental quantities Λ, t_i, and $(L_{ij})_0$. Also given are rigorous expressions for flows J_i in terms of these quantities as well as a proof that superposition of electrical and diffusion flow is valid. Values of l_{ij} are calculated for all systems for which sufficient experimental data exist, namely, seven alkali halide mixtures at total concentrations from 0.5 to 3 N. The cross coefficients are from 5 to 30% of main coefficients and thus cannot be neglected. It is found empirically that ternary l_{ij} can be closely approximated using binary l_{ij} data, yielding good estimates of t_i, Λ, and $(L_{ij})_0$. These l_{ij}, with thermodynamic derivatives approximated from binary data, yield good estimates of ordinary ternary diffusion coefficients $(D_{ij})_0$ from binary data alone. Such estimates are compared with experimental values. Explicit limiting expressions for l_{ij}/N, $(L_{ij})_0$, and $(D_{ij})_0$ at infinite dilution are given in terms of limiting ionic conductances. Limiting tracer and intradiffusion are briefly discussed. The friction coefficient formalism is briefly considered and values of ionic R_{ij} are presented.

I. Introduction

In paper I,[3] irreversible thermodynamics was used to provide a general macroscopic description of isothermal vector transport processes in electrolyte solutions. Binary systems were discussed in detail and equations for the fundamental transport coefficients, l_{ij}, were derived in terms of experimentally measured quantities. Values of solvent-fixed l_{ij} for several chlorides were presented and their concentration dependence discussed.

In this paper we extend the analysis to ternary isothermal systems, in particular to two binary electrolytes with a common ion in a neutral solvent.[4,5] The Onsager reciprocal relations (ORR) are assumed throughout. The l_{ij} are calculated from the limited data available for mixed chlorides at 25° and their behavior is discussed. Empirically it is found that very good estimates of ternary l_{ij} can be obtained from the l_{ij} of appropriate binary systems. If thermodynamic data are available, these estimates lead to good approximations for ternary diffusion coefficients.

Limiting expressions for thermodynamic diffusion coefficients, L_{ij}, and ordinary diffusion coefficients, D_{ij}, are given for some special cases.

(1) This work was performed under the auspices of the U. S. Atomic Energy Commission.

(2) Portions of this work were presented at the 94th AIME meeting in Chicago, Ill., Feb 1965, and at the 16th CITCE meeting in Budapest, Hungary, Sept 1965.

(3) D. G. Miller, *J. Phys. Chem.*, **70**, 2639 (1966).

(4) If there were no common ions, the system would be ternary for equilibrium processes but quaternary for transport processes.[5]

(5) B. R. Sundheim, *J. Chem. Phys.*, **27**, 791 (1957).

Expressions for and values of R_{ij} for the inverse description are presented for completeness.

II. Notation and General Equations

Equations from paper I will be distinguished by the prefix I. Consider two binary electrolytes, $C_{r_{1c}}A_{r_{1a}}$ and $D_{r_{2c}}A_{r_{2a}}$, with the anion A in common, which ionize as follows

$$C_{r_{1c}}A_{r_{1a}} \longrightarrow r_{1c}C^{z_1} + r_{1a}A^{z_3} \quad (1)$$

$$D_{r_{2c}}A_{r_{2a}} \longrightarrow r_{2c}D^{z_2} + r_{2a}A^{z_3} \quad (2)$$

where C and D are the cations, r the stoichiometric coefficients for ionization, and z_i the signed valences of the ions. These two electrolytes form a ternary system when dissolved in a neutral solvent. The solvent is denoted by subscript 0.

If μ_1, μ_2, and μ_3 are the chemical potentials in joules per mole of ions 1, 2, and 3, respectively, and if μ_{13} and μ_{23} are chemical potentials in joules per mole of the electrolytes as a whole, $C_{r_{1c}}A_{r_{1a}}$ and $D_{r_{2c}}A_{r_{2a}}$, respectively, then

$$\mu_{13} = r_{1c}\mu_1 + r_{1a}\mu_3 \quad (3)$$

$$\mu_{23} = r_{2c}\mu_2 + r_{2a}\mu_3 \quad (4)$$

Moreover because of charge conservation

$$r_{1c}z_1 + r_{1a}z_3 = 0 \quad (5)$$

$$r_{2c}z_2 + r_{2a}z_3 = 0 \quad (6)$$

If c_1 and c_2 are the concentrations in moles per liter of the electrolytes as a whole, $C_{r_{1c}}A_{r_{1a}}$ and $D_{r_{2c}}A_{r_{2a}}$, respectively, and N_1 and N_2 are the respective number of equivalents per liter, then

$$N_1 = r_{1c}z_1c_1 \qquad N_2 = r_{2c}z_2c_2 \quad (7)$$

The total number of equivalents per liter, N, is the same as the number of equivalents of the common ion 3 and is

$$N = r_{1c}z_1c_1 + r_{2c}z_2c_2 = -z_3(r_{1a}c_1 + r_{2a}c_2) = N_3 \quad (8)$$

There are four diffusing constituents, 1, 2, 3, and 0. However only three are independent because of a choice of reference frame and because of the Gibbs–Duhem equation.[3] It is convenient to choose the three ion flows for the independent set and to choose the solvent-fixed (SF) reference frame because transference numbers are defined on that frame.

According to irreversible thermodynamics,[3] our ternary system may be described by

$$J_i = \sum_{j=1}^{3} l_{ij}X_j \qquad i = 1, 2, 3 \quad (9)$$

where J_i are the *solvent-fixed* ion flows in moles/cm² sec, l_{ij} the *solvent-fixed* ionic transport coefficients, and X_j the thermodynamic forces, which for the usual one-dimensional case are

$$X_j = -\left[\frac{\partial u_j}{\partial x} + z_j\mathfrak{F}\frac{\partial \phi}{\partial x}\right] \qquad j = 1, 2, 3 \quad (10)$$

Here $\mathfrak{F}$ is the faraday in coulombs per equivalent, ϕ the electrical potential in volts, and x the distance in centimeters. The solvent flow, J_0, is zero on this reference frame.

Equation 9 requires nine l_{ij}. However because the sets J_i and X_i were chosen from $T\sigma$ and are independent, the ORR

$$l_{ij} = l_{ji} \qquad i, j = 1, 2, 3 \quad (11)$$

are valid.[3] Therefore only six l_{ij} are independent. To determine them, six independent experimental quantities are required. Six such quantities are the conductance, two of the three transference numbers, and three of the four diffusion coefficients.[6–10] As in paper I, we begin by deriving expressions for these six quantities in terms of the l_{ij}.

III. Experimental Quantities in Terms of l_{ij}

A. Conductance and Transference. The analysis of these cases is the same as in paper I. The results for conductance (analogous to eq I-18) are

$$\alpha = \sum_{k=1}^{3}\sum_{l=1}^{3} z_k l_{kl} z_l \quad (12)$$

with

$$\alpha = \lambda/\mathfrak{F}^2 = \Lambda N/1000\mathfrak{F}^2 \quad (13)$$

where α is defined by eq 13, λ is the specific conductance in $(\text{ohm cm})^{-1}$, and Λ is the equivalent conductance in $\text{cm}^2/\text{ohm equiv}$.

The transference number expression (analogous to eq I-22) is

$$t_k = \left[z_k\sum_{l=1}^{3} z_l l_{kl}\right]\Big/\alpha \qquad k = 1, 2, 3 \quad (14)$$

and is given in the Hittorf form but without superscript because the ORR will be assumed. As with binary systems, t_i depends on the reference frame whereas α, λ, and Λ do not.[3]

(6) There is a relation between the four diffusion coefficients owing to an ORR for pure diffusion.[7–9] This ORR is either a consequence of eq 11 (see eq 28 and 29) or results from an analysis of $T\sigma$ for pure diffusion.[10]

(7) G. J. Hooyman, *Physica*, **22**, 751 (1956).

(8) D. G. Miller, *J. Phys. Chem.*, **62**, 767 (1958); corrections, *ibid.*, **63**, 2089 (1959).

(9) P. J. Dunlop and L. J. Gosting, *ibid.*, **63**, 86 (1959).

(10) D. G. Miller, *ibid.*, **63**, 570 (1959); corrections, *ibid.*, **63**, 2089 (1959).

B. Diffusion. The analysis of pure diffusion in ternary systems is more complex than in binaries. The expression of Fick's law in terms of *solvent-fixed* flows and *solvent-fixed* diffusion coefficients, $(D_{ij})_0$, is[7,9]

$$J_{i3} = -\sum_{j=1}^{2}(\hat{D}_{ij})_0\frac{\partial c_j}{\partial x} \qquad i = 1, 2 \tag{15}$$

where the flows J_{i3} of electrolyte as a whole are

$$J_{13} = \frac{J_1}{r_{1c}} \qquad J_{23} = \frac{J_2}{r_{2c}} \tag{16}$$

For consistent units $(\hat{D}_{ij})_0$ is in l./cm sec and is related to SF $(D_{ij})_0$ in the usual units (cm²/sec) by

$$(\hat{D}_{ij})_0 = (D_{ij})_0/1000.027 \tag{17}$$

The irreversible thermodynamic description in terms of these SF flows is[11,12]

$$J_{i3} = -\sum_{j=1}^{2}(L_{ij})_0\frac{\partial \mu_{j3}}{\partial x} \qquad i = 1, 2 \tag{18}$$

where $(L_{ij})_0$ denotes SF thermodynamic diffusion coefficients in mole²/joule cm sec.

The $(D_{ij})_0$ can be related to the $(L_{ij})_0$ and conversely by the equations[7,9,11]

$$(\hat{D}_{ij})_0 = \sum_{k=1}^{2}(L_{ik})_0\mu_{kj} \qquad i, j = 1, 2 \tag{19}$$

and

$$\begin{aligned}
(L_{11})_0 &= \frac{\mu_{22}(\hat{D}_{11})_0 - \mu_{21}(\hat{D}_{12})_0}{\mu} \\
(L_{12})_0 &= \frac{\mu_{11}(\hat{D}_{12})_0 - \mu_{12}(\hat{D}_{11})_0}{\mu} \\
(L_{21})_0 &= \frac{\mu_{22}(\hat{D}_{21})_0 - \mu_{21}(\hat{D}_{22})_0}{\mu} \\
(L_{22})_0 &= \frac{\mu_{11}(\hat{D}_{22})_0 - \mu_{12}(\hat{D}_{21})_0}{\mu}
\end{aligned} \tag{20}$$

where

$$\mu = \mu_{11}\mu_{22} - \mu_{12}\mu_{21} \tag{21}$$

The quantity μ_{ij} for our systems is[10]

$$\mu_{ij} = \frac{\partial \mu_{i3}}{\partial c_j} = \hat{R}T\left[\frac{r_{ic}\delta_{ij}}{c_j} + \frac{r_{ia}r_{ja}}{r_{1a}c_1 + r_{2a}c_2} + r_i\frac{\partial \ln y_i}{\partial c_j}\right] \qquad i, j = 1, 2 \tag{22}$$

where $\hat{R}$ is the gas constant in joules/mole deg, T the absolute temperature in °K, δ_{ij} the Kronecker delta, y_i the moles per liter activity coefficient, and $r_i = r_{ic} + r_{ia}$.

The expressions for $(L_{ij})_0$ in terms of ionic l_{ij} are obtained below in a manner analogous to the binary case.

Although there are gradients of μ_i, the current density, I, is zero; *i.e.*

$$I = \sum_{k=1}^{3}z_k\mathfrak{F}J_k = \mathfrak{F}\sum_{k=1}^{3}\sum_{l=1}^{3}z_kl_{kl}X_l = 0 \tag{23}$$

Substituting eq 10 in eq 23 and solving for $\mathfrak{F}\partial\phi/\partial x$ yields

$$\mathfrak{F}\frac{\partial \phi}{\partial x} = -\frac{\sum_{k=1}^{3}\sum_{l=1}^{3}z_kl_{kl}(\partial\mu_l/\partial x)}{\sum_{k=1}^{3}\sum_{l=1}^{3}z_kl_{kl}z_l} \tag{24}$$

Upon substituting eq 24 into eq 9 and appropriately manipulating the sums, we obtain

$$J_i = -\frac{\sum_{j=1}^{3}\sum_{k=1}^{3}\sum_{l=1}^{3}l_{ij}l_{kl}z_k[z_l(\partial\mu_j/\partial x) - z_j(\partial\mu_l/\partial x)]}{\sum_{k=1}^{3}\sum_{l=1}^{3}z_kl_{kl}z_l} \qquad i = 1, 2, 3 \tag{25}$$

Although the term in square brackets involves unmeasurable individual ion chemical potentials, fortunately all the indicated combinations reduce to the measurable ones, *e.g.*

$$z_3\frac{\partial \mu_1}{\partial x} - z_1\frac{\partial \mu_3}{\partial x} = \frac{z_3}{r_{1c}}\frac{\partial \mu_{13}}{\partial x} \tag{26}$$

Evaluation of all such terms and division of the J_i expression by r_{ic} gives the result for pure diffusion

$$J_{i3} = \frac{J_i}{r_{ic}} = \frac{-\sum_{j=1}^{2}\left[\sum_{k=1}^{3}\sum_{l=1}^{3}\frac{z_kz_l}{r_{ic}r_{jc}}(l_{ij}l_{kl} - l_{il}l_{kj})\right]\frac{\partial \mu_{j3}}{\partial x}}{\sum_{k=1}^{3}\sum_{l=1}^{3}z_kl_{kl}z_l} \qquad i = 1, 2 \tag{27}$$

However (27) has precisely the same form as (18). Thus identification of terms yields the desired expression for pure diffusion $(L_{ij})_0$ in terms of ionic l_{ij}

$$(L_{ij})_0 = \frac{\sum_{k=1}^{3}\sum_{l=1}^{3}\frac{z_kz_l}{r_{ic}r_{jc}}(l_{ij}l_{kl} - l_{il}l_{kj})}{\sum_{k=1}^{3}\sum_{l=1}^{3}z_kl_{kl}z_l} \qquad i, j = 1, 2 \tag{28}$$

(11) J. G. Kirkwood, R. L. Baldwin, P. J. Dunlop, L. J. Gosting, and G. Kegeles, *J. Chem. Phys.*, **33**, 1505 (1960).

(12) L. A. Woolf, D. G. Miller, and L. J. Gosting, *J. Am. Chem. Soc.*, **84**, 317 (1962).

The expressions for $(D_{ij})_0$ in terms of l_{ij} are fairly complex and are omitted.

So far, the ORR's have not been used in this section. From eq 28 we see that the ORR's for the ionic l_{ij} (eq 11) imply the ORR

$$(L_{12})_0 = (L_{21})_0 \tag{29}$$

for pure diffusion, which can be derived independently for any ternary diffusion system, ionic or otherwise.[7,9,12] Equation 29, however, does not imply eq 11. A relation between the four $(D_{ij})_0$ is obtained[7] when eq 29 is introduced into eq 20, thus proving that only three are independent.

Equations 12, 14, and 28 are also valid for a system of $n - 1$ cations and a common anion if the k and l run from 1 to n and i and j run from 1 to $n - 1$. The case of a common cation is clearly described by the same equations after proper relettering.

C. The Six Experimental Quantities. The equations for the six independent experimental quantities in terms of the l_{ij} are now written out using eq 12, 13, 14, and 28

$$\alpha = \frac{\Lambda N}{1000\mathfrak{F}^2} = z_1(z_1l_{11} + z_2l_{12} + z_3l_{13}) + z_2(z_1l_{12} + z_2l_{22} + z_3l_{23}) + z_3(z_1l_{13} + z_2l_{23} + z_3l_{33}) \tag{30}$$

$$\alpha t_1 = z_1(z_1l_{11} + z_2l_{12} + z_3l_{13}) \tag{31}$$

$$\alpha t_2 = z_2(z_1l_{12} + z_2l_{22} + z_3l_{23}) \tag{32}$$

$$\alpha r_{1c}^2(L_{11})_0 = z_2^2(l_{11}l_{22} - l_{12}^2) + 2z_2z_3(l_{11}l_{23} - l_{12}l_{13}) + z_3^2(l_{11}l_{33} - l_{13}^2) \tag{33}$$

$$-\alpha r_{1c}r_{2c}(L_{12})_0 = z_1z_2(l_{11}l_{22} - l_{12}^2) + z_1z_3(l_{11}l_{23} - l_{12}l_{13}) + z_2z_3(l_{13}l_{22} - l_{12}l_{23}) + z_3^2(l_{13}l_{23} - l_{12}l_{33}) \tag{34}$$

$$\alpha r_{2c}^2(L_{22})_0 = z_1^2(l_{11}l_{22} - l_{12}^2) + 2z_1z_3(l_{13}l_{22} - l_{12}l_{23}) + z_3^2(l_{22}l_{33} - l_{23}^2) \tag{35}$$

IV. The l_{ij} in Terms of Measured Quantities

A. Expressions for the l_{ij}. The six equations 30–35 can be solved for the six coefficients l_{11}, l_{22}, l_{33}, l_{12}, l_{13}, and l_{23}. By analogy to the solution for the binary case, it is expected that $\alpha^2t_it_j/z_iz_j$ and one or more $(L_{ij})_0$ should be involved. Using this combination for $i = 1$, $j = 1$, and eq 33, one obtains an expression for l_{11} and similarly for l_{12} and l_{22}. Then l_{13} and l_{23} are obtained by substituting the previous results into eq 31 and 32, respectively. Finally l_{33} comes from eq 30 or from the expression for αt_3 analogous to eq 31 or 32.

The results are as shown in eq 36–41

$$l_{11} = \frac{\Lambda N t_1^2}{10^3\mathfrak{F}^2z_1^2} + r_{1c}^2(L_{11})_0 \tag{36}$$

$$l_{22} = \frac{\Lambda N t_2^2}{10^3\mathfrak{F}^2z_2^2} + r_{2c}^2(L_{22})_0 \tag{37}$$

$$l_{33} = \frac{\Lambda N t_3^2}{10^3\mathfrak{F}^2z_3^2} + r_{1a}^2(L_{11})_0 + 2r_{1a}r_{2a}(L_{12})_0 + r_{2a}^2(L_{22})_0 \tag{38}$$

$$l_{12} = \frac{\Lambda N t_1t_2}{10^3\mathfrak{F}^2z_1z_2} + r_{1c}r_{2c}(L_{12})_0 \tag{39}$$

$$l_{13} = \frac{\Lambda N t_1t_3}{10^3\mathfrak{F}^2z_1z_3} + r_{1c}r_{1a}(L_{11})_0 + r_{1c}r_{2a}(L_{12})_0 \tag{40}$$

$$l_{23} = \frac{\Lambda N t_2t_3}{10^3\mathfrak{F}^2z_2z_3} + r_{2c}r_{1a}(L_{12})_0 + r_{2c}r_{2a}(L_{22})_0 \tag{41}$$

with the units mole^2/joule cm sec. They are valid for strong or weak electrolytes.

These equations are clearly generalizations of the binary case[3] and reduce to that case if one of the electrolytes is at vanishing concentration. Thus if $D_{r_{2c}}$-$A_{r_{2a}}$ is missing, then $c_2 = 0$. By eq 22, $\mu_{22} = -\infty$ and hence $(L_{12})_0$ and $(L_{22})_0$ are 0 from eq 20. Moreover if $c_2 = 0$, then there is no ion D^{z_2} to carry any current, whence $t_2 = 0$. Consequently $l_{12} = l_{22} = l_{23} = 0$, and everything has reduced to the binary case. Finally $(L_{22})_0 = 0$ and $(L_{12})_0 = 0$ imply $(D_{21})_0 = 0$ by eq 19, which can be proved independently by an analysis of eq 15.

It can be shown that N is factorable from the $(L_{ij})_0$, leaving terms which are relatively concentration independent. Consequently all the l_{ij} go to zero at infinite dilution. It is therefore plausible to tabulate l_{ij}/N, which remain finite at all concentrations.

By analogy to the binary systems, it is expected that l_{12}/N, l_{13}/N, and l_{23}/N will be zero at infinite dilution. Moreover at finite concentrations l_{13}/N and l_{23}/N should be positive because of coulombic attraction. However l_{12}/N should (a) be negative because of coulombic repulsion and (b) be smaller because there are fewer encounters between ions 1 and 2 compared to 1 and 3 or 2 and 3 (since the concentration of 3 is greater than 1 or 2).

B. J_i in Terms of Ordinary Transport Quantities. Useful and rigorous expressions for SF J_i in terms of the usual transport quantities t_i, Λ, and $(L_{ij})_0$ or $(D_{ij})_0$ are obtained by substituting eq 36–41 into eq 9. After some algebra and recalling that the right-hand sides of eq 15 and 18 are the same for given i, we obtain the forms

$$-J_1 = \frac{\Lambda N t_1}{10^3 \mathfrak{F}^2 z_1}[\ ] + r_{1c}\left[(L_{11})_0\frac{\partial \mu_{13}}{\partial x} + (L_{12})_0\frac{\partial \mu_{23}}{\partial x}\right] =$$

$$\frac{\Lambda N t_1}{10^3 \mathfrak{F}^2 z_1}[\ ] + r_{1c}\left[(\hat{D}_{11})_0\frac{\partial c_1}{\partial x} + (\hat{D}_{12})_0\frac{\partial c_2}{\partial x}\right] \quad (42)$$

$$-J_2 = \frac{\Lambda N t_2}{10^3 \mathfrak{F}^2 z_2}[\ ] + r_{2c}\left[(L_{12})_0\frac{\partial \mu_{13}}{\partial x} + (L_{22})_0\frac{\partial \mu_{23}}{\partial x}\right] =$$

$$\frac{\Lambda N t_2}{10^3 \mathfrak{F}^2 z_2}[\ ] + r_{2c}\left[(\hat{D}_{21})_0\frac{\partial c_1}{\partial x} + (\hat{D}_{22})_0\frac{\partial c_2}{\partial x}\right] \quad (43)$$

$$-J_3 = \frac{\Lambda N t_3}{10^3 \mathfrak{F}^2 z_3}[\ ] + r_{1a}\left[(L_{11})_0\frac{\partial \mu_{13}}{\partial x} + (L_{12})_0\frac{\partial \mu_{23}}{\partial x}\right] +$$

$$r_{2a}\left[(L_{12})_0\frac{\partial \mu_{13}}{\partial x} + (L_{22})_0\frac{\partial \mu_{23}}{\partial x}\right]$$

$$= \frac{\Lambda N t_3}{10^3 \mathfrak{F}^2 z_3}[\ ] + r_{1a}\left[(\hat{D}_{11})_0\frac{\partial c_1}{\partial x} + (\hat{D}_{12})_0\frac{\partial c_2}{\partial x}\right] +$$

$$r_{2a}\left[(\hat{D}_{21})_0\frac{\partial c_1}{\partial x} + (\hat{D}_{22})_0\frac{\partial c_2}{\partial x}\right] \quad (44)$$

where [] is defined as

$$[\ ] = \frac{t_1}{z_1}\frac{\partial \mu_1}{\partial x} + \frac{t_2}{z_2}\frac{\partial \mu_2}{\partial x} + \frac{t_3}{z_3}\frac{\partial \mu_3}{\partial x} + \mathfrak{F}\frac{\partial \phi}{\partial x} \quad (45)$$

Substitution of eq 42–44 into the expression for I in eq 23 yields the relation

$$[\ ] = -\frac{10^3 \mathfrak{F} I}{N\Lambda} \quad (46)$$

Consequently we obtain the further useful results

$$J_1 = \frac{t_1}{z_1}\frac{I}{\mathfrak{F}} - r_{1c}\left[(\hat{D}_{11})_0\frac{\partial c_1}{\partial x} + (\hat{D}_{12})_0\frac{\partial c_2}{\partial x}\right] \quad (47)$$

$$J_2 = \frac{t_2}{z_2}\frac{I}{\mathfrak{F}} - r_{2c}\left[(\hat{D}_{21})_0\frac{\partial c_1}{\partial x} + (\hat{D}_{22})_0\frac{\partial c_2}{\partial x}\right] \quad (48)$$

$$J_3 = \frac{t_3}{z_3}\frac{I}{\mathfrak{F}} - r_{1a}\left[(\hat{D}_{11})_0\frac{\partial c_1}{\partial x} + (\hat{D}_{12})_0\frac{\partial c_2}{\partial x}\right] -$$

$$r_{2a}\left[(\hat{D}_{21})_0\frac{\partial c_1}{\partial x} + (\hat{D}_{22})_0\frac{\partial c_2}{\partial x}\right] \quad (49)$$

with similar equations when the square brackets containing D_{ij} terms are replaced by the corresponding square brackets containing L_{ij} terms.

Equations 47–49 represent a superposition of ion transport by current flow and diffusion flow. Consequently the analysis leading to them is a rigorous proof from irreversible thermodynamic principles that superposition of flows is valid in a ternary system, and obviously in an n-component system as well by an analogous argument.

V. Calculated Values of l_{ij} for Seven Systems

Data necessary for determining l_{ij}, namely, t_1, t_2, Λ, and $(L_{ij})_0$, are exceedingly scarce. The $(L_{ij})_0$ can be obtained from μ_{ij} and $(D_{ij})_0$ using eq 20. The $(D_{ij})_0$ in turn are obtained from partial molal volumes, $\bar{V}_{i3}$, and the volume-fixed (VF) diffusion coefficients $(D_{ij})_v$.[9,11,12] Ternary systems for which $(D_{ij})_v$ and other data exist are seven strong electrolyte mixtures, namely, five compositions of H_2O–NaCl–KCl[13] at 25° (systems IA–IE) and one composition each of H_2O–LiCl–KCl[14] and H_2O–LiCl–NaCl[14] at 25° (systems II and III, respectively). Values of $(L_{ij})_0$ have been calculated for systems I using experimental μ_{ij}[15] and for systems II and III using estimated μ_{ij} based on experimental ternary data at higher concentrations.[16]

There are some conductance data at 25° for NaCl–KCl mixtures from 0.1 to 4 m[17–20] and for LiCl–KCl mixtures from 0.001 to 0.2 N.[21–23] These data can be predicted at low concentrations by the mixture rule

$$\Lambda = x_1\Lambda_{13}^{\circ} + x_2\Lambda_{23}^{\circ} \quad (50)$$

where Λ_{i3}° is the conductance of the binary electrolyte at the same total equivalent concentration, N, of the mixture and where the "equivalent fractions" x_i are given by

$$x_i = \frac{N_i}{N_1 + N_2} \qquad i = 1, 2, 3 \quad (51)$$

$$x_3 = x_1 + x_2 = 1$$

Van Rysselberghe and Nutting[24] derived a formula which represents conductance data as well as or better than eq 50 for all salt mixtures for which it could be tested[24,25] and was within 0.1 conductance unit for NaCl–KCl mixtures[18] to 4 N (it was less satisfactory for HCl–NaCl mixtures[25]). This formula is

(13) H. Fujita and L. J. Gosting, *J. Phys. Chem.*, **64**, 1256 (1960).
(14) P. J. Dunlop, *ibid.*, **68**, 3062 (1964).
(15) D. G. Miller, *ibid.*, **69**, 3374 (1965).
(16) D. G. Miller, Lawrence Radiation Laboratory, UCRL-12462, March 1965.
(17) A. E. Stearn, *J. Am. Chem. Soc.*, **44**, 670 (1922).
(18) C. E. Ruby and J. Kawai, *ibid.*, **48**, 1119 (1926).
(19) D. A. MacInnes, I. A. Cowperthwaite, and T. Shedlovsky, *ibid.*, **51**, 2671 (1929).
(20) R. W. Bremner, T. G. Thompson, and C. L. Utterback, *ibid.*, **61**, 1219 (1939).
(21) H. Egner, *Medd. Vetenskapsakad. Nobelinst.*, **6**, No. 5, 1 (1923).
(22) K. A. Krieger and M. Kilpatrick, *J. Am. Chem. Soc.*, **59**, 1878 (1937); corrections, **61**, 3601 (1939).
(23) G. Kell and A. R. Gordon, *ibid.*, **81**, 3207 (1959).
(24) P. Van Rysselberghe and L. Nutting, *ibid.*, **56**, 1435 (1934).
(25) N. C. C. Li and H. Fang, *J. Chinese Chem. Soc.*, **6**, 32 (1938).

Table I

	IA	IB	IC	ID	IE	II	III
	A. Ionic l_{ij}/N for Seven Ternary Systems at 25°[a,b]						
$(l_{11}/N) \times 10^{12}$	2.43$_0$	3.12$_4$	1.64$_5$	2.36$_4$	2.01$_2$	2.00$_4$	1.95$_2$
$(l_{22}/N) \times 10^{12}$	3.63$_8$	2.41$_6$	4.79$_3$	3.58$_5$	3.19$_1$	3.24$_5$	2.15$_6$
$(l_{33}/N) \times 10^{12}$	7.30$_2$	7.08$_2$	7.24$_8$	7.06$_2$	6.14$_8$	7.16$_7$	7.03$_0$
$(l_{12}/N) \times 10^{12}$	−0.08$_9$	−0.10$_7$	−0.11$_0$	−0.13$_5$	−0.15$_6$	−0.10$_3$	−0.08$_2$
$(l_{13}/N) \times 10^{12}$	0.43$_1$	0.60$_8$	0.31$_4$	0.48$_0$	0.47$_1$	0.39$_0$	0.37$_4$
$(l_{23}/N) \times 10^{12}$	0.51$_0$	0.36$_7$	0.74$_5$	0.60$_0$	0.66$_5$	0.45$_5$	0.39$_7$
	B. Ionic and Diffusion Friction Coefficients for Seven Ternary Systems at 25°						
$R_{10} \times 10^{-9}$	−3.47	−3.58	−3.48	−3.61	−4.48	−4.77	−4.93
$R_{20} \times 10^{-9}$	−2.30	−2.36	−2.31	−2.35	−2.75	−2.35	−3.55
$R_{30} \times 10^{-9}$	−2.14	−2.16	−2.15	−2.18	−2.54	−2.14	−2.13
$R_{12} \times 10^{-9}$	27.5	25.1	24.8	21.4	11.2	44.8	55.8
$R_{13} \times 10^{-9}$	−51.1	−38.7	−38.0	−31.1	−14.2	−64.0	−64.5
$R_{23} \times 10^{-9}$	−40.5	−31.1	−30.2	−25.6	−12.5	−46.4	−61.9
$R_{11} \times 10^{-11}$	8.33	4.35	8.19	4.31	1.70	11.2	11.5
$R_{22} \times 10^{-11}$	5.56	5.58	2.84	2.84	1.08	6.93	10.4
$R_{33} \times 10^{-11}$	2.80	1.93	1.89	1.46	0.57	3.16	3.23
$R_{00} \times 10^{-7}$	4.59	7.36	6.70	9.54	36.1	4.79	5.28
$\mathfrak{R}_{10} \times 10^{-9}$	−5.62	−5.75	−5.64	−5.80	−7.06	−6.93	−7.11
$\mathfrak{R}_{20} \times 10^{-9}$	−4.42	−4.52	−4.46	−4.51	−5.25	−4.45	−5.60
$\mathfrak{R}_{12} \times 10^{-11}$	2.15	1.48	1.45	1.10	0.41	2.51	2.52
$\mathfrak{R}_{11} \times 10^{-11}$	10.10	5.51	9.32	5.14	1.98	13.12	13.47
$\mathfrak{R}_{22} \times 10^{-11}$	7.55	6.89	4.18	3.79	1.39	9.16	12.43
$\mathfrak{R}_{00} \times 10^{-7}$	4.59	7.36	6.70	9.54	36.13	4.79	5.28

[a] The compositions of these systems are: systems I, for NaCl and KCl, respectively: A (0.25 M, 0.25 M); B (0.5, 0.25); C (0.25, 0.5); D (0.5, 0.5); E (1.5, 1.5); system II: LiCl (0.25 M), KCl (0.2 M); and system III: LiCl (0.25 M), NaCl (0.2 M). [b] The units are mole²/joule cm sec for l_{ij} and joule cm sec/mole² for R_{ij} and $\mathfrak{R}_{ij}$.

$$\Lambda = [x_1\Lambda_{13}^{\bullet}(1 - t_1^{\bullet}) + x_2\Lambda_{23}^{\bullet}(1 - t_2^{\bullet})] \times \left[\frac{x_1}{(1 - t_1^{\bullet})} + \frac{x_2}{(1 - t_2^{\bullet})}\right] \quad (52)$$

where $t_1^{\bullet}$ and $t_2^{\bullet}$ are the transference numbers of cations 1 and 2 in their respective binary solutions at the same total concentration N as in the mixture. Since Λ at our concentrations are unavailable or not too accurate and since eq 52 is so successful as an interpolation formula, we have used it to calculate Λ for our seven cases, using the smoothed and critically reviewed binary data in paper I[3] for $t_i^{\bullet}$ and $\Lambda_{i3}^{\bullet}$.

There exist very little data for transference numbers in ternary systems. There are some Hittorf measurements on various alkali halides,[24] in particular for NaCl–KCl[26-28] and LiCl–KCl[26] up to 5 N. These relatively imprecise data can be fitted within the experimental error[26-28] (*i.e.*, <0.01 in t) by the equations

$$t_3 = (1 - t_1^{\bullet})(1 - t_2^{\bullet})/[x_1(1 - t_2^{\bullet}) + x_2(1 - t_1^{\bullet})] \quad (53)$$

$$t_1 = \frac{x_1 t_1^{\bullet} t_3}{(1 - t_1^{\bullet})} \qquad t_2 = \frac{x_2 t_2^{\bullet} t_3}{(1 - t_2^{\bullet})} \quad (54)$$

These equations are due to MacInnes[29] and were rederived by Van Rysselberghe[30] under much less restrictive hypotheses.

No accurate data in concentrated solutions exist, but there are some dilute solution moving boundary results, namely, t_3 in NaCl–KCl at 0.1 N,[19] t_i in HCl–KCl at 0.1 N,[31] and t_i in LiCl–KCl at 0.01 N.[32] Comparison of these data with the t_i predicted by eq 53 and 54 show agreement within 0.001. Because eq 53 and 54 give excellent results where they can be definitely tested and because they are within the experimental error in the more concentrated solutions, we have used them with the smoothed $t_i^{\bullet}$ data in paper I[3] to obtain the transference numbers for our seven cases.

(26) P. Van Rysselberghe and L. Nutting, *J. Am. Chem. Soc.*, **55**, 996 (1933).
(27) J. Dewey, *ibid.*, **47**, 1927 (1925).
(28) S. A. Braley and C. W. Rippie, *ibid.*, **49**, 1493 (1927).
(29) D. A. MacInnes, *ibid.*, **47**, 1922 (1925).
(30) P. Van Rysselberghe, *ibid.*, **55**, 990 (1933).
(31) L. G. Longsworth, *ibid.*, **52**, 1847 (1930).
(32) G. S. Kell and A. R. Gordon, *ibid.*, **81**, 3207 (1959).

We have used $\hat{R}$ = 8.3144 joules/mole deg, $\mathfrak{F}$ = 96,493 coulombs/equiv, and 25°C = 298.15°K.

In Table IA are the l_{ij}/N calculated from eq 36–41 using the above-mentioned t_1, t_2, Λ, and $(L_{ij})_0$ (whose values are given in the experimental columns of Tables II–VIII). These results are less certain than the binary l_{ij}, primarily because of uncertainties in t_i.

Because the concentration ranges and number of examples are limited, it is difficult to analyze the results systematically. However we note that (a) the cation–cation interaction is, as predicted, negative and smaller than l_{13} and l_{23} and (b) the l_{13} and l_{23} are from 5 to 30% of l_{ii}/N and are thus not negligible even at 0.5 N. The latter observation emphasizes the importance of l_{ij}, $i \neq j$, discussed in detail in paper I, and calls attention once again to the unreality of theories which take $l_{ij} = 0$.

VI. Estimation of Ternary Quantities from Binary Data

To avoid confusion in what follows between the notation of this paper and ref 3, we note that in the ternary description the cation–cation terms 11 and 22 both correspond to 11 in binaries, the cation–anion cross terms 13 and 23 correspond to 12 in binaries, and the anion–anion term 33 corresponds to 22 in binaries. The ternary cation–cation term 12 has no binary analog.

A. Approximations for l_{ij}/N. An important empirical observation is that the ternary l_{ij}/N are directly related to their binary analogs for these strong electrolyte systems. For example consider IA, where $x_1 = x_2 = 0.5$. The values of l_{11}/N and l_{22}/N are about half the values of l_{11}/N in the NaCl and KCl binaries, respectively, at the same total concentration N as in the ternary. Similarly, l_{13}/N and l_{23}/N are about half the l_{12}/N in the NaCl and KCl binaries, respectively, and l_{33}/N is about halfway between the l_{22}/N for the NaCl and KCl binaries. A similar relationship to equivalent fractions x_i holds for the other cases.

Although l_{12}/N has no analog in binary systems, it can be approximated within 10% for all seven systems except IA by the purely empirical eq 58 below.

These approximations can be written more explicitly as

$$l_{ii}/N = x_i(l_{11}^{\cdot}/N)_{i,N} \quad i = 1, 2 \tag{55}$$

$$l_{33}/N = x_1(l_{22}^{\cdot}/N)_{1,N} + x_2(l_{22}^{\cdot}/N)_{2,N} \tag{56}$$

LN
$$l_{i3}/N = x_i(l_{12}^{\cdot}/N)_{i,N} \quad i = 1, 2 \tag{57}$$

$$\frac{l_{12}}{N} = x_1x_2\left(\frac{l_{13}}{N}\frac{l_{23}}{N}\right)^{1/2} \tag{58}$$

where $(l_{11}^{\cdot}/N)_{i,N}$ denotes the term for cation i in the binary with the same anion as in the ternary, $(l_{22}^{\cdot}/N)_{i,N}$ is the anion term for the binary with cation i, and $(l_{12}^{\cdot}/N)_{i,N}$ is the cross term of cation i with anion 3 in the $i3$ binary. The superscript dots refer to binaries and the subscript N indicates that $(l_{ij}^{\cdot}/N)$ is to be evaluated in the binary at the same total equivalent concentration N as in the ternary.[33] This set of approximations, denoted by **LN**, seems very reasonable. It gives excellent estimates of l_{13}/N, l_{23}/N, and l_{33}/N, but the values of l_{11}/N and l_{22}/N are slightly low.

Closer examination of l_{11}/N and l_{22}/N shows that if $(l_{11}^{\cdot}/N)_i$ are evaluated at the equivalent concentration of the ion itself N_i in the ternary (rather than the total equivalent concentration N), the resulting estimates are greatly improved and very close. This second approximation set, denoted by **LNI**, is the same as **LN** except

LNI
$$l_{ii}/N = x_i(l_{11}^{\cdot}/N)_{i,Ni} \quad i = 1, 2 \tag{59}$$

where the subscript N_i means that the $l_{11}^{\cdot}/N$ is to be evaluated at N_i in the binary.

These two approximation schemes contain estimates of all the possible terms in a common anion system (*i.e.*, cation i–cation i, cation i–cation j, cation i–anion, and anion–anion). Therefore the extension to quaternary and higher order strong-electrolyte systems is immediate, making possible the estimation of transport properties of such systems using only binary data. A test awaits experimental data on such systems.

A third approximation set, denoted by **LL**, is equivalent to simplified electrolyte theories, *i.e.*

$$l_{ii}/N = x_i(l_{11}^{\cdot}/N)_{i,0} = x_i\Lambda_i^0/(10^3z_i^2\mathfrak{F}^2) \quad i = 1, 2 \tag{60}$$

LL
$$l_{33}/N = x_1(l_{22}^{\cdot}/N)_{1,0} + x_2(l_{22}^{\cdot}/N)_{2,0} = \Lambda_3^0/10^3z_3\mathfrak{F}^2 \tag{61}$$

$$l_{12}/N = l_{13}/N = l_{23}/N = 0 \tag{62}$$

where the subscript 0 indicates evaluation at infinite dilution and where Λ_i^0 is the ionic conductance of ion i at infinite dilution. This approximation is equivalent to one used by Wendt for the prediction of diffusion coefficients.[34]

The estimated values of l_{ij}/N from approximations **LN**, **LNI**, and **LL** are compared with experimental values in Tables II–VIII. These tables show that

(33) For 1–1 electrolytes, $N = c = S$, where S is the ionic strength. Therefore it is not yet clear whether evaluation of $(l_{ij}^{\cdot}/N)$ for mixtures with higher valence types should be at the same c, N, or S. Electrolyte theory suggests S at first thought.

(34) R. P. Wendt, *J. Phys. Chem.*, 69, 1227 (1965).

Table II: Estimated Ternary Properties at 25° for Strong Electrolytes from Data on Binaries[a,b]

IA H_2O–NaCl (0.25 M)–KCl (0.25 M)

	Exptl	LNIE	LNIB	LNB	LLB	LLM[c]	LK1	LK2
$(l_{11}/N) \times 10^{12}$	2.43	2.40	2.40	2.31	2.69	2.69		
$(l_{22}/N) \times 10^{12}$	3.64	3.64	3.64	3.60	3.95	3.95		
$(l_{33}/N) \times 10^{12}$	7.30	7.30	7.30	7.30	8.20	8.20		
$(l_{12}/N) \times 10^{12}$	−0.09	−0.12	−0.12	−0.12	0	0		
$(l_{13}/N) \times 10^{12}$	0.43	0.42	0.42	0.42	0	0		
$(l_{23}/N) \times 10^{12}$	0.51	0.52	0.52	0.52	0	0		
t_1	0.169	0.166	0.166	0.166	0.181	0.181		
t_2	0.268	0.268	0.268	0.267	0.266	0.266		
Λ	105.3	104.5	104.5	103.3	138.1	138.1		
$(L_{11})_0 \times 10^8 \hat{R}T$	0.261	0.259	0.259	0.251	0.273	0.273		
$(L_{12})_0 \times 10^8 \hat{R}T$	−0.075[d]	−0.076	−0.076	−0.073	−0.089	−0.089		
$(L_{22})_0 \times 10^8 \hat{R}T$	0.350	0.352	0.352	0.348	0.359	0.359		
$(L_{11})_v \times 10^8 \hat{R}T$	0.260	0.258	0.258	0.250	0.272	0.272	0.270	0.266
$(L_{12})_v \times 10^8 \hat{R}T$	−0.078[d]	−0.079	−0.079	−0.076	−0.092	−0.092	−0.088	−0.089
$(L_{22})_v \times 10^8 \hat{R}T$	0.345	0.347	0.347	0.344	0.355	0.355	0.355	0.349
$(D_{11})_v \times 10^5$	1.37	1.36	1.36	1.32	1.42	1.46		
$(D_{12})_v \times 10^5$	−0.00	−0.01	−0.00	0.00	−0.05	0.01		
$(D_{21})_v \times 10^5$	0.14	0.13	0.14	0.15	0.08	0.19		
$(D_{22})_v \times 10^5$	1.82	1.83	1.83	1.81	1.85	1.98		

[a] Units: l_{ij} in mole²/joule cm sec; Λ in cm²/ohm equiv; $(L_{ij})_0\hat{R}T$ and $(L_{ij})_v\hat{R}T$ in mole/cm sec; and $(D_{ij})_v$ in cm²/sec. [b] E refers to use of experimental activity coefficient derivatives,[15] B to derivatives estimated from binary data.[10] [c] The same as Wendt[34] except assume $\partial \ln \gamma_i/\partial m_j = 0$ instead of $\partial \ln y_i/\partial c_j = 0$ [d] The average of L_{12} and L_{21} calculated from experimental data.[15]

Table III: Estimated Ternary Properties at 25° for Strong Electrolytes from Data on Binaries[a,b]

IB H_2O–NaCl (0.5 M)–KCl (0.25 M)

	Exptl	LNIE	LNIB	LNB	LLB	LLM[c]	LK1	LK2
$(l_{11}/N) \times 10^{12}$	3.12	3.08	3.08	2.97	3.59	3.59		
$(l_{22}/N) \times 10^{12}$	2.42	2.43	2.43	2.38	2.63	2.63		
$(l_{33}/N) \times 10^{12}$	7.08	7.08	7.08	7.08	8.20	8.20		
$(l_{12}/N) \times 10^{12}$	−0.11	−0.10	−0.10	−0.10	0	0		
$(l_{13}/N) \times 10^{12}$	0.61	0.59	0.59	0.59	0	0		
$(l_{23}/N) \times 10^{12}$	0.37	0.38	0.38	0.38	0	0		
t_1	0.230	0.228	0.228	0.221	0.249	0.249		
t_2	0.186	0.186	0.186	0.184	0.182	0.182		
Λ	97.4	97.2	97.2	95.7	134.2	134.2		
$(L_{11})_0 \times 10^8 \hat{R}T$	0.472	0.471	0.471	0.459	0.501	0.501		
$(L_{12})_0 \times 10^8 \hat{R}T$	−0.103[d]	−0.102	−0.102	−0.097	−0.122	−0.122		
$(L_{22})_0 \times 10^8 \hat{R}T$	0.382	0.384	0.384	0.378	0.400	0.400		
$(L_{11})_v \times 10^8 \hat{R}T$	0.472	0.465	0.465	0.453	0.495	0.495	0.492	0.474
$(L_{12})_v \times 10^8 \hat{R}T$	−0.110[d]	−0.108	−0.108	−0.104	−0.128	−0.128	−0.120	−0.119
$(L_{22})_v \times 10^8 \hat{R}T$	0.378	0.380	0.380	0.373	0.395	0.395	0.393	0.381
$(D_{11})_v \times 10^5$	1.42	1.40	1.40	1.36	1.47	1.51		
$(D_{12})_v \times 10^5$	−0.01	−0.01	0.01	0.02	−0.06	0.01		
$(D_{21})_v \times 10^5$	0.09	0.10	0.11	0.12	0.06	0.13		
$(D_{22})_v \times 10^5$	1.82	1.83	1.83	1.80	1.88	1.97		

[a] Units: l_{ij} in mole²/joule cm sec; Λ in cm²/ohm equiv; $(L_{ij})_0\hat{R}T$ and $(L_{ij})_v\hat{R}T$ in mole/cm sec; and $(D_{ij})_v$ in cm²/sec. [b] E refers to use of experimental activity coefficient derivatives,[15] B to derivatives estimated from binary data.[10] [c] The same as Wendt[34] except assume $\partial \ln \gamma_i/\partial m_j = 0$ instead of $\partial \ln y_i/\partial c_j = 0$. [d] The average of L_{12} and L_{21} calculated from experimental data.[15]

Table IV: Estimated Ternary Properties at 25° for Strong Electrolytes from Data on Binaries[a,b]

IC H_2O–NaCl (0.25 M)–KCl (0.5 M)

	Exptl	LNIE	LNIB	LNB	LLB	LLM[c]	LK1	LK2
$(l_{11}/N) \times 10^{12}$	1.64	1.60	1.60	1.48	1.79	1.79		
$(l_{22}/N) \times 10^{12}$	4.79	4.80	4.80	4.75	5.26	5.26		
$(l_{33}/N) \times 10^{12}$	7.25	7.24	7.24	7.24	8.20	8.20		
$(l_{12}/N) \times 10^{12}$	−0.11	−0.11	−0.11	−0.11	0	0		
$(l_{13}/N) \times 10^{12}$	0.31	0.30	0.30	0.30	0	0		
$(l_{23}/N) \times 10^{12}$	0.74	0.76	0.76	0.76	0	0		
t_1	0.108	0.106	0.106	0.096	0.118	0.118		
t_2	0.347	0.348	0.348	0.349	0.345	0.345		
Λ	105.7	105.3	105.3	103.7	142.0	142.0		
$(L_{11})_0 \times 10^8 \hat{R}T$	0.281	0.274	0.274	0.256	0.294	0.294		
$(L_{12})_0 \times 10^8 \hat{R}T$	−0.099[d]	−0.097	−0.097	−0.089	−0.115	−0.115		
$(L_{22})_0 \times 10^8 \hat{R}T$	0.637	0.638	0.638	0.631	0.641	0.641		
$(L_{11})_v \times 10^8 \hat{R}T$	0.280	0.273	0.273	0.255	0.293	0.293	0.289	0.287
$(L_{12})_v \times 10^8 \hat{R}T$	−0.105[d]	−0.102	−0.102	−0.095	−0.120	−0.120	−0.113	−0.117
$(L_{22})_v \times 10^8 \hat{R}T$	0.620	0.621	0.621	0.615	0.624	0.624	0.629	0.617
$(D_{11})_v \times 10^5$	1.36	1.32	1.32	1.23	1.40	1.41		
$(D_{12})_v \times 10^5$	0.00	0.00	0.01	0.01	−0.02	0.00		
$(D_{21})_v \times 10^5$	0.19	0.20	0.22	0.25	0.13	0.24		
$(D_{22})_v \times 10^5$	1.84	1.84	1.84	1.83	1.83	1.98		

[a] Units: l_{ij} in mole²/joule cm sec; Λ in cm²/ohm equiv; $(L_{ij})_0\hat{R}T$ and $(L_{ij})_v\hat{R}T$ in mole/cm sec; and $(D_{ij})_v$ in cm²/sec. [b] E refers to use of experimental activity coefficient derivatives,[15] B to derivatives estimated from binary data.[10] [c] The same as Wendt[34] except assume $\partial \ln \gamma_i/\partial m_j = 0$ instead of $\partial \ln y_i/\partial c_j = 0$. [d] The average of L_{12} and L_{21} calculated from experimental data.[15]

Table V: Estimated Ternary Properties at 25° for Strong Electrolytes from Data on Binaries[a,b]

ID H_2O–NaCl (0.5 M)–KCl (0.5 M)

	Exptl	LNIE	LNIB	LNB	LLB	LLM[c]	LK1	LK2
$(l_{11}/N) \times 10^{12}$	2.36	2.31	2.31	2.16	2.69	2.69		
$(l_{22}/N) \times 10^{12}$	3.58	3.60	3.60	3.54	3.95	3.95		
$(l_{33}/N) \times 10^{12}$	7.06	7.04	7.04	7.04	8.20	8.02		
$(l_{12}/N) \times 10^{12}$	−0.14	−0.13	−0.13	−0.13	0	0		
$(l_{13}/N) \times 10^{12}$	0.48	0.45	0.45	0.45	0	0		
$(l_{23}/N) \times 10^{12}$	0.60	0.61	0.61	0.61	0	0		
t_1	0.165	0.164	0.164	0.152	0.181	0.181		
t_2	0.269	0.270	0.270	0.270	0.266	0.266		
Λ	98.5	98.4	98.4	96.4	138.1	138.1		
$(L_{11})_0 \times 10^8 \hat{R}T$	0.514	0.502	0.502	0.476	0.546	0.546		
$(L_{12})_0 \times 10^8 \hat{R}T$	−0.150[d]	−0.148	−0.148	−0.138	−0.177	−0.177		
$(L_{22})_0 \times 10^8 \hat{R}T$	0.698	0.701	0.701	0.690	0.718	0.718		
$(L_{11})_v \times 10^8 \hat{R}T$	0.509	0.497	0.497	0.471	0.541	0.541	0.533	0.522
$(L_{12})_v \times 10^8 \hat{R}T$	−0.162[d]	−0.160	−0.160	−0.150	−0.189	−0.189	−0.173	−0.177
$(L_{22})_v \times 10^8 \hat{R}T$	0.681	0.683	0.683	0.672	0.700	0.700	0.701	0.681
$(D_{11})_v \times 10^5$	1.39	1.36	1.35	1.28	1.46	1.46		
$(D_{12})_v \times 10^5$	−0.00	+0.00	0.02	0.02	−0.02	0.01		
$(D_{21})_v \times 10^5$	0.16	0.16	0.18	0.20	0.11	0.19		
$(D_{22})_v \times 10^5$	1.83	1.84	1.83	1.81	1.85	1.98		

[a] Units: l_{ij} in mole²/joule cm sec; Λ in cm²/ohm equiv; $(L_{ij})_0\hat{R}T$ and $(L_{ij})_v\hat{R}T$ in mole/cm sec; and $(D_{ij})_v$ in cm²/sec. [b] E refers to use of experimental activity coefficient derivatives,[15] B to derivatives estimated from binary data.[10] [c] The same as Wendt[34] except assume $\partial \ln \gamma_i/\partial m_j = 0$ instead of $\partial \ln y_i/\partial c_j = 0$. [d] The average of L_{12} and L_{21} calculated from experimental data.[16]

Table VI: Estimated Ternary Properties at 25° for Strong Electrolytes from Data on Binaries[a,b]

IE H_2O–NaCl (1.5 M)–KCl (1.5 M)

	Exptl	LNIE	LNIB	LNB	LLB	LLM[c]	LK1	LK2
$(l_{11}/N) \times 10^{12}$	2.01	2.03	2.03	1.68	2.69	2.69		
$(l_{22}/N) \times 10^{12}$	3.19	3.49	3.49	3.32	3.95	3.95		
$(l_{33}/N) \times 10^{12}$	6.15	6.16	6.16	6.16	8.20	8.20		
$(l_{12}/N) \times 10^{12}$	−0.16	−0.14	−0.14	−0.14	0	0		
$(l_{13}/N) \times 10^{12}$	0.47	0.43	0.43	0.43	0	0		
$(l_{23}/N) \times 10^{12}$	0.66	0.72	0.72	0.72	0	0		
t_1	0.158	0.160	0.160	0.130	0.181	0.181		
t_2	0.270	0.289	0.289	0.287	0.266	0.266		
Λ	81.6	84.8	84.8	79.9	138.1	138.1		
$(L_{11})_0 \times 10^8 \hat{R}T$	1.334	1.335	1.335	1.142	1.638	1.638		
$(L_{12})_0 \times 10^8 \hat{R}T$	−0.394[d]	−0.417	−0.417	−0.340	−0.532	−0.532		
$(L_{22})_0 \times 10^8 \hat{R}T$	1.896	2.030	2.030	1.944	2.154	2.154		
$(L_{11})_v \times 10^8 \hat{R}T$	1.289	1.293	1.293	1.105	1.587	1.587	1.51	1.36
$(L_{12})_v \times 10^8 \hat{R}T$	−0.494[d]	−0.521	−0.521	−0.440	−0.642	−0.642	−0.49	−0.50
$(L_{22})_v \times 10^8 \hat{R}T$	1.743	1.865	1.865	1.783	1.985	1.985	1.99	1.75
$(D_{11})_v \times 10^5$	1.40	1.39	1.38	1.19	1.70	1.45		
$(D_{12})_v \times 10^5$	0.10	0.08	0.13	0.12	0.16	−0.01		
$(D_{21})_v \times 10^5$	0.32	0.34	0.41	0.47	0.32	0.20		
$(D_{22})_v \times 10^5$	1.80	1.92	1.92	1.86	1.99	1.99		

[a] Units: l_{ij} in mole²/joule cm sec; Λ in cm²/ohm equiv; $(L_{ij})_0\hat{R}T$ and $(L_{ij})_v\hat{R}T$ in mole/cm sec; and $(D_{ij})_v$ in cm²/sec. [b] E refers to use of experimental activity coefficient derivatives,[15] B to derivatives estimated from binary data.[10] [c] The same as Wendt[34] except assume $\partial \ln \gamma_i/\partial m_j = 0$ instead of $\partial \ln y_i/\partial c_j = 0$. [d] The average of L_{12} and L_{21} calculated from experimental data.[15]

Table VII: Estimated Ternary Properties at 25° for Strong Electrolytes from Data on Binaries[a,b]

II H_2O–LiCl (0.25 M)–KCl (0.2 M)

	Exptl	LNIE	LNIB	LNB	LLB	LLM[c]	LK1	LK2
$(l_{11}/N) \times 10^{12}$	2.00	1.99	1.99	1.87	2.31	2.31		
$(l_{22}/N) \times 10^{12}$	3.24	3.26	3.26	3.20	3.51	3.51		
$(l_{33}/N) \times 10^{12}$	7.17	7.22	7.22	7.22	8.20	8.20		
$(l_{12}/N) \times 10^{12}$	−0.10	−0.10	−0.10	−0.10	0	0		
$(l_{13}/N) \times 10^{12}$	0.39	0.39	0.39	0.39	0	0		
$(l_{23}/N) \times 10^{12}$	0.46	0.45	0.45	0.45	0	0		
t_1	0.144	0.141	0.141	0.132	0.165	0.165		
t_2	0.255	0.256	0.256	0.254	0.250	0.250		
Λ	97.9	98.5	98.5	96.8	130.5	130.5		
$(L_{11})_0 \times 10^8 \hat{R}T$	0.199	0.198	0.198	0.188	0.215	0.215		
$(L_{12})_0 \times 10^8 \hat{R}T$	−0.054[d]	−0.054	−0.054	−0.051	−0.064	−0.064		
$(L_{22})_0 \times 10^8 \hat{R}T$	0.285	0.286	0.286	0.282	0.293	0.293		
$(L_{11})_v \times 10^8 \hat{R}T$	0.198	0.197	0.197	0.187	0.214	0.214	0.213	0.207
$(L_{12})_v \times 10^8 \hat{R}T$	−0.057[d]	−0.056	−0.056	−0.053	−0.067	−0.067	−0.064	−0.063
$(L_{22})_v \times 10^8 \hat{R}T$	0.283	0.284	0.284	0.279	0.290	0.290	0.291	0.281
$(D_{11})_v \times 10^5$	1.13	1.13	1.12	1.07	1.21	1.19		
$(D_{12})_v \times 10^5$	−0.00	0.01	0.02	0.03	−0.01	0.01		
$(D_{21})_v \times 10^5$	0.22	0.21	0.23	0.24	0.18	0.25		
$(D_{22})_v \times 10^5$	1.81	1.82	1.81	1.79	1.84	1.98		

[a] Units: l_{ij} in mole²/joule cm sec; Λ in cm²/ohm equiv; $(L_{ij})_0\hat{R}T$ and $(L_{ij})_v\hat{R}T$ in mole/cm sec; and $(D_{ij})_v$ in cm² sec. [b] E refers to use of experimental activity coefficient,[16] B to derivatives estimated from binary data.[10] [c] The same as Wendt[34] except assume $\partial \ln \gamma_i/\partial m_j = 0$ instead of $\partial \ln y_i/\partial c_j = 0$. [d] The average of L_{12} and L_{21} calculated from experimental data.[16]

Table VIII: Estimated Ternary Properties at 25° for Strong Electrolytes from Data on Binaries[a,b]

III H_2O–LiCl (0.25 M)–NaCl (0.2 M)

	Exptl	LNIE	LNIB	LNB	LLB	LLM[c]	LK1	LK2
$(l_{11}/N) \times 10^{12}$	1.95	1.99	1.99	1.87	2.31	2.31		
$(l_{22}/N) \times 10^{12}$	2.16	2.16	2.16	2.06	2.39	2.39		
$(l_{33}/N) \times 10^{12}$	7.03	7.01	7.01	7.01	8.20	8.20		
$(l_{12}/N) \times 10^{12}$	−0.08	−0.09	−0.09	−0.09	0	0		
$(l_{13}/N) \times 10^{12}$	0.37	0.39	0.39	0.39	0	0		
$(l_{23}/N) \times 10^{12}$	0.40	0.37	0.37	0.37	0	0		
t_1	0.159	0.159	0.159	0.150	0.179	0.179		
t_2	0.178	0.179	0.179	0.173	0.186	0.186		
Λ	87.8	88.0	88.0	86.0	120.1	120.1		
$(L_{11})_0 \times 10^8\hat{R}T$	0.191	0.195	0.195	0.185	0.211	0.211		
$(L_{12})_0 \times 10^8\hat{R}T$	−0.038[d]	−0.041	−0.041	−0.037	−0.048	−0.048		
$(L_{22})_0 \times 10^8\hat{R}T$	0.207	0.207	0.207	0.199	0.217	0.217		
$(L_{11})_v \times 10^8\hat{R}T$	0.190	0.194	0.194	0.184	0.210	0.210	0.209	0.199
$(L_{12})_v \times 10^8\hat{R}T$	−0.040[d]	−0.042	−0.042	−0.038	−0.049	−0.049	−0.047	−0.046
$(L_{22})_v \times 10^8\hat{R}T$	0.206	0.206	0.206	0.198	0.216	0.216	0.215	0.205
$(D_{11})_v \times 10^5$	1.10	1.13	1.13	1.08	1.22	1.21		
$(D_{12})_v \times 10^5$	0.10	0.11	0.12	0.12	0.10	0.12		
$(D_{21})_v \times 10^5$	0.19	0.16	0.17	0.18	0.15	0.19		
$(D_{22})_v \times 10^5$	1.35	1.34	1.34	1.29	1.40	1.46		

[a] Units: l_{ij} in mole²/joule cm sec; Λ in cm²/ohm equiv; $(L_{ij})_0\hat{R}T$ and $(L_{ij})_v\hat{R}T$ in mole/cm sec; and $(D_{ij})_v$ in cm²/sec. [b] E refers to use of experimental activity coefficient derivatives,[15] B to derivatives estimated from binary data.[10] [c] The same as Wendt[34] except assume $\partial \ln \gamma_i/\partial m_j = 0$ instead of $\partial \ln y_i/\partial c_j = 0$. [d] The average of L_{12} and L_{21} calculated from experimental data.[16]

LNI gives a very close estimate of the l_{ij}/N (no deviation greater than 0.05×10^{-12}) with the exception of l_{22}/N for system IE. Although approximation **LN** appears more "natural," nonetheless it gives low values of l_{ii}/N. The values of **LL** based on Λ_i^0 are all quite high and unrealistic at finite concentrations.

Two other approximations for l_{ij} have been proposed by Lane and Kirkaldy, one in terms of an exchange model[35] (denoted by **LK1**), the other in terms of a vacancy model[36] with a viscosity correction factor (denoted by **LK2**). Since they do not report values of l_{ij}/N, their approximations will be compared in Tables II–VIII in terms of their calculated volume-fixed thermodynamic diffusion coefficients $(L_{ij})_v$.[37,38]

With these approximation methods for l_{ij}, it is possible to estimate other transport properties of ternary systems from data on the appropriate binaries, as indicated below.

B. Estimates of t_1, t_2, and Λ. Estimates of t_1, t_2, and Λ based on the approximations **LNI**, **LN**, and **LL** together with eq 30–32 are given in Tables II–VIII.

For t_1 and t_2: these results show that **LNI** is very close, with no deviation in t_i greater than 0.003. However, deviations for **LN** and **LL** are as large as 0.01 and 0.02, respectively. As a measure of round-off error, we note that the back calculation of t_i using the experimental l_{ij}/N rounded to 0.01×10^{-12} gives deviations within 0.000_6.

For Λ: with **LNI** the deviations are within 0.9 conductance unit except for IE (3.1), and with **LN** within 2 units, estimated values being mostly low. The limiting values from **LL** are all very poor, being 30–50 units too high. For comparison, the back calculation of Λ using the rounded l_{ij}/N gives deviations within 0.2 conductance unit.

It is interesting to note that approximation **LN** can be related to the mixture rule for conductance (eq 50). Substituting for everything but l_{12}/N and identifying appropriate quantities yield

$$\Lambda = x_1\Lambda_{13}^{\circ} + x_2\Lambda_{23}^{\circ} + 2000z_1z_2\mathfrak{F}^2(l_{12}/N) \qquad (63)$$

However using this equation to estimate l_{12}/N gives a result which is a factor of 10 too small.

(35) J. E. Lane and J. S. Kirkaldy, *Can. J. Chem.*, **43**, 1812 (1965).

(36) J. E. Lane and J. S. Kirkaldy, *ibid.*, **44**, 4777 (1966).

(37) The $(L_{ij})_v$ are related to the $(L_{ij})_0$ by $\bar{V}_{i3}$ factors given in ref 11 and 12.

(38) Lane and Kirkaldy's models can also be used for nonelectrolyte mixtures and electrolyte–nonelectrolyte mixtures.

C. Estimates of $(L_{ij})_v$. Intercomparisons of approximations for $(L_{ij})_0$ and for $(L_{ij})_v$ are similar, as can be seen in Tables II–VIII. Therefore attention will be concentrated on $(L_{ij})_v$ both because they are more directly related to experiment and because Lane and Kirkaldy[35,36] used them for comparisons. Deviations are given in per cent because of the strong concentration dependence.

Back calculations with rounded l_{ij}/N yield maximum deviations of 0.3, 2.5, and 0.2% for $(L_{11})_v$, $(L_{12})_v$, and $(L_{22})_v$, respectively. Estimates by **LNI** give 3, 5, and 1% (except 7% for system IE), respectively. For **LN** the corresponding maximum deviations are 10 (except 16% for IE), 11, and 4%, with most L_{ii} low, especially L_{11}. For **LL**, the values are all high, especially for $(L_{12})_v$ with maximum deviations of 10, 22, and 5%, except for IE where the deviations are substantially higher. The Lane and Kirkaldy schemes give maximum deviations for **LK1** of 10 (except 15% for IE), 13 (except 18% for III), and 4% (except 14% for IE), and for **LK2** of 5, 15, and 1%.

The **LNI** estimates are excellent, even for IE where the over-all concentration is 3 N. Hence for mixed alkali chlorides at least, these ternary properties can be quite well estimated knowing the properties of the binaries. The next best is **LK2** with **LN** somewhat poorer, followed by **LK1** and **LL**. In general all schemes are better at lower concentrations.

D. Estimates of $(D_{ij})_v$. Ordinary diffusion coefficients $(D_{ij})_v$ are very hard to measure for multicomponent systems but are often needed in particular situations. Therefore estimation methods are very useful. An obvious one is to work backward from estimates of the l_{ij}/N as follows. If the appropriate thermodynamic quantities, μ_{ij}, are available from experiment or can be reasonably approximated, it is possible to use eq 19 and $(L_{ij})_0$ estimated from l_{ij} to compute estimated values of $(D_{ij})_0$. From $\bar{V}_{i3}$ and these $(D_{ij})_0$, we may then calculate the desired $(D_{ij})_v$ by the equation[11]

$$(D_{ij})_v = \sum_{k=1}^{2} \left(\delta_{ki} - \frac{c_i \bar{V}_{k3}}{1000} \right) (D_{kj})_0 \qquad i, j = 1, 2 \quad (64)$$

This idea was proposed by Wendt,[34] who used the approximation **LL** for l_{ij}/N and the rather drastic approximation for μ_{ij} that the molar activity coefficient, y_i, is independent of concentration. For strong electrolyte mixtures Wendt's estimates of D_{ij} were surprisingly good and required only limiting ionic conductances and $\bar{V}_{i3}$ as input data.

It is naturally expected (and observed) that better estimates of $(D_{ij})_v$ would be obtained from better estimates of both l_{ij}/N and μ_{ij}. We have therefore considered approximations **LNI**, **LN**, and **LL** for the l_{ij}/N together with various μ_{ij} approximations. These are: (a) μ_{ij} calculated from actual ternary thermodynamic data used to get the experimental l_{ij}/N (denoted by final letter E), (b) μ_{ij} estimated from binary activity data by the method in ref 10 (denoted by B), and (c) μ_{ij} based on the unrealistic approximation that the molal activity coefficient γ is concentration independent[39] (denoted by M).

Five estimates of $(D_{ij})_v$ are compared with experiment in Tables II–VIII. These are **LNIE**, based on binary l_{ij}/N and ternary thermodynamic data, **LNIB**, based wholly on binary data, **LNB**, also based only on binary data, **LLB**, based on limiting conductances but using binary μ_{ij}, and **LLM**, based on limiting conductances only.

Back calculations using rounded l_{ij}/N and the actual ternary thermodynamic data (E) yield maximum deviations of 0.00_5, 0.02, 0.02, and 0.00_8 for $(D_{11})_v$, $(D_{12})_v$, $(D_{21})_v$, and $(D_{22})_v$, respectively, compared to experimental errors of the order of 0.01 ($\times 10^{-5}$). For **LNIE** it is noteworthy that the maximum deviations are not much greater than experimental errors, namely, 0.04, 0.03, 0.03, and 0.01 (except 0.12 for IE). **LNIB**, based wholly on binary data, yields exactly the same maximum deviations as **LNIE** except that $\Delta D_{21} = 0.09$ for IE. The results for the others are progressively less satisfactory, namely, **LNB**: 0.13 (except 0.21 for IE), 0.03, 0.06 (except 0.15 for IE), 0.06; **LLB**: 0.12 (except 0.3 for IE), 0.06, 0.06, 0.06 (except 0.19 for IE); **LLM**: 0.11, 0.02 (except 0.11 for IE), 0.05 (except 0.12 for IE), 0.19.

Clearly excellent estimates of $(D_{ij})_v$ can be obtained at 1 N and below (with acceptable values even at 3 N) for alkali halide mixtures by means of **LNIB** which is based *wholly on binary data*. This scheme is thus recommended for such mixtures. The same closeness of prediction should hold for other 1–1 strong electrolyte mixtures, although acid or higher valence type of mixtures may not give as good results.

Naturally the best scheme requires the most input data. Thus **LNIB** requires $\bar{V}$, γ, t, Λ, and $(D)_0$ for the appropriate binaries at all concentrations, whereas **LLM**, which gives fair D_{ij} only because of fortuitous canceling of errors (as shown by the poor values of t_i and Λ), requires only limiting ion conductances and $\bar{V}$'s.

(39) This assumption, used instead of Wendt's, was made solely for our computational convenience and is of course nearly equivalent to his. The difference between them, discussed in ref 34, footnote 17, is significant only at higher concentrations.

Although we have not calculated D_{ij} from Lane and Kirkaldy's **LK2**,[36] the results should be good, as indicated by their good values for $(L_{ij})_v$. This scheme requires Λ_i^0, the limiting self-diffusion coefficient of the solvent, D^{0*}, the viscosity, η, of the mixtures (or estimates of it) at all concentrations, and $\bar{V}$ and γ for the binaries at all concentrations.

VII. Limiting Values of Transport Quantities at Infinite Dilution

To get an idea of the general relative concentration dependence and to obtain approximate tracer equations, it is useful to consider the various transport quantities at infinite dilution. The systematic analysis below leads easily to expressions in terms of Λ_i^0 (which for a given ion are independent of the other ions present). Some of the results (*e.g.*, for D_{ij}^0) have been obtained before but in different forms. In this section, reference frames will not be distinguished because the SF and VF reference frames become identical at infinite dilution, and quantities at infinite dilution will be denoted by a superscript 0.

A. Expressions for Ternary l_{ij}^0. We begin by considering the limiting values for the binary l_{ij}^*. As can be shown theoretically or experimentally,[3] $l_{12}^*/N \to 0$ and $(1 + c\mathrm{d} \ln y/\mathrm{d}c) \to 1$ at infinite dilution. Therefore using these conditions in eq I-41 and recalling that the ionic conductance, Λ_i, is defined by

$$\Lambda_i \equiv t_i\Lambda \tag{65}$$

we obtain the result for the diffusion coefficient at infinite dilution

$$D^0 = \frac{r\hat{R}T\Lambda_1^0\Lambda_2^0}{r_1z_1\mathfrak{F}^2\Lambda^0} \tag{66}$$

which is the Nernst–Hartley equation (eq I-47).

Substitution of eq 66 into I-41 for $i, j = 1, 2$ yields the following simple results for binary systems

$$\frac{l_{ii}^0}{N} = \frac{\Lambda_i^0}{10^3z_i^2\mathfrak{F}^2}; \quad \frac{l_{12}^0}{N} = 0 \qquad i = 1, 2 \tag{67}$$

For ternary systems, we substitute eq 67 in approximation schemes **LN** or **LNI** (since they are the same at infinite dilution) for l_{ii}/N and set $l_{ij}/N = 0$, $i \neq j$, either on theoretical grounds or as a generalization of results on binary systems. Recalling that $x_3 = 1$, we obtain the results below (which are eq 60–62 and are equivalent to Wendt's[34])

$$\frac{l_{ii}^0}{N} = \frac{x_i\Lambda_i^0}{10^3z_i^2\mathfrak{F}^2} \qquad i = 1, 2, 3 \tag{68}$$

$$\frac{l_{12}^0}{N} = \frac{l_{13}^0}{N} = \frac{l_{23}^0}{N} = 0$$

The l_{ii}^0/N depend on the relative concentration x_i, but the expressions

$$\frac{l_{ii}^0}{x_iN} = \frac{l_{ii}^0}{N_i} \qquad i = 1, 2, 3 \tag{69}$$

do not. In fact despite the restrictive assumptions of this section, this relation holds approximately at higher concentrations (compare IB, IC in Table I), and even with a change of over-all concentration up to 1 N (compare IA–ID, II, and III in Table I).

B. Expressions for Λ^0, t_i^0, L_{ij}^0/N, and D_{ij}^0. Upon substituting eq 68 in eq 30–35, we obtain the following trivial results for Λ^0 and t_i^0

$$\Lambda^0 = x_1\Lambda_1^0 + x_2\Lambda_2^0 + \Lambda_3^0 \tag{70}$$

$$t_i^0 = x_i\Lambda_i^0/\Lambda^0 \tag{71}$$

and the nontrivial results for L_{ij}^0/N[40]

$$\frac{L_{11}^0}{N} = \frac{x_1\Lambda_1^0(\Lambda^0 - x_1\Lambda_1^0)}{10^3(r_{1c}z_1)^2\mathfrak{F}^2\Lambda^0} \tag{72}$$

$$\frac{L_{12}^0}{N} = -\frac{x_1x_2\Lambda_1^0\Lambda_2^0}{10^3r_{1c}r_{2c}z_1z_2\mathfrak{F}^2\Lambda^0} \tag{73}$$

$$\frac{L_{22}^0}{N} = \frac{x_2\Lambda_2^0(\Lambda^0 - x_2\Lambda_2^0)}{10^3(r_{2c}z_2)^2\mathfrak{F}^2\Lambda^0} \tag{74}$$

We note that all L_{ij}^0/N are finite at infinite dilution and that L_{12}^0/N is negative. The nonzero value for L_{12}^0/N results from coupling due to the electroneutrality condition.[35] Note that L_{12}^0/x_1x_2N is constant for arbitrary x_i. However the $L_{ii}^0/x_iN = L_{ii}^0/N_i$ do depend on x_i; they could vary by a factor of 2 for alkali halide mixtures and substantially more for HCl mixtures.

To obtain expressions for D_{ij}^0, we substitute eq 72–74 into eq 19 and use the equation for μ_{ij} at infinite dilution

$$\mu_{ij} = \frac{\hat{R}T}{c_j}[r_{ic}\delta_{ij} + r_{ia}x_j] \quad \text{infinite dilution} \tag{75}$$

Equation 75 is obtained from eq 22, after noting that by the Debye–Hückel theory $c_j\partial \ln y_i/\partial c_j$ goes to 0 as $S^{1/2}$, where S is the ionic strength. The resulting expressions are ternary analogs of the Nernst–Hartley equation and are

$$D_{11}^0 = \frac{\hat{R}T\Lambda_1^0}{\mathfrak{F}^2\Lambda^0}\left[\frac{\Lambda^0}{z_1} - x_1\left(\frac{\Lambda_1^0}{z_1} + \frac{\Lambda_3^0}{z_3}\right)\right] \tag{76}$$

$$D_{12}^0 = -\frac{x_1r_{2a}\hat{R}T\Lambda_1^0}{r_{1a}\mathfrak{F}^2\Lambda^0}\left[\frac{\Lambda_2^0}{z_2} + \frac{\Lambda_3^0}{z_3}\right] \tag{77}$$

(40) Equations 72–74 can also be obtained by setting $l_{ij} = 0$ in eq 39–41, solving for L_{ij}, and using eq 71.

$$D_{21}^0 = -\frac{x_2 r_{1a} \hat{R}T\Lambda_2^0}{r_{2a}\mathfrak{F}^2\Lambda^0}\left[\frac{\Lambda_1^0}{z_1} + \frac{\Lambda_3^0}{z_3}\right] \quad (78)$$

$$D_{22}^0 = \frac{\hat{R}T\Lambda_2^0}{\mathfrak{F}^2\Lambda^0}\left[\frac{\Lambda^0}{z_2} - x_2\left(\frac{\Lambda_2^0}{z_2} + \frac{\Lambda_3^0}{z_3}\right)\right] \quad (79)$$

Equations 76–79 are the explicit formulas for the approximation used by Wendt for strong electrolytes at all concentrations.[34] These equations specialized to 1–1 electrolytes were given earlier in a different form by Gosting.[41,42]

We see that D_{12}^0/x_1 and D_{21}^0/x_2 are constant for arbitrary x_i, and inspection of Tables II–VI shows that this remains approximately true even as high as 3 N. Moreover since z_3 is negative they may be positive or negative depending on the relative sizes of Λ_i^0 and Λ_3^0 and can be fairly large if H^+ is a constituent. However the D_{ii}^0 do depend on x_i, although the variation is not large except for systems including H^+.

C. Tracer and Intradiffusion Expressions. For tracer quantities of constituent 2 in a solution of 1, we find that setting $x_1 = 1$ and $x_2 = 0$ reduces eq 72–74 to the binary case, with a Nernst–Hartley expression for L_{11}^0/N and with L_{12}^0/N and L_{22}^0/N both being zero.

The diffusion coefficients reduce to

$$D_{11}^0 = \frac{\hat{R}T\Lambda_1^0\Lambda_3^0}{\mathfrak{F}^2\Lambda^0}\left(\frac{1}{z_1} - \frac{1}{z_3}\right) = \text{Nernst–Hartley} \quad (80)$$

$$D_{12}^0 = -\frac{r_{2a}\hat{R}T\Lambda_1^0}{r_{1a}\mathfrak{F}^2\Lambda^0}\left[\frac{\Lambda_2^0}{z_2} + \frac{\Lambda_3^0}{z_3}\right] \quad (81)$$

$$D_{21}^0 = 0 \quad (82)$$

$$D_{22}^0 = \frac{\hat{R}T\Lambda_2^0}{z_2\mathfrak{F}^2} \quad (83)$$

where eq 80 is equivalent to eq 66. These equations were given in a different but equivalent form by Gosting.[41] Since $D_{21}^0 = 0$ (which can be shown to be true for tracer diffusion at arbitrary concentrations of constituent 1), the flow of 2 is a Fick's law flow; *i.e.*, there is no effect of 1 on 2. However, owing to the nonzero D_{12}^0, a finite flow of 1 is induced by the tracer's gradient.

We now turn to the case where constituent 2 is an isotopically labeled form of constituent 1. This labeled form is denoted by 1* and may be present in large amounts. The differences between 1 and 1* are assumed to be sufficiently small that their diffusion and other solution properties are the same.

In this circumstance, the limiting expressions for L_{ij}/N become

$$\frac{L_{11}^0}{N} = \frac{x_1\Lambda_1^0(\Lambda^0 - x_1\Lambda_1^0)}{10^3\mathfrak{F}^2(r_{1c}z_1)^2\Lambda^0} \quad (84)$$

$$\frac{L_{11*}^0}{N} = -\frac{x_1x_1^*(\Lambda_1^0)^2}{10^3\mathfrak{F}^2(r_{1c}z_1)^2\Lambda^0} \quad (85)$$

$$\frac{L_{1*1*}^0}{N} = \frac{x_1^*\Lambda_1^0(\Lambda^0 - x_1^*\Lambda_1^0)}{10^3\mathfrak{F}^2(r_{1c}z_1)^2\Lambda^0} \quad (86)$$

and the limiting expressions for the D_{ij} become

$$D_{11}^0 = \frac{\hat{R}T\Lambda_1^0}{\mathfrak{F}^2\Lambda^0}\left[\frac{\Lambda^0 - x_1\Lambda_1^0}{z_1} - \frac{x_1\Lambda_3^0}{z_3}\right] \quad (87)$$

$$D_{11*}^0 = -\frac{x_1\hat{R}T\Lambda_1^0}{\mathfrak{F}^2\Lambda^0}\left[\frac{\Lambda_1^0}{z_1} + \frac{\Lambda_3^0}{z_3}\right] \quad (88)$$

$$D_{1*1}^0 = -\frac{x_1^*\hat{R}T\Lambda_1^0}{\mathfrak{F}^2\Lambda^0}\left[\frac{\Lambda_1^0}{z_1} + \frac{\Lambda_3^0}{z_3}\right] \quad (89)$$

$$D_{1*1*}^0 = \frac{\hat{R}T\Lambda_1^0}{\mathfrak{F}^2\Lambda^0}\left[\frac{\Lambda^0 - x_1^*\Lambda_1^0}{z_1} - \frac{x_1^*\Lambda_3^0}{z_3}\right] \quad (90)$$

From these equations it is easy to show that

$$\frac{L_{11}^0}{N} + 2\frac{L_{11*}^0}{N} + \frac{L_{1*1*}^0}{N} = \frac{\Lambda_1^0\Lambda_3^0}{10^3(r_{1c}z_1)^2\mathfrak{F}^2\Lambda^0} = L_{\text{bNH}} \quad (91)$$

and that

$$D_{11}^0 + D_{11*}^0 + D_{1*1}^0 + D_{1*1*}^0 = \frac{2\Lambda_1^0\Lambda_3^0\hat{R}T}{\mathfrak{F}^2\Lambda^0}\left(\frac{1}{z_1} - \frac{1}{z_3}\right) = 2D_{\text{bNH}} \quad (92)$$

where the subscript bNH indicates the appropriate Nernst–Hartley expression for the binary system 13.

Two isotopically differing solutes[43] clearly form a *ternary* solution. However Albright and Mills[44] have shown how the ternary D_{ij} can be related to "pseudo" binary coefficients in two special cases. First, they showed that the binary diffusion coefficient $(D)_v$ for isotopically labeled constituents diffusing in the solvent without regard to labels is given in terms of ternary D_{ij} by the equation

$$(D)_v = (D_{11})_v + \frac{c_1^*}{c_1}(D_{11*})_v = (D_{1*1*})_v + \frac{c_1}{c_1^*}(D_{1*1})_v \quad (93)$$

which is valid at any concentration. Our notation has been used in eq 93. Substitution of the limiting

(41) L. J. Gosting, *Advan. Protein Chem.*, 11, 536 (1956).

(42) I. J. O'Donnell and L. J. Gosting in "The Structure of Electrolytic Solutions," John Wiley and Sons, Inc., New York, N. Y., 1959, Chapter 11.

(43) With our present notation, the two cations are chosen to be isotopically different.

(44) J. G. Albright and R. Mills, *J. Phys. Chem.*, 69, 3120 (1965). Their equations are derived for a ternary nonelectrolyte case, but the results are equally valid for ternary electrolyte systems.

eq 87 and 88 or 89 and 90 in eq 93 yields the Nernst–Hartley value of D^0, as would be expected.

Second, Albright and Mills related *intradiffusion* to binary processes. Intradiffusion is defined as follows.[44] Consider a solution which is homogeneous except that, in a part of the container, a portion of one constituent is replaced by an equal portion of the labeled form of that constituent. The resulting diffusion between the labeled and unlabeled forms at a constant concentration ($c_1 + c_1^*$) is called intradiffusion.[45] Because the total concentration of solute is constant, the ternary equations reduce to binary forms

$$J_1 = -D^\dagger \frac{\partial c_1}{\partial x} \tag{94}$$

$$J_1^* = -D^\dagger \frac{\partial c_1^*}{\partial x} \tag{95}$$

where $D^\dagger$ is the intradiffusion coefficient. Albright and Mills[44] have shown that in general

$$(D^\dagger)_v = (D_{11})_v - (D_{11^*})_v = (D_{1^*1^*})_v - (D_{1^*1})_v \tag{96}$$

Substitution of the limiting eq 87–90 in eq 96 yields the result

$$D^{\dagger 0} = \frac{\hat{R}T\Lambda_1^0}{\mathfrak{F}^2 z_1} \tag{97}$$

which upon relettering is the same as D_{22}^0 for the tracer diffusion case (eq 83).

VIII. The R_{ij} Representation

Although the writer believes the "friction coefficient" formalism (R_{ij}) to be less intuitive and straightforward than the "mobility" one (l_{ij}) used above, a number of R_{ij} results are presented for completeness. The ORR are assumed.

Because they simplify the expressions for the ionic "friction coefficients" R_{ij}, it is convenient to first consider the ternary diffusion friction coefficients $\mathfrak{R}_{ij}$ (analogous to the $(L_{ij})_0$). In terms of friction coefficients, ternary diffusion is described by the inverse of eq 18[46]

$$-\frac{\partial \mu_{i3}}{\partial x} = \sum_{j=1}^{2} \mathfrak{R}_{ij} J_{j3} \qquad i = 1, 2 \tag{98}$$

The $\mathfrak{R}_{ij}$ can be obtained from the $(L_{ij})_0$ by Cramer's rule, which yields

$$\mathfrak{R}_{11} = (L_{22})_0/L;\ \mathfrak{R}_{12} = -(L_{12})_0/L;\ \mathfrak{R}_{22} = (L_{11})_0/L \tag{99}$$

where

$$L = (L_{11})_0(L_{22})_0 - (L_{12})_0^2 \tag{100}$$

We obtain $\mathfrak{R}_{i0}$ from $\mathfrak{R}_{ij}$ by means of the equations[3,46]

$$\sum_j c_j \mathfrak{R}_{ij} = 0 \qquad i, j = 0, 1, 2 \tag{101}$$

We now turn to that form of the ionic R_{ij} formalism which is obtained by inverting eq 9. This form gives forces in terms of independent ion flows rather than velocity differences, namely

$$-\left(\frac{\partial \mu_i}{\partial x} + z_i \mathfrak{F} \frac{\partial \phi}{\partial x}\right) = \sum_{j=1}^{3} R_{ij} J_j \qquad i = 1, 2, 3 \tag{102}$$

The dependent solvent friction terms R_{i0} are obtained from eq 101 adapted to ion concentrations, namely

$$R_{i0} = -(1/c_0)[(r_{1c}R_{i1} + r_{1a}R_{i3})c_1 + (r_{2c}R_{i2} + r_{2a}R_{i3})c_2] \qquad i = 0, 1, 2, 3 \tag{103}$$

An analysis using eq 102 of the conductance, transference, and diffusion experiments similar to that in section IV leads to the following results

$$\alpha = (1/R^2)[z_1^2(R_{22}R_{33} - R_{23}^2) + z_2^2(R_{11}R_{33} - R_{13}^2) + z_3^2(R_{11}R_{22} - R_{12}^2) + 2z_1z_2(R_{13}R_{23} - R_{12}R_{33}) + 2z_1z_3(R_{12}R_{23} - R_{13}R_{22}) + 2z_2z_3(R_{12}R_{13} - R_{23}R_{11})] \tag{104}$$

$$t_1 = (1/\alpha)[z_1^2(R_{22}R_{33} - R_{23}^2) + z_1z_2(R_{13}R_{23} - R_{12}R_{33}) + z_1z_3(R_{12}R_{23} - R_{13}R_{22})] \tag{105}$$

$$t_2 = (1/\alpha)[z_1z_2(R_{13}R_{23} - R_{12}R_{33}) + z_2^2(R_{11}R_{33} - R_{13}^2) + z_2z_3(R_{12}R_{13} - R_{23}R_{11})] \tag{106}$$

$$\mathfrak{R}_{11} = r_{1c}^2R_{11} + 2r_{1c}r_{1a}R_{13} + r_{1a}^2R_{33} \tag{107}$$

$$\mathfrak{R}_{12} = r_{1c}r_{2c}R_{12} + r_{1a}r_{2c}R_{23} + r_{1c}r_{2a}R_{13} + r_{1a}r_{2a}R_{33} \tag{108}$$

$$\mathfrak{R}_{22} = r_{2c}^2R_{22} + 2r_{2c}r_{2a}R_{23} + r_{2a}^2R_{33} \tag{109}$$

where

$$R = (R_{11}R_{22}R_{33} + 2R_{12}R_{13}R_{23}) - (R_{12}^2R_{33} + R_{13}^2R_{22} + R_{23}^2R_{11}) = \det|R_{ij}| \tag{110}$$

Equations 104–110 may be solved directly for R_{ij} in terms of α, t_1, t_2, $\mathfrak{R}_{11}$, $\mathfrak{R}_{12}$, and $\mathfrak{R}_{22}$. Alternatively, since the matrix of coefficients **R** is the inverse of **l**,

(45) *Intradiffusion* can be *tracer diffusion* if the concentration of 1* is very small. However *tracer diffusion* can also refer to an essentially homogeneous solution with a tiny amount of a solute completely different from 1. *Self-diffusion* is *intradiffusion* in a system containing only isotopically different forms of the same species. These terms are discussed more completely in ref 44.

(46) For example, R. W. Laity, *J. Phys. Chem.*, **63**, 80 (1959).

the expressions for the inverse together with eq 36–41 can be used to get R_{ij}. Either route is very tedious. The results can be written in condensed form as

$$R_{ij} = \frac{z_i z_j}{\alpha} + \frac{z_i z_j}{z_3^2}\sum_{k,l}\frac{(\delta_{ik} - t_k)(\delta_{jl} - t_l)\Re_{kl}}{r_{ka}r_{la}} \qquad i, j = 1, 2, 3 \quad k, l = 1, 2 \qquad (111)$$

$$R_{i0} = \frac{z_i}{z_3 c_0}\sum_{k,l}\frac{(\delta_{ik} - t_k)\Re_{kl}c_l}{r_{ka}} = \frac{-z_i}{z_3}\sum_{k}\frac{(\delta_{ik} - t_k)\Re_{k0}}{r_{ka}} \qquad i = 1, 2, 3 \quad k, l = 1, 2 \qquad (112)$$

$$R_{00} = \Re_{00} \qquad (113)$$

These equations reduce to those of a binary system (eq I-72–77) when one of the salt constituents vanishes.

Equation 113 is an interesting theorem, which may be used as a calculational check. It could be anticipated because the solvent–solvent "friction" should be independent of whether one considers the transport of ions or of salts as a whole.

The values of R_{ij} and $\Re_{ij}$ for the seven ternary systems are given in Table IB. The general trends are analogous to the binary results.[3] Again the intuitive notion of "friction coefficient" seems completely inadequate, because "frictions" should all be of the same sign; yet R_{13} and R_{23} are of opposite sign to R_{12}. Moreover the solvent–solvent friction R_{00}, which intuitively should be relatively constant, is concentration dependent.

Fairly good estimates for ternary R_{11} and R_{22} can be made by taking the values of the appropriate binary R_{ii} at N_i, and for R_{13} and R_{23} by taking the cross term of the appropriate binary at N. The same is true for R_{33} and R_{30} by taking linear combinations of the appropriate binary terms at N. However estimates of R_{10} and R_{20} from binaries are poor at both N and N_i, and are low. Moreover the writer has not found any good way to relate R_{12} to R_{13} and R_{23} or to R_{10} and R_{20}. Consequently good estimates of t_i, Λ, and D_{ij} from binary R_{ij} data are not available—in contrast to the excellent estimates from binary l_{ij} data.

Values of R_{ij}^0 at infinite dilution can be obtained from the limiting values of l_{ij} and are useful in getting an idea of approximate concentration dependences. Recalling that $x_3 = 1$, we obtain

$$R_{ii}^0 = \frac{1}{l_{ii}^0} = \frac{10^3 z_i^2 \mathfrak{F}^2}{x_i N \Lambda_i^0} \qquad i = 1, 2, 3 \qquad (114)$$

$$R_{i0}^0 = \frac{10^3 z_i \mathfrak{F}^2 (2\delta_{3i} - 1)}{c_0 \Lambda_i^0} \qquad i = 1, 2, 3 \qquad (115)$$

$$R_{00}^0 = \frac{10^3 \mathfrak{F}^2 N}{c_0^2}\left[\frac{x_1}{\Lambda_1^0} + \frac{x_2}{\Lambda_2^0} + \frac{x_3}{\Lambda_3^0}\right] \qquad (116)$$

For R_{12}, R_{13}, and R_{23}, there are no simple limiting expressions without appeal to the Debye–Hückel theory or some other model. However by analogy to the binaries[3]

$$R_{ij} \propto \frac{1}{N^{1/2}} \qquad i \neq j; \quad i, j = 1, 2, 3 \qquad (117)$$

so that the R_{ij} of eq 117 are infinity at $N = 0$. It can also be shown by appropriate substitutions of limiting values that for $N > 0$

$$NR_{ij}^0 = 0 \qquad (118)$$

Consequently the use of limiting values as the concentration increases is increasingly in error because the R_{ij} in Table IB are in fact nonzero.

The pure diffusion $\Re_{ij}^0$ are given by

$$\Re_{ij}^0 = \frac{10^3 \mathfrak{F}^2 r_{ic} r_{jc} z_i z_j}{N}\left(\frac{1}{\Lambda_3^0} + \frac{\delta_{ij}}{x_i \Lambda_i^0}\right) \qquad i, j = 1, 2 \qquad (119)$$

$$\Re_{i0}^0 = -\frac{10^3 \mathfrak{F}^2 r_{ic} z_i}{c_0}\left(\frac{1}{\Lambda_i^0} + \frac{1}{\Lambda_3^0}\right) \qquad i = 1, 2 \qquad (120)$$

$$\Re_{00}^0 = R_{00}^0 \qquad (113)$$

It is a curious fact that

$$\Re_{12}^0 = r_{1a} r_{2a} R_{33}^0 \qquad (121)$$

We note from eq 114, 115, 119, and 120 that $N_i R_{ii}$, R_{i0}, $N\Re_{12}$, and $\Re_{i0}$, respectively, should be independent of N and x_i and be relatively constant. This is seen from Table IB to be approximately true up to 1 N for the seven systems. However the other R_{ij} and $\Re_{ij}$ quantities are expected to depend on x_i, as is also found from the data.

IX. Remarks

The generality of irreversible thermodynamics is clearly necessary for ternary electrolyte solutions because the cross coefficients l_{ij}, $i \neq j$, are significantly large even as low as 0.5 N. Setting them equal to zero is obviously as unsatisfactory here as it was in binary systems.[3]

We repeat an observation of paper I: although the l_{ij} are determined numerically from the one-dimensional special cases of t_i, Λ, and D_{ij}, the resulting l_{ij} and the general equations are valid in two or three dimensions and for any isothermal vector process no matter how complex.

The discovery that ternary l_{ij} can be estimated to

good approximation from binary data for strong electrolytes is useful in estimating usual transport coefficients such as t_i or D_{ij}, which are hard to measure.

An interesting application of these estimates is the generalization of Hafemann's[47] calculation of charge separation and liquid junction potentials. Hafemann used the simplified model that $l_{ij} = 0$, $i \neq j$, and by a step by step numerical calculation computed the motions of all the ions from the instant of forming a sharp, free diffusion, liquid junction boundary. With our estimation procedure it is now possible to include the cross terms, thereby eliminating his worst approximations. The coding of course will be more complex, but good agreement with experiment should be obtained.

Finally, we emphasize that transference number and diffusion data in ternary electrolyte solutions are very scarce and badly needed. It is hoped that experimentalists will increasingly turn their attention to these situations.[48]

Acknowledgments. The author wishes to thank Robert Carpenter and Guy McMillan for their aid in computer calculations.

(47) D. R. Hafemann, *J. Phys. Chem.*, **69**, 4226 (1965).

(48) NOTE ADDED IN PROOF. A paper on tracer diffusion by Rastas (J. Rastas, *Acta Polytech. Scand., Chem. Met. Ser.*, **50**, 37 (1966)) has just come to the author's attention in which eq 36–41 have been independently derived. This interesting paper also contains a comparison of experimental tracer data with tracer quantities estimated from the Onsager–Fuoss theory rather than LL-type approximations

Electron Spin Resonance Studies of Aromatic Hydrocarbons Adsorbed on Silica–Alumina. I. Perylene

by G. M. Muha

Esso Research and Engineering Company, Linden, New Jersey 07036 *(Received August 22, 1966)*

An analysis is presented of the electron spin resonance (esr) spectrum of the perylene radical cation generated on a silica–alumina catalyst surface. The magnitude of the larger proton hyperfine-coupling constants are shifted by 4% from the corresponding values obtained when the radical cation is prepared in sulfuric acid solution. The shift is discussed in terms of an electrostatic perturbation of the radical-cation π-electron distribution due to the presence of the counterion. The severe line-width effects which are also observed are discussed in terms of a modulation of the anisotropic hyperfine and g-tensor interactions. It is found that the line-width variation can be satisfactorily described by a polynomial equation in the nuclear spin quantum number of the equivalent proton groups provided that the value of the correlation time for the radical-cation motion is chosen to be comparable to that found in solution. From this result it is argued that the radical cation is relatively unrestricted in its motion and by implication, perhaps the counterion, *i.e.*, electrophilic agent, is also somewhat unrestricted in its movements on the surface.

Examples of the generation and stabilization of radical ions on the surface of solids have been known for some time.[1] Recently, this technique has been used to study the nature of the catalytically active sites on the surface of silica–alumina catalysts. These surface sites are thought to function, in some broad sense, as an acid[2] and induce a carbonium ion type of reaction in an adsorbed hydrocarbon.[3] When aromatic hydrocarbons are used, optical studies[4-7] indicate the presence of a radical cation in addition to the "classical" carbonium ion. Electron spin resonance (esr) studies[4,8,9] confirm the presence of a paramagnetic material adsorbed on the surface.

To date, the principal use of these esr results has been to demonstrate certain features of the electrophilic sites responsible for the oxidation of the aromatic hydrocarbons. For example, it has been found that the intensity of the esr signal from the adsorbed species is decreased by a hydrogen reduction treatment of the catalyst[6,10-13] and also (to a varying degree) by base exchange.[7,9,11,13,14] In addition, the number of paramagnetic entities per unit surface area is approximately equal to the number of surface sites active in the generation of carbonium ions.[15]

Little attention has been given to some of the aberrant features observed in the esr spectra of these

(1) D. Bijl, H. Kainer, and A. C. Rose-Innes, *Nature*, **174**, 830 (1954).

(2) G. A. Olah in "Friedel-Crafts and Related Reactions," Vol. 1, G. A. Olah, Ed., Interscience Publishers, Inc., New York, N. Y., 1963, p 201.

(3) *Cf.* H. H. Voge in "Catalysis," Vol. 6, P. P. Emmett, Ed., Reinhold Publishing Corp., New York, N. Y., 1958, p 407.

(4) M. Okuda and T. Tachibana, *Bull. Chem. Soc. Japan*, **33**, 863 (1960).

(5) R. M. Roberts, C. Barter, and H. Stone, *J. Phys. Chem.*, **63**, 2077 (1959).

(6) W. K. Hall, *J. Catalysis*, **1**, 53 (1962).

(7) A. Terenin, V. Barachevsy, E. Kotov, and V. Kalmogarov, *Spectrochim. Acta*, **19**, 1797 (1963).

(8) J. J. Rooney and R. C. Pink, *Proc. Chem. Soc.*, 70 (1961); *Trans. Faraday Soc.*, **58**, 1632 (1962).

(9) D. M. Brouwer, *Chem. Ind.* (London), 177 (1961); *J. Catalysis*, **1**, 372 (1962).

(10) J. K. Fogo, *J. Phys. Chem.*, **65**, 1919 (1961).

(11) H. Imai, Y. Ono, and T. Keii, *ibid.*, **69**, 1082 (1965).

(12) F. R. Dollish and W. K. Hall, *ibid.*, **69**, 4402 (1965).

(13) B. D. Flockhart and R. C. Pink, *J. Catalysis*, **4**, 90 (1965).

(14) R. P. Porter and W. K. Hall, *ibid.*, **5**, 366 (1966).

(15) See ref 8 and 9; also see A. E. Hirschler and J. O. Hudson, *ibid.*, **3**, 239 (1964); A. E. Hirschler, *ibid.*, **5**, 390 (1966).

surface-generated radicals. In this and in the following papers of this series,[16] this aspect of the problem will be considered. It will be seen that by disentangling some of the physical and chemical interactions that manifest themselves in the line-width variations, exchange effects, and line shifts observed in these spectra, information concerning the nature of the surface interactions in this catalyst system can be obtained. Thus, in this paper, attention is directed to perylene and an analysis of the effects of the counterion on its esr spectrum. In II, a study is made of chemical- and electron-exchange effects as exhibited in the anthracene spectrum. In III, a measure of the oxidation strength of the electrophilic sites on this catalyst surface is given along with a discussion of the significance of the results of I and II to the theory of the action of this catalyst. Finally in IV, a discussion of the line-width effects in the spectra of methyl-substituted anthracenes is given which further illustrates some aspects of the nature of adsorption on this surface.

Experimental Section

Esr Spectrometer. X-Band spectra were obtained with a Strand Model 600 spectrometer equipped with a Varian V-4531 variable-temperature cavity. The modulation amplitude and microwave power level were set below the point at which line broadening or saturation effects could be observed in the recorded spectrum. A lock-in reference frequency of 6 kHz and a field modulation frequency of either 6 or 3 kHz were used. The latter frequency was used for second-derivative presentation, the former for first-derivative presentation. When a second-derivative presentation was used, a multisection filter was placed between the modulation amplifier and the modulation coils to reduce the line distortion from a small admixture of the first-derivative signal.[17]

"Line-sharpened" spectra[18] were recorded by using a modulation wave form consisting of a superposition of three odd-harmonic frequencies.[19] In our instrument, these frequencies were 6, 2, and 1.2 kHz.

Spectrum Calibration. The magnetic field was calibrated with a Harvey Wells F502 nmr gaussmeter, the frequency of which was monitored by a Hewlett-Packard 524C frequency counter. The g values were obtained by comparison with a diphenylpicrylhydrazil (DPPH) sample ($g = 2.0036$) sealed in a capillary and placed concentric with and internal to the sample tube. The spin concentration was measured relative to the signal from a Cr^{3+}-doped ruby sample securely mounted inside the microwave cavity and oriented so as to give a single line in a region (*ca.* $g =$ 4) not overlapping the sample line.[20] The comparison of the microwave susceptibility per gram of sample and the ruby standard was made on the basis of the integrated area obtained by doubly integrating the first-derivative curve. The reproducibility of this type of measurement is estimated as $\pm 10\%$. The conversion of the relative spin concentration to absolute units was made by calibrating the ruby standard in terms of known weights of DPPH and $CuSO_4 \cdot 5H_2O$. The absolute measurements are estimated to be correct within $\pm 60\%$. For quantitative measurements on those adsorbed aromatics exhibiting hyperfine structure, the modulation amplitude was deliberately raised to a level such that a single modulation-broadened line was obtained in the recorded spectrum.[21]

Chemicals. The aromatics, deuterated aromatics, and solvents used in this study were obtained from commercial suppliers. Some were repurified before use and all were checked for decomposition or other impurities by suitable physical techniques. In addition, in those aromatic systems permitting, the esr spectrum of the sulfuric acid generated radical cation was examined for spurious lines. All deuterated aromatics were found to be at least 96 atom % deuterium as determined by mass spectroscopy.[22] Solvents were stored for 24 hr over "activated" silica–alumina (see below) prior to use.

Catalyst. The catalyst samples used in this study were taken from the same lot of an American Cyanamid Aerocat AAA silica–alumina cracking catalyst containing *ca.* 22% Al_2O_3. Organic contaminants were removed by heating in air for 24 hr at 500°.

The catalyst samples were "activated" by heating the decontaminated material in the esr tube at 500° in either an air or a hydrogen atmosphere. When activated in air, the samples were heated for 2 hr in an open-ended tube and then sealed (while still hot) with a tight-fitting rubber septum cap. A solution of the aromatic was introduced through the septum by means of a hypodermic syringe. Samples heated in a hydrogen atmosphere were similarly treated except the cell was equipped in addition with a stopcock and the

(16) G. M. Muha, *J. Phys. Chem.*, 71, 640 (1967). In the text, these papers will be referred to as II, III, and IV, respectively.

(17) J. Gendell, J. H. Freed, and G. K. Fraenkel, *J. Chem. Phys.*, **41**, 949 (1964).

(18) L. C. Allen, H. M. Gladney, and S. H. Glarum, *ibid.*, **40**, 3135 (1964).

(19) S. H. Glarum, *Rev. Sci. Instr.*, **36**, 771 (1965).

(20) L. S. Singer, *J. Appl. Phys.*, **30**, 1463 (1959).

(21) K. Halbach, *Phys. Rev.*, **119**, 1230 (1960); J. S. Hyde and H. W. Brown, *J. Chem. Phys.*, **37**, 368 (1962).

(22) The mass spectral analyses of these compounds were kindly performed by Dr. Theresa Mao.

heating period extended to 24 hr with frequent changes of the hydrogen atmosphere.

Deuterated catalyst surfaces were prepared by substituting deuterium in the activation step above[23] or by refluxing the sample with a large excess of deuterium oxide for 2 hr.[24] Both techniques gave identical results as judged from the esr results. The latter technique, being simpler, was used to prepare the deuterated samples used in all experiments except where specifically noted. The completeness of the deuterations obtained by each technique was checked by following (with esr) the chemical-exchange effects of certain aromatic radical cations adsorbed on the surface. These exchange effects are discussed in other sections of this and subsequent papers in this series.[16]

Catalyst samples heated in a hydrogen or deuterium atmosphere exhibited a weak esr signal, several hundred gauss wide and centered at $g = 2.0$. This signal could be detected only by using high microwave power and large modulation amplitudes; thus it caused no difficulties in interpreting the spectrum of the radical cations. The signal probably arises from paramagnetic[25] or ferromagnetic[26] impurities. Catalyst samples heated in air did not exhibit a resonance.

Results

g Value and Hyperfine-Coupling Constants. The esr spectrum of a benzene solution of perylene adsorbed on silica–alumina is given in Figure 1a. The perylene:catalyst concentration ratio for this spectrum corresponds to ~95% surface saturation.[27]

The odd shapes of the various hyperfine lines is particularly striking. This asymmetry has not previously been reported and is easily missed if the field is overmodulated. From the second-derivative presentation (Figure 1B), it is evident that the asymmetry arises because of the overlapping of individual hyperfine lines. The line-sharpened first-derivative spectrum[18] (Figure 1C) allows most of the lines to be resolved; however, serious discrepancies in the relative intensities are apparent.

These discrepancies are not unexpected, for the line-sharpening technique works best when all the lines have the same width,[18] a condition not obtained in the present case. For the spectrum shown in Figure 1C, the spectrometer settings were arbitrarily chosen[19] to give the narrowest width to the line in the center of the spectrum.

Because of the asymmetry of the lines, it is difficult to measure the g value of the spectrum; also, care must be exercised in superimposing the three presentations shown in Figure 1. To circumvent these difficulties, each presentation was independently calibrated with a

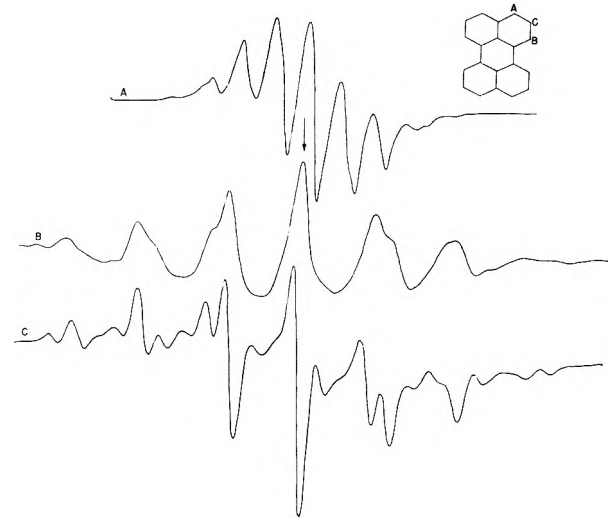

Figure 1. First-derivative (A), second-derivative (B), and line-sharpened (C) spectra of the perylene radical cation generated on a silica–alumina catalyst. In (A), the horizontal scale is 40% that of the other two spectra. The arrow in (B) corresponds to a value of $g = 2.0025$.

g scale. The figure is then drawn to align these scales. The spectrum g value ($=2.0025$) is taken to correspond to the center peak in the second-derivative presentation.

The poor resolution coupled with the variation in the widths of the individual hyperfine lines precludes an unambiguous identification of the radical present. Thus in this paper we reverse the procedure and assume that a perylene radical cation gives rise to the spectrum. An analysis of the spectrum then will serve to define any special features of the radical cation when prepared on this surface. There can be little doubt concerning the validity of this assumption, for the optical spectrum of perylene adsorbed on silica–alumina correlates well with that obtained from perylene dissolved in sulfuric acid.[28] The measured g value quoted above corresponds to that measured for the perylene radical cation in sulfuric acid;[29] thus this result is consistent with the assumption.

(23) The hydrogen and deuterium treatments of these samples were kindly performed by Dr. D. J. C. Yates.

(24) S. G. Hindin, G. A. Mills, and A. G. Oblad, *J. Am. Chem. Soc.*, **73**, 278 (1951).

(25) P. A. Berger and J. F. Roth, *J. Catalysis*, **4**, 717 (1965).

(26) L. S. Singer and D. N. Stamires, *J. Chem. Phys.*, **42**, 3299 (1965).

(27) We define 100% surface saturation as that point at which the addition of further increments of the aromatic does not increase the integrated esr intensity. For a further discussion of concentration effects, see II.

(28) See ref 6 and 9. Both of these investigators agree that the radical cation is present; however there appears to be a disagreement as to whether a carbonium ion is also present.

(29) B. G. Segal, M. Kaplan, and G. K. Fraenkel, *J. Chem. Phys.*, **43**, 4191 (1965).

The hyperfine-coupling constants can be obtained by computing a theoretical spectrum to fit the experimental second-derivative spectrum. This procedure is necessary because the overlapping of lines with different widths and relative intensities causes the apparent center of the line to shift from the true value by an unknown amount. For a Lorentzian line, the second derivative is given by

$$\frac{d^2\chi''}{dH^2} = -\frac{4SN}{\pi\Delta H}\frac{6x^2 - 2}{(1 + x^2)^3}$$

where S is the instrumental sensitivity factor, $x = (^1/_4\Delta H)^{-1}$, $(H - H_0)$ is the reduced independent variable, and ΔH is the line width of the line centered at H_0 with degeneracy N.

Approximate values for the coupling constants in ring positions A and B (see Figure 1) can be obtained from the line-sharpened spectrum (Figure 1C). Coupling in the C position is expected to be small and is neglected for the present. These values, together with an initial estimate of ΔH, were refined by a least-squares procedure for two groups of lines (numbered 4, 5 and 4′, 5′ in Figure 2B).[30] From this fit, the values $a_A = 3.92$ and $a_B = 3.16$ gauss were obtained.[31] In sulfuric acid solution, the corresponding values are 4.11 and 3.09, respectively.[32]

To test the reliability of this result, the theoretical fit to the lines at the center of the spectrum (numbered 2, 1, 2′ in Figure 2B) were computed next. This procedure is not entirely arbitrary, for now only one parameter, ΔH, can be varied for each line; the instrumental sensitivity, line position, and perhaps the most critical factor, the zero value of the ordinate, have been fixed by the previous iteration. The result is shown in the center region of Figure 2C. The close agreement between the computed and experimental curves lends credence to the method.

The stick spectrum corresponding to the values of the coupling constants determined above is plotted in Figure 2B. (Four lines of intensity $^1/_{36}$ that of the center line are not shown.) A comparison of this spectrum with the experimental result (Figure 2A) shows discrepancies between the relative heights of corresponding lines. These discrepancies arise because the experimental spectrum exhibits a variation in the line widths of the individual hyperfine lines.[33] Such variations are a manifestation of the interactions between the radical and the solvent, surface, other radicals, etc. It is possible to extend the iterative computation to these other lines and thus determine the line widths and their variation. However, to minimize computational labor we resort to another scheme.

Under certain conditions, the line-width variation

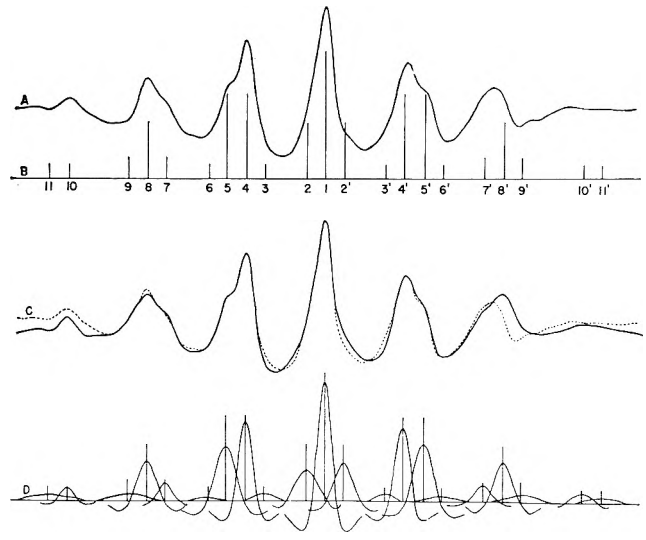

Figure 2. Second-derivative (A) and stick spectrum (B) of the perylene radical cation generated on a silica–alumina catalyst. In (B), the lines are numbered as in Table I. In (C), a comparison of the theoretical spectrum (solid line) computed by eq 1 with the experimental result (dotted line) is given. In (D), the individual lines (widths listed in Table I) making up (C) are shown. In (B), (C), and (D), four lines of degeneracy $^1/_{36}$ that of the center line are not included.

can be expressed as a simple polynomial in the total nuclear spin quantum numbers of the equivalent groups of protons,[34,35] *viz.*

$$H = A + BM_A + CM_B + DM_AM_B + EM_A^2 + FM_B^2 \quad (1)$$

where the coefficients A, B, ..., can be expressed in terms of certain spectral densities describing the interaction. We use this expression to determine the widths of the remaining lines.

To determine the six unknowns in eq 1, the values of ΔH for six of the lines computed above are used. Thus the values $A = 1.6$, $B = -0.05$, $C = 0.05$, $D = -0.2$, $E = 0.65$, and $F = 0.05$ are obtained. With these coefficients, the value of ΔH for the remaining

(30) In the actual computation, the iteration was limited to negative values of the dependent variable since significant contributions are made to the wings from adjacent lines. Also small contributions from lines 6, 3 and 6′, 3′ were included. (Note that Figure 2B is inverted with respect to the usual convention.)

(31) Shifts of up to ±35 mgauss in either $|a_A|$ or $|a_B|$ (but not both) could be tolerated in the parameters used in the iteration. However, the over-all fit of the computed to the experimental curve including *all* lines (to be discussed next, see Figure 2C) was much poorer.

(32) A. Carrington, F. Dravnieks, and M. C. R. Symons, *J. Chem. Soc.*, 947 (1959).

(33) J. H. Freed and G. K. Fraenkel, *J. Chem. Phys.*, **39**, 326 (1963).

(34) D. Kivelson, *ibid.*, **27**, 1087 (1957); **33**, 1094 (1960).

(35) A. D. McLachlan, *Proc. Roy. Soc.* (London), **A280**, 271 (1964).

lines can be computed. A summary of the results is given in Table I. The resulting calculated spectrum is given in Figure 2C and the individual line shapes are shown in Figure 2D.[36]

Table I: Results of the Line-Width Determination

Line no.[a]	M_A	M_B	Degeneracy	Line width: Least-square fit	Line width: From eq 1
11	−2	−1	4		3.9
10	−1	−2	4		2.0
9	−2	0	6		4.3
8	−1	−1	16		2.1
7	0	−2	6		1.7
6	−2	1	4		4.8
5	−1	0	24	2.3	
4	0	−1	24	1.6	
3	1	−2	4		2.7
2	−1	1	16	2.6	
1	0	0	36	1.6	
2′	1	−1	16	2.3	
3′	−1	2	4		3.0
4′	0	1	24	1.7	
5′	1	0	24	2.2	
6′	2	−1	4		4.5
7′	0	2	6		1.9
8′	1	1	16		2.1
9′	2	0	6		4.1
10′	1	2	4		2.1
11′	2	1	4		3.8

[a] The numbering of the lines is shown in Figure 2B. Four lines of unit degeneracy are not included.

The over-all fit of the computed to the experimental curve is quite satisfactory except for the misalignment of the base line of the computed curve at high and low field and the overestimation of the region in the vicinity of line 8′. However, eq 1 certainly is an adequate first approximation with which to discuss the nature of the interactions giving rise to the line-width variations.

Effect of Solvents and the Aromatic Concentration. Within the interval 25–95% surface saturation,[27] the spectral resolution, line-width variation, and coupling constants are not appreciably changed by the perylene:catalyst concentration ratio nor the choice of solvent. In the present experiments, carbon disulfide, carbon tetrachloride, hexane, benzene, and perdeuteriobenzene were used as solvent.

Below 25% surface saturation, the signal-to-noise ratio of the spectrum degrades to such an extent that the second-derivative presentation is of marginal value in the direct measurement of the coupling constants; the first-derivative presentation, however, still exhibits the asymmetry noted above.

It is likely that even below 25% surface saturation, the solvents have little effect on the line widths or coupling constants, for it is possible to obtain resolved hyperfine spectra without the use of a solvent by distilling the aromatic, *in vacuo*, onto the surface of the catalyst.[7,10] This method of preparation was not used in the present study since it was found that the mixing between the aromatic and the catalyst was nonuniform at the higher concentration levels and interradical-exchange effects became important (see II). At the lower concentration levels, the signal-to-noise ratio was poor and the second-derivative presentation could not be used. However, the first-derivative spectrum again exhibited asymmetry.

It is possible to remove the solvent by a vacuum-manipulation technique after the radicals have been formed. In this case, the same coupling constants and line-width variation are obtained as reported above. However, it is not possible to demonstrate that all of the solvent has been removed, and for this reason arguments concerning solvent effects based on this technique are not entirely convincing.

Temperature Effects. The appearance of the esr spectrum is essentially unchanged within the temperature interval defined by the boiling and freezing points of the particular solvent used. As the temperature is lowered below the freezing point of the solvent, the hyperfine lines quickly broaden, and at 77°K only a faint trace of the hyperfine structure remains. Anisotropy in the g tensor (as exhibited in a glass average) is too small an effect to account for this residual structure.

Discussion

Hyperfine-Coupling Constants. In the preceding section, it was noted that the hyperfine-coupling constants are shifted ~4% from the values observed in sulfuric acid. In the present section we wish to consider the possibility that this shift is caused by a modulation of the isotropic magnetic interactions. This type of modulation effect can arise from internal vibrations and rotations as well as fluctuating solvent or counterion complexes with the radical cation.[33]

It is difficult to get an accurate quantitative estimate of the magnitude of the shift, for it is known that when line-width effects are large, static and dynamic frequency shifts[37] must be considered.

(36) In summing the contributions from the individual lines that combine to form Figure 2C, it is necessary to adopt some cutoff procedure concerning the wings of the line. For this purpose, the wings were truncated at the point at which they contribute less than 10% to the peak of the next adjacent line.

(37) G. K. Fraenkel, *J. Chem. Phys.*, 42, 4275 (1965).

For $|a_B|$, the measured shift is ~0.12 gauss,[31] a value two orders of magnitude too large as estimated from a simple second-order calculation,[38] The complete theory of the shift[37] is too complex to be applied to the present problem, and since the contribution from this type of correction appears to be small, it will be neglected. In this connection we note that in the case of anthracene (see II) and 9,10-dimethylanthracene (see IV), shifts in the values of the larger coupling constants are again observed, but corrections due to static and dynamic effects are shown to be small. This point can be established with reasonable precision from the spectra of partially deuterated molecules.

Coupling-constant shifts of a similar magnitude have been observed for the protons in the anthracene radical anion generated by electrolytic[39] and alkali metal reduction[40] and in various radical cations prepared in antimony trichloride[41] and pentahalide[42] solvents. Much larger effects are observed in radicals having polar substituent groups.[43,44]

The effect is ascribed (in the case of alternant aromatic hydrocarbons) to a redistribution of the π-electron density caused by fluctuation solvent complexes[43] or an electrostatic perturbation due to the counterion.[40] An explanation based on the latter mechanism is the more plausible for the present system since, as noted above, it is possible to prepare the radical cation in the absence of solvent. Thus the surface (*i.e.*, the counterion) interaction must be the major cause of the isotropic modulation effects.

In principle, it should be possible to demonstrate a dependence of the magnitude of the coupling constant on temperature, concentration, and solvent.[40] In the case of a solid catalyst system this is not practical, for in addition to the handicap of poor resolution, the "counterion concentration" is fixed by the choice of catalysts[45] and the surface heterogeneities lead to local concentration fluctuations (see II). Indeed, one of the more striking observations concerning the experiments with any of the aromatics studied[16] is that the line-width variation and coupling constants are sensibly invariant over the range 25–95% surface saturation. This result suggests that the radical–counterion interactions are a *major effect* in these catalyst systems.

Shifts in the magnitude of a coupling constant can be understood in terms of a model involving a dissociative equilibrium between the radical–counterion complex and the individual components.[43] In the complex the value of the coupling constant will differ from that in the uncomplexed "free" radical. The experimental value is the average of these two values each weighted by the lifetime of the respective species.

Unfortunately, data are not available to allow an estimate of the lifetimes nor the coupling constant for the complexed and "free" perylene radical cation. However consider the electrostatic perturbation approach.[40] As determined experimentally, the magnitude of a_A decreases while that of a_B increases. Thus the π-electron distribution is modified to increase the average charge density in the center of the molecule. (We use the Hückel approximation and thus the electronic density is proportional to the spin density.) Presumably then, the time-average location of the counterions is over the center of the molecule as would be required for the electrostatic perturbation to be effective.[40]

Therefore, when compared to the coupling constants measured in sulfuric acid, the silica–alumina results indicate that either the counterion has a closer distance of approach or, more probably, the complex has a longer lifetime. If the counterion were relatively immobile compared to its counterpart in solution, line-width effects would be more pronounced than experimentally observed. The question of the counterion mobility is considered again briefly in the next section and more fully in III.

If the counterion is paramagnetic, the lifetime of the complex must be shorter than the inverse of the hyperfine splitting to preclude the possibility of quantum mechanical exchange broadening.[35,46] Thus the lifetime would be shorter than 10^{-7} sec. If the lifetime of the complex could be lengthened by lowering the temperature, it might be possible to observe $\Delta M = 1,2$ transitions[47] in a triplet complex similar to that observed in ketyl systems.[48] As noted earlier, only the broad line due to the radical cation is observed and the fact that a faint trace of structure is still visible at 77°K indicates that some surface mobility is retained even at this temperature.

(38) R. W. Fessenden, *J. Chem. Phys.*, **37**, 747 (1962).

(39) J. R. Bolton and G. K. Fraenkel, *ibid.*, **40**, 3307 (1964).

(40) A. H. Reddoch, *ibid.*, **43**, 225 (1965).

(41) E. C. Baughan, T. P. Jones, and L. G. Stoodley, *Proc. Chem. Soc.*, 274 (1963).

(42) I. C. Lewis and L. S. Singer, *J. Chem. Phys.*, **43**, 2712 (1965).

(43) J. G. Gendell, J. H. Freed, and G. K. Fraenkel, *ibid.*, **37**, 2832 (1962).

(44) P. Ludwig, T. Layloff, and R. N. Adams, *J. Am. Chem. Soc.*, **86**, 4568 (1964).

(45) The counterion concentration apparently depends on the oxidation potential of the aromatic used. A discussion of this effect is given in III.

(46) J. D. Currin, *Phys. Rev.*, **126**, 1995 (1962).

(47) J. H. van der Waals and M. S. Groot, *Mol. Phys.*, **2**, 333 (1959).

(48) N. Hirota and S. I. Weissman, *J. Am. Chem. Soc.*, **86**, 2538 (1964).

If the counterion is diamagnetic, again a relative motion within the complex can give rise to a shift in the coupling constant,[49] but in this case the result of the present experiment does not permit an estimate of the lifetime of the complex.

Line-Width Effects. In the preceding discussion only the isotropic modulation effects introduced by the relative motion of the counterion with respect to the radical cation were considered. More generally, it is necessary to consider other perturbations in addition, *e.g.*, internal vibrations, random molecular tumbling, exchange interactions, etc. Each of these introduces a fluctuating time-dependent force on the spin system and thus results in a modulation of both the isotropic and anisotropic magnetic parameters. These modulation effects manifest themselves in a line-width variation among the different hyperfine lines of the esr spectrum.

The complete theory of the effect[33] is too complex to apply to the present data. Thus in the following, an approximate analysis[35] is used to estimate the effects arising from the anisotropic hyperfine interaction and the anisotropic part of the g tensor. Exchange and counterion effects are considered as an afterthought. The treatment is crude, for it assumes an arbitrary separation of the different contributions to the line width; nevertheless the agreement is quite remarkable.

In eq 1, an expression is given which describes the line widths in terms of the resultant nuclear spin quantum numbers of the individual groups of equivalent nuclei. A similar equation can be derived theoretically[35] in which the average line width (T_2^{-1}) of each hyperfine line is evaluated in terms of the inner product of the anisotropic hyperfine and g tensors. The result is[50-52]

$$(JT_2)^{-1} = K - 4898M_A + 2138M_B + 306M_C - 1490M_AM_B - 212M_AM_C - 103M_BM_C + 3800M_A^2 + 10M_B^2 + 0.7M_C^2 \quad (2)$$

where

$$J = (4J_0 + 3J_1)(60 \times 10^{-12})^{-1}$$

$$K = 6370(7J_0 + 10J_1)(4J_0 + 3J_1)^{-1} - 2075$$

and J_0 and J_1 are the spectral densities of the interactions at zero and the microwave frequency, respectively.

Equation 2 shows that terms involving M_C make a minimal contribution to the line widths, a result which follows from the small coupling constant in this position. This result presumably accounts for the success in the attempted fit between the computed and experimental spectrum (Figure 2C) even though M_C was neglected.

A comparison of eq 1 and 2 shows that the signs of the various terms[53] are correctly predicted. The relative magnitude of the corresponding coefficients, however, exhibit considerable disagreement.[54] Such a result is not surprising, for in addition to errors introduced through approximations inherent in the theory and in the calculation of the tensor components, the above treatment considers only the anisotropic effects. Line-width effects also arise from isotropic modulation[43] and exchange effects;[46] to a first approximation both of these contributions give rise to a variation that is symmetrical about the center of the spectrum and thus contribute to K and quadratic terms in M. (Other relaxation mechanisms also contribute to K that are independent of M.[55])

These factors notwithstanding, it is possible to obtain an order of magnitude agreement between the larger coefficients in eq 1 and 2 if spectral densities corresponding to a correlation time of $\sim 10^{-9}$ sec are chosen; this value is comparable to that found for radicals in solution.[35] Such a result, coupled with the correct prediction of the signs of the coefficients, indicates that the theory gives adequate agreement with experiment and, therefore, at least the principal features of the interaction are correctly described.

Such a result is quite remarkable, for on first viewing, the poor resolution and exaggerated line-width effects would suggest that a relaxation theory designed for radicals in solution might require major modification before it was applied to the problem of radicals on a surface. That such is not the case suggests that the radical cation is quite unrestricted in its movements (as opposed to being bound to a fixed catalytically active site on the surface). By implication then, the counterion may also be mobile since counterion effects are important to the description of the shift in the magnitude of the coupling constants. Such a picture

(49) E. de Boer and E. L. Mackor, *J. Am. Chem. Soc.*, 86, 1513 (1964).

(50) The anisotropic hyperfine tensor is obtained from the measured coupling constant[51] using $Q = 23$. The components of the anisotropic g tensor are obtained from theoretical considerations.[52] Throughout the calculation, the microwave frequency is taken to be 9200 mHz.

(51) H. M. McConnell and J. Strathdee, *Mol. Phys.*, 2, 129 (1959).

(52) A. J. Stone, *ibid.*, 7, 311 (1964).

(53) The signs of the coupling constant in positions A and B are the same and opposite to that in position C. See E. de Boer and E. L. Mackor, *ibid.*, 5, 493 (1962).

(54) It has been reported that this theory also accounts for the line-width effects observed in the perylene–sulfuric acid system;[35] however a numerical evaluation of the terms was not given. Also the experimental data on the solution line widths have not been published; thus a comparison with the present results is not possible.

(55) P. W. Atkins and D. Kivelson, *J. Chem. Phys.*, 44, 169 (1966).

is in good agreement with an older model of this catalyst surface,[56] but it has not been included in some of the more recent discussions. This question concerning counterion mobility as well as the nature of the counterion is discussed more fully in III.

Finally, we note that in the perylene–catalyst system discussed here, electronic and chemical-exchange effects can also be studied. The results so obtained for perylene parallel those for anthracene. Since partially deuterated compounds were available in the study of the latter aromatic hydrocarbon, the esr spectra are simpler to understand. Thus a brief discussion of the perylene exchange results will be included with those of anthracene given in II.

Acknowledgment. During the course of the work reported in this and the subsequent papers in this series, the writer benefited from the thoughtful criticisms and helpful suggestions of Drs. S. Bank, M. T. Melchior, and D. J. C. Yates. Their assistance is gratefully acknowledged.

(56) A. G. Oblad, S. G. Hindin, and G. A. Mills, *J. Am. Chem. Soc.*, 75, 4096 (1953).

Electron Spin Resonance Studies of Aromatic Hydrocarbons Adsorbed on Silica–Alumina. II. Anthracene

by G. M. Muha

Esso Research and Engineering Company, Linden, New Jersey 07036 *(Received August 22, 1966)*

An analysis is presented of the line-width and exchange effects exhibited in the electron spin resonance (esr) spectrum of the anthracene radical cation generated on a silica–alumina catalyst surface. The line-width effects and the magnitude of the proton hyperfine-coupling constants are discussed in terms of isotropic and anisotropic modulation of the magnetic parameters due to fluctuations in the radical-cation environment. The results parallel those obtained for perylene on this surface. When the aromatic concentration is in excess of that required to saturate the radical-forming ability of the catalyst, both chemical and electron-exchange effects are observed. The latter effect is discussed in terms of an electron-transfer mechanism with neutral aromatic molecules. Chemical exchange involves surface protons and occurs after the radical concentration has reached a limiting value; thus it is argued that proton transfer is not involved in radical-cation formation.

In the preceding paper,[1] an analysis of the electron spin resonance (esr) spectrum of the perylene radical cation formed on a silica–alumina surface was presented. From the analysis, it was argued that the observed line-width effects and the shifts in the values of the hyperfine-coupling constants (relative to those in sulfuric acid) could be understood in terms of a combination of effects arising from a random tumbling motion and a dissociative equilibrium of a complex between the radical cation and its counterion. Also, exchange effects were noted, but the system was not convenient to study the effect.

(1) G. M. Muha, *J. Phys. Chem.*, 71, 633 (1967), hereafter referred to as I.

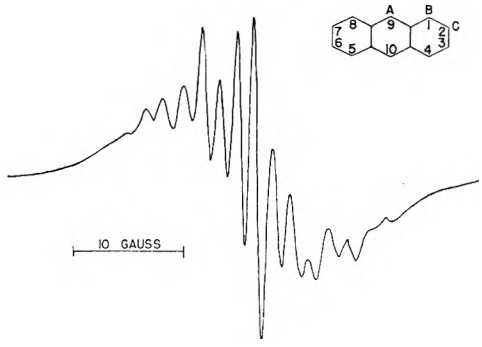

Figure 1. First-derivative spectrum of the anthracene radical cation adsorbed on a silica–alumina catalyst.

In the present paper, a more detailed analysis is presented of the several exchange effects occurring in aromatic systems adsorbed on this catalyst. Anthracene is particularly convenient for this study because of the ready availability of partially deuterated compounds and also because the length of time required to complete the chemical exchange is sufficiently long enough to allow the effect to be followed by the esr technique. Again, as in the case of perylene, line-width effects are evident and the magnitude of the hyperfine-coupling constants appear to be shifted from those exhibited in sulfuric acid solution; a brief discussion of these effects is also included.

A description of the experimental techniques, equipment, and preparation of the reagents is given in I.

Hyperfine-Coupling Constants. The esr spectrum of anthracene adsorbed on silica–alumina (Figure 1) under conditions in which exchange effects are unimportant (see below) exhibits severe line-width effects. There is little doubt that the spectrum corresponds to the anthracene radical cation since the optical spectrum shows the expected characteristic adsorption bands.[2] Additional evidence in support of this conclusion can be obtained from a measurement of the hyperfine-coupling constants.

The proton-coupling constant in the A position (a_A) can be determined by using as a starting material the partially deuterated molecule $C_{14}H_2D_8$.[3] The expected triplet is shown in Figure 2A. From this spectrum, the value $a_A = 6.65$ gauss is obtained.

A value for the proton-coupling constant in the B position can be obtained by adjusting the initial concentration so that four surface hydrogens exchange with four deuterium atoms in $C_{14}H_2D_8$ to give $C_{14}H_6D_4$. (Details of this procedure are given below.) From the resulting spectrum (Figure 2C), the value $a_B = 3.16$ gauss is obtained; the corresponding stick spectrum is shown in Figure 2D.

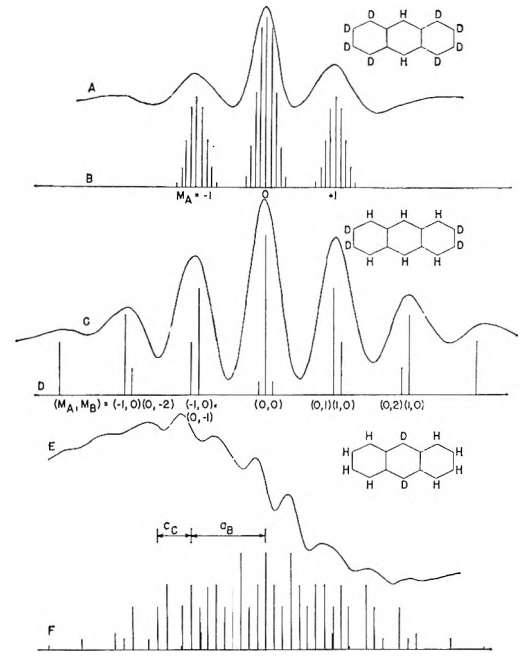

Figure 2. Experimental and theoretical stick spectra for three partially deuterated anthracene radical cations on silica–alumina. A second-derivative presentation is used in (A) and (C); (F) is a first-derivative presentation. In (B) and (D), deuterium hyperfine effects from the C positions are not included; in (B), the deuterium coupling from the B positions is included.

The coupling constant in the C position is small and not directly obtainable through the use of partially deuterated compounds since the presence of deuterium in the A positions gives a splitting of comparable size. In sulfuric acid solution,[4] the three coupling constants are $a_A = 6.53$, $a_B = 3.06$, and $a_C = 1.38$ gauss. The two values given above are similar in magnitude to the solution values; thus we evaluate a_C for the silica–alumina case by showing that a reasonable agreement is obtained if the sulfuric acid value is assumed.

To accomplish this, a deuterium-exchanged surface and $C_{14}H_{10}$ are used as starting materials; the aromatic concentration is adjusted (see discussion below) to observe the slow exchange of deuterium into the A positions. The resulting spectrum is shown in Figure 2E and the corresponding stick spectrum in Figure 2F. (In the latter figure, the expected hyperfine coupling from deuterium in the A position, a_A^D =

(2) W. K. Hall, *J. Catalysis*, 1, 53 (1962).

(3) We adopt the notation $C_{14}H_2D_8$ to represent the compound anthracene-1,2,3,4,5,6,7,8-d_8. By analogy, the notation $C_{14}H_6D_4$ represents the compound anthracene-2,3,5,6-d_4. The identification with the different ring positions is given in Figure 1.

(4) J. R. Bolton and G. K. Fraenkel, *J. Chem. Phys.*, 40, 3307 (1964).

1.02 gauss, is included.) The agreement is good and thus, in the following, a value of $a_C = 1.35$ gauss will be assumed.

Each of the spectra shown in Figure 2 were independently calibrated with a g scale. The figure is drawn to align these scales. The g value of the spectrum ($=2.0025$) is taken to correspond to the center of the largest peak in the second-derivative presentation shown in Figure 2B. This value is identical with that reported for the anthracene radical cation prepared in sulfuric acid.[5]

The values quoted above for a_A and a_B in the case of silica–alumina appear to differ from the corresponding values in sulfuric acid. It is difficult to determine if this is a real effect, for in the present case, the measurements are made on broad lines and the differences are small. A statistical analysis of the results for five identically prepared samples indicated a mean-square deviation of ± 0.06 gauss with the mean values of a_A and a_B quoted above. Thus it would appear that the difference is significant.

Corresponding shifts of the same relative magnitude were observed in the perylene radical cation generated on this surface.[1] There it was argued that the shifts reflected a difference in the lifetime of the radical–counterion complex, perhaps due to the effect of the catalyst surface. In the anthracene case, the argument can be made somewhat stronger.

The magnitude of a given coupling constant is thought to depend on the electrostatic perturbation of the π-electron system due to the presence of the counterion.[6] To compare the effect of the counterion then, the shift should be measured relative to the coupling constant of the "free" or uncomplexed radical. The coupling constant of the free anthracene radical cation is not known;[4] however, it has been computed for the radical anion.[6] As a first approximation it might be expected that the direction of the shift would be independent of whether the counterion was an anion or a cation. On this basis, the predicted effect of the counterion electrostatic perturbation is to increase $|a_A|$ and $|a_C|$ and to decrease $|a_B|$.[6] This is the observed shift of the silica–alumina values relative to those in sulfuric acid. Thus the counterion seems to have a larger effect when present on the catalyst surface than in solution—a conclusion analogous to that drawn from the perylene results.

Line-Width Effects. In Figure 3 a comparison is given between the complete anthracene spectrum and the stick spectrum obtained by using the coupling constants deduced above. A discrepancy between the relative height of corresponding lines in these two spectra is evident. Such a discrepancy can arise if the

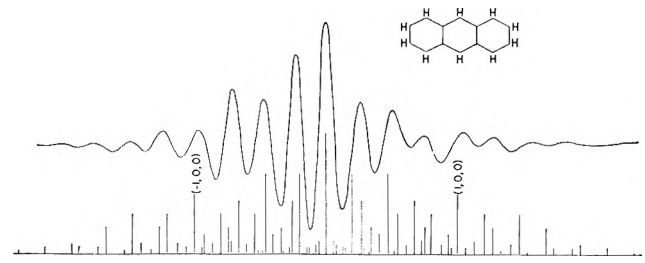

Figure 3. Second-derivative spectrum and theoretical stick spectrum of the anthracene radical cation adsorbed on silica–alumina.

experimental spectrum exhibits a variation in the widths of the individual hyperfine lines; the variation arises from a fluctuating time-dependent interaction at the different proton sites due to internal vibrations, complexes with the counterion and solvent, random molecular tumbling of the radical, exchange phenomena, etc.[7]

The line-width variation can be understood[7] in terms of a modulation of both the isotropic and anisotropic magnetic parameters, again in a fashion analogous to the perylene system.[1] In the present case, the spectrum is too complicated to attempt to obtain the line widths by a least-square procedure as was done with perylene; rather we content ourselves with considering an approximate theory involving only the modulation of the anisotropic hyperfine and the anisotropic part of the g tensor.[8] In the case of anthracene, the following dependence[9-11] of the average line width (T_2^{-1}) on the total nuclear magnetic quantum number of the various equivalent proton groups can be derived

$$(JT_2)^{-1} = 8315K - 7220 + 5480M_A^2 + 2380M_B^2 + 268M_C^2 + 5086M_AM_B - 1110M_AM_C - 519M_BM_C - 5753M_A - 2691M_B + 663M_C$$

where

$$J = (4J_0 + 3J_1)(60 \times 10^{-12})^{-1}$$

$$K = (7J_0 + 10J_1)(4J_0 + 3J_1)^{-1}$$

(5) B. G. Segal, M. Kaplan, and G. K. Fraenkel, *J. Chem. Phys.*, **43**, 4191 (1965).

(6) A. H. Reddoch, *ibid.*, **43**, 225 (1965).

(7) J. H. Freed and G. K. Fraenkel, *ibid.*, **39**, 326 (1963).

(8) A. D. McLachlan, *Proc. Roy. Soc.* (London), **A280**, 271 (1964).

(9) The anisotropic hyperfine tensor is obtained from the coupling constants[10] using $Q = 23$. The components of the anisotropic g tensor are estimated from theory.[11] The microwave frequency is taken to be 9200 mHz.

(10) H. M. McConnell and J. Strathdee, *Mol. Phys.*, **2**, 129 (1959).

(11) A. J. Stone, *ibid.*, **7**, 311 (1964).

and J_0 and J_1 are the spectral densities of the interactions at zero and the microwave frequency, respectively.

Since the isotropic hyperfine splittings of anthracene are negative,[4] positive values of M_I occur at high field. Thus the principal lines (M_A, 0, 0) and (0, M_B, 0) are expected to be narrower (and therefore have a higher peak height) at high field, while (0, 0, M_C) should be broader at high field.

It is simplest to check the predicted behavior by noting the line-width variations in the partially deuterated samples (Figure 2); the agreement is seen to be complete for both $C_{14}H_2D_8$ and $C_{14}H_6D_4$ insofar as the predicted trend is concerned.

In the above comparison, contributions from the deuterated positions are neglected. This is a reasonable approximation if only the variation in line width is considered, for the deuterium contribution should be proportional to its magnetogyric ratio,[7] which is ~15% that of a proton. In a quantitative comparison the deuterium contribution, as well as that arising from isotropic modulation effects, would have to be included.

If deuterium hyperfine effects are neglected, it is possible to use the general theory of relaxation[7] to develop an equation that describes the line-width variation in $C_{14}H_2D_8$. This equation includes both isotropic and anisotropic terms; it indicates that the *difference* in the widths of the outside lines arises from two contributions—one, the isotropic and the other, the anisotropic dipolar g-tensor interaction.[12] These contributions add to the low-field ($M_A = -1$) and subtract from the high-field ($M_A = +1$) line width. Experimentally, an intensity ratio[13] of 0.83:1.58:1.0 (low to high field) is observed; thus the sum of these two contributions accounts for ~8% of the line width.

Although the theories discussed above correctly predict the observed trends in the line widths of the partially deuterated compounds, the situation is less than clear when the full anthracene spectrum is considered (Figure 3). Overlapping among the different lines renders consideration of the expected trends in the line widths of the principal lines impossible. Also, in the case of the lines (−1, 0, 0) and (1, 0, 0) it is seen that the stick spectrum and the experimental spectrum appear to be displaced with respect to each other.

It is possible that this displacement arises from the effect of static and dynamic frequency shifts[14] in the line positions, a result expected whenever line-width effects are large. In the case of the $C_{14}H_{10}$ spectrum, it is not possible to analyze these position shifts further, for the overlapping of adjacent lines is too severe. For the partially deuterated molecules (Figure 2), the intervals between the hyperfine lines exhibit no trend attributable to a shift. A similar result is observed in the case of 9,10-dimethylanthracene.[15] Thus it is likely that the displacement arises from either a cumulative error in the values of the hyperfine-coupling constants or an extreme line-width effect,[15] or both.

Exchange Effects. In radical-cation systems, three phenomena can occur that would be described as due to exchange effects. The first is a quantum mechanical spin exchange[16] between the radical and the counterion or other radicals. A second possibility is an electron exchange (or transfer) between the radical cation and the counterion[17] or neutral aromatic molecules.[18] Finally, a chemical exchange can occur between the protons in the aromatic radical cation and those in the remainder of the chemical system.

In the systems studied in this series of papers, all three of these phenomena are occurring, depending in degree on the experimental conditions. The discussion given below separates, in an approximate fashion, the chemical- and electron-exchange effects based on the concentration range. Spin-exchange effects are either small or constant in their contribution within the range of experimental variables accessible in the present experiments.

Chemical Exchange. In the discussion of the hyperfine-coupling constants given above, chemical-exchange effects were used to determine approximate values for the coupling constants. The mechanism by which this chemical exchange takes place is of interest in its own right, for it is intimately related to the surface interaction occurring on this catalyst. Thus in this section we present the experimental evidence concerning chemical exchange.

To this end, it will be necessary to discuss the radical cation:catalyst concentration ratio. It is difficult to devise a suitable system of units to express this ratio, for the redox "equivalent weight" of the catalyst is unknown and apparently depends on the aromatic that is used.[19] Also, not all of the aromatic molecules

(12) This result can be obtained by extending the discussion given in section VII of ref 7.

(13) The line widths are taken to be proportional to the product of the derivative height and the square of the derivative width. See R. N. Rogers and G. E. Pake, *J. Chem. Phys.*, **33**, 1107 (1960).

(14) G. K. Fraenkel, *ibid.*, **42**, 4275 (1965).

(15) G. M. Muha, *J. Phys. Chem.*, in press.

(16) *Cf.* G. E. Pake, "Paramagnetic Resonance," W. A. Benjamin, Inc., New York, N. Y., 1962, Chapter 4.

(17) W. I. Aalbersberg, J. Gaaf, and E. L. Mackor, *J. Chem. Soc.*, 905 (1961).

(18) N. Hirota and S. I. Weissman, *J. Am. Chem. Soc.*, **86**, 253 (1964); A. Ishitani and S. Nagakura, *Bull. Chem. Soc. Japan*, **38**, 367 (1965).

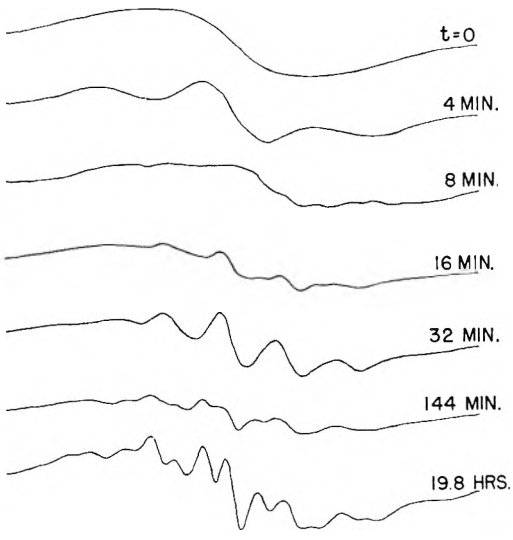

Figure 4. Time development of the esr spectrum of the perdeuterioanthracene radical cation showing the changes caused by a slow chemical exchange of surface protons with ring deuterium atoms.

adsorbed on this surface are converted to the radical cation. For these reasons, the concentration unit used will be simply the molarity of the aromatic solution. For this unit to be meaningful, the catalyst weight and the solution volume must be given; thus we adopt a standard catalyst weight of 0.1 g and a standard aromatic volume of 5 ml.[20]

The dependence of the chemical exchange on the concentration is easily established by equilibrating different concentrations of perdeuterioanthracene with the catalyst. It is found that below 5×10^{-4} M, no exchange is observed for periods up to 26 hr, the integrated intensity of the esr spectrum remaining sensibly constant. Within the concentration range 5×10^{-4} to 10^{-3} M, the exchange proceeds to completion (*i.e.*, all ten deuterium atoms are replaced by hydrogen) in $\sim$20 hr. The various steps in the exchange are shown by the changes in the esr hyperfine patterns (Figure 4). Chemical analysis showed that up to a concentration of $\sim 10^{-3}$ M, there is no anthracene remaining in the solvent above the catalyst. Also, at a concentration of $\sim 10^{-3}$ M, the esr intensity reaches its maximum value, indicating that the surface has become saturated. The uncertainty in the concentration at which saturation occurs is $\pm 20\%$; it arises principally from the experimental error inherent in the comparison of the esr intensities from a series of identically prepared catalyst samples.

In the concentration range 10^{-3} to $\sim 9 \times 10^{-3}$ M, the time required to complete the chemical exchange was much shorter, all of the deuterium being exchanged within 4 hr at the upper limit. The integrated esr intensity was unchanged, but now anthracene was present in the supernatant liquid. At concentrations above 10^{-2} M, electron exchange occurs and the hyperfine pattern disappears (see below).

Over the entire concentration range quoted above, it was observed that the radical concentration reached its final value within the first minute after mixing the component, thus the exchange follows the radical formation.[21] Also, the results were independent of the solvent used. (In these experiments benzene, perdeuteriobenzene, hexane, carbon tetrachloride, and carbon disulfide were used. The latter solvent is used at the highest concentration ranges because of the limited solubility of anthracene.)

As a corollary to these experiments, spectra were also recorded from samples in which the ratio of the solution volume to the catalyst weight was scaled so as to hold constant the number of molecules of aromatic available to the catalyst (*e.g.*, 50 ml of 10^{-4} M rather than 5 ml of 10^{-3} M). The results for a number of these runs showed that the time to complete the exchange corresponded to the solution concentration rather than the total number of molecules present.

Further, it was possible to slow down significantly the exchange by decanting the supernatant aromatic-containing liquid and substitute pure solvent. The exchange rate could then be increased again by adding the aromatic back to the solvent. On the other hand, the total radical concentration could not be reduced by substituting pure solvent for the supernatant liquid. Thus, in this sense, radical formation is an irreversible effect.

The dependence of the exchange time of the aromatic concentration in the solution phase suggests an effect involving physical adsorption of molecules on the surface, an expected result.

Another point of interest concerning the chemical exchange is the ultimate source of the hydrogen atoms. The absence of an effect on the exchange with carbon disulfide and carbon tetrachloride rules out the

(19) G. M. Muha, *J. Am. Chem. Soc.*, in press.

(20) In the perylene study, the concentration ratio was given in terms of the fractional surface saturation of the catalyst insofar as radical-forming ability was concerned. This unit is not convenient, for discussing the present results for exchange effects appear only when the surface is almost completely saturated.

(21) It might be argued that exchange did occur much earlier, perhaps during the process of radical formation; the absence of hyperfine structure might then be due to an anisotropic broadening effect arising from some peculiarities of a surface interaction and resulting in a restricted motion of the radical cation. That this is not the case is easily established by using $C_{14}H_2D_8$ and a deuterated catalyst as starting materials. In this case, the expected triplet of lines is observed immediately; these hyperfine lines then gradually decay and only a single broad resonance remains.

solvents as the source. Similarly, full exchange is observed when perdeuterioanthracene is used as a starting material; thus the protons cannot originate from the aromatic molecule. Finally, to rule out solution impurities as a source of the protons, the experiments were repeated with a deuterated surface and perdeuterioanthracene dissolved in benzene and also perdeuteriobenzene. No proton hyperfine was observed within any of the concentration ranges; thus it is concluded that the ultimate source of the hydrogen must be the surface.

During the course of these experiments, attempts were made to obtain the spectrum corresponding to one hydrogen atom exchanged into the perdeuterioanthracene rings, *i.e.*, $C_{14}HD_9$. All attempts were unsuccessful; the spectrum obtained always corresponded to $C_{14}H_2D_8$. At the lowest concentration at which exchange occurs, 5×10^{-4} *M*, the conversion of $C_{14}D_{10}$ to $C_{14}H_2D_8$ requires 20 min; thus it is possible to follow the reaction with esr. At this concentration, the appearance of the first hyperfine lines occurs at ~3 min after mixing. The resulting spectrum is shown in Figure 5A. From this spectrum, it is not possible to decide if a doublet (due to $C_{14}HD_9$) or a triplet is observed. That the latter is the case is clearly shown in the corresponding second-derivative spectrum (Figure 5B).

The result is of interest, for it implies that the radical cation is formed first, eventually exchanges one deuterium atom,[21] and then, in a length of time that is short compared to that required to accomplish the first exchange, replaces a second deuterium with hydrogen.

To appreciate this argument, consider the possible alternatives. If all the radicals were formed in an identical environment or if the chemical exchange were in some way intimately connected with radical formation, the length of time to effect the first exchange would be roughly the same for all molecules. Most certainly a doublet would have to be observed unless the second exchange followed right after the first, which is the above hypothesis.

Alternatively, consider the radicals to be formed in a number of environments (sites) each with a different length of time required to effect the first exchange. Depending on the distribution in the "exchange times" involved, a superposition of a doublet and a triplet spectrum with different relative intensities might be expected. The doublet lines would fall between the lines of the triplet; thus five equally spaced lines would be expected. The resolution might be poor, but at least more than three lines should be observed. (For example, see Figure 4 where a superposition of the triplet with hydrogen exchanging in the B position is shown.) The experimental results (Figure 5), however, show only the triplet, hence the above hypothesis.

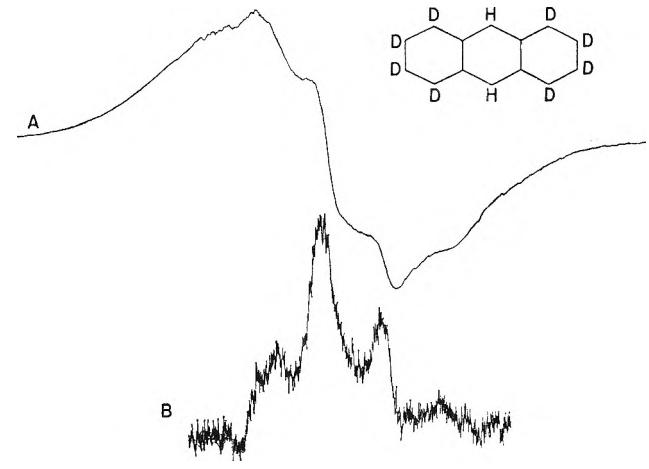

Figure 5. First- (A) and second-derivative (B) presentations of the initial hyperfine lines that appear in the spectrum of perdeuterioanthracene adsorbed on silica–alumina. The hyperfine lines arise from the chemical exchange of ring deuterium atoms with surface protons.

The fact that the first hyperfine lines occur within 3 min of mixing, but that 20 min is required to complete the exchange in the *meso* positions, argues that the distribution in "exchange times" is broad, possibly arising from the heterogeneous nature of the surface. The broad distribution precluded any attempt to measure an isotope effect or to estimate rate constants for the chemical exchange.

In summary then, in this section it has been shown that (1) there is no chemical exchange until the surface is nearly saturated in its capacity to generate radicals, (2) the exchange occurs with surface hydrogens (3) at a rate that depends on the concentration of the aromatic in the solution phase, and finally (4) the time required to complete the exchange of a deuterium in the 10 position after the 9 position is exchanged is short compared to the time for the first deuterium to exchange.

The results described here also apply qualitatively to perylene,[1] tetracene,[19] and methyl-substituted anthracenes[15] in respect to the concentration dependence; however, the time to complete the exchange varies markedly.

Electron-Exchange Effects. Above a concentration of $\sim 10^{-2}$ *M*, the hyperfine lines disappear and the line width narrows (Figure 6). One measure of the effect is the peak-to-peak separation in the first-derivative presentation; a better one is the second moment of the spectrum, for this quantity takes into account possible changes in the line shape. Both measures are given in

Table I. From this table it is seen that dipolar effects are important, for the replacement of hydrogen by deuterium in both the molecule and the surface decreases the line width and the second moment.

Table I: Line-Width Effects in the Presence of Electron Exchange

Concn,[a] *M* — Perdeuterio-anthracene	Peak-to-peak separation, gauss	Second moment[c]
Satd soln	3.6	12.3
10^{-2}	5.1	14.6
10^{-3} [b]	8.1	19.7
10^{-4} [b]	8.9	27.2
10^{-5} [b]	~8.9	31.6
Anthracene		
Satd soln	6.3	18.3
Perdeuterio-anthracene-deuterated surface		
10^{-4}	4.7	11.5

[a] Carbon disulfide used as a solvent in all cases. [b] Measurements made on spectrum recorded before hyperfine observed. [c] Computed from the first-derivative spectrum by numerical integration. The integration limits were taken to be the points at which the wings of the curve disappear into the base-line noise.

If the line narrowing were the result of spin-exchange effects, the second moment should remain constant,[16] and the hyperfine lines coalesce and shift to the unsplit Zeeman frequency.[22] The predicted constancy of the second moment under similar circumstances has been observed in the perylene–molecular oxygen system.[17]

In the present system, the second moment changes appreciably with concentration and the hyperfine lines are found to broaden and disappear rather than coalesce and shift. To establish the latter point, a 10^{-3} *M* sample was prepared (Figure 7A), then the supernatant liquid decanted and replaced (without shaking) by a 10^{-2} *M* solution. The spectra given in Figures 7B and 7C show the time development as the higher concentration diffuses into the catalyst bed. The hyperfine lines can be made to reappear by washing the catalyst with pure solvent. The integrated esr intensity remains constant during this series of manipulations, but as seen in Figure 7B, the hyperfine lines do not return to full intensity. We have no explanation for the lack of complete reversibility.

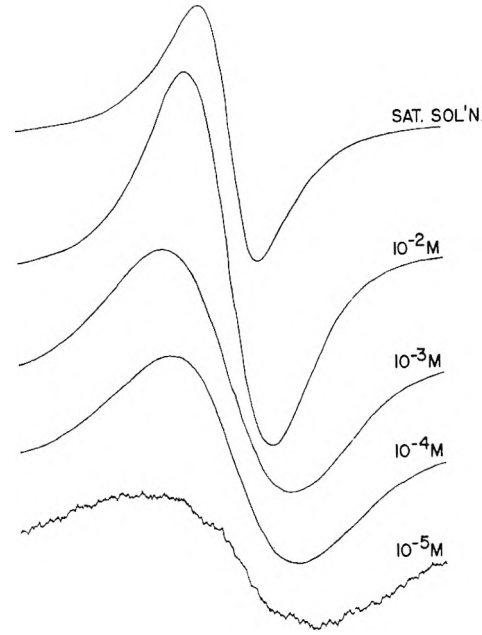

Figure 6. First-derivative spectra of perdeuterioanthracene radical cation on silica–alumina as a function of aromatic concentration. These spectra correspond to the first five entries in Table I.

From this evidence it is concluded that the spin-exchange phenomenon does not explain the observed behavior. Most certainly the phenomenon is occurring, but apparently its contribution is small or perhaps constant in its effect within the concentration range accessible. The latter result would be obtained if the spin exchange occurred principally between the radical and its counterion.[17] As an alternative explanation of the observed behavior, the possibility of an electron-transfer mechanism is considered.

In the concentration range in which the line narrowing occurs, the radical concentration remains constant with increasing aromatic concentration. A similar behavior has been reported in aromatic ketyl systems generated by alkali metal reduction.[18] There it was observed that at higher concentrations the hyperfine lines collapse, and the resulting spectrum was that associated with the counterion (*i.e.*, the alkali metal). The phenomena was explained in terms of a transfer process between the radical and neutral aromatic molecules in which the counterion and the electron spin are transferred together.[23]

The analogy between the concentration dependence exhibited in the present system and that in the ketyl

(22) D. Kivelson, *J. Chem. Phys.*, **33**, 1094 (1960); J. D. Currin, *Phys. Rev.*, **126**, 1995 (1962).

(23) P. J. Zandstra and S. I. Weissman, *J. Am. Chem. Soc.*, **84**, 4408 (1962).

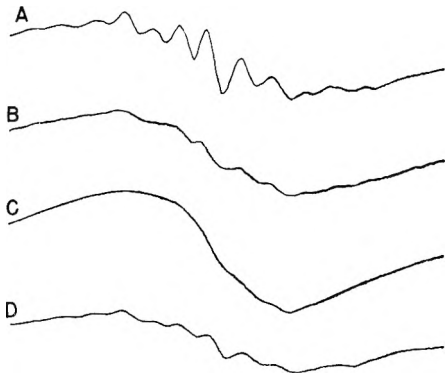

Figure 7. First-derivative spectra of the anthracene radical cation (A) showing the changes observed when an excess of solid anthracene is added to the solution above the catalyst (B), allowed to diffuse into the catalyst bed (C), and finally removed by washing with solvent (D).

system is clear and thus we offer the hypothesis that the explanation of the phenomena is the same in both cases. The effect of the increasing aromatic concentration in the present system is then to shorten the average lifetime of the radical cations. Also, as discussed below, an electron transfer (*via* the counterion) to neutral aromatic molecules offers a convenient mechanism to explain the *chemical*-exchange phenomena as well.

A search was made over a region of the magnetic field 1200 gauss wide and centered on $g = 2$ in an attempt to detect additional lines arising from the counterion hyperfine interaction. No such lines were found. Presumably then, the counterion either has zero nuclear spin or its hyperfine contribution is obscured by the radical-cation line.[24]

Finally, we note that nuclear magnetic resonance (nmr) techniques can also be used to study the various exchange phenomena. In the limit of strong exchange, theory predicts a paramagnetic shift of the proton nmr line.[25] Attempts were made to observe this effect in the higher concentration range by using perdeuterioanthracene and a hydrogen catalyst as starting materials. Unfortunately, the experiments were inconclusive for the sensitivity was low even with exaggerated sample sizes (~3 g of catalyst). Work is continuing on other aspects of this approach.

Anthracene Derivatives. In the discussion given above concerning chemical-exchange effects, it was shown that the first step in the protodedeuteration occurred in the 9,10 positions as expected.[26] For this reason a series of chemical-exchange studies was undertaken in which these positions were modified by introducing other substituent groups. Thus the experiments were repeated with 9-methyl- and 9,10-dimethylanthracene, 9,10-dihydroanthracene, 9-bromo- and 9,10-dibromoanthracene, and anthraquinone.

The first two compounds listed are especially interesting, for the methyl groups are not expected to be susceptible to chemical exchange on this acid surface.[27] Such a result was found. The analysis of the resulting spectrum provides other information, particularly from the line-width variations, and a full discussion is given in the fourth paper in this series.[15]

The dihydro derivative gave identically the same hyperfine pattern and line-width variation as anthracene;[28] however, the catalysts turned bright orange rather than the usual green observed with anthracene. The chemical-exchange behavior parallels that of anthracene.

The bromo derivatives are photosensitive; thus the experiments were conducted in a darkened laboratory.[19] The monobromo compound gave the same esr spectrum as anthracene, but the dibromo compound gave a single broad asymmetric line covering a region of ~125 gauss. Both spectra were more intense than that of anthracene, possibly due to secondary oxidation of the aromatic by liberated bromine. No chemical-exchange studies were attempted.

The semiquinone intermediate of anthraquinone is paramagnetic, but since it is stable only in basic solution,[29] an esr signal was not expected on the acid surface. Contrary to prediction, however, a resolved spectrum of low intensity was observed at high microwave power (Figure 8). The interval between the lines is ~2.3 gauss, which is much larger than the value reported for the hyperfine-coupling constant of the radical anion[30] prepared by more conventional techniques. Since the semiquinone is an intermediate

(24) There can be little doubt that chemical exchange continues after electron-exchange effects set in; however, the point is not easily established experimentally. The technique used involved reversing the electron-exchange effects after fixed periods of time by replacing the solution with solvent; thus the hyperfine lines again become visible. The method is subject to error, for the resulting spectra are complicated and it is difficult to reproduce any given spectrum obtained after some chosen time interval. However, chemical-exchange effects were clearly evident and thus the results were sufficient to establish the point.

(25) H. M. McConnell and D. B. Chestnut, *J. Chem. Phys.*, 28, 107 (1958).

(26) V. Gold and F. A. Long, *J. Am. Chem. Soc.*, 75, 4543 (1953).

(27) A. I. Shatenshtein, "Isotopic Exchange and the Replacement of Hydrogen in Organic Compounds," Consultants Bureau, New York, N. Y., 1962.

(28) The oxidation of this compound to anthracene in an acidic media is expected; *cf.* "Dictionary of Organic Compounds," Vol. II, J. Heilbron, *et al.*, Ed., Oxford University Press, New York, N. Y., 1953, p 197.

(29) E. S. Gould, "Mechanism and Structure in Organic Chemistry," Henry Holt and Co., New York, N. Y., 1959, p 679.

(30) G. Vincow and G. K. Fraenkel, *J. Chem. Phys.*, 34, 1333 (1961).

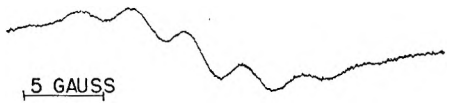

Figure 8. First-derivative esr spectrum of anthraquinone adsorbed on silica–alumina.

in the quinone–hydroquinone equilibrium, it is possible that the heterogeneous nature of the surface allows some small quantity of the semiquinone to stabilize in spite of the predominantly acid nature of the surface. Such a result would explain the low intensity. However, it does not seem possible that the surface interaction could shift the coupling constants by such a large amount. The problem is under investigation at the present time.

Exchange Mechanism. Considerable evidence has been accumulated on the mechanism of exchange in the case of aromatic molecules in nonoxidizing media.[31] The intermediate in the mechanism is usually a carbonium ion. Apparently exchange studies in radical-cation systems in solution have not yet been undertaken.

In the case of the aromatic–catalyst system considered in the present work, optical studies[2] have shown the presence of carbonium ions and physically adsorbed molecules on this surface in addition to radical cations. Thus in the following an exchange mechanism based on a carbonium ion "intermediate" is proposed. Also convenient use is made of the electron-transfer data and the presence of physically adsorbed molecules.

It was established above that the radical cation is formed first, then a relatively long time elapses before chemical-exchange effects are observed. To suggest a possible mechanism for the chemical exchange, it is then necessary to consider the radical cation as the "starting material." Also the addition of aromatic in excess of that required to saturate the surface does not increase the radical-cation concentration. Thus this excess presumably increases the concentration of the physically adsorbed molecules, the carbonium ions, or both.

If the plausible assumption is made that the carbonium ions are able to undergo chemical exchange with the surface, then the mechanism by which the radical cations undergo protodedeuteration might arise from an equilibrium reaction involving an interconversion of the carbonium ion and the radical cation. Such a step would be equivalent to the transfer of a hydrogen *atom;* thus proton hyperfine (doublet with separation of ~500 gauss) might be expected by analogy with the ketyl results.[18] As noted above, no such lines were found.

Alternatively, an equilibrium between the carbonium ion and the adsorbed neutral molecules might be considered. Such an interconversion would supply a mechanism to obtain deuteration of the neutral molecules. Then, arguing from the electron-exchange data, the radical cation could undergo chemical exchange by an equilibrium interconversion involving an electron transfer to a neutral molecule (again by analogy with the ketyl results).

Specifically, we visualize the sequence

$$C_{14}D_{10} + (SH) \rightleftharpoons C_{14}D_{10}H^+ + (S)^- \rightleftharpoons C_{14}D_9H + (SD)$$

$$C_{14}D_9H + (C_{14}D_{10})\cdot^+ \rightleftharpoons (C_{14}D_9H)\cdot^+ + C_{14}D_{10}, \text{ etc.}$$

The last step represents the electron exchange; the first step represents the generation of the carbonium ion and its equilibrium with the physically adsorbed molecules. The symbol (SH) is chosen to represent, in a noncommittal fashion, the source of protium from the surface. In this discussion we assume that the electron-exchange step occurs only with the neutral molecules that are physically adsorbed. Such an assumption seems reasonable since the radical-cation ions are bound to the immediate vicinity of the surface by the requirement by local charge neutrality; *viz.*, the counterion must be nearby (as evidenced by the line-width analysis).[32]

The sequence suggested above is clearly a hypothesis, for the present experimental results do not serve to determine uniquely any of the individual steps. The sequence has the obvious advantage of interconnecting all the exchange phenomena involved in a plausible manner and, further, is based on an analogy[18] with effects observed in chemical systems that are more easily and completely defined. For these reasons, we believe that the sequence serves to outline at least some of the major chemical interactions on this surface.

However, questions remain, for no account has been taken of the dipositive ions present on this surface.[19] Also perylene probably does not form a "classical" carbonium ion on this surface.[33] Thus the intermediate involved in the transfer of a surface proton is

(31) V. Gold in "Friedel-Crafts and Related Reactions," Vol. II, Part II, G. A. Olah, Ed., Interscience Publishers, Inc., New York, N. Y., 1964, p 1253; ref 27, Chapter 2.

(32) Attempts were made to determine whether the aromatic molecules in the solution phase were deuterated at approximately the same rate as the radical cations; the method involved the analysis (by nmr and mass spectroscopy) of the perdeuterated molecules in solution for the presence of hydrogen exchanged from the surface. The results were inconclusive because of the relatively low sensitivity of the techniques used; a tritium-labeling technique might work, but has not yet been attempted.

(33) See ref 2, but *cf.* D. M. Brouwer, *J. Catalysis,* 1, 372 (1962).

in question. However, perylene behaves differently than anthracene in other respects[19] and thus may simply represent an anomalous case.[34]

The steps in the proposed sequence are written as equilibrium reactions, for we visualize a dynamic situation on the catalyst surface as opposed to a relatively static situation that would result if each radical cation were bound to a fixed immobile surface site (*i.e.*, counterion).[1] In the first step the equilibrium shifts to the right at low aromatic concentrations since the exchangeable hydrogen is present in large excess. For example, in the case of silica–alumina, there are $\sim 10^{20}$ OH groups on our standard-size catalyst sample.[35] The standard volume of solution even at 10^{-3} M contains $\sim 3 \times 10^{18}$ molecules or 3×10^{19} deuterium atoms to be exchanged. Thus a fully exchanged radical cation is expected in accordance with the observed esr results.

At the highest concentration used, there are 1.5×10^{21} atoms to be exchanged. Thus a distribution of the available deuterium between the catalyst and the radical cation is expected; consequently a different hyperfine pattern should be observed. Such a result may explain the complicated esr spectra that were obtained when this effect was investigated.[24]

The position of the equilibrium in the second line depends on the proximity of the radical cation to the neutral molecules; thus it would be expected to depend in a sensitive fashion on the concentration. Such is the observed dependence.

Data are not available for chemical-exchange rates in oxidizing acids; in DBr, anthracene is completely exchanged in less than 30 min.[27] On silica–alumina, at 10^{-3} M, the complete exchange requires 3 hr. Since chemical exchange is a diffusion-controlled process,[31] the difference in the two cases may be qualitatively understood in terms of a lower diffusion constant in the silica–alumina case caused by the essentially two-dimensional process involved.

Quantitative assessment of the difference is more complicated, for the heterogeneous nature of the surface must be taken into account. For example, there is no reason to believe that the simple physical mixing of the components does not result in local concentration gradients which are corrected in a length of time that is long with respect to the occurrence of the first chemical exchange. This factor, possibly compounded with others not yet suspected, may conspire to cause the *meso* positions to complete their exchange in a time short compared to the time required to initiate the first exchange.

Finally, we note that throughout the above discussion we have used the terms "counterion" and "source of exchangeable hydrogen" without attempting to indicate the nature or role of the corresponding species. A discussion of the properties of these species and resulting implications concerning the nature of the acidity of this catalyst forms the basis of the following paper.[19]

(34) An attempt was made to use esr to follow the chemical exchange of perylene with the surface. The results were unsatisfactory, for perylene has two proton-coupling constants of the same magnitude; thus the partially deuterated spectrum is too complicated to analyze. (Compare, for example, the anthracene spectrum shown in Figure 2D.) Also the similarity in the coupling constants implies a similar charge density at these positions and thus a comparable chemical-exchange rate. This possibility may explain why perylene appears to exchange completely much more rapidly than anthracene.

(35) W. K. Hall, H. P. Leftin, F. J. Cheselske, and D. E. O'Reilly, *J. Catalysis*, **2**, 506 (1963). For computational convenience, we take the surface area to be 333 m^2/g.

Intramolecular Hydrogen Bonding and Potential Functions of Carboxylic and Percarboxylic Acids

by W. V. F. Brooks and Clyde M. Haas

Department of Chemistry, Ohio University, Athens, Ohio *(Received August 23, 1966)*

To study the nature of the forces between the acidic hydrogen and the carbonyl oxygen atoms in organic acids, a normal coordinate analysis has been carried out for monomeric formic, acetic, trifluoroacetic, performic, and peracetic acids. The results indicate weak O···H forces in the carboxylic acids and considerably stronger O···H forces in the percarboxylic acids.

Introduction

The planar configuration of monomeric carboxylic acids, with the acidic hydrogen *cis* to the carbonyl oxygen,[1-7] must be due to some combination of π bonding between the carbon and oxygen atoms, steric effects, intramolecular hydrogen bonding, intramolecular dipole–dipole interactions, etc. Since the intramolecular forces, however they are classified, are part of the molecular potential function, the determination of force constants from vibrational frequencies is a method for investigating the nature and the magnitude of the forces responsible for this planar configuration. Formic, acetic, and trifluoroacetic acids were chosen as typical carboxylic acids for which adequate data are available, and as molecules small enough to be handled by the available computing equipment.[8] Performic and peracetic acids were also treated because the percarboxyl group is probably also planar and the extra oxygen permits an arrangement more favorable to hydrogen bonding.[9]

While vibrational analyses of some of these molecules have been done previously,[1,10,11] no provision was made for forces acting between the acid hydrogen and the carbonyl oxygen. This study includes O···H stretching and additional bending coordinates.

Data and Computation

The models used for the carboxyl and percarboxyl groups are shown in Figures 1 and 2 and the parameter values are given in Table I. The models and values are based upon electron diffraction data,[3,5] microwave data,[2,6] and an assumed percarboxyl structure.[8] It is also assumed that the carboxyl group is identical in the three carboxylic acids and that the methyl and trifluoromethyl groups are tetrahedral. The percarboxylic acid problems were simplified by replacing the methyl group of peracetic acid with a single particle

Table I: Structural Parameters of Molecules Studied

Bond description	Length, A	Angle description	Angle, degrees
C—C	1.54	R—C=O	125
C—F	1.35	R—C—O	110
C—H	1.09	C—O—H	107
C—O	1.36	C—O—O	105
C=O	1.25	O—O—H	100
O—H	0.97		
O—H (per acids)	1.02		
O—O	1.49		

(1) T. Miyazawa and K. S. Pitzer, *J. Chem. Phys.*, **30**, 1076 (1959).
(2) G. H. Kwei and R. F. Curl, Jr., *ibid.*, **32**, 1592 (1960).
(3) I. L. Karle and J. Karle, *ibid.*, **22**, 43 (1954).
(4) J. H. N. Loubser, *ibid.*, **21**, 2231 (1953).
(5) J. Karle and L. O. Brockway, *J. Am. Chem. Soc.*, **66**, 574 (1944).
(6) R. E. Kagarise, *J. Chem. Phys.*, **27**, 519 (1956).
(7) M. Davies and O. Thomas, *Discussions Faraday Soc.*, **9**, 335 (1950).
(8) IBM 1620-I computer with 40,000 digits of core memory.
(9) P. A. Giguere and A. W. Olmos, *Can. J. Chem.*, **30**, 821 (1952).
(10) (a) O. Thomas, *Discussions Faraday Soc.*, **9**, 339 (1950); (b) K. Nakamoto and S. Kishida, *J. Chem. Phys.*, **41**, 1554 (1964).
(11) R. Blinc and D. Hadzi, *Spectrochim. Acta*, **12**, 82 (1959).

Table II: Force Constants[a] for Carboxylic and Percarboxylic Acids

Coord no.	Bonds	Molecules HCOOH	CH_3COOH	CF_3COOH	HCOOOH	CH_3COOOH
1	R—C	4.728	4.784	4.958	4.819	3.924
2	C=O	9.609	9.451	9.925	9.004	9.293
3	C—O	5.203	5.046	5.609	5.453	5.200
4	O—H	7.162	7.265	7.238	5.910	5.659
5	O···H	0.011	0.094	0.005	0.660	0.525
13	O—O				4.284	2.832
...	C—H or C—F	4.728	4.876	5.657	4.819	
1	C—C		4.784	4.958		3.924
9 or 10	C—O—H or (O—O—H)	0.744	0.736	0.847	0.488	0.375
8	O=C—O	2.125	1.128	0.830	2.302	1.545
9	C—O—O				0.729	0.762
10 or 11	O—H···O	0.0	0.0	0.0	0.108	0.191
11 or 12	C=O···H	0.0	0.0	0.0	0.961	1.307
...	H—C—H or F—C—F		0.518	1.220		
...	H—C—C or F—C—C		0.716	1.121		
6	R—C=O	0.602	1.734	1.627	0.612	1.747
7	R—C=O	0.702	1.511	1.225	0.622	1.657
...	R—C out-of-plane wag	0.387	0.894	0.702		
...	C—CX_3 torsion		0.027	0.027		
...	COOH out-of-plane bend	0.496	0.653	0.582		
1, 3	R—C/C—O		1.106	0.341		1.005
2, 3	C=O/C—O	−0.365				
...	C—F/C—F			1.665		
...	C—C/C—F			1.024		
3, 13	C—O/O—O				−0.753	
1, 8	R—C/O=C—O					−0.593
3, 7	C—O/R—C—O	0.328	0.510			0.134
3, 9	C—O/C—O—H	−0.425	0.138			
2, 9	C=O/C—O—H	0.112				
...	R—C/H—C—O		0.434			
...	H—C—C/H—C—C		−0.009			
...	R—C wag/COOH out-of-plane	−0.132	0.117	0.223		

[a] Units are mdynes/A for stretching constants, mdyne A/(radian)^2 for bending constants, and mdynes/radian for bend–stretch interaction constants.

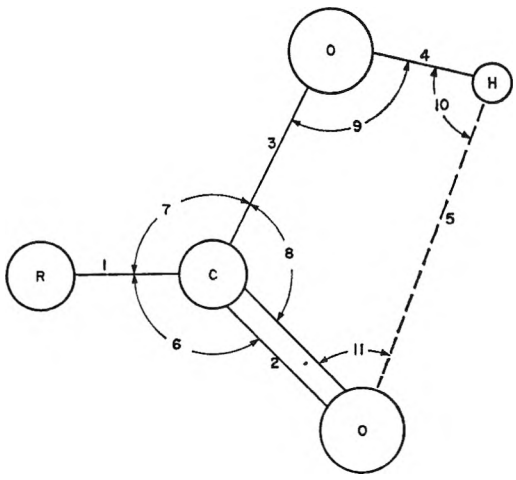

Figure 1. Carboxylic acid coordinates.

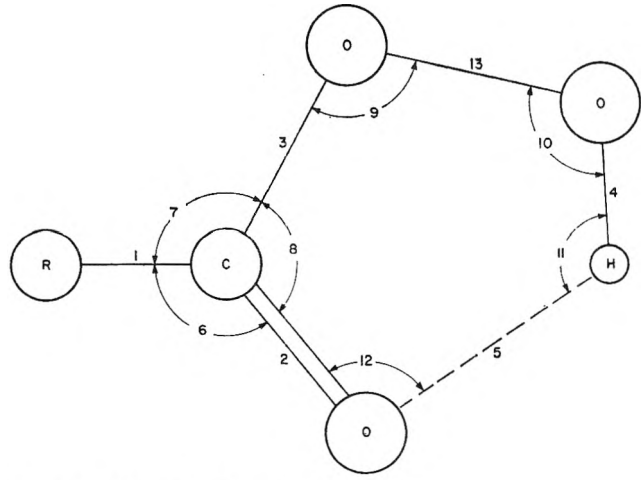

Figure 2. Percarboxylic acid coordinates.

Table III: Selected Force Constant Values[a]

Bond	Molecule	Value	Source
O—H stretch	RCOOH	7.2	This work
	RCOOOH	5.8	This work
	RCOOH	6.9*	*b*
	$(RCOOH)_2$	4.7*	*c*
	HNO_3	7.1	*d*
	HCO_3^- (cryst)	3.2*	*e*
	HCO_3^-	6.5	*f*
	CH_3OH	7.6	*g*
	H_2O	8.1	*h*
	H_2O_2	7.3	*i*
O···H stretch	RCOOH	0.06	This work
	RCOOOH	0.6	This work
	$HOOCCH{=}CHCO_2^-$	1.1*	*j*
	$(RCOOH)_2$	0.4*	*c*
	HCO_3^- (cryst)	0.76*	*e*
C=O stretch	RCOOH	9.7	This work
	RCOOOH	9.2	This work
	RCOOH	11.2*	*b*
	$(RCOOH)_2$	10.0*	*c*
	H_2CO	12.4	*k*
	HCO_3^-	9.1	*f*
	...	11.8–13.4	*l*
C—O stretch	RCOOH	5.3	This work
	RCOOOH	5.3	This work
	RCOOH	4.6*	*b*
	$(RCOOH)_2$	4.0*	*c*
	HCO_3^-	5.45 ± 0.15	*f*
	CH_3OH	5.15	*g*
	...	5.0–5.8	*k*
X—O—H bend (X = C, O, or H)	RCOOH	0.8	This work
	RCOOOH	0.44	This work
	$HOOCCH{=}CHCO_2^-$	0.1	*j*
	HCO_3^-	0.84	*f*
	HNO_3	0.88	*d*
	CH_3OH	0.79	*g*
	H_2O	0.70	*h*
	H_2O_2	0.90	*i*

[a] Values are rounded and averaged. Units are the same as in Table II. Values followed by * are from Urey–Bradley force fields. [b] Ref 10b. [c] Ref 16. [d] G. E. McGraw, D. L. Bernitt, and I. C. Hisatsune, *J. Chem. Phys.*, **42**, 237 (1965). [e] K. Nakamoto, Y. A. Sarma, and H. Ogoshi, *ibid.*, **43**, 1177 (1965). [f] Ref 18. [g] Ref 14. [h] T. Oka and Y. Morino, *J. Mol. Spectry.*, **8**, 9 (1962). [i] P. A. Giguere and O. Bain, *Can. J. Chem.*, **56**, 340 (1951). [j] K. Nakamoto, Y. A. Sarma, and G. T. Behnke, *J. Chem. Phys.*, **42**, 1662 (1965). [k] T. Oka and Y. Morino, *J. Phys. Soc. Japan*, **16**, 1235 (1961). [l] Ref 12, p 175.

of mass 15.035 and treating only the in-plane vibrations.

The bond coordinates for in-plane motions are shown in Figures 1 and 2. The only unusual feature is that the acid hydrogen atom is treated as equivalent to the other atoms in a four (carboxyl)- or five (percarboxyl)-membered ring system. All the bond coordinates are listed in Table II with the final values of the force constants. For the out-of-plane coordinate of the carboxyl group, a bending of the four-membered ring was chosen instead of the usual torsion coordinate in order to avoid making an early judgment as to the kind of motion involved.

The Wilson F and G matrix method[12] was used with a valency force field. G matrix formulation, solution of the secular equations, and determination of the best values of the force constants were done by digital

(12) E. B. Wilson, Jr., J. C. Decius, and P. C. Cross, "Molecular Vibrations," McGraw-Hill Book Co., Inc., New York, N. Y., 1955.

Table IV: Calculated and Observed[a] Frequencies of Formic Acid

Assignment	HCOOH		HCOOD		DCOOH		DCOOD	
	Obsd	Calcd	Obsd	Calcd	Obsd	Calcd	Obsd	Calcd
O—H stretch	3570	3583	2632	2613	3570	3584	2632	2613
C—H stretch	2943	2958	2948	2959	2220	2224	2232	2223
C=O stretch	1770	1796	1772	1776	1756	1747	1742	1722
H—C bend	1387	1383	...	1367	970	972	1040	1034
C—O—H bend	1229	1244	990	975	...	1240	945	934
C—O stretch	1105	1125	1178	1172	1143	1152	1171	1161
H—C out-of-plane	1033	1035	...	1033	...	870	873	871
COOH out-of-plane	669	674	529	524	661	665	515	508
O=C—O bend	638	633	573	569	632	631	569	568

[a] Observed frequencies from ref 15 except for two lowest frequencies of each molecule which are from T. Miyazawa and K. S. Pitzer, *J. Chem. Phys.*, **32**, 1592 (1959).

Table V: Calculated and Observed[a] Frequencies of Acetic Acid

Assignment	CH_3COOH		CH_3COOD		CD_3COOH		CD_3COOD	
	Obsd	Calcd	Obsd	Calcd	Obsd	Calcd	Obsd	Calcd
O—H stretch	3546	3610	2653	2632	3640	3610	2660	2632
C—H stretch	3027	3028	3021	3032	2225	2256	2237	2257
C—H stretch	2935	2910	2940	2910	2111	2097	2111	2097
C=O stretch	1770	1777	1770	1770	1760	1767	1760	1760
H—C—H bend	1431	1439	1434	1440	1060	1037	...	1037
H—C—C and H—C—H bends	1403	1406	1403	1403	1065	1056	1060	1058
C—O—H bend	1284	1316	974	968	1335	1327	1000	964
C—O stretch	1192[b]	1219	1284	1273	1217	1221	1280	1282
H—C—C bend	1068[b]	1053	1057[b]	1053	820	814	812	813
CH_3 rock	996	968	950	940	926	968	925	940
C—C stretch	846[b]	853	837[b]	822	790	802	785	781
O—H rock	650	673	546	509	...	673	...	509
CH_3—C bend	564	561	564	559	...	495	...	486
O=C—O bend	536	536	535	519	...	531	...	532
CH_3 torsion	...	221	...	221	...	167	...	167

[a] Observed frequencies from W. Weltner, *J. Am. Chem. Soc.*, **77**, 3941 (1955), except where indicated otherwise. [b] J. K. Wilmshurst *J. Chem. Phys.*, **25**, 1171 (1956).

computer, using modifications of Schachtschneider's FORTRAN programs.[13] The main program is designed to adjust the values of the force constants until calculated and observed frequencies are in the best agreement possible. The adjustment of force constants was done independently for each molecule so that, for example, each value for the O–H stretching constant represents an independent determination. The only constant transferred from another molecule was the torsion constant for the methyl and trifluoromethyl groups which was taken from methanol.[14]

The percarboxylic acids posed a problem since the data are insufficient to determine even the diagonal force constants uniquely. The calculations for performic acid illustrate the method used. Eight frequencies are available and there are thirteen diagonal force constants to be found. A set of starting values of the thirteen constants was chosen, and ten of these were held fixed while the best values of the three "variable" constants were found. Then these three were fixed for the next step, and three other constants became "variables" and their best values were found. This was continued with different combinations of constants held fixed until calculated and observed frequencies agreed. This procedure cannot lead to reliable values of all the constants, and the values found

(13) J. H. Schachtschneider, Technical Report No. 263-62, Shell Development Corp., Emeryville, Calif., 1962.

(14) C. M. Haas, Thesis, Ohio University, 1965.

will in general be very much dependent upon the starting values chosen. Nevertheless, the results can give significant values for constants (such as O–H or C–H stretchings) of groups with normal vibrations that are separable or almost separable from the other vibrations of the molecule.

Results and Discussion

Table II lists the final values of the force constants and Table III gives selected force constants from this and other studies. The observed and calculated frequencies and assignments are listed in Tables IV through VIII.

Table VI: Calculated and Observed[a] Frequencies of Trifluoroacetic Acid

	CF_3COOH		CF_3COOD	
Assignment	Obsd	Calcd	Obsd	Calcd
O—H stretch	3587	3603	2648	2626
C=O stretch	1826	1836	1823	1826
C—O stretch	1415[b]	1417	...	1412
C—O—H bend	1300	1307	1039	1026
C—F stretch	1244	1248	1243	1249
C—F stretch	1182	1170	1187	1169
C—C stretch	825	821	798	798
CF_3 rock	781[b]	790	781[b]	778
O—H rock	661[b]	654	...	490
O=C—O bend	580[b]	585	...	558
CF_3—C bend	507[b]	500	...	497
F—C—F bend	436[b]	440	...	438
F—C—F and F—C—C bends	...	326	...	324
F—C—C bend	...	271	...	267
CF_3 torsion	...	53	...	53

[a] Observed frequencies from N. Fuson, M. Josien, E. A. Jones, and J. R. Lawson, *J. Chem. Phys.*, **20**, 1627 (1952), unless indicated otherwise. [b] R. E. Kagarise, *ibid.*, **27**, 519 (1957).

Table VII: Calculated and Observed[a] Frequencies for Performic Acid

	HCOOH	
Assignment	Obsd	Calcd
O—H stretch	3367	3367
C—H stretch	2987	2987
C=O stretch	1739	1739
O—O—H bend	1453	1453
H—C bend	1340	1340
C—O stretch	1243	1243
O—O stretch	859	859
O=C—O bend	810	810
Hydrogen bond stretch	...	437

[a] Reference 9.

Table VIII: Calculated and Observed[a] Frequencies for Peracetic Acid

	CH_3COOOH	
Assignment	Obsd	Calcd
O—H stretch	3310	3310
C=O stretch	1760	1760
O—O—H bend	1450	1450
C—O stretch	1248	1249
O—O stretch	868	868
C—C stretch	861	861
O=C—O bend	656	656
CH_3—C bend	...	513
Hydrogen bond stretch	...	411

[a] Reference 9.

The agreement between calculated and observed frequencies is satisfactory except for the methyl group rocking and the out-of-plane motion of the carboxyl group in acetic acid. The perfect agreement for the percarboxylic acids is the result of having more force constants to adjust than the number of frequencies. The assignments for formic acid are in general agreement with previous assignments by Miyazawa and Pitzer,[1] Millikan and Pitzer,[15] and Nakamoto and Kishida.[10b] The acetic acid assignments differ from Nakamoto and Kishida only in a reversal of the assignments for the 1284- and 1192-cm^{-1} bands.

The three sets of carboxyl group constants show some significant differences, especially in bending and interaction constants, but the O···H, C=O, C—O, and O—H stretching constants are sufficiently consistent in value that it is appropriate to consider the three molecules together. The O···H stretching constant is the most obvious measure of hydrogen-bonding forces, and the low values (compared to formic and acetic acid dimers)[16] indicate either weak forces or a situation in which opposing forces leave only a small resultant. The small C=O···H and O—H···O bending constants seem to confirm this. The O—H stretching constants have values slightly lower than would be expected if there were no hydrogen bonding.[17]

The C=O and C—O constants are of interest as indicators of the carbon–oxygen bonding. The C=O constants are roughly midway in value between single- and double-bond constants. This can be easily ex-

(15) R. C. Millikan and K. S. Pitzer, *J. Chem. Phys.*, **27**, 1305 (1957).

(16) K. Nakamoto and S. Kishida, *ibid.*, **41**, 1558 (1964).

(17) G. Herzberg, "Infrared and Raman Spectra of Polyatomic Molecules," D. Van Nostrand Co., Inc., New York, N. Y., 1951, p 193.

plained in terms of a delocalization of π electrons so that the C=O bond has only partial double-bond character. A shift of π electrons from one bond into another will presumably decrease the first stretching constant and increase the second, compared to isolated double and single bonds, respectively. However, a simple comparison of carboxyl group force constants with single-bond constants from alcohols and ethers may not be appropriate since both σ and π bondings change in going from tetrahedral to planar configuration. Therefore, it is interesting that the C–O force constants all have values within the range expected for carbon–oxygen single bonds. The bicarbonate ion (HCO_3^-) should have bonding similar to the carboxyl group but with π electrons delocalized among three carbon–oxygen bonds. The reported C–OH stretching constant[18] for the bicarbonate ion is close to the average of the C–O constants from the three carboxylic acids.

The inertia defect[19] was calculated for the ground state of formic acid (HCOOH); the calculated and observed[20] values are 0.07418 and 0.07709 amu/A^2, respectively.

Despite the uncertainties, the O···H, O—H, C—O, and C=O stretching constants for the two percarboxylic acids are consistent and appropriate for molecules with strong intramolecular hydrogen bonding. The carbon–oxygen constants are also in agreement with the values from the carboxylic acids. The inconsistencies of some of the other constants serve as a reminder that the data for the percarboxylic acids are not sufficient to define the potential functions.

Summary

A valency force field, including constants for hydrogen bonding coordinates, has been found for each of the five acids studied. The values of the force constants indicate strong intramolecular hydrogen bonding in monomeric percarboxylic acids, weaker hydrogen bonding in the monomeric carboxylic acids, and delocalization of π electrons in the O=C—O groups. The partial double-bond character of the C—OH bond accounts for the planarity of the carboxyl group, but the bond does not show a significant increase in force constant compared to carbon–oxygen single bonds in other molecules.

Acknowledgment. The authors thank the Ohio University Research Committee for financial support, the staff of the Numerical Computation Laboratory at the Ohio State University for their generous assistance, Dr. Jerry Schachtschneider for his computer programs, and especially the National Science Foundation whose grant supporting the Ohio University Computer Laboratory made this work possible.

(18) D. L. Bernitt, K. O. Hartman, and I. C. Hisatsune, *J. Chem. Phys.*, **42**, 3553 (1965).

(19) T. Oka and Y. Morino, *J. Mol. Spectry.*, **6**, 472 (1961).

(20) R. Wertheimer, *Arch. Sci.* (Geneva), **10**, 184 (1957).

The Dielectric Constant of Water and Heavy Water between 0 and 40°

by G. A. Vidulich,[1] D. F. Evans, and R. L. Kay[2]

Mellon Institute, Pittsburgh, Pennsylvania 15213 *(Received August 29, 1966)*

The dielectric constant of H_2O and D_2O was determined at several temperatures between 0 and 40° using a new design of capacitance cell and a transformer ratio arm bridge in the frequency range 0.5–100 kHz. The electrodes of the cell were completely guarded and shielded and consisted of platinum films fused onto the surfaces of two concentric Pyrex cylinders. Water of extremely low conductance (0.6–0.8 $\times$ 10^{-7} ohm^{-1} cm^{-1} at 25°) was used. The values at 25° for ϵ_{H_2O} and ϵ_{D_2O} were 78.39 and 78.06, respectively. The equations $\log \epsilon_{H_2O} = 1.94404 - 1.991 \times 10^{-3}t$ and $\log \epsilon_{D_2O} = 1.94275 - 2.013 \times 10^{-3}t$ fitted the data to better than 0.05% for t between 0 and 40°. A detailed comparison is made with the more recent work reported in the literature.

Introduction

The dielectric constants of liquids and their temperature dependence are of considerable importance in the electrochemical investigation of electrolytes. Although dielectric constants generally can be measured with considerable ease, the relatively high conductance of liquids of electrochemical interest introduces a complication that can result in serious errors. We have designed and constructed cells[3] for the measurement of absolute dielectric constants in which polar liquids can be maintained at an exceedingly low conductivity. These cells are of the three-terminal or guarded-electrode type, are completely shielded, and are ideally suited for rapid measurements on transformer bridges.

Owing to its importance both as a solvent and as a secondary dielectric standard, the absolute dielectric constant of water was reinvestigated. Recent precise determinations[4,5] of the dielectric constant of H_2O at several temperatures disagree somewhat, particularly at lower temperatures. Both of these results are significantly lower than the generally accepted but older values reported by Wyman and Ingalls.[6] Our results are in best agreement with the data of Owen[5] and the unpublished data of Lees.[7] We have reported preliminary values[8] of our results, but here we report our final values after an extensive investigation of bridge errors and the effect of varying the cell design and the cell constant.

Our measurements were extended to D_2O at 0, 5, 25, and 40°. The only other extensive investigation of the absolute dielectric constant of D_2O and its temperature dependence was by Malmberg,[9] using the same apparatus employed previously for H_2O,[4] thereby permitting another comparison with our method. Our data for the ratio $\epsilon_{H_2O}:\epsilon_{D_2O}$ are in better agreement with those of Wyman and Ingalls[6] than with those of Malmberg.

Apparatus and Experimental Procedure

Cells. Full particulars concerning the design and construction of the cells have been published elsewhere.[3] Essentially, the cells consisted of concentric glass cylinders with platinum-film electrodes fused onto the inner surface of the outer cylinder (the high-potential electrode) and the outer surface of the inner cylinder. The platinum film on the inner cylinder extends from the sealed bottom right through the standard type joint joining the two cylinders. The guarded or low-potential electrode is separated from

(1) Adapted in part from a Ph.D. Thesis submitted to Brown University, 1964.

(2) To whom all correspondence should be addressed.

(3) G. A. Vidulich and R. L. Kay, *Rev. Sci. Instr.*, **37**, 1662 (1966).

(4) C. G. Malmberg and A. A. Maryott, *J. Res. Natl. Bur. Std.*, **56**, 1 (1956).

(5) B. B. Owen, R. C. Miller, C. E. Milner, and H. L. Cogan, *J. Phys. Chem.*, **65**, 2065 (1961).

(6) J. Wyman, Jr., and E. N. Ingalls, *J. Am. Chem. Soc.*, **60**, 1182 (1938).

(7) W. L. Lees, Ph.D. Thesis, Harvard University, 1949.

(8) G. A. Vidulich and R. L. Kay, *J. Phys. Chem.*, **66**, 383 (1962).

(9) C. G. Malmberg, *J. Res. Natl. Bur. Std.*, **60**, 609 (1958).

the guard electrodes on either side by narrow gaps less than 0.15 mm wide scratched through the platinum film. Conventional coaxial cables and BNC connectors are used to join the outermost electrode to the high-potential side of the bridge (see below), the guarded electrode to the low-potential or detector side of the bridge, and the guard electrodes to the ground. The complete outer surface of the cell is electrically shielded by a silver coating and protected by a thin vinyl coating.

The significant dimension of the various cells used in this investigation are given in Table I, where r_2 (cm) and r_1 (cm) are the radii of the high- and low-potential electrodes, respectively, and l (cm) is the length of the low-potential or guarded electrode. C_0 (pf) is the approximate vacuum capacitance of the cell.

Table I: Cell Dimensions

Cell	r_2, cm	r_1, cm	l, cm	C_0, pf
A	1.2	0.8	1.5	2.2
B	1.15	0.8	1.7	2.5
C	1.2	0.9	2.4	4.6
D	1.2	0.9	2.5	4.6
E	1.2	0.9	3.0	5.4
F	1.2	0.8	6.0	8.3
G	1.2	0.8	6.3	8.8

Bridges. The results presented here for H_2O can be divided into two sets of data—one set measured in the Chemistry Department at Brown University using a modified Cole–Gross bridge[10] (CG bridge) and a second set measured at the Mellon Institute using a General Radio Type 1615A capacitance bridge (GR bridge). The type of bridge used is the only feature distinguishing these two sets of data. Both of these Wheatstone type bridges have inductively coupled, or transformer, ratio arms[11] which permit the determination of small capacitances with considerable accuracy. They are ideally suited in connection with guarded or three-terminal electrodes since all admittances to ground are reflected equally across the mutual windings of the ratio arms and consequently do not affect the bridge balance. This eliminates the need for a lead correction, at times a source of serious error in other methods.

A Hewlett–Packard Type 200CD oscillator, a Rohde and Schwarz Type UBM tunable amplifier, and a Hewlett–Packard Model 120AR oscilloscope were used in conjunction with both bridges.

The modified CG bridge has been described in detail by Vidulich,[1] and only the schematic shown in Figure 1 is included here. A potential is applied by the oscillator to the transformer ratio arms, M and M′, containing a grounded center tap. Zero balance of the bridge is obtained by the small air capacitors, C_1 and C_1'. Several trimming capacitors and resistors are not shown. Conductance balance is obtained by the "wye" network consisting of a metal film resistor, R_1, and a ten-turn, 200-ohm, precision helipot, R_2. By selecting R_1 = 20 kilohms, 200 kilohms, or 2 megohms, conductance ranges of 50, 5, or 0.5 μmho were obtained. R_2' is a fixed 200-ohm resistor that equalizes the transformer loading. The capacitance of the cell containing the high-potential electrode, H, the guarded electrode, L, and the grounded guard electrodes, G, is balanced by two General Radio Type 1422 capacitances[12] connected externally in parallel. These precision capacitors had ranges from 5 to 110 pf and from 50 to 1100 pf, permitting capacitances as high as 1200 pf to be measured to 0.005 pf. The sensitivity of the bridge is better than 0.01% or 1×10^{-4} pf, whichever is greater.

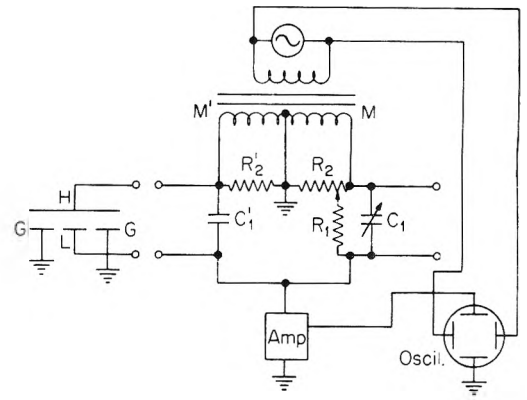

Figure 1. Schematic diagram of Cole–Gross (CG) bridge circuit.

Although the measurement of absolute dielectric constants does not require absolute capacitance measurements, it is necessary to calibrate the two precision capacitors relative to each other. This was accomplished in 1-pf steps for the smaller capacitor and 100-pf steps for the larger capacitor by an iteration procedure using a 1-pf standard capacitor and a dummy variable capacitor. No backlash was detected when turning the dial in either direction, and the maximum deviation from linearity was found to be 0.2% for capacitances greater than 10 pf, the minimum capaci-

(10) R. H. Cole and P. M. Gross, Jr., *Rev. Sci. Instr.*, **20**, 252 (1949).

(11) The advantages and limitations in the use of transformer ratio arms are discussed in the *General Radio Experimenter*, **36**, No. 8, 4 (1962).

(12) *General Radio Experimenter*, **35**, No. 8, 10 (1961).

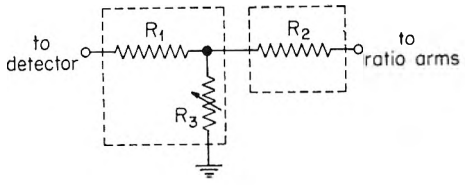

Figure 2. Diagram of auxiliary conductance network.

tance measured directly in the determination of cell constants. This iteration procedure, as well as the process of zeroing the bridge, was aided considerably by switches (not shown in Figure 1) which permitted as many as two capacitors on either side of the bridge to be switched in or out of the circuit.

Although the GR bridge is also a transformer ratio arm bridge, it differs in a number of essential features from the CG bridge. Instead of externally connected variable capacitors, the GR bridge contains eight highly precise fixed capacitors that can be connected internally to any one of ten equally placed taps on one side of the ratio arm. The unknown capacitance can also be attached at any one of four taps on the opposite side of the ratio arms producing multipliers of 1, 10, 10^2, and 10^3. The bridge gives a six-figure digital readout for capacitance in the range 1–10^6 pf. Although this bridge contains a "wye" resistance network of essentially the same type as in the CG bridge, the range was not correct for our purpose. It was necessary to attach an external auxiliary conductance network as shown in Figure 2 for a conductance range of 0.1–10 μmhos. R_1 and R_2 are both 10-kilohm metal film resistors situated in separate shielded containers to minimize the capacitance across the resistors, and R_3 is a 1-kilohm helipot. The accuracy claimed for this bridge is $0.01\% + 3 \times 10^{-5}$ pf for the frequency and capacitance ranges used in our measurements ($f \leq 20$ kHz; $C < 10^3$ pf).

Cell Constants. The variable capacitances used in conjunction with the Cole–Gross bridge did not extend to low enough values for the direct measurement of the capacitance of the cells filled with dry nitrogen, although the bridge sensitivity was sufficient for that purpose. Owing to this latter fact, the cell constants were obtained by an iteration procedure so that the cell constant was obtained by the actual measurement of over 10 pf. This procedure involved balancing the cell and an auxiliary variable capacitor against the precision variable capacitor in a number of steps until 10 pf was reached. Reproducible cell constants could be obtained only if the cell was thoroughly dried. For this purpose, the cell was placed in a vacuum chamber that was restored to atmospheric pressure repeatedly with dry nitrogen. This procedure was repeated until the cell constant would be reproduced to 0.05%. The cell constant under these conditions is given[13] by $C_0 = C_{N_2}/1.0005$. No difference to within 0.01% was observed in the cell constant when measured at temperatures between 0 and 40° in a water bath or when measured outside the bath in air, demonstrating the excellence of the electrical shielding. This negligible temperature dependence is in keeping with the coefficient of expansion of Pyrex glass.

The cell constant could be determined directly on the General Radio bridge without the iteration procedure owing to the extended capacitance range available. If the cell was dried as outlined above, the cell constant was reproduced in repeated measurements to better than 0.02% and the frequency dependence was established to be less than 0.02% for $f \leq 20$ kHz.

Procedure. In order to obtain reproducible results, it was necessary to clean the cells with chromic acid solution followed by a leaching with conductivity water until the specific conductance of fresh samples of conductivity water at 25° was less than 8×10^{-8} ohm^{-1} cm^{-1} and increased by less than 10% per hour. This process generally required 2 days if care was exercised in excluding the cleaning solution from the standard taper joint at the top of the cell. All the results reported here were carried out on water samples with specific conductances between 0.6 and 0.8×10^{-7} ohm^{-1} cm^{-1} at 25° as measured in the dielectric cell.

The measurements for H_2O were carried out in the following manner. The leached cell was filled with water by attaching it directly to the ion-exchange column. The cell was thermostated in a water bath to within ±0.01° of the stated temperature as determined by a platinum resistance thermometer. After measuring the capacitance of the cell in the frequency range 1–200 kHz, the cell was dried and the cell constant redetermined. This procedure was repeated until the cell constant was reproduced to better than 0.05% and the water capacitance to better than 0.02%.

The D_2O measurements were carried out in a similar manner except that the cell was filled in a drybox. The following sequence of measurements was made: H_2O, N_2, D_2O, N_2, and H_2O, so that a direct comparison between D_2O and H_2O could be made. The result for D_2O was not recorded unless those for H_2O and N_2 agreed to 0.02 and 0.05%, respectively.

Normal Water (H_2O). A high grade of conductivity

(13) A. A. Maryott and F. Buckley, National Bureau of Standards Circular 537, U. S. Government Printing Office, Washington, D. C., 1953.

water with a specific conductance between 0.6 and 0.8 $\times 10^{-7}$ ohm^{-1} cm^{-1} was obtained by passing distilled water through a 4-ft mix-bed ion-exchange column (Reagent Grade Amberlite MB-1).

Heavy Water (D_2O). Conductivity grade D_2O was prepared by passing distilled D_2O (Atomic Energy Commission normal O^{18} content) through a deuterated mix-bed ion-exchange column in a drybox as described by Swain and Evans.[14] The first 100 ml passed through the column was discarded if the column was not in regular use. The final product had a specific conductance of 0.4–1.0 $\times 10^{-7}$ ohm^{-1} cm^{-1} and a density of 1.10439 g ml^{-1}, indicating an isotopic purity[15] of 99.89%.

Errors and Corrections

A number of corrections were applied to the measured capacitances. The calibration corrections for the General Radio Type 1422 variable capacitors have already been described. The capacitors in the GR bridge required no calibration.

A correction must be applied for the effective capacitance of the resistors in the conductance balancing network. The magnitude of this correction in the CG bridge was determined by measuring liquids of varying conductance and known capacitance on various overlapping conductance ranges. A consistent set of corrections was obtained that varied linearly with the setting of R_2 in Figure 1, but they changed the dielectric constant by less than 0.01 unit. The effective capacitance in the auxiliary conductance network used with the GR bridge as shown in Figure 2 was measured for each 0.1-μmho step directly on the bridge by assuming that the "wye" resistance network built into the bridge contained no residual capacitance. The correction to the measured capacitance due to the capacitance of the auxiliary resistors amounted to approximately 0.1% at most and could be determined to at least 10%. The effective capacitance of the resistors in the "wye" network in the bridge was determined in the following way. Cells A and D were filled with samples of water with increasing conductance covering the range 0.6–12 $\times 10^{-7}$ ohm^{-1} cm^{-1}. The measured capacitances for cell A after correction as outlined above are shown in Figure 3 as a function of the reciprocal frequency. The slight increase in capacitance as the frequency decreases to low values is due to electrode polarization and increases in magnitude as the conductance increases. The sharp increase at higher frequencies is due to lead inductance and ratio arm tapping errors. The significant feature of this plot is that the extrapolated value C_∞, which eliminates polarization errors, is different for each curve and increases

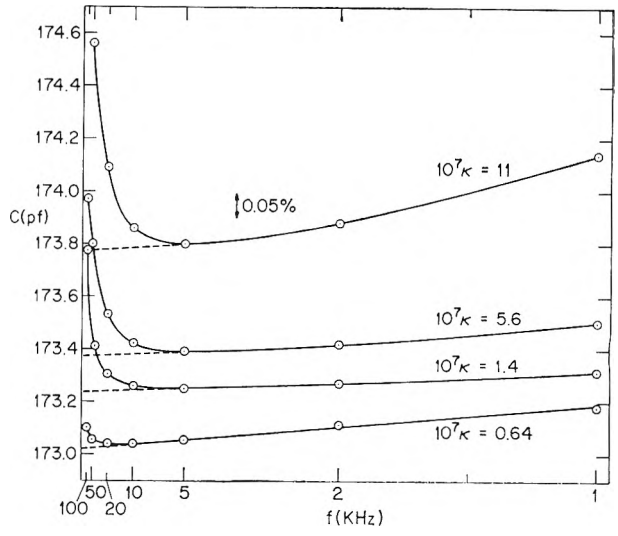

Figure 3. Frequency dependence of the capacitance of cell A containing H_2O of various conductances.

with increased conductance. If an effective capacitance of -2.5×10^{-3} pf is attributed to the full-scale resistance network in the bridge and the calibration curve for the auxiliary conductance network is recalculated, these values of C_∞ can be corrected to give the constant values given in the third and sixth columns of Table II. The constancy of the corrected C_∞ for both cells indicated that our calibration curves are valid and that we have successfully determined all residual capacitances associated with the networks used to balance the cell conductance.

Table II: The Effect of -2.5×10^{-3} pf Effective Capacitance in the General Radio Type 1615A Bridge Conductance Network Resistors

$10^7\kappa$	C_∞	Cor C_∞	$10^7\kappa$	C_∞	Cor C_∞
	Cell A			Cell D	
11.0	173.77	173.07	12.0	362.50	360.87
5.6	173.37	173.02	8.8	362.05	360.95
1.4	173.24	173.03	3.2	361.34	360.91
0.68	173.04	173.00	0.83	361.05	360.94
0.64	173.02	172.98	0.76	361.05	360.95

(14) C. G. Swain and D. F. Evans, *J. Am. Chem. Soc.*, 88, 383 (1966). We are indebted to Professor Swain for donation of this resin which had been equilibrated with D_2O for 6 months. The removal of all exchangeable protons had been followed by density measurements.

(15) I. Kirshenbaum, "Physical Properties and Analysis of Heavy Water," McGraw-Hill Book Company, Inc., New York, N. Y., 1951, p 14.

Owing to the extremely low conductance of the water used in this investigation, electrode polarization was kept to a minimum and extrapolation to infinite frequency was extremely easy, as shown in the bottom curve of Figure 3. The total capacitance changes by less than 0.1% between 1 kHz and the extrapolated value at infinite frequency. The extremely low polarization correction required for the CG bridge values has already been noted.[8] Similar results were obtained for all the runs for both H_2O and D_2O at every temperature. It should be pointed out that failure to correct for the lead inductance at high frequencies does not affect the linear extrapolation of the measured capacitance to infinite frequency. The fractional change in capacitance due to this inductive effect is given by $\Delta C/C = (2\pi)^2 f^2 CL$. Vidulich[1] has shown that the lead inductance for these cells varies between 3 and 12 μhenries. At 20 kHz, the lead inductance can introduce less than 0.01% error in the measured values. The somewhat higher values shown in Figure 3 at high conductances are due to the tapping errors in the multiplier circuit of the GR bridge.

Possible errors associated with the dielectric cell such as improper guarding, end effects, and errors associated with the finite size of the gap between guard and guarded electrodes have been discussed in detail already.[3] It is necessary to state here only that it would appear that guard-gap errors constitute the limiting factor in determining the accuracy of the measurements. It has been shown that the guard gap in cell B could introduce an error of about 0.1%. The cells with longer guarded electrodes should introduce proportionately smaller errors.

Results

The results obtained for the dielectric constant of H_2O at several temperatures are given in Table III. The dielectric constants in columns ϵ_{CG} and ϵ_{GR} are the averages of several measurements on a number of cells measured on the CG and GR bridges, respectively. The ϵ_{GR} values are consistently 0.04 unit greater than ϵ_{CG}. We have no explanation for this difference, although it amounts approximately to what we estimate to be the uncertainty in our measurements. The final ϵ_{H_2O} is the average of ϵ_{CG} and ϵ_{GR}, or in those cases where only ϵ_{CG} was measured, it is equal to $\epsilon_{CG} + 0.02$ to compensate for the higher values obtained for ϵ_{GR} at the other temperatures. The difference between the final average ϵ_{H_2O} and that calculated from

$$\log \epsilon_{H_2O} = 1.94404 - 1.991 \times 10^{-3} t \qquad (1)$$

is given by $\delta\epsilon$ in the last column.

The average values of the dielectric constant of D_2O at different temperatures using cells, A, C, and E are given in Table IV. The difference between the measured ϵ_{D_2O} and that calculated from

$$\log \epsilon_{D_2O} = 1.94275 - 2.013 \times 10^{-3} t \qquad (2)$$

is given by $\delta\epsilon$ in the last column.

Table III: The Dielectric Constant of H_2O

t, °C	ϵ_{CG}	ϵ_{GR}	Final ϵ_{H_2O}	$\delta\epsilon$, eq 1
0	87.89	87.93	87.91	(0.00)
5	85.87	...	85.89	−0.03
10	(83.95)[a]	83.98	83.96	−0.01
15	(82.09)[b]	...	(82.11)	0.04
20	80.18	...	80.20	−0.01
25	78.37	78.41	78.39	(0.00)
40	73.17	...	73.19	0.01

[a] Interpolated from a plot of ϵ_{CG} *vs.* t. [b] Single determination.

Table IV: The Dielectric Constant of D_2O

t, °C	ϵ_{D_2O}	$\delta\epsilon$, eq 2
0[a]	87.65[a]	(0.00)
5	85.61	−0.03
25	78.06	0.00
40	72.84	0.02

[a] Supercooled D_2O, fp 3.8°.

The effect of varying the cell constant and the bridge can be seen in Figure 4 where, at each temperature, the differences between the ϵ obtained from each individual

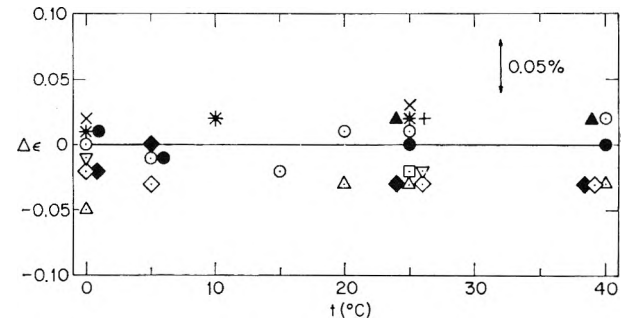

Figure 4. Illustration of the effect of cell constant and bridge on the measured ϵ. $\Delta\epsilon$ for the various cells given in Table I is defined by $\Delta\epsilon = \epsilon$(measured) − ϵ(eq 1). The subscripts CG and GR refer to the Cole–Gross and General Radio bridges, respectively. $\epsilon_{CG}(H_2O)$: ○, A; □, B; △, C; ◇, E; ⬡, F. $\epsilon_{GR}(H_2O)$: *, A; ×, D; +, G. $\epsilon_{CG}(D_2O)$: ●, A; ▲, C; ◆, E.

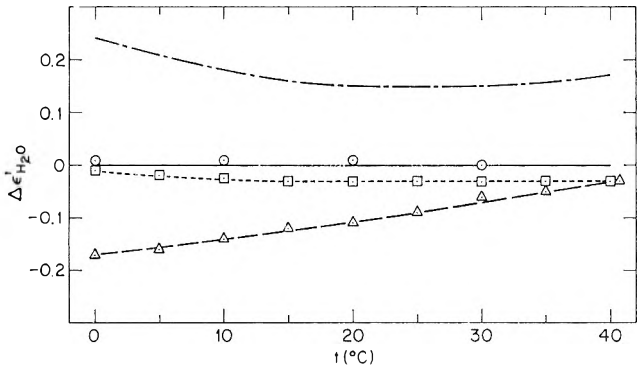

Figure 5. Comparison of the differences between the values of ϵ_{H_2O} obtained by various workers and those reported here, $\Delta\epsilon' = \epsilon$(lit.) $- \epsilon$(this research): △, NBS;[4] — — —, Wyman and Ingalls;[6] ○, Lees;[7] □, Owen.[5]

cell and the final average are plotted for each temperature. The D_2O results are included in this graph by the filled symbols. It can be seen that there is no definite trend in the differences that can be attributed to cell constant, but the slightly higher values obtained with the GR bridge are evident although they amount to less than 0.03%. The cell constants used varied by a factor of 4 and produced a total spread in ϵ of less than 0.06%.

Discussion

Our data for H_2O are compared to the results of other recent and precise investigations in Figure 5. Here the differences between the data of Wyman and Ingalls,[6] Owen and co-workers,[5] Lees,[7] and Malmberg and Maryott,[4] and our present data (eq 1) are plotted. We have not considered several earlier works owing to a general lack of experimental details or to the fact that a comparative method was used. Malmberg and Maryott have discussed some of these earlier investigations, particularly in respect to possible errors. Needless to say, there is considerable disagreement in these earlier results that is not always easily explained. Although the temperature dependence of the data of Wyman and Ingalls, obtained by a resonance method, is in good agreement with our own, their data are consistently higher than ours by more than 0.15 unit in ϵ. The much more precise data of Malmberg and Maryott[4] approach our own only at the higher temperatures, and at 0° their ϵ is 0.17 unit lower than our point. This is three times the estimated error in either set of measurements. The agreement between our data and the microwave data of Owen[5] and the data of Lees,[7] who also used a bridge method, is excellent at all temperatures, as can be seen in Figure 5. This agreement with an entirely different method and also with a similar method, the lack of any significant dependence of ϵ on cell constant, the use of two different bridges, the direct determination of the capacitance associated with the resistance networks, the extremely low-electrode polarization encountered due to the low conductance of the water used, and the excellent reproducibility of the measurements add considerably to the reliance to be placed on the accuracy of our data. Possibly the most significant difference between our measurements and those of Maryott and Malmberg is in the conductance of the water used. They used water of ten times greater conductivity and consequently encountered considerably greater electrode polarization. However, their correction for this effect was still small and will not explain the differences, particularly in the temperature coefficient. In the bridge method used in both investigations, errors tended to produce a lower value of ϵ, and on this basis our data are to be preferred. If anything, we believe our data to be on the low side due to errors associated with the finite size of guard gap required.[3]

The temperature dependence of our data for D_2O agrees well with the two precise determinations that have been reported,[6,9] but the absolute values differ significantly, as shown in Figure 6. Malmberg's data[9] are 0.1–0.15 lower than ours. Since Wyman and Ingalls[6]

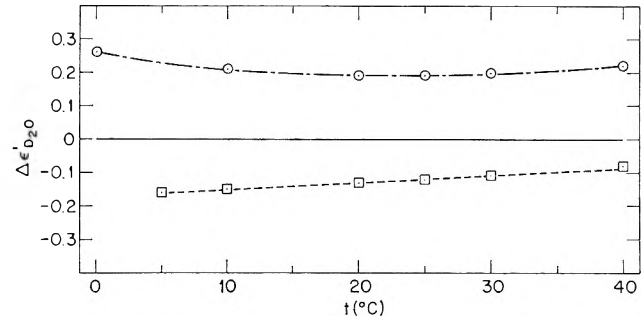

Figure 6. Comparison of the differences between the values of ϵ_{D_2O} obtained by other workers and those reported here, $\Delta\epsilon'_{D_2O} = \epsilon$(lit.) $- \epsilon$(this research): □, NBS;[9] ○, Wyman and Ingalls.[6]

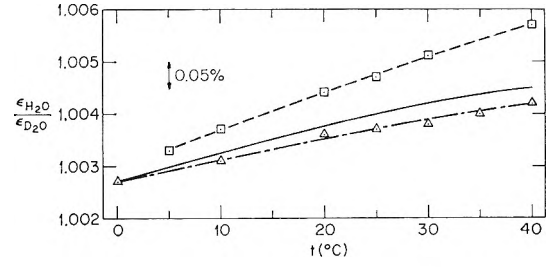

Figure 7. Comparison of $\epsilon_{H_2O}/\epsilon_{D_2O}$: □, NBS;[4,9] △, Wyman and Ingalls;[6] ———, this research.

determined only the ratio $\epsilon_{H_2O}:\epsilon_{D_2O}$, their value for ϵ_{D_2O} depends on their ϵ_{H_2O} data. A plot of this ratio, shown in Figure 7, shows their data for D_2O will be in good agreement with our own if our ϵ_{H_2O} are used. This ratio, using ϵ_{D_2O} of Malmberg[9] and ϵ_{H_2O} of Malmberg and Maryott,[4] differs by a small but significant amount (0.1%) from our ratio. There appears to be a consistent difference of about 0.15 unit in ϵ between our data for D_2O and H_2O and those measured at the National Bureau of Standards, with a difference in the temperature coefficient for H_2O that is difficult to explain.

Acknowledgment. The authors are indebted to Professor R. H. Cole of Brown University for the use of his laboratory for some of these measurements and for his interest and suggestions during the course of the work. This work was supported by the U. S. Atomic Energy Commission under Contract AT-(30-1)2727 and by the Office of Saline Water, U. S. Department of the Interior, under Contract No. 14-01-0001-359.

Electromotive Force Studies in Aqueous Solutions at Elevated Temperatures. VIII. The Thermodynamic Properties of Hydrochloric Acid–Lanthanum Chloride Mixtures[1]

by M. H. Lietzke and R. W. Stoughton

Chemistry Division, Oak Ridge National Laboratory, Oak Ridge, Tennessee *(Received September 19, 1966)*

The activity coefficient of HCl in HCl–$LaCl_3$ mixtures has been studied to 175°. At constant temperature and ionic strength, the logarithm of the activity coefficient of HCl in the mixtures varies linearly with the ionic strength fraction of $LaCl_3$ in conformity with Harned's rule. The activity coefficient of $LaCl_3$ in the mixtures was calculated by using the parameters describing the variation of the logarithm of the activity coefficient of HCl in the mixtures and those for the variation of the activity coefficient of $LaCl_3$ with ionic strength in pure $LaCl_3$ solutions at 25°.

Previous papers in this series have described our investigations into the thermodynamic properties of HBr–KBr,[2] HCl–NaCl,[3] and HCl–$BaCl_2$[4] mixtures over a wide range of temperature. The present study represents an extension of this work to a mixture containing a salt of the 3–1 valence type. Only a few such mixtures have been previously investigated, and these only at 25°. Randall and Breckenridge[5] observed that in mixtures of this type a plot of the logarithm of the activity coefficient of the acid in mixtures at constant ionic strength was a nearly linear function of the ratio of the mean molality of the acid to the molality of pure acid at the same ionic strength. Mason and Kellam[6] found that at a total ionic strength

(1) Research sponsored by the U. S. Atomic Energy Commission under contract with the Union Carbide Corp.

(2) M. H. Lietzke and R. W. Stoughton, *J. Phys. Chem.*, **67**, 2573 (1963).

(3) M. H. Lietzke and R. W. Stoughton, *ibid.*, **69**, 2395 (1965).

(4) M. H. Lietzke and R. W. Stoughton, *ibid.*, **70**, 756 (1966).

(5) M. Randall and G. F. Breckenridge, *J. Am. Chem. Soc.*, **49**, 1435 (1927).

of 1.0, a plot of the logarithm of the activity coefficient of HCl *vs.* the molality of HCl was linear in the system HCl–$CeCl_3$. Harned and Gary[7] observed the same behavior in the HCl–$AlCl_3$ system. In the present study emf measurements of the cell

$$Pt\text{–}H_2(p)|HCl(m_2),\ LaCl_3(m_3)|AgCl\text{–}Ag$$

have been combined with values of the activity coefficient of $LaCl_3$[8] to compute the thermodynamic properties of both HCl and $LaCl_3$ in HCl–$LaCl_3$ mixtures.

Experimental Section

The high-temperature, high-pressure experimental apparatus and the preparation of electrodes and solutions were the same as described previously.[9,10] Since this apparatus was built for moderate accuracy over a wide temperature range rather than for maximum accuracy at low temperatures, the accuracy in the latter range is not as great as that claimed by other investigators.[11] The emf measurements were carried out in the temperature range 25–175° in solutions of total ionic strength 0.5 and 1.0 in which the ratio of HCl to $LaCl_3$ was varied. The emf values taken at the same temperature were reproducible to *ca.* ±0.5 mv. No drift of emf with time was observed.

Results and Discussion

In treating the results, the hydrogen pressure was calculated by subtracting the vapor pressure of the solution from the observed total pressure, while the vapor pressure of the solution was obtained by taking the vapor pressure of water at the temperature of measurement from the steam tables[12] and correcting for the presence of $LaCl_3$ and HCl in solution by Raoult's law. No correction was made for the amount of HCl in the vapor phase since it was previously found unnecessary to do so below 250° in pure HCl solution.[9] Each emf value was corrected to 1.00 atm of hydrogen pressure by subtracting $(RT/2\mathfrak{F})\ \ln f_{H_2}$, where the hydrogen fugacity, f_{H_2}, was taken equal to the hydrogen pressure. The solubility of AgCl was neglected and the ionic strength was taken to be equal to $m_{HCl} + 6m_{LaCl_3}$. The corrected emf values, E, at each ionic strength were plotted as a function of temperature and the values corrected to the round values of the temperature, 25, 60, 90, 125, 150, and 175°. The temperature of measurement was never more than 1° from the corresponding round temperature. These corrected values are given in Table I.

The activity coefficient, $\gamma_\pm$, of HCl at each temperature and set of concentrations in the mixtures was evaluated by using the Nernst equation and previous values[13] of the standard potential, E^0, of the Ag, AgCl electrode, except that 0.2223 v was used instead of 0.2220 v at 25°. In eq 1, m_2 and m_3 are the

$$E = E^0 - \frac{RT}{\mathfrak{F}} \ln [m_2(m_2 + 3m_3)] - \frac{2RT}{\mathfrak{F}} \ln \gamma_\pm \quad (1)$$

molalities of HCl and $LaCl_3$, respectively, while T is the absolute temperature, R is the gas constant, and $\mathfrak{F}$ is the faraday.

A plot of $\ln \gamma_\pm$ *vs.* ionic strength fraction of $LaCl_3$ was made at each temperature and at the total ionic strengths, 0.5 and 1.0. Also included in these plots were the values for pure HCl[13] at all temperatures. In all cases the plots were linear within experimental error in conformity with Harned's rule.

Expressions for $\gamma_\pm$ of HCl and $LaCl_3$ in the Mixtures. The activity coefficients of HCl was smoothed as to HCl and $LaCl_3$ concentrations and temperature and those of $LaCl_3$ were evaluated as follows. In accordance with the treatment in the previous papers[2-4] the excess free energy of the solution G^e, *i.e.*, excess over the molality and Debye–Hückel terms, was expressed as

$$\frac{G^e}{RT} = 2n_2 \ln \gamma_2{}^e + 4n_3 \ln \gamma_3{}^e = 2\sum_{ij} B_{ij} \frac{n_i n_j}{w} + 2\sum_{ijk} C_{ijk} \frac{n_i n_j n_k}{w^2} \quad (2)$$

where n represents the numbers of moles of each solute, w is the number of kilograms of water, and the sums are taken over each solute i, j, k = 2 (for HCl) to 3 (for $LaCl_3$). B_{ij} and C_{ijk} are interaction coefficients to be determined from the data.

Then for the HCl

$$2 \ln \gamma_2{}^e = \frac{\bar{G}_2{}^e}{RT} = \frac{\partial}{\partial n_2}\left(\frac{G^e}{RT}\right) = 4\sum_i B_{2i} m_i + 6\sum_{ij} C_{2ij} m_i m_j \quad (3)$$

(6) C. M. Mason and D. B. Kellam, *J. Phys. Chem.*, **38**, 689 (1934).

(7) H. S. Harned and R. Gary, *J. Am. Chem. Soc.*, **77**, 4696 (1955).

(8) H. S. Harned and B. B. Owen, "The Physical Chemistry of Electrolytic Solutions," 3rd ed, Reinhold Publishing Corp., New York, N. Y., 1958, p 566.

(9) R. S. Greeley, W. T. Smith, Jr., R. W. Stoughton, and M. H. Lietzke, *J. Phys. Chem.*, **64**, 652 (1960).

(10) M. B. Towns, R. S. Greeley, and M. H. Lietzke, *ibid.*, **64**, 1861 (1960).

(11) H. S. Harned and B. B. Owen, *ibid.*, **64**, 456 (1960).

(12) "VDI-Wasserdampftafeln," 4th ed, E. Schmitt, Ed., Springer-Verlag, Berlin, 1956.

(13) M. H. Lietzke and R. W. Stoughton, *J. Phys. Chem.*, **68**, 3043 (1964).

Table I: Values of the Emf in Volts for the Cell, Pt-$H_2(p)$|HCl(m_2), $LaCl_3(m_3)$|AgCl-Ag, and Deviations[a] of the Emf Values Calculated from Smoothed Activity Coefficients

		t, °C					
m_2	m_3	25	60	90	125	150	175
0.3766	0.0217	0.2818	0.2648	0.2466	0.2213	0.2018	0.1790
		0	0	0	−25	−4	+5
0.2520	0.0418	0.2996	0.2830	0.2644	0.2400	0.2205	0.1995
		−1	0	0	−5	−23	−6
0.1242	0.0630	0.3243	0.3104	0.2964	0.2766	0.2573	0.2344
		0	0	−5	+22	+17	−3
0.7661	0.0417	0.2479	0.2247	0.2038	0.1735	0.1519	0.1311
		0	0	0	0	−18	+19
0.5056	0.0912	0.2627	0.2441	0.2237	0.1979	0.1779	0.1543
		−1	−1	−8	+4	+20	+16
0.2541	0.1254	0.2890	0.2743	0.2549	0.2293	0.2098	0.1865
		+2	0	+4	−5	−3	−22

[a] The deviations are given below each emf as observed emf values less the values calculated from smoothed activity coefficients. Thus, a positive deviation indicates that the emf reported here is algebraically larger.

while for the $LaCl_3$

$$4 \ln \gamma_3^e = \frac{\bar{G}_3^e}{RT} = 4\sum_i B_{i3}m_i + 6\sum_{ij} C_{ij3}m_i m_j \quad (4)$$

Hence

$$\ln \gamma_2^e = 2I\left[B_{22} + \left(\frac{B_{23}}{6} - B_{22}\right)X_3\right] + 3I^2\left[C_{222} + \left(\frac{C_{223}}{3} - 2C_{222}\right)X_3 + \left(C_{222} + \frac{C_{233}}{36} - \frac{C_{223}}{3}\right)X_3^2\right] \quad (5)$$

and

$$\ln \gamma_3^e = I\left[\frac{B_{33}}{6} + \left(B_{23} - \frac{B_{33}}{6}\right)X_2\right] + \frac{I^2}{2}\left[\frac{C_{333}}{12} + \left(C_{233} - \frac{C_{333}}{6}\right)X_2 + \left(\frac{C_{333}}{12} + 3C_{223} - C_{233}\right)X_2^2\right] \quad (6)$$

In eq 5 and 6, X represents the ionic strength fraction of the designated component in the mixture and I represents the ionic strength of the solution given by $I = m_2 + 6m_3$. Since, as mentioned above, Harned's rule appears to hold for the HCl in the mixtures, the coefficient in parentheses of the X_3^2 term in eq 5 is zero.

The total ln γ_2 is obtained by adding the Debye–Hückel term to eq 5 and 6. This term was assumed to be $\mathbb{S}\rho^{1/2}\sqrt{I}/(1 + 1.5\sqrt{I})$ for the HCl and $3\mathbb{S}\rho^{1/2}\sqrt{I}/(1 + 1.5\sqrt{I})$ for the $LaCl_3$, where $\mathbb{S}$ is the limiting slope for a 1–1 electrolyte and ρ is the density of water which corrects the ionic strength to a volume basis as required by the Debye–Hückel theory.

The activity coefficients of HCl in the HCl–$LaCl_3$ mixtures were fitted by the method of least squares using eq 5 with the coefficient of the X_3^2 term set to zero. As in our previous studies of electrolyte mixtures[2-4] it was found possible to express the B coefficients with equations of the type

$$B_{iq} = B'_{iq} + B''_{iq}/T + B'''_{iq} \ln T \quad (7)$$

and the C coefficients with equations of the type

$$C_{ijq} = C'_{ijq} + C''_{ijq}/T \quad (8)$$

Thus, in this system also, the contribution of the B terms is much more important than the C terms (at least in the ionic strength range studied) and hence the difficulty in determining as many parameters in the C coefficients.

The values of B'_{22}, B''_{22}, B'''_{22}, B'_{23}, B''_{23}, B'''_{23}, C'_{222}, C''_{222}, C'_{223}, and C''_{223} were obtained directly by the least-squares fit, while the values of C'_{233} and C''_{233} were obtained by the application of Harned's rule: $C_{222} + C_{233}/36 - C_{223}/3 = 0$. The additional parameters needed for calculating ln γ_3^e by eq 6, namely the coefficients B_{33} and C_{333}, were evaluated by the method of least squares using activity coefficient data on pure $LaCl_3$ solutions.[8] Since the activity coefficient of $LaCl_3$ has been measured only at 25°, the values of

Table II: Parameters of B and C Coefficients (Eq 7 and 8) for the HCl–$LaCl_3$ System over the Range 25–175°

$B'_{22} = 2.52103$	$B''_{22} = -87.0994$	$B'''_{22} = -0.380853$
$B'_{23} = 29.1766$	$B''_{23} = -1596.85$	$B'''_{23} = -4.17835$
$C'_{222} = 0.0303565$	$C''_{222} = -9.44179$	
$C'_{223} = -0.0602743$	$C''_{223} = 19.8402$	
$C'_{233} = -1.816124$	$C''_{233} = 577.98684$	

At 25°

$B_{33} = 0.0484593$ $C_{333} = 0.00128873$

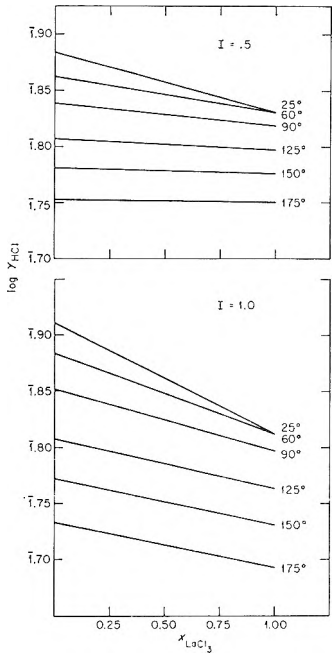

Figure 1. Log γ_{HCl} *vs.* X_{LaCl_3} in HCl–$LaCl_3$ mixtures.

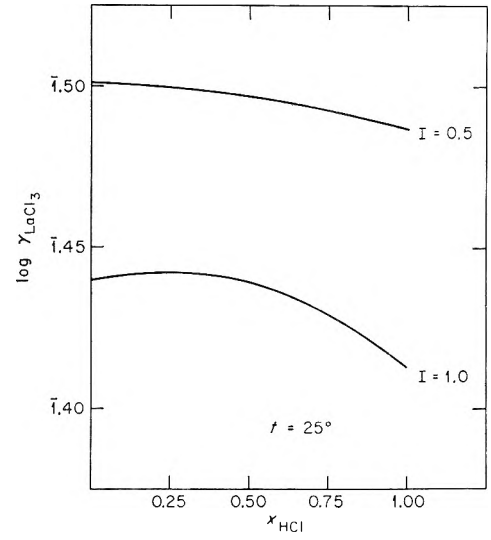

Figure 2. Log γ_{LaCl_3} *vs.* X_{HCl} in HCl–$LaCl_3$ mixtures.

B_{33} and C_{333} were determined at this temperature only. Hence it was possible to compute the activity coefficient of $LaCl_3$ in the HCl–$LaCl_3$ mixtures at this temperature only.

The parameters for calculating the various B and C coefficients (on a common log basis) are given in Table II. Activity coefficients of HCl and $LaCl_3$ in the mixtures at $I = 0.5$ and 1.0 calculated using these parameters are shown plotted in Figures 1 and 2. Since the experimental solutions used were not at exactly $I = 0.5$ and 1.0, the activity coefficient values calculated from the observed emf values are not shown in the figure. However, values of the emf E were calculated using the previously determined E^0 values and the B and C values for the smoothed activity coefficients (Table II) for each experimental point. The algebraic difference between the observed E values and those calculated are given below the observed E values in Table I.

The relationship between the B and C coefficients as defined by eq 7 and 8 and the α coefficient of Harned's rule is given by eq 9. In this equation, α_{23}

$$\alpha_{23} = 2\left(B_{22} - \frac{B_{23}}{6}\right) + 3I\left(2C_{222} - \frac{C_{223}}{3}\right) \qquad (9)$$

is the coefficient designated by Harned as α_{12}. When eq 9 is solved at 25° using the parameters given in Table II, then a value of $\alpha_{23} = 0.1061$ is obtained at $I = 0.5$ and $\alpha_{23} = 0.0991$ at $I = 1.0$. This latter value may be compared with $\alpha_{23} = 0.0614$ for HCl in HCl–$AlCl_3$ mixtures and with $\alpha_{23} = 0.0870$ for HCl in HCl–$CeCl_3$ mixtures, both at $I = 1.0$.

It is interesting to compare the activity coefficient behavior observed in the HCl–$LaCl_3$ system with that obtained in the previous mixtures studied. The plots of log γ_{HCl} *vs.* X_{LaCl_3} (Figure 1) are very similar to the corresponding plots in the HCl–$BaCl_2$ mixtures except that at both $I = 0.5$ and 1.0, the activity coefficient of HCl at 25° decreases even more rapidly as X_3 increases relative to the plots at the higher temperatures than it does in the HCl–$BaCl_2$ mixtures. In

contrast, the plots of log γ_{LaCl_3} *vs.* X_{HCl} (Figure 2) at both $I = 0.5$ and 1.0 resemble more nearly the plots of log γ_{KBr} *vs.* X_{HBr} than those of either log γ_{NaCl} *vs.* X_{HCl} or log γ_{BaCl_2} *vs.* X_{HCl}.

It is also interesting to observe that at constant ionic strength, plots of the logarithm of the activity coefficient of HCl in the HCl–$LaCl_3$ mixtures *vs.* the molality of HCl are linear, just as was observed by others in the HCl–$CeCl_3$[6] and the HCl–$AlCl_3$[7] mixtures.

Excess and Total Partial Molal Quantities. The excess partial molal enthalpy (over that given by the Debye–Hückel term) and entropy (over that given by the molality and Debye–Hückel terms) may be readily evaluated as was done previously.[2]

$$\bar{S}_q^e = -4R\left[\sum_i B'_{iq}m_i + (\ln T + 1)\sum_i B'''_{iq}m_i\right] - 6R\left[\sum_{ij} C'_{ijq}m_im_j + (\ln T + 1)\sum_{ij} C'''_{ijq}m_im_j\right] \quad (10)$$

$$\bar{H}_q^e = 4R\left[\sum_i B''_{iq}m_i - T\sum_i B'''_{iq}m_i\right] + 6R\left[\sum_{ij} C''_{ijq}m_im_j - T\sum_{ij} C'''_{ijq}m_im_j\right] \quad (11)$$

where $q = 2$ for HCl and 3 for $LaCl_3$.

Similarly, the total partial molal thermodynamic quantities for either solute are given by the following equations.

$$\bar{G}_q - \bar{G}^0_q = RT\left\{\ln\left[m_q(m_2 + 3m_3)^{a_q}\right] - \frac{A_q S\rho^{1/2}\sqrt{I}}{1 + 1.5\sqrt{I}} + A'_q \ln \gamma_q^e\right\} \quad (12)$$

$$\bar{S}_q - \bar{S}^0_q = R\left\{-\ln\left[m_q(m_2 + 3m_3)^{a_q}\right] + \frac{A_q\sqrt{I}}{1 + 1.5\sqrt{I}}\left[\frac{\partial}{\partial T}(TS\rho^{1/2})\right]\right\} + \bar{S}_q^e \quad (13)$$

$$\bar{H}_q - \bar{H}^0_q = \bar{L}_q = -\frac{A_qR\sqrt{I}}{1 + 1.5\sqrt{I}} \times \left[(TS\rho^{1/2}) - T\frac{\partial}{\partial T}(TS\rho^{1/2})\right] + \bar{H}_q^e = \frac{A_qR\sqrt{I}}{1 + 1.5\sqrt{I}}\left[T^2\frac{\partial}{\partial T}(S\rho^{1/2})\right] + \bar{H}_q^e \quad (14)$$

where S is the limiting slope for the mean activity coefficient for a 1–1 electrolyte, $a_q = 1$, $A_q = 2$, and $A'_q = 2$ for $q = 2$ (HCl), while $a_q = 3$, $A_q = 12$ and $A'_q = 4$ for $q = 3$.

Acknowledgment. The authors wish to express their sincere appreciation to John T. Turk and W. D. Armstrong for performing the experimental emf measurements, and to R. W. Whitfield, Jr., for his assistance with the calculations.

Structure and Electrolyte Properties in Bolaform Electrolytes. II. The Conductance of Potassium Salts of Several Rigid Bolaform Disulfonic Acids in Dioxane–Water Mixtures at 25°

by Bert R. Staples[1] and Gordon Atkinson

Department of Chemistry, University of Maryland, College Park, Maryland 20740
(Received August 23, 1966)

The conductances of potassium benzenesulfonate, potassium *p*-benzenedisulfonate, potassium 4,4′-biphenyldisulfonate, and potassium 4,4′′-terphenyldisulfonate in dioxane–water mixtures of 0–70% dioxane content were measured at 25°. The data have been interpreted by means of the Fuoss–Onsager equation using the Fuoss–Edelson technique. The Fuoss–Edelson method for unsymmetrical charge type (bolaform) electrolytes was tested using this series of salts in which the charge separation on the divalent anion increased so that the ion deviated further and further from spherical symmetry. The distances of closest approach which were determined were compared with those found using the Fuoss association model.

Introduction

The application of strong polyvalent electrolytes such as the benzenesulfonates[2] to conductance measurements established a somewhat unique base line, from which further and more meaningful comparisons of conductance data could be made.

It has been demonstrated that alkali metal and alkaline earth salts of *p*-benzenedisulfonic acid, H_2-BDS, are unassociated in water.[3] It was also shown that the Fuoss–Onsager equation can be applied to 2–2 and 1–2 salts of this type. Some of the effects of higher terms in the equation were also examined using these salts. The salts have also formed a basis for comparing association of 2–2 electrolytes in mixed solvents having dielectric constants lower than that of water.[4]

An understanding of ion–ion interaction is important, since it determines the validity of any conclusions drawn concerning the interaction of the ion with the solvent. The interaction between a pair of ions depends on the charge, size, structure, and sometimes the dipole moment of the ions as well as the solvent properties. Further dependence lies in the interaction of the solvent molecules with the ions. This investigation deals more closely with the effects of size and structure on ion association and related electrolyte properties.

Atkinson and co-workers have investigated arylpolysulfonates, including potassium *p*-benzenedisulfonate (K_2BDS) and 4,4′-biphenyldisulfonate (K_2BPDS), illustrating a systematic size increase of the anion. These aryldisulfonates are much to be preferred over alkyldisulfonates, since they possess a certain rigidity with little tendency to bend or coil as do long-chain alkyldisulfonates. This rigidity allows a more meaningful interpretation of results, since the distance separating the sulfonate groups is well defined. A study of this very useful systematic increase in the size, and at the same time, the charge separation, of an anion produced fruitful results.

Rice[5] has examined models for a theoretical treat-

(1) Taken in part from an M.S. Thesis submitted to the Graduate School of the University of Maryland.

(2) C. J. Hallada and G. Atkinson, *J. Am. Chem. Soc.*, **83**, 3759 (1961).

(3) G. Atkinson and S. Petrucci, *J. Phys. Chem.*, **67**, 337 (1963).

(4) G. Atkinson and C. J. Hallada, *J. Am. Chem. Soc.*, **84**, 721 (1962).

(5) S. A. Rice, *ibid.*, **80**, 3207 (1958).

ment of bolaform salts to obtain transport properties, and Atkinson[6] has applied these models to bolaform salts in water. Since the treatment of such a model has been presented in previous papers, it need not be repeated here.

For the diquaternary ammonium bolaform ions investigated by Fuoss,[7] Rice found that the Peterlin[8] model of beads separated by massless rods was superior to the rigid ellipsoid model. Using the rigid bolaform ions such as the 4,4′-biphenyldisulfonate ion, $BPDS^{2-}$, Atkinson found that the rigid ellipsoid model enabled one to calculate accurately the frictional coefficient of $BPDS^{2-}$ from the parameters of the benzenesulfonate ion, BS^-. Both of these results seem valid since, in the case of the diquaternary ammonium salts, a nonrigid polymethylene chain separates the charge sites, but a rigid aryl framework lies between the charge sites of the $BPDS^{2-}$ ion.

Thompson, Rice, and Nagasawa[9] have measured the diffusion coefficients of K_2BDS, K_2BPDS, and potassium 4,4″-terphenyldisulfonate, K_2TPDS. They find that the Perrin rigid ellipsoid gives a very accurate description of that property.

Starting with a relatively simple 1–1 salt, potassium benzenesulfonate (KBS), a base line is established to describe the behavior of this type of salt in dioxane–water mixtures. Using the KBS as a foundation, the effect of charge separation on the conductance, association, and the distance of closest approach, a_J, of the ions is determined. Other potassium salts of aryldisulfonates representing a systematic increase in size and charge separation, a sort of "polymeric series," are investigated. The salts which form this series of rigid, charge-separated anions are potassium benzenesulfonate (KBS), potassium *p*-benzenedisulfonate (K_2BDS), potassium 4,4′-biphenyldisulfonate (K_2BPDS), and potassium 4,4″-terphenyldisulfonate (K_2TPDS).

The conductances of this series of salts are measured in dioxane–water mixtures to force association due to the decreasing dielectric constant of the solvent mixtures. This enables one to observe the effect on association of the separation of charge on the anion.

From the distance of closest approach obtained through the Fuoss–Onsager equation, one should be able to tell whether the cation has any preference of position with respect to the anion when an ion pair of the type $(KX)^-$ is formed. The cation might prefer to associate with the anion at a 4 (or 4′) *para* position, immediately in contact with the sulfonate group (Figure 1a), or it might prefer to take up a position somewhat between the two sulfonate groups, at a sort of an "electrostatic equilibrium position" (Figure 1b).

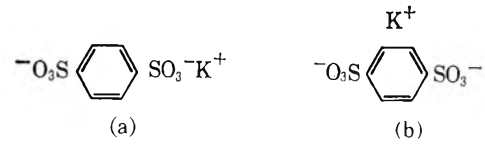

Figure 1. Position of the potassium ion in (a) the associated species 1, and (b) the associated species 2.

Experimental Section

All salts with one exception were prepared as previously described.[3,10]

Potassium 4,4″-Terphenyldisulfonate (K_2TPDS). Exhaustive sulfonation of *p*-terphenyl (Eastman Organic Chemicals, Rochester, N. Y., Item 2103) produced H_2TPDS which was then converted to the K_2-TPDS. The K_2TPDS was recrystallized three times from conductivity water.

These salts were analyzed for total cation (anion) content by converting the potassium salt to the acid using a Dowex-50 cation-exchange resin, then titrating the acid with a standard solution of NaOH. A Metrohm potentiograph, E336, and automatic titrator were used to obtain an automatic differential plot for the equivalence point. The NaOH was standardized using a stock solution of conductance-quality KCl, which was converted to HCl by the same cation-exchange resins.

All salts were dried at 110° to the anhydrous form and stored over $CaCl_2$ and under vacuum, even though there was no indication that they were very hygroscopic.

Purification of Solvents. The conductivity water for the first half of the measurements was prepared by passing distilled water through two Barnstead Bantam mixed-bed ion-exchange cartridges (Type 0808) yielding water with a specific conductivity of about 0.7×10^{-6} ohm^{-1} cm^{-1} at 25°. The water for the remaining measurements was obtained by distilling distilled water in a Barnstead water still, Catalog No. EPR 1/2, Barnstead Still and Sterilizer Co., Boston, Mass. Conductivity water was then obtained with a specific conductivity of about 0.9×10^{-6} ohm^{-1} cm^{-1} at 25°.

The Union Carbide *p*-dioxane was purified by standard techniques[11] and had a boiling point of 101.5–101.7° and a melting point of 11.65° which compared quite well with the literature values,[12] bp 101.5° and mp 11.7°.

(6) G. Atkinson and S. Petrucci, *J. Phys. Chem.*, **67**, 1880 (1963).
(7) O. V. Brody and R. M. Fuoss, *ibid.*, **60**, 156 (1956).
(8) A. Peterlin, *J. Chim. Phys.*, **47**, 6, 699 (1950).
(9) G. Thomson, S. A. Rice, and M. Nagasawa, *J. Am. Chem. Soc.*, **85**, 2537 (1963).
(10) M. Yokoi and G. Atkinson, *ibid.*, **83**, 4367 (1961).
(11) C. A. Kraus and R. A. Vingee, *ibid.*, **56**, 513 (1934).

The precision conductance setup as described by Dike[13] was employed as before. A Leeds and Northrup constant temperature bath, Catalog No. 4956, was utilized to give a temperature control of ±0.001°.

Flask-type conductance cells were used. Solutions were prepared by the weight-dilution method and all experimental details appear in previous papers.[4,14]

Calculations of Ionic Equivalent Conductances in Dioxane–Water Mixtures. Since the Fuoss–Edelson[15] method for treating unsymmetrical electrolytes requires the use of both limiting ionic equivalent conductances, $\lambda_{\pm}^0$ and Λ^0, the limiting ionic equivalent conductance for the potassium ion had to be calculated for dioxane–water mixtures. Starting with the data of Owens and Waters,[16] which give the Λ^0 for HCl in dioxane–water mixtures and the experimentally determined transference numbers for the H^+ in dioxane–water mixtures, one may calculate the limiting ionic equivalent conductance of the chloride ion by

$$T_- = 1 - T_+; \quad \lambda_-^0 = \Lambda^0 T_-^0 \qquad (1)$$

Then from a plot of $\lambda_{Cl^-}^0$ for the dioxane–water mixtures for which Fuoss and Lind[17] report Λ^0 values of the conductance of KCl in dioxane–water, one calculates the limiting ionic equivalent conductance of the potassium ion, $\lambda_{K^+}^0$, simply from Kohlrausch's law: $\lambda_{K^+}^0 = \Lambda^0 - \lambda_{Cl^-}^0$. Then a plot of $\lambda_{K^+}^0$ *vs.* per cent dioxane determines the value of $\lambda_{K^+}^0$ for the particular mixture of dioxane–water being investigated.

Results

The actual conductance results are given in Table I. When the limiting-law plots showed that there was no association or only very slight association, the data were treated by means of the Fuoss–Onsager equation for unassociated electrolytes. The equation is

$$\Lambda = \Lambda^0 - S\sqrt{C} + EC \log C + JC \qquad (2)$$

where Λ^0 is the equivalent conductance at infinite dilution and S, E, and J are theoretical terms defined by Fuoss.[18] A Λ' *vs.* C plot evaluated J and hence a_J, where Λ' is defined as $\Lambda + S\sqrt{C} - EC \log C = \Lambda^0 + JC$. This gives Λ^0 as the intercept and J as the slope. With the new Λ^0, a better Λ' and hence a better J is obtained.

If one assumes that the distance of closest approach for a given salt in all mixtures of dioxane–water is approximately the same as that in water, since the ions should show preference to hold water molecules in their coordination sphere rather than nonpolar dioxane molecules, one may obtain K_A values by using the Λ_K *vs.* $\Lambda f_{\pm}^2 C\gamma$ plot described by Fuoss.[19] From the conductance equation (at top of next column)

$$\Lambda' = \Lambda + S\sqrt{C\gamma} - EC\gamma \log C\gamma = \Lambda^0 + JC\gamma - K_A \Lambda f_{\pm}^2 C\gamma \qquad (3)$$

one may define $\Lambda_K \equiv \Lambda' - JC\gamma = \Lambda^0 - K_A \Lambda f_{\pm}^2 C\gamma$, where $f_{\pm}^2$ is the Debye–Hückel mean activity coefficient and γ is the fraction of unassociated ions. Then knowing a Λ^0 and an a_J, a set of Λ_K values may be calculated. To smooth the data, a plot of Λ_K *vs.* $\Lambda f_{\pm}^2 C\gamma$ will yield Λ^0 as the intercept and K_A as the slope.

Using Atkinson's[5] a_J value of 3.18 A for KBS in water, Λ_K values were calculated and the K_A values for KBS were obtained as described above.

If the Fuoss[20] model applies for these dioxane–water mixtures, then a_0 may be calculated from the slope of a plot of $\log K_A$ *vs.* $1/D$ by

$$K_A = K_A^0 e^b \qquad (4)$$

and

$$\log K_A = \log K_A^0 + 0.4343b \qquad (5)$$

where $b = \epsilon^2/a_K DkT$ and $(0.4343)\epsilon^2/kT = 243.3 \times 10^{-8}$ for a 1–1 electrolyte at 25°.

A plot of $\log K_A$ *vs.* $1/D$, Figure 2, yields a Fuoss a_K value of 3.4 A from the slope. Since the K_A values for KBS were rather small, being comparable to those of KCl in dioxane–water,[17] a large uncertainty in these K_A values was encountered.

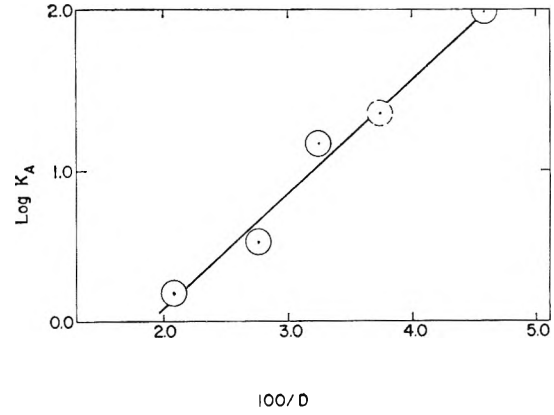

Figure 2.

(12) "Handbook of Chemistry and Physics," 38th ed, C. D. Hodgman, Ed., Chemical Rubber Publishing Co., Cleveland, Ohio, 1956.

(13) P. H. Dike, *Rev. Sci. Instr.*, 2, 379 (1931).

(14) G. Atkinson, M. Yokoi, and C. J. Hallada, *J. Am. Chem. Soc.*, 83, 1570 (1961).

(15) R. M. Fuoss and D. Edelson, *ibid.*, 73, 269 (1951).

(16) B. B. Owens and G. W. Waters, *ibid.*, 60, 2371 (1938).

(17) R. M. Fuoss and J. E. Lind, Jr., *J. Phys. Chem.*, 65, 999 (1961).

(18) R. M. Fuoss and F. Accascina, "Electrolyte Conductance," Interscience Publishers Inc., New York, N. Y., 1959.

(19) R. M. Fuoss, *J. Am. Chem. Soc.*, 81, 2659 (1959).

(20) R. M. Fuoss, *ibid.*, 80, 5059 (1958).

Table I: Conductance Results[a-c]

KBS

0% Dioxane		35.94% Dioxane	
$C \times 10^4$	Λ	$C \times 10^4$	Λ
1.8539	107.279	3.9743	56.124
4.0755	106.573	7.0027	55.654
6.3302	106.114	11.953	55.116
12.673	105.207	16.946	54.684
19.024	104.563	24.938	54.138
		31.716	53.801

49.68% Dioxane		56.36% Dioxane		66.52% Dioxane	
$C \times 10^4$	Λ	$C \times 10^4$	Λ	$C \times 10^4$	Λ
1.8948	45.238	3.7218	42.345	2.0713	35.791
6.3486	44.026	5.7988	41.457	5.7723	33.883
10.676	43.326	8.6547	40.654	9.6693	32.517
17.414	42.529	11.744	40.008	14.967	31.158
25.463	41.816	15.664	39.370	20.694	30.073
35.420	41.121			27.884	28.995
				33.376	28.309
				41.215	27.506

K_2BDS

35.94% Dioxane		47.76% Dioxane	
$C \times 10^4$	Λ	$C \times 10^4$	Λ
3.4413	59.823	1.9021	49.349
6.2619	58.800	4.0654	47.822
11.155	57.460	8.5183	45.717
17.288	56.245	15.806	43.495
26.653	54.976	26.897	41.395
36.471	54.024		

54.79% Dioxane		59.14% Dioxane		65.59% Dioxane	
$C \times 10^4$	Λ	$C \times 10^4$	Λ	$C \times 10^4$	Λ
0.66281	43.898	1.6246	39.585	1.0757	32.826
2.1900	42.247	2.8519	37.867	2.4778	29.794
3.9479	40.177	5.4787	35.466	5.1989	26.800
6.0343	38.774	8.5767	33.636	8.2794	24.976
9.7153	37.011	15.018	31.244	12.994	23.172
15.931	35.053	25.148	29.062	18.383	21.872
22.079	33.680			22.414	21.137

K_2BPDS

24.17% Dioxane		46.83% Dioxane	
$C \times 10^4$	Λ	$C \times 10^4$	Λ
2.3769	73.906	1.1648	49.943
4.5757	73.245	2.0663	49.264
6.8160	72.500	3.5578	48.395
9.4883	71.785	4.6675	47.862
12.612	71.102	6.8891	46.970
15.914	70.469	9.6428	46.020
		12.684	45.253
		17.112	44.397

52.27% Dioxane		59.14% Dioxane		68.69% Dioxane	
$C \times 10^4$	Λ	$C \times 10^4$	Λ	$C \times 10^4$	Λ
1.0804	45.500	0.86887	41.094	2.3474	26.400
2.2859	44.530	2.5021	38.587	4.4619	23.881
3.2770	43.798	4.1283	36.929	6.4060	22.468
5.2771	42.627	5.6683	35.821	9.1299	21.116
7.7475	41.522	8.0555	34.540	12.168	20.063
9.8468	40.788	12.594	32.795	14.365	19.468
14.636	39.458	17.456	31.514	15.934	19.111
18.559	38.498			17.129	18.867
				17.992	18.709

K_2TPDS

0% Dioxane		41.94% Dioxane		46.83% Dioxane	
$C \times 10^4$	Λ	$C \times 10^4$	Λ	$C \times 10^4$	Λ
0.18672	116.000	1.3234	50.364	0.72870	45.285
0.58250	114.739	2.4687	49.594	1.6309	44.414
1.1499	113.801	3.7284	48.964	3.2708	43.380
1.8595	113.091	5.1224	48.417	4.5116	42.820
2.3945	112.691	6.9594	47.834	7.4265	41.801
3.1441	112.243	8.8585	47.346	10.099	41.140
4.5837	111.572	11.729	46.737	12.521	40.615
6.2168	111.009	14.223	46.303		

52.27% Dioxane		58.32% Dioxane	
$C \times 10^4$	Λ	$C \times 10^4$	Λ
0.48053	44.984	1.0653	37.229
1.2024	43.463	2.4501	35.795
2.8310	41.606	4.3420	34.322
4.2392	40.749	6.0695	33.381
6.6478	39.579	7.7880	32.651
9.3889	38.713	10.156	31.843
11.445	38.142	13.969	30.838
		18.703	29.924

[a] Percentages are w/w %. [b] Concentrations are moles $l.^{-1}$. [c] Λ is in ohm^{-1} cm^2 equiv^{-1}.

Conductance parameters for unsymmetrical electrolytes were obtained by the Fuoss–Edelson[15] technique. A formal, theoretical basis for applying the Fuoss–Onsager equation and its related data treatment methods to unsymmetrical electrolytes is lacking. However, such data treatment techniques have proven greatly superior to other methods of data fitting. The assumption that a correct a_J value can be readily obtained is not strictly true, but no theory relating an unsymmetrical "J" term to the ion-size parameter has been put forth. Until such a theory does come to light, we feel that it is acceptable to use the same basic assumptions of the model of a charged ion surrounded by its ionic atmosphere, which has been proven successful for symmetrical electrolytes, to arrive at probable a_J values for unsymmetrical electrolytes. The

Table II: Conductance Parameters

% Dioxane	Λ^0	λ_+^0	λ_-^0	J	a_J	K_A	$\Lambda^0\eta_0$	D
				KBS				
0.0	108.51	73.52[a]	34.99	...	(3.18)[b]	...	0.971	78.54
35.94	57.51	38.65	18.86	318.2	4.11	1.6	0.942	48.06
49.68	46.45	30.28	16.17	~307	~2.2	3.5	0.886	36.25
56.36	43.35	27.95	15.40	~450	~2.1	14.3	0.854	30.51
66.52	38.12	24.50	13.62	2097	5.16	95.4	0.744	21.78
				K_2BDS				
0.0	131.95	73.52[a]	58.43	(2118)[b]	(4.58)[b]	...	1.181	78.54
35.94	64.00	38.65	25.35	3625	4.13	...	1.047	48.06
47.76	52.92	31.19	21.73	5405	3.33	36.0	0.993	37.90
54.79	46.20	28.48	17.72	7740	3.11	118.6	0.906	31.86
59.14	43.60	27.03	16.57	10803	3.12	292.8	0.864	28.12
65.59	36.35	24.77	11.58	18360	3.28	1063.0	0.710	22.58
				K_2BPDS				
0.0	122.51	73.52[a]	48.99	...	(4.50)[b]	...	1.096	78.54
24.17	77.18	49.29	27.89	3104	5.46	...	1.065	58.18
46.83	52.91	31.64	21.27	5845	4.27	23.1	0.985	38.71
52.27	48.51	29.39	19.12	7418	3.79	52.2	0.943	34.02
59.14	43.83	27.03	16.80	11324	3.32	256.0	0.868	28.12
68.69	33.60	23.67	9.93	25836	3.52	980.0	0.649	19.92
				K_2TPDS				
0.0	116.08	73.52[a]	42.46	2654	7.10	~11.6	1.039	78.54
41.94	52.77	34.19	18.58	4687	4.94	4.12	0.932	42.94
46.83	47.13	31.62	15.51	5460	4.64	51.2	0.884	38.71
52.27	45.82	29.39	16.43	7360	4.15	214.0	0.890	34.02
58.32	40.28	27.29	12.99	10163	3.77	~139.4	0.797	28.83
				NA_2TPDS				
0.0	92.06	50.11[a]	41.95	1890	6.0	4.1	0.824	78.54

[a] Limiting ionic conductance of K^+ in water taken from H. S. Harned and B. B. Owens, "The Physical Chemistry of Electrolyte Solutions," 3rd ed, Reinhold Publishing Corp., New York, N. Y., 1958, Chapters 4 and 8. [b] Values in parentheses are taken from previous investigations.[3,6,10]

major wrong assumption which is made is that the ion is spherical, but the ion is most probably ellipsoidal, as borne out by the good agreement with Rice's treatment.

A good approximation for the association constant was obtained from the Fuoss–Edelson technique for unsymmetrical electrolytes. This K_A was then used in the Fuoss–Onsager equation to obtain an estimated a_J. In most cases, the Λ'–C method was used to obtain an a_J value. Data for all salts are presented in Table II.

Associated Symmetrical Electrolytes. When the limiting-law plots indicated association, the data were treated by means of the Fuoss–Onsager[19] equation for associated electrolytes

$$\Lambda = \Lambda^0 - S\sqrt{C\gamma} + EC\gamma \log C\gamma + JC\gamma - K_A f_\pm^2 \Lambda C\gamma \quad (6)$$

The Fuoss "Y–X" method of determining the three parameters, Λ^0, a_J, and K_A, was used and has been presented in other works.[19] A series of successive approximations was programmed for an IBM 7090/7094 computer and the "best" Λ^0, a_J, and K_A values were found. The details of the computer program are available from the authors.

Associated Unsymmetrical Electrolytes. The problem of treating unsymmetrical electrolytes lies in the fact that the associated species MA^- still conducts. The Fuoss–Edelson technique was used in the data analysis for the unsymmetrical electrolytes. The basic assumptions made were (1) the second association to form the nonconducting species as $M^+ + MA^- = M_2A$ was negligible at such low concentrations; (2) the limiting ionic conductance of the associated species, MA^-, is approximately equal to one-half the limiting ionic conductance of the anion, A^{2-}, since the

charge is one-half and the size of the ion is approximately the same; and (3) the approximate single anionic activity coefficient, $f_{=}$, could be estimated from

$$-\log f_{=} = (250.3Z^2\sqrt{3N})/D^{3/2} \quad (7)$$

where $Z = Z_{A^{2-}} = -2$.

Using other approximations described by Fuoss and Edelson, Λ^* is defined

$$\Lambda^* \equiv \Lambda^0\gamma_1 \quad (8)$$

where

$$\gamma_1 = \frac{\Lambda}{\Lambda^0}\left(\frac{1}{1 + 0.5\frac{\lambda_{=}^0}{\Lambda_0}}\right)\left(\frac{1}{1 - \frac{S}{\Lambda_0}\sqrt{N}} + \frac{\lambda_{=}^0}{2\Lambda}\right) \quad (9)$$

with N being the normality of the solution and

$$N' \equiv Nf_{=} \quad (10)$$

Finally, arriving at the hopefully linear relationship

$$\Lambda^* = \Lambda^0 - \frac{K_{A_1}}{\Lambda^0}(\chi) \quad (11)$$

where

$$(\chi) = N\Lambda^*(\Lambda^* - 0.5\Lambda^0)$$

Then a plot of Λ^* *vs.* (χ) should give a slope of $-K_{A_1}/\Lambda^0$, in the dilute range, and Λ^0 as intercept. Where the first association constant was small (in less than 50% dioxane), linear plots of Λ^* *vs.* (χ) were obtained. As association increased so that K_{A_2} was no longer negligible, a slight upward curve was observed. These were still approximately linear in the very dilute range, however, so that K_{A_1} could be estimated. The majority of the calculations were programmed for the IBM 7090/7094 computer (FORTRAN). The results were all hand plotted to guard against the taking of an incorrect slope due to a curving plot. Examples of Λ' *vs.* C graphs and Λ^* *vs.* χ are shown in Figures 3 and 4, respectively. An example of a curving Λ^* *vs.* χ plot and how the K_{A_1} was estimated is included in Figure 4 (K_2BDS in 65.59% dioxane).

The nonlinearity of the Λ^* *vs.* χ plots of the K_2TPDS both in water and dioxane–water mixtures seems to indicate that the Fuoss–Edelson technique cannot be applied very successfully to an electrolyte containing such a large ion. However, the theory does appear adequate for the other salts investigated. Failure to obtain an a_K value from the slope of the log K_{A_1} *vs.* $1/D$ plot in line with the other three salts considered, 5.0 A for K_2BDS, 4.6 A for K_2BPDS, but 3.0 A for K_2TPDS, points to either an inadequate estimation of

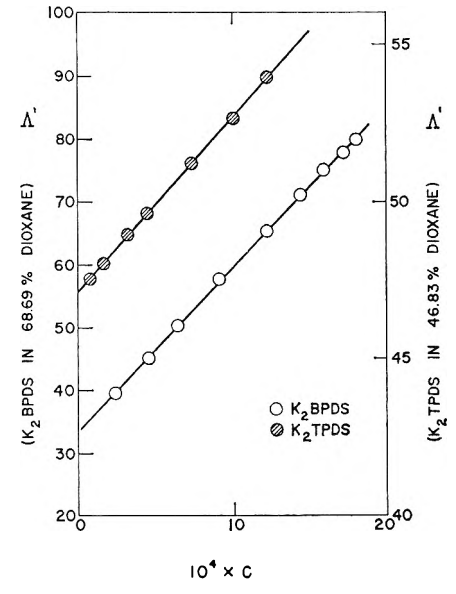

Figure 3.

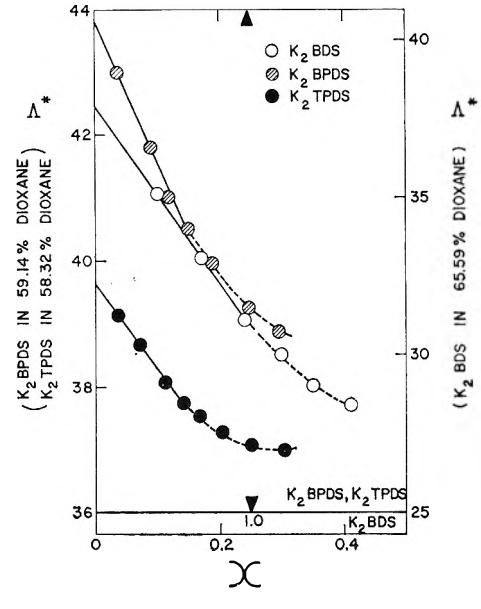

Figure 4.

the association constants or a breakdown in the Fuoss model for large, nonspherical ions, or some combination of effects. The a_J and a_K distance of closest approach parameters are contrasted in Table III.

Conclusions

1. The Fuoss–Edelson data treatment technique works adequately for the unsymmetrical salts examined in this paper with the possible exception of K_2TPDS.

2. The a_K values (determined from a plot of log K_{A_1} *vs.* $1/D$) show an unexpected trend for the bola-

Table III: The Distance of Closest Approach

Salt	Thermodynamic (Fuoss) a_K, A	Conductance (Fuoss–Onsager) a_J, A
KBS	3.4	(3.2)[5]
K_2BDS	5.0	3.6
K_2BPDS	4.6	4.2
K_2TPDS	3.0	4.5

form ions decreasing as the charge separation (and anion size) increases. This can possibly be attributed to a breakdown of the Fuoss association theory as the anions deviate more and more from the spherical model of the theory. On the other hand, if it is a real effect, it could reflect the increasing tendency of the cation to associate with a given sulfonate group rather than occupy an equilibrium position between the sulfonate groups. A simple coulombic calculation shows that the end position should be favored in the $TPDS^{2-}$ case, but not in the BDS^{2-} or $BPDS^{2-}$ cases.

3. It would be of real value to extend this work to the alkyldisulfonate case so that the effect of chain flexibility could be investigated.

Acknowledgments. The authors wish to express their gratitude to the National Institutes of Health for their support under Grant GM 9232. The machine computation used in this research was supported under NASA Grant NsG-398 to the Computer Science Center of the University of Maryland.

The Kinetics of Ion Association in Manganese Sulfate Solutions. II. Thermodynamics of Stepwise Association in Water

by Gordon Atkinson and S. K. Kor

Department of Chemistry, University of Maryland, College Park, Maryland *(Received September 13, 1966)*

Ultrasonic absorption was measured in aqueous $MnSO_4$ solutions at 20, 25, and 30° in the frequency range 2–250 Mc. The data are interpreted in terms of the Eigen three-step ion-association mechanism using a Bjerrum association constant for the first step. From the rate constants obtained, it is possible to calculate ΔF, ΔH, and ΔS for each of the three steps. The mechanism of the association process is discussed in terms of the thermodynamic parameters obtained.

The investigation of the details of ion association and complexation in solution has been put on a new level by the relaxation techniques so imaginatively developed by Eigen and his co-workers.[1] These techniques, coupled with the increased realization of the importance of ion association in biological systems,[2] have made the investigation of this very classical electrolyte problem a central theme in modern physical and inorganic solution chemistry. In fact, the dominant picture of Eigen's results—the consideration of all ion association as a multi-step process—demands a reconsideration of most if not all of the traditional

(1) M. Eigen and L. de Maeyer in "Technique of Organic Chemistry," Vol. VIII, Part 2, Interscience Publishers, Inc., New York, N. Y., 1963, Chapter 18.

(2) *E.g.*, G. L. Eichhorn in "Chemistry of the Coordination Compounds," J. Bailer, Ed., Reinhold Publishing Corp., New York, N. Y., 1956, Chapter 21.

theoretical approaches to the kinetics and thermodynamics of ion–ion interactions in solution. The most promising relaxation technique for the detailed examination needed is ultrasonic absorption and we have adopted this as our primary approach.

Recently,[3] we have published a study of $MnSO_4$ ion association in water and some mixed solvent systems at 25°. The basic interpretation is the three-step ion association process postulated by Eigen and Tamm.[4] However, the use of all three measured relaxation frequencies led to some differences in the actual kinetic parameters. The three-step process is detailed below. Step I is the diffusion-controlled

$$\underset{a}{Mn^{2+}(aq) + SO_4^{2-}(aq)} \underset{k_{21}}{\overset{k_{12}}{\rightleftharpoons}} \underset{b}{Mn^{2+}(W)_xSO_4^{2-}} \quad (I)$$

$$\underset{b}{Mn^{2+}(W)_xSO_4^{2-}} \underset{k_{32}}{\overset{k_{23}}{\rightleftharpoons}} \underset{c}{Mn^{2+}(W)_ySO_4^{2-}} \quad (II)$$

$$\underset{c}{Mn^{2+}(W)_ySO_4^{2-}} \underset{k_{43}}{\overset{k_{34}}{\rightleftharpoons}} \underset{d}{Mn^{2+}(W)_zSO_4^{2-}} \quad (III)$$

approach of the completely hydrated ions, while steps II and III represent the successive loss of waters of hydration from between the ions. States b, c, and d are all ion-pair states where $(W)_x$, $(W)_y$, and $(W)_z$ represent water molecules between the ions. None of the ion-pair states contributes to the solution conductance.[3] In the simplest picture, $z = 0$ and state d represents a contact ion pair with sulfate oxygens occupying one (or more) positions in the first coordination sphere of the Mn^{2+} ion. The numerical results are summarized later in this paper.

To examine the details of the above picture further, we have measured the ultrasonic absorption of aqueous $MnSO_4$ solutions as a function of temperature. The traditional approach[5] to such data has been to plot some logarithmic function of the relaxation frequency against $1/T$ and to obtain an apparent activation energy. Yet as will be shown, the relaxation frequency may depend on up to six rate constants and will also contain temperature-dependent thermodynamic functions. Therefore, we have analyzed our data in a more detailed way in terms of the temperature dependence of the individual rate constants. It is, then, possible to obtain good estimates of ΔF, ΔH, and ΔS for each step in the association process as well as the conventional activation parameters.

Experimental Section

All measurements were made by the transmitted-pulse technique.[6–8] In the frequency range 2–60 Mc, a 1-m path length apparatus was used.[9] For the frequency range 30–300 Mc, a new apparatus was constructed. This apparatus uses a conventional pulse technique comparing the pulse received after transmission through the solution with a standard pulse obtained from a pulse-modulated signal generator. This apparatus will be more completely described in an article being prepared. The cell is a 1-in. path length two-crystal interferometer similar to that used by Litovitz and co-workers.[10] Frequency measurements were made with a BC-221 in the range from 1 to 20 Mc and a Gertsch FM-3 in the range from 20 to 200 Mc.[11] In each case the frequency is known to better than 0.2%. The absorption coefficient, α, can be determined to approximately ±5% in the frequency range covered, although duplicate runs often agree to 2% or better.

Aqueous $MnSO_4$ solutions at 25° exhibit absorption maxima (on a plot of $\alpha\lambda$ *vs.* ν) at approximately 200, 30, and 3 Mc. These maxima correspond very roughly to steps I, II, and III, respectively. However, the 30-Mc peak is very temperature dependent and, because of its lower amplitude, shows a regrettable tendency to hide under the surrounding peaks. For this reason, the temperature range covered was only 20–30°. The temperature was controlled to ±0.05° at each temperature measured. However, the very limited range makes our conclusions necessarily tentative. The high-frequency data (up to 250 Mc/sec) will be published separately in an article dealing with diffusion-controlled steps in 2–2 electrolyte solutions.

The $MnSO_4$ used was AR grade weighed as a stoichiometric monohydrate. Mn analyses were done both by EDTA titration and by redox titration after preliminary bismuthate oxidation. The water used was doubly distilled conductance water.

Data Treatment

For a three-step association process, the rate constants are related to the measured relaxation times by eq 1–4[4]

(3) G. Atkinson and S. K. Kor, *J. Phys. Chem.*, **69**, 128 (1965).

(4) M. Eigen and K. Tamm, *Z. Elektrochem.*, **66**, 107 (1962).

(5) *E.g.*, S. K. Kor and G. S. Verma, *J. Chem. Phys.*, **29**, 9 (1958).

(6) J. Andreae, T. Bass, E. L. Heasell, and J. Lamb, *Acustica*, **8**, 131 (1956).

(7) J. R. Pellam and J. K. Galt, *J. Chem. Phys.*, **14**, 608 (1946).

(8) T. Pinkerton, *Proc. Phys. Soc.* (London), **B62**, 286 (1949).

(9) G. Atkinson, S. K. Kor, and R. L. Jones, *Rev. Sci. Instr.*, **35**, 1270 (1964).

(10) *E.g.*, T. A. Litovitz and E. H. Carnevale, *J. Appl. Phys.*, **26**, 816 (1955).

(11) Gertsch Products, Inc., 3211 Los Angeles 16, Calif.

$$(1/\tau_I) = 2\pi\nu_{mI} = k_{21} + k_{12}' \quad (1)$$

where

$$k_{12'} = k_{12}\sigma C\gamma_\pm^2\left(2 + \frac{\partial \ln \gamma_\pm^2}{\partial \ln \sigma}\right) \quad (2)$$

$$(1/\tau_{II}) = 2\pi\nu_{mII} = k_{32} + \left(\frac{k_{12'}}{k_{12'} + k_{21}}\right)k_{23} = k_{32} + k_{23'} \quad (3)$$

$$(1/\tau_{III}) = 2\pi\nu_{mIII} = k_{43} + \left(\frac{k_{23}}{k_{23'} + k_{32}}\right)k_{34} = k_{43} + k_{34'} \quad (4)$$

where σ is the degree of association in step I at C, C is concentration of $MnSO_4$, $\gamma_\pm$ the mean activity coefficient of ions in state a at concentration C, ν_{mi} the frequency of maximum absorption for concentration C, and τ_i the relaxation time for step i. In the data analysis, we have made the following assumptions.

1. Step I can be described using the Fuoss–Bjerrum association model.[12] An equilibrium constant can be calculated for a given temperature with the Fuoss equation and a distance parameter equal to the sum of the ionic radii plus the diameter of two water molecules. The calculations of the rate constant are not very sensitive to the actual distance chosen.

2. The activity coefficient, $\gamma_\pm$, can be calculated using the extended Debye–Hückel equation. Brubaker has demonstrated the excellence of this for an unassociated 2–2 salt.[13] The measured activity coefficients for $MnSO_4$ include a contribution from association and cannot be used.

3. Activity coefficients can be ignored for states b, c, and d. Rice has shown that the activity of dipoles is not very sensitive to changes in the charge separation.

With these assumptions, we can define a quantity $\theta(C)$ as

$$\theta(C) = \sigma C\gamma_\pm^2\left(2 + \frac{\partial \ln \gamma_\pm^2}{\partial \ln \sigma}\right)_c \quad (5)$$

and write

$$2\pi\nu_{mI} = k_{21} + k_{12}[\theta(C)] \quad (6)$$

$$2\pi\nu_{mII} = k_{32} + \left[\frac{\theta(C)}{K_{12} + \theta(C)}\right]k_{23} = k_{32} + \Phi(C)k_{23} \quad (7)$$

$$2\pi\nu_{mIII} = k_{43} + \left[\frac{\Phi(C)k_{23}}{k_{32} + \Phi(C)k_{23}}\right]k_{34} \quad (8)$$

where d is defined in eq 9.

$$K_{12} = \frac{C_a^2\gamma_\pm^2}{C_b} \quad (9)$$

A small computer program is used to calculate $\theta(C)$ for a given K_{12}. Plots of $2\pi\nu_{mi}$ *vs.* the quantities in brackets in eq 6, 7, and 8 are straight lines yielding the rate constants as slope and intercept. This method is very useful for smoothing the (ν_{mi}, C) data.

The amplitudes of the relaxation maxima can be used to calculate approximate values for ΔV for each step of the ion-association process. The equations are derived and discussed by Eigen and Tamm.[14] Unfortunately, for reactions involving a ΔH, it is difficult to be certain of the ΔV values. The problem is further exacerbated by the occurrence of ΔV in a squared term and the fact that the thermodynamic parameters are coupled in the same way that is indicated by the rate-constant expression.

Results

At least two different concentrations (0.01, 0.05, and 0.10 M) were run at each of the three temperatures, 20.0, 25.0, and 30.0°. Figure 1 shows a typical relaxation spectrum for a given temperature and concentration. At least two duplicate runs were always made. For single relaxations, the Mikhailov technique[15] can be used for data analysis to obtain the relaxation frequencies. However, in the case of multiple relaxations, the following approach has proved necessary. The measured excess absorption per wavelength, $\alpha'\lambda$, can be written as

$$(\alpha'\lambda)_{exptl} = (\alpha'\lambda)_I + (\alpha'\lambda)_{II} + (\alpha'\lambda)_{III}$$

where

$$(\alpha'\lambda)_i = 2(\alpha'\lambda)_{i,max}\frac{\omega\tau_i}{1 + \omega^2\tau_i^2}$$

In the case of $MnSO_4$, the peaks for steps I and III are large and can be evaluated using a graphical technique to give τ_I, $(\alpha'\lambda)_{I,max}$, τ_{III}, and $(\alpha'\lambda)_{III,max}$. Then, τ_{II}, $(\alpha'\lambda)_{II,max}$ is obtained from

$$2(\alpha'\lambda)_{II,max}\frac{\omega\tau_{II}}{1 + \omega^2\tau_{II}^2} = (\alpha'\lambda)_{exptl} - [(\alpha'\lambda)_I + (\alpha'\lambda)_{III}]_{calcd}$$

The parameters found for steps II and III are given in Table I. The relaxation frequencies are then treated

(12) R. M. Fuoss and C. A. Kraus, *J. Am. Chem. Soc.*, 79, 3304 (1957).

(13) C. H. Brubaker, Jr., and P. G. Rasmussen, *J. Phys. Chem.*, 67, 330 (1963).

(14) M. Eigen and K. Tamm, *Z. Elektrochem.*, 66, 93 (1962).

(15) I. G. Mikhailov, *Dokl. Akad. Nauk SSSR*, 89, 991 (1953).

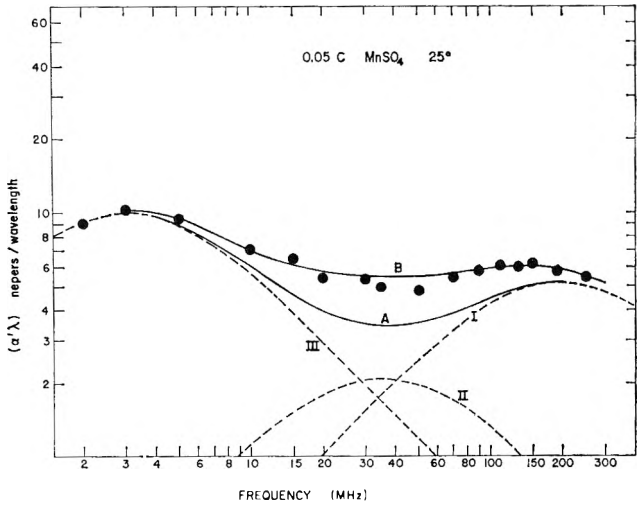

Figure 1.

as described under the data treatment section above to yield the rate constants. These results are summarized in Table II together with the individual step equilibrium constants.

Table I: Relaxation Parameters for $MnSO_4$ in H_2O

Concn, C	Step III ν_m, Mc/sec	Step III $10^4(\alpha'\lambda)$, nepers	Step II ν_m, Mc/sec	Step II $10^4(\alpha'\lambda)$, nepers
		20°		
0.01	...	...	...	...
0.05	2.4	10.1	38.0	2.0
0.10	2.5	19.6	39.0	3.8
		25°		
0.01	2.7	3.2	32.0	0.6
0.05	3.1	10.1	34.0	2.1
0.10	3.3	18.4	35.0	3.7
		30°		
0.01	...	...	...	...
0.05	4.1	10.1	38.0	2.0
0.10	4.5	17.3	39.0	3.6

With the present high-frequency apparatus it was not possible to go high enough in frequency to completely define the step I relaxation frequency. The estimated value at 25° was in good agreement with the assumption of a diffusion-controlled step. For the 20 and 30° data, only the calculated K_{12} is necessary for further data treatment.

The derived activation parameters are given in Table III. Step II is distinctly exothermic while step III is definitely endothermic. We can now calculate approximate thermodynamic functions for the three steps by the following straightforward approach. All parameters are given for the process written as association, not dissociation: (a) ΔF_i° from $-RT \ln K$; (b) ΔH_i° from $(\Delta H_R^{\circ\ddagger} - \Delta H_f^{\circ\ddagger})$; and (c) ΔS_i° from $(\Delta H_i^\circ - \Delta F_i^\circ)/T$. The derived values are presented in Table IV.

Table II: Rate Constants for $MnSO_4$ Ion Association[a]

	20.0°	25.0°	30.0°
$10^{-10} \times k_{12}$, M^{-1} sec^{-1}	...	4.2	...
$10^{-8} \times k_{21}$, sec^{-1}	...	8.0	...
K_{12}, M (Bjerrum)	0.02022	0.01920	0.01856
$10^{-7} \times k_{23}$, sec^{-1}	6.52	6.73	6.94
$10^{-8} \times k_{32}$, sec^{-1}	1.64	1.87	2.12
K_{23}	2.52	2.78	3.05
$10^{-7} \times k_{34}$, sec^{-1}	3.46	4.75	6.62
$10^{-7} \times k_{43}$, sec^{-1}	1.03	1.35	1.73
K_{34}	0.297	0.284	0.261

[a] More figures are carried than is justified by the accuracy of the data so that rounding off errors are not propagated.

Table III: $MnSO_4$ Association in Water, $\Delta H^{\circ\ddagger}$ Values (kcal/mole)

	Forward	Reverse
Step II	0.68	3.91
Step III	10.4	8.72
	I	II	III

"free" ions a $\rightleftharpoons$ pair b (solvent separated) $\rightleftharpoons$ pair c (solvent separated) $\rightleftharpoons$ pair d (contact)

Table IV: Stepwise Thermodynamic Functions

	Step I	Step II	Step III	Σ (this work)	Σ (thermo)
ΔF°, kcal/mole[a]	−2.3	0.6	−0.7	−2.9	−3.07
ΔH°, kcal/mole[a]	1.5	−3.2	1.6	3.2	3.37
ΔS°, eu/mole[a]	13	−13	8	21	22.6

[a] ΔF_Σ°, ΔS_Σ°, ΔH_Σ° (thermo) from G. H. Nancollas, *J. Chem. Soc.*, 3934 (1959). The estimated errors in ΔF° and ΔH° are ±30% and the error in ΔS° is ±40%.

The Σ values refer to the over-all process, that is, K_Σ is defined by

$$K_\Sigma = \frac{[2] + [3] + [4]}{[1]^2\gamma_\pm^2}$$

The last column contrasts the Σ values with those found by classical thermodynamic methods. It should be noted that the step I values are from the calculated Bjerrum association constants and that the Σ values are calculated from the K_Σ values, not from the weighted average of the three steps. This causes a discrepancy that is not outside the error of the method.

Discussion of Results

As Eigen has previously stated, step I is very definitely the diffusion-controlled approach of the two ions. Our "measured" rate, based on an assumed Bjerrum K_{12}, is $4.2 \times 10^{10}\ M^{-1}\ \text{sec}^{-1}$, while Eigen's assumed rate based on the diffusion coefficients was $4 \times 10^{10}\ M^{-1}\ \text{sec}^{-1}$. This very adequate agreement is good support for the essential correctness of the Debye approach to the diffusion step.[16] This has implications beyond the immediate scope of this paper since the same model is used for the basis of the classical equations governing salt and solvent effects on ion–ion processes in solutions. It encourages us in our belief that processes like step I can be adequately described using the conventional solution parameters: solvent dielectric constant, solvent viscosity, ion charges, and ionic strength. It should be noted that step I is the only step involving a substantial $\Delta F°$. As has been pointed out,[17,18] the various bivalent metal ions should behave almost identically in this step since they are still completely hydrated. A synthesis of the two previous statements shows the basic reason why the various 2–2 sulfates have almost identical activity coefficients in water.[19] Step I is definitely endothermic (as is the over-all process) with a substantial positive $\Delta S°$ overriding the positive $\Delta H°$ to give a negative $\Delta F°$. One can further examine the entropy term along the lines suggested by Gurney.[20] Gurney divides the entropy change into cratic and unitary terms with the cratic term depending only on a change in the number of particles.

$$\Delta S° = \Delta S_u° + \Delta S_c° = 13 \text{ eu}$$

For $\Delta n = -1$ (two ions going to one ion pair), $\Delta S_c° = -8.0$ eu/mole. Therefore

$$\Delta S_u° = 13 \text{ eu} + 8 \text{ eu} = 21 \text{ eu}$$

It is apparent that we have a strong net disordering effect in spite of the cratic, ordering term. At the present time, it is only possible to attribute this to rather profound changes in the solvent shell surrounding the ion pair and/or a possible release of first-shell coordinated water.[21] Steps II and III represent the expulsion of water molecules from between the Mn^{2+} and SO_4^{2-} ions. From the close correspondence between k_{34} and the rate of exchange of H_2O on the Mn^{2+} ion, step III seems primarily dependent on cation properties. Presumably then, step II depends more on the anion. Both steps are small free energies caused by counterbalancing of enthalpy and entropy effects. Unfortunately, the $\Delta H°$ and $\Delta S°$ terms are small enough that many possible mechanisms could be proposed to account for them. It should be pointed out that the most probable source for the entropy changes is rearrangement of the solvent shell immediately around the ion pair. What effect changes in symmetry of the SO_4^{2-} ion have on the terms is very hard to discuss quantitatively. In fact, a definitive statement of how many of the SO_4^{2-} oxygens can and will coordinate to the Mn^{2+} does not seem possible.

In view of the very limited temperature range and limited accuracy of ultrasonic data, further speculation seems fruitless at this point. Work is in progress on other salt systems and on direct evaluation of the thermodynamic parameters of the diffusion-controlled step. When these data become available, we hope that a more definitive discussion of the problem will be possible.

Acknowledgment. We wish to acknowledge the support of the Army Research Office (Durham) through Grant No. DA-ARO(D)-31-124-G502. We also wish to express our gratitude to Dr. H. Tsubota for his aid in the analytical chemistry.

(16) P. Debye, *Trans. Electrochem. Soc.*, 82, 265 (1942).

(17) J. E. Prue in "Chemical Physics of Ionic Solutions," B. E. Conway and R. G. Barradas, Ed., John Wiley and Sons, Inc., New York, N. Y., 1966, Chapter 9.

(18) G. Atkinson, see ref 17, p 281.

(19) R. A. Robinson and R. H. Stokes, "Electrolyte Solutions," Butterworth and Co., Ltd., London, 1954, Appendix 8.10.

(20) R. W. Gurney, "Ionic Processes in Solution," McGraw-Hill Book Co., Inc., New York, N. Y., 1953.

(21) J. F. Duncan and D. L. Kepert in "The Structure of Electrolytic Solutions," W. J. Hamer, Ed., John Wiley and Sons, Inc., New York, N. Y., 1959, Chapter 25.

Mechanism of Oxygen Isotopic Exchange in Mixtures of Carbon Monoxide and Oxygen in a Quartz Vessel

by E. A. Th. Verdurmen

F.O.M.—Instituut voor Atoom, en Molecuulfysica, Amsterdam, The Netherlands *(Received October 3, 1966)*

The mechanism of the oxygen isotopic exchange processes occurring in a thermally reacting dry mixture of natural CO and O_2, predominantly enriched in the $^{18}O^{18}O$ species, has been studied between 500 and 580° and within the pressure range 28–144 torr, in a quartz reaction vessel. Three independent processes occur: (1) formation of CO_2; (2) oxygen isotopic exchange between CO and O_2; and (3) scrambling of oxygen isotopes in O_2. Scrambling and CO–O_2 isotopic exchange are retarded practically equally by the addition of considerable amounts of foreign gases, He, Ar, Xe, N_2, CO_2, and SF_6, whereas the rate of CO_2 formation remains practically constant. Relative efficiencies of the various foreign gases for retardation of the exchange processes have been obtained. Both scrambling and CO–O_2 isotopic exchange are completely inhibited by the addition of small amounts of NO. The processes involved show similar apparent activation energies between 30 and 35 kcal/mole. The formation of CO_2 is mainly a surface process. Scrambling and CO–O_2 isotopic exchange are interpreted in terms of gas-phase chain reactions. The chain carriers are oxygen atoms, originating from a wall reaction between CO and O_2, and excited CO_2 (singlet) molecules formed by radiationless transition from the CO_2 (triplet) association complex of CO and O. Chain termination occurs both by wall recombination of oxygen atoms and by gas-phase third-order reactions. The CO–O_2 isotopic exchange is determined by the reactions $O + CO \rightarrow CO_2^*$ (triplet) $\rightarrow CO + O$, and scrambling is ascribed to $O + O_2 \rightarrow O_3^* \rightarrow O_2 + O$ and CO_2^{**} (singlet) $+ O_2 \rightarrow CO_2^*$ (triplet) $+ O_2$. No marked deactivation of excited CO_2 has been observed. Addition of foreign gases favors third-order gas-phase termination and consequently reduces the O atom partial pressure. The inhibitory effect of NO is ascribed to very small amounts of NO_2, formed by slow reaction of NO with the O_2 reactant, and acting as an O atom scavenger. The ratio of the rate constant k_{25} of $O + O_2 \rightarrow O_3^*$ and the rate constant k_{28} of $O + CO \rightarrow CO_2^*$ (triplet) has been obtained at 500°, $k_{25}/k_{28} = 7.1 \pm 0.2$.

Introduction

Generally, the study of isotopic exchange reactions can demonstrate the existence of otherwise nondetectable processes, or can provide information on the elementary steps of a known but complicated chemical process. Such a complicated system is a thermally reacting dry mixture of CO and O_2. It exhibits the phenomenon of the first and second explosion limits.[1,2] The explosion is of the chain-branching type. Oxygen atoms and excited CO_2 (triplet) molecules[3] next to the carbon suboxides,[4] C_2O and C_3O_2, are proposed as the chain carriers or as important intermediates. The explosion peninsula starts above 600°.[5] Below that temperature, a slow formation of CO_2 is observed. In a previous paper,[6] it has been reported that in addition,

(1) G. J. Minkoff and C. F. H. Tipper, "Chemistry of Combustion Reactions," Butterworth and Co. (Publishers) Ltd., London, 1962, p 58.

(2) B. Lewis and G. von Elbe, "Combustion, Flames and Explosions of Gases," Academic Press Inc., New York, N. Y., 1961, p 71.

(3) S. W. Benson, "The Foundations of Chemical Kinetics," McGraw-Hill Book Co., Inc., New York, N. Y., 1960, p 460.

(4) P. Harteck and S. Dondes, *J. Chem. Phys.*, **27**, 1419 (1957).

(5) P. G. Dickens, J. E. Dove, and J. W. Linnett, *Trans. Faraday Soc.*, **60**, 539 (1964).

above 450°, oxygen isotopic exchange occurs between CO and O_2 as an independent gas-phase process, whereas the attendant formation of CO_2 is mainly a surface process. The preliminary study involved left the following problems unsolved: (a) are the intermediates mentioned, and particularly are oxygen atoms important in the exchange mechanism; (b) is a possibly formed excited CO_2 molecule sufficiently long lived to take part in the reactions; (c) does oxygen scrambling in O_2 occur (O_2–O_2 isotopic exchange); (d) if oxygen atoms are important intermediates, what is their origin?

The present paper reports the results of an attempt to obtain a more complete understanding of the processes occurring in a slowly and thermally reacting dry[7] mixture of CO and O_2 in a quartz vessel. The oxygen isotopic exchange between the reactants and the formation of CO_2 have been followed directly and simultaneously as a function of reaction time by continuous analysis of reactants and products with a mass spectrometer. The results indicate that oxygen atoms act as chain carriers in the oxygen exchange between the reactants.

Experimental Section

Apparatus. The experiments were performed in a reaction vessel constructed of Vitreosil quartz, i.d. 39 mm, volume 200 cc, supplied with a small quartz leak (3×10^{-5} l. torr sec^{-1}, at a pressure difference of 75 torr and at room temperature) to the ionization chamber of an Atlas CH4 mass spectrometer. As shown in Figure 1, the reaction vessel was placed in a resistance-heated furnace consisting of a copper cylinder, tightly surrounding the vessel and provided with external windings, and heat-insulating material. The furnace temperature was maintained constant within ±0.5° at 500° by means of a temperature controller. Control was applied to the furnace current by the changing resistance of a Pt resistance thermometer, fitted into the copper cylinder as indicated in Figure 1. The temperature gradient along the reaction vessel was less than 2° at 500°. Temperatures were measured by thermocouples (chromel–alumel) fitted outside the reaction vessel and inside the copper cylinder. The reactor was separated from the vacuum line by an indium stopcock. This particular vacuum line and the attendant pumping system were used exclusively for the evacuation of the reactor. The reactants inlet at the reactor side consisted of about 100 cm of capillary tube, i.d. 2 mm, partly cooled at −78° to prevent interference of condensable impurities (*e.g.*, mercury vapor from the manometer and the Toepler pump). The inlet system consisted of a 500-cc vessel for premixing of reactants, mercury manometer, Toepler pump, gas-condensing device equipped with a Pyrex leak (3×10^{-2} l. torr sec^{-1}, at a pressure difference of 760 torr and at room temperature) to allow slow evaporation of liquid, and three 1000-cc volumes to store purified gases. The reactor was connected to the mass spectrometer by way of 60 cm of copper tubing, i.d. 6 mm, provided with a stainless steel high-vacuum valve (bore 12 mm) to the mass spectrometer ionization chamber, and separated from the vacuum line by a glass stopcock. The inlet system and the glass–copper tubing between the reactor and the mass spectrometer were joined to a separate vacuum line. The copper tubing and the stainless steel valve were bakeable, respectively, at 150 and 130°.

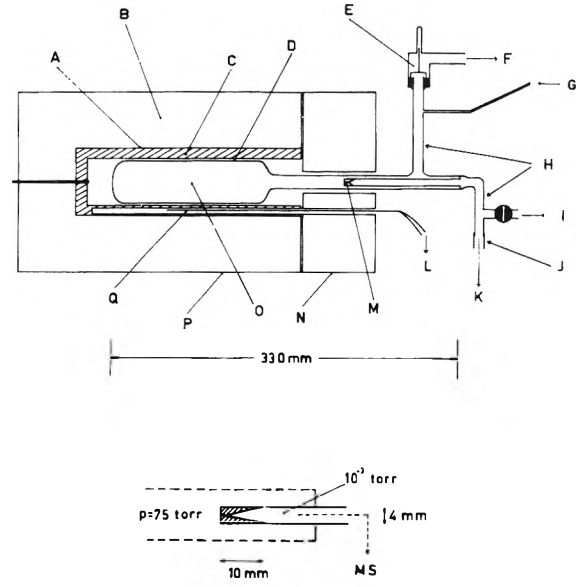

Figure 1. The reactor and its connections; the quartz leak. A, external windings; B, heat-insulating material; C, copper cylinder; D, Vitreosil; E, indium stopcock; F, to vacuum line I; G, reactants inlet (Pyrex); H, graded seal (Vitreosil–Pyrex); I, to vacuum line II; J, Kovar; K, to mass spectrometer ionization chamber; L, to temperature controller; M, leak; N, cover; O, reaction vessel; P, furnace; Q, Pt resistance element; MS, mass spectrometer.

Sampling Device. The actual size of the quartz leak can be estimated from graphs of ion beam intensity against reactor pressure, as shown in Figure 2. Ion beam intensity and gas pressure in the reactor show a linear relation over the whole pressure range. However, there is a change of slope at about 10 torr, very probably cor-

(6) E. A. Th. Verdurmen and C. A. Bank, *J. Inorg. Nucl. Chem.*, 25, 1521 (1963).

(7) Though it has been shown in the preliminary investigation[6] that small amounts of water do not influence the exchange rate, in the present experiments water has been carefully removed from the reactor, the inlet system, and the reactants.

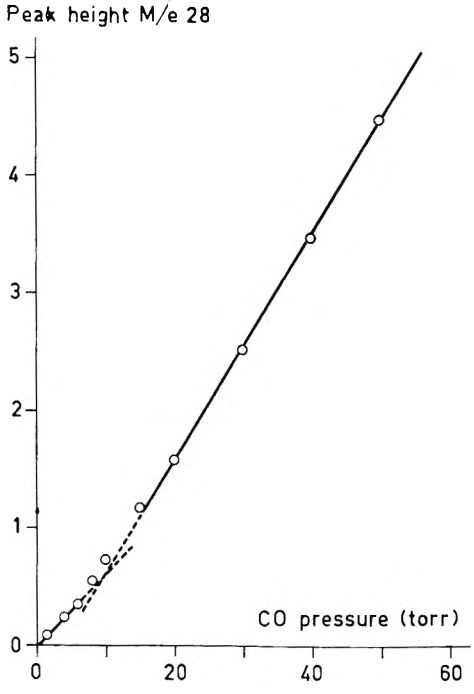

Figure 2. Peak height m/e 28 in the mass spectrum, as a function of CO pressure in the reactor, at room temperature.

responding to the transition from molecular to viscous flow through the leak. Consequently, the size of the leak was of the order of the mean free path at a pressure of 10 torr at room temperature, *i.e.*, about 5×10^{-3} mm. The total volume of the tubing on the low-pressure side of the leak was about 30 cc. Under operating conditions (gas pressure in the reactor 75 torr, and flow 3×10^{-5} l. torr sec^{-1}), the pressure just behind the leak could be estimated to be of the order of 10^{-3} torr. Thus, the total amount of gas in the tubing was equal to the flow through the leak in about 0.5 sec. Pressure reduction in the reactor as a result of the continuous sampling through the leak was about 0.5% in 45 min. Consequently, the sampling did not disturb the kinetics. The response of the system showed some delay. Pressure changes in the reactor mass spectrometrically were detected after about 1 sec. Peak heights approached their ultimate values, within 1% of initial difference, after about 30 sec. Since concentration changes in the present experiments were slow relative to these 30 sec, they could be followed adequately in this system.

The shape of the leak was that of a divergent nozzle.[8] The (maximum) mass rate of flow, above the critical-pressure ratio, is given by

$$G' = A\rho C f(\gamma) \qquad (1)$$

where A is the area of the leak, ρ is the density of the gas on the high-pressure side of the leak, C is the root mean square velocity of the molecules, and $f(\gamma)$ is a complicated function of $\gamma = C_p/C_v$ (the ratio of the specific heats of the gas at constant pressure and at constant volume). This kind of sampling by a mass spectrometer through a leak at pressures for which the mean free path of the molecules is small compared to the diameter of the leak, has been considered theoretically and experimentally by Barber, Farren, and Linnett.[9] According to their treatment, for a particular two-component gas mixture the ratio of the number of molecules per unit volume, n_1 and n_2, in the mass spectrometer is given by

$$\frac{n_1}{n_2} = \frac{p_1}{p_2}\left[\frac{M_1}{M_2}\right]^{1/2}$$

where p_1 and p_2 are the partial pressures, and M_1 and M_2 the molecular weights of the components in the reactor. If ion beam intensity I, concentration n, and ionization efficiency S, are related by $I = Sn$, then the following expression can be derived

$$\frac{p_1}{p_2} = \frac{I_1 S_2}{I_2 S_1}\left[\frac{M_2}{M_1}\right]^{1/2} \qquad (2)$$

In the present investigation, measured isotope ratios in CO and O_2 were compared with a standard, so that fractionation effects cancelled out. However, product CO_2 was determined relative to the original amount of CO, and no standard was present, so that a mass discrimination correction had to be applied (*vide infra*).

Materials. Natural carbon monoxide was prepared from purified carbon dioxide by reaction on charcoal at 1000°. Natural oxygen was made by gentle heating of $KMnO_4$. A small amount of $^{18}O_2$ was obtained by electrolysis of $H_2{}^{18}O$ (90%). Carbon dioxide, sulfur hexafluoride, nitrogen, helium, argon, and xenon were purest available materials. Nitric oxide was prepared by the action of moderately concentrated nitric acid on copper. Carbon monoxide and oxygen were purified by repeated condensation in a liquid nitrogen trap at −196°, followed by slow evaporation collecting a middle fraction. Carbon dioxide, nitric oxide, and sulfur hexafluoride were purified by repeated bulb-to-bulb distillation. Nitrogen was passed through a column of charcoal at −196°. The remaining gases were used without further treatment. The purity of the gases was checked by mass spectrometric analysis.

In none of the samples was molecular hydrogen detected, indicating that the concentration of H_2 in the

(8) A. B. Cambel and B. H. Jennings, "Gas Dynamics," McGraw-Hill Book Co., Inc., New York, N. Y., 1958, Chapter 7.

(9) M. Barber, J. Farren, and J. W. Linnett, *Proc. Roy. Soc.* (London), **A274**, 293 (1963).

samples was below 3×10^{-5}. The mass spectrum of the residual gas in the ionization chamber always showed a rather small peak of H_2O^+. Thus the mass spectrometric analysis was not suitable for the detection of traces of H_2O in the samples. The present drying method is similar to that of Gordon and Knipe.[10] These investigators observed that addition of 0.004% H_2O to their dried CO–O_2 mixtures had a marked effect upon the position of the second explosion limit. Consequently, the concentration of H_2O in their dried mixtures must have been smaller than 1×10^{-4}. It seems fairly safe to conclude that the present drying method provides samples containing less than 0.01% H_2O. Other impurities (mainly nitrogen) did not exceed 0.1%.

Treatment of Vessel. Formation of carbon dioxide in this system (below 600°) appears to be mainly a surface process.[11] At room temperature, the silica surface is believed to be covered with OH groups and possibly with physically adsorbed water molecules.[12,13] Heating at 120° during some hours removes completely the physically adsorbed water, but the OH groups are retained. When the temperature is raised, water begins to be lost by formation of oxygen bridges between two adjacent hydroxyl groups. According to Zhadanov[14] and de Boer, *et al.*,[13] these oxygen bridges can be converted back to OH groups by exposure to liquid water. It has been observed that the catalytic formation of CO_2 from CO and O_2 at a quartz surface is the higher the less the number of hydroxyl groups attached to the silica surface.[11] Therefore, to suppress the CO_2 formation, before mounting, the reaction vessel was treated with water at 95° during 5 hr. Thus, total and partial pressure changes due to conversion of CO and O_2 into CO_2 and interference of product CO_2 were reduced as far as possible. At 500° generally not more than a few per cent of the maximum possible conversion into CO_2 was measured after 45 min of reaction time. The crushed silica (Vitreosil), used in a number of experiments, was treated in a similar way.

Procedure. The water-treated reaction vessel, mounted into the furnace and connected to the vacuum line and the inlet system, was baked for 3 hr at 120° under vacuum. Then the temperature was raised to 500° and the vessel was evacuated for at least 10 hr to below 1×10^{-6} torr, measured by an ionization gauge. Before admitting a gas mixture, the vessel was evacuated for 2 hr to below 1×10^{-6} torr at the reaction temperature (between 500 and 580°). The reactants were premixed, except in the experiments with nitric oxide. This gas was admitted before or simultaneously with the remaining reactants, or it was added to a reacting mixture as indicated in the experiments involved. Admission of reactants occurred by expansion from the premixing vessel. The gas pressure in the reactor was measured by a mercury manometer connected to the premixing vessel. The experiments were performed with natural CO and enriched O_2. The oxygen sample used (^{18}O content about 3%) was obtained by mixing natural oxygen and oxygen containing 90% ^{18}O isotope. The enrichment of the O_2 thus predominantly was in the $^{18}O^{13}O$ species, so that next to isotopic exchange between CO and O_2 the rate of attainment of statistical equilibrium of the ^{18}O in O_2 (scrambling) could be measured. Recording of peak heights, corresponding to concentrations of isotopic CO, isotopic O_2, and isotopic CO_2 molecules, generally was started about 40 sec after admission of reactants to the reactor. The range m/e 28–46 was continuously scanned during 45 min, so that the corresponding concentrations were measured directly as a function of time. Before each series of experiments, pure oxygen gas was passed through the ionization chamber, by way of the conventional mass spectrometer inlet system, for 2 hr to condition the ion source. After that time, the ratios of the peak heights m/e 28 to m/e 32, and m/e 44 to m/e 32, appeared to be practically constant and relatively small (see Reduction of Data).

Applied Rate Expressions. In this study it is assumed that the isotopic exchanges are ideal; thus isotope effects are not considered. The well-known first-order rate expression for isotopic exchange of the general type

$$AX_n + BX_{m-1}X^* \rightleftarrows AX_{n-1}X^* + BX_m$$

where X* and X are isotopes of a particular element, is given by

$$S = -\frac{1}{t}\frac{nmab}{na + mb}\ln(1 - F) \qquad (3)$$

S is the gross rate of exchange; a and b are the partial pressures of the reactants AX_n and BX_m; $F = (x_t - x_0)/(x_\infty - x_0)$ is the exchange fraction; x_t is the fractional content of tracer in AX_n or BX_m at time t, and x_0 and x_∞ are the values for this fraction at $t = 0$ and $t = \infty$. The kinetics of the present isotopic exchange reactions are complicated by a nonrandom distribution of isotopes in one of the reactants. However, it is

(10) A. S. Gordon and R. H. Knipe, *J. Phys. Chem.*, 59, 1160 (1955).

(11) C. A. Bank and E. A. Th. Verdurmen, *ibid.*, 67, 2869 (1963).

(12) J. C. Greaves and J. W. Linnett, *Trans. Faraday Soc.*, 55, 1355 (1959).

(13) J. H. de Boer, M. E. A. Hermans, and J. M. Vleeskens, *Proc. Koninkl. Ned. Akad. Wetenschap.*, B60, 45 (1957); B61, 85 (1958).

(14) S. P. Zhadanov, *Dokl. Akad. Nauk SSSR*, 68, 99 (1949).

easily derived that also in this case the general expression (3) can be applied.

The general expression relating the rate of a reaction and the partial pressures of the reactants is

$$S = ka^q b^r \qquad (4)$$

wherein q and r can be integers or fractional numbers.

The following symbols are used in this study: (i) for formation of CO_2, rate S_{CO_2}, pressure $a = p_{O_2}$, pressure $b = p_{CO}$; (ii) for oxygen isotopic exchange between CO and O_2, rate S_{CO-O_2} abbreviated S_{CO}, exchange fraction F_{CO-O_2}, abbreviated F_{CO}, pressure $a = p_{O_2}$, pressure $b = p_{CO}$, $n = 2$, and $m = 1$; (iii) for oxygen exchange between O_2 and O_2 (scrambling), rate $S_{O_2-O_2}$ abbreviated S_{sc}, exchange fraction $F_{O_2-O_2}$ abbreviated F_{sc}, pressure $a = b = p_{O_2}$, $n = m = 2$.

Reduction of Data. The peak heights m/e 28 and 30 were corrected for the contribution of oxygen and carbon dioxide. These corrections were relatively small (a few per cent, rarely 10%). The addition of some of the foreign gases (N_2, Ar, SF_6) forced further correction at, respectively, m/e 28; m/e 36; and m/e 32, 34, and 36.

The starting point of the reaction in all performed experiments was arbitrarily fixed on the time $t = 2$ min after expanding the reactants into the reactor.

From the corrected peak heights at m/e 28 and 30, ^{18}O contents in CO were calculated, and hence the corresponding exchange fractions F_{CO} were found as a function of time. From the corrected peak heights at m/e 32, 34, and 36, the product of mass ratios $^{34}/_{32}$ and $^{34}/_{36}$ was obtained as a function of time. The oxygen samples used (^{18}O content about 3%) showed initial values of the product of about 0.005. The limiting value at equilibrium is 4.0. The product values were reduced to exchange fractions, F_{sc}, using calculated curves of the product of mass ratios $^{34}/_{32}$ and $^{34}/_{36}$ as a function of exchange fraction. The measurement of the scrambling of isotopes in O_2 was complicated by the decrease in ^{18}O content of O_2, due to the simultaneous isotopic exchange between O_2 and CO. However, the latter exchange was relatively slow. The decrease in ^{18}O content of O_2 generally was a few per cent, rarely 10%, of the initial value after 45 min reaction time. The exchange fractions F_{sc} were corrected for this decrease, assuming that the $^{34}O_2$ and the $^{36}O_2$ content in O_2 are equally reduced as a result of the $CO-O_2$ exchange. The amount of product CO_2 was determined from the ratio of the corrected peak height m/e 44 to the corrected peak height m/e 28, the latter correlating with the CO partial pressure in the reactor. The ratio was corrected for the difference between the ionization efficiencies of CO and CO_2, and a mass discrimination correction was applied (*vide supra*).

Results

In this system three different processes occur: (a) formation of CO_2; (b) isotopic exchange between CO and O_2; (c) scrambling of oxygen isotopes in O_2 (*i.e.*, isotopic exchange between O_2 and O_2).

Figure 3, a typical plot of log $(1 - F)$ *vs.* reaction time t, demonstrates that both the isotopic exchange $CO-O_2$ and the scrambling of oxygen isotopes in O_2 fit in with expression 3: the relation between ln $(1 - F)$ and the reaction time t is obviously linear. For all performed experiments such linear relations have been found.[15] Consequently, it is justified to calculate the exchange rates S_{CO} and S_{sc} from the slopes of the straight lines in the log $(1 - F)$ *vs.* t plots, by substitution into expression 3.

The rates S_{CO_2}, S_{CO}, and S_{sc} have been measured as a function of O_2 pressure at constant CO pressure, and as a function of CO pressure at constant O_2 pressure at 500°. Plots of log S *vs.* log p can provide information on the magnitude of the numbers q and r in expression 4 and the applicability of the expression with certain q and r values over a particular pressure range. Such plots for the experiments mentioned are shown in Figures 4 and 5. In the latter, measurements have been included performed in a reaction vessel partly packed with crushed silica (Vitreosil) increasing the surface to volume ratio fivefold. The following observations are shown in these figures. (1) There is a striking difference in order of magnitude between

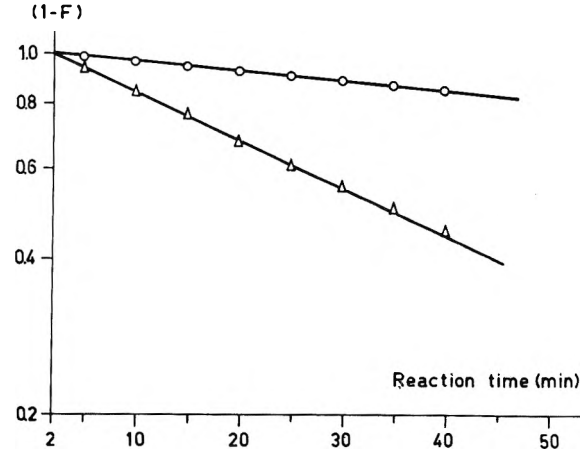

Figure 3. Typical logarithmic plot of $(1 - F)$ *vs.* reaction time for scrambling in O_2 and for $CO-O_2$ isotopic exchange at 500°; CO (24 torr), O_2 (24 torr); O, F_{CO}, △, F_{sc}.

(15) Except for experiments in which very small amounts of NO were present (*vide* Figure 10).

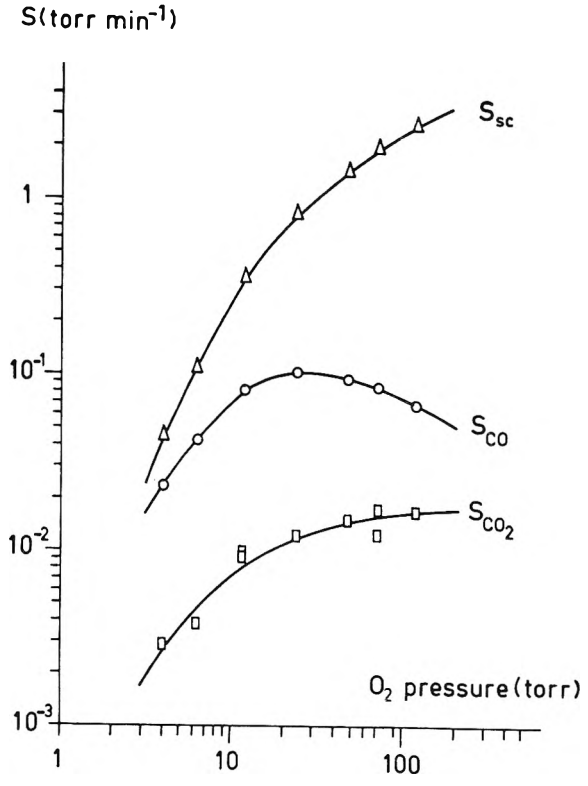

Figure 4. Log–log plot of reaction rate S *vs.* O_2 pressure at constant pressure of CO (24 torr) at 500°; △, S_{sc}; ○, S_{CO}; □, S_{CO_2}.

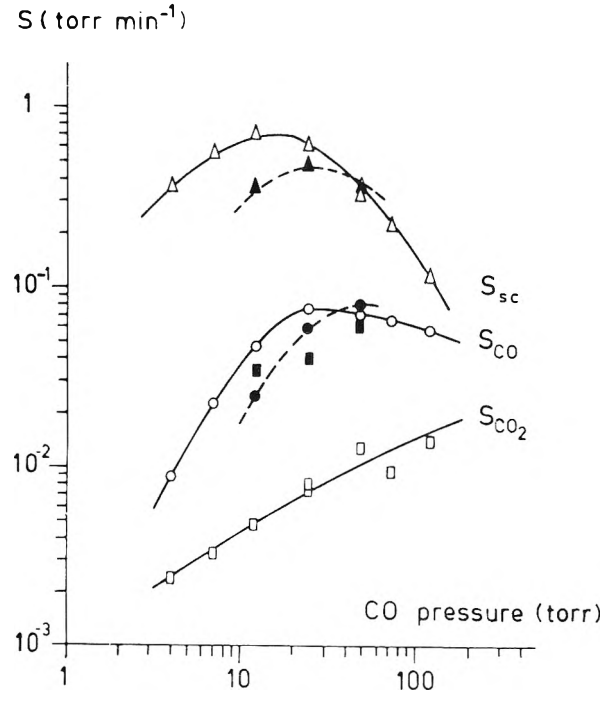

Figure 5. Log–log plot of reaction rate S *vs.* CO pressure at constant pressure of O_2 (24 torr) at 500°; △ and ▲, S_{sc}; ○ and ●, S_{CO}; □ and ■, S_{CO_2}; shaded marks: surface to volume ratio increased fivefold.

S_{CO_2}, S_{CO}, and S_{sc}, at each applied pressure. (2) It is obvious that none of the curves shown, except that of S_{CO_2} in Figure 5, can be described by a particular expression (4) with constant numbers q and r over the whole pressure range. (3) Increasing the surface to volume ratio fivefold results in a roughly fivefold increase of S_{CO_2}, whereas S_{CO} and S_{sc} remain virtually constant. (4) The observed maxima in the curves S_{CO} and S_{sc} (Figure 5) are shifted to higher partial pressures of CO, if the surface to volume ratio is increased.

Considering the nature of the occurring processes, observation 1 is a strong indication that these processes are independent. At each particular pressure in Figures 4 and 5, the number of CO_2 molecules formed per unit of time is much smaller than the number of exchanges CO–O_2 per unit of time, the latter number being much smaller than the number of exchanges O_2–O_2 per unit of time. So the measured scrambling of oxygen isotopes in O_2 cannot occur as a result of oxygen isotopic exchange between CO and O_2, nor can the latter exchange occur as a result of CO_2 formation. Observation 3 confirms the conclusion of the preliminary study[6] that the CO_2 formation is mainly a surface process, whereas the isotopic exchange reactions occur in the gas phase. From the shape of the curves, observation 2, it can be concluded that the isotopic exchange processes do not occur by the simple gas-phase reactions

$$C^{16}O + {}^{18}O^{16}O \longrightarrow C^{18}O + {}^{16}O^{16}O \qquad (5)$$

$${}^{16}O^{16}O + {}^{18}O^{18}O \longrightarrow {}^{16}O^{18}O + {}^{16}O^{18}O \qquad (6)$$

Some experiments have been performed studying scrambling of oxygen isotopes in pure oxygen. Even at 600°, practically no scrambling was measured within the reaction time (45 min). However, as is clearly shown in Figure 6, addition of a small amount (2%) of CO immediately starts scrambling at a considerable rate at 500°. This observation indicates that the reactive species in the scrambling process is formed in a reaction in which CO is involved.

The temperature dependence of the three processes has been determined by performing experiments at various temperatures between 500 and 580°. The measured rates of both isotopic exchange reactions and the measured rate of CO_2 formation are logarithmically plotted as a function of reciprocal temperature, for two different mixtures, in Figure 7. The straight lines are a least-squares fit to experimental data. From

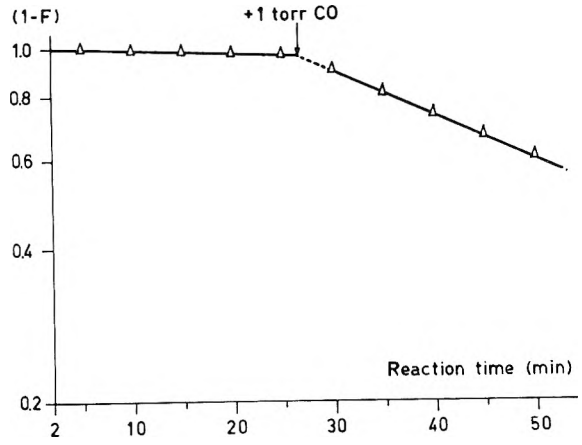

Figure 6. Logarithmic plot of $(1 - F)$ *vs.* reaction time, for scrambling in O_2 at 500°; O_2 (50 torr); CO added at time indicated.

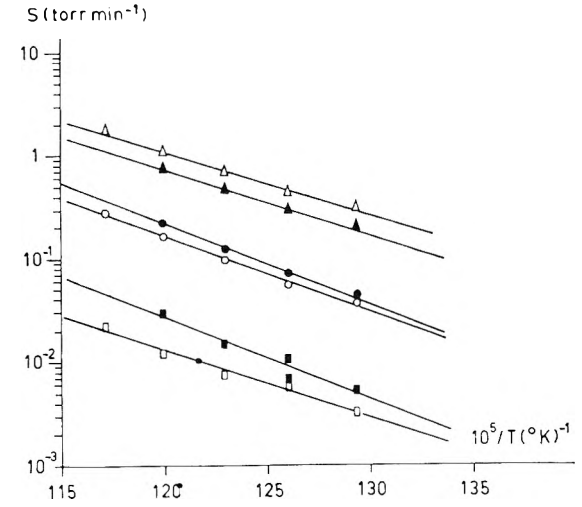

Figure 7. Logarithmic plot of reaction rate S *vs.* reciprocal temperature: △ and ▲, S_{sc}; ○ and ●, S_{CO}, □ and ■, S_{CO_2}; open marks: CO (24 torr), O_2 (24 torr); shaded marks: CO (48 torr), O_2 (24 torr).

the slopes of these lines, apparent[16] activation energies have been obtained, that are reported in Table I. The apparent activation energies obtained do not show much difference, though the value relating to the isotopic exchange CO–O_2 appears to be higher than the remaining apparent activation energies (about 30 kcal/mole) by a few kcal/mole.

In order to determine the possible occurrence of excited intermediates with lifetimes of kinetic significance, experiments have been performed in which considerable amounts of foreign gases were added: He, Ar, Xe, N_2, CO_2, and SF_6. The striking effect of these additions is that scrambling and CO–O_2 isotopic exchange are retarded practically equally, whereas the rate of CO_2 formation remains practically constant. It is easily found from the data reported in Table II that the ratio S_{sc}/S_{CO} does not depend upon foreign-gas pressure.

Table I: Over-all Apparent Activation Energies for Scrambling in O_2, Isotopic Exchange CO–O_2, and Formation of CO_2[a]

Process	Apparent activation energy, kcal/mole: Mixture I[b]	Mixture II[c]
Scrambling in O_2	28.5 ± 2.3	29.5 ± 1.4
Isotopic exchange CO–O_2	34.0 ± 1.4	36.4 ± 1.8
Formation of CO_2	30.0 ± 2.5	36.7 ± 5.5

[a] Observed in CO–O_2 mixtures in a quartz vessel between 500 and 580°. [b] Mixture of CO (24 torr) and O_2 (24 torr). [c] Mixture of CO (48 torr) and O_2 (24 torr).

Table II: Value of $f(S) = S_{sc}[CO]/S_{CO}[O_2]$ as a Function of Foreign-Gas Pressure, for Addition of Various Foreign Gases[a]

Foreign-gas pressure, torr	f(S) for addition of: He	Ar	Xe	N_2	CO_2	SF_6
0	8.04	...[b]	7.36	7.89	...[b]	7.74
12	7.87	8.25	7.56	7.99	7.72	8.15
24	7.40	7.96	7.29	7.89	8.19	8.21
48	7.35	8.21	7.15	7.71	7.65	7.23
72	7.57	8.16	...[b]	7.69	7.14	...[b]

[a] Observed in mixtures of CO (24 torr) and O_2 (24 torr) in a quartz vessel, at 500°. [b] Not measured.

Plots of the reciprocal of S_{CO} *vs.* foreign-gas pressure and plots of the reciprocal of S_{sc} *vs.* foreign-gas pressure show essentially straight lines. The rates S_{CO_2}, S_{CO}, and S_{sc}, measured in a series of particular foreign-gas additions, have been compared to the rates in the original CO–O_2 mixture that were measured preceding the series. Though, generally, the reproducibility of S_{CO} and S_{sc} within a series of experiments was quite good (about ± 5%), a comparison of the rates in similar experiments of different series showed larger scattering (about ± 35%). Therefore, in order to compare the particular effects of the added gases, the intercepts of the straight lines obtained in the plots of reciprocal S *vs.* foreign-gas pressure had to be reduced to one particular value of reciprocal S at zero foreign-gas pressure. The particular effects of the added gases are shown in Figures 8 and 9, being plots of reciprocal S_{CO} and reciprocal S_{sc} *vs.* foreign-gas pressure. In

(16) Apparent, since the particular activation energies obtained do not necessarily apply to an individual reaction.

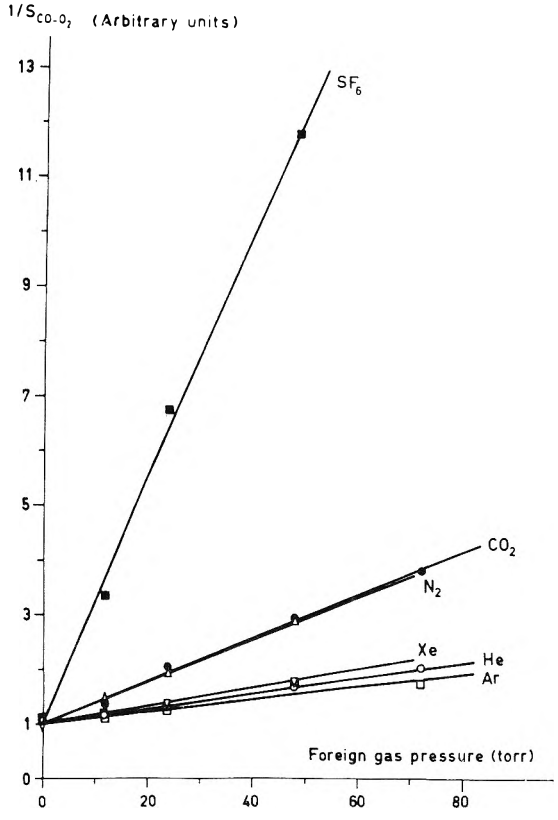

Figure 8. Reciprocal of the rate of isotopic exchange CO–O_2 plotted as a function of foreign-gas pressure, for various foreign gases, CO (24 torr) and O_2 (24 torr) at 500°. Straight lines are least-squares fit to experimental data; slope × 10^2: ○, He, 1.46 ± 0.03; □, Ar, 1.16 ± 0.34; ▽, Xe, 1.68 ± 0.05; △, N_2, 3.88 ± 0.16; ●, CO_2, 3.97 ± 0.45; ■, SF_6, 22.7 ± 6.2.

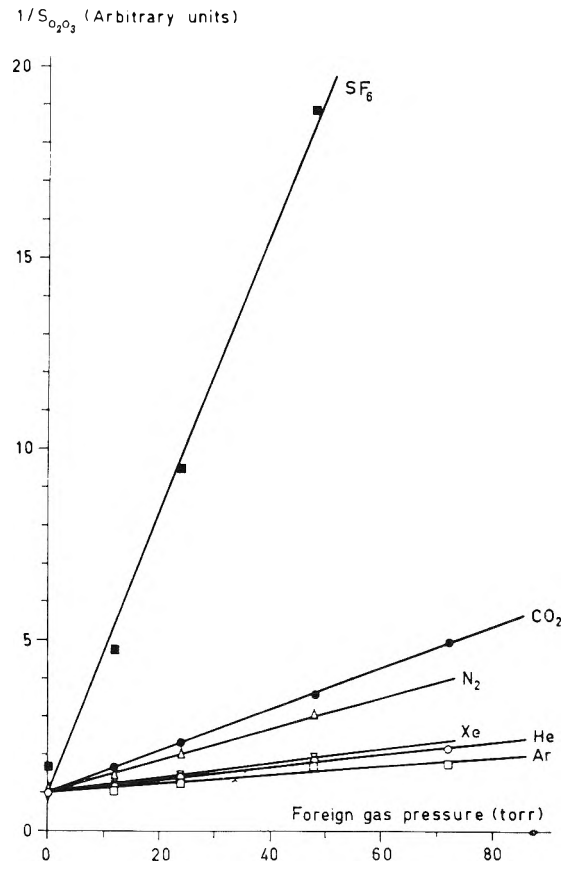

Figure 9. Reciprocal of the rate of scrambling in O_2 plotted as a function of foreign-gas pressure, for various foreign gases; CO (24 torr), O_2 (24 torr) at 500°. Straight lines are least-squares fit to experimental data; slope × 10^2: ○, He, 1.62 ± 0.07; □, Ar, 1.14 ± 0.32; ▽, Xe, 1.85 ± 0.03; △, N_2, 4.09 ± 0.26; ●, CO_2, 5.44 ± 0.18; ■, SF_6, 36.6 ± 20.8.

Table III the rate of CO_2 formation at different foreign-gas pressures, for addition of various foreign gases, has been given. Considering that within a series of experiments the reproducibility of S_{CO_2} appeared to be about ±15%, it can be concluded from the data of Table III that the rate of CO_2 formation in these experiments was practically constant. (The effect of SF_6 needs some qualification.) Figures 8 and 9 demonstrate the observed linear relation between the foreign-gas pressure and the reciprocals of the exchange rate S_{CO} and S_{sc}. Moreover, it is obvious from these figures that the various foreign gases are not equally effective. Relative efficiencies have been calculated from the slopes of the straight lines compared to the slope of the straight line for N_2 addition. These efficiencies and their standard deviations are reported in Table IV. The efficiency of N_2 has been set equal to unity owing to the supposition that the effect of N_2 does not differ appreciably from the foreign-gas effect of CO, a main component of the mixture. Taking into account the standard deviations mentioned, Table IV shows that the relative efficiencies for retardation of scrambling hardly differ from the relative efficiencies for retardation of isotopic exchange CO–O_2. Since

Table III: Rate of CO_2 Formation at Different Foreign-Gas Pressures, for Addition of Various Foreign Gases[a]

Foreign-gas pressure, torr	S_{CO_2}, (torr min^{-1}) × 10^3, for addition of—				
	He	Ar	Xe	N_2	SF_6
0	3.1	...[b]	7.6	4.9	6.9
12	3.8	4.9	8.0	6.0	3.1
24	4.2	5.3	9.1	6.0	2.7
48	4.2	6.0	9.6	6.0	2.2
72	4.2	6.4	...[b]	6.0	...[b]

[a] Observed in mixtures of CO (24 torr) and O_2 (24 torr) in a quartz vessel, at 500°. [b] Not measured.

Table IV: Relative Efficiencies of Various Foreign Gases in the Retardation of the Scrambling in O_2 and the Isotopic Exchange $CO-O_2$[a,b]

Foreign gas	Scrambling in O_2	Isotopic exchange $CO-O_2$
He	0.40 ± 0.03	0.38 ± 0.02
Ar	0.28 ± 0.08	0.30 ± 0.09
Xe	0.45 ± 0.03	0.43 ± 0.02
N_2	1.00 ± 0.09	1.00 ± 0.06
CO_2	1.33 ± 0.10	1.02 ± 0.12
SF_6	8.9 ± 5.1	5.8 ± 1.6

[a] Observed in mixtures of CO (24 torr) and O_2 (24 torr) in a quartz vessel at 500°. [b] The efficiency of N_2 has been set equal to unity.

the slope of the N_2 line in Figure 8 practically equals the slope of the N_2 line in Figure 9, respectively (3.88 ± 0.16) × 10^{-2} and (4.09 ± 0.26) × 10^{-2}, the former observation further illustrates the conclusion that the scrambling in O_2 and the isotopic exchange $CO-O_2$ are retarded practically equally by addition of foreign gases.

If the retardation of exchange rates, as a result of added foreign gases, is produced by deactivation of excited intermediates, it is not probable that these gases will have quite the same effect on different intermediates. Therefore, it is more likely that the main effect of addition of foreign gases is reducing the partial pressure of a common intermediate of both scrambling and $CO-O_2$ isotopic exchange. The almost equal efficiencies of He and Xe, and generally the order and relative magnitude of the efficiencies of the particular foreign gases, clearly suggest that neither adsorption nor diffusion in this system are rate-controlling processes.

If oxygen atoms are an intermediate in this system, the addition of an O atom scavenger should inhibit the otherwise occurring processes in which O atoms are involved. In order to test this hypothesis, some experiments have been performed in which small amounts of NO were added. The third-order reaction of NO with O atoms is a fast and consequently efficient reaction. Therefore, NO is considered to be an efficient O atom scavenger. Generally, NO retards all chain reactions in which paramagnetic radicals propagate the reaction chains. Figures 10 and 11 are combined plots of log $(1 - F)$ *vs.* reaction time and of pressure of product CO_2 *vs.* reaction time. In the experiments shown in Figure 10, the reactants, CO, O_2, and NO, were admitted to the reactor simultaneously. In the experiments of Figure 11, NO was added to a reacting mixture roughly at $t = 21$ min and $t = 30$ min. Both figures illustrate the following significant observations.

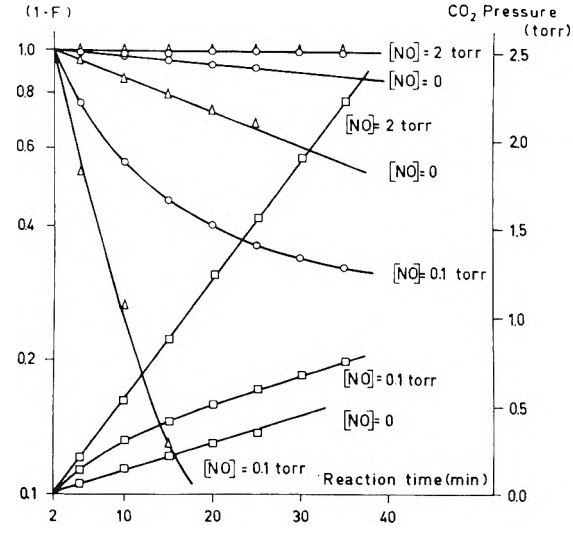

Figure 10. Logarithmic plot of $(1 - F)$ *vs.* reaction time and plot of pressure of product CO_2 *vs.* reaction time for mixtures of CO (48 torr) and O_2 (24 torr) and various amounts of NO at 500°; O, F_{CO}; △, F_{sc}; □, p_{CO_2}.

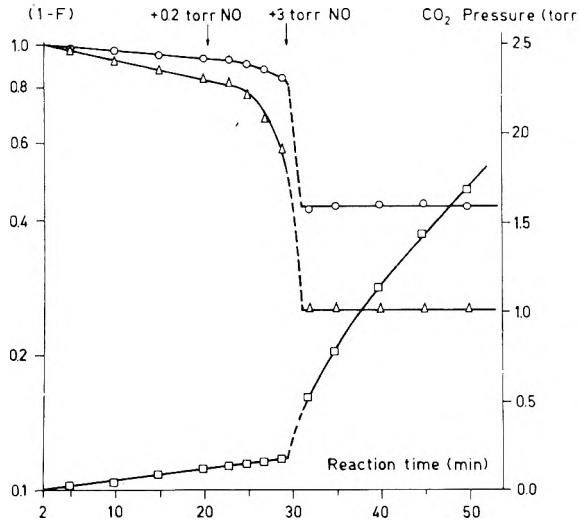

Figure 11. Logarithmic plot of $(1 - F)$ *vs.* reaction time and plot of pressure of product CO_2 *vs.* reaction time for mixtures of CO (48 torr) and O_2 (24 torr) at 500°. NO added at times indicated. O, F_{CO}; △, F_{sc}; □, p_{CO_2}.

(1) Small amounts of NO (concentrations roughly 3%) suffice to inhibit both scrambling and $CO-O_2$ isotopic exchange completely. (2) Very small amounts of NO (concentration roughly 0.3%) markedly accelerate both scrambling and $CO-O_2$ isotopic exchange. (3) The rate of CO_2 production remains constant by the addition of very small amounts of NO, but at higher NO concentrations it is considerably enhanced.

Regarding Figure 11, it has to be considered that the nitric oxide was introduced through the reactants inlet

so that it took some time before mixing was complete. Hence, after addition of the second amount of NO, at $t = 30$ min, the ultimate inhibition is preceded by acceleration of both isotopic exchange processes. Figure 10 clearly demonstrates that at very small NO concentrations no linear relation is found between ln $(1 - F)$ and the reaction time t, for both scrambling and CO–O_2 isotopic exchange. Obviously, there is no difference in the effect of NO whether it is added simultaneously with the remaining reactants or is introduced to a reacting mixture. Therefore, NO does not act upon the initiating reactions, but rather interferes in the propagating steps of the reaction process.[17] Apart from its accelerating effect at very small concentrations, the general behavior of NO in this system—complete inhibition of exchange processes by a relatively small amount of NO—is that of chain breaking by the inhibitor. As will be argued in the Discussion section, the inhibitory effect of NO addition should be ascribed to very small amounts of NO_2, produced by slow reaction of the added NO and the O_2 reactant.

Discussion

Reactive Species. The main information about the nature of the reactive species is obtained from the effect of the added inert foreign gases and the effect of NO addition. It has been concluded that the main foreign-gas effect is reducing the partial pressure of a common intermediate of both scrambling and CO–O_2 isotopic exchange. Considering the nature of both isotopic exchange processes, it is likely that this intermediate will be one of the species O_2, O_3, O_2*, and O.[18]

The shape of the curves in Figures 4 and 5 eliminates O_2 as the common intermediate: reactions 5 and 6 have been rejected. O_3 shows rapid reaction with NO,[19] but it has the disadvantage that its concentration is not expected to be reduced by the addition of inert gases. Recently, some chemical reactions of the metastable lowest-lying known excited states of oxygen, $O_2(^1\Delta_g)$ and $O_2(^1\Sigma_g^+)$, have been studied.[20–22] No rapid reaction with NO was observed.[21–24] Apart from their long radiative lifetime, these states appear to be very stable with respect to molecular collisions. Winer and Bayes[25] observed at 23° and at a pressure of 10 torr, in a 20-mm i.d. reaction tube, that wall deactivation of $O_2(^1\Delta_g)$ completely predominates gas-phase deactivation. It has been found in the present investigation that the concentration of the intermediate is considerably reduced by the addition of foreign gas at pressures below 100 torr. Vibrationally excited O_2 in the electronic ground state at 500° probably will be easily deactivated by collision.[26] Thus it cannot set up long chains and, therefore, should occur in rather high concentrations. On the contrary, the observation that a relatively small amount of NO completely inhibits the exchange processes is a strong argument for occurrence of a chain mechanism involving free atoms in very small concentrations. Since, additionally, oxygen atoms are generally believed to occur as important intermediates in this system at slightly higher temperatures[1–3] (above 600°), it seems justified to assume that oxygen atoms act as the common intermediate in the present processes too.

The scrambling of oxygen isotopes in O_2 and the CO–O_2 isotopic exchange observed in this system thus are ascribed to the independent processes

$$O + O_2 \longrightarrow O_2 + O \qquad (7)$$

$$O + CO \longrightarrow CO + O \qquad (8)$$

Termination and Initiation. Termination of chains involving oxygen atoms can occur by wall recombination of O atoms, reaction 9, or by the gas-phase third-order reactions 10 and 11

$$O + O + W \longrightarrow O_2 + W \qquad (9)$$

$$O + O_2 + M \longrightarrow O_3 + M \qquad (10)$$

$$O + CO + M \longrightarrow CO_2 + M \qquad (11)$$

The direct recombination in the gas phase is too slow to be of importance. Indicating the rate of O atom formation by R_O, a steady-state treatment yields the following expression for the O atom concentration in the stationary state

$$[O] = \frac{R_O}{k_{10}[O_2][M] + k_{11}[CO][M] + k_9} \qquad (12)$$

(17) V. N. Kondratev, "Chemical Kinetics of Gas Reactions," Pergamon Press Ltd., Oxford and London, 1964, p 606.

(18) The intermediates CO_2*, C_2O, and C_3O_2, probably occurring in this system at slightly higher temperatures,[3,4] are all produced by reactions involving O atoms.

(19) H. S. Johnson and H. J. Crosby, *J. Chem. Phys.*, **22**, 689 (1954).

(20) R. E. March, S. G. Furnival, and H. I. Schiff, *Photochem. Photobiol.*, **4**, 971 (1965).

(21) M. A. A. Clyne, B. A. Thrush, and R. P. Wayne, *ibid.*, **4**, 957 (1965).

(22) L. W. Bader and E. A. Ogryzlo, *Discussions Faraday Soc.*, **37**, 46 (1964).

(23) S. J. Arnold, E. A. Ogryzlo, and H. Witzke, *J. Chem. Phys.*, **40**, 1769 (1964).

(24) L. Elias, E. A. Ogryzlo, and H. I. Schiff, *Can. J. Chem.*, **37**, 1680 (1959).

(25) A. M. Winer and K. D. Bayes, *J. Phys. Chem.*, **70**, 302 (1966).

(26) Lipscomb, *et al.*, measured at room temperature very different efficiencies for deactivation of vibrationally excited O_2 ($v = 8$) in the electronic ground state: CO_2, one in 7000 collisions; Ar and N_2, one in more than 10^7 collisions. In the present study, the efficiencies of the various foreign gases are relatively in the same order of magnitude (the efficiencies of N_2 and CO_2 are almost equal). F. J. Lipscomb, R. G. W. Norrish, and B. A. Thrush, *Proc. Roy. Soc.* (London), **A233**, 455 (1956).

wherein wall recombination of oxygen atoms has been regarded as a first-order process, according to Greaves and Linnett.[12] The rate constant k_9 can be calculated from the recombination coefficient of oxygen atoms on Vitreosil,[12] γ (500°) = 1.4 × 10^{-2}, and the vessel dimensions: k_9 (at 500°) = 355 sec^{-1}. The rate constant k_{10}[M = O_2] can be obtained from data by Benson and Axworthy,[27] k_{10} = 2.96 × 10^7 exp(890/RT) l.^{2} $mole^{-2}$ sec^{-1}, at 500° reduced to k_{10} = 1.5 × 10^{-34} cm^6 $molecule^{-2}$ sec^{-1}. The rate constant k_{11} can be calculated from data by Kondratev and Ptichkin,[28] k_{11} (at 428°K) = 2.96 × 10^{13} cm^6 $mole^{-2}$ sec^{-1}, and data by Clyne and Thrush[29] regarding the activation energy of the reaction: 3.7 kcal/mole; k_{11} (at 500°) = 5.6 × 10^{-34} cm^6 $molecule^{-2}$ sec^{-1}. Thus, at 500° k_{10} and k_{11} are in the same order of magnitude.

In order to determine the order of magnitude of the O atom concentration in the present experiments, it is assumed that the measured rate of scrambling is given by the rate of the isotopic exchange reaction

$$O + O_2 \longrightarrow O_2 + O \qquad (7a)$$

The rate constant of this reaction has been determined by Herron and Klein[30] and by Brennen and Niki.[31] Assuming the reaction has the same small negative activation energy as reaction 10, the rate constant at 500° is given by k_{7a} = 0.4 × 10^{-12} cm^3 $molecule^{-1}$ sec^{-1} The rate of reaction 7a is represented by

$$S_{7a} = k_{7a}[O_2][O] \qquad (13)$$

In a mixture of CO(24 torr) and O_2 (24 torr) at 500°, a scrambling rate S_{sc} = 0.379 torr min^{-1}, *i.e.*, 8.8 × 10^{13} molecules cm^{-3} sec^{-1} has been measured. By substitution into expression 13, the concentration of O atoms is found to be [O] = 6.3 × 10^8 atoms cm^{-3}. Then the rate of O atom formation, R_O, required to maintain this concentration is calculated from expression 12: R_O = 3.2 × 10^{11} atoms cm^{-3} sec^{-1}.

As is shown in Figure 6, scrambling of oxygen isotopes in O_2 occurs under condition that CO is present, so that obviously the reactive intermediates, O atoms, are formed in a reaction in which CO is involved. This reaction might be

$$CO + O_2 \longrightarrow CO_2 + O \qquad (14)$$

Sulzmann, *et al.*,[32] determined the rate constant of this reaction in the temperature range 2400–3000°K, in a shock-wave experiment

$$k_{14} = (3.5 \pm 1.6) \times 10^{12} \exp[-(51000 \pm 7000)/RT]\ cm^3\ mole^{-1}\ sec^{-1}$$

Hence, it is expected that the over-all apparent activation energies in the present system will exceed 44 kcal/mole. The actual apparent activation energies reported in Table I evidently are much smaller than the 51 ± 7 kcal/mole observed by Sulzman in reaction 14. Consequently, the gas-phase reaction 14 can be rejected as an important source of O atoms in this system.

The most likely alternative is a similar process (15) occurring at the wall of the reaction vessel

$$CO + O_2 \xrightarrow{\text{wall}} CO_2 + O \qquad (15)$$

It is shown in Figure 5 that the rate of CO_2 formation is proportional to the surface to volume ratio of the vessel. Consequently, the CO_2 production is mainly a surface process, and it is not unlikely that the process (15) is involved. In the mixture of CO (24 torr) and O_2 (24 torr) at 500°, a CO_2 formation rate S_{CO_2} = 0.012 torr min^{-1}, *i.e.*, 2.8 × 10^{12} molecules cm^{-3} sec^{-1}, has been measured. If the CO_2 formation is attended with the simultaneous production of an O atom, the experimentally determined value of S_{CO_2} should equal the rate of O atom formation. However, it can be expected that only part of the produced O atoms actually will escape from the wall into the gas phase. In the mixture of CO (24 torr) and O_2 (24 torr), the deduced value of R_O is about 11% of the measured rate S_{CO_2}.

If chains are started at the wall of the vessel, the observation that the isotopic exchange rates S_{sc} and S_{CO} remain virtually constant in spite of the enhancement of the surface to volume ratio demonstrates that chain breaking at the wall should be important too. Considering expression 12, both R_O and k_9 are proportional to the surface to volume ratio. By substitution of the rate constants k_9, k_{10}, and k_{11}, it is found that, in a mixture of CO (24 torr) and O_2 (24 torr), a fivefold enhancement of the surface to volume ratio will increase the O atom concentration by a factor of 1.3. Actually, this effect had to be measured by comparison of experiments in a reaction vessel partly packed with crushed silica, with similar experiments in an unpacked vessel. Since the reproducibility of S_{sc} and S_{CO} in such experiments of different series appeared to be about ±35%, the expected small enhancement of the O

(27) S. W. Benson and A. E. Axworthy, *J. Chem. Phys.*, **42**, 2614 (1965).

(28) V. N. Kondratev and I. I. Ptichkin, *Kinetika i Kataliz*, **2**, 492 (1961).

(29) M. A. A. Clyne and B. A. Thrush, *Proc. Roy. Soc.* (London), **A269**, 404 (1962).

(30) J. T. Herron and F. S. Klein, *J. Chem. Phys.*, **40**, 2731 (1964); **41**, 1285 (1964); **44**, 3645 (1966).

(31) W. Brennen and H. Niki, *ibid.*, **42**, 3725 (1965).

(32) K. G. P. Sulzmann, B. F. Myers, and E. R. Bartle, *ibid.*, **42**, 3969 (1965).

atom concentration could not be measured. The observed experimental scattering should have its origin in the activity of the surface that obviously is not invariable. The condition of the wall, *e.g.*, the number of OH groups at the silica surface, will determine not only the rate of CO_2 production,[11] and consequently the rate of O atom formation, but also the fraction of O atoms that leaves the wall. Moreover, the less OH groups at the silica surface the higher will be the recombination coefficient for oxygen atoms on the wall.[12] Thus the dependence of the O atom concentration in the gas phase upon the surface conditions is rather complicated.

Summarizing, the initiation and wall termination of chains in this system is interpreted in terms of the reactions

$$CO + O_2 \xrightarrow{\text{wall}} CO_2 + O_{wall} \quad (16)$$

$$O_{wall} + O_{wall} \longrightarrow (O_2)_{wall} \quad (17)$$

$$O_{wall} \longrightarrow O_{gas} \quad (18)$$

$$\text{surface–O*} + O_{gas} \longrightarrow \text{surface–} + (O_2)_{gas} \quad (19)$$

$$\text{surface–} + O_{gas} \xrightarrow{\text{rapid}} \text{surface–O*} \quad (20)$$

The mechanism of wall recombination of oxygen atoms on Vitreosil, reactions 19 and 20, has been discussed by Greaves and Linnett.[12] Oxygen atoms from the gas phase recombine with loosely bound oxygen atoms, O*, that have been adsorbed from the gas phase.

Propagation. Isotopic exchange of oxygen atoms with O_2 has been studied by Herron and Klein.[30] Their results have been interpreted in terms of the mechanism

$$O + O_2 \rightleftarrows O_3^* \quad (21, 21')$$

$$O_3^* + M \longrightarrow O_3 + M \quad (22)$$

The rate constants k_{21}' and k_{22} were found to be at room temperature, $k_{21}' = 1.8 \times 10^9$ sec^{-1} and $k_{22} = 4 \times 10^{11}$ cm^3 mole^{-1} sec^{-1}; *i.e.*, 0.7×10^{-12} cm^3 molecule^{-1} sec^{-1}. The stationary-state concentration of O_3 is given by

$$[O_3^*] = \frac{k_{21}[O_2][O]}{k_{21}' + k_{22}[M]} \quad (23)$$

and the rate of exchange by

$$S_{21}' = k_{21}'[O_3^*] \quad (24)$$

Assuming that no temperature corrections in k_{21}' and k_{22} have to be applied, it is easily calculated that at 500° and total pressures below 100 torr, holds: $k_{22}[M]/k_{21}' < 5 \times 10^{-4}$. Consequently, in the exchange mechanism, deactivation of the excited association complex O_3^* is not a predominant process.

Direct isotopic exchange of oxygen atoms with CO has not been studied so far. In the present investigation the observation that S_{CO_2} is proportional to the surface to volume ratio demonstrates that at most, very small amounts of CO_2 are formed in the gas phase. The observation that even the total rate of CO_2 formation, S_{CO_2}, is small with regard to the related S_{CO} and S_{sc}, and the fact that S_{CO_2} is practically not influenced by addition of foreign gases, suggest that CO_2 formation by deactivation of an eventual excited complex CO_2^* is not an important process in the exchange mechanism. The rate of CO_2 formation by the third-order gas-phase reaction (11) is given by $S_{11} = k_{11}[CO][O][M]$. Substitution of $[O] = 6.3 \times 10^8$ atoms cm^{-3} (*vide supra*) yields, for a mixture of CO (24 torr) and O_2 (24 torr) at 500°, a rate $S_{11} = 7.7 \times 10^{10}$ molecules cm^{-3} sec^{-1}, *i.e.*, about 3% of the measured value of $S_{CO_2} = 2.8 \times 10^{12}$ molecules cm^{-3} sec^{-1}. The conclusion that the main effect of foreign-gas addition is reducing the partial pressure of the atomic oxygen intermediate is another argument against marked deactivation of a possibly formed association complex CO_2^* in the gas phase.

Thus far it is likely that the propagation reactions for scrambling in O_2 and for CO–O_2 isotopic exchange actually are represented by

$$O + O_2 \qquad O_3^* \longrightarrow O_2 + O \quad (25)$$

$$O + CO \longrightarrow (CO_2^* \longrightarrow) CO + O \quad (26)$$

The rate of reaction 25 should equal the measured scrambling rate. The CO–O_2 isotopic exchange will occur successively by reaction 26 and reaction 25. Since it has been observed that the scrambling rate uniformly exceeds the rate of CO–O_2 isotopic exchange, the latter should equal the rate of reaction 26. Then the following relation is easily found

$$\frac{S_{sc}}{S_{CO}} = \frac{k_{25}[O_2]}{k_{26}[CO]} \quad (27)$$

Consequently, the experimentally determined value of $S_{sc}[CO]/S_{CO}[O_2]$ should be constant for all performed experiments at a particular temperature. Tables V and II show that $f(S) = S_{sc}[CO]/S_{CO}[O_2]$ does not depend on total pressure as it does not on foreign-gas pressure. On the contrary, it is clearly shown in Figure 12 that $f(S)$ as a function of the mixing ratio is not constant. It is found that $f(S)$ is proportional to the mixing ratio $[CO]/[O_2]$. It appears that the individual measurements at constant O_2 pressure (open

circles) do not fit to the straight line as well as the measurements at constant CO pressure (shaded circles). However, the estimated relative accuracy of the individual measurements in this figure, *i.e.*, ±10%, and the observation shown in Table V that f(S) obviously

Table V: Value of f(S) = $S_{sc}[CO]/S_{CO}[O_2]$ as a Function of Total Pressure at 500° and at 540°[a]

Total pressure, torr	f(S) At 500°	f(S) At 540°
36	6.80	6.04
54	6.90	5.78
72	6.86	5.86
108	6.72	5.85

[a] Mixing ratio $[CO]/[O_2] = 0.50$.

does not depend on total pressure suggest that the apparent difference is not significant. Admittedly, the observation shown in Figure 12 demonstrates that the exchange mechanism is more complicated than supposed thus far. Consequently, next to oxygen atoms another reactive intermediate has to be of kinetic significance. It has been concluded that neither deactivation of O_3* nor deactivation of CO_2* is an important process in the exchange mechanism. However, molecular oxygen, which has a triplet ground state, $O_2(^3\Sigma_g^-)$, can facilitate spin reversal. Thus, if triplet–singlet transitions are involved, as can be expected for reaction of CO and O in their ground electronic states, molecular oxygen can act without simultaneous deactivation.

The present observations can be adequately interpreted in terms of the mechanism

$$O + O_2 \longrightarrow O_3^* \longrightarrow O_2 + O \qquad (25)$$

$$O(^3P) + CO(^1\Sigma^+) \rightleftarrows CO_2^*(\text{triplet}) \qquad (28, 29)$$

$$CO_2^*(\text{triplet}) \longrightarrow CO_2^{**}(\text{singlet}) \qquad (30)$$

$$CO_2^{**}(\text{singlet}) + O_2(^3\Sigma_g^-) \longrightarrow CO_2^*(\text{triplet}) + O_2(^3\Sigma_g^-) \qquad (31)$$

If the isotopic exchange between CO and O occurs by redissociation of the excited association complex CO_2*, this molecule has to be in a triplet state. As far as knowledge of CO_2 electronic energy levels is available, the lowest triplet state of CO_2 observed ($^3B_2$) should have its vibrational zero level not more than 45 kcal/mole below the energy of $CO(^1\Sigma^+) + O(^3P)$.[29,33] Using the Rice–Ramsperger–Kassel model for unimolecular decomposition,[34] the lifetime of this triplet CO_2

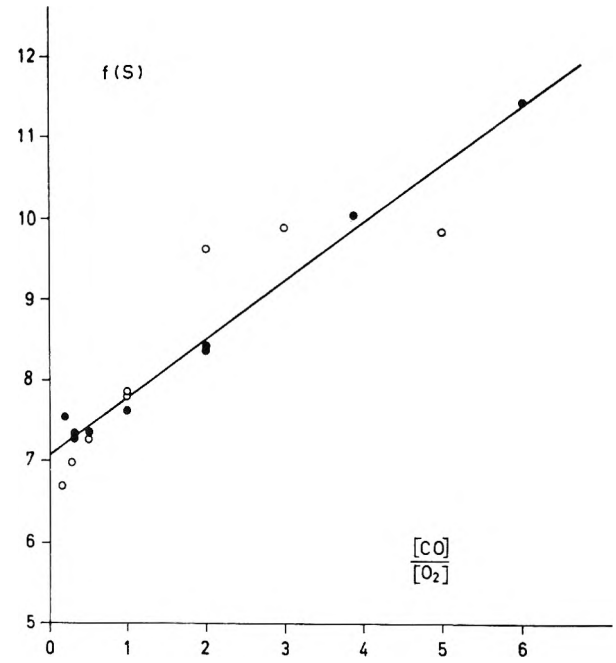

Figure 12. Plot of f(S) = $S_{sc}[CO]/S_{CO}[O_2]$ *vs.* the mixing ratio $[CO]/[O_2]$ at 500°; ○, at constant pressure of O_2 (24 torr); ●, at constant pressure of CO (24 torr). Estimated relative accuracy of the individual measurements, ±10%. The straight line is a least-squares fit to experimental data.

can be estimated to be 6×10^{-11} sec, that is too short to participate in molecular collisions below 100 torr (time between collisions longer than 6×10^{-10} sec). However, it is likely that crossing of potential energy surfaces will occur, so that the excited triplet CO_2* may undergo radiationless transitions. Gordon and Knipe[10] considered only the triplet surfaces and thus spin-allowed transitions. Mahan and Solo[35] and Clyne and Thrush[29] considered also spin-forbidden transitions. It has been supposed that the upper state of the CO flame band emission, $CO_2(^1B_2)$, is entered by radiationless transition from the $CO_2(^3B_2)$ state.[29] If the association complex CO_2*(triplet) produced in reaction 28 undergoes radiationless transition to a singlet CO_2 state, as in reaction 30, this singlet CO_2 does not correlate with $CO(^1\Sigma^+) + O(^3P)$ and consequently cannot dissociate with the available energy. Its lifetime, apart from deactivation by collision, depends on its probability to undergo further radiationless transitions and it may be sufficiently long to enable the molecule to take part in reactions. Since deactivation is not a predominant process in this system, the reaction that remains is spin reversal by

(33) R. N. Dixon, *Proc. Roy. Soc.* (London), **A275**, 431 (1963).
(34) *Cf.* ref 3, p 231.
(35) B. H. Mahan and R. B. Solo, *J. Chem. Phys.*, **37**, 2669 (1962).

reaction with O_2, reaction 31. It is not unlikely that scrambling of oxygen isotopes in O_2 occurs simultaneously in this reaction.

Stationary-state concentrations of CO_2*(triplet) and CO_2**(singlet) are easily derived to be

$$[CO_2^*] = \frac{k_{28}[CO][O] + k_{31}[O_2][CO_2^{**}]}{k_{29} + k_{30}}$$

$$[CO_2^{**}] = \frac{k_{30}[CO_2^*]}{k_{31}[O_2]}$$

By elimination of $[CO_2^{**}]$, an expression for $[CO_2^*]$ is obtained

$$[CO_2^*] = \frac{k_{28}}{k_{29}}[CO][O]$$

If the CO–O_2 isotopic exchange is determined by reaction 29 and the scrambling in O_2 by reactions 25 and 31, the following rate expressions can be derived

$$S_{CO} = k_{28}[CO][O] \tag{32}$$

and

$$S_{sc} = k_{25}[O_2][O] + \frac{k_{30}}{k_{29}}k_{28}[CO][O] \tag{33}$$

Thus it has been assumed that there are two paths for scrambling in O_2: the direct reaction (25), and that by way of the CO–O exchange mechanism, reaction 31. The ratio of S_{sc} and S_{CO} then is given by

$$\frac{S_{sc}}{S_{CO}} = \frac{k_{25}[O_2]}{k_{28}[CO]} + \frac{k_{30}}{k_{29}} \tag{34}$$

and consequently

$$f(S) = \frac{S_{sc}[CO]}{S_{CO}[O_2]} = \frac{k_{25}}{k_{28}} + \frac{k_{30}}{k_{29}}\frac{[CO]}{[O_2]} \tag{35}$$

Expression 35 is consistent with the observation that $f(S)$ is proportional to the mixing ratio $[CO]/[O_2]$. The slope and intercept of the plot in Figure 12 thus can be interpreted, respectively, as k_{30}/k_{29} and k_{25}/k_{28}. By the method of least squares it is found that $k_{30}/k_{29} = 0.7 \pm 0.1$ and $k_{25}/k_{28} = 7.1 \pm 0.2$, at 500°.

The temperature dependence of $f(S)$ is shown in Figure 13, a logarithmic plot of reciprocal $f(S)$ *vs.* reciprocal temperature, for two different mixtures. The straight lines are least-squares fits to experimental data. Both lines show the same slope, corresponding with an apparent activation energy 6.9 ± 0.9 kcal/mole. This number actually is the difference in the apparent activation energies of the CO–O_2 isotopic exchange and the scrambling process. Its interpretation in relation to rate constants of individual reactions is

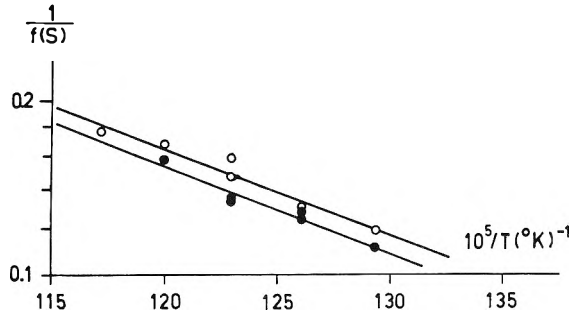

Figure 13. Logarithmic plot of reciprocal $f(S)$ *vs.* reciprocal temperature. Open circles: CO (24 torr), O_2 (24 torr); shaded circles: CO (48 torr); O_2 (24 torr).

rather difficult in consequence of the nature of expression 35. Since, for the mixtures involved, the term $(k_{30}/k_{29})([CO]/[O_2])$ is a few times smaller than k_{25}/k_{28}, and possibly k_{29} and k_{30} will not depend on temperature, the observed 6.9 ± 0.9 kcal/mole approximately equals the difference in activation energies between reaction 28 and reaction 25. This conclusion, however, needs some qualification. Provided reactions 25 and 28 have the same activation energies as observed for third-order formation of O_3 and CO_2, respectively, about −1 kcal/mole[27] and about 4 kcal/mole,[29] the expected difference in activation energies is 5 kcal/mole, in rather good agreement with the observed 6.9 ± 0.9 kcal/mole.

Regarding the nature of the CO_2**(singlet) formed in reaction 30, it can be stated that its lifetime, τ, has to be long enough to undergo molecular collisions: $\tau > 10^{-9}$ sec. Since no important deactivation of excited CO_2 has been observed, reaction 31 has to be effective and CO_2**(singlet) should be relatively stable with respect to collisional deactivation, also by CO_2. Generally, an electronically excited molecule in one of its higher vibrational levels has a high probability of transfer of vibrational energy into translational energy of a colliding particle, in contrast with a vibrationally excited molecule in the electronic ground state.[36] Moreover, to assure a sufficiently long lifetime of CO_2**-(singlet) with respect to radiationless transition, the excited singlet molecule should have a rather large amount of energy to relocalize before it can pass into another state by radiationless transition. Therefore, it is not unlikely that the CO_2**(singlet) actually is vibrationally excited CO_2 in its electronic ground state.

Effect of Reactant Concentrations. By substitution of expression 12 into 32 and 33, the following expressions for S_{CO} and S_{sc} are obtained: eq 36

$$S_{CO} = k_{28}[CO]\frac{R_O}{k_{10}[O_2][M] + k_{11}[CO][M] + k_9} \tag{36}$$

(36) *Cf.* ref 17, p 390.

and eq 37 respectively.

$$S_{sc} = \left\{k_{25}[O_2] + \frac{k_{30}}{k_{29}}k_{28}[CO]\right\} \times \frac{R_O}{k_{10}[O_2][M] + k_{11}[CO][M] + k_9} \quad (37)$$

If the rate of O atom formation, R_O, is determined by reaction 16, its dependence upon reactant concentrations will equal the reactant-concentration dependence of the rate of CO_2 formation in reaction 16. Provided that the CO_2 is practically exclusively produced by reaction 16, the rate dependence involved is shown by S_{CO_2} in Figures 4 and 5. At constant CO pressure (Figure 4), S_{CO_2} is proportional to $[O_2]$ at low pressures, and is increasing less and less than proportional at higher O_2 pressures. At constant O_2 pressure (Figure 5), S_{CO_2} is roughly proportional to $[CO]^{1/2}$ over the whole pressure range. Considering that $[M] = [CO] + [O_2]$, and that at 500° holds $k_{25}/k_{28} = 7.1$, $k_{30}/k_{29} = 0.7$, and $k_{11}/k_{10} = 3.7$, from expressions 36 and 37 the following shape of the curves in Figures 4 and 5 can be expected. At low partial pressures of O_2 or CO, the predominant term in the denominator of (36) and (37) is k_9. At relatively high partial pressures of O_2 or CO, respectively, the terms $k_{10}[O_2][M]$ and $k_{11}[CO][M]$ will be predominant. Considering in addition the deduced pressure dependence of R_O, in Figure 4 the S_{CO} will increase roughly proportional with $[O_2]$ at low O_2 pressures. At relatively high O_2 pressures, the rapid increase of the denominator (becoming quadratic in $[O_2]$) ultimately results in a decrease of S_{CO} for increasing $[O_2]$. In a similar way, it is expected that S_{sc} at low O_2 pressures will increase with somewhat less than $[O_2]^2$, and at relatively high O_2 pressures will pass through a maximum. The S_{sc} maximum should occur at a higher O_2 partial pressure than the S_{CO} maximum as a consequence of the fact that the numerator of (36) is less dependent upon $[O_2]$ than the numerator of (37) is. It is easily seen that S_{CO} and S_{sc} in Figure 5 should show similar curves. At low CO pressures, S_{CO} should increase roughly with $[CO]^{3/2}$, and S_{sc} roughly with $[CO]^{1/2}$. The rate constant for wall recombination of oxygen atoms, k_9, is proportional to the surface to volume ratio. Therefore, for experiments performed in a vessel with enlarged surface to volume ratio, the term k_9 in the denominator of (36) and (37) is relatively more important. Consequently, the maxima in S_{CO} and S_{sc} should be shifted to higher partial pressures (Figure 5). The observations shown in Figures 4 and 5 are in good agreement with all these considerations.

Expressions for the reciprocals of S_{CO} and S_{sc} as a function of foreign-gas pressure can easily be obtained from (36) and (37). For a mixture of CO (24 torr) and O_2 (24 torr)

$$\frac{1}{S_{CO}} = \frac{k_{10}[M] + k_{11}[M] + \frac{k_9}{[CO]}}{k_{28}R_O} \quad (38)$$

and

$$\frac{1}{S_{sc}} = \frac{k_{10}[M] + k_{11}[M] + \frac{k_9}{[CO]}}{\left\{k_{25} + \frac{k_{30}}{k_{29}}k_{28}\right\}R_O} \quad (39)$$

Consequently, a plot of reciprocal S_{CO} and of reciprocal S_{sc} *vs.* foreign-gas pressure should yield straight lines. The slopes of these lines are given, respectively, by a_{CO} and a_{sc}

$$a_{CO} = \frac{k_{10} + k_{11}}{k_{28}R_O}; \quad a_{sc} = \frac{k_{10} + k_{11}}{\left\{k_{25} + \frac{k_{30}}{k_{29}}k_{28}\right\}R_O} \quad (40)$$

Actually, these linear relations between the reciprocals of the exchange rates and the foreign-gas pressure have been observed, as shown in Figures 8 and 9. The various slopes for different foreign gases obviously relate to the values of $(k_{10} + k_{11})$ for the particular foreign gases. The relative efficiencies of the different foreign gases for retardation of S_{CO} should equal the corresponding relative efficiencies for retardation of S_{sc}, as it actually has been observed (Table IV). It has been calculated that at 500°, $k_{11}/k_{10} = 3.7$. Therefore, the relative efficiencies of the different foreign gases practically may be considered equal to the relative efficiencies of the particular third bodies, M, in the third-order[37] reaction 11. Some qualification is required regarding the fact that k_{10} and k_{11} have been obtained by extrapolation from other temperatures. Considering expressions 38 and 39, the retarding effect of a particular amount of foreign gas should be smaller the higher the value of k_9. In Figure 14, the retarding effect of CO_2 addition is compared for experiments in which k_9, proportional to the surface to volume ratio, has different values. Obviously, the retardation of both S_{CO} and S_{sc} is considerably smaller in the packed vessel, in agreement with the expectations.

(37) At total pressures below 1 torr, second-order formation of CO_2 has been observed.[35] The present data: the shape and position of the curves in Figures 4 and 5 and the difference between the observed foreign-gas efficiencies and the known[27] efficiencies of M in reaction 10, suggest that the gas-phase CO_2 formation in the present system, reaction 11, is a third-order process.

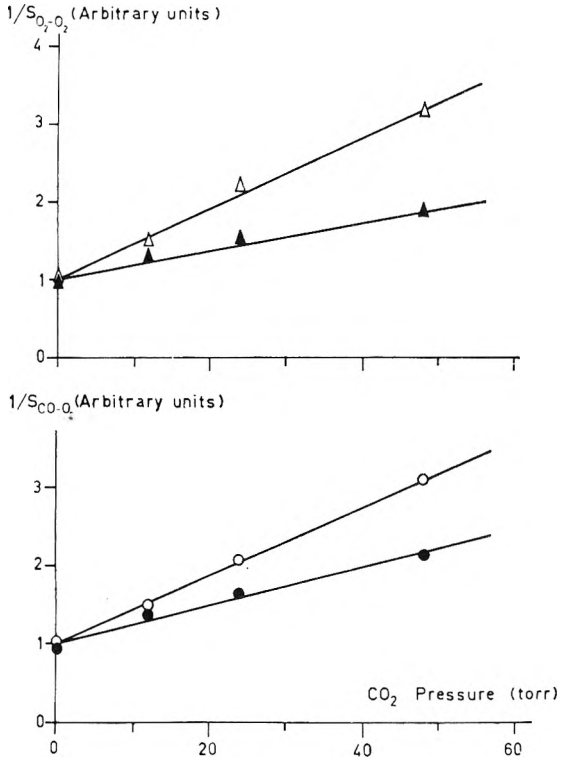

Figure 14. Plot of the reciprocal of the rate of scrambling in O_2 and of the reciprocal of the rate of CO–O_2 isotopic exchange *vs.* the pressure of added CO_2 for two different surface to volume ratios, CO (48 torr) and O_2 (24 torr), at 500°; open marks, unpacked vessel; shaded marks, packed vessel, surface to volume ratio increased fivefold. Straight lines are least-squares fit to experimental data; slope × 10^2; △, 4.56 ± 0.26; ▲, 1.84 ± 0.18; ○, 4.40 ± 0.16; ●, 2.48 ± 0.25.

Effect of NO. If the O atom concentration is reduced as a result of the fast reaction

$$NO + O + M \longrightarrow NO_2 + M \qquad (41)$$

the stationary-state concentration of oxygen atoms is given by

$$[O] = \frac{R_O}{k_{10}[O_2][M] + k_{11}[CO][M] + k_9 + k_{41}[NO][M]} \qquad (42)$$

The rate constant k_{41} can be obtained from data by Klein and Herron,[30] $k_{41} = 1.44 \times 10^{15} \exp(1930/RT)$ cm^6 mole^{-2} sec^{-1} (M = N_2) at 500°, reduced to $k_{41} = 1.4 \times 10^{-32}$ cm^6 molecule^{-2} sec^{-1}. By substitution of the rate constants k_{10}, k_{11}, k_9, and k_{41} into expression 42, it is easily calculated, for a mixture of CO (48 torr) and O_2 (24 torr), that the amount of NO required to reduce the O atom concentration to 0.1 of its original value should exceed 35 torr. Actually, 0.1 of this amount suffices to inhibit the exchange processes completely. Consequently, reaction 41 cannot explain the observed effect of NO. However, it is not unlikely that the oxygen atoms actually are removed by the very fast reaction with NO_2, produced in the slow reaction of NO and the O_2 reactant.

$$O + NO_2 \longrightarrow NO + O_2 \qquad (43)$$

The rate constant k_{43} can be obtained from data by Klein and Herron,[30] $k_{43} = 1.95 \times 10^{13} \exp(-1060/RT)$ cm^3 mole^{-1} sec^{-1} at 500° reduced to $k_{43} = 1.7 \times 10^{-11}$ cm^3 molecule^{-1} sec^{-1}. Thus in expression 42, the term $k_{41}[NO][M]$ should be replaced by $k_{43}[NO_2]$. It is easily calculated that, in the mixture involved, an amount of 0.03 torr NO_2 will reduce the O atom concentration to 0.1 of its initial value. The slow reaction of NO and O_2 is a third-order process

$$2NO + O_2 \longrightarrow 2NO_2 \qquad (44)$$

The rate constant k_{44} has been determined by Ashmore, Burnett, and Tyler[38] at 500°: $k_{44} = 1.6 \times 10^{-38}$ cm^6 molecule^{-2} sec^{-1}. The rate of NO_2 formation in a mixture of CO (48 torr), O_2 (24 torr), and NO (3 torr) is found to be $S_{44} = 6.5 \times 10^{-4}$ torr sec^{-1}. Thus, the required amount of 0.03 torr NO_2 is formed in about 45 sec. This time is sufficiently short to allow the conclusion that the inhibitory effect of NO in this system can be ascribed to very small amounts of NO_2 produced by slow reaction of NO and O_2.

The considerably enhanced CO_2 formation observed after addition of not too small amounts of NO then can be ascribed to the reaction

$$CO + NO_2 \longrightarrow CO_2 + NO \qquad (45)$$

The rate constant k_{45} has been measured between 500 and 800°K by Brown and Crist,[39] $k_{45} = 0.48 \times 10^9 \exp(-27800/RT)$ l. mole^{-1} sec^{-1}, at 500° reduced to $k_{45} = 1.2 \times 10^{-20}$ cm^3 molecule^{-1} sec^{-1}. The rate of CO_2 formation by reaction 45 in a mixture of CO (48 torr), O_2 (24 torr), NO (3 torr), and NO_2 (0.1 torr) is found to be $S_{45} = k_{45}[CO][NO_2] = 1.1 \times 10^{13}$ molecules cm^{-3} sec^{-1}, *i.e.*, 4.9×10^{-2} torr min^{-1}. This rate is in good agreement with the observed rates. Thus, it appears that in the mixture involved, the rate of NO_2 formation, S_{44}, practically equals the rate of NO_2 removal, S_{45}, so that the estimated partial pressure of NO_2 (*i.e.*, 0.1 torr) actually corresponds to the steady-state concentration of NO_2 in the mixture.

Experimental information regarding the remarkable acceleration of both isotopic exchange processes

(38) P. G. Ashmore, M. G. Burnett, and B. J. Tyler, *Trans. Faraday Soc.*, 58, 685 (1962).

(39) F. B. Brown and R. H. Crist, *J. Chem. Phys.*, 9, 840 (1941).

by addition of very small amounts of NO, unfortunately, is rather limited. Since at higher concentrations of NO the exchange processes are completely inhibited, it is unlikely that NO itself, either in the gas phase or by a wall reaction, can act as the extremely reactive intermediate. The data rather suggest that as long as sufficient oxygen atoms are available, NO addition will give rise to the occurrence of another reactive intermediate. If the CO_2**(singlet) intermediate is preferentially deactivated by NO, the induced intermediate might be excited nitric oxide, NO*, formed by energy transfer in the reaction

$$CO_2{}^{**}(\text{singlet}) + NO(^2\Pi) \longrightarrow CO_2(^1\Sigma_g{}^+) + NO^*(^2\Pi) \quad (46)$$

Vibrationally excited NO in its electronic ground state probably can set up sufficiently long chains. Thus, the accelerated exchange processes should be ascribed to

$$NO^* + O_2 \longrightarrow O_2 + NO^* \quad (47)$$

$$NO^* + CO \longrightarrow CO + NO^* \quad (48)$$

and NO* should be a more efficient chain carrier than O is. In case of increasing NO partial pressure, the concentration of O atoms, and consequently of CO_2**(singlet) and NO* molecules, is reduced as a result of reaction 43, and ultimately all exchange processes are inhibited. It has to be remarked that this interpretation of the accelerating effect is only tentative.

Even in a mixture of very small amounts of NO with CO and O_2, slow formation of NO_2 by reaction 44 will occur. Therefore, it is expected that the accelerated exchange processes in such a mixture will show decreasing rates as a function of reaction time. As shown in Figure 10, this effect actually has been measured: the slopes of the log $(1 - F)$ *vs.* reaction time curves for the mixture with NO (0.1 torr) are continuously decreasing with reaction time, and so, consequently, do the exchange rates. This observation underlines the conclusion that the inhibitory effect of NO can be ascribed to very small amounts of NO_2 formed by slow reaction of NO with the O_2 reactant.

Remark on Hydrogen-Containing Impurities. It is supposed that no hydrogen-containing intermediates take part in the reactions. As mentioned, the concentration of H_2 in the samples was below 3×10^{-5} and that of H_2O very probably below 1×10^{-4}. A possible source of H_2O in the samples might be the formation of H_2O by reaction of two adjacent OH groups at the silica surface. It is easily calculated from the known[12,13] number of hydroxyl groups at the surface (8/100 A^2) and the inner surface of the reaction vessel (180 cm^2) that the process involved yields at most 7×10^{16} molecules of H_2O. However, this formation of H_2O is a relatively slow process, so that in the particular experiments only a very small part of this number actually will enter the gas phase during the reaction time. Moreover, after several series of experiments at 500°, the rate of CO_2 formation, under otherwise comparable conditions, was virtually unchanged, indicating that the number of OH groups at the surface was not considerably reduced.[11] Thus, the introduction of H_2O by reaction of OH groups at the surface is certainly sufficiently small to maintain the H_2O concentration in the samples below 1×10^{-4}. It has been observed in the preliminary investigation[6] that the addition of small amounts of water (0.3%) does not influence the CO–O_2 exchange. However, in this case the H_2O concentration in the samples possibly was higher than in the present experiments as a result of a less thorough drying method. Consequently, the former observation does not exclude an effect of water that is measurable only in very low concentrations. The formation of reactive hydrogen-containing intermediates from H_2 or H_2O probably occurs by reaction with O atoms.[40] It has been found in the present study that the concentration of O atoms at the temperatures involved is extremely small. Therefore, it is not expected that traces of H_2 or H_2O will influence the exchange rates.

Acknowledgments. The author wishes to thank Professor Dr. J. A. A. Ketelaar and Professor Dr. J. Kistemaker and Dr. A. E. de Vries for helpful discussions and suggestions. A considerable part of the experiments and of the reduction of data has been performed by Miss A. Tom, whose reliable assistance is gratefully acknowledged. This work was part of the research program of the Stichting voor Fundamenteel Onderzoek der Materie (Foundation for Fundamental Research on Matter) and was made possible by financial support from the Nederlandse Organisatie voor Zuiver-Wetenschappelijk Onderzoek (Netherlands Organization for the Advancement of Pure Research).

(40) *Cf.* ref 1, p 79.

Structure and Properties of Amorphous Silicoaluminas. III.

Hydrated Aluminas and Transition Aluminas

by A. J. Léonard,[1a] F. Van Cauwelaert,[1b] and J. J. Fripiat[1c]

Laboratoire de Physico-Chimie Minérale, Agronomic Institute of the University of Louvain, Héverlé-Louvain, Belgium *(Received October 17, 1966)*

The structure of amorphous aluminas and of some transition aluminas has been studied using the generalized Fourier synthesis. The comparison of electron density distribution functions obtained for hydrated gels and gels calcined at various temperatures up to 700° with similar distribution functions computed from structure models has led to interesting conclusions. Amorphous hydrated gels obtained in acid or alkaline solutions behave differently on dehydration. Gels obtained in acid solutions evolve at 300° toward a partially hydrated phase in which a spinel-like structure is realized in contrast with those precipitated in alkaline solution which acquire a boehmite-like structure at 300°. At higher temperature, both series have a spinel-like structure but with an excess of tetrahedral aluminum cations in the case of the samples obtained initially in acid conditions. This suggests a differentiation between the η and γ transition forms. The structural characteristics of hydrated alumina gels reveal a disorganization in the distribution of aluminum cations, the degree of disorganization being higher for the samples obtained by acid precipitation. This and the thermal behavior mentioned above are believed to result from the prolonged presence of aquo groups. The significance of the estimation of the relative content of tetrahedral aluminum cations from the shift of the Al Kα fluorescence line has been checked with respect to the Al(IV) content in spinel-like structures. The agreement between both sets of measurements was reasonable when gibbsite and sodium zeolite were used as reference materials.

I. Introduction

Transition aluminas are obtained from the dehydration of aluminum trihydrates (gibbsite, bayerite, and nordstrandite) or monohydrate (boehmite) according to various decomposition sequences. A great deal of effort has been devoted to the study of these sequences as shown in Table I.[2-14] More details may be found in the excellent review published by Newsome, Heiser, Russell, and Stumpf.[15] For the sake of clarity, the Alcoa nomenclature will be used in this paper.

Among the reasons for the broad interest in this field are the high surface areas and the catalytic properties displayed by transition aluminas. Activation is produced by heating aluminum trihydrates or monohydrate (boehmite) at rather high temperatures (500–900°). The two main transition aluminas used in catalysis are the η and γ species. Maciver, *et al.*,[16] have studied particularly their surface properties and have concluded that η alumina differs from γ

(1) (a) The University of Louvain; (b) Aspirant van het N.F.W.O.; (c) The University of Louvain and M.R.A.C. (Tervurent).

(2) (a) G. W. Brindley and J. O. Choe, *Am. Mineralogist*, **46**, 771 (1961); (b) J. F. Brown, D. Clark, and W. W. Elliott, *J. Chem. Soc.*, 84 (1953).

(3) H. C. Stumpf, A. S. Russell, J. W. Newsome, and C. M. Tucker, *Ind. Eng. Chem.*, **B42**, 1398 (1950).

(4) H. Saalfeld, *Clay Minerals Bull.*, **3**, 249 (1958).

(5) B. C. Lippens, Doctoral Thesis, Technische Hogeschool, Delft, The Netherlands, 1961.

(6) U. Hauschild, *Z. Anorg. Allgem. Chem.*, **324**, 15 (1963).

(7) E. J. W. Verwey and E. L. Heilmann, *J. Chem. Phys.*, **15**, 174 (1947).

(8) E. Kordes, *Z. Krist.*, **91**, 193 (1935).

(9) H. Ginsberg, W. Hüttig, and G. Strunk-Lichtenberg, *Z. Anorg. Allgem. Chem.*, **293**, 204 (1957).

(10) H. P. Rooksby and C. J. M. Rooymans, *Clay Minerals Bull.*, **4**, 234 (1961).

Table I

A. Decomposition Sequences of Alumina Hydrates (h, Hydrothermal Treatment)

Starting material		Ref
Gibbsite	$\xrightarrow[270°]{}$ χ $\xrightarrow[970°]{}$ κ	2a
Gibbsite	$\rightarrow$ boehmite $\rightarrow \gamma \rightarrow \theta \rightarrow \alpha$	2b
Gibbsite	$\rightarrow$ boehmite $\xrightarrow[400°]{}$ χ $\xrightarrow[750°]{}$ γ $\xrightarrow[1050°]{}$ κ $\xrightarrow[1150°]{}$ $\theta \rightarrow \alpha$	3
Gibbsite	$\xrightarrow[300°,h]{}$ boehmite $\xrightarrow[900°]{}$ θ	4
Bayerite	$\rightarrow$ boehmite $\rightarrow \eta \rightarrow \theta \rightarrow \alpha$	3
Bayerite	$\xrightarrow[230°]{}$ η $\xrightarrow[850°]{}$ θ $\xrightarrow[1100°]{}$ α	5
Nordstrandite	Same as bayerite	6
Boehmite	$\xrightarrow[450°]{}$ γ $\xrightarrow[750°]{}$ δ $\xrightarrow[900°]{}$ $\theta \rightarrow \alpha$	3, 5

B. Structure of Transition Aluminas

Form	Structure	Ref
η	Spinel cubic or tetragonal (cubic close packing of oxygen atoms with tetrahedral and octahedral aluminum sites)	7, 8
γ	Spinel cubic	9
	tetragonal	4
δ	Spinel orthorhombic	3
	tetragonal	10
χ	Spinel cubic	3
	hexagonal	2a, 11
κ	Spinel hexagonal	2a, 11
θ	monoclinic	12, 13, 14

alumina, not only in its pore-size distribution but also in the fact that the water content of γ alumina is greater than that of η alumina. Both types develop surface acidity as they are heated up to 900° but the strength of the acid sites is greater in the case of η alumina. These observations, associated with many others not reviewed here, suggest structural differentiations between the various transition forms. Unfortunately our knowledge of these structures is rather poor. With the exception of the spinel form (η), the species are mainly characterized by the dimensions of the unit cell and by some indications on their crystallographic system (Table I).

The microcrystalline state of these substances and the poor quality of their X-ray diffraction patterns preclude the application of refined methods of structure determination. Moreover, the earlier works by Brown, *et al.*,[2] and by Tertian and Papée[17] have shown that the combination of heating rate, particle size, and pressure produces various decomposition sequences and thus complicated mixtures of transition forms. For instance, the two reaction paths given for gibbsite in Table I correspond, respectively, to the decomposition of a fine-grained mineral for the first and of coarse particles for the second. In the case of a broad range of particle size, dehydration would give possibly a mixture of χ and γ aluminas.

Brindley and Choe,[2a] using electron diffraction by single crystals, have suggested an interesting way to obtain more detailed information. It is possible to follow the decomposition mechanisms by recording the electron diffraction pattern of one specified particle and to determine subsequently the corresponding structure evolution. However, because of preferential orientations of the reciprocal lattice with respect to the electron beam, the number of parameters obtained in this manner is too restricted for complete structure determinations. Moreover in the case of extremely well-dispersed materials, as those used for catalysts, electron diffraction patterns cannot be obtained. In view of the limitations of the standard X-ray and electron diffraction techniques, we have approached this problem from a completely different viewpoint. The transition aluminas will no longer be considered as

(11) G. W. Brindley, *Am. Mineralogist*, **46**, 1187 (1961).

(12) J. A. Kohn, G. Katz, and J. D. Broder, *ibid.*, **42**, 398 (1957).

(13) R. F. Geller, *J. Chem. Phys.*, **33**, 676 (1960).

(14) H. Saalfeld, *Neues Jahrb. Mineral. Abhandl.*, **95**, 1 (1960).

(15) J. W. Newsome, H. W. Heiser, A. S. Russell, and H. C. Stumpf, "Alumina Properties," Technical Paper No. 10, Aluminum Co. of America, Pittsburgh, Pa., 1960.

(16) D. S. Maciver, H. H. Tobin, and R. T. Barth, *J. Catalysis*, **2**, 485 (1963).

(17) R. Tertian and D. Papée, *J. Chim. Phys.*, **55**, 341 (1958).

crystalline but as amorphous materials and a method especially suited for amorphous substances will be applied. From the diffuse scattering of a monochromatized X-ray beam, the radial electron density is computed with respect to an arbitrarily chosen origin. The successive maxima in this distribution correspond to the various interatomic vectors. This technique, initially proposed by Warren[18-20] for studying the structure of glasses, gives the mutual arrangements of atoms within a sphere of about a 5-A radius; for longer distances from the center, the successive maxima corresponding to various interatomic distances overlap. Fripiat, Léonard, and Baraké[21] have applied such a method to hydrated silica gels, but as far as we know, neither the amorphous alumina hydrates nor the transition aluminas obtained from their dehydration process have been studied in that manner. This will be the main topic of this contribution. To obtain detailed information, reference data are required: these will be obtained by computing the electron density distribution from known comparable structures, namely, gibbsite, bayerite, boehmite, or the η spinel structure. As in the latter type of oxygen atom arrangement, the distribution of aluminum in tetrahedral or octahedral sites is an important feature; the method used previously[22] and based on the shift of the aluminum Kα emission line will also be applied. Infrared spectra in the range where the Al octahedra and tetrahedra vibrations are observed will also give some useful information.

II. Procedures

(a) *Generalized Fourier Synthesis.* The method, developed originally by Warren for studying structures of amorphous materials, is based on the relationship between the radial electron density and the length of interatomic vectors. In the simplest case of a monoatomic substance the basic relationship is

$$4\pi r^2\rho(r) = 4\pi r^2\rho_0 + (2r/\pi)\int_0^\infty si(s)\sin sr ds \quad (1)$$

where ρ is the electron density, r the distance from an arbitrary atom taken as origin, and $s = (4\pi \sin\theta)/\lambda$. In eq 1

$$i(s) = I(s)/Nf(s) - 1 \quad (2)$$

where $I(s)$ is the intensity of the X-ray radiation diffracted by an indifferently oriented lattice, N is the effective number of atoms in the sample, and $f(s)$ is a function of the diffraction angle θ such that

$$f(s) = I_0\frac{e^4}{2m^2c^4R^2}f_A^2(1 + \cos^2 2\theta) \quad (3)$$

where I_0 is the intensity of the radiation reaching the sample and f_A the atomic scattering factor. R, e, m, and c are the distances from the scattering electron, the electron charge and mass, and the light velocity, respectively. For a substance containing more than one atomic species, eq 1 becomes

$$\sum_m K_m 4\pi r^2\rho_m = \sum_m K_m 4\pi r^2\rho_0 + (2r/\pi)\int_0^\infty si(s)\sin sr ds \quad (4)$$

the summation being extended to all the atoms contained in the stoichiometric unit. K_m is the effective electron number of atomic species m defined as the ratio f_m/f_e where f_m and f_e are the atomic scattering coefficient and the mean electron scattering coefficient, respectively. The latter is equal to $\sum_m f_m/\sum_m Z_m$ where Z_m is the atomic number. The electron density, ρ_m, is thus a function of the mean electron density (ρ_0) per cubic angstrom, of s, and of $i(s)$. Hence

$$\rho_0 = \frac{Nd \times 10^{-24}\sum_m K_m}{M} \quad (5)$$

where d is the specific weight and M the molecular weight. In eq 4, $i(s)$ has the same meaning as in eq 2 and becomes

$$i(s) = \frac{I_{coh} - \sum_m f_m^2}{f_e^2} \quad (6)$$

where

$$I_{coh} = I_{exp} - I_{incoh} \quad (7)$$

In this work the atomic scattering coefficients and the contribution of the incoherent intensity were taken from the "International Tables for Crystallography."[23] The calculations were made as shown previously for silica gels by Fripiat, Léonard, and Baraké,[21] using an IBM 1620 computer. In the calculation of K_m, 16 electrons were attributed to aluminum and 7 electrons to oxygen. This mathematical artifice has no influence on the final results provided that the total number of electrons is constant in the stochiometric unit, but it

(18) B. E. Warren and N. S. Gingrich, *Phys. Rev.*, **46**, 368 (1934).

(19) B. E. Warren, H. Krutter, and O. Morningstar, *J. Am. Ceram. Soc.*, **19**, 202 (1936).

(20) B. E. Warren, *J. Appl. Phys.*, **8**, 645 (1937).

(21) J. J. Fripiat, A. Léonard, and N. Baraké, *Bull. Soc. Chim. France*, 122 (1963).

(22) A. Léonard, S. Suzuki, J. J. Fripiat, and C. De Kimpe, *J. Phys. Chem.*, **68**, 2608 (1964).

(23) "International Tables for X-Ray Crystallography," Vol. III, The Kynoch Press, Birmingham, England, 1962, p 202, 250.

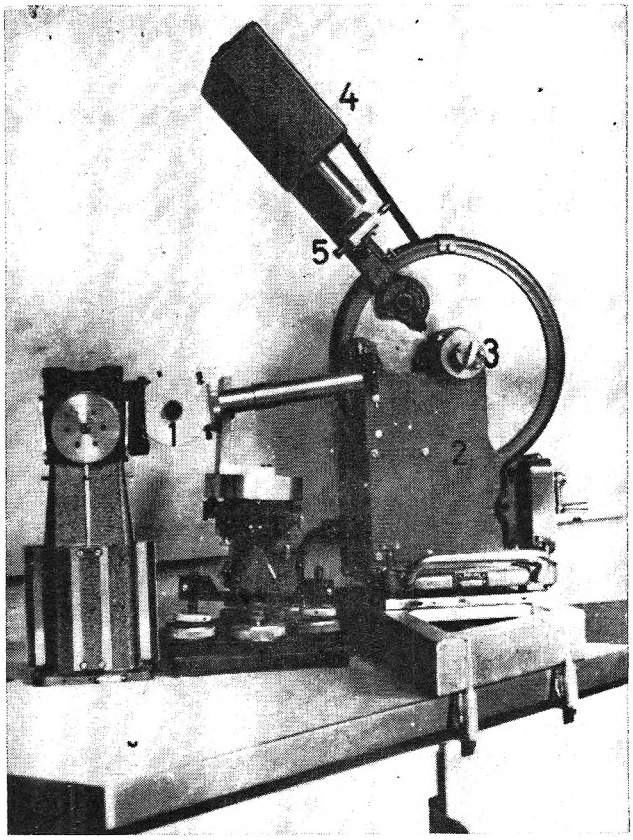

Figure 1. Instrument used for recording X-ray scattering curve and to compute the radial distribution of electron density.

produces a better resolution in the electron density distribution.

The instrument used in this work is shown in Figure 1; the X-ray beam was first monochromatized by means of a curved asymmetrical quartz crystal (1), the goniometer (2) being adjusted for fitting the focalization conditions; the distance between the monochromator and the sample (3) was 325 mm and the distance between the sample and the scintillation detector (4) was 180 mm. A molybdenum (λ 0.709 A) "fine-focus" target was used at 54 kv and 14 ma. The $K\alpha_2$:$K\alpha_1$ intensity ratio has been reduced from one-half to one-eighth. As proposed by McKinstry and Short,[24] the contribution of the harmonics was suppressed by discriminating at 44 ± 12 v. In the diffracted beam the number of pulses was between 150 and 1500 counts/sec; this is appreciably below the maximum speed of discrimination, *i.e.*, 4500 pulses/sec.

The diffraction spectra were recorded by scanning the 2θ domain between 4 and 162° by steps of 2θ = 1°, using the technique of fixed counts (16×10^3 pulses). The maintenance of a correct geometry was checked before and after every determination by recording the diffraction spectrum of a thin sheet of muscovite, using a narrow receiving slit of 0.8 mm (5 of Figure 1) as compared with the 6-mm asymmetrical aperture used for the amorphous substances.

The following corrections were made on the experimental data. Let x be the sample thickness and x_∞ the "infinite thickness" defined by Cullity[25]

$$I = I_{\text{exp}}\left[1 - \frac{\exp(-2\mu x_\infty/\sin\theta) - \exp(-2\mu x/\sin\theta)}{1 - \exp(-2\mu x/\sin\theta)}\right] \quad (8)$$

where μ is the linear absorption coefficient. The important contribution of the X-ray scattering by the air has been measured and subtracted from I_{exp}, as proposed by Zarzycki.[26] The experimental values have also been corrected for the double polarization effect undergone by the diffracted beam according to Azaroff.[27]

It is well known that neglecting the end terms of a Fourier series creates a perturbation[28] and raises a series of oscillations in the electron density distribution.[29] Taking into account the wavelength of the Mo $K\alpha_1$ radiation, the upper limit of the Fourier integral in eq 4 was s = 17.5 for 2θ = 162°. These oscillations have the strongest intensity near the origin of the radial distribution. Their amplitude decreases progressively as the radius increases and finally disappears at about 4 A. These so-called "ghosts" were observed mainly below 2.0 A. They modify the shape of the band appearing in the electron density distribution for radii between 1.5 and 2.1 A (band I), which is obviously due to the Al–O interatomic vectors. Above 2 A, the weak peak at 2.3 A, which appears in some cases, is probably a ghost too. Moreover, according to Becherer, *et al.*,[30] if the limit of the Fourier integral is extended to higher s values as by Richter, *et al.*,[31] the lack of convergence of I_{coh} and $\sum_m f_m^2$ in eq 6 may also modify the relative intensities of the electron density maxima since $f_e \to 0$ for $s \to \infty$. It is believed that the limit adopted in this work represents a compromise which minimizes the errors due to the end terms of the

(24) H. A. McKinstry and M. A. Short, *Z. Krist.*, **114**, 278 (1960).

(25) B. D. Cullity, "Elements of X-Ray Diffraction," Addison-Wesley, London, 1959, p 188.

(26) J. Zarzycki, *J. Phys. Radium*, **175**, 44A (1956).

(27) L. V. Azaroff, *Acta Cryst.*, **8**, 701 (1955).

(28) H. Krebs and F. Schultze-Gebhardt, *ibid.*, **8**, 412 (1955).

(29) H. Lipson and W. Cochran, "The Determination of Crystal Structures," Bell and Sons, London, 1953, p 291.

(30) G. Becherer, O. Brümmer, and G. Herms, *Silikat Tech.*, **13**, 339 (1962).

(31) H. Richter, G. Breitling, and F. Herre, *Z. Naturforsch.*, **9**, 390 (1954).

Fourier integral and the effect of the lack of convergence of I_{coh} and $\sum_m f_m^2$.

(*b*) *X-Ray Fluorescence Spectroscopy and Infrared Spectroscopy.* The method for determining the coordination numbers of aluminum and silicon from the shift of the Al Kα and Si Kα fluorescence lines has been described previously.[22] The samples prepared for recording the diffraction spectra and computing the radial electron density distribution were also used for X-ray fluorescence. The X-ray spectrometer was equipped with a chromium target, a pentaerythritol analyzer, and a flow counter, the settings being as follows: X-ray generator, 50 kv, 20 ma; collimator aperture, 160 μ; discrimination, 39 ± 12 v; scanning speed, $^1/_8°$ min^{-1}.

KBr pellets (5‰) were used for recording the infrared spectra in the 400–1200-cm^{-1} region with a Beckman IR12 spectrometer.

III. Materials

The hydrated alumina gels were prepared from a 0.25 *N* $AlCl_3 \cdot 6H_2O$ solution by precipitation with a 4 *N* NaOH solution.

Two series of gels were studied according to the pH at which the precipitation was carried out. The G series was obtained from gels precipitated at pH 4.5 and purified by dialysis at 50° for 3 (G_I), 4 (G_{II}), 5 (G_{III}), and 7 (G_{IV}) days, respectively. The B series was prepared from gels precipitated at pH 8 and purified by dialysis at the same temperature and for the same periods of time (B_I, B_{II}, B_{III}, and B_{IV}).

The samples were then dried under vacuum at 20°

Table II: Number of Water Molecules per Al_2O_3 Unit (WC) and Specific Surface Area (S_0, m²/g)

Pretreatment temp, °C	G series	I	II	III	IV
20	WC	3.67	3.04	3.23	3.68
	S_0	4	9	4	5
300	WC	2.00	1.39	1.38	1.51
	S_0	7	8	8	107
550	WC	1.18	0.86	1.02	0.99
	S_0	27	37	29	305
	B series				
20	WC	3.39	3.14	3.41	2.72
	S_0	158	235	224	243
300	WC	0.91	1.39	1.48	1.14
	S_0	301	286	296	287
550	WC	0.50	0.09	0.40	0.14
	S_0	247	208	276	240

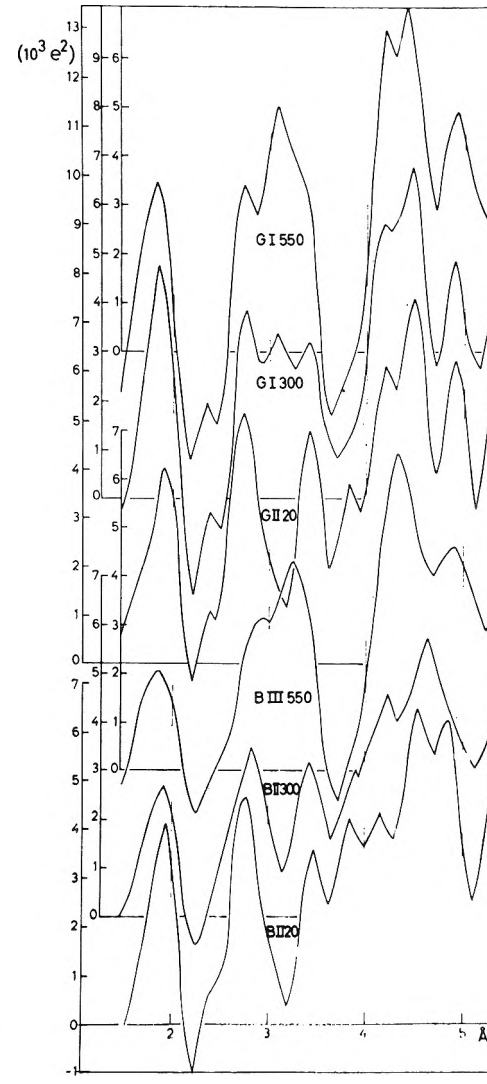

Figure 2. Some examples of radial distribution functions of electron density.

($G_{I,20}$–$G_{IV,20}$ or $B_{I,20}$–$B_{IV,20}$) or heated at 300 or 550° to constant weight ($G_{I,300}$–$G_{IV,550}$ and $B_{I,300}$–$B_{IV,550}$). In summary, four different samples of each series, dried or calcined at 20, 300, and 550°, were studied. Their water contents, obtained by measuring the weight loss at 1000°, and their BET (N_2 at −196°) surface areas are shown in Table II. In addition, two samples belonging to the G and B series were calcined at 700° (G_{700} and B_{700}).

For the X-ray diffraction and fluorescence methods, the samples were prepared by molding a pellet of 5-mm thickness and 30-mm diameter under a pressure of 500 kg/cm².

As shown by Gastuche and Herbillon,[32] the con-

(32) M. C. Gastuche and A. Herbillon, *Bull. Soc. Chim. France*, 1404 (1962).

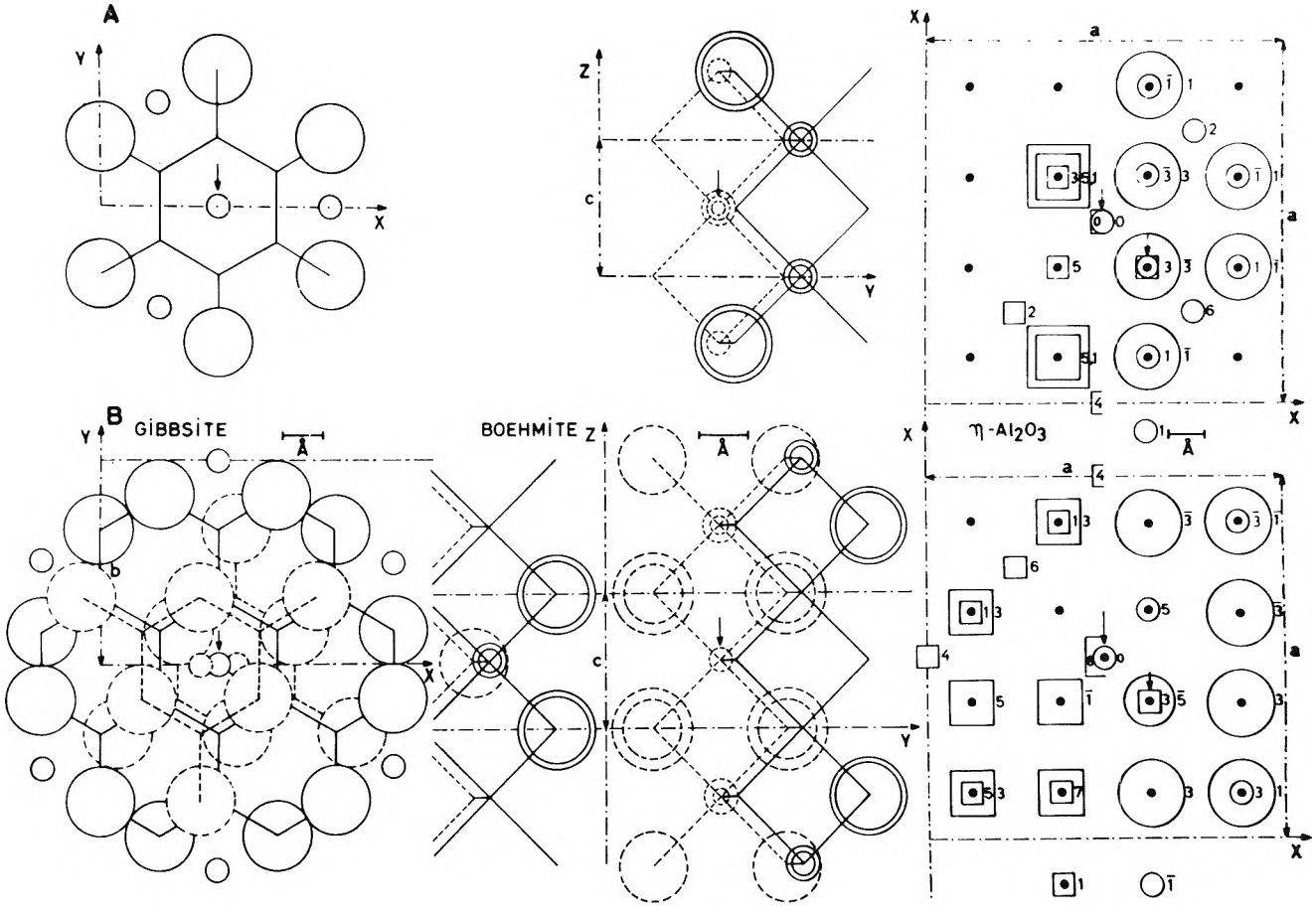

Figure 3. Projections of the characteristic framework of gibbsite, boehmite, and η-Al_2O_3 showing the interatomic vectors contributing to bands II (upper part A) and III (lower part B) of the radial distribution function of the electron density. Gibbsite: xy projection of the octahedral layer; A, second coordination shell of a specified aluminum atom (small circle at the center). The Al–O and Al–Al interatomic vectors contributing to band II involve the various atoms shown here. The atoms represented by dashed lines belong to the upper or lower hexagonal rings shifted with respect to the reference plane on the left or on the right, respectively. Boehmite: yz projection; % height: $x = 0.75$, ——; $x = 0.25$, – – – –. A, oxygen and aluminum atoms in the second coordination sphere of the aluminum atom at the center. The differentiation of atoms exactly superposed is obtained by using small (aluminum) and larger circles (oxygen or hydroxyl) of slightly different diameters. B, atoms contributing to band III are shown with respect to aluminum at the center. η-Al_2O_3: the heights in eighths of the cubic cell are represented by figures against each atom. For the sake of clarity, half the environment of each kind of aluminum is represented: on the left, □, Al(VI) and on the right, ○, Al(IV). Al(IV) and Al(VI) atoms lie in even or odd shells, respectively.

tinuous dialysis under the conditions explained above leads to the formation of gibbsite for the G series and to the formation of bayerite for the B series. These crystalline species are obtained after about 10–12 days. According to Fripiat and Pennequin,[33] the dialysis process results at first in a depolymerization of the initial coarse particles. The molecular weights of the fully depolymerized particles obtained after 2–3 days are of the order of magnitude of 10.000 in the G series and of 50.000 in the B series. After this first step, a polymerization process occurs which leads to the progressive formation of crystalline trihydrates. The first intense diffraction lines typical for gibbsite or bayerite are observed after 6–7 days. Therefore the periods of time chosen in the G as well as the B series cover the whole polymerization process preceding crystallization.

The G samples dried at 20° or calcined at 300° are amorphous. The samples calcined at 550° show X-ray diffraction spectra similar to those obtained by Tertian and Papée[17] and attributed to χ alumina. After the thermal treatment at 700°, a mixture of γ and χ aluminas is found. In the B series the $B_{I,20}$–$B_{III,20}$ samples are amorphous while the $B_{IV,20}$ sample contains some pseudoboehmite. The same crystalline form is found for the B_{300} samples while the four B_{550}

(33) J. J. Fripiat and M. Pennequin, *Bull. Soc. Chim. France*, 1655 (1965).

samples exhibit diffraction patterns similar to that of η alumina. B_{700} contains the same transition species.

IV. Results of the Generalized Fourier Analysis

As shown by some examples in Figure 2, the radial distribution functions obtained for the various samples may be split into three main "bands," *i.e.*, band I from 1.5 to 2.1 A, band II from 2.4 to 3.7 A, and band III from 3.9 to 5.2 A. They will be discussed separately. This division is founded on the distribution of the interatomic Al–O, O–O, or Al–Al vectors in gibbsite,[34] bayerite,[35] boehmite,[35] and η alumina.[7]

In order to decompose one band into its various components and to compute the respective contributions of the corresponding interatomic vectors, a gaussian distribution of the electron density is assumed. The amplitude "y" of a component is related to the distance x from the maximum of the peak by the relation

$$y = ke^{-h^2x^2} \qquad (9)$$

where k is the maximum amplitude; h is related to half band width, h_w, by the relationship $h = \sqrt{\pi}/h_w$. The surface of such a peak (which is comparable to a Patterson peak for crystalline substances) is equal to ZZ' e^2 A, where Z and Z' are the atomic numbers of the opposite atoms at both ends of the vector under consideration. Since the position of the maximum of each peak can be foreseen from the various reference structures, half-widths are the experimental data required to compute the gaussian distributions. The half-width of an O–O vector was obtained from the data published previously on silica gels.[21] The half-width for the Al–O vector was computed from the Al–O peak perfectly resolved in $B_{I,20}$ at 3.5 A while h_w for the Al–Al vector was obtained from the Al–Al peak in the G_{20} series after the weighted contributions of O–O and Al–O have been subtracted. In summary, the h_w values were, respectively, 0.187 A for Al–Al, 0.26 A for Al–O, and 0.39 A for O–O. These half-widths were considered as independent of the coordination state and used indiscriminently for the resolution of bands I, II, and III. Such a procedure is justified by the good fit between the band shape computed from the experimental data and those obtained from the combination of the various components.

In order to give an idea about the various interatomic vectors involved in bands II and III, we have reproduced in Figure 3A and B the respective environments of an aluminum atom in the main structures.

The study of band I which contains the Al–O contribution has been quite deceiving; it has been impossible to observe any significant modification for the various treatments. A reason for this is probably to be found in the perturbation arising from unoccupied octahedral holes. The dispersion of Al–O distances in trihydrates provokes a distribution of the Al–O vectors similar to that obtained for the species where both Al(IV) and Al(VI) cations are present. On the contrary, a great deal of information has been obtained from band II which shows the most drastic modifications when the samples are progressively dehydrated at increasing temperature.

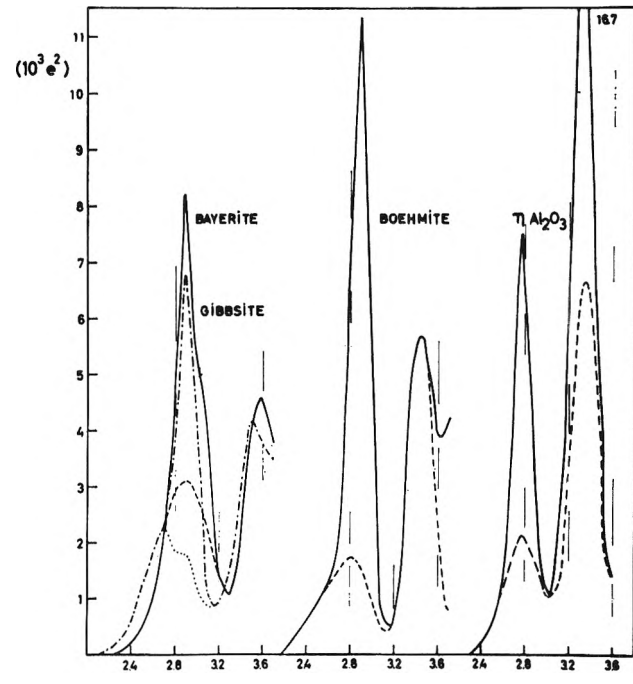

Figure 4. Radial electron distribution in gibbsite, bayerite, boehmite, and η-Al_2O_3 in the band II domain.

(*a*) *Band II (2.4–3.7 A).* Taking into account the various vectors which are possibly involved in band II according to the model structures, the calculated profiles shown in Figure 4 were obtained. The bands computed from gibbsite and bayerite result from the superimposition of O–O and Al–O distributions (dotted or broken lines), respectively, and from the Al(VI)–Al(VI) contributions (not shown). Likewise, for boehmite and η-Al_2O_3, the band is made from the O–O and Al–O contributions (broken lines) and of the Al–Al contributions (not shown). In η-Al_2O_3, the peak centered on 2.8 A represents the Al(VI)–Al(VI) vectors while the peak at 3.3 A is mainly due to the Al(IV)–Al(VI) vectors. The Al(IV)–Al(IV) vectors contribute to the deformation of the right wing of the peak centered on 3.3 A. The electron density distributions of Figure

(34) H. Saalfeld, see ref 14.

(35) H. Bosmans, personal communication, to be published.

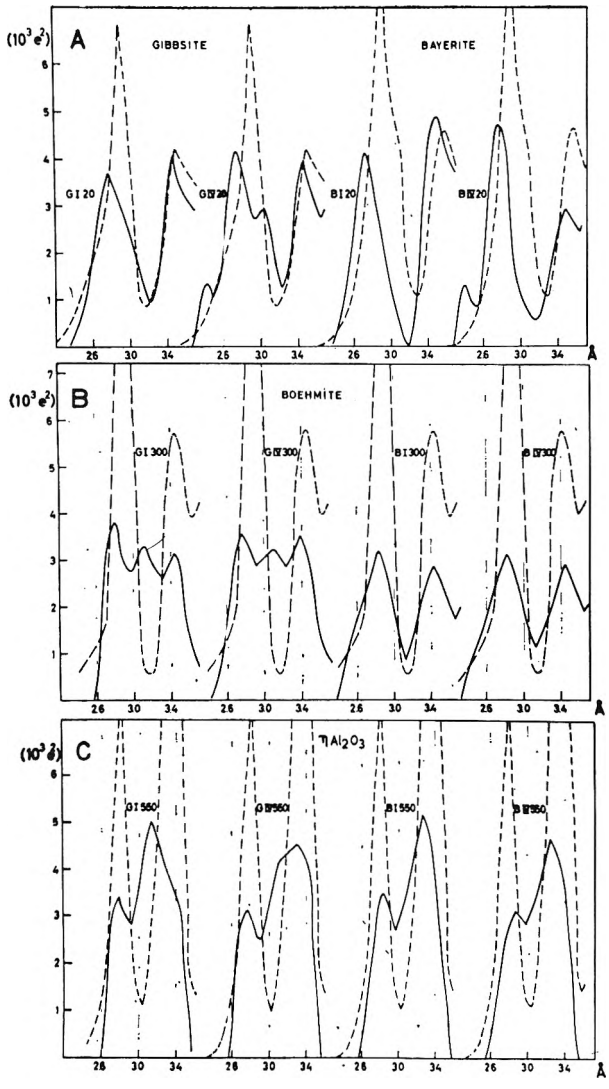

Figure 5. Band II: ——, experimental radial distributions; – – – –, computed radial distributions for the specified models.

4 may then be compared to the experimental profiles of band II.

For the low-temperature samples, $G_{I,20}$, $G_{IV,20}$, and $B_{I,20}$, it is observed in Figure 5A that the second peak at 3.45–3.5 A fits the position well and even the intensity of the peak computed either for gibbsite or bayerite while the first peak at 2.85 A is appreciably shifted toward a lower radius and is less intense than expected. The electron distribution curve obtained for $B_{IV,20}$ is more comparable to the band computed for boehmite. This is in agreement with the presence of some pseudo-boehmite detected in this sample by the usual X-ray diffraction procedure.

The small peak at 2.3 A in $G_{IV,20}$ and $B_{IV,20}$ originates from a ghost, as already explained. The rather intense peak at 3.05 A in $G_{IV,20}$ is weaker in $G_{III,20}$ and $G_{II,20}$ and it appears as a weak shoulder in $G_{I,20}$. It might thus represent a significant feature in the aging of hydrated alumina gels in acid medium. Since the first peak at 2.85 A in gibbsite, bayerite, and boehmite represents mainly Al(VI)–Al(VI) contributions while the second is almost entirely due to Al–O or O–O contributions, the comparison between the observed and computed radial electron distributions for the low-temperature samples suggests that the organization of the oxygen layers is more readily achieved than the adequate distribution of the aluminum cations. From this respect the lack of organization seems to be still higher in the G series than in the B series. This may be correlated with the prolonged presence of aquo groups[36] in the former since the dialysis process at low pH (G series) tends to maintain more of these aquo groups as shown by the measurement of the molecular weights in the course of the polymerization process,[33] by infrared spectroscopy,[37] and also by the higher water contents (Table II).

Let us consider the samples heated at 550°. The bands obtained for $G_{I,550}$, $G_{IV,550}$, $B_{I,550}$, and $B_{IV,550}$, are shown in Figure 5C where they are compared to the band computed from the structure of η-Al_2O_3 (Figure 4). It is obvious that the contribution of the Al(VI)–Al(VI) vectors around 2.8 A fits almost exactly the position of the first peak of band II. The situation for the second component is different. The experimental band between 3 and 3.5 A is much broader than that computed for η-Al_2O_3, especially for the G series. As this second component contains mainly the contributions of the Al(VI)–Al(IV) and of the Al(IV)–Al(IV) vectors (the latter on the right wing of the band), it is concluded that structural disorganization in transition aluminas may be mainly attributed to a disorganization in the distribution of fourfold coordinated aluminum cations.

When the O–O and Al–O contributions, normalized for the intensity obtained from the experimental distributions, are subtracted, the contributions of the Al(VI)–Al(VI) vectors may be distinguished from those of Al(IV)–Al(VI) or Al(IV)–Al(IV) vectors as shown in Figure 6A.

The situation for the G and B samples heated at 300° is more complex. According to their constitutional water contents, and especially for the B series, a "boehmite-like" structure could be expected in agreement with Stumpf, *et al.*[3] However according to Saalfeld[4]

(36) J. C. Baylar, "The Chemistry of the Coordination Compounds," Reinhold Publishing Corp., New York, N. Y., 1956, p 451.

(37) J. J. Fripiat, F. Van Cauwelaert, and H. Bosmans, *J. Phys. Chem.*, **69**, 2458 (1965).

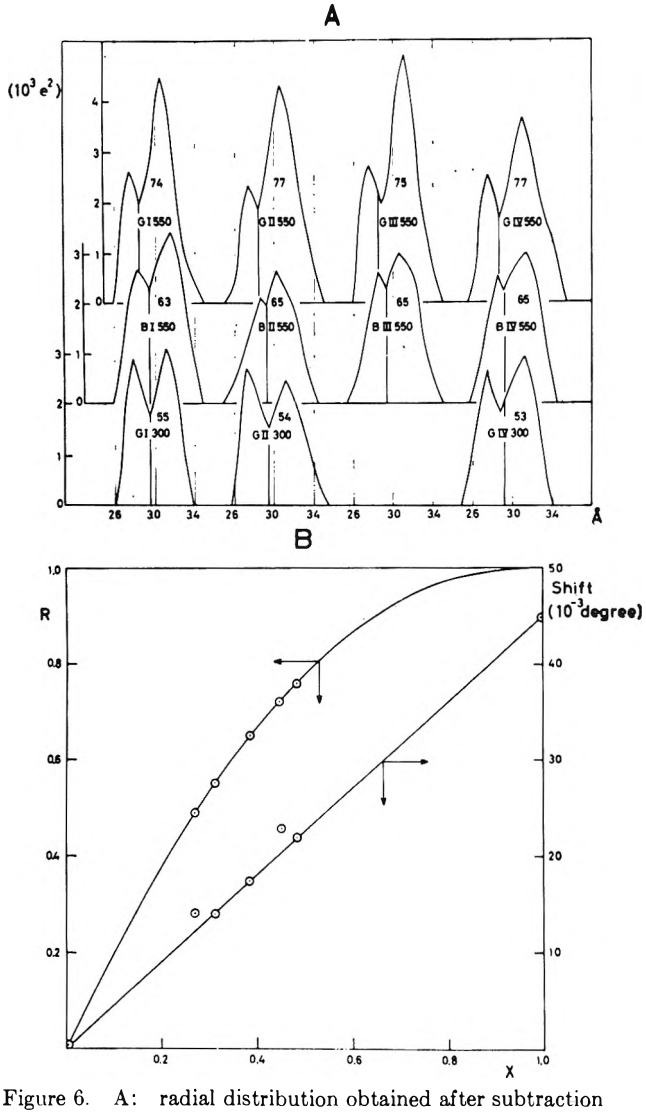

Figure 6. A: radial distribution obtained after subtraction of the Al–O and O–O contributions. Enclosed figures represent the R values defined by eq 12. B: upper curve, variation of R with respect to X calculated according to eq 12 for $N = 11$; lower line, relationship between the shift of the Al Kα line and X. The two extreme values are those observed for gibbsite ($X = 0$) and a sodium zeolite ($X = 1$).

and Brindley and Choe[2a] the yield of boehmite from gibbsite on atmospheric heating is appreciable only when large parent crystals are used. As the theoretical electron distribution of boehmite and those obtained for the B_{300} samples (Figure 5B) show a well-marked similarity, it may be assumed that a boehmite-like structure is formed. The same conclusion, however, does not hold for the G series; a third peak is observed approximately at 3.1 A, *i.e.*, in the region where the mixed Al(VI)–Al(IV) contributions appear in the high-temperature G and B samples (Figure 5C). In order to check this observation, the Al–O and O–O contributions for boehmite, normalized as usual, have been subtracted from the distribution functions. The two peaks assigned previously to the Al(VI) and Al(IV) contributions appear very distinctly, as shown in Figure 6A.

The G and B series heated at 550° and the G series heated at 300° should then contain appreciable amounts of fourfold coordinated aluminum. The same situation exists for the G_{700} and B_{700} samples which shows electron distribution functions very similar to those obtained at 550°.

(*b*) *The Al(IV) Contents and the Spinel-like Structures.* Let N_6 and N_4 be the number of sixfold and fourfold coordinated aluminum cations, respectively, and let N be the number of aluminum cations in one "structure unit." The numbers of Al(IV)–Al(IV) and Al(VI)–Al(VI) vectors in this unit are $0.5N_4 \cdot (N_4 - 1)$ and $0.5\,N_6(N_6 - 1)$, respectively, if the volume of the unit is chosen in such a way that it contains the aluminum cations present in the second coordination sphere of only one specified Al. The number of Al(IV)–Al(VI) vectors is then N_4N_6. If s is the electron density associated with one vector, the contributions of each of the Al(IV)–Al(IV) and of the Al(VI)–Al(IV) vectors to the peak area of band II, corrected for Al–O and O–O, are

$$S_{4-4} = 0.5N_4(N_4 - 1)s \qquad S_{4-6} = N_4N_6s \quad (10)$$

The ratio of the area of these vectors to that of band II is then

$$R = \frac{S_{4-4} + S_{4-6}}{S_{4-4} + S_{4-6} + S_{6-6}} = \frac{N_4(N_4 - 1) + 2N_4N_6}{N_6(N_6 - 1) + 2N_4N_6 + N_4(N_4 - 1)} \quad (11)$$

Let X be N_4/N and $(1 - X)$ be N_6/N, then

$$R = \frac{X[N(2 - X) - 1]}{N - 1} \quad (12)$$

It may be easily shown that N ranges approximately between 8 and 14 in oxide structures, according to their organization. Between these limits, R does not change appreciably with N for one given value of X. Consequently, the variation of R with respect to X has been plotted as shown in Figure 6B, assuming N to be equal to 11. In order to estimate R, band II, from which the contributions of Al–O and O–O have been subtracted, has been divided into two regions, the first corresponding to the contribution of Al(VI)–Al(VI), the second to the contributions of Al(IV)–Al(VI) or Al(IV)–Al(IV) (Figure 6A). The area under the curve for the latter has been determined be-

tween 2.9 and 3.4 A and it was divided by the total surface area of band II. This ratio was considered as a measurement of R and the corresponding X values were derived from eq 12. These results are given in Table III. The values obtained for X may be checked as follows. The shift (Δ) of the Al Kα fluorescence line observed between the positions of this line for both bayerite and gibbsite on the one hand and for a sodium zeolite on the other hand is measured. A linear relationship is assumed to exist between Δ and X, considering $X = 0$ for the crystalline aluminum trihydrate and $X = 1$ for the sodium zeolite, as shown in Figure 6B. The shifts obtained for the G and B samples are measured and reported with respect to X. As shown in Figure 6B, they fit the straight line reasonably well. This agreement between two sets of completely independent results supports the interpretation of band II for the calcined samples but it raises an important question above the number of tetrahedral Al cations which may be accomodated in spinel-like structures.

In a true spinel, one-third of the aluminum cations are on the tetrahedral sites, as proposed by Verwey[38] according to the composition $[Al_{7.1}\square_{0.9}](IV)[Al_{14.2}\square_{1.8}](VI)O_{32}$; such a structure is very unstable unless some cations, Na, Li, or H, substitute the lattice defects. In particular, Kordes[8] has proposed for Li or H samples the composition $Al_8(IV)Al_{12}H_4(VI)O_{32}$, for which $X = 0.40$, while the structure $Al_8(IV)Al_{14}Na_2(VI)O_{32}$ with $X = 0.36$ was assigned to β alumina by Bragg, *et al.*[39] Datta and Roy[40] have expressed the view that the normal and inverse spinel structures may form a continuous sequence and that the cation distribution is essentially a function of the temperature and the pressure of formation. A structure in which there is a random distribution of the cations in the tetrahedral and octahedral sites appears possible. In such a case, X should reach 0.5 as reported by Rooksby[10] for θ alumina. It is particularly striking (1) that the maximum value of X, derived from the measurement of R, has never exceeded 0.50 (Table III) and (2) that all the samples studied here always have a water content which is much above that required for the stabilization of a spinel structure.

Table III: R, Relative Contributions of the Al(IV)–Al(VI) and Al(IV)–Al(IV) Vectors to Band II; X, Relative Content in Fourfold Coordinated Aluminum Obtained from Eq 12, and Δ, Shift of the Al Kα Line (10^{-3} deg)

Sample	$G_{I,300}$	$G_{II,300}$	$G_{III,300}$	$G_{IV,300}$	Av values
R	0.55	0.54	...	0.53	0.54
X	0.33	0.32	...	0.31	0.32
Δ	13	16	13	13	14
	$G_{I,550}$	$G_{II,550}$	$G_{III,550}$	$G_{IV,550}$	
R	0.74	0.77	0.75	0.77	0.76
X	0.44	0.50	0.46	0.44	0.46
Δ	22	(29)	23	22	22
				$G_{IV,700}$	
R				0.73	0.73
X				0.45	0.45
Δ				23	23
	$B_{I,550}$	$B_{II,550}$	$B_{III,550}$	$B_{IV,550}$	
R	0.63	0.65	0.65	0.65	0.65
X	0.37	0.39	0.39	0.39	0.39
Δ	18	16	16	21	18
				$B_{IV,700}$	
R				0.49	0.49
X				0.33	0.33
Δ				14	14
	$G_{I,20}$	$G_{II,20}$	$G_{III,20}$	$G_{IV,20}$	$\Delta = -1$
	$B_{I,20}$	$B_{II,20}$	$B_{III,20}$	$B_{IV,20}$	$\Delta = +1$
	$B_{I,300}$	$B_{II,300}$	$B_{III,300}$	$B_{IV,300}$	$\Delta = +3$

The thermal evolution up to 300° of the B and G series is very different, although the hydrated samples dried at 20° under vacuum or the samples treated at 550° or above have comparable structures. The G series is characterized by low surface areas as compared with the B series (Table II). This observation is in contradiction with the conclusions of Lippens,[5] since a boehmite-like structure seems to appear in the B samples treated at 300° in spite of the fact that the high values of the surface area suggest the existence of very fine-grained materials.

(c) *Band III (3.9–5.2 A).* The contributions of the various interatomic vectors to this band were computed from the structure models, as shown in Figure 7. In each case band III contains three peaks, but their relative intensities and their positions are different. The most intense peak in gibbsite (5.05 A) is mainly due to the contribution of Al(VI)–Al(VI) vectors (dashed line) while the Al–O vectors are mainly responsible for the weaker components at 4.15 and 4.45 A (dotted–dashed line). In boehmite, Al(VI)–Al(VI) vectors account almost completely for the sharp peak at 4.97 A and for a large proportion of the peak at 4.69 A. In η-Al_2O_3, the second and the third peaks are also almost entirely due to Al(VI)–Al(VI) and Al(VI)–

(38) E. J. W. Verwey, *Z. Krist.*, **91**, 65 (1935).

(39) W. L. Bragg, C. Gottfried, and J. West, *ibid.*, **77**, 255 (1931).

(40) R. K. Datta and R. Roy, *Nature*, **191**, 169 (1961).

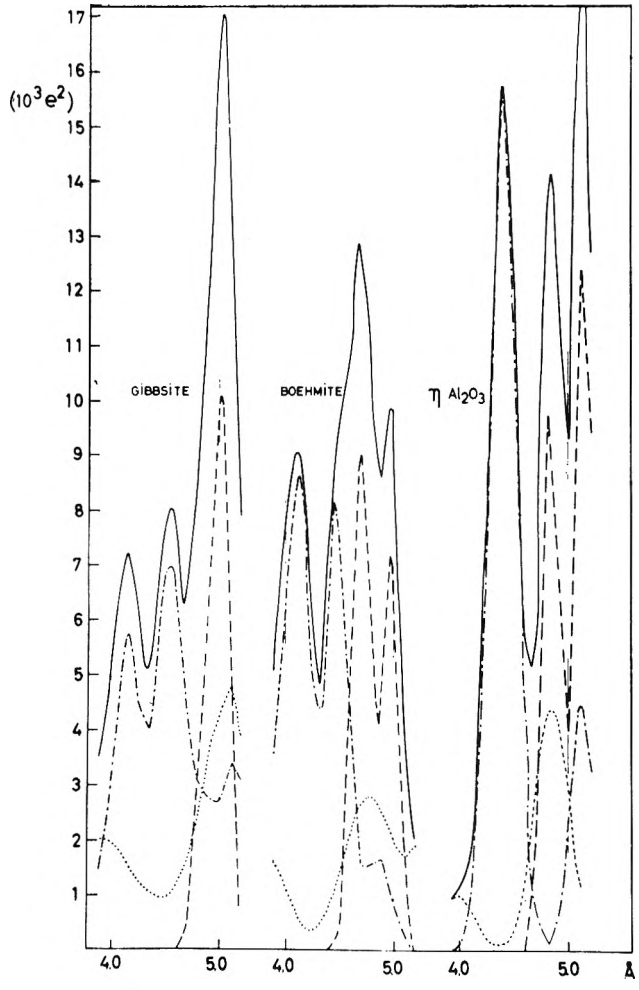

Figure 7. Radial distributions of the electron density in gibbsite, boehmite, and η-Al_2O_3 in the band III domain: ...., contribution of the O–O vectors; — · —, contribution of the Al–O vectors; – – – –, contribution of the Al–Al vectors.

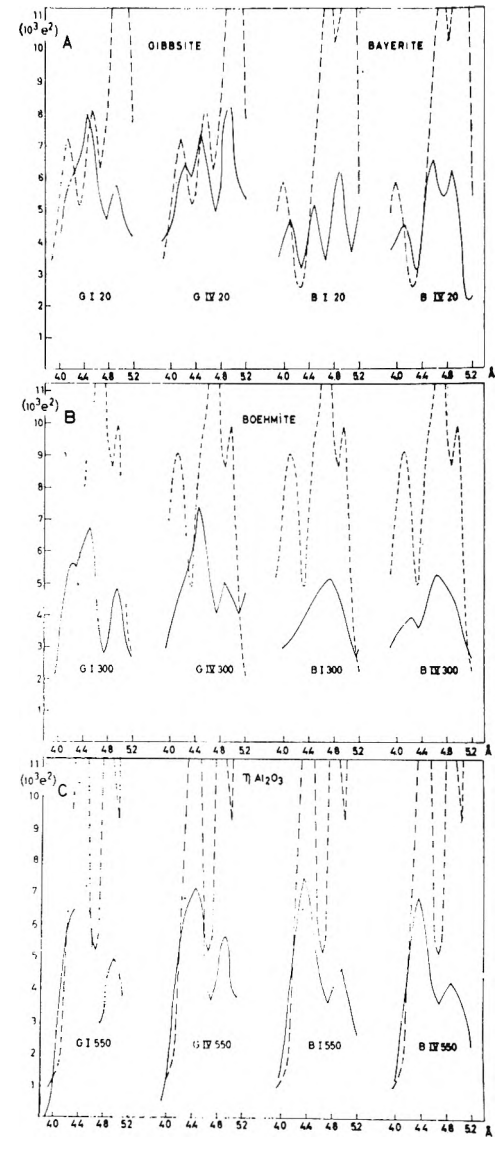

Figure 8. Band III: ———, experimental radial distributions; – – – –, computed radial distributions for the specified models.

Al(IV) vectors, respectively, while the first component is relevant to the Al–O contributions.

As shown in Figure 8A, the three peaks predicted from the gibbsite structure are quite well observed in the $G_{IV,20}$ and $B_{I,20}$ but the relative intensity of the third peak at 5.0 A is lower than that expected. This discrepancy would again indicate some disorganization in the distribution of the Al(VI)–Al(VI) vectors. The third peak being still weaker in $G_{I,20}$, the aging of the G samples would correspond to an increasing order in the distribution of octahedral aluminum cations. The band obtained for $B_{IV,20}$ is more similar to that computed from boehmite, in agreement with the presence of some pseudoboehmite detected by the usual X-ray diffraction procedure. Therefore, as far as the low-temperature samples are concerned, the conclusions derived from the examination of band III are in good qualitative agreement with those obtained from band II.

With the same restrictions about the relative intensities, the bands computed for the G_{550} and B_{550} series (Figure 8C) suggest the presence of spinel-like aluminas. For the samples heated at 300°, the differences delineated in band II between the B and the G samples are found again in band III. It is clear that the G_{300} samples are much more similar to the B_{650} and G_{550} series, and thus to spinel-like samples, than the B_{1300} samples. The latter have an electron density distribution function closer to that computed for boehmite assuming some disorganization

Table IV: Infrared Band Assignments in the 1200–400-Cm^{-1} Frequency Range[a]

Boehmite[41]	Gibbsite[35]	Bayerite[35]	Oxide[42]
1160 (w) Hydrogenic deformation mode	1030 (i) Hydrogenic deformation mode	1000 (s) Broad band (doublet)	
1080 (s) Hydrogenic deformation mode	970 (w) Hydrogenic deformation mode		870–700 cm^{-1} condensed Al tetrahedra
755 (s) Hydrogenic torsion mode	750 (s) ν_3 of AlO_6 octahedra	750 (s) ν_3 of AlO_6 octahedra	800–650 cm^{-1} isolated tetrahedron
618 (i) ν_3 of AlO_6 octahedra			742–572: AlO_6 octahedra
522 (s) ν_4 of AlO_6 octahedra	525 (i) ν_4 of AlO_6 octahedra	525 (i) ν_4 of AlO_6 octahedra	
422 (m) Skeletal mode of Al–O layers			

[a] i, intense; s, strong; m, medium; w, weak.

in the distribution of the Al(VI)–Al(VI) vectors. Consequently the comparison of bands III and II leads essentially to the same conclusions. Of course, the larger the radius of the domain under investigation, the more marked is the disorder due to the amorphous character.

V. Infrared Spectroscopy

The interesting domain for structure determinations lies between 1200 and 400 cm^{-1} as shown in Table IV. The fundamental modes of vibration of aluminum octahedra and of aluminum tetrahedra occur in this region, as well as the deformation modes of constitutional hydroxyls. Figure 9 shows the spectra obtained for the G_{IV} and B_{IV} samples treated at 20, 300, and 550° and the evolution of the G_{20} samples with respect to the time. The latter are representative of those obtained for the other series under similar conditions.

The structural evolution in the course of the dialysis may be summarized as follows. The end member of the series ($G_{IV,20}$) exhibits a spectrum similar to that of gibbsite, although the amorphous character precludes a good resolution of the main bands. Beyond this stage, the OH deformation band at 1030 cm^{-1} seems to be replaced by a broad band centered on 900 cm^{-1}. The bands corresponding to the ν_3 and ν_4 vibrations of AlO_6 octahedra, at 750 and 525 cm^{-1}, are present at the earlier steps of the evolution. In the B_{20} samples the situation is similar for these bands but the OH deformation at 1160 cm^{-1} occurs at the same frequency as in boehmite.

The samples belonging to the G_{300}, G_{550}, and B_{550} series have similar spectra characterized by a broad band between 900 and 500 cm^{-1}. The ratio of the absorbance in the 800–900-cm^{-1} region to the absorbance

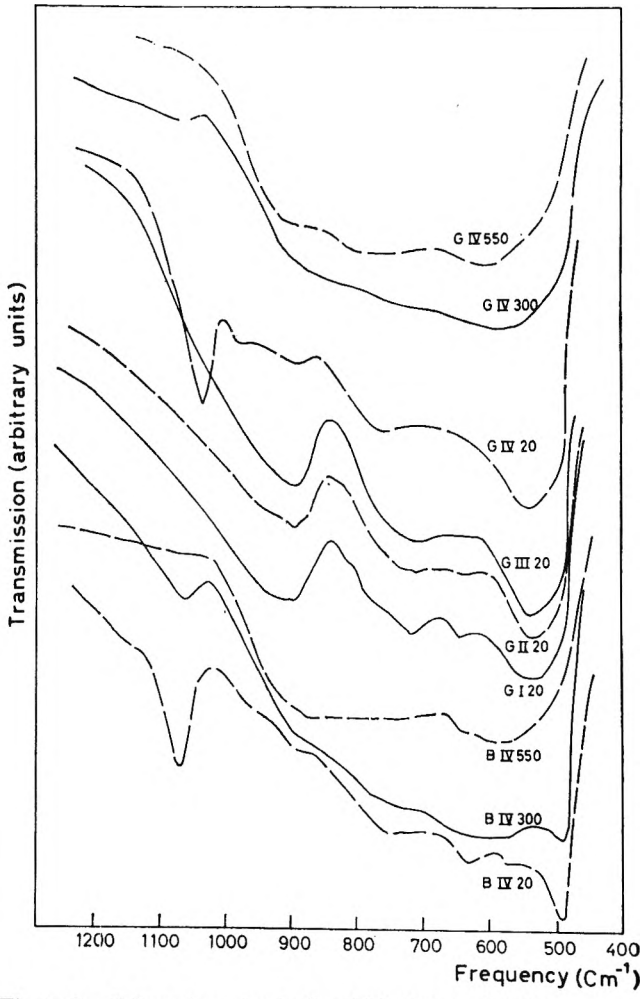

Figure 9. Infrared spectra in the 1200–400-cm^{-1} region.

(41) J. J. Fripiat, H. Bosmans, and P. Rouxhet, to be published.
(42) P. Tarte, *Silicates Ind.*, **28**, 345 (1963).

Table V: Structure Evolution with Respect to Temperature

		Temp, °C			
		20	300	550	700
G series	RD	Gibbsite-like	Spinel-like	Spinel-like	Spinel-like
	XRD	Amorphous	Amorphous	χ alumina	$\chi + \gamma$ alumina
	X	...	0.32	0.46	0.45
B series	RD	Gibbsite-like	Boehmite-like	Spinel-like	Spinel-like
	XRD	Amorphous (B_{IV}, some ps.bh)[a]	Amorphous	η alumina	η alumina
	X	...	...	0.39	0.33

[a] ps.bh, pseudoboehmite.

in the 500–600-cm^{-1} region follows roughly the contents in tetrahedral aluminum. It may thus be concluded that this broad band contains on its high frequency side the vibrations of aluminum tetrahedra and on its low frequency side the vibrations of aluminum octahedra. This is in agreement with observations made previously on silicoaluminas.[22]

The structural organization revealed by the electron density distribution is thus reflected by the infrared spectra. It is, however, important to point out that an appreciable degree of organization achieved within a sphere of 5-A radius restores to only a limited extent the spectral characteristics of crystalline substances.

VI. Discussion

Table V summarizes the structure evolution deduced from the radial distribution of electron density (RD) from the X-ray diffraction (XRD) data and shows the average relative content in fourfold coordinated aluminum (X).

The terms gibbsite-like, boehmite-like, and spinel-like are used to express the similarity of the observed radial distribution functions with those computed from the known models; they mean that within a sphere of an approximately 5-A radius and centered either on an aluminum or an oxygen atom, the structural organization displayed by these models is achieved approximately. The main differences between the G and the B series obtained by precipitating aluminum cations in acid or alkaline solutions are (1) the boehmite-like and spinel-like structures observed after partial dehydration at 300° of the B and G series, respectively, (2) the higher content in fourfold coordinated aluminum in the G series, and (3) the presence of a well-defined transition species in the B_{550} and in the B_{700} samples (η alumina). In order to understand these remarks, it is of interest to consider the possible mechanisms of transformation of gibbsite into boehmite and of boehmite into η-Al_2O_3. As emphasized by Ervin,[43] the basic principle consists of a migration of Al cations within relatively fixed arrangements of oxygen anions. The possible tetrahedral and octahedral coordinations of aluminum facilitate this movement and these transformation processes belong, therefore, to the class of ordered solid-state reactions. Brindley[44] has reviewed the mechanisms proposed by Saalfeld and Rooksby in order to interpret these reactions and has shown that the apparently complex relations between the lattices of gibbsite, boehmite, and η-Al_2O_3 turn out to have rather simple structural interpretations, namely, the maintenance of a nearly constant oxygen framework.

It has been shown several times in the presentation of the experimental results that the main discrepancy observed at the various pretreatment temperatures between the observed electron density distributions and those computed for gibbsite (or bayerite), boehmite, and η-Al_2O_3 was mainly due to a disorganization of the Al–Al vectors. This seems in perfect agreement with the basic assumption that it is the occasional migration paths followed by the aluminum cations in the course of dehydration or their distribution in the hydrated samples which are mainly responsible for the lack of crystalline organization.

Moreover the difference observed in the thermal behavior of the G_{20} and of the B_{20} samples when heated at 300° depends probably to some extent on a higher concentration of aquo groups in the gels obtained in acid medium. The persistence of randomly distributed H_2O ligands probably inhibits the ordered dehydration process. Oxygen vacancies are created by removing H_2O molecules, leaving a less organized structure. Accordingly, protons still present behave as stabilizing

(43) G. Ervin, *Acta Cryst.*, **5**, 103 (1952).

(44) G. W. Brindley, *Progr. Ceram. Sci.*, **3**, 1 (1963).

agents of the spinel structure and this would explain higher contents in fourfold coordinated aluminum in the G_{550} and G_{700} than in the B_{550} and B_{700} samples. A somewhat similar mechanism has been invoked by Peri[45] for the formation of γ alumina surfaces from hydrated alumina gels. From an application of the Monte Carlo method, Peri has shown that the removal of hydroxyl pairs from ideal OH surface would amount to a maximum of 67% of the original content insofar as no defects are formed. With defect formation, OH removal may reach 91%, while to obtain complete dehydration, migration of surface atoms is necessary. In the rather well-organized structure of the B_{20} samples, removing OH to obtain a boehmite-like structure is achieved readily. In the less organized structure of the G_{20} samples the same process leads to the formation of a spinel-like structure. Heating above 550° produces similar spinel-like structures in both series but with a higher content of defects in the G series.

Assuming that the evolution observed for the G and B series is due to the more or less marked persistence of aquo groups, the thermal behavior of crystalline species according to their particle-size distribution may be explained. Small-grained materials are usually obtained by a fast precipitation process under conditions less favorable to achieve a good structural organization. These conditions may maintain more aquo groups and thus orient the thermal evolution up to 300° toward highly defective species.

In order to correlate the bulk structures to catalytic properties, it would be necessary to know to what extent the surface is an image of the atomic arrangement within the solid. From the statistical study made by Peri[45] on the surface dehydroxylation process, such a connection is not obvious. However it seems highly probable that the less organized the starting materials, the more defective will be the surface. A spinel-like structure which contains an excess of tetrahedral aluminum with respect to the spinel composition is less stable and thus richer in defects. For samples with surface areas of the same order of magnitude, such as $B_{IV,550}$ and $G_{IV,550}$ (Table II), the latter would have a more energetic surface than the former since the Al(IV) relative contents in the bulk is 10% higher. This would explain why transition aluminas characterized by similar structures may have different catalytic properties as observed for the γ and η forms.

Acknowledgments. We want to express our appreciation to Professor Meinguet and Miss Leboutte of the Computer Center of the university for their helpful cooperation in the numerical calculation of the electron density distribution. The part taken by Dr. Bosmans in the discussion has also been very fruitful.

(45) J. B. Peri, *J. Phys. Chem.*, 69, 220 (1965).

Radiolysis of Cyclohexane and a Mixture of Cyclohexane and Benzene[1]

by Kent H. Jones

Sandia Laboratory, Albuquerque, New Mexico *(Received June 20, 1966)*

The higher radiolytic yield of low molecular weight hydrocarbons for vapor-phase cyclohexane in comparison to liquid-phase cyclohexane is inferred to be due to the lower vapor density and not due to phase difference. Some of the effects of phase, temperature, and density on the effectiveness of benzene in decreasing the radiolytic hydrogen yield (protection) when mixed with cyclohexane have been determined. The abrupt change in hydrogen yield at the critical temperature of cyclohexane in a benzene–cyclohexane mixture is attributed to a difference in the liquid and vapor structures. Protection decreases with increasing temperature and eventually disappears at 315°. Protection is affected by density in the vapor phase at 285°; this change in protection is attributed to energy transfer.

Introduction

The radiation chemistry of cyclohexane has been extensively studied[2] and the combination of benzene with cyclohexane has been frequently employed for studying the deposition and localization of energy in organic mixtures.[3] In the present study an attempt has been made to compare the vapor phase with the liquid phase by examining the radiolytic processes in cyclohexane and in a mixture of cyclohexane and benzene at high vapor densities.

Experimental Section

Phillips research grade cyclohexane was purified by successive passes through silica gel until the cyclohexane concentration was less than 0.001 mole % as shown by gas chromatography. Phillips research grade benzene was used as received.

Deaerated samples in 16- or 50-ml cells were irradiated for 30 min by γ-rays from a 30,000-curie Co^{60} source at a dose rate of *ca.* 10^{21} ev/l. min, as determined by the Fricke dosimeter $\{G[Fe(III)] = 15.6\}$. Calculation of dose for the organic compounds was based on the assumption that dose rate is proportional to electron density and that the dose rate is unaffected by temperatures over the range studied. All dosimetry was done at room temperature. Sample drying, degassing, and analysis have been described elsewhere.[4]

At the temperatures and densities employed in these studies, pressures up to 40 atm were obtained. In order to prevent breakage of the Pyrex radiolysis cells, a special steel cylinder was constructed in which were placed the sealed radiolysis cell containing the sample and, exterior to the radiolysis cell, an amount of cyclohexane needed to maintain an outside pressure equal to the pressure inside the Pyrex cell when the steel cylinder was heated to the desired temperature.

Results

Table I shows the G values at 300° for hydrogen, cyclohexene, and dicyclohexyl as a function of density

Table I: Yields from γ-Irradiated Cyclohexane Vapor at 300°

Density, g/cc	$G(C_6H_{10})$	$G(C_{12}H_{22})$	$G(H_2)$
0.0079	2.6	0.5	8.7
0.0158	2.0	0.3	6.3
0.047	2.3	0.8	5.6
0.079	2.4	1.2	6.3
0.11	2.0	0.5	5.7
0.14	1.9	1.1	5.4
0.42	1.7	1.1	5.7

(1) This work was supported by the U. S. Atomic Energy Commission. Reproduction in whole or in part is permitted for any purpose of the U. S. Government.

(2) For a recent paper containing pertinent references, see L. M. Theard, *J. Phys. Chem.*, 69, 3292 (1965).

(3) For example, see J. Blackford and P. J. Dyne, *Can. J. Chem.*, 42, 1165 (1964).

(4) K. H. Jones, W. Van Dusen, and L. M. Theard, *Radiation Res.*, 23, 128 (1964).

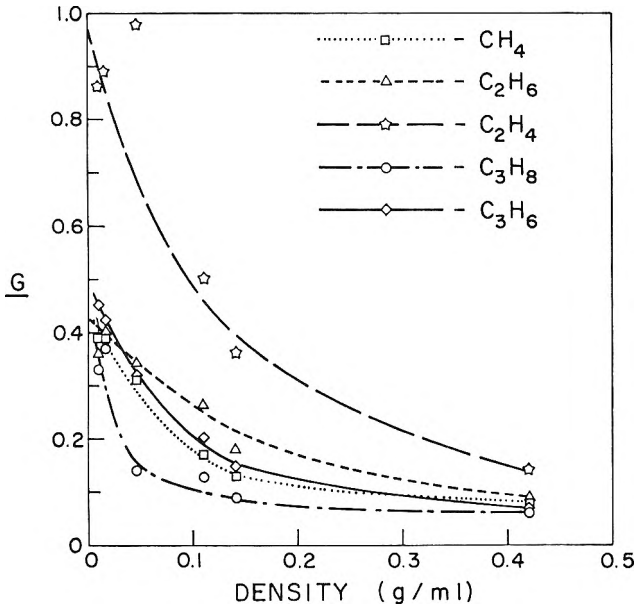

Figure 1. Yields from γ-irradiated cyclohexane vapor at 300°.

of pure cyclohexane vapor. These yields, which are independent of density, are similar to the corresponding yields reported for cyclohexane liquid[5] and low-density cyclohexane vapor.[2] Figure 1 shows that the radiolysis yields of low-molecular weight hydrocarbon products (methane, ethane, ethylene, propane, and propylene) are not density independent but decrease with increasing density of cyclohexane vapor. The low-density yields are comparable to vapor-phase yields at a lower temperature and atmospheric pressure[2] and the high-density yields are comparable to yields from cyclohexane liquid at room temperature.[6] Therefore, it is inferred that the difference in yield is not due simply to a difference in phase but is dependent on the density of cyclohexane.

Table II shows $g(H_2)$ and $\Delta g(H_2)$ (difference between pure cyclohexane and mixture) for various densities of cyclohexane–benzene vapor-phase mixtures of uniform composition (the electron fraction of benzene = 0.325) at 285°. At this temperature, which is just greater than the critical temperature (281°) of cyclohexane, $G(H_2)$ for pure cyclohexane is approximately 6.2. Decrease of $g(H_2)$, number of hydrogen molecules formed from cyclohexane per 100 ev absorbed by cyclohexane [$g(H_2) = G(H_2)$ for pure cyclohexane], is used as a measure of the effect of benzene. There is a measurable decrease of $g(H_2)$ at a solution density of about 0.04 g/ml [$\Delta g(H_2) = 0.2$]; with increasing density $\Delta g(H_2)$ increases further to a value of 1.7.

Experiments were performed to determine the effect of temperature on the reduction of hydrogen yield from cyclohexane by benzene. Samples of 8 or 9 ml of the benzene–cyclohexane mixture in which the benzene electron fraction was 0.325 were irradiated in 16-ml cells at temperatures ranging from 30 to 340°. The quantity of mixture was such that, upon heating, the liquid expanded to fill the cell completely prior to being converted to a vapor. Therefore, the density of the vapor (0.43 g/cc) was the same as the density of the liquid at temperatures above 270°. The results are presented in Figure 2, which shows that $g(H_2)$ increases with increasing temperature. There is an abrupt increase of $g(H_2)$ from 3.5 to 4.4 at the critical temperature of cyclohexane. Beyond the critical temperature $g(H_2)$ increases approximately linearly to the value of pure cyclohexane at a temperature of 315°. In addition Figure 2 shows the effect of temperature on $g(H_2)$ for 4-cc samples of the benzene–cyclohexane mixture (benzene electron fraction = 0.325) irradiated in 50-ml cells. The samples were of sufficiently low density and high temperature to ensure that all benzene and cyclohexane were in the vapor phase. The density of these mixtures was less than one-sixth the density of the other samples included in this figure.

Table II: Effect of Density on $g(H_2)$ in Vapor-Phase Benzene–Cyclohexane Mixture at 285° (Electron Fraction of Benzene = 0.325, $G(H_2)_{benzene}$ = 0.2, $G(H_2)_{cyclohexane}$ = 6.2)

Density, g/cc	$g(H_2)$	$\Delta g(H_2)$
0.035	6.0	0.2
0.07	5.8	0.4
0.10	5.2	1.0
0.13	5.2	1.0
0.24	4.7	1.5
0.41	4.7	1.5
0.41	4.3	1.9

Figure 3 shows hydrogen yield for pure cyclohexane as a function of temperature for 5.5 ml of cyclohexane irradiated in 16-ml cells. At low temperature the cyclohexane is predominantly in the liquid phase. The vapor-phase fraction increases with increasing temperature (at 270° the cyclohexane is 29% vapor) until complete conversion to the vapor phase occurs at the critical temperature (281°).

Discussion

Radiolysis yields of certain products of pure cyclohexane vapor decrease with increasing density. This

(5) S. Z. Toma and W. H. Hamill, *J. Am. Chem. Soc.*, **86**, 1478 (1964).

(6) S. Sato, K. Kikuchi, and S. Shida, *J. Chem. Phys.*, **41**, 2216 (1964).

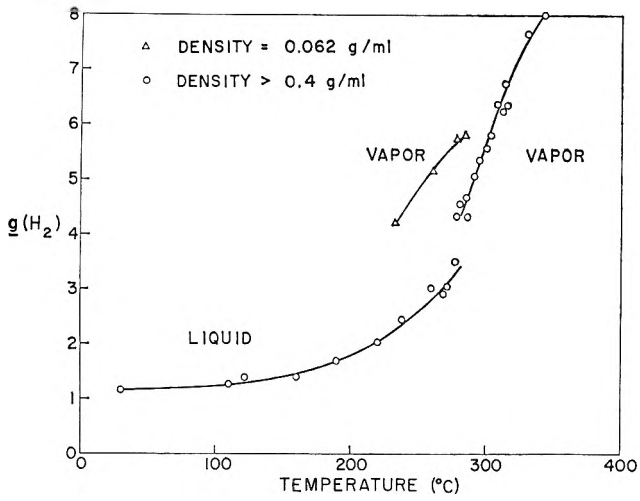

Figure 2. Effect of temperature on $g(H_2)$ in benzene–cyclohexane mixture. Electron fraction of benzene = 0.325.

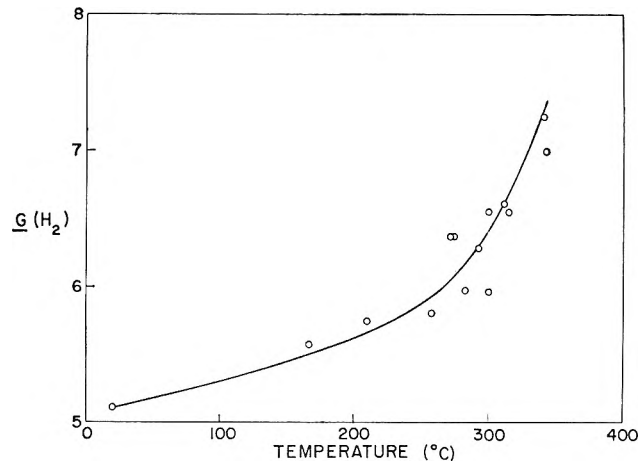

Figure 3. Effect of temperature on $G(H_2)$ of pure cyclohexane.

effect may be explained by the "cage" theory of limiting diffusion of precursors of these products[7] or by collisional deactivation of the precursors by surrounding molecules.[8]

Hydrogen yield decreases with increasing density of cyclohexane–benzene mixtures in the vapor phase under the conditions described in Table II. This decrease may be due to transfer of energy from cyclohexane to benzene, or may be due to hydrogen atom scavenging by benzene. However, inasmuch as the ratio of benzene to cyclohexane is constant at all densities in these mixtures, the relative probabilities of hydrogen atom scavenging and of abstraction to form hydrogen should not be affected. Therefore it is concluded that energy transfer is operative under these conditions in protecting the cyclohexane in the presence of benzene.

The abrupt increase in hydrogen yield at the critical temperature of cyclohexane (Figure 2) in changing from liquid to vapor implies an effect in the cyclohexane–benzene mixture attributable to phase. (Density, temperature, and composition are unchanged.) There is an apparent distinguishing characteristic of the liquid structure which may be some type of intermolecular bonding not present in the vapor phase which inhibits energy localization and thus accounts for this difference between the two phases.

Acknowledgments. The author is grateful to Dr. L. M. Theard for helpful discussions of this work and to D. R. Begeal and L. L. Stephenson for experimental assistance.

(7) L. Kevan and W. F. Libby, *J. Chem. Phys.*, **39**, 1288 (1963).

(8) Y. Toi, D. B. Peterson, and M. Burton, *Radiation Res.*, **17**, 399 (1962).

Time Variation of Ionic and Neutral Evaporation from Alkali Metal Iodides on a Heated Platinum Surface

by Hiroyuki Kawano[1] and Hokotomo Inouye

Research Institute for Scientific Measurements, Tohoku University, Gojyo-Dori, Sendai, Japan
(Received July 14, 1966)

The thermal emission of an alkali metal ion from its iodide on a metal surface is affected by the presence of another alkali metal iodide. For a detailed investigation of this phenomenon, the time variation of the alkali metal ion emission from one- and two-component systems of alkali metal iodides fixed on a platinum wire heated to constant temperature was examined with a mass spectrometer. (1) For the one-component systems the emission patterns of Li^+, Na^+, K^+, Rb^+, and Cs^+ were essentially the same. (2) In the two-component systems a "suppression effect" occurred. The emission pattern of the lighter alkali metal ion, M_L^+, was quite different from the corresponding pattern in the one-component system. In addition, the integrated ion currents of Li^+, Na^+, K^+, and Rb^+ were reduced to 60, 40, 60, and 40% by the presence of NaI, KI, RbI, and CsI, respectively. The effects were not observed for the heavier alkali metal ion, M_H^+. (3) Time variation of the vaporization of both ions and neutral particles was simultaneously examined with NaI–KI and KI–RbI mixtures. It was found that the reduced Na^+ emission (40%) produced by the presence of KI and the reduced K^+ emission (60%) produced by the presence of RbI were accompanied by an increase in Na (30%) and K (20%) evaporation in the form of neutral particles, respectively. (4) As a mechanism of this effect it is proposed that recombination of M_L^+ and I^- on the filament surface is enhanced by the presence of M_HI.

Introduction

When a mixture of sodium and potassium salts is heated on a metal surface, K^+ emission first occurs and Na^+ emission does not occur until the K^+ emission has decreased, even though in the absence of the potassium salt the surface temperature is high enough to produce Na^+ emission. In short, the emission of an alkali metal ion from its salt molecule on a metal surface can be altered by the presence of another alkali metal salt on the same surface. This phenomenon was first found by Dempster[2a] and later, in connection with experiments in ion microscopy, by Sasaki[2b] and by Popp and Walcher.[3] Hofmann[4] and Kaminsky[5] studied the phenomenon mass spectrometrically using biological tissue sections. The nature of their source material limited their observations to the emission of Na^+ and K^+. Since the mechanism responsible for the change in emission is not yet fully understood, the present authors have endeavored to obtain further information on this phenomenon. The features of the present experiments, in which a mass spectrometer was used to identify the positive ions and to measure their magnitudes, may be summarized as follows.

(1) A definite volume of an aqueous solution of a known concentration of an alkali metal iodide or of a binary mixture of alkali metal iodides was transferred to a substrate wire, F_I. In this way both the composition and the total amount of the sample could be determined in advance.

(1) H. K. is very grateful for a fellowship to The Sakkokai Foundation.

(2) (a) A. J. Dempster, *Phys. Rev.*, **11**, 316 (1918); (b) N. Sasaki, *J. Appl. Phys.*, **19**, 1050 (1948).

(3) G. Popp and W. Walcher, *Ann. Phys.*, **20**, 293 (1957).

(4) R. Hofmann, *ibid.*, **20**, 295 (1957).

(5) M. Kaminsky, "Advances in Mass Spectrometry," J. D. Waldron, Ed., Pergamon Press Ltd., London, 1959, p 125.

(2) Time variation of positive ion emission was examined for both one- and two-component systems. By comparing the results, the effect of a heavier alkali metal iodide, M_HI, on the emission of a lighter alkali metal ion, M_L^+, from its iodide, M_LI, could be investigated for a variety of systems.

(3) To investigate the mechanism of the above effect, emission patterns of both ions and neutral particles evaporating from F_1 was examined simultaneously by ionizing the particles on another heated filament, F_2.

This paper describes the results obtained in these experiments and discusses a mechanism for the observed effect.

Experimental Section

The mass spectrometer used in this work was a 180°-deflection, single-focusing type, with an ion path 2.6 cm in radius. As shown in Figure 1, the ion source contained double filaments of F_1 and F_2, which were made of a platinum wire 0.2 mm in diameter. The central part of the sample filament, F_1, was coiled into a spiral to facilitate coating with the sample solution and to limit the ion-emitting area. The second filament, F_2, was mounted parallel to F_1 in order to ionize neutral particles evaporating from the sample iodide on F_1. The central part of F_2 was coiled into a spiral to secure a larger ionizing surface. In order to increase the ion current from F_1 to the ion-accelerating system, F_1 was surrounded with the shield plate, S. The potentials of F_1 and F_2 were both positive with regard to the plate, P_1. A grid, G, was inserted between the filaments and held at a potential equal to that of F_2 (and lower than that of F_1) to keep F_1 from being bombarded by electrons emitted from F_2. F_1 and F_2 were heated to 1080 ± 20 and 920 ± 20°, respectively, with stabilized alternating currents. Filament temperatures were determined from measurements of electric resistance and kept constant by monitoring heating currents. Temperature equilibrium could be attained in about 10 sec after a heating current was applied. By applying an appropriate potential difference between F_1 and F_2, ions emitted from F_1 (primary ions), $M^+(1)$, and those from F_2 (secondary ions), $M^+(2)$, could be separated, since the radii of curvature of their paths in the analyzing magnetic field would be different because of their different linear velocities. The magnetic field was supplied by a permanent magnet with a field of 4500 gauss (for Li^+ and Na^+) and 6870 gauss (for Na^+, K^+, Rb^+, and Cs^+).

Prior to a run the filaments were thoroughly flashed at about 1300° *in vacuo* to remove occluded sodium and potassium impurities. After flashing, 1 μl of the aqueous sample solution was placed on F_1 with a microhypodermic syringe. The concentration of each alkali metal iodide in every solution was 0.075 mole/l. The LiI, NaI, and KI were of commercial "guaranteed reagent" grade. The RbI was obtained from E. Merck AG., Darmstadt, Germany, and the CsI from the Harshaw Chemical Co. Analysis of each reagent by the above mass spectrometer showed no alkali metal impurities which might affect the results.

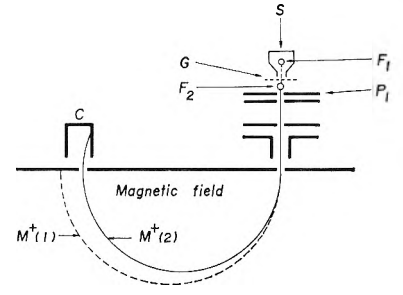

Figure 1. Schematic diagram of the mass spectrometer used in the present work.

Mass spectra were obtained by voltage scanning. The process is said to cause a mass discrimination effect. However, it was not necessary to take this into account in the present work, because the comparison of ion intensities was always confined to the same ion species in a given experiment. A series of peaks of the ion under study was measured by successive scannings, and the time variation of ion emission, accompanied with depletion of the sample material, was obtained by plotting the peak heights against the time, t, that had elapsed after the heating current of F_1 was turned on.

Results

1. Emission Curves of Primary Ions. At first only primary ions were examined. During the experiments both G and F_2 were removed from the ion source.

(1) One-Component Systems. Figure 2 shows a typical emission pattern of $Na^+(1)$. Similar patterns were observed for $Li^+(1)$, $K^+(1)$, $Rb^+(1)$, and $Cs^+(1)$ emitted from one-component systems of the corresponding iodides. An appreciable ion current was observed as soon as the heating current of F_1 was turned on (A), but the emission decreased rapidly and reached a minimum value (B) in about a minute. It then increased rapidly (C) until it reached a maximum (D) within the next few minutes, after which it decreased monotonically along the course indicated by D, E, and F. All the emission curves were reproducible within the experimental error of ±15%. They were used as comparison references for two-component systems.

(2) Two-Component Systems. The emission curves of $Li^+(1)$ and $Na^+(1)$ obtained from a two-component

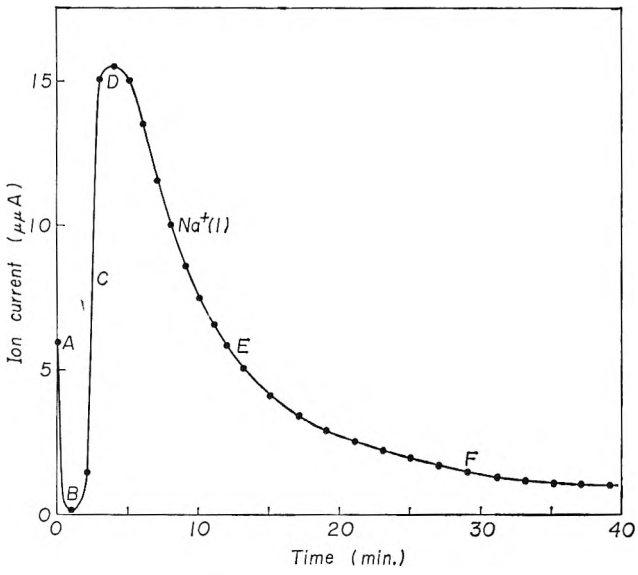

Figure 2. Time variation of $Na^+(1)$ emission from NaI on a platinum wire (F_1) heated to 1080°.

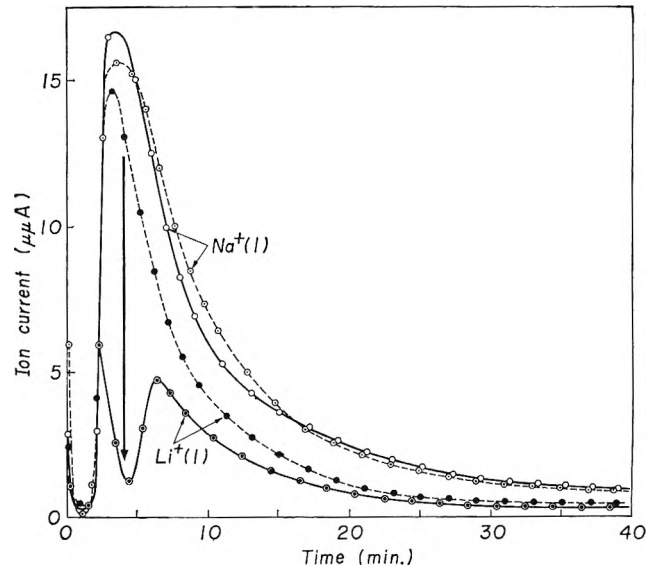

Figure 3. Emission patterns obtained for $Li^+(1)$ and $Na^+(1)$ from a LiI–NaI mixture (1:1 in mole ratio) and for $Li^+(1)$ from pure LiI and $Na^+(1)$ from pure NaI (broken lines).

system of LiI and NaI are shown in Figure 3 (solid lines). A curve of $Li^+(1)$ emission from a one-component system of LiI is also given for comparison (broken line). In both systems the $Li^+(1)$ emission shows a minimum at about 1 min. In the two-component system, however, after about 2 min, the $Li^+(1)$ emission ceases to increase and begins to decrease, giving rise to its first maximum, whereas the $Na^+(1)$ emission continues to increase. After passing the second minimum at about 4 min, the $Li^+(1)$ current increases to a second maximum at about 7 min. The second maximum always appears after the $Na^+(1)$ emission begins to decrease. Thus the presence of NaI produces a marked change in the emission pattern of $Li^+(1)$, as indicated with an arrow in Figure 3. Its integrated emission current is reduced to 0.6 ± 0.1 of that in the one-component system of LiI, although the amount of LiI on F_1 was the same in both systems. On the other hand, the pattern of the $Na^+(1)$ emission in the two-component system (solid line) was essentially the same as in the one-component system of NaI (broken line) and the magnitudes of the $Na^+(1)$ currents were also essentially the same. Thus the $Li^+(1)$ emission from LiI is suppressed by the presence of NaI on the same surface.

The same effect was observed also for two-component systems (1:1 in mole ratio) of NaI–KI, KI–RbI, and RbI–CsI. The results obtained are summarized in Figure 4, which shows the time variation of the ion intensity ratio, γ, of two- to one-component systems. The value of γ for $M_L^+(1)$ decreases remarkably in the range of about 2–10 min, after which it gradually

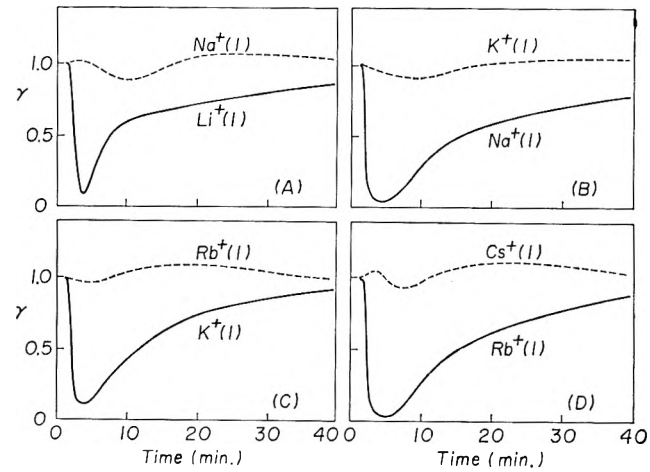

Figure 4. Time variation of the primary ion intensity ratio, γ, of two- to one-component systems: A, LiI–NaI, LiI, and NaI systems; B, NaI–KI, NaI, and KI systems; C, KI–RbI, KI, and RbI systems; and D, RbI–CsI, RbI, and CsI systems.

reaches unity. On the other hand, γ for $M_H^+(1)$ is always in the neighborhood of unity. The deviation is less than ±10% and within the limits of the experimental error of this work. The integrated ion currents of the $Na^+(1)$, the $K^+(1)$, and the $Rb^+(1)$ ions emitted from the NaI–KI, the KI–RbI, and the RbI–CsI systems are reduced to 0.4 ± 0.1, 0.6 ± 0.1, and 0.4 ± 0.1 of those in the one-component systems of the corresponding iodides, respectively.

These results show that in a binary system of alkali metal iodides the above effect always occurs in the di-

rection of decreasing atomic number, as in the series, Cs → Rb → K → Na → Li. Namely, the emission pattern of a primary ion on the right in this series is changed and the magnitude of its current is reduced by the presence of an element (in the form of the iodide) on the left. The reverse effect does not occur. The observed effect, which will be referred to hereafter as the "suppression effect," shows the following characteristics.

(1) When the emission curve of $M_H^+(1)$ begins to rise at about 2 min, the emission curve of $M_L^+(1)$ ceases to rise and begins to fall, thereby producing a maximum.

(2) After passing its first maximum the $M_L^+(1)$ emission does not begin to increase until the $M_H^+(1)$ emission has passed its own maximum.

(3) Not only are the individual values of the $M_L^+(1)$ emission from the M_LI–M_HI systems reduced, but the total integrated currents are also distinctly smaller, ranging from 40 to 60%. There is no evidence that the $M_L^+(1)$ emission in the two-component systems persists longer than in the one-component systems of M_LI.

2. Emission Curves of Primary and Secondary Ions. Since the above results made the authors feel that the reduced M_L^+ emission might be associated with an increase in the quantity of M_L evaporating in the form of neutral particles from F_1, evaporation of the neutral particles also was studied by ionizing them on F_2.

(1) One-Component Systems. Figure 5 is the emission curves of $K^+(1)$ and $K^+(2)$ obtained from a KI system. As in Figures 2 and 3, the peak heights in the mass spectra were plotted against t. (F_2 was at temperature at all times.) As shown in the figure, the emission pattern of $K^+(2)$ is the same as that of $K^+(1)$. Quite similar results were obtained for one-component systems of NaI and RbI.

(2) Two-Component Systems. The emission curves for a binary system of NaI–KI are shown in Figure 6. As described above, the pattern of $K^+(1)$ is the same as that in the one-component system (Figure 5), whereas that of $Na^+(1)$ is much changed and depends on the emission of $K^+(1)$. This change in pattern, however, is found for neither $Na^+(2)$ nor $K^+(2)$.

Little change was found in the emission currents of $K^+(1)$ and $K^+(2)$ from the NaI–KI system relative to those from the KI system. On the other hand, the presence of KI gave rise to changes in the ion currents of both $Na^+(2)$ and $Na^+(1)$, as indicated by the open and the solid arrows, respectively, in Figure 7. The integrated emission current of $Na^+(2)$ in the NaI–KI system increases to 1.3 ± 0.1 of that in the NaI system, while that of $Na^+(1)$ decreases to 0.4 ± 0.1.

Similar changes were observed for the K^+ emission

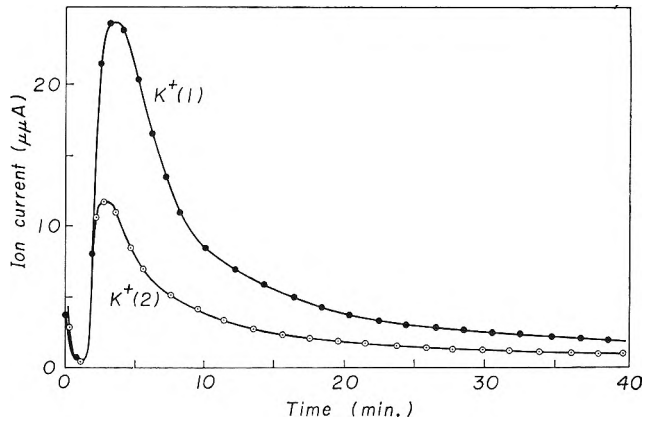

Figure 5. Emission patterns of $K^+(1)$ and $K^+(2)$ obtained for a KI system.

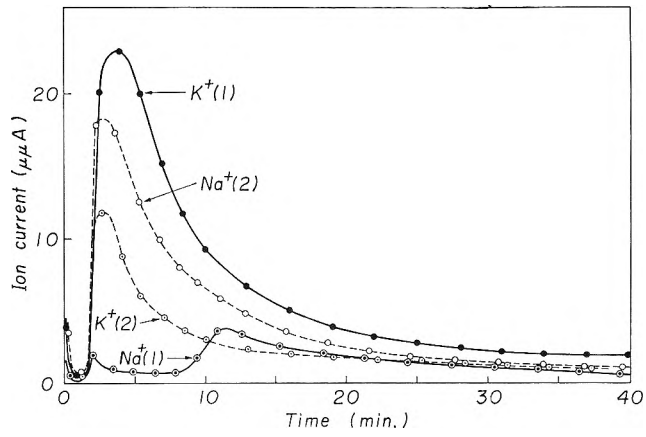

Figure 6. Emission patterns of the primary and the secondary ions obtained from a NaI–KI mixture (1:1 in mole ratio).

from a KI–RbI mixture (Figure 8). The integrated emission current of $K^+(2)$ in the mixture increases to 1.2 ± 0.1, while that of $K^+(1)$ decreases to 0.6 ± 0.1 of that from the KI system. These changes, however, were not found for the Rb^+ emission.

Discussion

The results obtained in this work show that in the M_LI–M_HI system the emission current of $M_L^+(1)$ decreases, unlike that of $M_L^+(2)$ which increases, and that both changes take place in the same time interval. The authors conclude that the reduced $M_L^+(1)$ emission is caused by an increase in the vaporization of neutral particles due to the presence of the iodide, M_HI. They will discuss the mechanism of this suppression effect.

1. Change of Work Function. Kaminsky[5] suggested that the observed effect of K on Na^+ emission might be due to change in work function of the metal surface. The change, however, could not explain the present

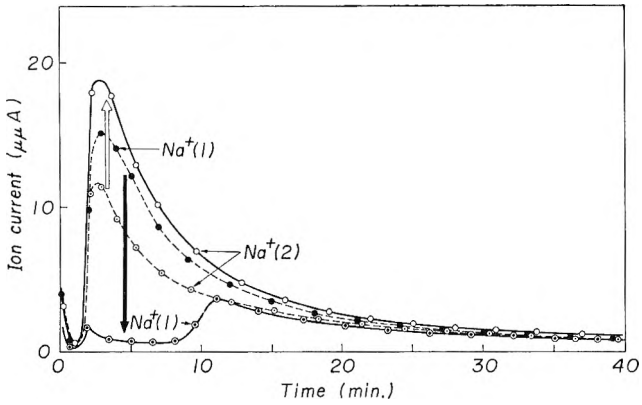

Figure 7. Changes in the amount of emission current observed for $Na^+(1)$ and $Na^+(2)$ due to the suppression effect. The broken and the solid curves were obtained with pure NaI and with an NaI–KI mixture (1:1 in mole ratio), respectively.

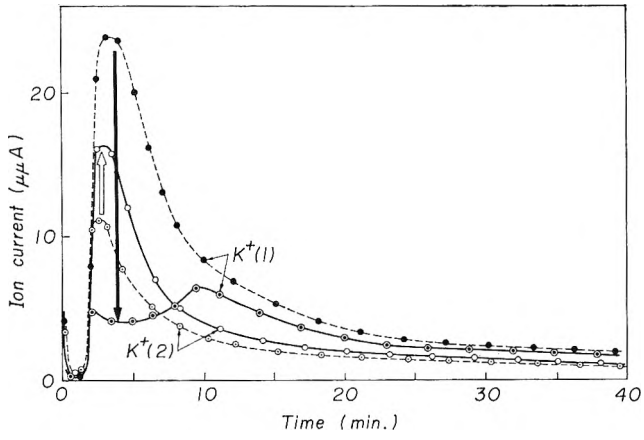

Figure 8. Changes in the amount of emission current observed for $K^+(1)$ and $K^+(2)$ due to the suppression effect. The broken and the solid curves were obtained with pure KI and with a KI–RbI mixture (1:1 in mole ratio), respectively.

result that only the $M_L^+(1)$ emission was reduced while the $M_H^+(1)$ emission was not affected. Besides, when a metal surface is covered with thousands of molecular layers of sample material, as is in this work, it is doubtful whether surface conditions of the substrate metal affect the ion emission from the surface of the sample material.[6]

2. Charge Transfer. As a mechanism of the suppression effect, a charge-transfer reaction, $M_L^+ + M_H \rightarrow M_L + M_H^+$, on the metal surface was suggested.[2b] Suppose that the suppression effect were caused by the above reaction, an increase in $M_H^+(1)$ emission and a decrease in M_H evaporation (*i.e.*, in $M_H^+(2)$ emission) should occur simultaneously with decrease in $M_L^+(1)$ emission. Such a result, however, has not been found in this work.

3. Recombination. Since all of the alkali metal iodides are ionic in character and their melting points are in the range of 450–750°, they melt and are probably to a considerable extent dissociated into ions when they are heated to a temperature of 1080°, as in the present work. A phenomenon similar to electrolysis of a molten salt can occur on the surface, since a drawing-out potential for a positive ion is applied between F_1 and P_1.

It is also well known that vapor from a molten alkali metal halide in a metallic crucible does not consist of the alkali metal atoms and the halogen molecules but of alkali metal halide molecules.[7-9] Accordingly, the authors assume that the neutral particles evaporating from an alkali metal iodide on a heated filament surface also consist of alkali metal iodide molecules. This assumption and the fact that the suppression effect only occurs with respect to $M_L^+(1)$ led the authors to take a recombination reaction of M_L^+ and I^- on F_1 into consideration.

A calculation along a course similar to the Born–Haber cycle gives the result that $M_H^+(1)$ is more easily emitted from the molten salt mixture on a metal surface. On the other hand, when two equilibria, $Na^+ + I^- \rightleftarrows NaI$ and $K^+ + I^- \rightleftarrows KI$, are coexistent, the following relation holds

$$\frac{K_{NaI}}{K_{KI}} = \frac{[NaI]/[Na^+]}{[KI]/[K^+]} = \frac{f_{NaI}f_{K^+}}{f_{Na^+}f_{KI}} \exp\{(E_{NaI} - E_{KI})/kT\}$$

where K is the equilibrium constant, f is the partition function, and E_{MI} is the energy liberated in the reaction $M^+ + I^- \rightarrow MI$. If the following conditions are assumed

$$f_{NaI}f_{K^+}/f_{Na^+}f_{KI} \cong 1$$

and

$$E_{NaI} - E_{KI} > kT$$

then

$$\frac{d}{d[I^-]}\left\{\frac{[NaI]}{[Na^+]}\right\} > \frac{d}{d[I^-]}\left\{\frac{[KI]}{[K^+]}\right\}$$

Addition of KI to NaI causes an increase in the iodide ion concentration and makes the equilibria shift to the

(6) In this work special attention was not paid to the platinum surface conditions. Reproducible results, however, could be obtained within a reasonable experimental error. This fact is thought to be another evidence that surface conditions have no serious effect on the results and that the suppression effect occurs in the volume or near the surface of the molten sample salts.

(7) L. Friedman, *J. Chem. Phys.*, 23, 477 (1955).

(8) J. Berkowitz and W. A. Chupka, *ibid.*, 29, 653 (1958).

(9) R. F. Porter and R. C. Schoonmaker, *ibid.*, 29, 1070 (1958).

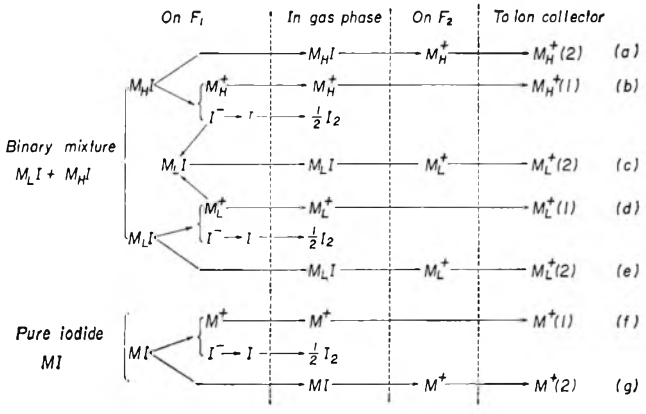

Figure 9. Scheme of the ion emission processes occurring in this work.

right. The magnitude of the shift or degree of increase in the iodide molecule–alkali ion concentration ratio is much larger for NaI than for KI. A similar result is obtained, more or less, for every pair of the iodides.

Although the above assumptions hold in a gas reaction, the authors are not sure whether the same result holds in the melt. It seems likely, however, that a similar tendency probably holds for the strength of interaction between a cation and an iodide ion in the melt. Lumsden,[10] for instance, has pointed out in his theoretical treatment of molten mixtures of alkali metal halides that in a mixture of two alkali metal halides with a common anion the cation with smaller ionic radius combines more strongly with the anion because of its stronger polarizing force and is less mobile in the mixture than in the pure melt.

These considerations lead to the conclusion that in a binary system of the alkali metal iodides, M_LI and M_HI, the heavier ion, M_H^+, is emitted almost independent of the presence of M_LI and emission of the lighter ion, M_L^+, is, on the other hand, suppressed because of the recombination with I^- on the emitting surface. The ionization processes which are supposed to occur in the present work are shown schematically in Figure 9. The processes b, d, and f cause thermal ionic emission from the iodides on F_1 (the primary ions). The processes a, e, and g are due to surface ionization on F_2 of the neutral molecules evaporating from F_1 (the secondary ions). The process c giving an additional $M_L^+(2)$ emission is assumed to explain the suppression effect; in a two-component system of M_LI–M_HI, some of the M_L^+ ions that would be emitted as $M_L^+(1)$ ions in the one-component system of M_LI recombine on the surface of F_1 with the I^- ions supplied by $M_H^+I^-$ and evaporate as neutral molecules.

The authors believe that the suppression effect could be explained by this model without conflict with their experimental results.

(10) J. Lumsden, *Discussions Faraday Soc.*, **32**, 138 (1961).

The Carbon Tetrachloride Sensitized Photooxidation of Leuco Ethyl Crystal Violet

by A. MacLachlan

Contribution No. 1243 from the Central Research Department, Experimental Station, E. I. du Pont de Nemours and Company, Wilmington, Delaware *(Received July 19, 1966)*

Based on direct observation of many of the reaction intermediates, a mechanism for halocarbon-sensitized oxidation of leuco ethyl crystal violet to the corresponding dye is presented. Sensitization occurs out of the leuco dye's singlet and triplet states and leads to a radical-ion intermediate rather than the triphenylmethyl radical directly. Rate constants of most of the reactions are given. Solvent effects on the various steps are studied.

Introduction

In the 1940's, G. N. Lewis and his associates demonstrated a number of stepwise photooxidation reactions of organic molecules contained in rigid glasses. They were able to distinguish electron ejection, triplet-state excitation, and bond-dissociation reactions.[1-4] The luminescence phenomena noted[4] were further investigated by Linschitz[5] in a study of the origin of the delayed luminescence as it applied to electron ejection and trapping by the solvent and added solutes. Convincing evidence for the ejection of an electron into lithium diphenylamide and other compounds was obtained by recording the absorption spectrum of the solvated electron. In a second paper, Linschitz[6] and co-workers identified conclusively the radical ion formed by photoejection of an electron from N,N'-diphenyl-*p*-phenylenediamine.

The technique of time-resolved fluorescence spectroscopy and the flash photolysis technique[7] offer the possibility of examining these same reactions and intermediates in fluid solvents even at room temperature. This paper reports the application of these high-speed techniques to the study of the mechanism of halocarbon-sensitized photooxidation of tris(*p*-N,N-diethylaminophenyl)methane known as leuco ethyl crystal violet (LECV). Halocarbon-sensitized oxidation of amines is a well-known and very general reaction.[8] LECV was selected for study because of its easily characterized oxidation product, the strongly absorbing ethyl crystal violet dye.

Experimental Section

A. Equipment. Fluorescence yield measurements were made using 2×10^{-4} *M* solutions of LECV in ethanol. The 2537-A line of mercury was used as the exciting wavelength. Samples were placed in 1-cm quartz cells.

Fluorescence quantum yields were made by comparison of the integrated fluorescence spectrum of the LECV with the fluorescence emission of a quinine bisulfate solution whose fluorescence quantum yield[9] is taken as 0.51.

Fluorescence lifetime values were obtained by P. C. Hoell of this laboratory using a subnanosecond phase fluorimeter. This instrument consists of an exciting light, modulated at 10 Mc, which is absorbed by the sample and reemitted as coherently modulated fluorescence. A phase shift occurs, the magnitude of

(1) G. N. Lewis, D. Lipkin, and T. T. Magel, *J. Am. Chem. Soc.*, **63**, 3005 (1941).

(2) G. N. Lewis and M. Kasha, *ibid.*, **66**, 2100 (1944).

(3) G. N. Lewis and D. Lipkin, *ibid.*, **64**, 2801 (1942).

(4) G. N. Lewis and J. Bigeleisen, *ibid.*, **65**, 2414 (1943).

(5) (a) H. Linschitz, M. L. Berry, and D. Schweitzer, *ibid.*, **76**, 5833 (1954); (b) J. Eloranta and H. Linschitz, *J. Chem. Phys.*, **38**, 2214 (1963).

(6) H. Linschitz, J. Rennert, and T. M. Korn, *J. Am. Chem. Soc.*, **76**, 5839 (1954).

(7) G. Porter, *Proc. Roy. Soc.* (London), **A200**, 284 (1950).

(8) (a) R. H. Sprague, H. L. Fletcher, and E. Wainer, *Phot. Sci. Eng.*, **5**, 98 (1961); (b) D. P. Stevenson and G. M. Coppinger, *J. Am. Chem. Soc.*, **84**, 149 (1962).

(9) W. H. Melhuish, *J. Phys. Chem.*, **64**, 762 (1960); **65**, 229 (1961).

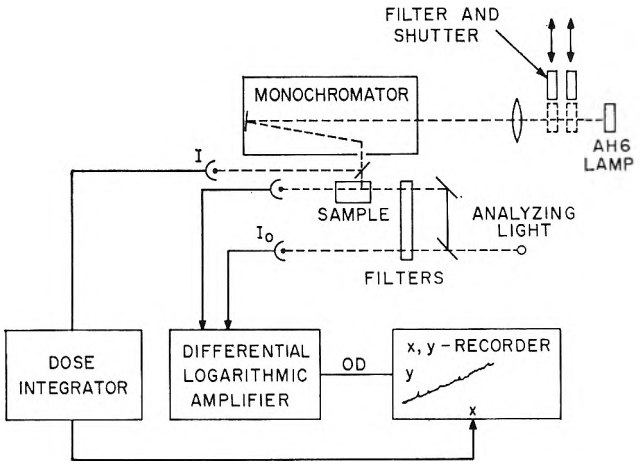

Figure 1. Photolyzing monochromator with continuous analysis.

which can be related to the lifetime of the fluorescence state by the expression

$$\tan(\omega t') = \omega\tau$$

where t' is the phase delay, ω is $2\pi f$ (f = 10 Mc), and τ is the lifetime of the fluorescing state. At small angles, the phase delay is equal to the lifetime.

Quantum yield measurements of color (Φ_C) were made on an apparatus designed by P. C. Hoell. Figure 1 presents a block diagram of the experimental arrangement. The sample to be irradiated is placed in a 1-cm path length quartz cell, the photolyzing wavelength is selected by adjustment of the monochromator, and then the shutter is opened. Optical density is followed by a double-beam spectrometer wherein OD is presented to the x axis of an x–y recorder. The total dose is monitored by deflecting a small fraction of the light leaving the monochromator to a phototube and integrating circuit. Integrated dose is then fed to the y axis of the recorder. Graphs of OD *vs.* dose are obtained, the slopes of which are directly proportional to the quantum yield, Φ_C. Quantum yields were placed on an absolute basis by taking advantage of the known quantum yield of crystal violet leuco nitrile (Φ = 1 in ethanol).[10] The color produced is the same species as the oxidized LECV and thus it is merely a matter of comparing slopes.

B. Flash Photolysis. The flash photolysis apparatus was similar to that described by Porter.[7] The flash duration has a half-width of 4 μsec. The analyzing lamp was operated from a 6-v storage battery.

Samples are deoxygenated by flushing for 10 min with purified argon. Argon pressure was used to drive the sample through the flash photolysis cell.

Results

A. Quantum Yields. It is readily demonstrated that LECV photooxidizes in the presence of a wide variety of materials (halocarbons, quinones, and other electron-deficient molecules) and yields the intensely colored cationic dye (λ_{max} 5900 A, ϵ 110,000 l./mole-cm). Halocarbons are an especially convenient series of sensitizers since they may be obtained pure and their structures may be varied. The major part of this study will be concerned with CCl_4 as a sensitizer.

The absorption spectrum of a 2×10^{-4} M solution of LECV in ethanol, in the presence of 0.1 M CCl_4, is given in Figure 2. No obvious effects of CCl_4 were observed on the LECV spectrum. However, photolysis with 3200-A light, thus photolyzing into the leuco dye, yields the dye cation only when CCl_4 is present. Quantum yields (Φ_C) are given in Table I. There is a marked effect of CCl_4 concentration when oxygen is present and a negligible effect over the range studied when it is absent.

Table I: Effect of CCl_4 Concentration and Oxygen and the Color Quantum Yield in Ethanol

LECV, M	CCl_4, M	O_2 present?	Φ_C
2×10^{-4}	0.005	Yes	0.36
2×10^{-4}	0.01	Yes	0.52
2×10^{-4}	0.03	Yes	0.61
2×10^{-4}	0.05	Yes	0.65
2×10^{-4}	0.1	Yes	0.68
2×10^{-4}	0.001	No	1.09
2×10^{-4}	0.005	No	1.14
2×10^{-4}	0.03	No	1.17
2×10^{-4}	0.1	No	1.16

An important clue to the reason for the variation in Φ, values can be obtained by examining the singlet-state reactions of LECV. The reactions to be considered are

	rate	
$DH + h\nu \longrightarrow DH^*$		(1)
$DH^* \longrightarrow h\nu' + \text{heat} + DH$	$k_f(DH^*)$	(2)
$DH^* \longrightarrow \text{heat} + DH$	$k_I(DH^*)$	(3)
$DH^* \longrightarrow T$	$k_T(DH^*)$	(4)
$DH^* + Q \longrightarrow \text{product}$	$k_Q(DH^*)(Q)$	(5)

where DH is LECV, with D representing the complete

(10) A. H. Sporer, *Trans. Faraday Soc.*, **57**, 983 (1961).

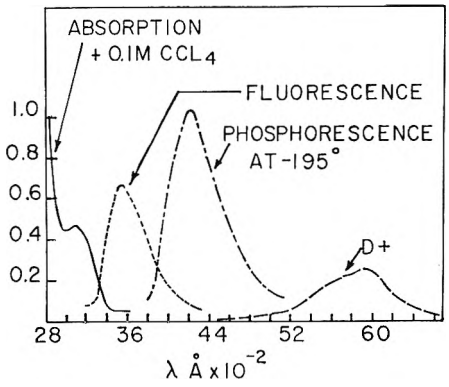

Figure 2. Spectral properties of LECV in ethanol.

molecule except for the single hydrogen atom (H) on the triphenylmethyl central carbon atom, DH* is the first-excited singlet state, T is the triplet, Q is an added quencher molecule (CCl_4), and k_f, k_I, k_T, and k_Q are the rate constants for fluorescence, internal conversion, conversion to a triplet state, and quenching, respectively. The fluorescence and phosphorescence spectra of LECV are shown in Figure 2. By measurement of fluorescence yields for 2×10^{-4} M LECV as a function of CCl_4 concentration, the curve given in Figure 3 was obtained. Since all the processes for loss of DH* are first order (pseudo first order for quenching), the slope of the line as plotted in Figure 3 is given by the Stern–Volmer equation. Furthermore, a plot of

$$\frac{1}{\Phi_f} = \frac{1}{\Phi_{f0}} + \frac{k_Q}{k_f}[Q]$$

the reciprocal lifetime (τ) of the state DH* *vs.* CCl_4 concentration yields at 2×10^{-4} M LECV a straight line (Figure 4) whose slope is k_Q. From the values ob-

$$\frac{1}{\tau} = \frac{1}{\tau_0} + k_Q[Q]$$

tained in Figures 3 and 4, there are two independent means of obtaining k_f. If τ_0, the mean lifetime, and Φ_{f0}, the fluorescence yield of DH* in the absence of Q, are used, k_f is found to be 12×10^7 sec^{-1}. Using the slopes of Figures 3 and 4, $k_Q = 15.9 \times 10^9$ M^{-1} sec^{-1} and $k_I = 7.1 \times 10^7$ sec^{-1} showing satisfactory agreement.

From the curves of DH* quenching, it is seen that at concentrations of CCl_4 lower than 0.005 M, there is no probability of reacting with DH* during its lifetime. However, the Φ_C reported in Table I demonstrates efficient oxidation at these CCl_4 concentrations in the absence of oxygen. This must mean that DH* converts to another species, either an intermediate free radical or the triplet state. Furthermore, these

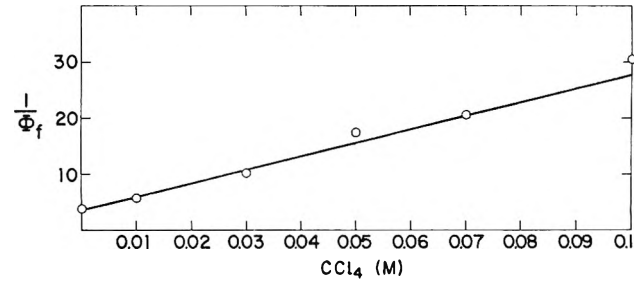

Figure 3. Plot of $1/\Phi_f$ *vs.* CCl_4 for LECV in ethanol.

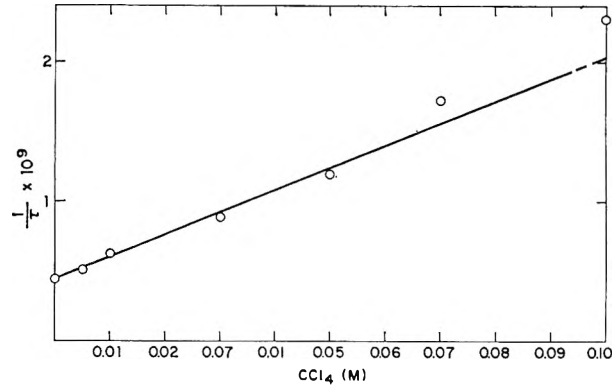

Figure 4. Plot of $1/\tau$ *vs.* CCl_4 in ethanol.

states then react with CCl_4 to produce D^+. Oxygen strongly inhibits this reaction.

B. The Triplet State. Two test sfor the participation of the triplet state were used.

(1) The phosphorescence curve in Figure 2 places the triplet of LECV at 4200 A and, thus, if triplet–triplet quenching is to be observed, a molecule must be used with a triplet emission to a longer wavelength. Naphthalene[11] phosphoresces at 4700 A and should be an excellent quencher if triplet states are involved. Table II presents the results of naphthalene quenching on Φ_C. Photolysis was carried out with 3400-A light, a wavelength where all of the energy is being absorbed by the LECV. Carbon tetrachloride was added at a concentration such that no singlet-state quenching attributable to it could occur.

(2) While it is possible that the previous results can be explained by arguing that efficient radical scavenging by naphthalene would yield the same experimental effect, a direct observation of the triplet state of naphthalene, produced by the quenching reaction, would be unequivocable evidence. This evidence was obtained by the flash photolysis technique.

(11) G. Porter and F. Wilkinson, *Trans. Faraday Soc.*, **57**, 1686 (1961).

Table II: Naphthalene Quenching of Φ_C[a]

LECV, *M*	CCl_4, *M*	Naphthalene, *M*	Relative quantum yield
10^{-3}	10^{-3}	...	1
10^{-3}	10^{-3}	10^{-3}	0.8
10^{-3}	10^{-3}	3×10^{-3}	0.35

[a] All runs were made in the absence of oxygen.

Filters and concentration were adjusted so that practically all the photolyzing light was absorbed by the LECV. In the absence of LECV, 0.003 *M* naphthalene in ethanol yields only an indication of the triplet–triplet absorption at 4100 A. When 2×10^{-4} *M* LECV is added, the 4100-A transient increases markedly in intensity. Combining this direct observation with the quantum yield data in Table II serves to identify the triplet state of LECV as the major product of the unquenched singlet state.

C. Reaction Intermediates. Investigation of the rate of D^+ formation with flash photolysis revealed some interesting solvent effects. Observation of D^+ at 5900 A as a function of time after the photolysis flash (half-width 4 μsec) demonstrated that in nonviscous polar solvents (methanol, ethanol) the D^+ is formed with appreciable delay, while in viscous (glycerol) or nonpolar solvents (CCl_4, cyclohexane), the D^+ formation is instantaneous.

Examination of the kinetics of D^+ formation reveals that good first-order kinetics are obeyed over the entire range of the slow part of the traces. Table III presents the first-order rate constants determined for a number of runs and sensitizers.

Table III: Slow Rate of D^+ Formation

Sensitizer	*M*	Solvent	k, sec^{-1}
Carbon tetrachloride	10^{-3}	Ethanol	29
Carbon tetrachloride	2×10^{-3}	Methanol	34
Carbon tetrachloride	5×10^{-3}	Ethanol	24
Hexachloroethane	10^{-3}	Ethanol	19 (1)
Chloroform			29 (1)
Carbon tetrachloride	(20%)	Ethanol	23
Cardon tetrachloride	0.04	Ethanol	20, 20, 22

The transient curves in ethanol and methanol are always composed of two distinct parts. A fraction of the D^+ is formed with a rate that follows the flash and the remainder is generated in the slow first-order process. Solvent viscosity is not the sole characteristic feature that determines the presence or absence of the two reactions because glycerol also suppresses the slow part. The mechanism below is consistent with all of the data.

$$DH^* + CCl_4 \longrightarrow \dot{DH}^+ + \dot{CCl}_4^- \quad (6)$$

$$\dot{DH}^+ + \dot{CCl}_4^- \longrightarrow D^+ + HCl + :CCl_2 + Cl^- \quad (7)$$

$$DH + \dot{CCl}_4^- \; (\cdot CCl_3 + Cl^-) \longrightarrow \dot{DH}^+ + CCl_3^- + Cl^- \quad (8)$$

$$\dot{DH}^+ \rightleftharpoons D\cdot + H^+ \quad (9)$$

$$\dot{DH}^+ + D\cdot \longrightarrow D^+ + DH \quad (10)$$

Reaction 6 is an electron-exchange reaction from either singlet or triplet DH, which yields the Würster-type ion radical, $\dot{DH}^+$. The $\dot{CCl}_4^-$ formed is still capable of oxidizing DH^+ to D^+ and does so to the extent dictated by its proximity to $\dot{DH}^+$ and the rate of reaction. Reaction 7 will be favored by an increase in viscosity as was observed with glycerol. The prior formation of the ion radical $\dot{DH}^+$ is favored over a direct formation of D because of the dramatic solvent effect. At high dielectric constants, as in ethanol and methanol, the ion would be expected to have greater stability than in a solvent of lower dielectric constant, like CCl_4 or cyclohexane. The intermediate $\dot{DH}^+$ formed from the sensitized oxidation of DH was easily observed at $-85°$ in methanol through the employment of esr spectroscopy. The single-line spectrum observed by photolysis of a 5% CCl_4–95% MeOH solution of 10^{-4} *M* DH could not be resolved to obtain hyperfine structure. On warming, in the absence of further photolysis, the radical disappeared and the characteristic 5900-A absorption of D^+ appeared.

Reaction 8 expresses the further possible reactions of the reduced CCl_4, either in the form of $\dot{CCl}_4^-$ or $\cdot CCl_3$. It is necessary to invoke these additional oxidizing species because of the quantum yield data in Table I. It can be seen from the reactions leading to D^+ that a quantum yield of one would be expected.

The precursor to D^+ can be observed at 4800 A. Because of its much lower extinction coefficient, meaningful kinetics could not be obtained; however, the lifetime for decay corresponded to the lifetime for D^+ formation. There are no protonated forms of D^+ that have an absorption maximum at 4800 A. The intermediate $\dot{DH}^+$ must attain the final oxidation state, D^+, at the rate and kinetic order found for the slow part of the D^+ formation. Reactions 9 and 10 represent the most probable manner in which this is accom-

plished. The first-order kinetics observed for D^+ formation dictate a prior equilibrium process as in (9) and furthermore make the D· formation the rate-determining step. Addition of 10^{-4} *M* HCl to the solution increased the lifetime of $D\dot{H}^+$ to 100 msec in agreement with the equilibrium nature of reaction 9. However, with all the other potentially protonating sites on LECV, this cannot be taken as proof for reaction 9.

Summary

Reactions 1–9 represent a plausible reaction scheme for the halocarbon-sensitized oxidation of LECV. The identity of the actual sensitizing steps in the reaction with the processes studied by Lewis and coworkers[1–4] and Linschitz[5,6] in the solid state at low temperatures suggests that many of these previously studied reactions can be examined at room temperature using the flash photolysis technique.

This work also supplies direct proof that both the singlet state and triplet state can interact with the sensitizers. Whether the singlet state is converted first to the triplet state by the sensitizer and then reacts cannot be ascertained from these data.

Acknowledgments. The author is deeply indebted to P. C. Hoell for his measurement of the fluorescence lifetimes of LECV and for all the instruments he has made available to our research staff, a number of which are mentioned in the Experimental Section. Thanks are also due to R. G. Bennett for many helpful discussions concerning fluorescence lifetimes, to V. F. Hanson for providing the flash photolysis apparatus, to C. Yembrick and R. Dessauer for getting the author interested in the problem, and finally to J. M. White for his assistance in carrying out many of the experiments.

Proton Resonance Spectra of Selected Mono-, Di-, and Trisubstituted Silanes[1]

by H. J. Campbell-Ferguson, E. A. V. Ebsworth, A. G. MacDiarmid, and T. Yoshioka

University Chemical Laboratory, Cambridge, England, and Department of Chemistry and the Laboratory for Research on the Structure of Matter, University of Pennsylvania, Philadelphia, Pennsylvania 19104 *(Received June 20, 1966)*

The proton nuclear magnetic resonance spectra of $H_2Si(OCH_3)_2$, $H_2Si(OSiH_3)_2$, $H_2Si[N(CH_3)_2]_2$, $HSi(OCH_3)_3$, $HSi(OSiH_3)_3$, $HSi[N(CH_3)_2]_3$, $HSiBr_3$, and $HSiI_3$ have been examined and proton chemical shift and $J_{^{29}SiH}$ data for these compounds are presented. The values are compared with analogous data for H_nSiX_{4-n} (X = F, Cl, Br) compounds and with values for the corresponding methane derivatives where available. In all cases, the chemical shifts of the protons attached directly to the central silicon or carbon move downfield with increasing substitution, with the exception of the series H_nSiX_{4-n} (X = F, $N(CH_3)_2$, OCH_3, $OSiH_3$), where an unexpected upfield shift is observed. Possible reasons for the different trends in chemical shift values and certain relationships between $J_{^{29}SiH}$ values are discussed.

In the course of some investigations into the reactions of silyl compounds, we have measured the proton resonance spectra of $SiHBr_3$, $SiHI_3$, and compounds of formula SiH_nX_{4-n}, where X = OCH_3, $OSiH_3$, or $N(CH_3)_2$. The chemical shifts are presented in Table I and coupling constants in Table II, together with the corresponding parameters for the other halomonosilanes. Long-range H–H coupling was not detected.

The way in which the chemical shifts change with increasing substitution depends on the substituent in an interesting way. In the chloro-, bromo-, and iodosilanes, τ(SiH) decreases with increasing substitution (Table I), as does τ(CH) in the analogous series of halomethanes, including the fluorides.[2] This is the direction in which the chemical shifts would be expected to change if they were determined by changes in σ-electron density at carbon and silicon, respectively.

In marked contrast, it has previously been noticed that in the fluorosilanes, τ(SiH) actually increases with increasing substitution; the data in Table I show that a similar over-all upfield shift occurs with increasing oxygen and nitrogen substitution at a silicon atom. Since the factors that determine the SiH chemical shift are still ill defined, it is at present impossible to offer an explanation for the effect of fluorine, oxygen, or nitrogen substitution; but it is interesting that these three elements are commonly believed to form the

Table I: Chemical Shift Values for SiH_nX_{4-n}[a]

Compound	τ(SiH)	Compound	τ(SiH)	$\tau(CH_3)$	$\tau(OSiH_3)$
SiH_3Cl[b]	5.41	SiH_3F[b]	5.24	...	...
SiH_2Cl_2[b]	4.60	SiH_2F_2[b]	5.29	...	...
$SiHCl_3$[b]	3.93	$SiHF_3$[b]	5.49	...	...
SiH_3Br[b]	5.83	$SiH_2N(CH_3)_2$[c]	5.64	7.51	...
SiH_2Br_2[b]	4.83	$SiH_2[N(CH_3)_2]_2$	5.62	7.49	...
$SiHBr_3$	3.70	$SiH[N(CH_3)_2]_3$	5.87	7.56	...
SiH_3I[b]	6.56	SiH_3OCH_3	5.51	6.58	...
SiH_2I_2[b]	5.97	$SiH_2(OCH_3)_2$	5.58	6.48	...
$SiHI_3$	5.51	$SiH(OCH_3)_3$	5.91	6.51	...
		SiH_3OSiH_3[b]	5.39	...	5.39
		$SiH_2(OSiH_3)_2$	5.46	...	5.33
		$SiH(OSiH_3)_3$	5.82	...	5.34

[a] All measurements carried out in cyclohexane solutions. Values given are extrapolated to infinite dilution except for the methoxy- and siloxysilanes, which were all measured at 25% (vol.) concentration. Conversions to τ scale based on C_6H_{12} being 1.44 ppm downfield from $(CH_3)_4Si$. Error in values quoted is $\leq \pm 0.01$ ppm. [b] E. A. V. Ebsworth and J. J. Turner, *J. Phys. Chem.*, **67**, 805 (1963). [c] J. C. Thompson, private communication.

(1) A portion of this study was supported by the Advanced Research Projects Agency, Office of the Secretary of Defense, Washington, D. C.

(2) A. A. Bothner-by and C. Naar-Colin, *J. Am. Chem. Soc.*, **80**, 1728 (1958); E. A. V. Ebsworth, "Volatile Silicon Compounds," Pergamon Press Inc., New York, N. Y., 1963, p 23.

Table II: Coupling Constant Parameters for SiH_nX_{4-n}[a]

Compound	$J_{^{29}SiH}$(obsd), cps	$J_{^{29}SiH}$(obsd) (SiH_3O-), cps	$J_{^{13}CH}$(obsd) (CH_3N-), cps	$J_{^{29}SiH}$(add), cps	Δ,[b] cps	100Δ/ J(obsd)	D	D/n
SiH_3F	229.0 ± 0.6[c]	...	...	...	...	...	0.3625	0.3625
SiH_2F_2	282 ± 3[c]	...	...	255.5	−26.5	9.40	1.0294	0.5147
$SiHF_3$	381.7 ± 1.5[c]	...	...	282.0	−99.7	26.12	2.1318	0.7106
SiH_3Cl	238.1 ± 0.2[c]	...	...	...	...	...	0.4821	0.4821
SiH_2Cl_2	288.0 ± 0.4[c]	...	...	273.7	−14.3	4.96	1.1008	0.5504
$SiHCl_3$	362.9 ± 0.2[c]	...	...	309.3	−53.6	14.77	1.9361	0.6454
SiH_3Br	240.5 ± 0.3[c]	...	...	...	...	...	0.5133	0.5133
SiH_2Br_2	289.0 ± 0.6[c]	...	...	278.5	−10.5	3.63	1.1126	0.5563
$SiHBr_3$	357.3	...	...	316.5	−40.8	11.42	1.8768	0.6256
SiH_3I	240.1 ± 0.2[c]	...	...	...	...	...	0.5081	0.5081
SiH_2I_2	280.5 ± 0.2[c]	...	...	277.7	−2.8	1.00	1.0114	0.5057
$SiHI_3$	325.1	...	...	315.3	−9.8	3.11	1.5266	0.5089
SiH_3OCH_3	216.2	...	...	...	...	...	0.1902	0.1902
$SiH_2(OCH_3)_2$	247.6 ± 0.6[d]	...	...	229.9	−17.7	7.15	0.6046	0.3023
$SiH(OCH_3)_3$	297.9 ± 0.3[d]	...	...	243.6	−54.3	18.23	1.2170	0.4057
SiH_3OSiH_3	221.5 ± 0.2[d]	221.5 ± 0.2[d]	...	...	...	...	0.2622	0.2622
$SiH_2(OSiH_3)_2$	256.6 ± 0.3[d]	222.9 ± 0.6[d]	...	240.5	−16.1	6.27	0.7184	0.3592
$SiH(OSiH_3)_3$	316.0 ± 0.5[d]	223.4 ± 0.6[d]	...	259.5	−56.5	17.88	1.4245	0.4748
$SiH_3N(CH_3)_2$	205.7 ± 0.5[e]	...	134.6	...	...	...	0.0450	0.0450
$SiH_2[N(CH_3)_2]_2$	217.6 ± 0.4	...	133.4 ± 0.5	208.9	−8.7	4.00	0.2093	0.1046
$SiH[N(CH_3)_2]_3$	235 ± 1.0	...	135 ± 2	212.1	−22.9	9.74	0.4417	0.1472

[a] D and D/n values were recalculated in this study. A value of $J_{^{29}SiH}(SiH_4)$ = 202.5 cps was used in all calculations. (See ref 9.) [b] Δ = $J_{^{29}SiH}$(obsd) − $J_{^{29}SiH}$(add). [c] E. A. V. Ebsworth and J. J. Turner, *J. Chem. Phys.*, **36**, 2628 (1962). [d] Error is expressed in terms of a 95% confidence limit from the arithmetic mean. See R. B. Dean and W. J. Dixon, *Anal. Chem.*, **23**, 636 (1951). [e] J. C. Thompson, private communication.

strongest (p → d)π bonds to silicon. Such π bonding seems to be weaker to germanium[3] than to silicon; in the fluorogermanes, τ(GeH) decreases with increasing fluorine substitution, as in the other halogermanes so far studied.[4]

Malinowski[5] calculated ^{13}CH coupling constants for the simple halomethanes CH_2Cl_2, $CHCl_3$, CH_2Br_2, and CH_2I_2, as well as for other more complex molecules from the experimentally determined ^{13}CH coupling constants in CH_3X and CH_4, using a relationship which, for such compounds, may be expressed as

$$J_{^{13}CH}(CH_{4-n}X_n) = J_{^{13}CH}(CH_4) + n[J_{^{13}CH}(CH_3X) - J_{^{13}CH}(CH_4)] \quad (1)$$

Good agreement between the calculated $[J_{^{13}CH}(\text{add})]$ and experimental $J_{^{13}CH}$ values was obtained in all cases; however, subsequent calculations for CH_2F_2, CHF_3, $CH_2(OCH_3)_2$, and $CH(OCH_3)_3$ gave poor agreement between the calculated and experimental values.[6]

When a similar treatment was applied by Juan and Gutowsky[7] to ^{29}SiH coupling constants of analogous silicon compounds, the agreement between the calculated and experimental values was always very poor. This treatment has been extended to the compounds studied in this investigation; and the differences, Δ, between the calculated $[J_{^{29}SiH}(\text{add})]$ and experimental ^{29}SiH coupling constants are given in Table II. It can be seen that Δ decreases in the order F > $-OCH_3$ > $-OSiH_3$ > Cl > Br > $-N(CH_3)_2$ > I for SiH_2X_2 compounds. For $SiHX_3$ compounds, the order is the same except for the fact that the position of the $-OCH_3$ and $-OSiH_3$ groups is reversed. The value of Δ increases with increasing substitution.

The percentage deviations, $100\Delta/J_{^{29}SiH}$, which are probably somewhat more significant, also follow the same general order, except that in the case of SiH_2X_2 compounds the positions of Br and $N(CH_3)_2$ are reversed, while in the case of the $HSiX_3$ species the order is followed exactly.

More recently, Reeves[8] has calculated deviation

(3) J. E. Griffiths and K. B. McAfee, Jr., *Proc. Chem. Soc.*, 456 (1961).

(4) E. A. V. Ebsworth, S. G. Frankiss, and A. G. Robiette, *J. Mol. Spectry.*, **12**, 299 (1964).

(5) E. Malinowski, *J. Am. Chem. Soc.*, **83**, 4479 (1961).

(6) N. Muller and P. I. Rose, *ibid.*, **84**, 3973 (1962).

(7) C. Juan and H. S. Gutowsky, *J. Chem. Phys.*, **37**, 2198 (1962).

(8) L. W. Reeves, *ibid.*, **40**, 2128 (1964).

Table III: $J_{^{13}CH}$ Parameters for CH_nX_{4-n}[a]

Compound	$J_{^{13}CH}$(obsd), cps	$J_{^{13}CH}$(add), cps	Δ,[b] cps	$100\Delta/J$(obsd)	D	D/n
CH_3F	149[c]	...	...	...	0.3664	0.3664
CH_2F_2	185[d]	173	−12	6.49	0.8645	0.4322
CHF_3	238[e]	197	−41	17.23	1.5164	0.5055
CH_3Cl	150[c]	...	...	...	0.3810	0.3810
CH_2Cl_2	178[c,f]	179	1	0.56	0.7717	0.3859
$CHCl_3$	209[c,f]	206	−3	1.43	1.1699	0.3900
CH_3Br	152[c]	...	...	...	0.4101	0.4101
CH_2Br_2	178[g]	179	1	0.56	0.7717	0.3859
$CHBr_3$	206[c]	206	0	0.00	1.1327	0.3776
CH_3I	151[c,f]	...	...	...	0.3956	0.3956
CH_2I_2	173[c]	177	4	2.25	0.7043	0.3522
CHI_3	...	...	...	...	...	...
CH_3OCH_3	140[e]	...	...	...	0.2327	0.2327
$CH_2(OCH_3)_2$	162[e]	155	−7	4.32	0.5526	0.2763
$CH(OCH_3)_3$	186[e]	170	−16	8.60	0.8776	0.2925

[a] D and D/n values were recalculated in this study. A value of $J_{^{13}CH}(CH_4) = 125$ cps was used in all calculations (see ref 9). [b] $\Delta = J_{^{13}CH}$(obsd) − $J_{^{13}CH}$(add). [c] N. Muller and D. E. Pritchard, *J. Chem. Phys.*, **31**, 1471 (1959). [d] N. Muller, *ibid.*, **36**, 359 (1962). [e] See ref 6. [f] G. V. D. Tiers, *J. Phys. Chem.*, **64**, 373 (1960). [g] See ref 5.

parameters "D" for a number of compounds, among which were many analogous carbon and silicon molecules. For such compounds

$$D_{M-H} = [(J_{M^a-H}/\gamma_M\gamma_H)^{1/2} - (J_{M^a-H}/\gamma_M\gamma_H)^{1/2}] \quad (2)$$

where J_{M^a-H} is the coupling constant in MH_4, J_{M^a-H} is the coupling constant in the substituted molecule (MH_nX_{4-n}), and γ_M and γ_H are the corresponding gyromagnetic ratios. Values of D and D/n for the compounds discussed by Reeves[9] as well as for the compounds studied in this investigation are given in Tables II and III.

It can be seen from Table II that the variation in the deviation parameters per bond, D/n, within a given series of silicon compounds, descreases in the order F > CH_3O ≅ SiH_3O > Cl > Br > $N(CH_3)_2$ > I. It is interesting to note that this order is essentially identical with that obtained from the Δ or $100\Delta/J_{^{29}SiH}$ values, which are obtained from a somewhat different method of approach. For the carbon compounds listed, the value of D/n is very much more constant within a given series, and it varies appreciably only for the fluoromethanes. For any given series, the variation of D/n values is very much greater for the silicon compounds than for the analogous carbon species, with the exception of the iodides.

It might be stressed that, in certain extreme cases, a series of some silicon compounds behaves more "additively" than a series of carbon compounds. For example, $100\Delta/J_{^{13}CH}$ for CH_2F_2 = 6.49%, whereas $100\Delta/J_{^{29}SiH}$ = 1.00% for SiH_2I_2. Also, the variation in D/n values for the fluoromethanes is 0.1391, while that for the iodosilanes is 0.0032. If it is assumed that (p → d)π bonding between fluorine and carbon is small in the fluoromethanes, then it appears possible that the "abnormal" behavior of the fluoromethanes may be due to polarization of the carbon by the fluorine atoms. If this should be the case, then the greater "abnormal" behavior in analogous silicon compounds may be due to the greater polarizability of silicon as compared to carbon, as suggested by Juan and Gutowsky.[7]

It is noteworthy that the relative magnitude of $100\Delta/J_{^{29}SiH}$ or D/n for a given subsituent might reasonably represent its relative polarizing power. π bonding might also contribute to the deviations, but it seems unwise to attempt to relate them primarily to π-bonding effects and to use one explanation for "abnormal" effects in the substituted methanes and another explanation of abnormalities observed in the substituted silanes.

Experimental Section

$SiH_2[N(CH_3)_2]_2$ and $SiH[N(CH_3)_2]_3$ were obtained according to the method described by Aylett and Peterson.[10] Tribromosilane was obtained by the reaction of $SiH[N(CH_3)_2]_3$ with HBr. Triiodosilane was obtained from the reaction of SiH_4 with HI in the presence of aluminum iodide catalyst at 110°.[11]

Methoxysilane was synthesized from $(SiH_3)_2S$ and

(9) P. T. Inglefield and L. W. Reeves, *J. Chem. Phys.*, **40**, 2424 (1964).

(10) B. J. Aylett and L. K. Peterson, *J. Chem. Soc.*, 3429 (1964).

(11) H. J. Emeléus, A. G. Maddock, and C. Reid, *ibid.*, 353 (1941).

CH_3OH.[12] The compounds $(CH_3O)_2SiH_2$ and $(CH_3O)_3SiH$ were prepared by the base-catalyzed condensation of CH_3OSiH_3.[13] The compounds $(SiH_3O)_2SiH_2$ and $(SiH_3O)_3SiH$ were obtained by the base-catalyzed condensation of $(SiH_3)_2O$.[13] The nmr spectra of $SiHBr_3$ and $SiHI_3$ were measured using a Perkin-Elmer HR10 spectrometer operating at 60 Mc/sec. The dimethylaminosilanes were recorded using a Varian Associates V4300B spectrometer operating at 40 Mc/sec; and the methoxy- and siloxysilanes were measured with a Varian Associates HR60 spectrometer, Model 4300D, with flux stabilizer, operated at 60 Mc/sec.

Acknowledgment. H. J. C.-F. wishes to acknowledge the receipt of a maintenance grant from the D.S.I.R. during the time that these experiments were being performed.

(12) G. S. Weiss and E. R. Nixon, *Spectrochim. Acta*, **21**, 903 (1965).

(13) T. Yoshioka and A. G. MacDiarmid, Abstracts of 149th National Meeting, American Chemical Society, Detroit, Mich., Sept 1964, p 5M.

Reaction Boundaries and Elution Profiles in Column Chromatography

by L. W. Nichol, A. G. Ogston, and D. J. Winzor

Russell Grimwade School of Biochemistry, University of Melbourne, Victoria, Australia, Department of Physical Biochemistry, John Curtin School of Medical Research, Australian National University, Canberra, Australian Capital Territory, Australia, and C.S.I.R.O. Wheat Research Unit, North Ryde, New South Wales, Australia

(*Received June 27, 1966*)

The relationships between the forms of migration boundaries within a chromatographic column and the forms of the elution profiles are examined by a method which makes use of constituent concepts of concentration and velocity of migration. The treatment applies to any procedure of column chromatography in which a plateau of all solute concentrations is ensured throughout the experiment. It is shown that the constituent concentration of any solute species in the effluent fluid is at any moment identical with that in the mobile solution within the column which reaches the exit plane at that time. In addition, equations are derived in both differential and integrated form describing essential features of the elution profiles obtained with systems affected by chemical or physical interaction. It is concluded that the equations are formally identical with those obtained previously to describe migration patterns obtained in moving boundary experiments not involving a stationary phase, provided elution volumes are substituted directly for velocity terms. The conclusion is in agreement with other workers who considered the case of chemically reacting systems subjected to column chromatography.

Theoretical discussion of the forms of migration boundaries in interacting systems has been along two lines. Gilbert[1,2] and Gilbert and Jenkins[3] did pioneer work in describing boundaries in freely migrating, chemically interacting systems; Ackers and Thompson[4] have applied their method to the behavior of a polymerizing system in gel filtration. A later alternative approach uses "constituent" concepts of velocity and concentration:[5,6] this approach has been developed in

(1) G. A. Gilbert, *Discussions Faraday Soc.*, **20**, 68 (1955).

(2) G. A. Gilbert, *Proc. Roy. Soc.* (London), **A250**, 377 (1959).

(3) G. A. Gilbert and R. C. L. Jenkins, *ibid.*, **A253**, 420 (1959).

(4) G. K. Ackers and T. E. Thompson, *Proc. Natl. Acad. Sci. U. S.*, **53**, 342 (1965).

detail for freely migrating systems[7-11] and has certain advantages.[11] It has also been applied (in one form) both theoretically and experimentally to gel filtration.[7-9] Recently Gilbert[12] has examined the relationships of velocities and concentrations within a gel filtration column to the elution volumes and concentrations in the eluate; he pointed out an error made by Nichol and Winzor[8,9] (who used the constituent approach) through simply replacing velocities in the column by reciprocal elution volumes in their version of the Johnston–Ogston equation[9,13] and the moving-boundary equation[6] applied to a hypersharp boundary.[3,8]

Although we agree with Gilbert's conclusions,[12] we have undertaken a further and more general examination of the application of the constituent approach to column chromatography, hoping to eliminate any confusion caused by his use of constituent quantities, as well as to establish more clearly the relationship between the effluent profile and the situation within the column. To conflate the treatment of freely migrating with that of chromatographic systems, we choose to regard the latter as a special aspect of the former.

Special Features of Chromatographic Migration. Chromatographic systems differ from freely migrating systems in the following ways.

(i) In addition to the mobile components (solvent and solutes), the chromatographic system contains a component or phase (which we term G), which is uniformly distributed between two limiting planes which define the ends of the column. The velocity of G is zero, and it vanishes across a sharp boundary at each limiting plane.

(ii) When a solution is applied to the column, which was originally filled with solvent, a sharp initial boundary of all mobile solutes is formed at the entry plane. This boundary then migrates down the column as an "ascending" boundary system, followed by a plateau of uniform composition. After establishment of the plateau, replacement of inflowing solution by solvent similarly creates an initially sharp "descending" boundary at the entry plane.

(iii) Both the solvent (S) and solutes (X = A, B, etc.) interact with G. These interactions may be represented by

$$\begin{aligned} S + G &\rightleftarrows SG \\ X + G &\rightleftarrows XG \end{aligned} \qquad (1)$$

without specifying the natures of the interactions; they could, for example, be partitions, adsorptions, or chemical interactions. Components SG and all XG have zero velocity; the constituent velocities of S and each X are therefore determined by the positions of the equilibria represented by eq 1.

(iv) Interactions between mobile solutes *in solution* of the type

$$A + B \rightleftarrows C \qquad (2)$$

may also occur. Although all components A, B, and C migrate at the same velocity as that of free solvent, the constituent velocities of A and B are not identical, since interactions of the type expressed in eq 2 affect the interactions with G (eq 1).

(v) Although it is convenient *in the first place* to describe migration in terms of concentrations and velocities within the column, the experimental observation is a relationship between composition and volume of eluate.

Assumptions, Definitions, and Symbols. As usual[3,11] we assume that all equilibria (of both types represented by eq 1 and 2) are established at rates infinitely great compared with that of migration, and that diffusion is negligible.

The positions of the equilibria represented by eq 1 are defined by μ_X, the fraction of each X which is free. The values of μ_X will always depend on the nature of X and G and on the amount of G per unit volume of column. According to the *nature* of the interactions, they may be dependent on or independent of composition with respect to mobile components. Equilibria in free solution (eq 2) are assumed to be governed by the simple mass action law.

The column is of unit total cross-sectional area; a fraction, ϕ, is occupied by mobile solvent or solution and a fraction χ by G itself; the remaining fraction is occupied by immobile S and X (in states represented by SG and XG).

Concentrations are defined as follows: (i) c_X is the concentration of X and $\bar{c}_X$ its constituent concentration in the mobile solution in the column; (ii) c_X' and $\bar{c}_X'$ are

(5) A. Tiselius, *Nova Acta Regiae Soc. Sci., Upsaliensis*, 7, No. 4, 1 (1930).

(6) L. G. Longsworth in "Electrophoresis, Theory, Methods and Applications," M. Bier, Ed., Academic Press Inc., New York, N. Y., 1959, p 91.

(7) L. W. Nichol and D. J. Winzor, *J. Phys. Chem.*, **68**, 2455 (1964).

(8) L. W. Nichol and D. J. Winzor, *Biochim. Biophys. Acta*, **94**, 591 (1965).

(9) D. J. Winzor and L. W. Nichol, *ibid.*, **104**, 1 (1965).

(10) L. W. Nichol and A. G. Ogston, *J. Phys. Chem.*, **69**, 1754 (1965).

(11) L. W. Nichol and A. G. Ogston, *Proc. Roy. Soc.* (London), **B163**, 343 (1965).

(12) G. A. Gilbert, *Nature*, **210**, 299 (1966).

(13) J. P. Johnston and A. G. Ogston, *Trans. Faraday Soc.*, **42**, 789 (1946).

the corresponding quantities in the inflowing solution. In addition to these definitions it is also convenient to define (iii) $\bar{c}_X{}^I$ as the constituent concentration of X itself within the column (*i.e.*, including forms X and XG but not including products of X resulting from chemical equilibria in the mobile solution) and (iv) $\bar{\bar{c}}_X$ as the constituent concentration of X in all forms within the column (in the absence of chemical equilibria in the mobile solution $\bar{c}_X{}^I$ and $\bar{\bar{c}}_X$ are identical). The following relationships for the system A + B $\rightleftarrows$ C (X = A, B, and C) follow from these definitions

$$\frac{c_A{}'c_B{}'}{c_C{}'} = \frac{c_Ac_B}{c_C} = K \tag{3}$$

$$\bar{c}_A = c_A + c_C = c_A + \frac{c_Ac_B}{K} \tag{4}$$

$$\bar{c}_A{}^I = \phi c_A/\mu_A \tag{5}$$

$$\bar{\bar{c}}_A = \bar{c}_A{}^I + \bar{c}_C{}^I \tag{6a}$$

$$= \phi\left[\frac{c_A}{\mu_A} + \frac{c_C}{\mu_C}\right] \tag{6b}$$

$$= \phi\left[\frac{c_A}{\mu_A} + \frac{c_Ac_B}{\mu_CK}\right] \tag{6c}$$

(Of the definitions given $\bar{\bar{c}}_A$ corresponds with Gilbert's[12] W; it is not clear to us whether his w represents $\bar{c}_A$ or c_A.)

v is the linear velocity of solvent within the column. The values of v_X (the linear velocity of mobile X) and of $\bar{v}_X$ (the constituent velocity of X in the mobile phase) are necessarily the same as v. $\bar{v}_X{}^I$ and $\bar{\bar{v}}_X$ are constituent velocities corresponding to the definitions of $\bar{c}_X{}^I$ and $\bar{\bar{c}}_X$. u is the linear velocity, within the reaction boundary system in the column, of a lamina of constant composition, all forms of all components being taken into consideration.[11] $\bar{u}_X$ is the median velocity of a boundary of *constituent* X between two neighboring plateaus.

$\dot{V}$ is the rate of inflow of solvent or solution, l is the length of the column between limiting planes, V_u is the volume that has flowed into (or out of) the column between the time of establishment of a sharp initial boundary at the entry plane and the time at which a lamina of velocity u reaches the exit plane, and V_0 is the volume of mobile solution between entry and exit planes.

Relationships between Velocities, Volumes, and Concentrations. From the definitions given, it is immediately obvious that

$$\dot{V} = \phi v \tag{7}$$

The time taken for a lamina moving with velocity v to traverse the column is l/v and the volume that has flowed during this time is

$$V_0 = \dot{V}l/v = l\phi \tag{8}$$

which is the void volume of the column. Similarly, a lamina moving at velocity u emerges after a volume flow

$$V_u = \dot{V}l/u \tag{9}$$

There is thus a reciprocal relationship between velocities within the column and corresponding elution volumes.

Consider now the conservation of constituent X across the entry plane of the column; this demands that

$$V\bar{c}_X{}' = \bar{\bar{v}}_X\bar{\bar{c}}_X \tag{10}$$

Since the velocity of XG is zero, we may write

$$\bar{\bar{v}}_X = \frac{\phi\bar{v}_X\bar{c}_X}{\bar{\bar{c}}_X} = \frac{\phi v\bar{c}_X}{\bar{\bar{c}}_X} \tag{11}$$

From eq 7, 10, and 11 it follows that

$$\bar{c}_X \equiv \bar{c}_X{}' \tag{12}$$

Equation 12 applies to each constituent (X = A, B, C). Moreover, the same conservation equations apply across the exit plane, and it therefore follows that all constituent concentrations in the effluent fluid are at any moment identical with those in the mobile solution which reaches the exit plane at that time. Since the same conditions of chemical equilibrium hold for both, the two fluids are at every moment identical in all respects. The profile of composition of the effluent therefore exactly reproduces the profile of composition in the *mobile* phase of a moving-boundary system; it does not reproduce, through it corresponds to, the profile of composition of the boundary *as a whole;* neglect of this fact was responsible for the mistaken use of the reciprocals of elution volumes by Nichol and Winzor,[8,9] to which reference has been made.

Relationships between the Equations for Boundary and Elution Profiles. The equations of conservation, which lead to the boundary equations, may be stated generally in terms of the inclusive constituent quantities $\bar{\bar{c}}$ and $\bar{\bar{v}}$. One such equation can be written for each constituent. In differential form these equations are

$$u = \mathrm{d}(\bar{\bar{v}}_X\bar{\bar{c}}_X)/\mathrm{d}\bar{\bar{c}}_X \tag{13}$$

In principle, solution of this set of equations describes uniquely the whole reaction boundary profile in terms of the relationship between u and the various concentrations. However, to arrive at practical solutions it is necessary to specify each $\bar{\bar{v}}_X$ as a function of composition,

which in the type of case considered requires definition both of the equilibria occurring in solution and their equilibrium constants, and of the composition dependence of each μ_X. By use of eq 8, 9, and 11, eq 13 can be rewritten in terms of elution volumes instead of velocities

$$V_u = \frac{V_0}{\phi}\frac{d\bar{c}_X}{d\bar{c}_X} \tag{14}$$

and solution of this set of equations gives, with the same limitations, a description of the elution profile.

The correspondence between eq 13 and 14 may be illustrated by simplified examples.

(i) With no interactions in solution, $\bar{c}_X$ and $\bar{\bar{c}}_X$ can be replaced by c_X and $\bar{c}_X$[I], respectively, and, from eq 5, eq 14 becomes

$$V_u = V_0\frac{d(c_X/\mu_X)}{dc_X} \tag{15}$$

which is the analog, in our terms, of Gilbert's[12] eq 3. The boundary and elution profiles depend on the composition dependence of μ_X. If these are independent of composition, eq 15 reduces to

$$V_u = V_0/\mu_X \tag{16}$$

showing that there is an independent, sharp elution front for each component of the solution.

(ii) μ_X is composition independent, but there is an equilibrium A + B $\rightleftarrows$ C in solution. From eq 4 and 6c eq 14 can be written, for constituents A and B

$$\left\{\left(V_u - \frac{V_0}{\mu_A}\right) + \left(V_u - \frac{V_0}{\mu_C}\right)\frac{c_B}{K}\right\}dc_A + \left(V_u - \frac{V_0}{\mu_C}\right)\frac{c_A}{K}dc_B = 0 \tag{17a}$$

$$\left\{\left(V_u - \frac{V_0}{\mu_B}\right) + \left(V_u - \frac{V_0}{\mu_C}\right)\frac{c_A}{K}\right\}dc_B + \left(V_u - \frac{V_0}{\mu_C}\right)\frac{c_B}{K}dc_A = 0 \tag{17b}$$

These equations are of exactly the same forms as eq 21a and 21b of Nichol and Ogston[11] for free migration of the system A + B $\rightleftarrows$ C, with replacement of u, v_A, v_B, and v_C in the latter equations by V_u, V_0/μ_A, V_0/μ_B, and V_0/μ_C, respectively; they can be handled in exactly the same way.

Integral Forms of Equations for Elution Profiles. Integration of each eq 13 across a boundary between two adjacent plateaus gives

$$\bar{u}_X = \frac{\int u d\bar{\bar{c}}_X}{\int d\bar{\bar{c}}_X} = \frac{\Delta\bar{\bar{v}}_X\bar{\bar{c}}_X}{\Delta\bar{\bar{c}}_X} \tag{18}$$

which is the integrated form of the Johnston–Ogston equation. Integration of eq 14 likewise gives

$$\bar{V}_X = \frac{V_0}{\phi}\frac{\Delta\bar{\bar{c}}_X}{\Delta\bar{c}_X} \tag{19}$$

It should be noted that the values of $\bar{u}$ and $\bar{V}$ for different constituents are in general not identical, but each corresponds to the median[10] of the boundary with respect to a particular constituent. Again, we apply this to two cases: (i) There is no chemical interaction in solution. If integration is performed between two phases α and β across a boundary where X does not vanish, by use of eq 4, 5, and 6c, eq 19 becomes

$$\left(\bar{V}_X - \frac{V_0}{\mu_X{}^\alpha}\right)c_X{}^\alpha = \left(\bar{V}_X - \frac{V_0}{\mu_X{}^\beta}\right)c_X{}^\beta \tag{20}$$

which is Winzor and Nichol's[9] equation, as corrected by Gilbert,[12] with X = B and $V_0/\mu_X{}^\alpha$ and $V_0/\mu_X{}^\beta$ replacing $V_X{}^\alpha$ and $V_X{}^\beta$, respectively.

(ii) μ_X is composition independent, but there is an equilibrium A + B $\rightleftarrows$ C in solution. Equation 19 can be written for (say) the A constituent, with the use of eq 4 and 6c

$$\bar{V}_A = V_0\frac{\Delta^{\alpha\beta}\left(\frac{c_A}{\mu_A} + \frac{c_Ac_B}{\mu_CK}\right)}{\Delta^{\alpha\beta}\left(c_A + \frac{c_Ac_B}{K}\right)} \tag{21}$$

Equation 21 may be rearranged to give an expression similar to eq 20, but with elution volume and concentration terms written as constituent quantities. In this form it is recognized as the moving boundary (or flux) equation used by Nichol and Winzor to determine K for migrating systems of the type A + B $\rightleftarrows$ C in which both sharp[7] and hypersharp[8] boundaries are predicted theoretically (*cf.* Figure 1a and 2b of ref 11). However, in the latter treatment[8] eq 21 was incorrectly applied in that reciprocals of elution volumes were employed; the corrected data have been presented by Gilbert.[12]

Discussion

In summary, it may be concluded that eq 16, 17a, 17b, 20, and 21 find direct analogs with equations presented earlier to describe the effects of physical[11,13] or chemical[11,3] interactions on migration patterns obtained by moving-boundary methods not involving a stationary phase. The relationship between the constituent concentration of any solute species in the effluent from a chromatographic column and mobile phase within the column shown in the discussion of eq 12 and the recognition that elution volumes

must replace velocity terms in earlier equations[11,13] permit direct application of previous theory to the chromatographic case. Ackers and Thompson[4] and Gilbert[12] in their treatments of chemically reacting systems have also stressed the necessity of direct substitution of elution volumes for velocity terms. It is hoped that the generalized approach based on the concept that essential features of migration patterns are determined by the dependence of constituent velocities of each constituent species on total composition may lead to a clearer understanding of elution profiles obtained in frontal analysis and affected by either chemical or physical interaction.

Acknowledgment. We are grateful to Dr. G. A. Gilbert for drawing our attention to the error mentioned, in advance of the publication of his paper.[12]

The Dehydration of Porous Glass

by M. J. D. Low and N. Ramasubramanian

School of Chemistry, Rutgers, The State University, New Brunswick, New Jersey *(Received August 23, 1966)*

A microbalance was used to follow the kinetics of dehydration of porous glass *in vacuo* at constant temperatures from 25 to 800°. The kinetics of water sorption and desorption by the degassed surfaces was measured. Infrared spectra of degassed specimens were obtained. Physically adsorbed water as well as some tightly bound water could be removed at 25°. Degassing above 600° produces surfaces containing isolated hydroxyls. The amount of water retained after a sorption–desorption cycle is a maximum with samples degassed near 300°. It is proposed that geminal hydroxyls responsible for this maximum are destroyed. The percentage of the sorbed water which is retained increases with samples degassed above 600°. This effect is produced by boron migrating to the surface of the glass.

Recent infrared spectroscopic studies of the dehydration and hydration of porous glass surfaces provided evidence for the existence of B–OH structures on the surface of highly degassed specimens.[1-3] The intensity of the absorption band at 3703 cm^{-1} attributed to B–OH groups was higher than would be expected if the boron were evenly distributed, the results indicating the boron concentration to be higher at the surface than within the bulk of the glass. However, it was not possible to detect surface B–OH groups on specimens which had been degassed under mild conditions. These effects thus raised some doubt about the stability of the surface of these adsorbents, because it was not clear if the boron enrichment at the surface occurred during the manufacture of the glass or came about as a result of the high-temperature degassing. The present experiments were performed to provide some information on this topic as well as on dehydration and rehydration of porous glass surfaces.

Experimental Section

The general procedures described elsewhere were employed.[2] Pressures of approximately 10^{-6} torr were produced with conventional high-vacuum systems. Spectroscopic measurements were made with a Perkin-

(1) M. J. D. Low and N. Ramasubramanian, *Chem. Commun.*, in press.

(2) M. J. D. Low and N. Ramasubramanian, *J. Phys. Chem.*, **70**, 2740 (1966).

(3) N. Ramasubramanian and M. J. D. Low, submitted.

Elmer Model 521 spectrophotometer. Samples of Corning Code 7930 porous glass were purchased from Corning Glass Co. in the form of 1-mm thick plates.

Gravimetric Procedure. The kinetics of dehydration and of water sorption and desorption were measured with a Gulbransen-type vacuum microbalance having a sensitivity of 10^{-6} g/10^{-4} cm.[4] It was desirable to observe the dehydration over a wide temperature range and to avoid any potential changes which might be caused by heating. Consequently, the specimens used for gravimetric work were used without subjecting them to the procedure of heating in oxygen that is sometimes necessary to remove the impurities which can be adsorbed from the air and give the glass a yellowish color. The glass as received was clear and colorless. Some duplicate sets of experiments established that identical infrared results were obtained with untreated specimens and with specimens that had been treated in oxygen at 650°.

Specimens weighing about 100 mg were used, all taken from one batch of glass. After a specimen had been suspended in the balance, the balance case was evacuated. After about 2 min, when the pressure had fallen to 10^{-3} torr, a preheated furnace was brought up around the balance leg containing the specimen. Weight-loss measurements were then made.

A fresh specimen was used at each constant temperature. At the end of a series of dehydration measurements at one particular temperature the specimen was cooled to room temperature *in vacuo*. The specimen was then exposed to H_2O vapor at room temperature at pressures near 4 torr ($P/P_0 \sim 0.25$), and the weight increase caused by H_2O sorption was followed for some time. The balance chamber was then opened to the pumps, and the desorption of H_2O in a dynamic vacuum of 10^{-3} to 10^{-6} torr was followed. Each weight change–time plot obtained in this manner shows an abrupt change in slope at the beginning of the desorption portion.

The initial dehydration weight loss was calculated on the basis of the weight of the fresh specimen in dry air. The subsequent water sorption and desorption on the same specimen were calculated on the basis of the weight of the specimen at the end of the initial dehydration process.

Results and Discussion

Initial Dehydration. The weight losses produced by heating fresh specimens *in vacuo* at various constant temperatures are shown by the plots of Figure 1. The general behavior observed during the first few minutes was identical with that described by Rand,[5] who degassed porous glass at temperatures up to 300°. Appreciable weight decreases occurred within a few minutes at degassing temperatures of 200° and higher. Approximately 90% of the total weight decrease to be found at any one temperature occurred within the first hour of degassing. After the initial, quasi-explosive desorption had occurred, weight loss was continuous at each temperature.

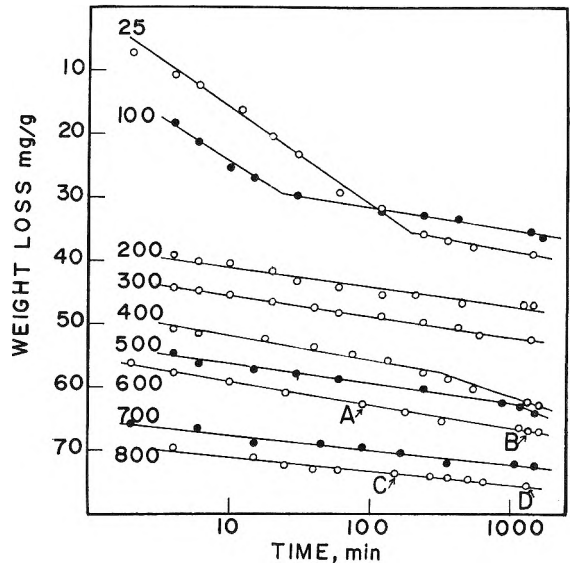

Figure 1. Initial dehydration. A fresh specimen was used to follow the weight loss *in vacuo* at each of the constant temperatures shown beside each plot. Infrared spectra were obtained with specimens degassed to stages corresponding to the points A–D. The degassing temperature is indicated beside each plot.

The plots of Figure 1 indicate that two over-all processes and three temperature regions are involved in the vacuum activation of porous glass. The plots fall into three groups of degassing temperatures, *i.e.*, below 200, 200–600, and above 600°. Below 200° the initial desorption was relatively small and was followed by a rapid but decelerating weight decrease. The latter abruptly changed after some time, the rate of weight decrease then approximating the slow rates observed at 200° and above.

The initial desorption and the rapid process occurring below 200° are ascribed to the desorption of physically adsorbed water, in general concurrence with the conclusions reached by others.[5-7] However, the abrupt changes in slope of the 25 and 100° plots are considered

(4) E. A. Gulbrausen, *Advan. Catalysis*, **5**, 119 (1953).

(5) M. J. Rand, *J. Electrochem. Soc.*, **109**, 402 (1962).

(6) L. H. Little and M. V. Mathieu, *Actes Congr. Intern. Catalyse*, 2e, *Paris*, 1, 771 (1961).

(7) T. H. Elmer, I. D. Chapman, and M. E. Nordberg, *J. Phys. Chem.*, **66**, 1517 (1962).

to mark the end of the desorption of physically adsorbed water (taken as approximately 35 mg/g near the "break" in the two plots) and the beginning of the removal of more tightly bound species. This would mean that all of the physically adsorbed water can be removed from porous glass at room temperature. This conclusion agrees with those of Young,[8] Benesi and Jones,[9] and Kiselev and Lygin,[10] who believe that physically adsorbed water was completely removed from silica by room-temperature evacuation.

Benesi and Jones based their conclusion on the disappearance of a band near 1640 cm^{-1} ascribed to the ν_2 fundamental of water. However, as pointed out by Elmer, Chapman, and Nordberg,[7] the presence of a band near 1640 cm^{-1} which decreased sharply in intensity up to 200° was reported by Little and Mathieu.[6] Elmer, Chapman, and Nordberg stated that, from studies in their and other laboratories, activation temperatures of about 180° are needed to obtain maximum water vapor adsorption on porous glass at relatively low pressures, that it is difficult to see why this should be so if all the physically adsorbed water has been driven off at room temperature and no condensation reaction is postulated below 180°, and that infrared bands in the region around 3600 cm^{-1} are decreasing in width below 200° and above room temperature. They consequently conclude that physically adsorbed water is present in porous glass at temperatures up to 200°. This discrepancy becomes much less important if due account is taken of the fact that various workers have used widely varying techniques. Infrared spectra of porous glass pumped for 1 hr were recorded after the specimen had cooled to room temperature at a pressure of 0.2 torr, for example.[7] Differences in sample thickness, pumping speed, degassing time, and the like could readily lead to the spectral observation of physically adsorbed water after a short 200° degassing. Also as will be shown later, room-temperature degassing or "activation" was as effective as activation at 200° for the sorption of H_2O at room temperature, again indicating that physically adsorbed water was removed below 200°.

The initial desorption which occurs at 200° and above is greater than the weight loss of approximately 35 mg/g ascribed to physical adsorption, so that some tightly bonded species must also be rapidly removed during the first few minutes of degassing. The slow processes subsequent to these initial, rapid desorptions are ascribed solely to the removal of tightly bound species.

As shown by the 25 and 100° plots of Figure 1, slow weight losses occurred subsequent to the occurrence of the breaks which are taken to mean the end of the desorption of physically adsorbed water. The rates of the slow weight decrease are similar to those observed at higher temperatures. This similarity, the plausibility of the removal of physically adsorbed water below 200°, and the retention of some water after the sorption–desorption cycles described later lead to the conclusion that the slow processes below and above 200° are similar in nature, *i.e.*, that the removal of species more tightly bound than physically adsorbed water is involved. However, it is not necessary that only a dehydroxylation is involved. As the slow process at 100 and 25° occurred below the temperature of 180° at which Young found silanol groups to begin to condense,[8] a desorption of molecular water strongly bound to the hydroxylated surface could account for all or most of the slow weight loss below 200°. A combination of such a desorption with dehydroxylation could occur at higher temperatures or, at least, at the lower temperatures of the range of 200–600°. Dehydroxylation proper could occur in the highest temperature range above 600°.

Water is given off continuously, at all temperatures, as shown by the plots of Figure 1 and also by the detailed infrared spectra described elsewhere.[2] In contrast to the statement by Elmer, Chapman, and Nordberg, whose spectra indicated that there was a finite amount of water which could be removed at a given temperature and that a steady state could be achieved in 1 hr,[7] a steady state was not observed in the present work. Significant changes occurred even after long periods of degassing.

Some infrared spectra of specimens at various stages of degassing are shown in Figure 2. Individual specimens were degassed within an infrared cell, because it was not feasible to make simultaneous infrared and gravimetric measurements. The temperatures and periods of degassing used to bring the specimens to the stages of dehydration shown by the spectra A–D of Figure 2 are those used to cause the weight losses indicated by the points marked A–D of Figure 1.

The weight loss required to reach stages A or C in Figure 1 is 20–40 times greater than that needed to go from stages A or C to stages B or D, respectively. The spectra corresponding to these stages of weight loss show, however, that significant changes occurred when small amounts of water were desorbed. These and other spectra[2] show that not only are long pumping periods at high temperatures required in order to remove the majority of the hydrogen-bonded hydroxyl

(8) G. J. Young, *J. Colloid Sci.*, **13**, 67 (1958).

(9) H. A. Benesi and A. C. Jones, *J. Phys. Chem.*, **63**, 179 (1959).

(10) A. V. Kiselev and V. I. Lygin, *Colloid J.* (U.S.S.R.), **21**, 561 (1960).

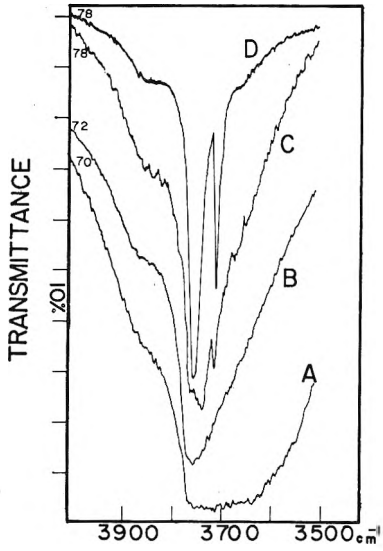

Figure 2. Various stages of dehydration. Porous-glass specimens were degassed in an infrared cell under conditions identical with those used in the gravimetric study. Spectra A–D were obtained with specimens degassed to the states A–D marked on Figure 1. The ordinates of the spectra were displaced. The numbers by each spectrum near the left ordinate indicate the per cent transmittance at that point.

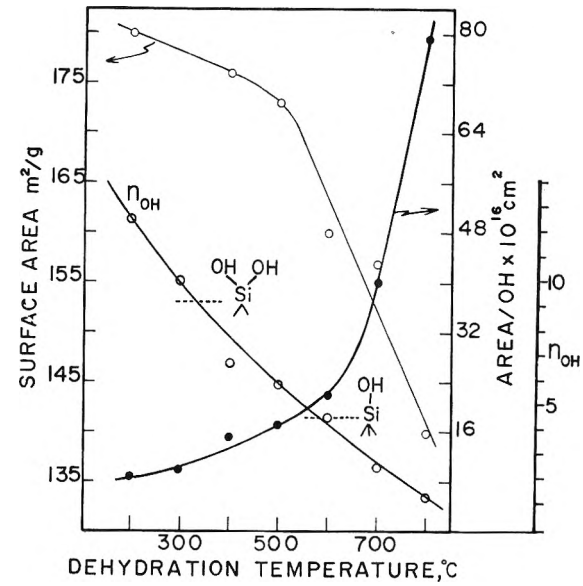

Figure 3. Effects of degassing temperature. n_{OH} is the number of OH groups per 100 A² of surface. The horizontal dotted lines mark the n_{OH} conditions where one surface silicon carries a single OH group or geminal OH groups.

groups which cause the asymmetry of the 3748-cm^{-1} silanol band but also that the development of the sharp 3703-cm^{-1} B–OH band occurs only during the last stages of degassing.

Gravimetric and similar spectroscopic data were used to estimate the surface hydroxyl concentrations of specimens after various degassing. For example, a specimen degassed at 800° for 4 hr decreased in weight by 1.5 mg/g on degassing at 800° for an additional 16 hr. The spectra of another specimen degassed under the same conditions showed that the area of the two sharp OH bands decreased by 80 mm² as measured with a planimeter. The area of the OH bands was 140 mm² after a 20-hr degassing at 800°. If it is assumed that only small errors are introduced by comparing the data of two samples and by neglecting the small contribution to the total hydroxyl area of the small, broad band on the low-frequency side of the 3703-cm^{-1} band, then the area of 140 mm² corresponds to 2.65 mg of H_2O/g. If one H_2O molecule corresponds to two surface OH groups, that amount of H_2O is equivalent to 1.8×10^{20} OH groups per gram. Consistent results were obtained with several pairs of infrared and gravimetric data. Some estimates of surface hydroxyl concentrations obtained in this manner are given in Figure 3. Also shown are the nitrogen BET surface areas on which the hydroxyl concentration estimates are based.

The surface area decreased with increasing temperature, but significant decreases occurred only above 500°. Analogous results were reported by Elmer, Chapman, and Nordberg,[7] who heated porous glass *in vacuo* and found that small but steady contractions occurred with increasing temperature, but that the shrinkage process was greatly accelerated above 900°. As shown by Figure 3, the total surface area decreased by about 20%, although the area per hydroxyl group increased by a factor of 8. This implies that the predominant dehydroxylation reaction over the temperature range studied involved a condensation of adjacent silanol groups to form siloxane bridges on the glass surface, rather than a simultaneous dehydroxylation and consolidation. Consequently, although the simple surface dehydroxylation would be expected to diminish with increasing temperature, the dehydroxylation–consolidation reactions which would lead to a marked rearrangement of the glass structure would not be dominant until 900°.

Figure 3 also shows n_{OH}, the number of OH groups per 100 A² of surface, as a function of the dehydration temperature. In their study of chemisorption and physical adsorption of water on silica, DeBoer, Hermans, and Vleeskens[11–14] concluded that a condi-

(11) J. H. DeBoer, M. E. A. Hermans, and J. M. Vleeskens, *Proc. Koninkl. Ned. Akad. Wetenschap.*, **B60**, 45 (1957).

(12) J. H. DeBoer, M. E. A. Hermans, and J. M. Vleeskens, *ibid.*, **B60**, 54 (1957).

tion of $n_{OH} = 4.6$ corresponded to a surface where all silicon atoms were covered with *one* hydroxyl group.[14] Conditions of $n_{OH} > 4.6$ would mean the bonding of more than one hydroxyl group per silicon atom.

Assuming that a comparison of silica and porous glass is valid, the decline of the value of n_{OH} to below 4.6 at temperatures above 600° implies that the surface hydroxyl concentration of the porous glass had fallen well below the "monolayer" coverage where every surface silicon atom carried one hydroxyl group. Under such conditions at least some of the surface hydroxyl groups would be isolated and not interact with their neighbors. Similar information can be deduced from the shapes and positions of the bands of the two sharp hydroxyl groups. Both the silanol band and the B–OH band, such as those of spectrum D of Figure 2, become sharper and lose most of the asymmetry of the low-wavenumber sides of the bands after prolonged high-temperature degassing. The band positions simultaneously shift to higher wavenumbers at 3745 cm^{-1} for the silanol band and 3703 cm^{-1} for the B–OH band.[2] Such effects indicate that isolated hydroxyl groups which do not interact with their environment to any great extent are produced by degassing at temperatures above 600°, *i.e.*, in the highest of the three temperature regions suggested by the kinetics of Figure 1.

The kinetics of the slow weight losses can be represented by an Elovich type of equation,[15] as shown by the plots of Figure 1. The kinetic representation is of a practical rather than theoretical interest, because the over-all weight-loss mechanism is very complex and incorporates various steps of surface migration, reaction, desorption, and mass transport within the pore system of the solid. However, although the observed weight loss is a summation of several simultaneous processes, the kinetics can be used in a limited, qualitative manner to indicate changes or trends, such as the division of the 200–800° region near 600°. This division is more clearly shown by the plots of Figure 4, which are derived from the data of Figure 1. A correction was made, based on the reasonable assumption that the rate of removal of tightly bound species is a function of the amount of tightly bound species remaining on the surface, as follows. Infrared and gravimetric data were used to estimate that the amount of water removable after point D in Figure 1 was approximately 2.6 mg/g. A total of 75.4 mg/g was removed up to point D, so that a complete dehydration would involve the removal of 78 mg/g of water. Taking the amount of physically adsorbed water as 35 mg/g, the maximum amount of tightly bound water is approximately 43 mg/g. The ratio of the amounts of tightly bound water removed to that

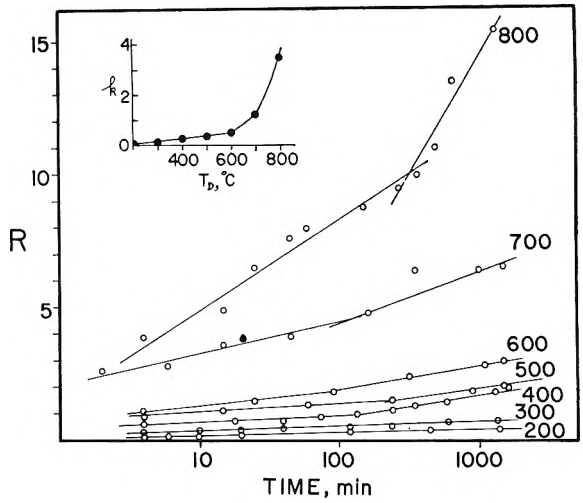

Figure 4. Corrected dehydration kinetics. R is the ratio of amounts of tightly bonded water removed and on the surface. The insert shows the variation of k, the slope of the plots (up to 100 min) as a function of degassing temperature, T_D. The degassing temperature is shown beside each plot.

remaining, R, was then computed, $R = (W_t - 35)/(78 - W_t)$, to result in the plot of Figure 4. W_t is the weight loss occurring after t min, from Figure 1. A comparison of rates can be made in terms of the slopes, k, of the plots.[15] As shown by the insert of Figure 4, the value of k of the first linear segment of each plot (up to about 100 min) increases slowly up to 600° with increasing degassing temperature, T_D. Above 600° there is a marked increase in k, suggesting the division of the temperature range near 600°.

The various data thus suggest that the initial dehydration produced porous-glass surfaces (a) freed from physically adsorbed water at all temperatures, (b) fully hydroxylated below about 600°, some surface silicon atoms possibly carrying more than one hydroxyl group, (c) on which some molecular water was strongly bound to the hydroxylated surface at the lower temperatures, and (d) incompletely hydroxylated above about 600°, an appreciable fraction of the hydroxyls being "free." Water sorption experiments were then carried out with such surfaces.

Water Sorption and Desorption. The weight changes observed on the sorption and desorption of water at room temperature are shown in Figure 5. The sorption rates may be compared in terms of the slopes of the plots, k'. The insert of Figure 5 shows k' to decline above 300°. The average value of 15.8 of the

(13) J. H. DeBoer and J. M. Vleeskens, *Proc. Koninkl. Ned. Akad. Wetenschap.*, **B60**, 234 (1957).
(14) J. H. DeBoer and J. M. Vleeskens, *ibid.*, **B61**, 2 (1958).
(15) M. J. D. Low, *Chem. Rev.*, **60**, 267 (1960).

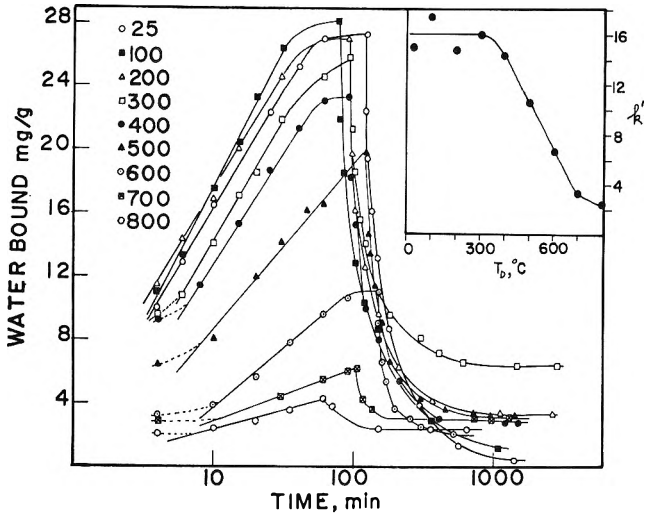

Figure 5. Water sorption and desorption. The key shows the degassing temperatures. Sorption occurred at 4 torr of water pressure. The insert shows the variation of k', the slope of the linear portions of the sorption plots.

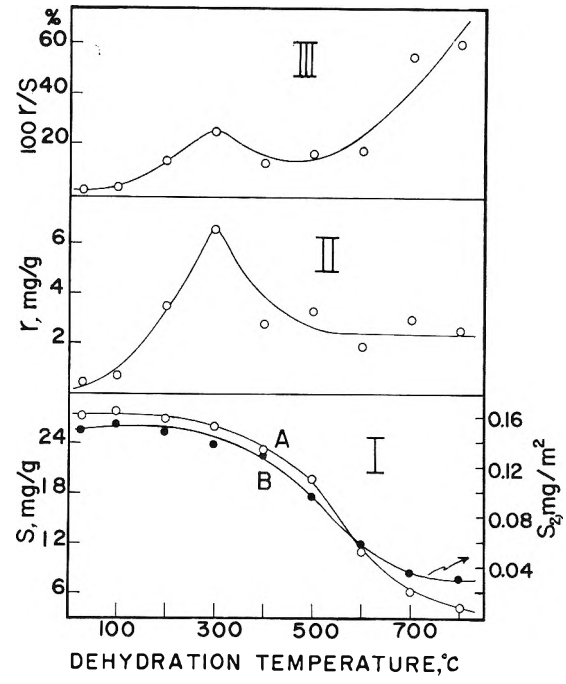

Figure 6. Sorption–desorption effects. S is the amount of water sorbed after 60 min and r is the amount of water retained by the surface after a sorption–desorption cycle.

slopes of the four plots at the lowest temperatures is close in numerical magnitude to the value of -15.5 of the slopes of the rapid weight losses of the 25 and 100° plots of Figure 1. This indicates that the water sorption on samples degassed at temperatures below 400° occurred at approximately the same rate as the process at 25 and 100° which was ascribed to the desorption of physically absorbed water.

The data of Figure 5 were used to construct the plots of Figure 6. Part I of Figure 6 shows in plot A the total amount of water sorbed after 60 min, S_1 mg/g, as a function of the degassing temperature. If the decrease in surface area with increasing degassing temperature is considered, plot B results, showing the total amount of water sorbed in units of S_2 mg/m². As many sorptions, particularly the copious ones at the lower degassing temperatures, were nearing completion, these plots closely approximate saturation curves. Part II of Figure 6 shows the variation of the amount of water retained, r mg/g, with degassing temperature. The value of r at any one temperature is the difference in the weights of the sample at the end of the initial dehydration and at the end of the desorption step. Part III of Figure 6 gives the value of $100\,r/S_1\%$.

The total amounts of water sorbed by samples degassed at temperatures below 400° are somewhat less than the amounts of water desorbed during the initial degassings at 25 and 100°. However, the top five sorption plots of Figure 5 bend toward the abscissa, so that the sorption reactions were near or at completion after about 100 min. The untreated samples and those after water sorption subsequent to degassing below 300° were therefore in similar although not identical states, *i.e.*, saturated as far as physical adsorption is concerned, differences in amounts of water sorbed being caused by differences in the water vapor pressure over the untreated samples and during the sorption experiments.

The plots of Figure 5 and part I of Figure 6 show that there was little change in sorption with specimens degassed at temperatures below 300°. The water removed during the initial degassing at those temperatures consequently had little effect on the subsequent water sorption. Similar results have been reported by Rand[5] with low-temperature degassings. The present results, however, show that the conditions of activation are crucial in determining the sorption of water, in direct contrast to the statements of Rand concerning the futility of prolonged vacuum activation and the lack of criticality of activation conditions for the preparation of porous-glass getters.

The absence of a desorption-produced effect would imply that the initial degassing involved the removal of physically adsorbed water, because this would not affect the sorptive properties of the surface. However, as shown by part II of Figure 6, small amounts of sorbed water were retained by the surface, which consequently indicates that the surfaces were slightly affected by degassing at the lowest temperatures. These effects thus support the earlier conclusions that the degassing

below 200° involved mainly the desorption of physically adsorbed water but also caused the removal of small quantities of more tightly bound species.

Changes in S_1, r, r/S_1, and the kinetics also indicate that more than one process was involved in the sorption on samples degassed at higher temperature. The kinetics of Figure 5 are subject to limitations similar to those of the initial dehydration but are useful qualitatively.

The desorption kinetics are shown in Figure 7. As shown by the insert of Figure 7, there is little change in the value of k'' (the slope of the plots up to about 100 min) below 300°, a small change in the range 300–500°, but a marked decrease above 500°. The low-temperature k'' values near 10 for the desorption are smaller than k or k' values of the initial dehydration or the water sorption. Above 600° the k'' values were smaller than the value of $k \sim -3$ found for the slow weight losses at 200° and above of the plots of Figure 1. Also, as shown by Figures 5 and 7, the deceleration of the desorptions decreased after about 100 min. These effects thus suggest that the desorption involved the removal of both physically adsorbed and tightly bound water, the amount of physically adsorbed water decreasing with increasing degassing temperature.

A general decrease in sorbed water with increasing degassing temperature is shown by the plots of part I of Figure 6, the decrease paralleling that of n_{OH}. As shown by infrared spectra,[2,7,16] when porous glass is degassed in the range 200–600°, a broad, asymmetric band near 3600 cm^{-1} ascribed to hydrogen-bonded hydroxyls decreases in intensity, but there is little change in the 3745-cm^{-1} band ascribed to isolated silanol groups. The decrease in water sorption is consequently associated with the decline in intensity of the broad band, water sorption occurring on polymerized rather than on isolated surface hydroxyl groups.[16]

Some of the sorbed water is strongly bound to the surface and cannot be removed by pumping for long periods at room temperature. As shown by part II of Figure 6, the amount of residual water, r, increases, approximately one-quarter of the total amount of water sorbed by a sample degassed at 300° being retained. The r values must only be taken as approximate values because, as indicated by the 25 and 100° plots of Figure 1 and the discussion above, some tightly bound water can be removed by pumping at room temperature. The value of r then declines and becomes roughly constant at higher degassing temperatures. The results thus indicate the occurrence of some process by which water can be strongly bound and which decreases with degassing temperatures above 300°. Kawasaki, Senzaki, and Tsuchiya arrived at a similar conclusion.[17] They studied water sorption at 30° by porous glass degassed at temperatures up to 450° and concluded that there were two states of adsorbed water molecules, or reversible and irreversible adsorption, and that the adsorption sites decreased by heat treatment above about 300° cannot be easily rehydrated by water sorption to regenerate the original surface. Also, Rand reported that a 12-hr degassing at 300° caused an irreversible weight loss, it being inferred that some of the adsorption sites and a disproportionate number of the more energetic ones were permanently removed.

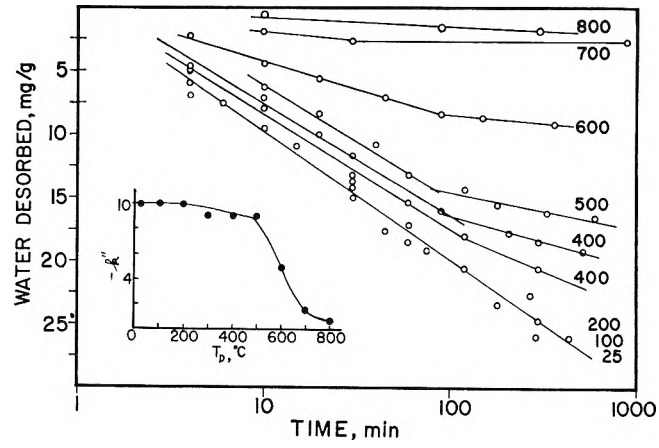

Figure 7. Desorption kinetics. k'' is the slope of the plots up to 100 min. The degassing temperature is shown beside each plot. The plots were constructed from the desorption portions of the plots of Figure 5.

It is interesting to note that the r maximum at 300°, as well as the 300° temperature mentioned by Kawasaki, Senzaki, and Tsuchiya and by Rand, is close to the degassing temperature at which the value of n_{OH} is 9.2, according to plot C of Figure 3. However, the latter is based on the assumption of the validity of comparison of silica and glass surfaces, so that the close correspondence between the temperatures at which $n_{OH} = 9.2$ and at which r is a maximum may be fortuitous. A surface for which $n_{OH} > 4.6$ implies the existence of some general hydroxyls in the absence of chemisorbed molecular water.[13] The importance of geminal hydroxyl groups, which have been postulated on many occasions, is strongly stressed by Hockey.[18] Young, for example,[8] finding that above about 180° silanol groups on the silica surface started to condense to form silica–oxygen bonds, proposed a mechanism involving the splitting of one water molecule from two

(16) A. N. Sidorov, *Opt. Spectry.*, 8, 434 (1960).

(17) K. Kawasaki, K. Senzaki, and I. Tsuchiya, *J. Colloid Sci.*, 19, 144 (1964).

(18) J. A. Hockey, *Chem. Ind.* (London), 57 (1965).

neighboring pairs of geminal hydroxyls as alternative to the formation of strained siloxane bridges. Such a mechanism may account for the 300° maximum in r and for the results of Kawasaki, Sensaki, and Tsuchiya and of Rand. This would imply that dehydration at low temperatures would cause the formation of a half-dehydroxylated surface grouping which, after adsorbing water, would be restored to form a pair of adjacent silicon atoms each having geminal hydroxyl groups. The sorbed water would thus be relatively strongly bound. Degassing at temperatures above 300° would cause further, irreversible dehydroxylation of the half-dehydroxylated state, so that the amount of tightly bound water would diminish.

Alternately, geminal hydroxyl groups might be adsorption sites having steric and energetic characteristics suitable for the bonding of molecular water in a stronger manner than physical adsorption. This could imply that, after physically adsorbed water had been removed near room temperature, degassing at low temperatures caused the desorption of such strongly bonded molecular water. The adsorption sites would then be freed and active for subsequent adsorption. Heating above 300° could destroy the geminal configuration and cause a decrease in the amount of strongly bound molecular water, as with Young's mechanism.

According to either mechanism, the amount of tightly bound water should decrease with increasing degassing temperature. However, although a general decline in water sorption was found, shown by part I of Figure 6, the amount of water retained remains approximately constant, as shown by part II of Figure 6. The ratio r/S_1 or the percentage of the sorbed water which was retained, $100r/S_1$, increases at degassing temperatures above 600°. Similarly, the decline with increasing degassing temperatures of the amount of water sorbed falls off above 600°, as shown by plot B of part I of Figure 6. These effects indicate that some mechanism by which water can be strongly bonded became important above 600°. Silanols cannot be connected with these effects, because the number of silanols decreases with increasing degassing temperature, as shown by the present results and by infrared spectroscopic data described elsewhere.[2] It has been shown, however, that the 3703-cm^{-1} band ascribed to surface B–OH groups is developed only after degassing under severe conditions[2] and that boron on the porous-glass surface can act as adsorption center and permit the reaction of water with the otherwise hydrophobic glass surface.[3] These results furnish strong support for the conclusion that the migration of boron to the glass surface is responsible for the effects observed with samples degassed at temperatures above 600°. Further support for this mechanism comes from experiments in which the degassing time was varied.

For example, water sorption and desorption were measured after degassing a specimen for periods of 0.5 and 9 hr. The total water sorption decreased by 50%, whereas the r decreased by 20%, after the additional 8.5-hr period. The value of $100r/S_1$ consequently increased from 40 to 70%. Similarly, with a specimen degassed at 800° for 0.5 and 14 hr, the value of $100r/S_1$ increased from 50 to 70%. Such results show that increased severity of degassing increased the reactivity of the surface. In terms of the boron-migration mechanism, the increased degassing period permitted an increase in the surface boron concentration to occur.

According to Sidorov,[16] the adsorption of water by porous glass is determined by perturbed hydroxyl groups in the case of hydrated surfaces and by "centers of the second kind," *i.e.*, silicon or oxygen atoms,[19-21] in the case of highly degassed surfaces; after heating porous glass at temperatures above 550°, the water adsorption takes place predominantly on centers of the second kind. The state of water bonded to the latter was considered to be intermediate between the physisorbed and chemisorbed states. In view of the present results it seems likely that the centers of the second kind can be equated with surface sites formed from boron atoms. These sites could adsorb a portion of the sorbed water and permit a portion to react with the siloxane groups of the surface and consequently become quite strongly bonded. The over-all binding effect could then be "intermediate."

Acknowledgment. This work was supported by the Office of Naval Research through Contract Nonr 404 (19) and, in part, by NSF Grant GP 1434. We are grateful to Dr. F. Ciapetta for making possible the loan of a cathetometer from W. R. Grace and Co.

(19) A. N. Sidorov, *Zh. Fiz. Khim.*, **30**, 995 (1956).

(20) M. Folman and D. J. C. Yates, *Proc. Roy. Soc.* (London), **A246**, 32 (1958); *Trans. Faraday Soc.*, **54**, 1684 (1958); *J. Phys. Chem.*, **63**, 183 (1959).

(21) N. Sheppard, *Spectrochim. Acta*, **14**, 249 (1959).

Adsorption of Sodium Dodecyl Sulfate at Various Hydrocarbon–Water Interfaces

by Selwyn J. Rehfeld

Shell Development Company, Emeryville, California *(Received September 2, 1966)*

This paper presents interfacial tension data for the adsorption of highly purified sodium dodecyl sulfate from aqueous solutions at the air–water and water–*n*-hexane, *n*-octane, *n*-nonane, *n*-decane, *n*-heptadecane, 1-hexene, 1-octene, cyclohexane, cyclohexene, benzene, *n*-butylbenzene, or carbon tetrachloride interfaces. The influence of these organic liquids upon the critical micelle concentration and the adsorption isotherms is described. Also, it is demonstrated that plots of interfacial tension *vs.* the logarithms of surfactant concentration can be fitted by a polynomial of second degree below the critical micelle concentration. The derivative of this empirical equation is substituted into the Gibbs adsorption equation and an adsorption isotherm of the form $\Gamma_{-} = (z_1/2RT) + (z_2/RT) \ln m_{\pm}$ is obtained for all the interfaces, where z_1 and z_2 are constants.

Introduction

Although a number of investigations[1-4] have been reported in the literature concerning the adsorption of sodium dodecyl sulfate (NaDDS) at hydrocarbon–water interfaces, only *n*-decane,[2] *n*-heptane (at 50°),[3] and petroleum ether[4] have been used as the hydrocarbons. The critical micelle concentration (cmc) of the NaDDS used in these experiments was 7.95,[2] 8.1 (at 50°),[3] and 8.0[4] m*M*. The adsorption isotherms computed for the *n*-decane– and petroleum ether–water interfaces were similar, and when the bulk concentration of NaDDS reached the cmc, the area occupied per adsorbed NaDDS molecule at these surfaces was 48 A.[2,4] Interfacial tension data for the adsorption of an impure NaDDS (cmc ~7 m*M*) at selected organic liquid–water interfaces[1] (benzene, cyclohexane, and chlorobenzene and nitrobenzene) suggested that the adsorbed film was considerably more expanded at benzene– and cyclohexane–water interfaces than at the air–water interface. For the chlorobenzene–water interface the film properties were closely similar to those on water and at the nitrobenzene–water interface the surface film appeared to be more condensed. The cmc of NaDDS in the presence of these organic liquids was not reported.

The present investigation represents an extension of these earlier studies in an attempt to explore further the dependence of the cmc and adsorption isotherms upon the addition of various organic liquids.

Experimental Section

Materials. The organic liquids were research grade and exceeded a purity of 99.5 mole %. All the organic liquids were doubly distilled before using. The *n*-alkanes, cyclohexane, and cyclohexene were passed repeatedly through columns of silica gel until no absorption occurred in the spectral region of 220–350 mμ as measured by a Cary 14 spectrophotometer. The water used in these experiments was triply distilled.

Interfacial Tension Measurements. Interfacial tension measurements were made at 25.0 ± 0.1° employing the drop-volume method;[5] the equilibrium drop volume was obtained within 5 min. The volumes of at least 10–15 drops were measured for each determination. The surface tension of the various bottles of triply distilled water used was 71.8 ± 0.1 dynes cm^{-1}. Interfacial tensions of the purified organic liquids *vs.* water are given in Table I. These interfacial tension values were found to be in excellent agreement with those given in the literature, ±0.5 dyne cm^{-1}

(1) E. J. Hutchinson, *J. Colloid Sci.*, **3**, 531 (1948).

(2) E. G. Cockbain, *Trans. Faraday Soc.*, **50**, 874 (1954).

(3) W. Kling and H. Lange, *Proc. Intern. Congr. Surface Activity, 2nd, London, 1957*, **1**, 295 (1957).

(4) D. A. Haydon and J. N. Phillips, *Trans. Faraday Soc.*, **54**, 698 (1958).

(5) W. D. Harkins, "Physical Methods of Organic Chemistry," Vol. I, A. Weissberger, Ed., Interscience Publishers, Inc., New York, N. Y., 1949.

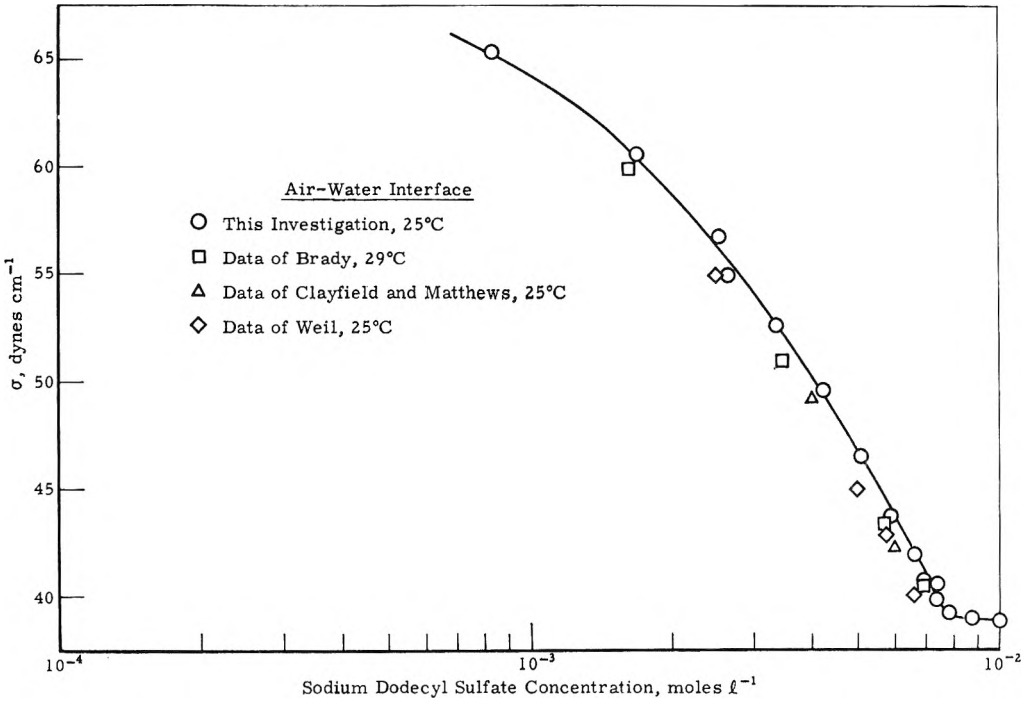

Figure 1. Surface tension of sodium dodecyl sulfate at the air–water interface.

(references given in parentheses). No literature values were found for the unsaturated hydrocarbons.

Preparation of Sodium Dodecyl Sulfate (NaDDS). The sodium dodecyl sulfate used in this experiment was prepared using a method described in the literature[6] in which 1-dodecanol was sulfated using reagent grade chlorosulfonic acid followed by neutralizing the dodecyl acid sulfate with a sodium salt. (Eastman White Label 1-dodecanol was redistilled in a column with approximately twenty theoretical plates at atmospheric pressure before using. Before distillation, the 1-dodecanol contained 3.5 wt % n-C_{14} and after distillation the impurity was less than 0.3 wt % as determined by gas–liquid chromatographic analysis.) The surfactant was recovered from the aqueous phase by successive extractions with 1-butanol and then crystallized from 1-butanol. The recovered surfactant was then Soxhlet extracted with n-hexane to remove unreacted alcohol after which it was recrystallized from redistilled methanol followed by repeated crystallizations from triply distilled water.

The purity of the sodium dodecyl sulfate was determined by measuring the cmc by three different methods: (i) the average of five electrical conductivity measurements at 25° gave a cmc of 8.25 ± 0.03 × 10^{-3} mole/l., (ii) the average of three density measurements gave a cmc of 8.20 ± 0.08 × 10^{-3} at 25°, and (iii) surface tension–log concentration curves showed

Table I: Interfacial Tensions of the Pure Organic Liquid *vs.* High-Purity Water

Oil–water interface	Interfacial tension,[a] ergs cm^{-2}		Dipole moments[b]
n-Heptadecane	53.2		0.0
n-Decane	51.7	51.9[c]	0.0
n-Nonane	50.9		0.0
n-Octane	50.7	51.2,[c] 50.2[d]	0.0
n-Hexane	50.5	50.4,[c] 50.2[e]	0.0
1-Octene	43.7		0.34
1-Hexene	31.3		0.34
Cyclohexane	49.6	50.0[d]	0 2
Cyclohexene	43.5		0.28
Benzene	34 4	34.1[d]	0.0
n-Butylbenzene	40.1	40.1[f,g]	0.35
Carbon tetrachloride	44.8	45.0,[f] 43.7[d]	...

[a] Maximum variations ±0.2 erg cm^{-2}. [b] A. L. McClellan, "Tables of Experimental Dipole Moments," M. H. Freeman and Co., San Francisco, Calif., 1963. [c] R. Aveyard and D. A. Haydon, *Trans. Faraday Soc.*, **61**, 2255 (1965). [d] D. J. Donahue and F. E. Bartell, *J. Phys. Chem.*, **56**, 480 (1952). [e] F. Franks and D. J. G. Ives, *J. Chem. Soc.*, 741 (1960). [f] "International Critical Tables." [g] J. E. Shewmaker, C. E. Vogler, and E. R. Washburn, *J. Phys. Chem.*, **58**, 945 (1954).

(6) E. E. Dreger, G. I. Keim, G. D. Miles, L. Shedlovsky, and J. Ross, *Ind. Eng. Chem.*, **36**, 610 (1944).

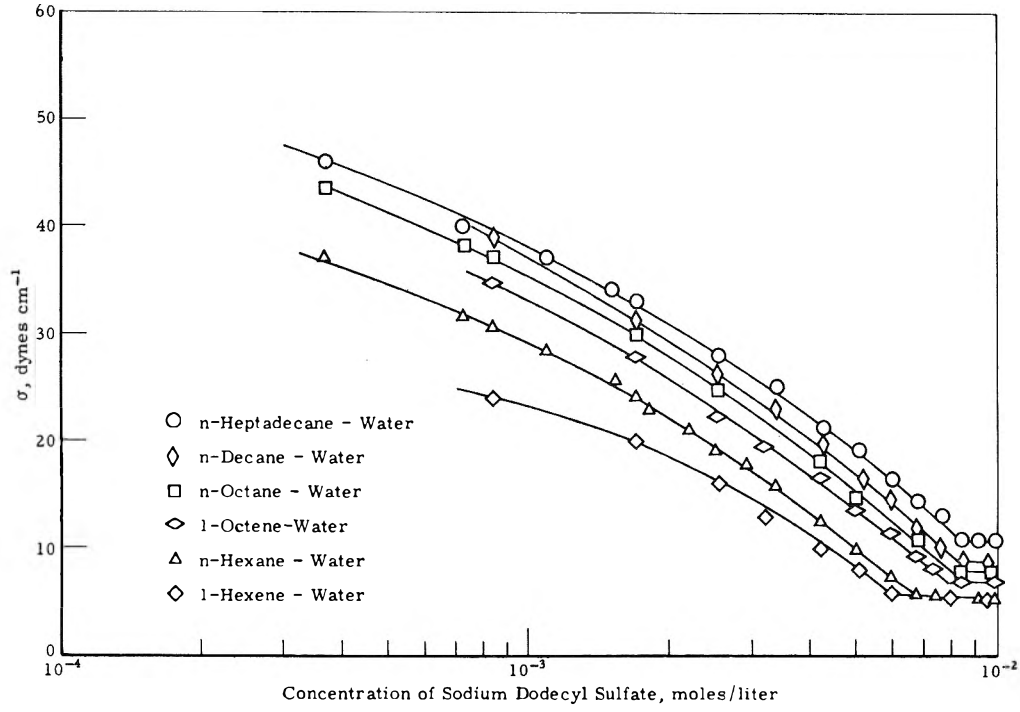

Figure 2. Interfacial tension at the hydrocarbon–water interface as a function of sodium dodecyl sulfate concentration.

no minimum and gave a cmc of 8.10 ± 0.05 × 10^{-3} mole/l. at 25°. These values are in agreement with the average of the values reported in the literature for the cmc of "pure" sodium dodecyl sulfate, 8.10 ± 0.10 × 10^{-3} mole/l. at 25°.

Results and Discussion

Interfacial Tension Measurements of Surfactant Solutions. A plot of the measured interfacial tension at the air–water interface as a function of NaDDS concentration is shown in Figure 1; these values are compared with those given in the literature for "pure" NaDDS.[7-9] The literature values were ~1.5 dynes cm^{-1} lower than those obtained in this investigation, suggesting that the NaDDS used in our study was of a higher purity. Plots of the interfacial tension at the various organic liquid–water interfaces as a function of NaDDS concentration are shown in Figures 2 and 3. (Note: The average standard deviation was ±0.3 dyne cm^{-1}.) Interfacial tension data given in the literature for the adsorption of NaDDS at the *n*-decane–water interface[2] were also ~1.5 dynes cm^{-1} lower, undoubtedly due to the impurities in the NaDDS.

Interfacial tension/ln concentration data were fitted to the Taylor series using multiple regression analysis; a polynomial of second degree was found to be adequate; thus

$$\sigma = z_0 + z_1 \ln m_{\pm} + z_2 \ln^2 m_{\pm} \qquad (1)$$

where $m_{\pm}$ is the surfactant concentration in moles per liter. All calculated values of σ fell within the limits of error of the measurements and the sum of the residual squares was considerably less than the values computed for the coefficients. Further terms (cubic, etc.) did not improve the fit; *i.e.*, the sum of the squares exceeded the values computed for the coefficients. Values computed for z_0, z_1, and z_2 and the standard error are given in Table II.

(Note: Literature data for surface or interfacial tension of aqueous nonelectrolytes, weak electrolytes, and strong electrolytes *vs.* natural logarithm of activity also were found to be adequately fitted by a polynomial of a second degree. Examples are given in Table III.)

The interfacial tension measurements were used to determine the cmc of the aqueous NaDDS solutions as well as to compute the amounts of surfactant adsorbed at the various interfaces. First, we will present the data on the effect of the dissolved organic liquids upon the cmc followed by a section on the computations of the adsorption isotherms.

It is of some interest to note that the organic molecules which have π electrons gave much lower interfacial

(7) A. P. Brady, *J. Phys. Chem.*, **53**, 56 (1949).

(8) E. J. Clayfield and J. B. Matthews, *Proc. Intern. Congr. Surface Activity, 2nd, London, 1957*, **1**, 172 (1957).

(9) I. Weil, *J. Phys. Chem.*, **70**, 133 (1966).

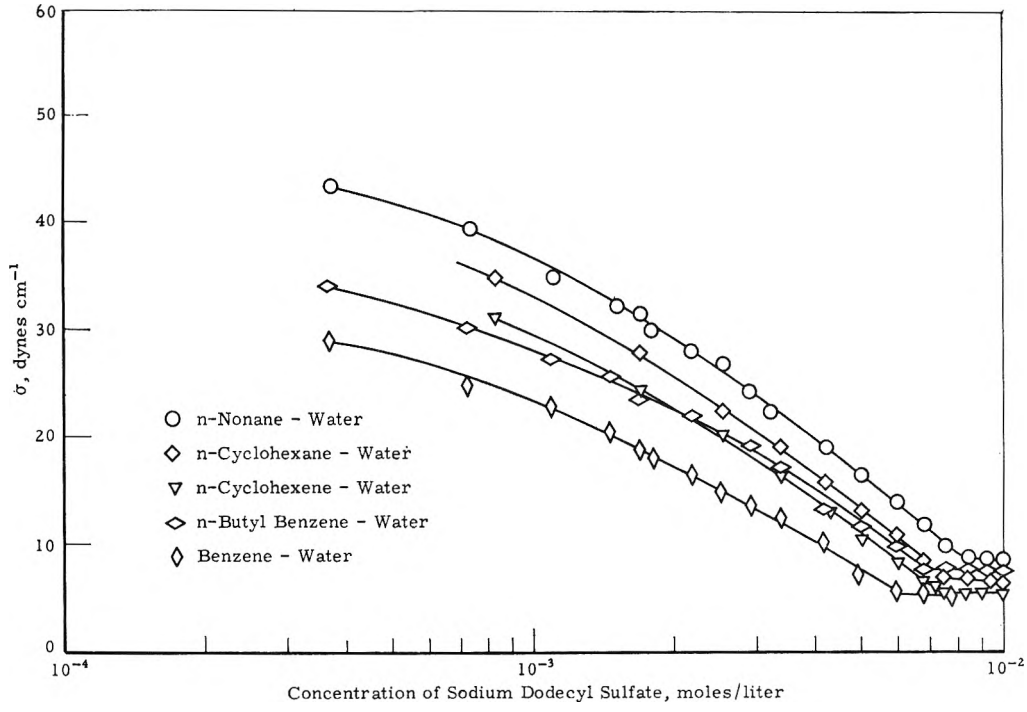

Figure 3. Interfacial tension at various hydrocarbon–water interfaces as a function of sodium dodecyl sulfate concentration.

Table II: Coefficients Computed from Fitting Eq 3

Type of interface *vs.* water	z_0, dynes cm^{-1}	z_1, dynes cm^{-1}	z_2, dynes cm^{-1}
n-Heptadecane	−102.3 ± 3.7	−31.5 ± 1.2	−1.62 ± 0.09
n-Decane	−108.6 ± 5.2	−32.5 ± 1.8	−1.65 ± 0.15
n-Nonane	−120.4 ± 3.6	−36.4 ± 1.2	−1.99 ± 0.09
n-Octane	−114.8 ± 3.3	−34.1 ± 1.1	−1.78 ± 0.08
n-Hexane	−139.3 ± 5.0	−41.7 ± 1.7	−2.37 ± 0.14
Cyclohexane	−121.3 ± 6.2	−35.5 ± 2.1	−1.90 ± 0.18
Cyclohexene	−124.2 ± 4.9	−36.1 ± 1.6	−2.01 ± 0.14
Octene-1	−115.9 ± 4.2	−34.3 ± 1.4	−1.85 ± 0.12
Hexene-1	−133.3 ± 7.1	−40.0 ± 2.3	−2.51 ± 0.19
Benzene	−100.0 ± 3.3	−28.4 ± 1.0	−1.54 ± 0.08
n-Butylbenzene	−115.8 ± 6.5	−34.8 ± 2.2	−2.02 ± 0.18
Carbon tetrachloride	−113.3 ± 2.6	−32.3 ± 0.8	−1.69 ± 0.06
Air	−118.0 ± 6.7	−46.6 ± 2.3	−2.92 ± 0.20

tensions than the *n*-alkanes whereas molecules with dipoles had only slightly lower interfacial tensions.

The decrease in the interfacial tension is probably due to the strong interaction of the water molecules with the π-electron orbitals,[10,11] *i.e.*, an induced dipole by polarization of the organic molecule by the water molecule.

Critical Micelle Concentrations. The concentrations at the inflection points in the interfacial tension curves, the cmc, in the presence of the various organic liquids are given in Table IV, column 1. (Note: Substituting the minimum value of σ into the empirical expression 1 gave the cmc; see column 2 in Table IV.) For the case of dissolved *n*-alkanes, the cmc decreases as the chain length is decreased. The introduction of unsaturation into *n*-C_6 and *n*-C_8 reduces the cmc relative to the saturated compounds. A decrease in the cmc due to the presence of unsaturation in the hydrocarbon is illustrated also by the lower cmc

(10) I. M. Goldman and R. O. Crisler, *J. Org. Chem.*, 23, 751 (1958).
(11) M. Oki and H. Iwamura, *Bull. Chem. Soc. Japan.*, 33, 717 (1960).

Table III: Coefficients and Standard Errors for the Fit of Surface or Interfacial Tension *vs.* Natural Logarithm of Activity for Various Aqueous Nonelectrolytes and 1:1 Electrolyte Solutions

	z_0, dynes/cm	z_1, dynes/cm	z_2, dynes/cm
Nonelectrolyte (25°)			
1-Butanol[a]	23.3 ± 0.5	−18.2 ± 0.4	−1.7 ± 0.1
Weak 1:1 electrolyte (25°)			
n-Propionic acid[b]	47.6 ± 0.3	−12.0 ± 0.3	−1.6 ± 0.1
n-Butanoic acid[b]	30.1 ± 0.4	−15.7 ± 0.4	−1.5 ± 0.1
Strong 1:1 electrolyte (25°)			
Sodium *n*-butyrate[b]	66.4 ± 0.4	−3.2 ± 0.4	−0.44 ± 0.08
Surfactant at petroleum ether–water interface (20°)			
Sodium dodecyl sulfate[c]	−98.6 ± 2.9	−29.4 ± 0.9	−1.5 ± 0.1

[a] W. D. Harkins and R. W. Wampler, *J. Am. Chem. Soc.*, **53**, 850 (1931). [b] F. M. Fowkes and W. D. Harkins, *ibid.*, **62**, 3377 (1940). [c] See ref 4.

Table IV: Critical Micelle Concentration, Organic Liquid Solubility in Water, Values of $\Delta(-\Delta G_s^\circ)$, z_2/RT, Γ_-^{cmc}, and A^2_{cmc}

	Cmc, m*M* (1)	Cmc, m*M* (2)	Soly (m_s), m*M*	$\Delta(-\Delta G_m^\circ)$,[a] cal/mole	z_2/RT,[g] moles × 10^{10} cm^{-2}	Γ_-^{cmc},[g] moles × 10^{10} cm^{-2}	A^2_{cmc},[g] area/molecule
n-Heptadecane	8.5	8.6	...	+40	0.65	3.25	51.0
n-Decane	8.2	8.2	...	...	0.66	3.39	49.0
n-Nonane	8.2	8.2	...	...	0.80	3.49	47.6
n-Octane	8.1	8.0	0.006[b]	20	0.71	3.45	48.3
n-Hexane	7.6	7.7	0.11[b]	90	0.95	3.67	45.2
1-Octene	7.9	7.8	0.04[c]	40	0.74	3.32	50.0
1-Hexene	6.1	6.1	0.67[c]	350	1.01	2.91	57.1
Cyclohexane	7.5	7.6	0.65[b]	90	0.76	3.43	48.3
Cyclohexene	7.1	7.1	1.94[d]	170	0.81	3.27	50.8
n-Butylbenzene	6.8	6.8	0.37[e]	220	0.81	3.08	54.1
Benzene	6.0	6.0	23.81[e]	370	0.62	2.56	64.9
Carbon tetrachloride	6.8	6.9	5.0[f]	210	0.68	3.12	53.1
Air	8.2	8.2[a]	...	...	1.17	3.78	43.9

[a] $m^\circ_\pm$ taken as 8.2 m*M*. [b] C. McAuliffe, *Nature*, **200**, 1092 (1963); also, *J. Phys. Chem.*, **70**, 1267 (1966). [c] L. Bastin and M. A. Muhs, to be published. [d] E. J. Farkas, *Anal. Chem.*, **37**, 1173 (1965). [e] R. Bahan and W. F. Claussen, *J. Am. Chem. Soc.*, **73**, 1571 (1951). [f] H. Stephen and T. Stephen, "Solubilities of Inorganic and Organic Compounds," Vol. I, Macmillan and Co., New York, N. Y., p 369. [g] These values were computed using the coefficients given in Table II; therefore, the variations in these computed values could be as large as 6–8% depending upon the standard error.

found for cyclohexene. Benzene, which is, of course, the most unsaturated molecule, reduced the cmc to its lowest value. The increase in the cmc found in the presence of *n*-heptadecane was reproducible, but the cause of this increase has not been resolved. (Note: Hydrocarbon solubilities in aqueous surfactant solutions below the cmc have been shown to be equal to their water solubilities.[12-14] The decrease in the cmc was found to be related to the water solubilities of the hydrocarbons (m_s) (see Table IV); the larger the water solubilities the greater the decrease in the cmc with the exception of CCl_4.)

To our knowledge, these are the first data to demonstrate the effect of dissolved organic liquids upon the cmc of NaDDS. Various investigators, using either

(12) M. E. L. McBain and E. Hutchinson, "Solubilization," Academic Press Inc., New York, N. Y., 1955, Chapter 3.

(13) G. K. Brashier, Thesis, Louisiana State University, 1964.

(14) A. S. Arambulo, Thesis, University of Illinois, 1964.

the electrical conductivity or dye method, have found that the presence of dissolved benzene, toluene, cyclohexane, *n*-hexane, *n*-octane, *n*-dodecane, *n*-heptadecane, and *n*-octadecane in the aqueous solutions of dodecylammonium chloride,[15,16] potassium carboxylate,[17] sodium alkyl sulfonates,[18] and potassium dodecyl sulfonates[18] caused a decrease in the cmc with the exception of *n*-heptadecane and *n*-octadecane. The presence of these two hydrocarbons had no detectable effect upon the cmc. The critical micelle concentrations of these surfactants were also reduced to their lowest values in the presence of benzene. Recently Nakagawa and Tori,[19] using nuclear magnetic resonance spectroscopy, measured the chemical shift of the benzene signal as a function of NaDDS concentration in deuterium oxide solutions of NaDDS saturated with benzene. These investigators found that no shift of the benzene proton position occurred below the cmc, but when the surfactant concentration reached the cmc, some of the benzene molecules were incorporated into the micelles; thus the benzene signal shifted.[19] The cmc found by this measurement, ~6.9 mM, was also lower than the cmc in the absence of benzene.

Two different models have been used in attempts to describe the micellization process

$$n(\text{monomer}) \rightleftharpoons (\text{micelle})_n \qquad (2)$$

One is an equilibrium process obeying the laws of mass action[20] and the other is a pseudo-phase separation.[15] Both of these models were reported to give the same semiempirical thermodynamic expression for the standard free energies of micellization,[21-24] namely, at constant temperature and pressure

$$\Delta G_m^\circ = 2RT \ln x_\pm \gamma_\pm \qquad (3)$$

where $x_\pm$ and $\gamma_\pm$ are the mole fraction and activity coefficient of the monomer just at the cmc (as defined by Phillips).[25] As previously pointed out by Herrmann and Benjamin,[21] the standard free energies of micellization obtained according to expression 3 depend on the concentration units used and on the choice of standard state. The solvated monomer standard state was taken as the hypothetical state of mole fraction unit; the micelle standard state was taken as the solvated micelle at mole fraction unit.[21] This process was presented diagrammatically by Herrmann and Benjamin[21] as

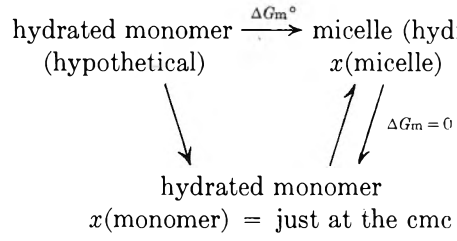

(4)

At the cmc in the ternary system—1:1 electrolyte, dissolved hydrocarbon, and water—the hydrocarbons are solubilized in the micelle–water interface[26] and the hydrocarbon core of the micelle.[12] This process may be described by the diagram shown in Figure 4. This model assumes that the hydrocarbon liquid in the micelle interior has the same activity as the excess hydrocarbon liquid at the oil–water interface and that the hydrocarbon dissolved in water is in the same state as the hydrocarbon dissolved in the surface of the hydrated micelle. Thus the standard free energy changes for these processes are zero. The standard free energy of micellization in the presence of organic liquids, ΔG_m°, represents in part the change in free energy due to the incorporation of the organic liquid into the micelle. The difference between the standard free energies of micellization in the presence of hydrocarbons

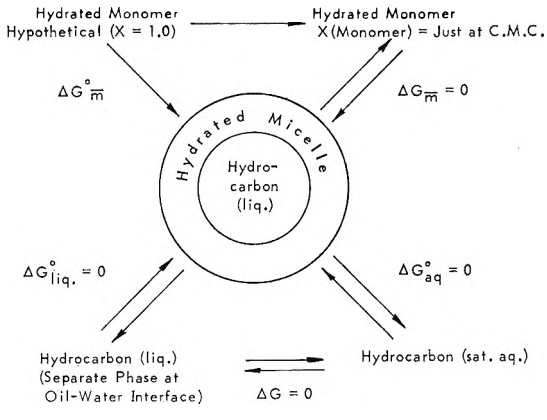

Figure 4. Diagram of micellization process in presence of organic liquids.

(15) E. Hutchinson, A. Inaba, and L. G. Bailey, *Z. Physik. Chem* (Frankfurt), **5**, 344 (1955).

(16) A. W. Ralston and R. N. Eggenberger, *J. Am. Chem. Soc.*, **70**, 983 (1948).

(17) H. B. Klevens, *J. Phys. Colloid Chem.*, **54**, 1012 (1950).

(18) W. Lim, *Bull. Chem. Soc. Japan*, **28**, 227 (1955).

(19) T. Nakagawa and K. Tori, *Kolloid-Z.*, **194**, 143 (1964).

(20) R. C. Murray and G. S. Hartley, *Trans. Faraday Soc.*, **31**, 183 (1935).

(21) K. W. Herrmann, *J. Phys. Chem.*, **66**, 295 (1962); L. Benjamin, *ibid.*, **68**, 3575 (1964).

(22) J. M. Corkill, J. F. Goodman, and S. P. Harrold, *Trans. Faraday Soc.*, **60**, 202 (1964).

(23) P. Molyneux, C. T. Rhodes, and J. Swarbrick, *ibid.*, **61**, 1043 (1965).

(24) H. F. Huisman, *Verhandel. Koninkl. Ned. Akad. Wetenschap. Afdel. Natuurk., Proc. Ser. B*, **67**, 407 (1964).

(25) J. N. Phillips, *Trans. Faraday Soc.*, **51**, 561 (1955).

(26) J. E. Eriksson, *Acta Chem. Scand.*, **17**, 1478 (1963).

($\Delta G_{\bar{m}}^{\circ}$) and in the absence of hydrocarbons (ΔG_m°), the reference state in this case, was computed using the expression

$$\Delta(-\Delta G_s^{\circ}) = \Delta G_{\bar{m}}^{\circ} - \Delta G_m^{\circ} = 2RT \ln x_{\pm}\gamma_{\pm}/x^{\circ}_{\pm}\gamma^{\circ}_{\pm} \quad (5)$$

where $\Delta(-\Delta G_s^{\circ})$ is the change in free energy due to solubilizing the organic liquid in the micelle and $x^{\circ}_{\pm}$ and $\gamma^{\circ}_{\pm}$ are the mole fraction and activity coefficient at the cmc in the absence of organic liquids (see Table IV). (Note: The ratio of the activity coefficients, $\gamma_{\pm}/\gamma^{\circ}_{\pm}$, since the change in concentration is small, was assumed to be unity.) The values of $\Delta(-\Delta G_s^{\circ})$ increased as the *n*-alkane chain length decreased. Solubilities of the *n*-alkanes in micelles increase as the *n*-alkane chain length decreases[12] (or as the hydrocarbon solubility in water increases); thus, the greater the *n*-alkane solubility in the micelle the larger the decrease in the value of $\Delta(-\Delta G_s^{\circ})$ (see Table IV). This was also true of the other homologous series; *e.g.*, benzene has the largest solubility in micelles[12] and had the largest value for $\Delta(-\Delta G_s^{\circ})$; whereas *n*-butylbenzene is less soluble in micelles[12] and had a corresponding smaller value for $\Delta(\Delta G_s^{\circ})$. We believe that these changes in the standard free energy arise from structural changes when these organic liquids are solubilized in the hydrated micelle surface and in the micelle interior. Before making any further speculations the adsorption isotherms were computed to determine if a correlation existed between the cmc and the concentration of NaDDS at the organic liquid–water interface when the bulk concentration is at the cmc.

Calculated Adsorption Isotherms. The surface "concentrations" of NaDDS as a function of the equilibrium concentration of surfactant in the bulk phase are calculated from interfacial tension data using the Gibbs adsorption equation. The equation for variations in composition in the surface of a 1:1 aqueous electrolyte solution, considering the surface layer as having a thickness of molecular dimensions at constant temperature, was derived by Guggenheim[27] as

$$-d\sigma/2RT = \Gamma_- d \ln a_{\pm} \quad (6)$$

where Γ_- is the surface "concentration" of NaDDS (anion), σ is the interfacial or surface tension, and $a_{\pm}$ is the mean activity of the ions Na^+ and DDS^-.

The term $d\sigma/d \ln a_{\pm}$ was evaluated by differentiating the empirical expression 1, assuming $a_{\pm} \cong m_{\pm}$, and substituting the derivative into expression 6; thus an expression for the adsorption isotherm is obtained, namely

$$-d\sigma/d\mu_{\pm} = d\sigma/2RT \, d \ln a_{\pm} = (z_1/2RT) + (z_2/RT) \ln m_{\pm} = \Gamma_- \quad (7)$$

The area per molecule is defined as $(\Gamma_- N_0)^{-1}$; thus expression 8 has the following form for changes in area per molecule *vs.* $\ln m_{\pm}$

$$-d\sigma/2kT \, d \ln a_{\pm} = (z_1/2kT) + (z_2/kT) \ln m_{\pm} = 1/A^2 \quad (8)$$

Values of the slope, z_2/RT, the amounts adsorbed at the cmc, Γ_-^{cmc}, and the corresponding areas occupied per molecule of NaDDS, A^2_{cmc}, are given in Table IV. The value of A^2_{cmc} computed for the air–water interface of 43.9 A^2 is within the range of values reported in the literature of 45 ± 5 A^2.[7-9] The value obtained for the *n*-decane–water interface of 49.3 A^2 was in good agreement with the literature value of 48.8 A^2.[2] The surface films at the benzene–water interface are more expanded (65 A^2) suggesting penetration or dissolving of benzene in the surface film.[1] Surface films of NaDDS were more closely packed at the *n*-alkane–water interface and the area per molecule at the cmc increased as a function of *n*-alkane chain length, 45–51 A^2. The surface films of NaDDS at the unsaturated hydrocarbon–water interface were more expanded than those at the saturated hydrocarbon–water interfaces. Also, note the expanded surface film in the presence of carbon tetrachloride.

Variations of the area per adsorbed NaDDS molecule at the various interfaces at the cmc are not easily explained without independent data concerning interactions between NaDDS, water, and the organic liquids. The fact that the presence of *n*-C_6 hardly changes the area per adsorbed NaDDS molecule at the interface while the benzene expands the area from 44 to 65 A^2 per molecule is interpreted as indicating far larger amounts of benzene are dissolved in the surface film as compared with *n*-C_6.

A correlation between the concentration of NaDDS at the oil–water interface and the cmc is observed for each homologous series (see Table IV). For example, as the solubility of the *n*-alkane decreased, the cmc increased and the concentration of NaDDS at the oil–water interface decreased. In the presence of the other organic liquids, the cmc increased with decreasing solubility, but the concentration of NaDDS at the oil–water interface increased. This implies that the surfactant film at the micelle–water interface becomes

(27) E. A. Guggenheim, "Thermodynamics," Interscience Publishers, Inc., New York, N. Y., 1957.

more expanded as the n-alkane solubility in the micelle decreases, whereas the direct opposite is implied for the other organic liquids. As the organic liquid solubilities in the micelle decrease, the micelle–water interface would be less expanded.

Acknowledgments. The author profoundly expresses his gratitude to Drs. J. W. Otvos, W. C. Simpson, and J. N. Wilson for helpful discussions and encouragement, and to G. V. Seastrom, Jr., for assistance in making duplicate interfacial tension measurements.

Acid–Base Properties of Quartz Suspensions[1]

by S. Storgaard Jørgensen and A. Tovborg Jensen

Chemical Laboratory, Royal Veterinary and Agricultural College, Copenhagen, Denmark
(Received October 17, 1966)

Narrow particle-size fractions of quartz, vitreous silica, and flint <20 μ, prepared by elutriation, were titrated back and forth several times with NaOH and HCl in the pH range 3–11. The titration curves of quartz were S shaped and showed hysteresis. It was shown that the major part of the protolysis capacity in the alkaline region was caused by silicic acid dissolving during titration. The protolysis capacity in the pH range 3–5 was unexpectedly high. It was shown to be due to a small iron impurity (0.03% Fe). The major part of the protolysis capacity in the range 5–9 was shown to be due to the quartz surface as such. The surface density of acid sites in the whole pH range 3–11 was estimated to 2.6 acid sites/100 A^2. As the protolysis capacity of HF-washed quartz was much lower than that of untreated quartz, it was concluded that the latter had a reactive surface layer different from that of the perfect crystal. Titration curves of vitreous silica were similar to those of quartz. The protolysis capacity of flint was higher than that of quartz and vitreous silica but increased only slightly with decreasing particle size. Hence it was concluded that flint has some kind of protolytically reactive inner surfaces in addition to outer surfaces. This was substantiated by X-ray investigation.

Introduction

It is reasonable to assume that the acid–base properties of suspensions of quartz and vitreous silica are confined to outer particle surfaces. If the acid–base sites are equally distributed over all surfaces, the protolysis capacity[2] must be proportional to the specific surface area of the particles. This assumption has, however, never been proved. It may also be assumed that suspended particles can both split off hydrogen ions instantaneously and reversibly and neutralize base at a slow rate; *i.e.*, they may exert "manifest" as well as "latent" acidity, in the terms of Bjerrum.[3]

The manifest acidity is assumed to be caused by ionization of hydrogen ions from surface hydroxyl groups. The nature and properties of these groups have been discussed by Boehm.[4] On amorphous silica,

(1) Taken in part from an unpublished thesis submitted by S. S. J. to the Veterinary and Agricultural College in partial fulfillment of the requirements for the L. Agro. degree.

(2) By "protolysis capacity" is understood equivalents of acid or base consumed in titration of 100 g of powder between definite pH values.

(3) N. Bjerrum, "Selected Papers," Ejnar Munksgaard, Copenhagen, Denmark, 1949, p 286.

(4) H. P. Boehm, *Angew. Chem.*, **78**, 617 (1966); *Angew. Chem. Intern. Ed. Engl.*, **5**, 533 (1966).

hydroxyl densities ranging from 2 to 5 OH/100 A^2 have been found by various methods.[4] From structural considerations, Stöber[5] calculated a surface hydroxyl density of about 5 OH/100 A^2 on crushed quartz. Experimentally (thermal dehydration), he estimated a density of about 3.6 OH/100 A^2.

The latent acidity is attributed to the acid–base properties of silicic acid formed by dissolution. Concentrations of monosilicic acid in "equilibrium" with different forms of amorphous silica have been found to lie within the range of 110–140 mg of SiO_2/l. in acid and neutral solutions at room temperature.[6-9] The solubility of quartz in water at 25° has been estimated to about 10 mg of SiO_2/l. by extrapolation from high-temperature experiments.[10,11] In alkaline solutions the solubility of silica is much larger than in acid and neutral solutions due to ionization of silicic acid.[6]

The dissolution of silica is slow, but only in the case of HF-washed quartz is it too slow to be recognized in titration curves of suspensions. It was noted by Holt and King[12a] that in water, silica dissolves rapidly at first, and later much more slowly. This has also been found by one of us[12b] in the case of precipitated amorphous silica. The dissolution rate increases with increasing alkalinity. It is therefore not possible to titrate the manifest acidity of any kind of silica without also titrating a part of the latent acidity. The combination of the two kinds of acidity causes the shape of a titration curve to depend on titration velocity. It also gives rise to hysteresis when a base-titrated suspension is titrated back with acid.

In the present investigation, protolysis capacities of four particle-size fractions <20 μ have been compared with specific surface areas calculated from sedimentation analysis. In the case of quartz, a semiquantitative separation of the manifest and the latent acidity has also been made.

Experimental Section

Samples. Quartz is an already powdered sample, 99% α quartz as shown by X-ray diffractometry. After volatilization with HF + H_2SO_4, 0.3% was left. In this residue aluminum and iron were detected. By boiling the fraction <2 μ with 4 N HCl, 0.03% Fe was brought into solution. The iron may originate from steel balls used for crushing the quartz. Its presence caused some trouble in the evaluation of titration curves as will be shown later. Unless otherwise stated, the iron impurity was not removed before titration.

Vitreous silica is clear "Vitreosil," completely amorphous to X-rays and completely volatile with HF + H_2SO_4.

Flint is a dark, Senonian specimen, uniform and free from calcium carbonate. By the X-ray diffractometry methods of Jensen, *et al.*,[13] the flint was compared with standard quartz (Riedel-de Haën). The area of the $10\bar{1}1$ quartz peak was 90% that of the standard. By comparing the half-width of the same peak with that of the standard quartz, an average crystal size of 312 A was estimated. After volatilization with HF + H_2SO_4, 0.3% was left.

Vitreous silica and flint were crushed in a steel mortar and then ground under methanol in a boron-carbide mortar. The powdered samples were separated at 20, 10, 4, and 2 μ by elutriation in 0.002 M sodium pyrophosphate by the method of Jensen and Hansen.[14] After elutriation, the fractions >2 μ were washed three times with water and dried at 110°. The particles <2 μ were flocculated by sodium chloride, washed Cl-free, and dried at 110°. On the quartz fractions 4–10, 2–4, and <2 μ, sedimentation analyses were carried out. Assuming spherical particles, the following specific surfaces were calculated from the size distributions found: 4–10 μ, 0.385; 2–4 μ, 0.93; and <2 μ, 3.16 m^2/g.

Cation-exchange capacities of the fractions <2 μ were determined by means of sodium ions at pH 7.65 as described by Jackson.[15] The following values were found: quartz, 4.9; flint, 6.3; and vitreous silica, 5.5 mequiv/100 g.

Titration Experiments. Acid–base titrations were performed by means of a Radiometer "Titrigraph." Powder (0.10–1.00 g) was suspended in 10 ml of deionized water or 1 M NaCl, titrated with 0.100 N HCl, and back-titrated with 0.100 N NaOH (carbonate-free). Suspensions were titrated back and forth several times. Titrations were either performed in the same liquid throughout or the suspension was centrifuged and the particles suspended in water after the first

(5) W. Stöber, *Kolloid-Z.*, **145**, 17 (1956).

(6) G. B. Alexander, W. M. Heston, and R. K. Iler, *J. Phys. Chem.*, **58**, 453 (1954).

(7) K. B. Krauskopf, *Geochim. Cosmochim. Acta*, **10**, 1 (1956).

(8) S. A. Greenberg and E. W. Price, *J. Phys. Chem.*, **61**, 1539 (1957).

(9) R. Siever, *J. Geol.*, **70**, 127 (1962).

(10) J. A. van Lier, P. L. de Bruyn, and J. T. G. Overbeek, *J. Phys. Chem.*, **64**, 1675 (1960).

(11) G. W. Morey, R. O. Fournier, and J. J. Rowe, *Geochim. Cosmochim. Acta*, **26**, 1029 (1962).

(12) (a) P. F. Holt and D. T. King, *J. Chem. Soc.*, 773 (1955); (b) S. S. Jørgensen, to be published.

(13) A. T. Jensen, C. J. Wøhlk, K. Drenck, and E. K. Andersen, *Danish Natl. Inst. Bldg. Res. Acad. Tech. Sci. Comm. Alkali Reactions Concrete, Progr. Rept., D*1, 37 (1957).

(14) E. Jensen and H. M. Hansen, *Soil Sci.*, **92**, 94 (1961).

(15) M. L. Jackson, "Soil Chemical Analysis," Prentice-Hall Inc., Englewood Cliffs, N. J., 1958, p 65.

base titration and after the following titrations. The centrifuged-off liquids were also titrated. During titration, the suspensions were vigorously stirred and CO_2-free air was bubbled through them. The instrument was equipped with two syringe burets (capacity 0.500 ml each) which could be used alternately so that back-titration with base could be performed immediately after titration with acid, and *vice versa*. Titrations were performed at 20–22°. Unless otherwise stated, a titration pH 3–11 took 10–15 min.

All titration curves were graphically corrected for the protolysis capacity of the solvent. For this correction were used titration curves for HCl titrated with NaOH the same day and under the same conditions as the suspensions. As the protolysis capacity of the solvent is rather large at low and high pH values, the capacity of the suspended mineral is not very accurately determined in these pH ranges. Titration curves are designated in the following way: I, titration with 0.100 *N* HCl from the initial pH to pH 3; II, subsequent titration with 0.100 *N* NaOH from pH 3 to pH 11; and III–V, subsequent titrations with acid, base, and acid pH 3–11.

Results

Quartz. From the curves of Figure 1 it is seen that the particles show buffer effect in the whole pH range investigated. A closer examination of the original curves indicated that the particles have a rather large protolysis capacity above pH 11, but only a very small one below pH 3. The corrected titration curves are in most cases S shaped and hysteresis effects are pronounced, especially in the most acid and the most alkaline regions. The protolysis capacity in the whole range 3–11 increases from one titration to the next, independent of the titrant used. (See Table I.)

The protolysis capacity of 0.50 g is larger than that of 1.00 g titrated in the same volume, this being more pronounced in the alkaline range. The capacity in the alkaline range also increases with increasing titration time. In the alkaline range, the protolysis capacity is greater in NaCl solution and the bending of the curve begins at a lower pH than in water. In titrations in NaCl solution, distinct buffer ranges between pH 4 and 5 are noticed in the base titrations but not in the acid titrations.

The titration curves can be divided into three parts, the two flat parts with pronounced hysteresis, pH 3–5 and pH 9–11, and the steep part with very little hysteresis, pH 5–9. In Table II the protolysis capacity in each part is expressed as acid sites/100 A^2 using the estimates of specific surface given above.

In the pH range 5–9, the protolysis capacity increases slightly from one titration to the next, independent of the titrant. The titrant consumption per 100 A^2 of different particle-size fractions is approximately the same. The average value from all titrations of the suspensions, 1.00 g, 4–10 μ; 1.00 g, 2–4 μ; and 0.50 g, <2 μ, titrated in the normal way in water, is 2.3 acid sites/100 A^2. The protolysis capacity in the pH range 3–5 is unexpectedly high. In the search for an explanation the iron impurity was found.

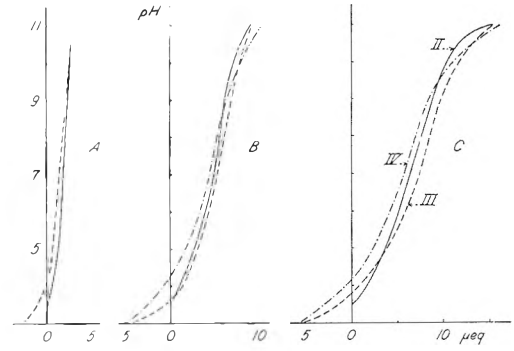

Figure 1. Corrected titration curves of quartz in water. Same liquid throughout: A, 1.00 g, 4–10 μ; B, 1.00 g, 2–4 μ; C, 0.50 g, <2 μ: ———, titration II; – – – –, titration III; — · —, titration IV.

In Figure 2 are shown titration curves of quartz <2 μ from which the iron had been removed by boiling with HCl and washing with deionized water. In these titrations the protolysis capacity in the acid range was much smaller both in water and in 1 *M* NaCl than in the titrations of untreated quartz.

In Figures 3 and 4 are shown titration curves of quartz suspended in pure water after titrations II–IV. The protolysis capacity of the particles in the pH

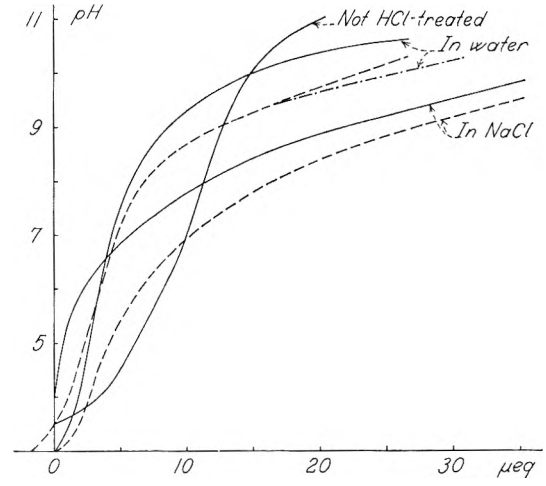

Figure 2. Corrected titration curves of 1.00 g of HCl-treated quartz, <2 μ. Same liquid throughout. Signatures as in Figure 1.

Table I: Titration of Quartz Suspensions. Same Liquid Throughout. Acid–Base Properties in the pH Range 3–11

	Initial pH	Acid/base consumption (cor) mequiv/100 g in titrations I	II	III	IV
1.00 g, 10–20 μ, in water	5.65	...	0.17	0.32	...
1.00 g, 4–10 μ, in water	5.30	0.06	0.27	0.56	...
1.00 g, 2–4 μ, in water	6.02	0.38	0.95	1.35	1.48
0.50 g, <2 μ, in water	7.10	0.50	3 13	4.40	4.45
1.00 g, <2 μ, in water	6.93	1.25	2.05	2.65	...
1.00 g, <2 μ, in water, 1.5 hr	6.85	0.91	3.50	...	...
1.00 g, 2–4 μ, in 1 *M* NaCl	4.62	0.16	1.35	1.75	1.90

Table II: Protolysis Capacity of Quartz Suspensions in Relation to Estimated Surface Areas

	Acid sites/100 A²								
	pH 3–5			pH 5–9			pH 9–11		
	II	III	IV	II	III	IV	II	III	IV
1.00 g, 4–10 μ, in water	1.9	5.9	...	1.7	2.5	...	0.6	0.5	...
1.00 g, 2–4 μ, in water	1.7	4.9	4.2	2.3	2.6	2.8	2.2	1.3	2.5
0.50 g, <2 μ, in water	1.4	3.6	3.1	1.9	2.3	2.3	2.6	2.5	3.1
1.00 g, <2 μ, in water	1.1	2.6	...	1.3	1.3	...	1.5	1.1	...
1.00 g, <2 μ, in water, 1.5 hr	0.8 (?)	...	...	1.6	...	...	4.3	...	...
1.00 g, 2–4 μ, in 1 *M* NaCl	1.3	3.4	2.7	3.2	3.6	3.8	4.3	4.3	5.8

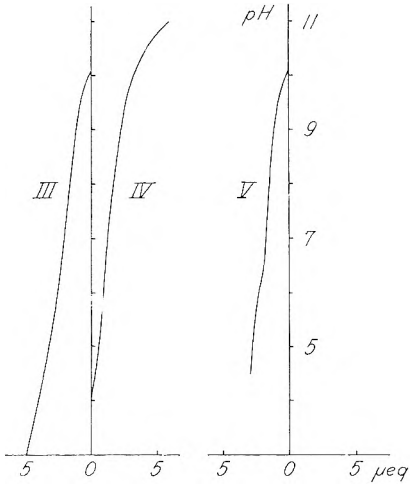

Figure 3. Corrected titration curves of 1.00 g of quartz, 2–4 μ, in water. Liquid centrifuged off and particles suspended in fresh water after each titration.

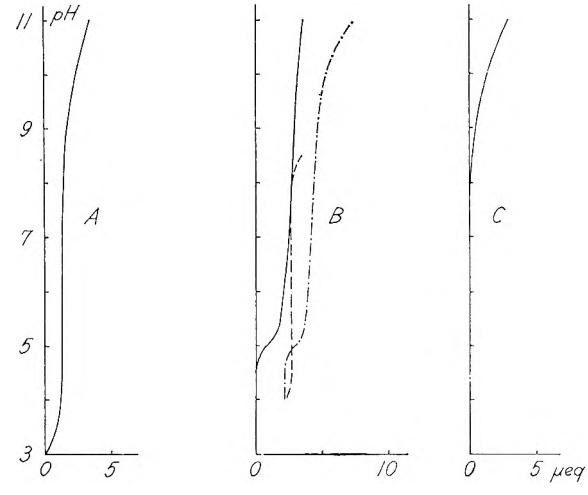

Figure 4. Corrected titration curves of centrifuged-off liquids: A, after titration II; B, after titration III; C, after titration IV; ———, base titration (in the cases A and C after acid titration and removal of absorbed CO_2); – – – –, back-titration with acid; — · —, subsequent base titration.

range 5–9 is equivalent to 1.3 acid sites/100 A². In the alkaline range, all the particle suspensions and all the liquids have a high protolysis capacity. In the acid range (pH 3–5), the protolysis capacity is "brought into solution" during titrations.

In the titration of quartz from which a surface layer of approximately 1100 A had been removed by treatment with HF, the protolysis capacity in titration II was about 40% of that of untreated quartz. In subsequent titrations of suspensions and centrifuged-off liquids there was no significant acid or base consumption.

Vitreous Silica. Titration data are given in Table III and Figure 5. Protolysis capacities are of the same magnitude as those of the corresponding quartz fractions, and the curves are very similar to those of HCl-treated quartz. The only appreciable difference is found in the most alkaline range, where the acid

Table III: Titration of Suspensions of Vitreous Silica. Same Liquid Throughout. Acid–Base Properties in the pH Range 3–11

	Initial pH	Acid–base consumption (cor) mequiv/100 g in titrations I	II	III	IV
1.00 g, 11.7–23.4 μ, in water	5.30	Not detectable			
1.00 g, 4.7–11.7 μ, in water	5.17	0	0.29	...	...
1.00 g, 2.34–4.7 μ, in water	5.10	0	0.70	0.90	...
0.75 g, <2.34 μ, in water	5.88	0.12	2.53	3.05	3.60[a]
1.00 g, 2.34–4.7 μ, in 1 *M* NaCl	5.33	0	1.00	1.53	1.80

[a] Titrated to pH 10.7 only.

Table IV: Titration of Suspensions of Flint. Same Liquid Throughout. Acid–Base Properties in the pH Range 3–11

	Initial pH	Acid–base consumption (cor) mequiv/100 g in titrations I	II	III	IV
1.00 g, 10.2–20.3 μ, in water	6.08	0.14	2.25	2.62	...
0.30 g, 4.1–10.2 μ, in water	4.85	0.30	2.30	3.16	3.50
0.15 g, 2.03–4.1 μ, in water	5.04	0.67	2.40	5.00	...
0.15 g, <2.03 μ, in water	5.78	0.73	5.16	6.60	7.26
0.15 g, 2.03–4.1 μ, in water, 1.5 hr	6.12	0.40	5.33	...	...
0.15 g, 2.03–4.1 μ, in 1 *M* NaCl	5.28	0	9.0	9.0	...

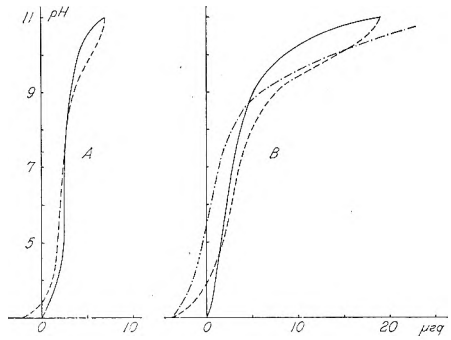

Figure 5. Corrected titration curves of vitreous silica in water: Same liquid throughout: A, 1.00 g, 2.34–4.7 μ; B, 0.75 g, <2.34 μ. Signatures as in Figure 1.

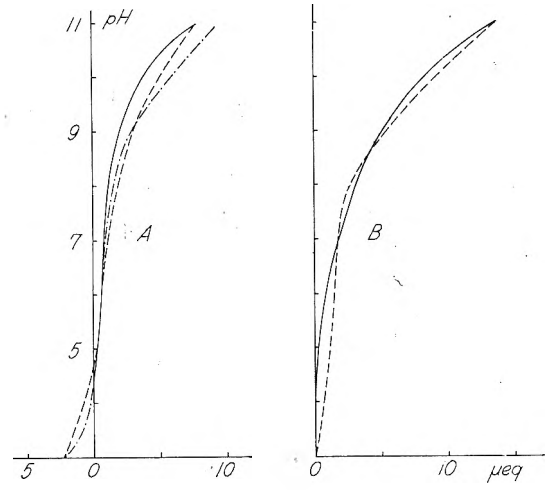

Figure 6. Corrected titration curves of flint. Same liquid throughout: A, 0.15 g, <2.03 μ, in water; B, 0.15 g, 2.03–4.1 μ, in 1 *M* NaCl. Signatures as in Figure 1.

titration curves of vitreous silica have an inflection point with maximum buffer capacity just below pH 10. In the titrations in NaCl solution, this inflection is also seen in the base titrations.

Flint. Titration data are given in Table IV and Figure 6. The protolysis capacity of this flint is much larger than those of the corresponding quartz and vitreous silica fractions and there is only a small increase in protolysis capacity with decreasing particle size. The general shape of the titration curves of different fractions is the same, but there are smaller differences between the curves obtained in water and 1 *M* NaCl than in the case of quartz and vitreous silica. In all flint titrations, the protolysis capacity in the acid range was low; in titration II there was no base consumption at all below pH 4.5.

Discussion

The protolysis capacity of quartz and of vitreous silica was shown to be confined to outer particle surfaces. The flint titrations indicated the presence of some kind of inner surfaces too. From X-ray line broadening, the total specific surface of the crystals is estimated to

be 70 m^2/g, which is 22 times that of the finest quartz fraction. This whole surface cannot be accessible to the solution in these fast titrations. The protolysis capacity is at most only nine times that of the corresponding quartz fraction. The smaller the particles, however, the greater the part of the inner surfaces coming into contact with the solution. This explains the increase in protolysis capacity with decreasing particle size.

The protolysis capacity of quartz is due partly to the surface as such and partly to material dissolving during titration. If the titration curve of the surface as such is linear in the whole pH range 3–11 with the same slope as in the range 5–9, the density of acid sites on the surface is 2.6/100 A^2. This figure, which is within the range of surface hydroxyl densities found on silica, is only a rough estimate. The particles are not spherical as assumed in the calculation of specific surface areas, and the protolysis capacity of the surface might be larger in the alkaline range.[16]

The major part of the protolysis capacity in the alkaline range is assumed to be due to dissolution of the surface layer as monosilicic acid, H_4SiO_4. The titrated solutions are very far from saturation, both with respect to amorphous silica and quartz. Therefore, the dissolution is going on during all titrations. The protolysis capacity in the pH range 3–5 was ascribed to the iron impurity. This might be present either as iron adsorbed on the quartz surface or as soluble silica–iron oxide complexes. The existence of such complexes was indicated by the experiments of Hazel, *et al.*[17]

From the titrations of HF-treated quartz, it is concluded that the untreated quartz had a surface layer much more reactive toward acids and bases than a "pure" quartz surface. It has been found[9,10] that crushed quartz has a surface layer a few hundred angstroms thick which is not completely amorphous but has a somewhat "loosened" quartz structure. This layer can be removed by hydrofluoric acid. What has been reported on in the present paper is not the acid–base properties of the surface of a perfect quartz crystal but those of a disturbed quartz surface. This kind of surface might well be much more common in nature than the perfect crystal surface.

Acknowledgments. The authors are deeply indebted to Dr. K. J. Pedersen for helpful discussions during the preparation of the manuscript. A research grant to S. S. J. from The Danish Government Fund for Scientific and Industrial Research is gratefully acknowledged. The titration equipment was placed at our disposal by The Carlsberg Foundation Grant to the Royal Veterinary and Agricultural College, Copenhagen.

(16) W. M. Heston, R. K. Iler, and G. W. Sears, *J. Phys. Chem.*, **64**, 147 (1960).

(17) F. Hazel, R. U. Schock, and M. Gordon, *J. Am. Chem. Soc.* **71**, 2256 (1949).

Ionization of Diketocyclobutenediol and Its Metal Complexes

by D. T. Ireland[1] and H. F. Walton

University of Colorado, Boulder, Colorado 80302 *(Received July 21, 1966)*

The second ionization constant of diketocyclobutenediol was measured by potentiometric titration and found to be 6.2×10^{-4} in 0.1 *M* KCl; it decreased slightly with rising temperature. The value of K_1 is about 2×10^{-2}. Ultraviolet absorption spectra confirmed the value of K_2. They did not permit determining K_1, but gave evidence of protonated species at high acidities. Preliminary measurements of the solubility of the iron(III) and copper(II) complexes were made. They indicate the formation of soluble anionic complexes of Fe(III).

The compound diketocyclobutenediol, $C_4H_2O_4$

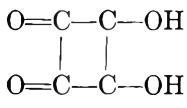

also known as "squaric acid," was first prepared by Cohen, Lacher, and Park,[2] who noted that it was a dibasic acid with pK_2 about 3. They also noted the colored complexes formed with certain metal ions, especially Fe(III).

We have now determined the second ionization constant, K_2, with fair accuracy and made an estimate of K_1. We have studied the ultraviolet absorption spectrum at various acidities and made preliminary measurements of the solubilities of its compounds with iron(III) and copper(II).

Experimental Section

Preparation of Diketocyclobutenediol. We used the procedure of Park, Cohen, and Lacher,[3] starting with trifluorochloroethylene, converting it to 1,2-diethoxy-3,3,4,4-tetrafluorocyclobutene[4,5] and hydrolyzing this with 50% sulfuric acid at 100°. The acid crystallized as a white solid. It was impure. Repeated recrystallization from hot water was only moderately effective in purifying it. Recrystallization of the potassium salt from aqueous methanol, followed by reconversion to the acid by cation exchange, was somewhat more efficient, but the best method of purification was absorption of the squarate ion from aqueous solution on a strong-base quaternary anion-exchange resin, Dowex-1, in the chloride form. The acid was eluted by warm 0.5 *M* hydrochloric acid and crystallized by evaporating the solution. One recrystallization from water, followed by drying in a vacuum desiccator, gave a product which assayed 99% purity or better by titration with standard base. The titration curve and absorbance curves here presented were obtained with acid purified in this way.

Potentiometric Titration. To determine the ionization constants, quantities of 0.5–1 mmole of squaric acid were dissolved in 50 ml of 0.10 *M* potassium chloride solution and titrated with carbonate-free potassium hydroxide using glass and calomel electrodes and a Beckman Model G pH meter. The titration was done in a three-necked 200-ml flask immersed in a constant temperature bath. A stream of nitrogen was passed in some tests to exclude atmospheric carbon dioxide. The standard of pH used to calibrate the cell was 0.050 *M* potassium acid phthalate, whose pH has been established by Bates[6] over a wide temperature range. Potassium tetroxalate was used as a secondary standard. Titrations were done at 0, 25, and 50°. Three different samples of acid, purified in the three different ways described above, gave pK_2 values agreeing to 0.05 unit (see Table I).

(1) Based on the M.S. Thesis of D. T. Ireland, University of Colorado, Boulder, Colo., 1963.

(2) S. Cohen, J. R. Lacher, and J. D. Park, *J. Am. Chem. Soc.*, **81**, 3480 (1959).

(3) J. D. Park, S. Cohen, and J. R. Lacher, *ibid.*, **84**, 2919 (1962).

(4) J. D. Park, M. L. Sharrah, and J. R. Lacher, *ibid.*, 71, 2337 (1949).

(5) S. Cohen, Thesis, University of Colorado, Boulder, Colo., 1959.

(6) R. G. Bates, "Determination of pH: Theory and Practice," John Wiley and Sons, Inc., New York, N. Y., 1964.

Absorption Spectra. These were measured between 220 and 300 mμ, using a Cary Model 14 recording spectrophotometer, 2-mm quartz cells, and solutions 2×10^{-4} *M* in squaric acid. Only the acid purified by ion exchange gave consistently reproducible spectra, and these spectra are shown in Figures 1 and 2.

Table I: Values of pK_2 at Ionic Strength 0.1

Sample	pK_2 at 0°	pK_2 at 25°	pK_2 at 50°
A	3.09	3.17	3.28
B	....	3.21	3.23

Solubility Measurements with Metal Complexes. Solutions of ferric salts or cupric salts were mixed with squaric acid, together with sodium or potassium hydroxide to adjust the pH, and the mixed solutions were left to stand at room temperature with occasional shaking for at least 7 days, and in some cases for 13 days. At the end of this time the pH was measured and the solution analyzed for iron or copper, the first photometrically with 1,10-phenanthroline, the second by titration with EDTA. The total squarate ion content was found by passing the solutions through small columns of cation-exchange resin to remove metal ions (blank experiments showed that no squarate ions were retained) then adding ammonia and measuring the ultraviolet absorption.

Results and Discussion

Titration Curves. A typical titration curve at 25° is shown in Figure 3. To interpret such curves, constant activity coefficients during titration were assumed and the contribution of hydroxyl ions to the ionic charge balance was ignored. Then this equation would describe the course of the curve

$$h^3 + h^2(b + K_1) - hK_1(b - a + K_2) + K_1K_2(b - 2a) = 0$$

where h is the hydrogen-ion concentration, a and b the stoichiometric concentrations of acid and base, and K_1 and K_2 the acid ionization constants.

This equation is derived by combining the electroneutrality and mass balance equations with the concentration quotients for K_1 and K_2.[7] However, we find the hydrogen-ion concentration, h, from the emf of the glass–calomel electrode pair; it is actually a single-ion activity based on the usual convention that the liquid-junction potential is zero. Since the last

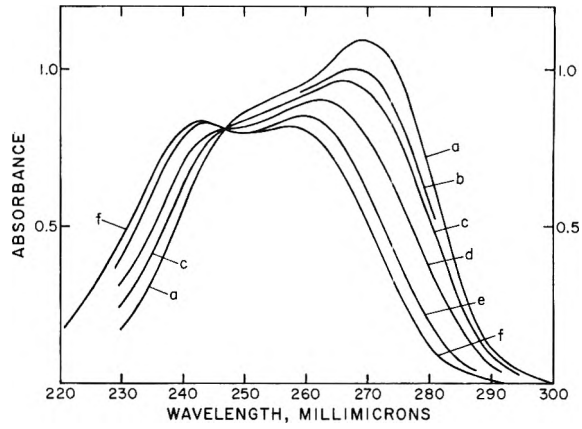

Figure 1. Absorption spectra at ionic strength 0.10; 2.00×10^{-4} *M* acid, 2-mm cells. pH values: a, 5.45 and 6.64 (coincident); b, 3.65; c, 3.42; d, 2.88; e, 1.96; f, 1.11.

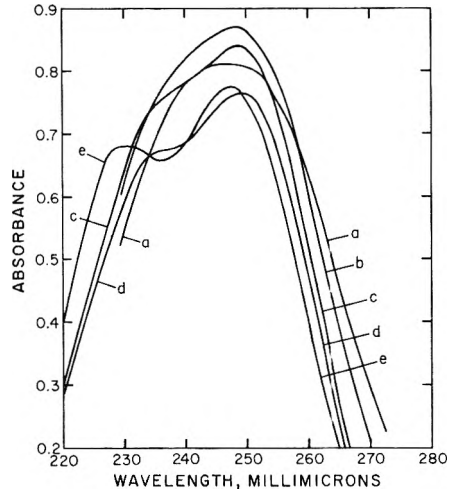

Figure 2. Absorption spectra; 2.00×10^{-4} *M* acid, 2-mm cells. a, 1.2 *M* HCl; b, 2.4 *M* HCl; c, 6 *M* HCl; d, 12 *M* HCl; e, 10 *M* $HClO_4$.

two terms in the equation are the largest, and since $K_2 << (b - a)$, the calculated value of K_2 is a hybrid concentration and activity quotient, $a_{H^+}m_{X^{2-}}/m_{HX^-}$.

By orthodox curve-fitting procedures the following values are found consistent with Figure 3.

$$K_1 = 2 \times 10^{-2}; \quad K_2 = 6.2 \times 10^{-4}$$

The probable error in K_2 is about $\pm 0.3 \times 10^{-4}$; that in K_1, assuming the pH readings to be reliable to within 0.04 unit, is almost 50%. We may consider that K_1 lies between 1 and 3×10^{-2} at 25° and ionic

(7) J. E. Ricci, "Hydrogen Ion Concentration," Princeton University Press, Princeton, N. J., 1952.

strength 0.1. We note in passing that neglect of the h^3 term in the region of pH 2.5 is equivalent to a pH error of 0.02–0.04 unit.

A less tedious way to find K_1 and K_2 is to select two points on the titration curve, one before and one after the half-neutralization point (*i.e.*, the point of addition of 1 mole of base to 1 mole of acid), and apply the computational method of Noyes,[8] discussed by Albert and Serjeant.[9] It is based on the equation given above, and the calculated constants agreed with those found by curve fitting.

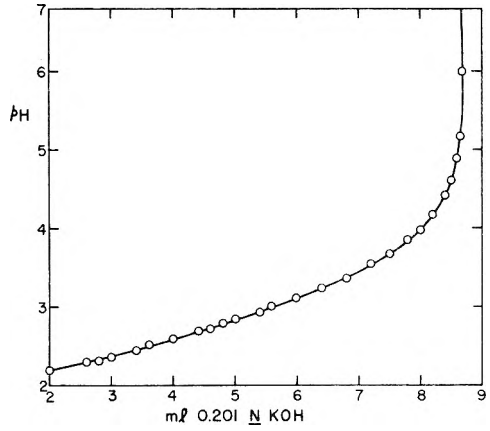

Figure 3. Titration curve: 100.9 mg of purified acid dissolved in 50 ml of 0.100 *M* KCl, temp 24.92°.

Values of K_2 from several titrations are summarized in Table I. Sample "A" of diketocyclobutenediol was purified solely by recrystallization from water; sample "B" was purified by the ion-exchange method.

Absorption Spectra. These are presented in Figures 1 and 2. The data of Figure 1 are at a constant ionic strength of 0.10, maintained by adding sodium chloride. The solutions of pH 3.42 and higher were buffered by the addition of potassium dihydrogen phosphate in 0.004 *M* concentration; this increased the absorbance slightly below 230 mμ but not above this wavelength. The other three solutions contained only hydrochloric acid in addition to sodium chloride. In every case the pH was measured with a Beckman Model G pH meter.

At the higher acid concentrations shown in Figure 2, no attempt was made to keep a constant ionic strength; the solutions contained only the acid named, plus squaric acid in concentration 2.00×10^{-4} *M*. The ordinates of the graphs give the absorbance in 2-mm cells. Thus the molar absorptivity is 2.54×10^4 at pH 5.45 and 270 mμ.

The data of Figure 1 show a good isosbestic point, and above pH 2 the absorbance at 269 mμ is a linear function of the fraction of acid ionized if we consider the acid to be monobasic with $K_a = 6.2 \times 10^{-4}$. For curve *e* (pH 1.96) the absorbance is less than that estimated in this way. These data, then, are consistent with a value for K_1 of the order 2×10^{-2}.

In the hope of obtaining a value for K_1 from spectroscopic data, a series of curves were recorded at ionic strength 1.0. They are not shown, as they were of no use for this purpose. The curves of Figure 2 show that at acidities of 1.0 *M* and higher, the absorption spectra change with acidity in a very complex manner. We suggest that in addition to the uncharged acid $C_4H_2O_4$, protonated species occur, and that the degree of hydration may also be a factor.

Solubilities of Metal Complexes. (a) The Iron(III) Complex. This compound precipitates slowly from solution when solutions of ferric salts are mixed with a slight excess of squaric acid and the pH is adjusted to a value between 1 and 3. The compound is deep purple; its supersaturated solutions have maximum absorbances at 540 mμ, and a series of tests in which Fe(III) chloride and the acid were mixed at constant total molarity but varying ratios showed the absorbance to be a maximum when the mole ratio was 1:1. The same conclusion was reached by analyzing the purplish-black solid which separated out; determinations of iron, carbon, and hydrogen agreed with the formula $Fe(C_4O_4)OH \cdot 3H_2O$. *Anal.* Calcd: C, 20.10; H, 2.95; Fe, 23.38. Found: C, 20.80; H, 2.96; Fe, 21.6. The compound retained its water of hydration even after storing in a vacuum desiccator over phosphoric anhydride for 1 month. The composition agrees with that found by West.[10]

A series of tests were made in which 0.0230 mmole of Fe(III) chloride and 0.388 mmole of squaric acid were mixed in the presence of hydrochloric acid with 5 *M* sodium hydroxide added to adjust the pH. The solutions after mixing were 0.22 *M* in sodium chloride. They were allowed to stand at room temperature. Precipitation was apparently complete after 10 days, for the solution composition did not change. Then the pH, iron concentration, and total squaric acid concentration were determined in the solution as previously described. Using our value of K_2, values of the "solubility product," $[Fe^{3+}][C_4O_4^{2-}][OH^-]$, were calculated. They were as follows: pH 1.61, log $K_{sp} = -20.35$; pH 2.08, log $K_{sp} = -19.61$; and pH 2.33, log K_{sp} =

(8) A. A. Noyes, *Z. Physik. Chem.*, **11**, 495 (1893).

(9) A. Albert and E. P. Serjeant, "Ionization Constants of Acids and Bases," Methuen and Co., London, 1962, p 52.

(10) R. West and H. Y. Niu, *J. Am. Chem. Soc.*, **85**, 2589 (1963).

-19.28. These are corrected for the association of the ferric iron with Cl^- and OH^-.[11] The increasing values of K with increasing pH suggest that soluble negatively charged iron–squarate complexes are formed, but lack of time precluded further investigation.

(*b*) *The Copper(II) Complex.* When solutions of squaric acid and copper(II) are mixed at pH values near 2, a yellow precipitate is formed. This was not investigated as extensively as the iron(III) complex, but values of the solubility product $[Cu^{2+}][C_4O_4^{2-}]$ of the order of 10^{-9} were obtained, and again it seemed that they increased with increasing pH; log K_{sp} was -9.3 at pH 1.18 and -8.8 at pH 2.50. The ionic strength was maintained at 0.10 with sodium nitrate.

Anal. Calcd for $CuC_4O_4 \cdot 2H_2O$: C, 22.7; H, 1.91; Cu, 30.0. Found: C, 22.9; H, 3.56; Cu 29.3.

Acknowledgments. Confirmatory work by Lois Schloemer and Jon Parcher is gratefully acknowledged. The carbon and hydrogen analyses were performed by Huffman Microanalytical Laboratories, Wheatridge, Colo.

(11) L. G. Sillén and A. E. Martell, "Stability Constants of Metal–Ion Complexes," The Chemical Society, London, 1964.

The Radiolysis of Ethanol. V. Reactions of the Primary Reducing Species in the Liquid Phase[1]

by J. C. Russell and G. R. Freeman

Chemistry Department, University of Alberta, Edmonton, Alberta, Canada *(Received June 27, 1966)*

A study has been made of the effects of temperature, acid, and nitrous oxide on the yields of the hydrogen precursors in the γ radiolysis of liquid ethanol. The yields of the free-ion solvated electrons and of those that undergo geminate recombination have been calculated and compared to the experimental results. The yields of the various reducing species at 25° were $G(H) = 2.0$, $G(e^-_{solv})_{fi} = 1.2$, G(geminate recombination) = 1.9, $G(X) = 0.8$, and $G(Y) = 1.0$. Species X reacts with acid to form hydrogen, but its identity is unknown. Species Y forms hydrogen at high temperatures and it might be an excited molecule.

Introduction

Recent studies of the radiolysis of liquid ethanol have shown that there are at least three precursors of hydrogen.[2,3] Furthermore, the hydrogen yield is increased by the addition of an inorganic acid to the ethanol before radiolysis.[2a] This effect has been attributed to scavenging of solvated electrons by the acid.[2a] The yield of solvated electrons (free ions) in ethanol has been estimated to be $G(e^-_{solv})_{fi} = 0.8$.[2b] In another study[3] it was estimated that $G(e^-_{solv})_{fi} = 0.9$ plus $G(e^-)_{sp} = 0.75$ for electrons scavenged in the spur.

Nitrous oxide in water is known to react with hydrated electrons with a high specific rate ($k_{e^-+N_2O} = 7 \times 10^9\ M^{-1}\ sec^{-1}$).[4,5] Nitrous oxide reacts with hydrogen atoms at a much slower rate ($k_{H+N_2O} = 2 \times 10^6\ M^{-1}\ sec^{-1}$).[6] Thus in a medium such as ethanol, where the bulk of the medium reacts rapidly with hydrogen atoms ($k_{H+C_2H_5OH} = 1.5 \times 10^7\ M^{-1}\ sec^{-1}$),[7] the reaction of hydrogen atoms with nitrous oxide is probably of no consequence.

The great advantage of nitrous oxide as a scavenger is that reaction with an electron gives rise to nitrogen which is easily measured and provides a direct measure of the extent of reaction.

Changing the temperature of ethanol over a wide range drastically alters the internal characteristics, such as the viscosity and dielectric constant, of the liquid. These changes might be expected to cause some variation in the yields or reactions of the hydrogen precursors.

The present study was initiated in order to obtain a more accurate measure of the yields of the hydrogen precursors, and in particular to compare the calculated and experimental yields of free-ion solvated electrons.

Experimental Section

Apparatus. The 10-ml samples were irradiated in Pyrex glass cells with a 38-mm o.d. bulb and a bulbous, easily cleaned break-seal. They were filled through a side arm which was sealed off after filling. Such cells, if strain free, will contain a pressure of 16 atm. The total volume of each cell was approximately 30 ml. The cells were cleaned with permanganic acid, rinsed with a dilute solution of HNO_3 and H_2O_2, and rinsed repeatedly with triply distilled water. They were then

(1) This work received financial support from the National Research Council of Canada.

(2) (a) G. E. Adams and R. D. Sedgewick, *Trans. Faraday Soc.*, **60**, 865 (1964); (b) J. J. Myron and G. R. Freeman, *Can. J. Chem.*, **43**, 381 (1965).

(3) E. Hayon and M. Moreau, *J. Phys. Chem.*, **69**, 4053 (1965).

(4) F. S. Dainton and D. B. Peterson, *Proc. Roy. Soc.* (London), **A267**, 443 (1962).

(5) S. Gordon, E. J. Hart, M. S. Matheson, J. Rabani, and J. K. Thomas, *Discussions Faraday Soc.*, **36**, 193 (1963).

(6) F. S. Dainton and D. C. Walker, *Proc. Roy. Soc.* (London), **A285**, 339 (1965).

(7) J. P. Sweet and J. Thomas, *J. Phys. Chem.*, **68**, 1363 (1964).

evacuated, heated with a flame, and pumped under vacuum for 1 hr before filling.

Irradiations were performed in a Gammacell 220 (Atomic Energy of Canada Ltd.) containing ^{60}Co. A glass dewar vessel fixed with epoxy resin to a metal positioning plate was used to hold the samples, which were fixed in a metal jig. All irradiations were performed with a liquid thermostating agent in the dewar; water was used for temperatures between 0 and 90°, ethanol was used for temperatures below 0°, and glycerol was used for temperatures above 90°. The temperature of the sample during any given irradiation was constant within ±1°.

The dose rate was adjusted for the slight difference caused by the differing electron densities of the baths at the various temperatures. The dose rate was approximately 5×10^{17} ev/ml min in ethanol and the total dose was 1.5×10^{17} ev/ml.

The yield of gaseous products was determined by refluxing the sample in a vacuum line and passing the gases so obtained through two traps cooled by liquid nitrogen. The pressure and volume were then measured in a Teopler–McLeod gauge and the gases analyzed by gas chromatography. A 2.5-m molecular sieve column, helium carrier gas, and a thermal conductivity detector were used.

The dielectric constant of ethanol was measured at different temperatures using a variable capacitor mounted in a stainless steel cell which held the liquid under measurement. The variable capacitor permitted the measurement of the stray capacitance of the system. A modified General Radio Type 1304-B beat frequency audio generator, with the experimental cell as an external frequency-determining capacitor, was used as an oscillator. The change in capacitance of the experimental cell was determined with a General Radio Type 1422-D standard variable capacitor connected in parallel. The oscillator frequency was maintained at 60 cps and monitored with an oscilloscope. The temperature of the cell was measured with an iron–constantan thermocouple in contact with the liquid.

Materials and Sample Preparation. Benzene-free absolute ethanol from the Reliance Chemical Co. was used. In order to remove the trace amounts of acetaldehyde present, 2 l. of the alcohol was refluxed for 2 hr with 3 g of 2,4-dinitrophenylhydrazine and 2 ml of concentrated sulfuric acid. It was then distilled through a column packed with glass helices into a reservoir attached to a vacuum line. During the refluxing and distillation, the alcohol and distillation system were protected from atmospheric oxygen and moisture by a stream of dry nitrogen. The purified ethanol was degassed and stored under vacuum in a Pyrex vessel.

Samples were prepared by vacuum distilling ethanol from the reservoir into a measuring tube and then redistilling it into the sample cell through the side arm. Nitrous oxide and/or hydrogen chloride were added by condensation onto the frozen sample, if required, and the cell was sealed off with the sample maintained at −196°.

Nitrous oxide was purified by trap-to-trap sublimation in a vacuum line, discarding the first and last portions, and stored in a Pyrex reservoir. It was always recondensed and pumped upon at −196° before use. Hydrogen chloride was subjected to a similar procedure and also stored in a Pyrex bulb.

Results

The yield of hydrogen at 25° and 1.5×10^{17} ev/ml was found to be $G(H_2) = 5.1 \pm 0.1$.

Figures 1–4 show the effect of the concentration of nitrous oxide on the yields of nitrogen and hydrogen. Those results marked "acidic" refer to experiments in which a low concentration (between 5×10^{-5} and 5×15^{-4} M) of hydrogen chloride was also added. The values for $G(N_2)$ have been corrected by a method which will be discussed later. The lines through the nitrogen yields were calculated theoretically following a method published elsewhere[8] and will be discussed later. The other lines were drawn to suit the experimental points.

A correction to the nitrogen yield was made for the direct radiolysis of nitrous oxide in the high concentration solutions. It was assumed that the amount of energy absorbed by the nitrous oxide was proportional to its electron fraction in the solution and that $G(N_2) = 10$ for direct radiolysis.[9]

The concentration of nitrous oxide in samples at −112° was calculated assuming that all the nitrous oxide dissolved at that temperature. At 25° data available[10] give $\alpha = 2.57$, where $\alpha = (273.1/T)(C_{liq}/C_{gas})$, and C_{liq} and C_{gas} are the concentrations of nitrous oxide in the liquid and gas phases, respectively. This permits the calculation of the concentration of nitrous oxide in the sample if the volume of the cell is known. The cell volumes were measured at the conclusion of each analysis. The available data on the solubility of nitrous oxide in ethanol only extend from 18 to 36°. However, it was found that a plot of α *vs.* $1/T$ gives a straight line, and this was extrapolated to give estimates for α at 90 and 145°. The values used were $\alpha_{90°} = 1.0$ and $\alpha_{145°} = 0.55$. An error in these

(8) G. R. Freeman, *J. Chem. Phys.*, in press.

(9) F. T. Jones and T. J. Sworski, *J. Phys. Chem.*, 70, 1546 (1966).

(10) "International Critical Tables," McGraw-Hill Book Co., New York, N. Y., 1926.

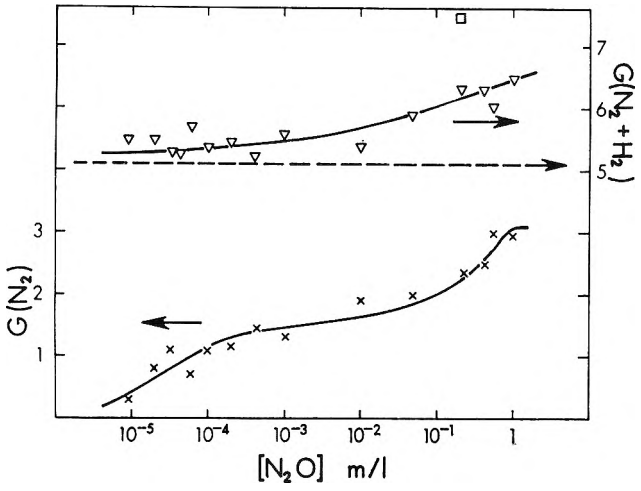

Figure 1. Effect of nitrous oxide concentration at −112°: ×, N_2; ▽, $N_2 + H_2$; □, $N_2 + H_2$ from acidic ethanol.

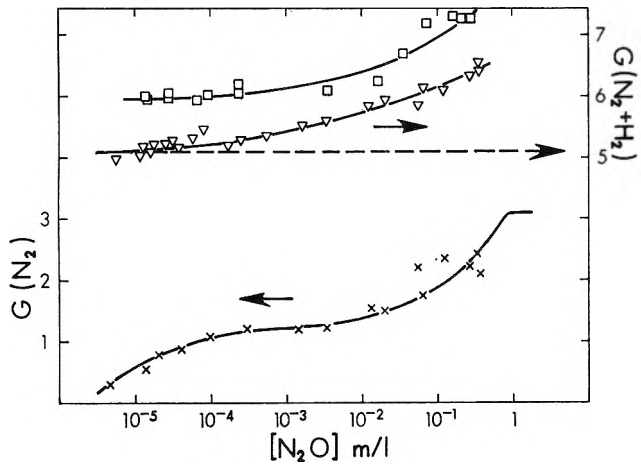

Figure 2. Effect of nitrous oxide concentration at 25°: ×, N_2; ▽, $N_2 + H_2$; □, $N_2 + H_2$ from acidic ethanol.

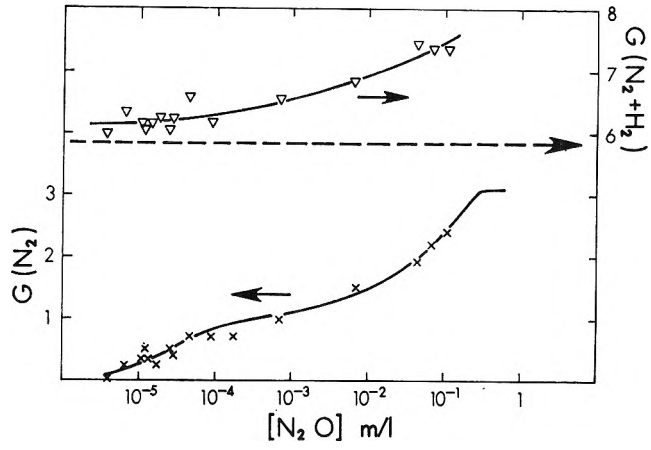

Figure 3. Effect of nitrous oxide concentration at 90°: ×, N_2; ▽, $N_2 + H_2$.

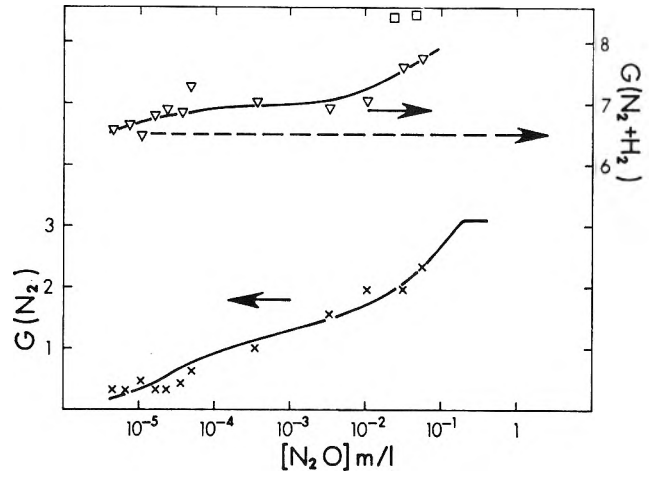

Figure 4. Effect of nitrous oxide concentration at 145°: ×, N_2; ▽, $N_2 + H_2$; □, $N_2 + H_2$ from acidic ethanol.

values would shift the entire concentration scale of Figures 3 and 4 by the corresponding amount, but it would not affect the shape of the curves.

The presence of hydrogen chloride at concentrations greater than 5×10^{-6} M increased $G(H_2)$ to 5.9 ± 0.1, independent of the acid concentration, in confirmation of the results of Fletcher.[11] At lower acid concentrations the value of $G(H_2)$ was less than 5.9. Acid concentrations as high as 1 M caused no increase above $G(H_2) = 5.9$.

A study was also made of the effect of high concentrations of hydrogen chloride and a relatively high concentration of nitrous oxide. The results are shown in the first four columns of Table I. The concentration of $C_2H_5OH_2^+$ was computed on the basis that $K_{diss} = 0.015$ for hydrogen chloride in ethanol.[12]

Figure 5 shows the yields of hydrogen as a function of temperature. It may be seen that the yields were independent of temperature between −112 and 25°. Between 25 and 150° the hydrogen yields rise by approximately 1.0 G unit. At all temperatures, and independent of the presence of nitrous oxide, the presence of hydrogen chloride raised the yields by 0.8 ± 0.1 G unit.

The results indicate that both temperature and acid may increase the over-all yield of hydrogen and nitrogen (the reduction yield). In the limit, each does this independent of the effect of the other. The yields of hydrogen as a function of temperature, with and without acid present (Figure 5), may be superimposed on the lines

(11) J. W. Fletcher, unpublished results.

(12) I. I. Bezman and F. H. Nerhock, *J. Am. Chem. Soc.*, 67, 1330 (1945).

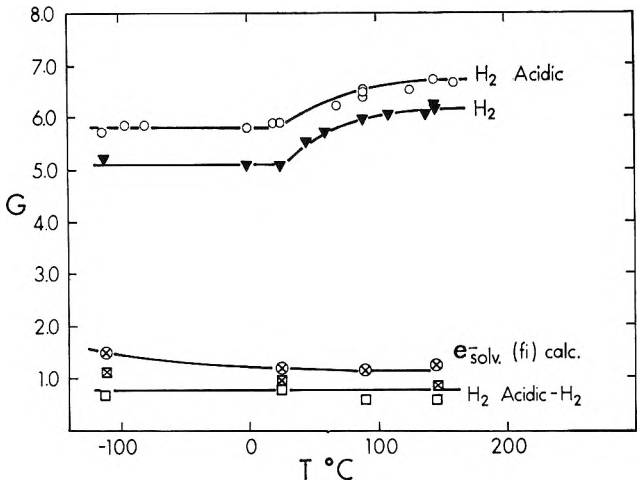

Figure 5. Effect of temperature: ▼, H_2 from pure ethanol; O, H_2 from acidic ethanol; □, H_2 from acidic ethanol − H_2 from pure ethanol; ⊠, (N_2 + H_2) from acid ethanol − (N_2 + H_2) from pure ethanol at ~0.1 *M* N_2O; ⊗, calculated yield of $(e^-_{solv})_{fi}$.

representing the yields at −112 to 25° and, if this is done, the points at the higher temperatures all lie within experimental error of a line drawn giving equal weight to all points. This line gives a rise in $G(H_2)$ = 1.0 ± 0.1 between 25 and 150°. There is a similar variation of $G(H_2)$ with temperature at both high and low concentrations of nitrous oxide.

Table I: Effect of High Concentrations of Acid on $G(N_2)$

$[C_2H_5OH_2^+]$, *M*	$[N_2O]$, *M*	$\frac{[N_2O]}{[N_2O] + 2[C_2H_5OH_2^+]}$	$G(N_2)$	$G(N_2)_{calcd}$
0.177	4.1×10^{-2}	0.103	0.42	0.28
0.125	3.4×10^{-2}	0.120	0.47	0.32
4.9×10^{-2}	4.1×10^{-2}	0.295	0.80	0.80
2.1×10^{-2}	3.8×10^{-2}	0.475	1.35	1.28

Experiments were not conducted at higher temperatures because above 150° the vapor pressure of ethanol rapidly exceeds that which may be contained within the glass cells used.

Knowledge of the dielectric constant is required for the nonhomogeneous kinetic calculations of scavenging and free-ion solvated electron yields. The dielectric constant, ϵ, of ethanol was measured over the temperature range −112 to 79°. The results are shown in Figure 6. An extrapolation of the curve was used to estimate ϵ at 90 and 145°. The values shown were determined at 60 cps.

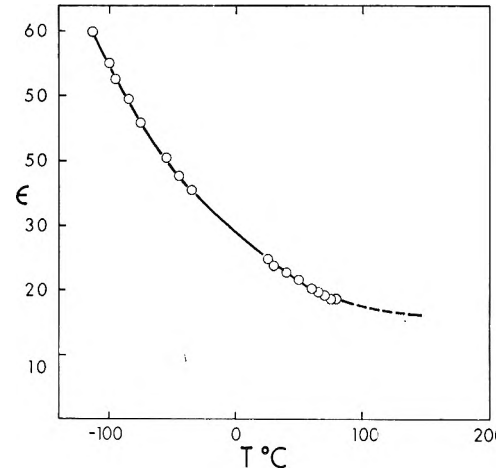

Figure 6. Dielectric constant as a function of temperature.

Discussion

The present results are consistent with those reported earlier,[2,3] but the previously suggested mechanisms require extension to explain the variation of the hydrogen and nitrogen yields as functions of temperature and acidity in both the pure ethanol and the ethanol–nitrous oxide systems.

In order to explain the acid effect adequately, it is necessary to postulate a species, to be represented by the symbol X, which reacts with hydrogen ions to give either H or H_2. This species does not react with N_2O and in the absence of H^+ does not give rise to hydrogen. The increased yields at higher temperatures appear to be due to another species, to be represented by Y, which must undergo competing reactions, one of which gives rise to hydrogen or a hydrogen atom, and the other leads to deactivation.

The mechanism which follows is an extension of that of Myron and Freeman.[2b] It is also based upon consideration of the fate of ionic species in irradiated liquids following a previously described approach.[8,13] The square brackets indicate that the species are inside a spur. The yields (in parentheses) specified for the reactions

$$CH_3CH_2OH \xrightarrow{\sim\sim} [CH_3CH_2OH^+ + e^-] \quad (1.1) \quad (1)$$

$$CH_3CH_2OH \xrightarrow{\sim\sim} [CH_3CHOH^+ + H + e^-] \quad (2.0) \quad (2)$$

$$CH_3CH_2OH \xrightarrow{\sim\sim} [X] \quad (0.8) \quad (3)$$

$$CH_3CH_2OH \xrightarrow{\sim\sim} [Y] \quad (1.0) \quad (4)$$

$$[e^-] \longrightarrow [e^-_{solv}] \quad (5)$$

(13) G. R. Freeman and J. M. Fayadh, *J. Chem. Phys.*, **43**, 86 (1965).

$$[C_2H_5OH^+ + C_2H_5OH] \longrightarrow [C_2H_5OH_2^+ + CH_3CH_2O] \quad (6)$$

$$[CH_3CHOH^+ + C_2H_5OH] \longrightarrow [CH_3CHO + C_2H_5OH_2^+] \quad (7)$$

$$[e^-_{solv} + C_2H_5OH_2^+] \longrightarrow [H + C_2H_5OH] \quad (1.9) \quad (8)$$

$$[e^-_{solv} + C_2H_5OH_2^+] \longrightarrow e^-_{solv} + C_2H_5OH_2^+ \text{ (free ions)} \quad (1.2) \quad (9)$$

are based on the experimental yields as well as the theoretical considerations. The yield of free-ion solvated electrons (free ions) was calculated according to Freeman and Fayadh[13] assuming G(total ionization) = 3.1. Those electrons which do not escape the spur will undergo geminate recombination with positive ions. The yield of solvated electrons as a function of time was calculated as previously described.[8] This indicated that at times of less than 10^{-10} sec the majority of the electrons had not yet undergone recombination and that they are therefore solvated before recombination can take place. The calculations will be discussed later.

The hydrogen atoms attack the ethanol.

$$H + CH_3CH_2OH \longrightarrow CH_3CHOH + H_2 \quad (10)$$

The free-ion solvated electrons decay giving rise to further hydrogen atoms.

$$e^-_{solv} + CH_3CH_2OH \longrightarrow H + CH_3CH_2O^- \quad (11)$$

At the low doses used in the present experiments, the concentration of the product acetaldehyde was always so low that reaction 12 was negligible.[2b]

$$e^-_{solv} + CH_3CHO \longrightarrow CH_3CHO^- \quad (12)$$

The addition of a low concentration of acid will cause reaction 11 to be replaced by reaction 13. However,

$$e^-_{solv} + CH_3CH_2OH_2^+ \longrightarrow H + CH_3CH_2OH \quad (13)$$

this would not alter the observed yield of hydrogen. Since small amounts of acid did cause the hydrogen yield to increase, a reactive species X must be postulated to undergo reactions 14 and 15. The data in Figures 1–5

$$X \longrightarrow \text{no product} \quad (14)$$

$$X + C_2H_5OH_2^+ \longrightarrow H \text{ or } H_2 + \text{products} \quad (15)$$

show that neither high concentrations of nitrous oxide nor high temperatures interfere with reaction 15. A high concentration of acid caused no further increase in hydrogen yield because it did not alter the number of hydrogen atoms formed.

Nitrous oxide will react with the free-ion solvated electrons in the bulk of the liquid, and if present in sufficient concentration will scavenge electrons within the spurs.

$$e^-_{solv} + N_2O \longrightarrow N_2 + O^- \quad (16)$$

$$[e^-_{solv} + N_2O] \longrightarrow [N_2 + O^-] \quad (17)$$

Reactions 16 and 17 should not alter the total gas ($H_2 + N_2$) yield. However, the yield does increase. Since the addition of acid above 10^{-5} M does not cause a further increase in the gas yield, the increase caused by nitrous oxide is unlikely to be due to electrons. This suggests that a secondary reaction of nitrous oxide occurs at the higher concentrations. Reaction 18 has been suggested to occur in the gas phase[14] and is a possible source of additional nitrogen in the present system. Reactions 19 and 20 would be in competition

$$O^- + N_2O \longrightarrow N_2 + O_2^- \quad (18)$$

$$O^- + C_2H_5OH \longrightarrow OH^- + CH_3CHOH \quad (19)$$

$$\longrightarrow OH + C_2H_5O^- \quad (20)$$

with reaction 18, inhibiting it except in the presence of substantial concentrations of nitrous oxide. Using the known values for the rate constants for the reactions H + C_2H_5OH[7] and H + N_2O,[6] the expected contribution to the nitrogen yield from the reaction of H + N_2O was calculated. This was found to be less than 10^{-2} G(H) under all experimental conditions.

Because of the apparent occurrence of a secondary reaction of nitrous oxide, the values of $G(N_2)$ in Figures 1–4 have been corrected by subtraction of the amount by which $G(N_2 + H_2)$ for that sample exceeded $G(H_2)$ in pure ethanol.

In the presence of a low concentration of nitrous oxide, a low concentration of acid would cause competition between reactions 13 and 16. The over-all yield would be $G(H_2 + N_2) = 5.9$, with $G(N_2)$ falling below the values found in the absence of acid. This was found experimentally. The results obtained at high concentrations of both acid and nitrous oxide indicate that competition between reactions 8 and 17 occurs (Table I).

In the presence of a high concentration of acid, reaction 21 should occur.

$$O^- + C_2H_5OH_2^+ \longrightarrow OH + C_2H_5OH \quad (21)$$

Since reactions 13, 16, 18, and 21 are assumed to be diffusion controlled, the acid should interfere with the secondary reaction of nitrous oxide, reaction 18, in a similar manner to which it interferes with reaction 16. The OH generated in reaction 21 would not attack the nitrous oxide but would react with the ethanol. The

(14) G. R. A. Johnson and J. M. Warman, *Nature*, **203**, 73 (1964).

value of $k(e^-_{solv} + H_3O^+)/k(e^-_{solv} + N_2O) = 3$ found in water[15] is probably due to the abnormally high diffusion coefficient of protons in water. The diffusion coefficient of protons in ethanol is probably also abnormally high, although less so than in water, so for the lack of a better value it is assumed that $k_{13}/k_{16} = 2$. Similarly, it is assumed that $k_8/k_{17} = k_{21}/k_{18} = 2$. The calculated nitrogen yields were therefore obtained using eq i.

$$G(N_2)_{calcd} = 2.7\frac{[N_2O]}{[N_2O] + 2[C_2H_5OH_2^+]} \quad \text{(i)}$$

At $[N_2O] = 4.0 \times 10^{-3}$ M, in the absence of acid, $G(N_2) = 2.7$, uncorrected for secondary reaction. Within the uncertainties in the effective acid concentrations and the rate constant ratios, the results indicate that nitrous oxide and acid compete for the same species. Although nitrous oxide does not compete with acid for species X, acid competes for all of the species with which nitrous oxide reacts.

The results in Figures 1–5 show that there is a species, to be represented as Y, which is sensitive to temperature but not to nitrous oxide or acid. At temperatures above 25°, reaction 23 proceeds at the expense of reaction 22.

$$Y \xrightarrow{\text{low temp}} \text{deactivation} \quad (22)$$

$$Y \xrightarrow{\text{high temp}} H \text{ or } H_2 + \text{products} \quad (23)$$

It is not possible to identify unambiguously the species Y. However, there are several definite requirements for any description of the species. It must undergo two competing reactions such as reactions 22 and 23. The relative rates of the two reactions change rapidly over the temperature range 25 to 90°. If the assumption is made that the rate of reaction 22 is temperature independent, then a crude estimate may be made of the energy of activation for reaction 23. This is of the order of 10 kcal/mole. Furthermore, the yield of species Y is unaffected by the addition of either hydrogen chloride or nitrous oxide. Species Y might be an excited molecule that is deactivated at low temperatures, but with the additional increment of thermal energy acquired at high temperatures it can decompose to yield H_2 or H.

The identity of the species X which reacts in the presence of acid to give hydrogen is elusive. The entity responsible for the observed effects must undergo reactions similar to (14) and (15). The suggestion of Adams and Sedgewick[2a] that the increased yield on addition of acid is due to scavenging of solvated electrons is not compatible with the present results. In the presence of low concentrations of acid, the free-ion solvated electrons do react to form hydrogen atoms. However, nuless the experiments are carried out at high doses, where acetaldehyde scavenging of the electrons is important, this would have no effect on the yield of hydrogen. The results indicate that there is competition between the acid and nitrous oxide for the solvated electrons. In addition to this, however, acid increases the over-all reduction yield by 0.8 G unit, and this is true even under conditions where the solvated electrons, including those which normally undergo geminate recombination, are scavenged by nitrous oxide.

The effect of acid on the radiolysis of ethanol will be the subject of another publication from this laboratory[11] and will be treated in greater detail there.

The yield of free-ion solvated electrons was computed using the nonhomogeneous kinetics of Freeman and Fayadh.[13] This approach takes into account the spectrum of initial ion separations and allows an approximate computation of the proportion which escape geminate recombination. If G(total ionization) is known or assumed, then the approximate yield of free ions may be calculated.

A spectrum of $N(y)$ *vs.* y, the number of ion pairs formed with an initial separation distance y, was computed for ethanol at each temperature.[13] The probability of escape, $\phi_{fi} = e^{-r/y}$, was computed for each value of y in the step function $N(y)$ *vs.* y, where $r = \xi^2/\epsilon kT$ and ξ is the charge on an ion (4.80×10^{-10} esu), ϵ is the dielectric constant, k is the Boltzmann constant, and T is the absolute temperature. G(free ion) is then given by the summation equation

$$G(\text{free ion}) = G(\text{total ionization})\frac{\sum N(y)\phi_{fi}}{\sum N(y)} \quad \text{(ii)}$$

The same general theory[8] permits an approximate calculation of the effect of a scavenger such as nitrous oxide which can interfere with the geminate recombination of the electrons. If Φ_- is the probability of reaction with the scavenger before geminate recombination takes place, then

$$\Phi_- = \phi_{fi} + \phi_-(1 - \phi_{fi}) \quad \text{(iii)}$$

where

$$\phi_- = 1 - (1 - f_- N_s)^{\beta_- \nu} \quad \text{(iv)}$$

and

$$\beta_- = \frac{1}{(u_+ + u_-)}\left[\frac{b_- D_-}{\lambda_-^2} + \frac{b_s D_s}{\lambda_s^2}\right] \text{ v/cm}^2 \quad \text{(v)}$$

(15) L. M. Dorfman and M. S. Matheson, *Progr. Reaction Kinetics*, 3, 237 (1965).

$$\nu = \frac{6\epsilon(y^3 - r_0^3)}{4.32 \times 10^{-7}} \text{ cm}^2/\text{v} \qquad \text{(vi)}$$

N_s is the mole fraction of the scavenger, $0 \leqslant f_- \leqslant 1$ is the encounter efficiency of reaction 17, D_- and D_s are the diffusion coefficients of the solvated electrons and scavenger, respectively, λ_- and λ_s are the respective average jump distances, b_- and b_s are the numbers of new neighbors encountered per jump, u_+ and u_- are the positive ion and electron mobilities, and r_0 is the encounter radius of reaction 8.

These equations were solved with the aid of the $N(y)$ *vs.* y spectrum. The lines on the experimental plots (Figures 1–4) were computed using the equation

$$G(\text{N}_2) = G(\text{total ionization})\frac{\sum N(y)\Phi_-}{\sum N(y)} \qquad \text{(vii)}$$

G(total ionization) was taken as 3.1 as this value gives the best fit with the experimental yields.

The equation

$$t_{gr} = \frac{\epsilon(y^3 - r_0^3)}{4.32 \times 10^{-7}(u_+ + u_-)} \text{ sec} \qquad \text{(viii)}$$

can be used to calculate the average geminate recombination time of ions with an initial separation distance y, and so can be used to convert the $N(y)$ *vs.* y spectrum into an $N(t_{gr})$ *vs.* t_{gr} spectrum.[8] Then the number of ions that survive at a time $t < 10^{-6}$ sec is given by

$$N(t) = \sum_{t_{gr}=t}^{\infty} N(t_{gr})(1 - \phi_{fi}) + \sum N(y)\phi_{fi} \qquad \text{(ix)}$$

The yield of solvated electrons that exists at time t in pure ethanol is then

$$G(e^-_{solv})_t = G(\text{total ionization})\frac{N(t)}{N(0)} \qquad \text{(x)}$$

where $N(0)$ is the number of solvated electrons at $t = 0$. The calculation showed that at times $<10^{-10}$ sec the majority of electrons, including those which will undergo geminate recombination, have not yet been neutralized and thus will have time to become solvated. For this reason, the electrons within the spur are written as solvated in the mechanism.

The calculation of the $N(y)$ *vs.* y spectrum requires knowledge of the density of the medium. Existing data[10] were used for the 25, 90, and 145° calculations. The density of ethanol was measured at −112° and found to be 0.903 ± 0.010 g/ml, and this value was used in the calculations.

The values of ϵ were taken from Figure 6. The value of β_- was adjusted by trial and error to give the best fit with the experimental yields. The final calculations for the 25° experiments were made using $\beta_- = 2.4 \times 10^{13}$ v/cm², which can be rationalized in terms of the following quantities.

$(u_+ + u_-) = 3 \times 10^{-3}$ cm²/v sec[16]

	$r_0 = 1.0 \times 10^{-7}$ cm
$b_- = 4$	$b_s = 4$
$D_- = 3 \times 10^{-5}$ cm²/sec	$D_s = 2 \times 10^{-5}$ cm²/sec
$\lambda_-^2 = 28 \times 10^{-16}$ cm²	$\lambda_s^2 = 28 \times 10^{-16}$ cm²

These quantities, especially D, will change with temperature. This variation is not precisely known, and the calculation is approximate. The most suitable value of β_- varied with temperature ($\beta_- = 1.0 \times 10^{13}$ v/cm² at −112°, 2.4×10^{13} at 25°, 7.9×10^{13} at 90°, and 1.9×10^{14} at 145°). This variation may be understood in terms of the variation of the values of the quantities in eq v. The calculations were made assuming f_- was unity.

The calculated nitrogen yields as a function of nitrous oxide concentration agree favorably with the experimental results (Figures 1–4). The low concentration regions, where only the free-ion solvated electrons would be scavenged, were computed on the basis of competition between reactions 11 and 16. The ratio of the rate constants k_{16}/k_{11} was adjusted to give the best fit with the experimental yields. The values of the ratios used were $k_{16}/k_{11} = 5.6 \times 10^5$ at −112°, 1.0×10^6 at 25°, 5.0×10^5 at 90°, and 5.4×10^5 at 145°. Thus the ratio was not sensitive to the temperature, although the temperature range and hence the variation in viscosity and other factors is very large. The value $k_{16} = 7 \times 10^9\ M^{-1}$ sec^{-1} in water at 25°[4,5] suggests that the reaction is diffusion controlled. Since the viscosity of ethanol changes drastically over the temperature range studied, the rate constant of reaction 16 would be expected to show similar changes. The ratio k_{16}/k_{11} does not, and this suggests that viscosity has a similar effect on k_{11} and k_{16}. If it is assumed that k_{16} has the same value in water and in ethanol at 25°, the value of k_{11} would appear to be approximately $6 \times 10^3\ M^{-1}$ sec^{-1} at this temperature. This implies a half-life for the free-ion solvated electron in ethanol of approximately 7 μsec. Myron and Freeman[2b] estimated the half-life to be 3 μsec at 25°. Since neither estimate is of great accuracy, the agreement is satisfactory.

The present results can be compared to those of Hayon and Moreau,[3] who studied the effect of $LiNO_3$,

(16) The corresponding sum of mobilities in water is 5.4×10^{-3} cm²/v sec if the migrating positive species is a proton; $u(H_{aq}^+) = 3.6 \times 10^{-3}$ cm²/v sec. See S. Glasstone, "Textbook of Physical Chemistry," D. Van Nostrand Co., New York, N. Y., 1946, p 909. $u(e_{aq}^-) = 1.8 \times 10^{-3}$ cm²/v sec; see footnotes of Table II, ref 8.

$NiCl_2$, and chloroacetic acid on the H_2 yield in ethanol. Their results show curves which are similar to those in Figures 1–4. They interpreted these in terms of $G(e^-_{solv})_{fi} = 0.90 \pm 0.10$ and the scavenging of electrons in the spurs to give $G(e^-)_{sp} = 0.75 \pm 0.10$. Thus they found a total of $G(e^-)_T = 1.65 \pm 0.2$. The present results and calculations are consistent with $G(e^-_{solv})_{fi} = 1.2$, $G(e^-_{solv})_{gr} = 1.9$, and $G(e^-_{solv})_T = 3.1$. The fact that a much higher value for the total yield of solvated electrons was found in the present work may indicate that the rates of reaction of the solutes used by Hayon and Moreau with the solvated electrons in ethanol are lower than they presumed. By comparison with the results of Adams and Sedgewick for the effect of acid,[2a] they concluded that increases in over-all yield on addition of some of the scavengers were due to scavenging of solvated electrons in the spurs. It is felt that an incomplete understanding of the true effects of acid on the radiolysis may have resulted in an incorrect comparison.

There is an apparent disagreement between the proposed mechanism and the previously accepted[2,3,17] yield of free-ion solvated electrons in γ irradiated ethanol. [G(free ion) = 0.9 ± 0.1, compared to the present estimate of 1.2.] Although the present estimate might be too high, it is quite possible that the previous estimates are too low because of the lack of good plateaus in the scavenger plots (see Figure 2 as well as ref 2 and 3). In effect, the concentration of scavenger required to react with all free-ion solvated electrons is not radically different from that which will begin to react in the spurs. In comparison, the case of water is quite different. A value of $k_{e_{aq}^- + H_2O} = 16\ M^{-1}\ sec^{-1}$ has been quoted.[18] This corresponds to a half-life of the order of 1 msec. Thus in very pure water the solvated electron has a long lifetime and may be scavenged efficiently by a low concentration of scavenger. This suggests why very good scavenger plots may be obtained in aqueous systems and not in ethanolic ones.

Taub, *et al.*,[17] estimated that $G(e^-_{solv})_{fi} = 1.0 \pm 0.3$, which is consistent with the present value of 1.2.

In conclusion, the reaction mechanism advanced may be used to explain the yields of primary reducing species and their variation under differing conditions. The simple mechanism for nonhomogeneous kinetics is as successful in treating the results as the limitations of the method could permit. This agreement must be considered further evidence in favor of the theory.[8] The shape of the scavenger curves is a function of the lifetime of the free-ion solvated electrons in the medium. The lifetime of free-ion solvated electrons in ethanol appears to be approximately 3–7 μsec compared to 1 msec in water. The existence of four distinguishable hydrogen precursors has been demonstrated. Species Y might be an excited molecule, but the identity of species X is unknown.

(17) I. A. Taub, D. A. Harter, M. C. Sauer, and L. M. Dorfman, *J. Chem. Phys.*, 41, 979 (1964).

(18) E. I. Hart, quoted by J. Rabani in "Solvated Electron," Advances in Chemistry Series, No. 50, American Chemical Society, Washington, D. C., 1965, p 251.

NOTES

Disproportionation and Combination Reactions of Isopropoxy Radicals with Nitric Oxide

by Barbara E. Ludwig and G. R. McMillan

Department of Chemistry, Western Reserve University, Cleveland, Ohio 44106 *(Received August 1, 1966)*

Meager information is available about the temperature dependence of disproportionation and combination reactions of simple radicals other than the alkyls. For the isopropoxy–nitric oxide pair, k_1/k_2 was found to be 0.15 at 26° and 0.20 at 77° from results of photolysis of diisopropyl peroxide in the presence of nitric oxide.[1] The data showed considerable scatter, especially at 77°, and we agree with Arden, Phillips, and Shaw[2]

$$(CH_3)_2CHO + NO \longrightarrow CH_3COCH_3 + HNO \quad (1)$$

$$\longrightarrow (CH_3)_2CHONO \quad (2)$$

(1) G. R. McMillan, *J. Am. Chem. Soc.*, 83, 3018 (1961).

(2) E. A. Arden, L. Phillips, and R. Shaw, *J. Chem. Soc.*, 5126 (1964).

Table I: Pyrolysis of Diisopropyl Peroxide–Nitric Oxide Mixtures, Typical Data at 120°

Pressures, mm			Yield, molecules × 10^{-18}			
$[(CH_3)_2CHO]_2$	NO	% decompn[a]	$(CH_3)_2CHONO$	$(CH_3)_2CO$	$(CH_3)_2CHOH$	$(CH_3)_2CO$[b]/$(CH_3)_2CHONO$
4.5	22.4	7.5	3.11	0.702	0.570	0.191
6.0	40.7	4.3	1.87	0.470	0.429	0.204
6.4	26.9	3.0	1.14	0.474	0.482	0.295[c]
7.3	2.8	5.6	3.94	1.11	0.980	0.225
10.1	38.6	4.5	4.68	1.28	0.826	0.232
13.2	41.4	2.2	2.24	0.575	0.479	0.211

[a] Of peroxide. [b] Corrected, see text. [c] Packed cell.

that the ratios obtained at the two temperatures are identical within experimental uncertainty. The ratio of rate constants for disproportionation to combination of ethoxy radicals with nitric oxide has been reported to display negligible temperature dependence, the values being 0.30 at 95° and 0.31 at 135°.[2] Because these constants are important for interpretation of the primary photochemistry of alkyl nitrites, nitrates, and nitro compounds, the isopropoxy–nitric oxide reaction was studied over a wide temperature range.

Diisopropyl peroxide[1,3] was purified by fractional distillation and gas chromatography. Even with careful exclusion of room light,[1] it was impossible to reduce the acetone content of the samples below about 0.05%. Mixtures of the peroxide vapor with nitric oxide were pyrolyzed in quartz vessels of approximately 200 ml volume. A cell was packed with quartz tubing to increase the surface:volume ratio by a factor of 9. Unreacted nitric oxide and products volatile at −160° were pumped away, and the condensable fraction was analyzed by gas chromatography at 32° on a 12-ft column of tricresyl phosphate on Chromosorb W.

The main products found were isopropyl nitrite, acetone, and isopropyl alcohol, with traces of acetaldehyde and methyl nitrite. Results are shown in Table I for some of the 120° experiments. The isopropyl alcohol is probably formed in large part by hydrolysis of isopropyl nitrite and was therefore added as a correction to the isopropyl nitrite yield before calculation of the last column in Table I. The isopropyl alcohol yield at a given temperature did not depend on the variables discussed below. Some hydrolysis of alkyl nitrites always is observed on the columns used in this study. In one experiment, a small amount of *t*-pentyl nitrite was mixed with peroxide and nitric oxide and the mixture was pyrolyzed at 120° in the usual manner. The gas chromatogram showed considerable *t*-pentyl alcohol.

Over the ranges indicated, the following variables were without effect on the acetone:isopropyl nitrite ratio: pressure of diisopropyl peroxide, 2.7–14.6 mm; pressure of nitric oxide, 2.8–46.9 mm; pressure of nitric oxide:pressure of peroxide, 0.35–8.58; per cent decomposition of peroxide 2.0–12.1%; time of reaction, 0.7–1440 min; added nitrogen, 200 mm. The effect of temperature is shown in Figure 1 for temperatures at which secondary pyrolysis of isopropyl nitrite is negligible as shown by experiments on isopropyl nitrite–nitric oxide mixtures.

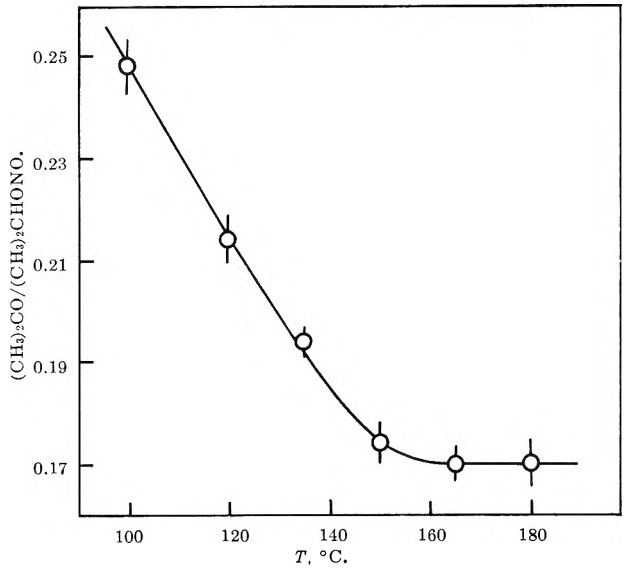

Figure 1. Temperature dependence of acetone:isopropyl nitrite ratio.

The mechanism of thermal decomposition of diethyl peroxide in the presence of nitric oxide has been discussed by Arden, Phillips, and Shaw.[2] The ratio of rate constants for disproportion to combination of ethoxy radicals with nitric oxide was calculated simply as the ratio of yields of the disproportionation and combination products. In the present system such a calculation is not generally valid. Figure 1 indicates a change in mechanism in the temperature range studied. Some side process, which the packed-cell results suggest

(3) W. A. Pryor, D. M. Huston, T. R. Fiske, T. L. Pickering, and E. Ciuffarin, *J. Am. Chem. Soc.*, **86**, 4237 (1964).

to be a surface reaction, makes a temperature-dependent contribution to the product ratio below 150°. At higher temperatures, this process is apparently overwhelmed, for the acetone to isopropyl nitrite ratio becomes temperature independent above about 160°. This constancy together with independence of the ratio of the other variables suggests the ratio be identified with k_1/k_2. The value thus obtained, 0.17, is the same as the grand average of low-temperature results (26–79°).[1] The disproportionation:combination ratio may therefore be taken as 0.17 over the range 26–180°. The isopropoxy–nitric oxide pair is evidently similar to alkyl–alkyl reactions in showing an inappreciable difference in activation energies between the two processes.

As has been pointed out,[2] a value of 0.17 for k_1/k_2 at 120° would fit well with a correlation showing the disproportionation to combination ratios for alkoxy radicals and nitric oxide to be proportional to the number of available hydrogen atoms, in contrast to results on alkyl–alkyl reactions. Such a correlation would not be expected from data on reactions of alkoxy radicals with methyl radicals, which indicate that isopropoxy disproportionates with methyl about twice as fast relative to combination as does methoxy.[4] Furthermore, a referee has pointed out that the correlation would be significant only if all the alkoxy–nitric oxide disproportionation:combination ratios were temperature independent, and this must be considered questionable in view of the apparent absence of disproportionation at 25° in the reaction of methoxy and ethoxy radicals with nitric oxide [5]

Acknowledgment. Grateful acknowledgment is made of support of this work by the Division of Air Pollution, Bureau of State Services, U. S. Public Health Service.

(4) Summarized in G. R. McMillan and J. G. Calvert, "Oxidation and Combustion Reviews," Vol. I, C. F. H. Tipper, Ed., Elsevier Publishing Co., Amsterdam, 1965, p 123.

(5) A. R. Knight and H. E. Gunning, *Can. J. Chem.*, 39, 1231, 2466 (1961).

Miscibility of Metals with Salts. VII. The Potassium–Potassium Sulfide System[1]

by A. S. Dworkin and M. A. Bredig

Oak Ridge National Laboratory, Oak Ridge, Tennessee
(Received September 8, 1966)

Our previous studies of metal–metal salt solutions[2] have dealt with systems of the type M–MX, M–MX_2, and M–MX_3, where M represents alkali, alkaline earth and rare earth metals, and X represents halide ions. This report on the phase equilibria in the K_2S–K system deals with an extension of the work to the first representative of systems M–M_2Y, where Y is a doubly charged chalcogenide ion, and where the anion-to-cation ratio is as much as a factor of 6 smaller than in the previous other extreme, the M–MX_3 systems. The significance of the stoichiometry for the electrical conductivity, *i.e.*, for the mobility of the metal electrons, was discussed earlier.[3]

The K_2S was prepared by slowly adding triply sublimed, carbon-free sulfur to excess potassium in an inert atmosphere at a controlled temperature of 180–200°. The excess potassium was then removed by distillation at 300–350° under high vacuum. The final product was analyzed for K, S, and O and found to be better than 99% K_2S with the major impurities being K and K_2O. The potassium contained less than 0.02% of other cations. All handling operations were performed under helium in a drybox.

The phase diagram was determined by thermal analysis (cooling curves). Inconel capsules with thermocouple wells were used as containers and a Pt—Pt–10% Rh thermocouple was used in conjunction with a Rubicon potentiometer and a Brown recorder to measure temperatures. The Inconel capsules were sealed under helium in a welding drybox. A rocking furnace permitted mixing of the components before each cooling curve was run.

The K–K_2S phase diagram is shown in Figure 1. The melting point T_m of 948° is considerably higher than the value of 912° reported in the literature.[4] However, the latter value was determined with K_2S which contained at least 5% impurity. The critical solution temperature T_c lies at about 900°, or about 50° below the melting point of the K_2S. The monotectic temperature T_{mon} is 883° and the monotectic concentration is 21 mole % K. The K_2S–K system thus resembles the KBr–K system except that T_c for the former lies about 180° higher.

The end of the miscibility gap at 63 mole % K is somewhat uncertain due to the very rapid increase in the sulfide solubility in the liquid metal just below the monotectic temperature. This rapid increase is, of

(1) Research sponsored by the U. S. Atomic Energy Commission under contract with the Union Carbide Corp.

(2) M. A. Bredig, "Mixtures of Metals with Molten Salts," in "Molten Salt Chemistry," M. Blander, Ed., Interscience Publishers, Inc., New York, N. Y., 1964.

(3) M. A. Bredig, *J. Chem. Phys.*, 37, 914 (1962).

(4) J. Goubeau, H. Kolb, and H. G. Krall, *Z. Anorg. Allgem. Chem.*, 236, 45 (1938).

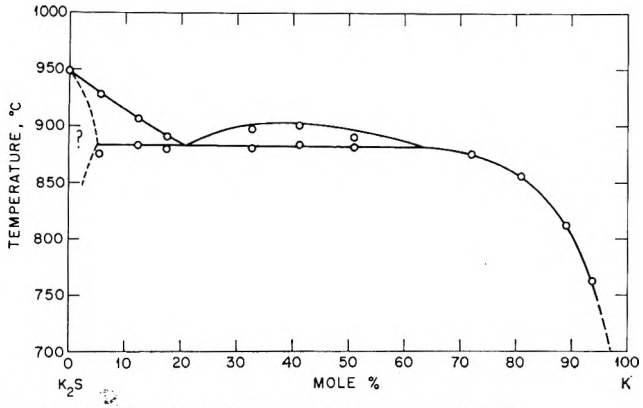

Figure 1. The phase diagram of the system K_2S–K.

course, connected with the fact that immiscibility in this system is close to being suppressed altogether. The liquid–liquid equilibrium curve was drawn as shown, namely, above rather than through the point at 51 mole % K, for two reasons: (1) to avoid having to accept an even more rapid, namely, infinitely steep increase in the K_2S solubility in liquid K near the monotectic temperature, which would be in disagreement with the existence of a finite, even though very small, region of immiscibility, and (2) because the appearance of the first cooling halt at 51 mole % K indicated some supercooling.

An attempt to interpret the liquidus near the melting point of K_2S in terms of solute species leads to the following results. From the experimental entropy of fusion of K_2S,[5] a melting point depression of

$$\frac{\Delta T}{nN_K} \approx \frac{RT_m}{\Delta S_m} = \frac{2 \times 1220}{3.16 \times 100} = 7.7°/\text{mole \% K}$$

is expected, if one assumes $n = 1$, for F-center-like or anion-like electrons singly occupying S^{2-} ion positions in the K_2S melt. If, however, the potassium metal electrons would pair up[6] in the sulfide melt to substitute for S^{2-}, $\Delta T/N_K$ would be $^1/_2 \times 7.7 = 3.85°$ per mole % of K. Observed is

$$\frac{T_m - T_{mon}}{N_{K(mon)}} = \frac{65}{21} = 3.1°/\text{mole \% K}$$

Although this experimental result appears at first glance to favor the second case, it actually cannot at this stage of the study be interpreted unambiguously, but rather in either one of two ways.

1. Electrons may occupy anion positions singly. In this case, a relatively large solubility of potassium metal in solid potassium sulfide near its melting point similar to that found for calcium in the anti-isomorphous calcium fluoride could explain the difference between $(\Delta T/N_K)_{theoret} = 7.7$ and $(\Delta T/N_K)_{exptl} = 3.1°$/mole % K. This case is supported by the straightness of the liquidus which is in disagreement with curvature due to positive deviation from Raoult's law as expected in a system with only partial miscibility of the components and as actually observed in the potassium–potassium halide systems. This is the case implied in Figure 1, where the curved solidus (dotted line) was drawn to reflect the assumed increasing positive deviation from Raoult's law, *i.e.*, a faster-than-linear increase of $\Delta N_K = N_K^{(l)} - N_K^{(s)}$ with increasing N_K.

2. If pairs of electrons would occupy S^{2-} positions in the K_2S melt and if at the same time the assumption of a rapidly increasing positive deviation from Raoult's law with increasing metal concentration were to be maintained, a comparatively much smaller solubility of K in solid K_2S would have to be assumed, perhaps of the order of 1 mole % at the monotectic temperature.

Direct experimental determination of the solid solubility or, still better, of the activity of potassium metal through measurement of the potassium vapor pressure of the solutions will be required in order to support better any assumption about the molecular structure of these solutions.

(5) A. S. Dworkin and M. A. Bredig, submitted for publication. (The entropy of fusion, 3.2 eu/mole, compares to the similarly low entropies of fusion of 4.2 and 3.4 for the anti-isomorphous substances CaF_2 and $SrCl_2$, respectively.)

(6) This possibility is suggested by the large cation-to-anion ratio and should be of sufficient interest also to be investigated in additively colored K_2S crystals.

The Nitrogen-14 Nuclear Quadrupole and Spin–Rotation Coupling Constants in Methyl Isocyanide and Methyl Cyanide

by M. K. Kemp,[1a] J. M. Pochan,[1b] and W. H. Flygare[1c]

Noyes Chemical Laboratory, University of Illinois, Urbana, Illinois *(Received August 12, 1966)*

Until recently, the quadrupole coupling constant of methyl isocyanide has proven to be too small to measure by microwave spectroscopy. The upper limit on the coupling constant has been lowered progressively in recent years. In 1947, Ring and co-workers[2] predicted

(1) (a) University of Illinois Fellow and National Science Foundation Summer Fellow; (b) National Science Foundation Summer Fellow; (c) Alfred P. Sloan Fellow.

a coupling constant of less than |1| Mc, and Kessler, *et al.*,[3] lowered this upper bound to |0.5| Mc in 1950. Early magnetic resonance work by Kuntz, Schleyer, and Allerhand[4] indicated a very low value for the ^{14}N field gradient. Recently, Loewenstein and Margalit[5] have stated an upper limit of |0.3| Mc by consideration of the ^{14}N nuclear magnetic resonance relaxation data for methyl cyanide (CH_3CN) and methyl isocyanide (CH_3NC). Since the exact value of the coupling constant is not known for CH_3NC and since there is interest in comparing correlation times[6] in liquids by magnetic resonance, we decided to measure the number using a high-resolution microwave spectrometer. We have also remeasured the ^{14}N nuclear quadrupole coupling constant in CH_3CN, and finally, we have obtained some information on the ^{14}N nuclear spin–rotation interaction in these molecules.

Experimental Section

The preparation of methyl isocyanide was carried out using straightforward procedures.[7] The sample was purified by microdistillation. An infrared spectrum showed that the sample contained only trace impurities and the sample was used without further purification. The high-resolution microwave spectrometer has been described elsewhere.[8]

The essential new features which make higher resolution possible are phase stabilization of the microwave frequency source and the use of large absorption cells. The large absorption cells enable the use of low pressures and power densities and decrease wall broadening, leading to narrow lines.

Results and Discussion

Previous investigators[3] give a value of 10,052.90 Mc for the rotational constant, B, in $^{12}CH_3{}^{14}N{}^{12}C$. We observed the transition $J = 0 \rightarrow 1$ at 20,105.80 Mc under very high resolution, yielding the spectrum shown in Figure 1. The nuclear quadrupole and spin–rotation interactions in a linear molecule or symmetric top are well characterized.[9] The rotational angular momentum, J, couples with the nuclear angular momentum I to give the resultant F. In the case of linear molecules,[10] or $K = 0$ symmetric top transitions, the energy involved is

$$E = -\chi_N f(I,J,F) + \frac{M_{bb}}{2}[J(J+1) - F(F+1) + I(I+1)] \quad (1)$$

where $f(I,J,F)$ is Casimir's function conveniently tabulated for a wide choice of I, J, and F,[9] χ_N is the nitrogen quadrupole coupling constant along the C–N–C bond axis, and M_{bb} is the spin–rotation constant perpendicular to the C_3 symmetry axis in CH_3NC and CH_3CN. For the $J = 0$ to $J = 1$ transitions studied here, in the case where $|\chi_N| > |M_{bb}|$, the spectra will be an asymmetric triplet with spacings given by eq 1. Thus, both the sign and magnitude of the nitrogen quadrupole coupling constant and spin–rotation constant are determined. The frequency markers on the spectrum in Figure 1 are every 10 kc. The expected intensity ratio of 1:5:3 is distorted in Figure 1. However, the absorption cell is an L-band cell[11] which has a cutoff frequency of about 1000 Mc compared to the 20,105-Mc signal that is being propagated in the guide. Propagation of a high frequency in a low-frequency wave guide leads to sharp power variations with frequency making relative intensities of molecular absorption, even over a small frequency range, unrealiable.

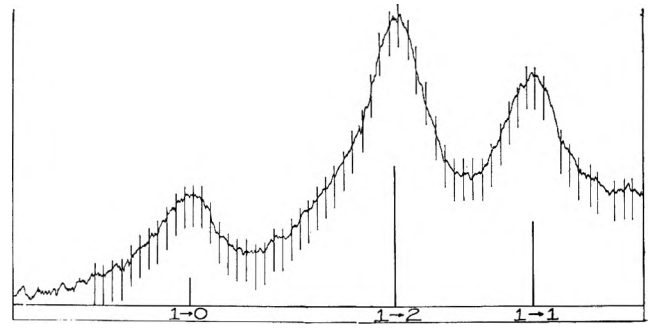

Figure 1. Observed and theoretically predicted nuclear quadrupole hyperfine transitions ($F \rightarrow F'$) and intensities in the $J = 0 \rightarrow 1$ rotational transition of CH_3NC. The markers are every 10 kc/sec.

Over 20 traces were taken of the $J = 0 \rightarrow J = 1$ transition in CH_3NC as shown in Figure 1 and average values of the differences were obtained. The average differences between the F transitions in Figure 1 are $[(F = 2) - (F = 0)] = 225 \pm 10$ kc/sec and $[(F =$

(2) H. Ring, H. Edwards, M. Kessler, and W. Gordy, *Phys. Rev.* **72**, 1262 (1947).

(3) W. Kessler, H. Ring, R. Trambarulo, and W. Gordy, *ibid.*, **79**, 54 (1950).

(4) I. D. Kuntz, P. von R. Schleyer, and A. Allerhand, *J. Chem. Phys.*, **35**, 1533 (1961).

(5) A. Loewenstein and Y. Margalit, *J. Phys. Chem.*, **69**, 4152 (1965).

(6) W. B. Moniz and H. S. Gutowsky, *J. Chem. Phys.*, **38**, 1155 (1963).

(7) A. Allerhand, "Infrared Spectroscopic Studies of Hydrogen Bonding in Solution," Dissertation, Princeton University, 1962, pp 125, 126.

(8) W. H. Flygare, *J. Chem. Phys.*, **41**, 206 (1964).

(9) C. H. Townes and A. L. Schawlow, "Microwave Spectroscopy," McGraw-Hill Book Co., Inc., New York, N. Y., 1955.

(10) See the analysis of $^{17}O^{12}C$ in ref 11.

(11) W. H. Flygare and V. W. Weiss, *J. Chem. Phys.*, **45**, 2785 (1966).

2) − (F = 1)] = −140 ± 5 kc/sec. Solving the two-parameter equations from eq 1 gives χ_N = 483 ± 17 kc/sec and M_{bb} = −3.0 ± 2.0 kc/sec.

Our value of χ_N is not in agreement with the value of |300| kc given by Loewenstein and Margalit.[5] Their value is an upper limit obtained from the ratio of the ^{14}N magnetic resonance line widths observed in liquid CH_3NC and CH_3CN at room temperature. In their analysis, they used the relation[6]

$$1/T_1 = \frac{3}{8}(e^2qQ/h)^2\tau_q \qquad (2)$$

where T_1 is the ^{14}N relaxation time and τ_q is the effective correlation time for quadrupolar relaxation of the ^{14}N. They assumed that $T_1 \leq T_2^*$, where $1/\pi T_2^*$ is the total apparent line width, and also made the reasonable approximation that τ_q is the same in the two liquids. However, less approximate determinations of the ^{14}N T_1 give 4.9 ± 0.8 msec for CH_3CN,[12] and 0.35 ± 0.1 sec for CH_3NC,[13] both liquids at room temperature. These T_1 values, when combined in eq 2 with an ^{14}N coupling constant of −4.21 Mc/sec (see below) for gaseous CH_3CN, and with the τ_c values assumed to be equal, lead to a predicted coupling constant of 500 ± 50 kc for CH_3NC in the gas phase. This is in agreement with the directly determined microwave value of 483 ± 17 kc/sec.

For the sake of completeness and interest in the ^{14}N spin–rotation interaction, we have remeasured the $J = 0 \rightarrow J = 1$ triplet in CH_3CN.[9] The results are [(F = 2) − (F = 0)] = −1896 ± 8 kc/sec and [(F = 2) − (F = 1)] = 1264 ± 4 kc/sec. Solving again the two-parameter equations from eq 1 gives χ_N = −4214 ± 16 kc/sec and M_{bb} = 0.0 ± 2.0 kc/sec.

Acknowledgment. We are indebted to Professor H. S. Gutowsky for communicating to us the T_{1N} determinations in CH_3NC and CH_3CN prior to publication. The support of the National Science Foundation is gratefully acknowledged.

(12) N. Boden, J. Deck, E. Gore, and H. S. Gutowsky, *J. Chem. Phys.*, **45**, 3875 (1966).

(13) E. Gore and H. S. Gutowsky, to be published.

Photosensitized Reactions of Cinnamate Esters

by H. G. Curme, C. C. Natale, and D. J. Kelley

Research Laboratories, Eastman Kodak Company, Rochester, New York 14650 *(Received June 27, 1966)*

In 1959, Minsk, Smith, Van Deusen, Wright, and Robertson[1,2] described the preparation of the cinnamic acid ester of poly(vinyl alcohol) and showed that, after exposure to light, it becomes insoluble in solvents in which the unexposed polymer is soluble. Although the inherent absorption and sensitivity of the cinnamate esters lie well into the ultraviolet region of the spectrum, these authors found that the esters can be sensitized to longer wavelengths with certain compounds that absorb farther toward the red than the cinnamate. Other authors have shown that infrared absorption[3] and sensitometric behavior[4] of the polymer are consistent with formation of cross-links through dimerization of the cinnamate groups during irradiation and that triplet energy levels[5] of sensitizers are such that sensitizers may reasonably be postulated to transfer triplet energy to cinnamate groups.

In this communication we present chemical evidence that the model compound, ethyl cinnamate, dimerizes when irradiated in the absorption bands of added sensitizers, and that irradiation of poly(vinyl cinnamate) produces spectral changes in the ultraviolet region similar to those shown by the model compound. Spectroscopic evidence is also presented to show that the triplet states of some of the sensitizers are involved in the reactions.

Comparison of the Photolysis of Poly(vinyl cinnamate) and of Ethyl Cinnamate

The sensitized cinnamate reactions are easily followed by changes in ultraviolet absorption. Figure 1 shows a typical absorption spectrum of a thin film of poly(vinyl cinnamate) (PVC) containing about 10 wt % of the sensitizer, Michler's ketone, henceforth referred to as MK. Samples were coated on a quartz plate and exposed to filtered light of 350-mμ wavelength and longer from a General Electric A-H4 mercury arc under vacuum at room temperature. The light was not absorbed by the polymer itself and produced no reaction in unsensitized films. In this particular experiment, the large decreases in the cinnamate absorption peak at 274 mμ were accompanied by very much smaller changes in the spectrum of the sensitizer (see the right side of the figure).

Table I shows the yields of disappearance of the cinnamate group for thin polymer films (<0.1 μ) containing three different sensitizers: Michler's ketone (MK), *p*-nitroaniline (PNA), and picramide (P).

(1) L. M. Minsk, J. G. Smith, W. P. Van Deusen, and J. F. Wright, *J. Appl. Polymer Sci.*, **2**, 302 (1959).

(2) E. M. Robertson, W. P. Van Deusen, and L. M. Minsk, *ibid.*, **2**, 308 (1959).

(3) A. Inami and K. Morimoto, *Kogyo Kagaku Zasshi*, **65**, 293 (1962).

(4) M. Tsuda, *J. Polymer Sci.*, **A2**, 2907 (1964).

(5) M. Tsuda, *Polymer Letters*, **2**, 1143 (1964).

Table I: Yields on Irradiation of Cinnamate Esters

Sensitizer	Atm	Initial: Moles of cinnamate/mole of sensitizer present	Initial: Quantum yield of loss of cinnamate	Initial: Quantum yield of loss of sensitizer	After long exposure: Time, hr	After long exposure: % decrease in absorption of cinnamate[a]	After long exposure: % decrease in absorption of sensitizer[b]	Wt % product
Substrate: poly(vinyl cinnamate)								
MK	Vac	29.8	0.25	...	17	80	10	...
MK	Air	29.8	0.16	...	16	79	21	...
PNA	N_2	7.8	0.08	...	17	69	64	...
PNA	Air	7.8	0.1	...	10	68	84	...
P	N_2	4.0	0.06	...	1	19	10	...
P	Air	4.0	0.06	...	6	36	28	...
Substrate: ethyl cinnamate								
PNA	Air	190	0.1	...	20	46	...	41[c]
P	Air	190	0.03	...	20	20	0	14[d]

[a] At the peak at 274 mμ for polymer films and at 277 mμ for ethyl cinnamate, the latter after subsequent dilution with methanol. [b] At the first peak in the visible or near-ultraviolet region. [c] Mol wt of product = 335; that of ethyl cinnamate dimer = 352. [d] Mol wt of product = 317.

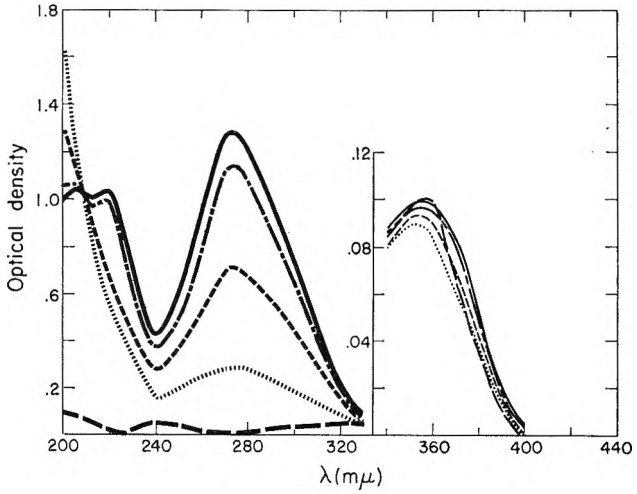

Figure 1. Optical densities of an MK-sensitized poly(vinyl cinnamate) layer irradiated at room temperature under vacuum: ———, no exposure; –·–·–·, 5-min exposure; – – – –, 15-min exposure; ———, 120-min exposure; —— —— ——, MK in poly(vinyl acetate), no exposure.

Quantum yields were calculated from initial rates of decrease of the cinnamate absorption at 274 mμ, coupled with measurements of light intensity by uranyl oxalate actinometry. In making these calculations, products of the reaction were assumed to show little absorption at 274 mμ relative to the cinnamate; results of experiments on ethyl cinnamate, given in the next paragraph, indicate that this assumption is justified. The sensitizers acted repeatedly in the process, as shown by the fact that several cinnamate groups reacted per original molecule of sensitizer originally present. This suggests that, in cases where sensitizers decompose, their decomposition may be a side reaction. As the graph shows, the rates of reaction decreased very rapidly during exposure, but the reactions could be driven to 70–80% decrease in peak height by long exposure. The spectra of the sensitizer, MK, showed relatively little change during irradiation in PVC if exposures were made in nonoxidizing atmospheres. However, PNA and P decomposed in the films even under nitrogen.

Solutions 0.03 *M* in sensitizer of PNA and P in liquid ethyl cinnamate (5.9 *M*) were exposed as 1-mm layers under air to the same wavelength radiation as the polymer films, except that a General Electric A-H6 mercury arc was used as source. The temperature in these experiments was held at 25°. As in the case of the polymer films, light was absorbed only by the sensitizers, and unsensitized ethyl cinnamate showed no reaction on irradiation. On subsequent dilution of the sensitized samples with methanol, spectral changes similar to those shown for poly(vinyl cinnamate) in the figure were found to have occurred. After irradiation, the unreacted ethyl cinnamate was pumped off and nonvolatile products were obtained. Their molecular weights, as determined by the boiling-point elevation of benzene, showed them to be predominantly dimers. Although the peak extinction coefficient of ethyl cinnamate in methanol is 22,400 l./mole cm, ab-

Table II: Emission of Sensitizers

Sensitizer	In PMMA at 77°K: Fluorescence max, mμ	In PMMA at 77°K: Phosphorescence max, mμ	Φ_P/Φ_F	In PVC at 77°K	Φ_F in PVC/Φ_F in PMMA: 77°K	Φ_F in PVC/Φ_F in PMMA: Room temp
MK	388	460	0.83	No phosphorescence	0.9	0.8
PNA	No fluorescence	517	...	No phosphorescence	...	...
P	467	No phosphorescence	...	No phosphorescence	1.5	1.7

sorbances of the products in this region were very low ($\epsilon_{max} \approx 500$ l./mole cm at 260 mμ), consistent with the loss of conjugation of the carbonyl with the phenyl group. Infrared absorption similar to that reported by Inami and Morimoto[3] was also observed. No attempt was made to resolve the mixture of truxillic and truxinic esters which are presumed to be the products.

Exposure of dilute solutions of ethyl cinnamate in methanol in the cinnamate absorption band produced a very different effect; the spectra rotated around an isosbestic point at 248 mμ, characteristic of isomerization of the *trans* form to the *cis*.[6] However, relative decreases of the absorption of both undiluted liquid ethyl cinnamate and poly(vinyl cinnamate) upon sensitized exposure were nearly the same at 248 mμ as at the peak. This indicates that very little permanent *trans–cis* isomerization occurred in the sensitized undiluted systems.

The spectra indicate slow photolysis of the sensitizers in solution in air.

Table I shows the yields of two of the irradiation experiments with ethyl cinnamate in air. The per cent reaction, as calculated from the gravimetric data, is seen to agree fairly well with the per cent drop of the cinnamate peak at 277 mμ. As with poly(vinyl cinnamate), the large number of dimer molecules produced per molecule of sensitizer initially present is clear evidence that the sensitizers are not destroyed during sensitizing.

The close similarity between the spectral changes in liquid ethyl cinnamate, which has been shown to produce dimer, and those in the PVC system is good evidence that the polymer is insolubilized by the formation of dimer-type cross-links. The quantum yields of reaction are of the same order of magnitude in both systems. The higher yields in the polymer films may actually be due to more favorable photochemical conditions; only a fraction of the exciting light was absorbed by the polymer films, but all of it was absorbed by the liquid samples. Inner filter effects from photolysis products of the sensitizers may have decreased the observed yields in the liquid.

Effect of Poly(vinyl cinnamate) on the Luminescence of Sensitizers

The mechanism of sensitization was investigated by comparing the luminescence of sensitizers in PVC and in poly(methyl methacrylate) (PMMA). Polymer films were from 3×10^{-3} to 1×10^{-1} *M* in the sensitizer in order to ensure that a large fraction of the exciting light was absorbed by the samples, which were a few thousandths of an inch thick. Light from a Bausch and Lomb SP-200 superpressure mercury arc was passed through a Bausch and Lomb high-intensity grating monochromator set at 365 mμ and through a 365-mμ interference filter onto the sample. The half band width of the monochromator was 10 mμ and of the interference filter approximately 20 mμ. Emitted light was analyzed by a 500-mm Bausch and Lomb grating monochromator and detected by an EMI 9558-R phototube. The output signal was recorded as a function of monochromator wavelength setting. In addition to measuring total luminescence, we could identify and observe bands due to luminescence with a lifetime of 5×10^{-4} sec or longer by means of a pair of rotating sector disks placed on either side of the sample. For the purpose of rough calculation, relative quantum yields (Φ) of short- and long-lived emissions (fluorescence and phosphorescence, respectively) were assumed to be proportional to peak heights on the traces of the total luminescent emission. A correction was made for the spectral response of the photometer by measuring its response to light from a lamp of known color temperature. In comparing fluorescence in PMMA to that of the same sensitizer in PVC, coatings with nearly the same sensitizer concentration and absorption were used. No phosphorescence was observed with any of the samples at room temperature. Results are summarized in Table II.

The two sensitizers which phosphoresce in PMMA (MK and PNA) have this emission quenched com-

(6) A. Smakula and A. Wassermann, *Z. Physik. Chem.*, **A155**, 353 (1931).

pletely in poly(vinyl cinnamate). At the same time, the two which fluoresce in PMMA show as much or more fluorescence in PVC. Borgman, *et al.*,[7] have reported that Michler's ketone does not fluoresce in methanol. The emission observed in our work persisted after several recrystallizations, but may be due to an impurity.

These experiments indicate that cinnamate does not remove energy from the excited singlet states of MK or P, but it does interact with the excited triplet states of MK, and probably of PNA, at least at 77°K. The transfer of triplet energy from sensitizer to cinnamate, followed by dimerization, is a likely mechanism of the reaction at room temperature. Liu, Turro, and Hammond[8] have shown that the dimerizations of isoprene and of butadiene photosensitized by MK and by a number of other compounds proceed by a similar mechanism.

(7) V. A. Borgman, I. A. Zhmyreva, V. V. Zelinskii, and V. P. Kolobkov, *Dokl. Akad. Nauk SSSR*, 131, 781 (1960).

(8) R. S. H. Liu, N. J. Turro, and G. S. Hammond, *J. Am. Chem. Soc.*, 87, 3406 (1965).

Magnetic Susceptibility Changes in Silver Powders during Oxidation–Reduction Cycling

by A. W. Czanderna[1]

Union Carbide Corporation, Chemicals Division, Research and Development Department, South Charleston, West Virginia *(Received August 11, 1966)*

A limited number of magnetic susceptibility measurements have been made when a paramagnetic gas is chemisorbed on a diamagnetic solid. These include the adsorption of oxygen or nitric oxide on alumina,[2-4] silica gel,[5] chromia,[6] and cuprous oxide.[7] These oxides all have relatively high surface areas compared with metal powders, and therefore it is not surprising that little if any work has been done on the latter.

The existence of O_2^-, which should be paramagnetic, on silver metal has been postulated,[8] and indirect evidence has been obtained that supports this hypothesis.[9] In recent studies,[10,11] it was demonstrated that silver powder may be cleaned satisfactorily by OAOR cycling.[12] The cleaned silver surface not only exhibited a constant surface area and reproducible chemisorption but also was not poisoned by bulk diffusion of soluble oxygen and did not adsorb hydrogen, carbon monoxide, carbon dioxide, or water.[11,13] Thus, the silver–oxygen system is of special interest because a detailed quantitative study of the magnetic susceptibility of adsorbed species appears to be feasible experimentally. The results of this type of study would be important for elucidating the nature of chemisorbed species.

For the method used in this study, the sample must not only retain the reproducible chemisorption characteristics as reported,[11] but also be suspended easily into a magnetic field of a Faraday apparatus[14] and be free of ferromagnetic contamination on the surface. It has been suggested that iron contamination on a silver surface can be removed by use of carbon monoxide;[9] therefore, this study was carried out to determine the efficiency of this treatment and to determine the effect of the necessary OAOR cycling in hydrogen at an elevated temperature on the ferromagnetic contamination of silver powder.

Experimental Section

To satisfy the geometry requirements of the susceptibility apparatus[14] and to maximize the sample to container ratio, the silver powder was pressed into cylinders 5 mm high and 2 mm in diameter about a coaxially positioned quartz fiber 0.2 mm in diameter. A special case-hardened iron mold was used to minimize introducing ferromagnetic contamination to the silver. The cylinders were compressed to about one-third of the bulk density of silver. Fourteen cylinders of the same mass (50 mg) were prepared. Three were kept as blanks and the remaining eleven were suspended in a vacuum system for purification treatment. For this, the samples were subjected to OAOR cycling at 400° using hydrogen as the reducing gas to reduce the silver surface and iron oxide present on the surface. The

(1) Clarkson College of Technology, Potsdam, N. Y. 13676.

(2) L. N. Mulay and L. K. Keys, *J. Am. Chem. Soc.*, 86, 4489 (1964).

(3) A. Solbakken and L. H. Reyerson, *J. Phys. Chem.*, 64, 1903 (1960).

(4) A. Solbakken and L. H. Reyerson, *ibid.*, 63, 1622 (1959).

(5) R. W. Zuehlke, *Dissertation Abstr.*, 22, 1432 (1961).

(6) K. Tarama, S. Teranishi, and K. Hattori, *Nippon Kagaku Zasshi*, 81, 1665 (1960).

(7) J. D. Cotton and P. J. Fenshaw, *J. Phys. Chem.*, 68, 1052 (1964).

(8) J. H. de Boer, *Advan. Catalysis*, 8, 76 (1956).

(9) J. T. Kummer, *J. Phys. Chem.*, 63, 460 (1959).

(10) A. W. Czanderna, *ibid.*, 68, 2765 (1964).

(11) A. W. Czanderna, *ibid.*, 70, 2120 (1966).

(12) OAOR cycling is repeated exposure of the sample to outgassing, oxygen adsorption, outgassing, and chemical reduction at a constant elevated temperature using the same ambient pressure in each adsorption and reduction step.

(13) A. W. Czanderna, *J. Colloid Interface Sci.*, in press.

(14) D. E. Soule, C. W. Nezbeda, and A. W. Czanderna, *Rev. Sci. Instr.*, 35, 1504 (1964).

oxygen and hydrogen pressure used was 10 torr. The cylinders were then cooled under a pressure of *ca.* 10^{-7} torr and exposed to 380 torr of carbon monoxide at 50°. This treatment results in the formation of adsorbed iron carbonyl if iron contamination is present on the surface. After evacuation, the cylinders were outgassed at 120° to desorb the iron carbonyl, which was trapped with liquid nitrogen and then pumped out. The treatment, described from the initial outgassing of the pressed cylinder to the final outgassing to desorb iron carbonyl, constitutes one OAOROCPD cycle. After each cycle, one cylinder was removed from the vacuum system except for the last cylinder which was treated to two cycles before being removed. All cylinders were exposed to the room ambient during removal.

The gases used during OAOROCPD cycling were obtained from the Air Reduction Co. in break-seal flasks. The silver powder and the vacuum system used have been described.[10] The surface area of the cylinders was determined by nitrogen adsorption at 78°K as previously described.[15]

Each cylinder was suspended in a Faraday apparatus[14] and the apparent susceptibility was measured as a function of the field strength at 25°. The measurement of the susceptibility was repeated three times for each sample. The data for each cylinder were evaluated by plotting the apparent susceptibility *vs.* reciprocal field for fields of 9.8 to 20.2 koersteds. The ppm of ferromagnetic impurity was calculated from the slope of the Honda–Owen plot.[16]

Results and Discussion

The ferromagnetic contamination of each cylinder is plotted as a function of the OAOROCPD cycle number in Figure 1. The average value of the three untreated samples, which are plotted as open squares, has been plotted at zero cycles. The minimum measurable ferromagnetic contamination, achieved after one cycle, is more than one order of magnitude smaller than for the untreated samples. This results from removal of ferromagnetic surface contamination. However, further cyclic treatment produces an increase in the ferromagnetism present in the silver up to a saturation level of 3 ppm after several cycles. The latter phenomenon probably results from agglomeration of iron dissolved in bulk silver into ferromagnetic domains. Since the rate of this process would be limited by solid-state diffusion, a saturation behavior would be expected.

The surface area of the silver powder in the compressed cylinders was 0.04 m^2/g compared with 0.09 m^2/g found after OAOR cycling of loosely packed silver powders. With the apparatus described,[14] the monolayer coverage of oxygen on this surface of about 1.5 μg could be determined with a precision of better than 10%.

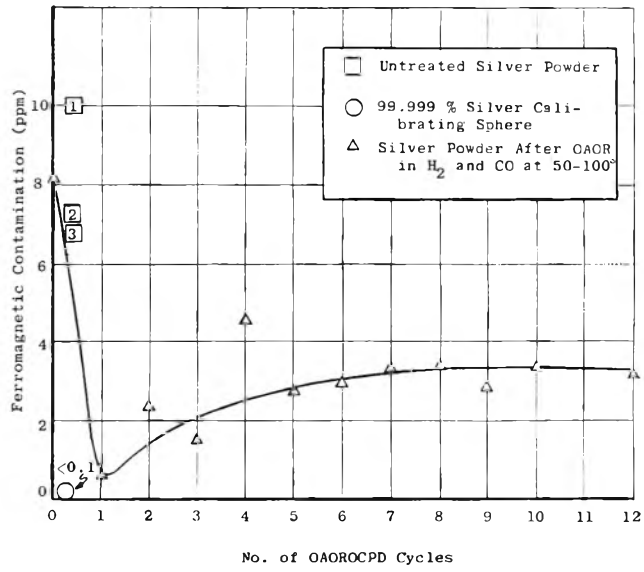

Figure 1. The ferromagnetic contamination of silver cylinders after OAOROCPD cycling. The size of the triangles exceeds the error associated with the susceptibility measurement.

The susceptibility of the silver was within experimental error of values reported on very high-purity silver shot.[14,17] Corrections to the raw data were made because of the diamagnetic contribution of the quartz fiber and the influence of the oversize samples on the values of $H\mathrm{d}H/\mathrm{d}z$.

The ferromagnetic contamination at 3 ppm is probably tolerable for susceptibility studies of oxygen adsorbed on silver because the studies would be carried out at constant field and the oxygen would not be able to react with the iron. The method of carbonyl purification of the surface is desirable because it produces a material which has the order of 0.3 ppm or less ferromagnetic contamination on the surface. It is presumed that particles of iron on the surface that are too small to form ferromagnetic domains would be readily removed by the action of carbon monoxide since it is evident larger particles can be eliminated with one OAOROCPD cycle.

(15) A. W. Czanderna, *J. Phys. Chem.*, **63**, 620 (1959).

(16) K. Honda, *Ann. Physik*, **32**, 1027 (1910); M. Owen, *ibid.*, **37**, 657 (1912).

(17) W. G. Henry and J. L. Rogers, *Phil. Mag.*, **1**, 223 (1956).

Acknowledgments. The author is grateful to Dr. D. E. Soule and Dr. F. G. Young for discussions. The assistance of Miss L. I. Forrest and C. W. Nezbeda in carrying out the experimental work is appreciated.

The Radiation-Induced Oxidation of Peptides in Aqueous Solutions[1]

by Harriette L. Atkins, Winifred Bennett-Corniea, and Warren M. Garrison

Lawrence Radiation Laboratory, University of California, Berkeley, California *(Received August 12, 1966)*

Radiolysis of certain compounds of the type $RCONHCHR_2$ in dilute aqueous solution containing O_2 leads to formation of labile peptide derivatives which are readily degraded on mild hydrolysis to give ammonia and carbonyl compounds as characteristic products.[2] It has been proposed[2,3] that such oxidation in the case of peptides derived from the simpler amino acids, glycine and alanine, is initiated by a preferential attack of the OH radical at the carbon–hydrogen position α to the nitrogen function. The over-all reaction scheme includes the radiation-induced step[4]

$$H_2O \longrightarrow H_2O_2, H_2, OH, H, e_{aq}^-, H^+ \quad (1)$$

followed by

$$OH + RCONHCHR_2 \longrightarrow H_2O + RCONH\dot{C}R_2 \quad (2)$$

$$O_2 + RCONH\dot{C}R_2 \longrightarrow RCONHC(O_2)R_2 \quad (3)$$

The reducing species, e_{aq}^- and H, are scavenged quantitatively by O_2 to form O_2^- and HO_2, which are related by the equilibrium[5] $HO_2 \rightleftarrows O_2^- + H^+$. Proposed reaction modes for removal of the intermediate peroxy radicals include

$$RCONHC(O_2)R_2 \longrightarrow RCON{=}CR_2 + HO_2 \quad (4)$$

$$HO_2 + RCONHC(O_2)R_2 \longrightarrow RCONHC(OOH)R_2 + O_2 \quad (5)$$

$$H_2O + RCONHC(OOH)R_2 \longrightarrow RCONH\dot{C}(OH)R_2 + H_2O_2 \quad (6)$$

where $RCON{=}CR_2$ represents a dehydropeptide and $RCONHC(OH)R_2$ the corresponding hydrate. Such compounds readily decompose on hydrolysis[6]

$$RCON{=}CR_2 + 2H_2O \longrightarrow RCOOH + NH_3 + R_2CO \quad (7)$$

$$RCONHC(OH)R_2 + H_2O \longrightarrow RCOOH + NH_3 + R_2CO \quad (8)$$

The above reaction scheme requires that the ammonia and carbonyl yields be in the relationship $G(NH_3) = G(R_2CO) = G_{OH}$ where the latter term represents the 100-ev yield for OH production in the radiation-induced step 1. We have measured ammonia and carbonyl yields in the γ-ray-induced oxidation of N-acetylglycine,[3c] glycine anhydride,[3d] N-acetylalanine, and alanine anhydride in oxygenated 0.1 M solution and we find for each system $G(NH_3) \simeq 3$, which value is consistent with recent measurements[7] of the maximal yield of OH radical in the γ radiolysis of water containing reactive solutes. On the other hand, we also find that carbonyl production in these simple peptide systems is not in accord with the quantitative requirements of the proposed oxidation scheme; the initial carbonyl yields are uniformly low with $G(R_2CO) \leq 0.8$. There is then the question as to whether this apparent discrepancy arises from (a) an incorrect formulation of the locus of initial OH attack or from (b) unspecified complexities in the chemistry of removal of the peroxy radicals $RCONHC(O_2)R_2$.

To obtain specific information on this point, we have employed Fe(III) instead of O_2 as the scavenger of intermediate radicals formed in the radiolysis of N-acetylalanine and N-acetylglycine. Heavy metal ions such as Fe(III) and Cu(II) oxidize organic free radicals in aqueous solution by electron transfer and by ligand transfer.[8] Such reactions in the case of the peptide radical $RCONH\dot{C}R_2$ would correspond to

$$RCONH\dot{C}R_2 + Fe(III) \longrightarrow RCON{=}CR_2 + Fe(II) + H^+ \quad (9)$$

$$RCONH\dot{C}R_2 + Fe(III) + H_2O \longrightarrow RCONHC(OH)R_2 + Fe(II) + H^+ \quad (10)$$

(1) This work was performed under the auspices of the U. S. Atomic Energy Commission, AEC Contract No. W-7405-eng-48.

(2) M. E. Jayko, B. M. Weeks, and W. M. Garrison, *Proc. Intern. Conf. Peaceful Uses At. Energy, Geneva, 2nd*, **29**, 30 (1958).

(3) (a) W. M. Garrison, M. E. Jayko, and W. Bennett-Corniea, *Radiation Res.*, **16**, 483 (1962); (b) W. M. Garrison and B. M. Weeks, *ibid.*, **17**, 341 (1962); (c) W. M. Garrison, *Radiation Res., Suppl.*, **4**, 148 (1964); (d) W. Bennett-Corniea and W. M. Garrison, UCRL-8988, Dec 1959.

(4) (a) A. O. Allen, *Radiation Res., Suppl.*, **4**, 54 (1964); (b) E. J. Hart, *Science*, **146**, 19 (1964).

(5) G. Czapski and H. J. Bielski, *J. Phys. Chem.*, **67**, 2180 (1963).

(6) J. P. Greenstein and M. Winitz, "Chemistry of the Amino Acids," John Wiley and Sons, Inc., New York, N. Y., 1961, p 843.

(7) E. Hayon, *Trans. Faraday Soc.*, **61**, 723 (1965).

(8) J. H. Baxendale and D. H. Smithies, *Z. Physik. Chem.*, **7**, 242 (1956); H. E. DeLaMare, J. K. Kochi, and F. F. Rust, *J. Am. Chem. Soc.*, **85**, 1437 (1963).

respectively. We note that the organic products of reactions 9 and 10 are identical with the postulated products of reactions 4 and 6.

Experimental Section

Solutions containing the acetylamino acid (Nutritional Biochemicals, twice recrystallized) plus ferric sulfate (CP) were adjusted to pH 3 with sulfuric acid to retain Fe(III) in solution, evacuated, and then irradiated with Co^{60} γ rays to a dose of not more than $\sim 5 \times 10^{18}$ ev/ml. Above this value the dose–yield curves were no longer linear. Dose was determined with the Fricke dosimeter, $G(Fe(III)) = 15.5$, $\epsilon_{Fe(III)}$ 2130 at 305 mμ and 22°. Immediately after irradiation, an aliquot was passed through a Dowex-50 column (1 cm × 10 cm), acid form, to remove iron. The eluent was made 2 *N* in hydrochloric acid, heated to 100° for 60 min, cooled, and assayed for α-keto acid and aldehyde through use of the 2,4-dinitrophenylhydrazine reagent.[9] A second aliquot was made 2 *N* in sodium hydroxide, allowed to stand 24 hr in the outer compartment of a Conway diffusion cell to liberate ammonia which was collected in 0.1 *N* sulfuric acid in the inner compartment, and assayed by the standard Tollen procedure. Control runs established that product hydrolysis and ammonia transfer were quantitative under these experimental conditions.

Results and Discussion

Ammonia production (Figure 1) in 0.1 *M* acetylalanine increases abruptly from $G(NH_3) = 0.7$ to $G(NH_3) = 4.3$ with increasing concentrations of Fe(III) up to $\sim 10^{-3}$ *M*. The ammonia yield then falls gradually to a limiting value of $G(NH_3) = 3.3$ at the higher Fe(III) concentrations. We also find under these conditions that pyruvic acid and ammonia are formed in equal molar yields. Yields of glyoxylic acid and ammonia from acetylglycine show this same quantitative relationship. Aldehyde yields from these systems are low, $G \simeq 0.1$.

At the higher (Fe(III))/(peptide) ratios of Figure 1, the reducing species, e_{aq}^- and H, are preferentially scavenged by Fe(III)

$$e_{aq}^- + Fe(III) \longrightarrow Fe(II) \qquad (11)$$

$$H + Fe(III) \longrightarrow Fe(II) + H^+ \qquad (12)$$

and under these conditions the yield for peptide oxidation *via* reaction 2 followed by reactions 9 and 10 is in accord with

$$-G(\text{peptide}) = G(NH_3) = G(RCOCOOH) \simeq 3.2 \simeq G_{OH} + G_{H_2O_2}$$

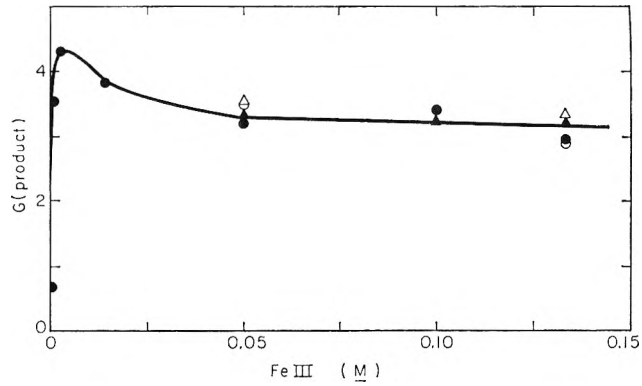

Figure 1. Effect of Fe(III) concentration on the yields of ammonia (●) and pyruvic acid (▲) from 0.1 *M* acetylalanine and of ammonia (○) and glyoxylic acid (△) from 0.1 *M* acetylglycine.

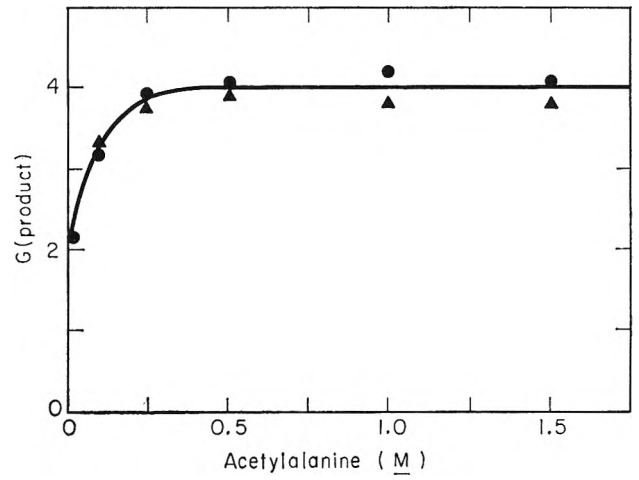

Figure 2. Effect of acetylalanine concentration on yields of ammonia (●) and of pyruvic acid (▲) from solutions containing 0.05 *M* Fe(III).

Hydrogen peroxide formed in the radiation-induced step 1 reacts rapidly with Fe(II) to give an additional yield of OH radicals.[10] The maximum in the yield curve shown in Figure 1 is attributed to the onset of the reaction

$$H + RCONHCHR_2 \longrightarrow RCONHCR_2 + H_2 \qquad (13)$$

in competition with reaction 12 as the Fe(III) concentration is reduced below 0.05 *M*. The $RCONHCR_2$ radicals from both reactions 2 and 13 are then available for oxidation by Fe(III) *via* steps 9 and 10. The H

(9) G. R. A. Johnson and G. Scholes, *Analyst*, **79**, 217 (1954); T. E. Friedemann and G. E. Haugen, *J. Biol. Chem.*, **147**, 415 (1943).

(10) F. Haber and J. Weiss, *Proc. Roy. Soc.* (London), **A147**, 333 (1934).

atoms involved in reaction 13 are derived from the radiation-induced step 1 and the conversion reaction

$$e_{aq}^- + H^+ \longrightarrow H \qquad (14)$$

which at pH 3 is in competition with reaction 11 at the lower Fe(III) concentrations. At Fe(III) concentrations below $\sim 10^{-3}$ M, the dimerization of $RCONH\dot{C}R_2$ radicals[3b] becomes competitive with reactions 9 and 10 and the ammonia yield is depressed accordingly.

If now the Fe(III) concentration is kept constant at 0.05 M and the acetylalanine concentration is increased over the range 10^{-3} to 1.5 M, it is found (Figure 2) that the ammonia and pyruvic acid yields are essentially equivalent and approach a limiting value of $G \simeq 3.9$ at acetylalanine concentrations above 0.25 M. At these higher (peptide)/(Fe(III)) ratios, the H atoms formed in the radiation-induced step 1 are not scavenged by Fe(III) but are preferentially removed *via* reaction 13. (The conversion reaction 14 at pH 3 is wholly quenched by 0.05 M Fe(III).) Hence we have the higher limiting oxidation yield which is in accord with the stoichiometry

$$-G(\text{peptide}) = G(NH_3) = G(R_2CO) \simeq 4.0 \simeq G_{OH} + G_{H_2O_2} + G_H$$

We conclude that the reaction of OH and H radicals with these peptide derivatives of the simpler amino acids, glycine and alanine, occurs essentially quantitatively at the α position as formulated in reactions 2 and 3.[11] The present data also establish the quantitative oxidation of $RCONHCR_2$ radicals by Fe(III) *via* reactions 9 and 10. In the case of acetylalanine such oxidation appears to occur almost exclusively through ligand transfer (reaction 10) since measurements of the optical absorption of the irradiated solutions (after removal of Fe(III)) reveal negligible absorption above 230 mμ when read differentially against unirradiated control solution. Absorption by control solutions containing authentic acetyldehydroalanine[12] (ϵ_{240} 6050) show that G values of >0.1 for reaction 9 would be detectable. To our knowledge the optical properties of acetyldehydroglycine have not been described.

The low carbonyl yields obtained when O_2 is used in place of Fe(III) as the radical scavenger are interpreted here as evidence that other more complex degradation reactions occur in parallel with the dehydrogenation and hydroxylation reactions 4–6. The nature of these more complex branching reactions of the peroxy radical $RCONHC(O_2)_2$ is presently under study.

(11) We refer to radical attack at the C–H linkage α to the nitrogen function as the characteristic peptide reaction. With the more complicated amino acid residues, attack may occur in parallel or exclusively at side-chain loci. See ref 3 and H. A. Sokol, W. Bennett-Corniea, and W. M. Garrison, *J. Am. Chem. Soc.*, **87**, 1391 (1965).

(12) We are indebted to Dr. B. M. Weeks for the sample of authentic acetyldehydroalanine which was prepared after the method of V. E. Price and J. P. Greenstein, *Arch. Biochem.*, **10**, 383 (1948).

COMMUNICATIONS TO THE EDITOR

The Absorption Spectrum of the Allyl Radical by Pulse Radiolysis[1]

Sir: The identification of the optical absorption spectrum of the allyl radical has been the subject of much discussion and various investigators have suggested widely different values for its absorption maxima.[2–7]

We have observed the absorption spectrum of the transient allyl radical in the pulse radiolysis of dilute solutions of allyl bromide in cyclohexane and have obtained a preliminary value for its absolute rate constant for termination.

All of the pulse radiolysis experiments were performed using the linear electron accelerator at Argonne National Laboratory. A typical run consisted in introducing a several-joule pulse of 13.5-Mv electrons into a 15-ml sample at 22°. Transient optical absorption analysis over a 16.0-cm optical path length was carried out in a manner similar to previous work.[8,9]

(1) Based on work performed under the auspices of the U. S. Atomic Energy Commission.

(2) D. M. Bodily and M. Dole, *J. Chem. Phys.*, **44**, 2821 (1966).

(3) M. B. Fallgatter and M. Dole, *J. Phys. Chem.*, **68**, 1988 (1964).

(4) D. A. Ramsay, *J. Chem. Phys.*, **43**, S18 (1965).

(5) C. L. Currie and D. A. Ramsay, *ibid.*, **45**, 488 (1966).

(6) S. Ohnishi, S. Sugimoto, and I. Nitta, *ibid.*, **39**, 2647 (1963).

(7) H. C. Longuet-Higgins and J. A. Pople, *Proc. Phys. Soc.* (London), **A68**, 591 (1955).

Figure 1 shows the absorption spectrum observed when a deoxygenated cyclohexane solution containing 5.0×10^{-2} M allyl bromide was irradiated. The following additional facts serve to characterize this absorption spectrum as that due to the allyl radical.

(a) No absorption in this region is observed when deoxygenated pure cyclohexane is irradiated, although the well-known cyclohexyl peroxy spectrum[10] is observed when oxygen is present. The rate constant for the second-order termination of cyclohexyl peroxy radicals is much smaller than the rate constant we measure; *viz.*, $k = 1.6 \times 10^6 M^{-1}$ sec^{-1}.

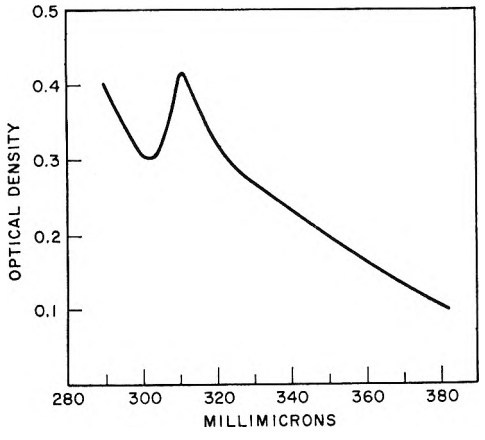

Figure 1. The absorption spectrum of the allyl radical.

(b) No absorption is observed when either allyl chloride or allyl alcohol, present at 5.0×10^{-2} M in deoxygenated cyclohexane, is irradiated.

(c) When the allyl bromide–cyclohexane solution is concentrated after irradiation, cyclohexyl bromide is observed as a final product by nmr, by mass spectrometry, and by gas–liquid partition chromatography, together with a smaller amount of an as yet unidentified product.

From (a) it is concluded that the transient spectrum is due to the presence of allyl bromide in the irradiated solution. Since the transient absorption is observed in allyl bromide solution, but not in allyl chloride or allyl alcohol solution, the 3100-A absorption appears to be due to the $CH_2 \cdots CH \cdots CH_2$ radical formed by bromine atom abstraction by cyclohexyl radicals. If the absorption were due to a radical formed by abstraction of a hydrogen atom from allyl bromide, a similar result would be expected in the allyl chloride and allyl alcohol solutions. This is not observed. Furthermore, the presence of an appreciable percentage of cyclohexyl bromide among the final products substantiates a mechanism involving bromine atom abstraction from the allyl bromide.

The 3100-A absorption due to the allyl radical disappears by a second-order process. A rate constant for this reaction, $k = (7.7 \times 10^5)\epsilon\ M^{-1}$ sec^{-1}, was obtained by a computer analysis of the absorption as a function of time using an adaptation[11] of the CHLOE system at Argonne. This value of k is good to about 20% when the correct value of ϵ is used. A tentative value for ϵ was calculated by means of end-product analysis: $\epsilon = 2.6 \times 10^3\ M^{-1}$ cm^{-1}. An exact evaluation of ϵ will be made based on the detailed examination of the reaction mechanism and a more precise determination of end products which is now in progress.

Acknowledgment. The authors gratefully acknowledge the assistance of Mr. E. Backstrom and Mr. B. E. Clifft in operating the Linac.

(8) J. Rabani, W. A. Mulac, and M. S. Matheson, *J. Phys. Chem.*, **69**, 53 (1965).

(9) E. J. Burrell, Jr., *ibid.*, **66**, 401 (1962).

(10) R. L. McCarthy and A. MacLachlan, *J. Chem. Phys.*, **35**, 1625 (1961).

(11) M. Sauer, "A Method for Automatic Analysis of Data on the Kinetics of Fast Chemical Reactions in the Form of Pictures of Oscilloscope Traces," Argonne National Laboratory Report ANL-7113, Oct 1965.

(12) Summer Resident Research Associate, Argonne National Laboratory.

(13) Resident Student Associate, Argonne National Laboratory.

CHEMISTRY DEPARTMENT
LOYOLA UNIVERSITY
CHICAGO, ILLINOIS 60626
E. J. BURRELL, JR.[12]

CHEMISTRY DIVISION
ARGONNE NATIONAL LABORATORY
ARGONNE, ILLINOIS
P. K. BHATTACHARYYA[13]

RECEIVED OCTOBER 26, 1966

Reply to Bond Lengths in Iron Pentacarbonyl

Sir: We wish to comment upon a recent communication to this journal by Donohue and Caron[1] concerning our investigation of iron pentacarbonyl by the gas-phase electron diffraction technique.[2]

The most significant question posed by Donohue and Caron is "whether the electron diffraction data are capable of detecting a difference of only 0.045 A between the two kinds of Fe–C bonds because of the high correlation between that difference and the vibrational amplitudes." This statement is mainly meaningful in the context of attempting to resolve two closely

(1) J. Donohue and A. Caron, *J. Phys. Chem.*, **70**, 603 (1966).

(2) M. I. Davis and H. P. Hanson, *ibid.*, **69**, 3405 (1965).

contiguous peaks of somewhat arbitrary widths in the radial distribution curve. In actual fact, the difference is established essentially by the nonbonded contributions to the scattering. Donohue and Caron's statement that our use of assumed values for the vibrational amplitudes in the Hedberg and Iwasaki[3] matrix least-squares method "virtually fixed the bond length difference before the refinement began" is not correct. This difference is not a sensitive function of the damping in our treatment.

Donohue and Caron's reference to the 2,3-dimethylbuta-1,3-diene investigation[4] is not particularly pertinent. A closer analogy to the present case would be the recent study on PF_5,[5] which, while more straightforward than that for $Fe(CO)_5$, involved much the same analytical procedure. The number of independent variables required to describe 2,3-dimethylbuta-1,3-diene is relatively high with respect to the total number of internuclear distances. Thus, while the distinction between the two nonequivalent C–C distances of the diene is largely dependent upon separation of the two bond contributions, the axial and trigonal bond lengths of $Fe(CO)_5$ may be obtained from the nonbonding contributions. We maintain our viewpoint that from a consideration of all of the nonbonded distances, in the framework of a simple molecular model of trigonal bipyramidal symmetry, there exists a reasonable probability of making the required distinction between axial and trigonal Fe–C bond lengths.

Since our results may be considered somewhat unexpected, they can, of course, be challenged on other grounds, namely, that our mathematical analysis has been inadequate or that the data may have contained systematic errors. Prompted by Donohue and Caron's criticism, we have made what we consider to be an exhaustive analysis of our present data using various starting models with numerous combinations of parameters involving distances and amplitudes and with different ranges of s. We have repeated what we feel was the critical stage of the analysis, namely, a refinement procedure involving three-dimensional parameters: the average Fe—C bond length, the C=O bond length, and the difference between the two Fe—C bond lengths. The Fe—C and Fe—O distances were all assumed equal to their respective mean values and the axial–trigonal difference was obtained solely from the other contributions to the scattering. The values shown in Table I are representative of our recalculations. They were obtained by using a starting model in which the axial bond was *longer* than the trigonal by 0.02 A in a modified least-squares program of the type recently described by Bartell.[6]

Figure 1 shows the outer part of the radial distribution curves. This is the region where the important nonbonded contributions are to be found. It can be seen that there is good over-all agreement between the experimental curve and the theoretical version for a model with the axial Fe–C bond being the shorter. Another theoretical version where the axial bond is the longer is seen to be less close to the experimental curve. We consider that our data require the shorter axial bond, within the probability indicated by our standard deviation.

Table I: The Molecular Structure of $Fe(CO)_5$

	r, A	σ, A
r(Fe—C), mean	1.823	0.0014
Δ(Fe—C), trigonal–axial	0.049	0.020
r(C=O), mean	1.136	0.0015

This does not preclude the possibility for systematic error. Since the problem is of considerable chemical interest and since the analysis certainly approaches the limits of credibility for the electron diffraction technique, we are planning to obtain new experimental data. We have also asked other electron diffraction groups to repeat the experiment, and the Oslo group has indicated that such an investigation will be made. A joint study by a number of laboratories on a rather subtle problem of this nature could help to establish the limits of consistency to be expected from various groups.

As indicated previously, our results may be considered to be unexpected, and this was pointed out by Donohue and Caron. However, there does not exist, in our view, unequivocal theoretical or experimental evidence for either bond being the longer. Owing to a regrettable oversight on our part, we were not aware of the Donohue and Caron refinement[7] of Hanson's data on solid iron pentacarbonyl.[8] This refinement suggests a longer axial bond in the solid. Nevertheless, examples of major structural changes in going from the solid to the gas phase are numerous, and a small modification can easily be possible. In this con-

(3) K. Hedberg and M. Iwasaki, *Acta Cryst.*, **17**, 529 (1964).

(4) L. Hedberg and K. Hedberg, American Crystallographic Association Meeting, Gatlinburg, Tenn., July 2, 1965.

(5) K. N. Hansen and L. S. Bartell, *Inorg. Chem.*, **4**, 1775 (1965).

(6) L. S. Bartell, D. A. Kohl, B. L. Carrol, and R. M. Gavin, Jr., *J. Chem. Phys.*, **42**, 3079 (1965).

(7) J. Donohue and A. Caron, *Acta Cryst.*, **17**, 663 (1964).

(8) A. W. Hanson, *ibid.*, **15**, 930 (1962).

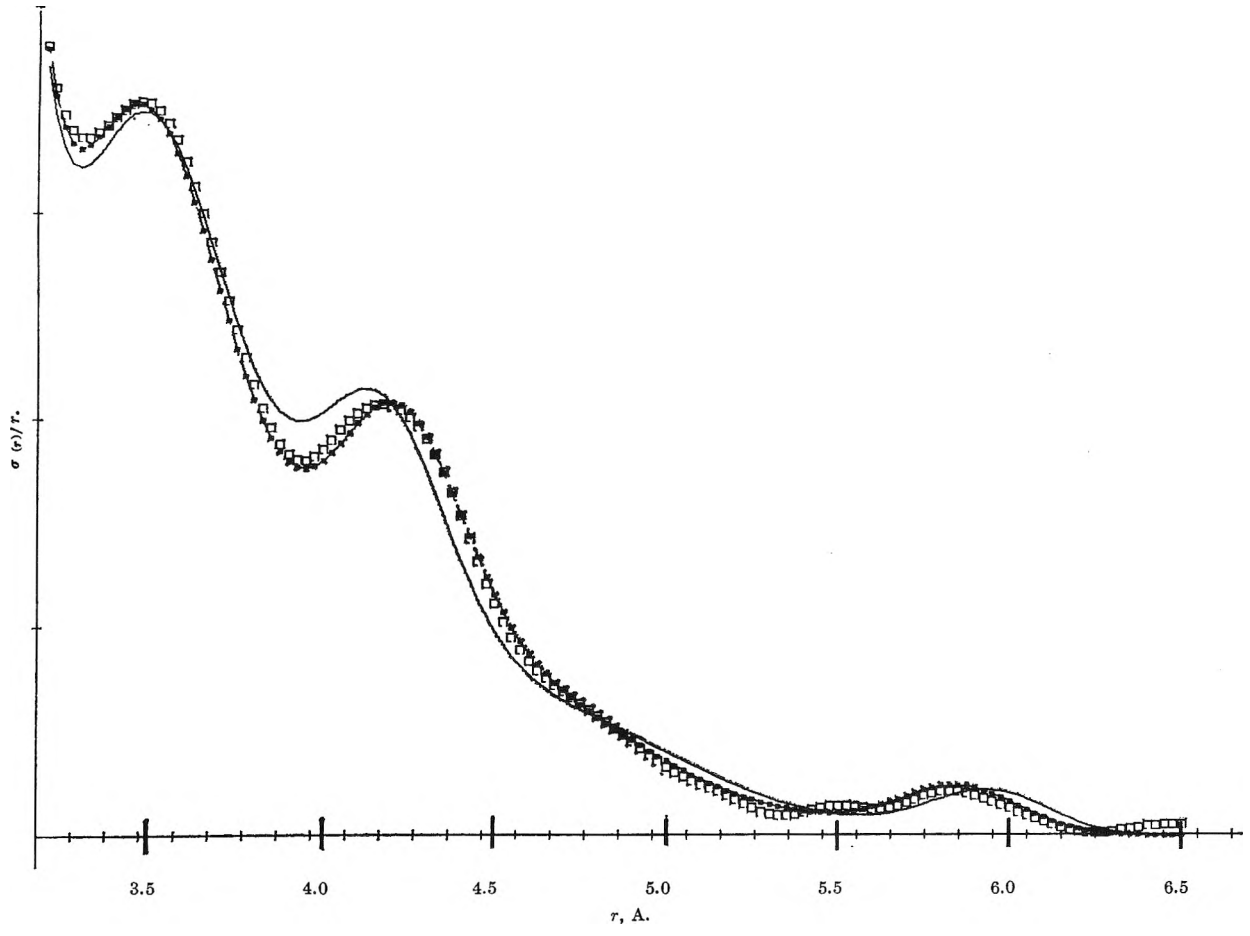

Figure 1. The radial distribution curve of $Fe(CO)_5$ in the region 3.2–6.5 A: □, experimental curve; *, $r(Fe–C)_{tr} - r(Fe–C)_{ax}$ = 0.048 A; ———, $r(Fe–C)_{ax} - r(Fe–C)_{tr}$ = 0.020 A. Damping factor = $\exp(-0.008s^2)$.

text, it is interesting to note that Donohue and Caron's value for the average Fe–C bond length differs by 0.03 A from ours.

From the point of view of theory, if one compares the orbital description of PF_5, in which the axial bonds are longer by 0.05 A, and $Fe(CO)_5$, a number of important differences are encountered. In PF_5 the d orbitals which might be used to stabilize the axial bonds are higher in energy than the s or p orbitals. Bartell has expressed doubts that the d-orbital contribution to bonding is at all significant, formulating his arguments in the context of the Rundle approach. In $Fe(CO)_5$, on the other hand, the d orbitals are of lower energy than the p and may consequently be expected to add to the stability of the axial bonds. There is the further factor of back-donation in $Fe(CO)_5$. A consideration of the respective symmetries of the occupied Fe orbitals and the antibonding CO orbitals show that multiple bonding is more favorable in the axial direction. On the basis of these considerations, a model in which the axial Fe–C bond is shorter does not appear unreasonable.

DEPARTMENT OF CHEMISTRY
THE UNIVERSITY OF TEXAS
AUSTIN, TEXAS 78712
M. I. DAVIS

DEPARTMENT OF PHYSICS
THE UNIVERSITY OF TEXAS
AUSTIN, TEXAS 78712
H. P. HANSON

RECEIVED SEPTEMBER 6, 1966

The Iron Pentacarbonyl Problem

Sir: The preceding letter by Davis and Hanson[1] contains a number of points which we feel deserve comment.

First, we beg to disagree that the most significant question posed by us[2] was whether the electron dif-

(1) M. I. Davis and H. P. Hanson, *J. Phys. Chem.*, 71, 775 (1967).

fraction data were detecting a difference of only 0.045 A between the two kinds of Fe–C bonds. Our principal point was (and is) that the crystal structure results[3] did not provide confirmation of the structure with shorter $(Fe–C)_{axial}$ bond lengths proposed by them.[4]

Davis and Hanson now[1] call attention to the fact that our average Fe–C bond length differs from theirs by 0.03 A, with the implication that the molecular structures in the gas and the solid may not be the same. Perhaps so, but the evidence *now* available does not support this view: in the gas,[1] $(Fe–C)_{mean} = 1.823 \pm 0.0014$ A, and in the solid,[3] $(Fe–C)_{mean} = 1.795 \pm 0.020$ A. The difference of 0.028 A, with a σ of 0.020 A, is significant at the 8% level, or clearly in the "not-significant" range, as defined by Cruickshank.[5]

Regarding the two closely contiguous and therefore unresolved peaks in the radial distribution function, no one can argue that there is not a high correlation between the separation between them and the vibrational amplitudes, as we have already pointed out.[2] This difficulty may be obviated in certain special cases, such as the example of PF_5[6] cited by Davis and Hanson. We are, however, unable to understand why they consider that the electron diffraction investigation of this molecule is germane to the present problem: the radial distribution function of PF_5 consists of four rather sharp, well-separated peaks, only *one* of which is composite, and it was accordingly a simple matter for Hansen and Bartell to determine, with a high degree of precision, the two variables which characterize the molecule and to conclude that the $(P–F)_{axial}$ bond distance was greater than the $(P–F)_{equatorial}$ bond distance by 0.043 ± 0.008 A. This situation is in sharp contrast to that in $Fe(CO)_5$, the radial distribution function of which has six peaks, two of which are rather well-defined shoulders and one of which, the outermost, is a rather ill-defined smear at about 5.9 A. Of these, five are composite and the position of the sixth, the outermost, does not depend directly on whether or not the two kinds of Fe–C bonds are equal in length. There is, accordingly, a serious resolution problem and the assumed vibration amplitudes, which have a marked effect not only on the width of the peaks but also on the positions of the shoulders, should be included as parameters in the refinement, together with the bond length difference.

We agree that other electron diffraction groups should repeat the experiment and for that reason see no point in making detailed comments on some rather curious features of the radial distribution functions presented by Davis and Hanson.[1]

Finally, we feel that a quantum mechanical discussion of this molecule is premature. Given a correct molecular structure, an MO description which "explains" that structure can usually be found.[7] In the present case, it would seem more prudent to wait until the structure is firmly established.

(2) J. Donohue and A. Caron, *J. Phys. Chem.*, **70**, 603 (1966).

(3) J. Donohue and A. Caron, *Acta Cryst.*, **17**, 663 (1964).

(4) M. I. Davis and H. P. Hanson, *J. Phys. Chem.*, **69**, 3405 (1965).

(5) D. W. J. Cruickshank, *Acta Cryst.*, **2**, 65 (1949).

(6) K. N. Hansen and L. S. Bartell, *Inorg. Chem.*, **4**, 1775 (1965).

(7) See, for example, A. G. Turner and F. S. Mortimer, *ibid.*, **5**, 906 (1966).

DEPARTMENT OF CHEMISTRY
UNIVERSITY OF PENNSYLVANIA
PHILADELPHIA, PENNSYLVANIA
J. DONOHUE

DEPARTMENT OF CHEMISTRY
UNIVERSITY OF MASSACHUSETTS
AMHERST, MASSACHUSETTS
A. CARON

RECEIVED DECEMBER 1, 1966

Comments on the Paper, "Cation Exclusion from Gels," by R. A. Horne

Sir: Horne[1] disagrees with us concerning our interpretation[2] of the exclusion of aqueous ions from part of the pore volume of high surface area materials. The fact of exclusion has been known for a long time, but up until recently there has been very little discussion as to its explanation. Redfern and Patrick[3] were unable to explain it. Plank[4] observed it for certain ions, referring to "negative adsorption" in certain cases, and Konyushka[5] reported it for aqueous nonelectrolytes in the pores of silica gel. We reported that when a silica gel adsorption column is just filled with aqueous hexachloroplatinic acid there is a depletion of the acid in the first part of the column with a corresponding enrichment in the latter part.[6]

We later made several studies of ion exclusion,[7] usually with silica gel, and we concluded[2] that the principal if not the only reason is a geometric one and that we consequently are measuring ion hydrate size

(1) R. A. Horne, *J. Phys. Chem.*, **70**, 1335 (1966).

(2) B. L. McConnell, K. C. Williams, J. L. Daniel, J. H. Stanton, B. N. Irby, D. L. Dugger, and R. W. Maatman, *ibid.*, **68**, 2941 (1964).

(3) S. Redfern and W. A. Patrick, *ibid.*, **42**, 497 (1938).

(4) C. J. Plank, *ibid.*, **57**, 584 (1953).

(5) (a) I. M. Konyushka, *Uch. Zap. Belorussk. Gos. Univ.*, 140 (1953); (b) *ibid.*, 282 (1956); (c) *Vestsi Akad. Navuk Belarusk. SSR, Ser. Fiz-Tekhn. Navuk*, 111 (1956).

(6) R. W. Maatman and C. D. Prater, *Ind. Eng. Chem.*, **49**, 253 (1957).

(7) See ref 2 and our earlier papers referred to therein.

when we observe exclusion. On the other hand, Horne, Konyushka, Plank, and others ascribe at least part of the effect to a preferential adsorption of water; some refer also to the exclusion from the smallest pores of the solute, but not of water molecules.

Unfortunately, Horne, Konyushka, and Plank do not take into account the geometric effect, an effect which by its nature must *always* be considered. If there is in addition preferential water adsorption or ion reaction, these effects are superimposed upon the geometric effect. The geometric effect arises when there is a difference between the sizes of the solute and solvent species. The larger species is effectively more dilute near the solution–solid interface. It is more dilute because, *for species touching the interface*, the distance between an *average* point (for a sphere, the center) of the geometric shape representing the larger species and the interface is greater than the corresponding distance for the smaller species. There is therefore a compensating enrichment of the larger species in the bulk phase. This effect becomes important where the interface area is several hundred square meters per milliliter of solution.

Horne states quite correctly that ion reaction with the surface must be included in any analysis of these systems; we have either repressed reaction or calculated its amount in all of our work.[7] He suggests that a correlation between our sizes and the viscosity B coefficient indicates we are really observing water structure at the interface, not ion hydrate size. We had, however, earlier shown[8] that correlation with the B coefficient is about as good as the B coefficient correlation with sizes determined in other ways.[9]

Our sizes scatter around those of Nightingale[9] and others and there is no doubt that our method, involving as it does an assumption of the size of the "average" water cluster and a knowledge of the pore size distribution, is less accurate than most other methods. These sources of error are not relevant to the discussion of the question of the reason for ion exclusion, since ion hydrates *are* of different sizes, and therefore the geometric argument given earlier *must* apply to at least some ions. One must make at least approximate calculations for each solution–solid experiment to determine whether or not the exclusion factor is important.

Is there on hydrated silica gel a water layer impermeable to ions? Our sizes, similar to those of others, calculated on the assumption there is no such layer, seem to be consistent with that assumption. However, the meaning of "size" varies from one method of determination to another and our experimental error is large. Yet it is interesting to note that the ions of $CsNO_3$ "see" exactly the same pore volume of silica gel as does water and the ions of $RbNO_3$ "see" almost as much. Even though some of these ions are structure breakers, it is generally true that the less an ion is able to hydrate, the more easily it penetrates all of the pore volume water penetrates. It is difficult to explain this fact on the basis of a hydration layer and it is easily explainable on the basis of ion hydrate size.

(8) R. W. Maatman, J. Netterville, H. Hubbert, and B. Irby, *J. Miss. Acad. Sci.*, 8, 201 (1962).

(9) E. R. Nightingale, Jr., *J. Phys. Chem.*, 63, 1381 (1959).

DEPARTMENT OF CHEMISTRY
DORDT COLLEGE
SIOUX CENTER, IOWA 51250
RUSSELL W. MAATMAN

RECEIVED OCTOBER 24, 1966

Double-Layer Perturbation without Equilibrium between Concentrations and Potential

Sir: In the application of the three recently proposed general equations[1,2] for the treatment of nonsteady-state electrode processes without *a priori* separation of charging and faradaic currents, one needs explicit forms of the time derivatives $(d\Gamma/dt)$ of the surface excesses of reactant and product. An explicit form of the $d\Gamma/dt$, based on equilibrium considerations, was proposed[2] and applied to impedance studies.[3] This relationship does not take into account the *nonequilibrium* between potential and the concentrations of reactant and product at the electrode for a finite exchange current i_0 different from zero. This concept of nonequilibrium is new in double-layer studies, to our knowledge, and is believed to be essential to the interpretation of nonsteady-state and periodic electrode processes. Application is made to the amalgam electrode $M^{z+} + ze = M(Hg)$, but ideas carry over to other processes.

The value of $d\Gamma/dt$ for nonequilibrium can be expressed either directly in terms of the variables involved or by correcting for nonequilibrium the $d\Gamma/dt$ corresponding to equilibrium. The two approaches are discussed and lead to the same final form of $d\Gamma/dt$. For the model previously[1,2] used, one has for a small perturbation and a finite i_0 different from zero

$$d\Gamma_+/dt = (\partial\Gamma_+/\partial c^s_+)_{c^s_M,E}(dc_+/dt)_{x=0} + (\partial\Gamma_+/\partial c^s_M)_{c^s_+,E}(dc_M/dt)_{x=0} + (\partial\Gamma_+/\partial E)_{c^s_+,c^s_M}(dE/dt) \quad (1)$$

(1) P. Delahay, *J. Phys. Chem.*, 70, 2067 (1966).

(2) P. Delahay, *ibid.*, 70, 2373 (1966).

(3) P. Delahay and G. G. Susbielles, *ibid.*, 70, 3150 (1966).

where Γ_+ is the surface excess of M^{z+}; c, the concentration; c^s, the bulk concentration; E, potential; x, distance from the electrode; t, time. When $i_0 \to \infty$, only two variables need be considered, instead of three in the writing of $d\Gamma_+/dt$; *i.e.*, it is not possible to vary E when both $c^s{}_+$ and $c^s{}_M$ are constant; likewise one cannot vary one of the c^s's while keeping constant the other c^s and E. However, this is not the case when i_0 is finite. Finally, only the last term on the right-hand side of eq 1 has to be retained when $i_0 = 0$ for the model used here.

In the other, intuitive approach we express $d\Gamma_+/dt$ as the sum of two components corresponding to equilibrium and nonequilibrium conditions. Thus one has for a finite i_0 different from zero

$$d\Gamma_+/dt = (\partial\Gamma_+/\partial c^s{}_+)_{c^s{}_M}(dc_+/dt)_{x=0} + (\partial\Gamma_+/\partial c^s{}_M)_{c^s{}_+}(dc_M/dt)_{x=0} + (\partial\Gamma_+/\partial E)_{c^s{}_+,c^s{}_M}(d\eta_{ct}/dt) \quad (2)$$

where η_{ct} is the charge-transfer overvoltage. The first two terms on the right-hand side of eq 2 correspond to the behavior of a reversible electrode for which Γ_+ at equilibrium is solely a function of the two independent variables $c^s{}_+$ and $c^s{}_M$. These terms in eq 2 account for the change of Γ_+ resulting from the variation of c_+ from $c^s{}_+$ to $(c_+)_{x=0}$ and the variation of E from the equilibrium value E_e to that corresponding to $(c_+)_{x=0}$ and $(c_M)_{x=0}$, namely, $E_e + \eta_d$, η_d being the diffusion overvoltage. The last term on the right-hand side of eq 2 accounts for the variation of Γ_+ when E varies from $E_e + \eta_d$ to $E_e + \eta_d + \eta_{ct}$. Note that $(\partial\Gamma_+/\partial c^s{}_+)_{c^s{}_M,E}$ in eq 1 is not the same as $(\partial\Gamma_+/\partial c^s{}_+)_{c^s{}_M}$ and that the same remark applies to $(\partial\Gamma_+/\partial c^s{}_M)_{c^s{}_+,E}$ and $(\partial\Gamma_+/\partial c^s{}_M)_{c^s{}_+}$.

Equation 2 can be written in the same form as eq 1 as follows. One has $dE/dt = d\eta/dt$, $\eta = \eta_d + \eta_{ct}$, and η_d is given by the Nernst equation. Hence one has for a small perturbation

$$d\Gamma_+/dt = [(\partial\Gamma_+/\partial c^s{}_+)_{c^s{}_M} - (RT/zF) \times (1/c^s{}_+)(\partial\Gamma_+/\partial E)_{c^s{}_+,c^s{}_M}](dc_+/dt)_{x=0} + [(\partial\Gamma_+/\partial c^s{}_M)_{c^s{}_+} + (RT/zF) \times (1/c^s{}_M)(\partial\Gamma_+/\partial E)_{c^s{}_+,c^s{}_M}](dc_M/dt)_{x=0} + (\partial\Gamma_+/\partial E)_{c^s{}_+,c^s{}_M}(dE/dt) \quad (3)$$

This result is of the same form as eq 1, and correlations between the different coefficients of the time derivatives are immediate. One could also derive eq 3 directly from eq 1 without splitting $d\Gamma_+/dt$ as was done in eq 2.

Expressions for $d\Gamma_M/dt$ and $d(q + zF\Gamma_+)/dt$ are similar to eq 1. These results ought to be used, rather than the forms previously written,[3] in the analysis of nonsteady-state and periodic electrode processes. Revised calculations have been completed for the electrode impedance and will soon be carried out for other relaxation processes.

Acknowledgment. This work was supported by the National Science Foundation and the Office of Naval Research. We thank Dr. J. E. B. Randles, University of Birmingham, and Dr. G. C. Barker, Atomic Energy Research Establishment, Harwell, for most valuable comments.

DEPARTMENT OF CHEMISTRY
NEW YORK UNIVERSITY
NEW YORK, NEW YORK 10003

P. DELAHAY
K. HOLUB
G. SUSBIELLES
G. TESSARI

RECEIVED NOVEMBER 14, 1966

Barium Ion Exchange of Linde 13-X

Sir: Recent articles[1,2] present data on alkaline earth ion exchange of the synthetic zeolite Linde 13-X (NaX). In ref 2 the data were presented as equilibrium data and the free energies for the complete conversion of NaX into the alkaline earth forms were computed from them. In both ref 1 and 2 the data indicate that a maximum of 74% of all the sodium ions in NaX can be replaced by Ba^{2+} ions. We began a study of alkaline earth exchange of NaX prior to the publication of the works cited above and are in essential disagreement with portions of them. The purpose of this communication is to report our Ba^{2+} ion-exchange data.

The contents of the anhydrous unit cell of the NaX crystals used in ref 1 and 2 and in our work are

$$Na_{86}[(AlO_2)_{86}(SiO_2)_{106}]$$

$$Na_{87}[(AlO_2)_{87}(SiO_2)_{105}]$$

and

$$Na_{85}[(AlO_2)_{85}(SiO_2)_{107}]$$

We have discussed lattice structure and cation locations in a previous paper.[3] For our present purpose it is sufficient to note that there are exchangeable cations located in two independent but interconnecting three-

(1) L. V. C. Rees and C. J. Williams, *Trans. Faraday Soc.*, **61**, 1481 (1965).

(2) R. M. Barrer, L. V. C. Rees, and M. Shamsuzzoha, *Inorg. Nucl. Chem.*, **28**, 629 (1966).

(3) H. S. Sherry, *J. Phys. Chem.*, **70**, 1158 (1966).

dimensional networks of cavities. One network of cavities contains 69–71 Na^+ ions per unit cell (depending on whether the crystal contains 85, 86, or 87 cations per unit cell) and has ports of 9-A free diameter. The other network of cavities contains 16 Na^+ ions per unit cell and has ports that are 2.5 A in free diameter.

Barium ions must diffuse through these windows in order to replace all the Na^+ ions. The Ba^{2+} ion has a Pauling radius of 1.35 A and a Goldschmidt radius of 1.43 A and should not be able to pass through the 2.5-A diameter ports. If this expectation is realized, an ion-exchange isotherm for this system based on an ion-exchange capacity of 85–87 Na^+ per unit cell should terminate at $Z_{Ba} = {}^{70}/_{86}$ or about 0.82, where Z represents the equivalent ionic fractional loading of Ba^{2+} ions. In Figure 1 we present the ion-exchange isotherm for the BaNaX system at 25° and 0.1 total normality. The experimental technique has been described in a previous publication.[4] The important point to note is that we have carefully allowed the reaction to reach equilibrium and find that the isotherm terminates at the point $Z_{Ba} = 0.82 \pm 0.02$. We can thus conclude with some confidence that Ba^{2+} cannot replace the 16 Na^+ per unit cell in the network of small cages, commonly called sodalite cages. This result is to be compared with termination point of $Z_{Ba} = 0.74$ shown by the authors of ref 1 and 2 in their Figures 5-C and 1-G, respectively. They could not conclude that the exclusion of Ba^{2+} ions from the network of small cavities is responsible for the low ion-exchange capacity of NaX for these ions because of the low value for maximum Ba^{2+} loading which was obtained.

We have very carefully determined whether or not our data are equilibrium data by tracing the Ba^{2+} with $^{133}Ba^{2+}$ and have found that the system takes about 4 days to reach the equilibrium state, especially at low Ba^{2+} loadings. At high loadings the reaction is faster. In this respect it resembles the BaNaA system.[4] In Figure 2 we have plotted the logarithm of the corrected selectivity coefficient, ${}^{N}K_{C}{}^{Ba}{}_{Na}$, defined by the equations

$$K = \frac{Z_{Ba} m_{Na}{}^2}{Z_{Na}{}^2 m_{Ba}} \frac{f_{Ba}}{f_{Na}{}^2} \frac{\gamma_{+Na}{}^2}{\gamma_{+Ba}}$$

$$K = {}^{N}K_{C}{}^{Ba}{}_{Na} \frac{f_{Ba}}{f_{Na}{}^2}$$

where K is the thermodynamic equilibrium constant, Z represents equivalent ionic fractions in the zeolite, m represents ionic molalities in solution, f represents rational activity coefficients for the ions in the zeolite phase, and γ represents single-ion molal activity coefficients in the solution phase. The ratio of the latter

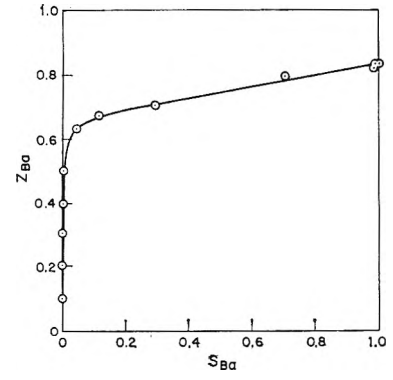

Figure 1. The ion-exchange isotherm for the BaNaA system at 0.1 total normality and 25°.

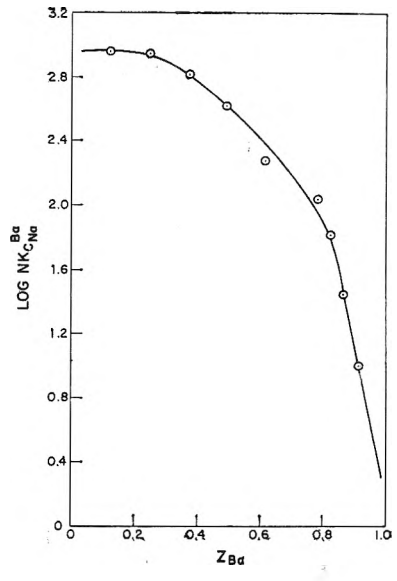

Figure 2. The corrected rational selectivity coefficient for the BaNaA system at 0.1 total normality and 25° as a function of zeolite composition.

are thermodynamically determinable from mean molal activity coefficients because the salts of the cations have a common anion, Cl^-. Again, our data must be compared with the data reported by the authors of ref 1 and 2 in their Figures 5-D and 2-G, respectively. Their data show that log ${}^{N}K_{C}{}^{Ba}{}_{Na}$ continuously increases with Ba^{2+} loading—if true, it is a very unique system—whereas our data show log ${}^{N}K_{C}{}^{Ba}{}_{Na}$ to be continuously decreasing with increasing Ba^{2+} loading—a result normally expected in ion-exchange systems. We have reason to suspect that the data on alkaline earth ion exchange reported in ref 1 and 2 do not represent equilibrium data because we have previously found[4]

(4) H. S. Sherry and H. F. Walton, *J. Phys. Chem.*, in press,

that in the alkaline earth–NaA systems maxima in selectivity plots reported by two of these authors[5] disappeared when the systems were allowed to reach equilibrium.

If 99% of the equilibrium Ba^{2+} loading is achieved, only a 1% error or less occurs in the heat of reaction reported in ref 2; however, because of the shape of the ion-exchange isotherm in Figure 1, a very great error results in the solution composition and, hence, in ${}^{N}K_{C}{}^{Ba}{}_{Na}$. Thus the standard free energy of reaction reported in ref 2 is in error. If we assume our selectivity plot (Figure 2) is correct, the standard free energy of complete exchange (replacement of 69 Na^+ per unit cell), calculated using the method of Gaines and Thomas,[6] is -1290 ± 10 cal/equiv of NaX at 25°. Using Barrer and co-workers' value for the standard enthalpy of complete exchange of -110 cal/equiv of NaX, we calculated a standard entropy change of $+3.96$ eu/equiv of NaX. These results should be compared to the values of -1168 cal, 0 ± 200 cal, and 3.9 ± 0.8 eu reported by Sherry and Walton[4] for the BaNaA system. For both the X and the A type of zeolite crystals, we believe that the small enthalpy of reaction indicates that there are no strong interactions between the Ba^{2+} ions and the anionic aluminosilicate framework; that is, the ions are "dissolved" in the zeolitic water.

(5) R. M. Barrer, L. V. C. Rees, and D. J. Ward, *Proc. Roy. Soc.* (London), **A273**, 180 (1963).

(6) G. L. Gaines and H. C. Thomas, *J. Chem. Phys.*, **21**, 714 (1953).

RESEARCH DEPARTMENT HOWARD S. SHERRY
CENTRAL RESEARCH DIVISION LABORATORY
MOBIL OIL CORPORATION
PRINCETON, NEW JERSEY

RECEIVED NOVEMBER 18, 1966

Simultaneous Voltammetric Generation of U(III) and Spectrophotometric Observation of the U(III)–U(IV) System in Molten Lithium Fluoride–Beryllium Fluoride–Zirconium Fluoride[1]

Sir: We wish to report a technique for the generation and characterization of small amounts of unusual oxidation states in molten salts and other solvents. In this technique the species are produced by linear-sweep voltammetry (or some other controlled-potential electrochemical method) at a *microelectrode located in the optical path of a spectrophotometer* and absorption spectra of the solution layer immediately surrounding the electrode are obtained a short time (<30 sec) after the beginning of electrolysis. The experimental setup employed for the generation and observation of U(III) in molten LiF–BeF_2–ZrF_4 (66:29:5 mole %) containing 2 wt % uranium (as UF_4) at 540° is shown in Figure 1. The platinum wire working electrode ($A = 0.1$ cm²) is visible in the optical aperture. The cell is a $^3/_8$-in. o.d. captive liquid cell[2a] which fits into a furnace especially designed for spectrophotometric studies of molten salts.[2a] Helium atmosphere is maintained within the furnace. The platinum wire auxiliary and quasi-reference electrodes are introduced below the working electrode using boron nitride insulating plugs. The position of the working electrode, which is insulated from the cell by means of a Teflon spacer, may be easily adjusted to the desired level from outside the furnace. The absorption spectra were obtained with a Cary Model 14-M spectrophotometer. The linear-sweep voltammograms were obtained with a controlled-potential voltammeter previously described.[3] Current–voltage curves similar to those reported by Mamantov and Manning[4] were obtained. The general

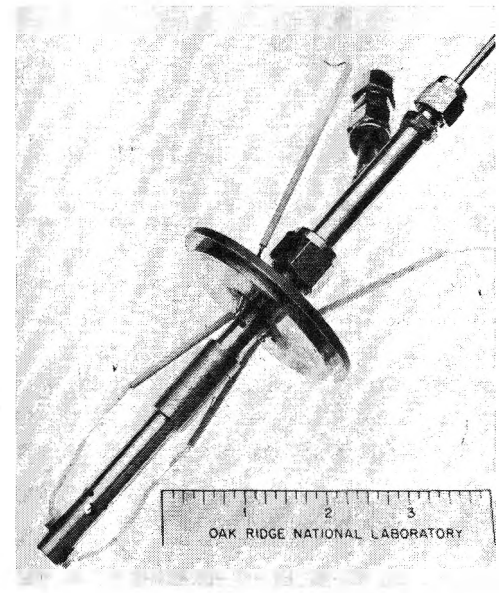

Figure 1. Combination voltammetric–spectrophotometric cell.

(1) Research sponsored by the U. S. Atomic Energy Commission under contract with Union Carbide Corp.

(2) (a) J. P. Young, *Anal. Chem.*, **36**, 390 (1964); (b) J. P. Young and J. C. White, *ibid.*, **31**, 1892 (1959), and modified in Analytical Chemistry Division Annual Progress Report ORNL-3537, Nov 15, 1963, p 26.

(3) D. J. Fisher, M. T. Kelley, W. L. Maddox, and R. W. Stelzner, USAEC Reprint ORNL-3537, p 16, 1963.

(4) G. Mamantov and D. L. Manning, *Anal. Chem.*, **38**, 1494 (1966).

spectra of U(IV) and U(III) in molten fluoride salts have recently been investigated in detail;[5] however, the resultant spectra of various mixtures of these two oxidation states have not been studied. Such results are shown in Figure 2. Initially the spectrum of U(IV) is observed (curve I); the spectra after successive periods of electrolysis are shown as curves II and III.

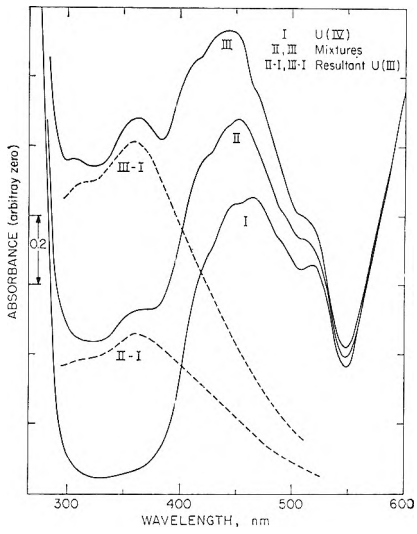

Figure 2. Spectra of U(IV)–U(III) mixtures in molten LiF–BeF_2–ZrF_4 at 540°.

Mathematical subtraction of I from II or III yields spectra of U(III).[5] At 360 nm, a pronounced increase in absorbance due to U(III) was obtained within 20 sec after reaching the limiting-current plateau. The absorbance decreased as soon as some of the U(III) was removed by the anodic sweep. The technique has been shown to be quite sensitive since only ~0.75 μequiv was generated in an average run and much less (~0.4 μequiv) was required for spectral observation.

Previous work in aqueous or organic solutions involved either large-scale electrolysis in which the solutions were contained in normal spectrophotometric cells[6,7] or the use of specialized techniques such as internal reflection spectroscopy using an optically transparent glass electrode[8] in order to observe the products of an electrochemical reaction. Our success in applying conventional spectrophotometry to the study of the solution in the vicinity of a microelectrode is due to the use of a small spectral port. The technique may be made more versatile by the use of a second working electrode, for example, a ring configuration,[9] which would be used for the electrochemical characterization of the reaction products.

Acknowledgment. We wish to acknowledge the help of Mr. D. L. Manning in this work.

(5) J. P. Young, to be published.

(6) I. Bergman, "Polarography 1964," Vol. II, G. J. Hills, Ed., Macmillan and Co., New York, N. Y., 1966, p 925.

(7) D. Cohen and W. T. Carnall, *J. Phys. Chem.*, **64**, 1933 (1960).

(8) W. N. Hansen, R. A. Osteryoung, and T. Kuwana, *J. Am. Chem. Soc.*, **88**, 1062 (1966).

(9) A. N. Frumkin and L. N. Nekrasov, *Dokl. Akad. Nauk SSSR*, **126**, 115 (1959).

OAK RIDGE NATIONAL LABORATORY
OAK RIDGE, TENNESSEE
J. P. YOUNG

DEPARTMENT OF CHEMISTRY
UNIVERSITY OF TENNESSEE
KNOXVILLE, TENNESSEE
GLEB MAMANTOV
F. L. WHITING

RECEIVED NOVEMBER 21, 1966

Reactions of Thiyl Radicals. I. Methylthiyl Recombination and Thionitrite Formation in the Photolysis of Methanethiol[1]

Sir: Current investigations in this laboratory indicate that recombination rather than disproportionation results from reaction of two RS radicals—the exact opposite of the known behavior of alkoxy radicals where recombination has been observed only for high molecular weight radicals.[2]

To establish the relative contribution of these reactions and that the presence of RS radicals in general can be unequivocally demonstrated by observing thionitrite formation when NO is present, we have reinvestigated the photolysis of gaseous CH_3SH. This system has been studied previously[3,4] and the main products are H_2 and methyl disulfide. The latter has not been determined quantitatively.

The photolysis with added NO was studied in a grease- and mercury-free vacuum system using an Hg resonance lamp. At P_{CH_3SH} = 100–200 torr and P_{NO} = 10–20 torr, no disulfide was found and the principal product recovered was CH_3SNO, identified by comparison of its gas-phase infrared spectrum with

(1) From the Ph.D. thesis of R. P. Steer to be submitted to the University of Saskatchewan, Saskatoon, Saskatchewan, Canada. The authors express their thanks to Mr. J. A. Copeck, who performed some of the preliminary experiments, and to the National Research Council and Imperial Oil Ltd. for financial support.

(2) P. Gray and A. Williams, *Chem. Rev.*, **59**, 239 (1959).

(3) N. P. Skerrett and N. W. Thompson, *Trans. Faraday Soc.*, **37**, 81 (1941).

(4) T. Inaba and B. deB. Darwent, *J. Phys. Chem.*, **64**, 1431 (1960).

that obtained by Philippe.[5] The thionitrite is susceptible to decomposition due to light and heat, but with careful handling it can be subjected to quantitative glpc analysis using a silicone 550–stearic acid column operated at 30°. At higher temperatures decomposition to NO and disulfide occurs on the column.

The pure substrate photolysis was examined in a conventional grease-free vacuum system with a filtered medium-pressure Hg arc (λ >2300 A). The products at decompositions <1%, identified by mass spectrometry, were H_2, $CH_3S_2CH_3$, and the previously unreported H_2S. 1,2-Ethanedithiol was not detected. H_2 and CH_4 were measured together in most experiments in a gas buret. Mass spectrometric analysis showed that the methane comprised 9.4 ± 0.6% of this fraction at CH_3SH pressures of 540, 247, and 130 torr and exposure times of 30 and 90 min. Methyl disulfide was measured in the gas buret and analyzed by glpc. Table I gives the product rates[6] as a function of substrate pressures for 15-min exposures.

Table I: Rates of Product Formation in the CH_3SH Photolysis

P_{CH_3SH}, torr	$R_{H_2+CH_4}$[a]	$R_{CH_3S_2CH_3}$[a]
55	7.02	6.63
130	7.90	7.08
252	9.04	8.25
408	10.0	9.56
540	10.9	11.4
741	11.1	11.1

[a] Average values, in μmoles/15 min, from at least two experiments.

The variation in over-all decomposition with increasing P_{CH_3SH} is consistent with increasing absorption by the substrate. Most significantly, however, the yields of (H_2 + CH_4) and $CH_3S_2CH_3$ are equal within experimental error at all pressures. The following mechanism, where R = H, CH_3, SH, is proposed

$$CH_3SH + h\nu \longrightarrow CH_3S + H \quad (1a)$$

$$CH_3SH + h\nu \longrightarrow CH_3 + SH \quad (1b)$$

$$R + CH_3SH \longrightarrow RH + CH_3S \quad (2)$$

$$2CH_3S \longrightarrow CH_3S_2CH_3 \quad (3)$$

The thionitrite formation confirms the presence of CH_3S and the relative H_2 and CH_4 yields indicate about 90% of the reaction is *via* eq 1a. The constancy of the proportion of CH_4 with pressure and time suggests that CH_3 is also a primary product. CH_3S formation in reaction 2 is consistent with the total absence of dithiol. The stoichiometry of this mechanism indicates that one molecule of disulfide is formed for each H_2 and for each CH_4 *or* H_2S. Thus the observed equality, $R_{H_2+CH_4} = R_{CH_3S_2CH_3}$, is strong evidence for eq 3 as the main terminal fate of CH_3S radicals. Any contribution from disproportionation would decrease the relative amount of disulfide.

If the absence of significant disproportionation characterizes RS reactions in general, it would effect an important simplification in the study of this species since disulfide is readily determined quantitatively, whereas disproportionation yields thioformaldehyde which trimerizes and is extremely difficult to determine in vacuum systems. The thionitrite-forming reaction should also be of general utility as a diagnostic text for the presence of thiyl radicals. Further studies on this system are currently underway.

(5) R. J. Philippe, *J. Mol. Spectry.*, **6**, 492 (1961).

(6) $R_{H_2+CH_4}$ values were reproducible to ±1%, while disulfide rates, likely due to some mechanical losses of this low volatility product, were ±3%.

DEPARTMENT OF CHEMISTRY AND CHEMICAL ENGINEERING — R. P. STEER
UNIVERSITY OF SASKATCHEWAN — B. L. KALRA
SASKATOON, SASKATCHEWAN, CANADA — A. R. KNIGHT

RECEIVED DECEMBER 9, 1966

Radiation-Induced Isomerization of Hexafluorobenzene[1]

Sir: Recent photochemical work has focused attention on valence isomers of aromatic compounds. Formation of Dewar benzene, prismane, benzvalene, and fulvene derivatives has been confirmed in the photolysis of alkylbenzenes.[2-4] Benzvalene[5,6] and Dewar hexafluorobenzene[7,8] have been isolated by photocon-

(1) Research supported by the U. S. Atomic Energy Commission.

(2) E. E. van Tamelen and S. P. Pappas, *J. Am. Chem. Soc.*, **84**, 3789 (1962).

(3) K. E. Wilzbach and L. Kaplan, *ibid.*, **87**, 4004, (1965).

(4) H. J. F. Angus, J. M. Blair, and D. Bryce-Smith, *J. Chem. Soc.*, 2003 (1960).

(5) K. Shindo and S. Lipsky, *J. Chem. Phys.*, **45**, 2292 (1966).

(6) J. K. Foote, M. H. Mallon, and J. N. Pitts, Jr., *J. Am. Chem. Soc.*, **88**, 3698 (1966). The benzvalene assignment is tentative.

(7) I. Haller, *ibid.*, **88**, 2070 (1966).

(8) G. Cammagi, F. Gozzo, and G. Cevidalli, *Chem. Commun.*, 313 (1966).

version of benzene and the fluorocarbon vapor, respectively. Since photolysis often yields products closely related to those obtained by radiolysis,[9] the work cited above suggested that similar valence isomerization might occur in radiolysis. (Radiation-induced *cis–trans* isomerization is well established.[9]) Results on the γ irradiation of hexafluorobenzene (I) are reported here.

Radiolysis of liquid or gaseous I[10] in a Co^{60} source at ambient temperature and at a dose rate of 7×10^6 rads/hr yielded several products. These were separated by gas chromatography using diisodecyl phthalate and/or Kel-F oil columns.[7] Liquid-phase irradiation yielded a fraction which had the same retention time as Dewar C_6F_6, hexafluorobicyclo[2.2.0]hexa-2,5-diene (II). This assignment was verified: the collected fraction showed the same infrared and mass spectra as authentic II obtained by photolysis.[7,11] Gas-phase radiolysis yielded two compounds with retention times similar to II. Upon infrared and mass spectral analyses, these were identified as C_6F_8, perfluorocyclohexadiene, and I. Since I and II have significantly different retention times, the C_6F_6 observed must be due to conversion of II at the thermal conductivity detector.[12] This was confirmed by chromatography of small amounts of authentic II; conversion to I also occurred. The valence isomer II was thus almost certainly produced in the gas phase and was unequivocally present in the liquid-phase irradiations.

Vapor-phase photoisomerization to II requires <115 kcal[8] (2537 A). We suggest therefore that isomer formation in radiolysis occurs largely by conversion from low-lying excited states. These may be formed by direct excitation, by ion–electron neutralization, or even by radical–fluorine recombination (the ionization potential of I is given as 230 kcal,[13] estimates of the C–F bond energy range from 145[13] to 108 kcal[14]).

We have established that valence isomerization occurs in the radiation chemistry of C_6F_6. The question now arises whether similar isomerization occurs in hydrocarbon radiolysis. Valence isomers of benzene and its derivatives have been isolated.[2–6] However, prismane, Dewar benzene, and benzvalene have not been obtained by liquid-phase photolysis of C_6H_6. In their study of benzvalene, Pitts, *et al.*,[6] have suggested that rapid collisional quenching of excited states prevents conversion to the isomer in condensed-phase photochemistry. The same processes which prevent photoisomerization may also apply to radiolysis. On the other hand, a greater range of excited states is obtained in radiolysis compared to photolysis. Collisional deexcitation may still leave states with sufficient energy to convert to the isomers which go undetected because of further reaction. In view of our results with C_6F_6, valence isomerization should at least be considered in the radiation chemistry of aromatic hydrocarbons.

(9) See, for example, R. A. Caldwell, D. G. Whitten, and G. S. Hammond, *J. Am. Chem. Soc.*, 88, 2659 (1966).

(10) C_6F_6, Imperial Smelting, was purified by preparative glpc and contacted with a sodium mirror. Samples were degassed to better than 10^{-6} torr.

(11) In the course of this work, we found that photolysis of liquid C_6F_6 with an unfiltered AH-6 mercury lamp also yielded II.

(12) II is heat sensitive.[8] If isomerization back to I occurred on the glpc column, the retention time would change.

(13) J. R. Majer, *Advan. Fluorine Chem.*, 2, 84 (1961).

(14) C. R. Patrick, cited by D. Bryce-Smith, B. E. Connett, and A. Gilbert, *Chem. Ind.* (London), 855 (1966).

Acknowledgments. We are indebted to Messrs. R. Smol and J. Forrest for their assistance.

BROOKHAVEN NATIONAL LABORATORY
UPTON, NEW YORK 11973
J. FAJER
D. R. MACKENZIE

RECEIVED DECEMBER 8, 1966

Corrections of Schlieren Data

Sir: In their articles,[1,2] Ford and Ford have claimed that important corrections should be applied to the data obtained from schlieren patterns.

The first correction, called "refraction correction δ_x," was deduced from geometrical constructions (Figures 1, 2, 3, ref 1).

It appears however, as explained below, that this correction δ_x is due to an error made in these constructions and that δ_x is actually nonexistent.

In their first article (see Figure 1, ref 1, to which we refer for the following discussion) Ford and Ford consider two rays passing through a cell in which there is a refractive index gradient. If the path of the bent ray through the solution is a parabola, the backward extension of its exit tangent intersects the center of the cell at the entry level, as described in ref 1.

The optical system, consisting of many refracting surfaces, starting with the cell window surfaces, is focused on a plane through the center of the cell, filled with solvent or solution. In other words, this plane and the plane of the photographic plate are conjugate image planes. So two rays coming (or appearing to come) from the same point in the center of the cell (point b)

(1) T. F. Ford and E. F. Ford, *J. Phys. Chem.*, 68, 2843 (1964).

(2) T. F. Ford and E. F. Ford, *ibid.*, 68, 2849 (1964).

intersect the plate at the same level in accordance with the definition of imaging and not at different levels b_0' and b_δ'.

The error in the constructions resulting in the different levels can be seen if one considers the contribution of the optical elements of the system to the imaging separately. The cell window (with solution to the left and air to the right of it) forms a virtual image of the center of the cell in a plane (plane I) somewhere between the window and this center. The collimating lens, in turn, forms a virtual image of plane I in a plane (plane II) situated to the left of the center of the cell, because the distance from plane I to the collimating lens is appreciably shorter than the focal distance of this lens. Plane II is the object plane "seen" by the optical elements following the collimating lens.

The two dashed lines in Figure 1, ref 1, being the rays traced backwards after their refraction by the collimating lens, intersect the center line of the cell at different levels b_0 and b_δ. However, they should have been traced backward further to plane II where they intersect.

In the second article[2] distortion and tilting of the schlieren curves was computed numerically. In connection with this the excellent and definitive work on this subject by Svensson,[3-5] which is not cited by Ford and Ford, should be mentioned. Since this work became known, workers with schlieren and interference optics have adopted the practice of focusing on a plane in the cell which is separated from the window nearest the camera by a distance equal to one-third (not one-half) of the thickness of the cell. By doing so, the tilting of the schlieren curves (Wiener skewness) is corrected for and the corrections of the sedimentation coefficients and the lag times, as given in ref 2, become negligible.

Furthermore, Svensson gives two equations (eq 63 and 110, ref 5) which give the distortion of a schlieren curve as a function of a number of parameters such as cell thickness, refractive index, and its derivatives. It might be interesting to see whether numerical calculations of the type done by Ford and Ford for an optical system focused on the one-third plane would give results in agreement with the equations given by Svensson.

(3) H. Svensson, *Opt. Acta*, **1**, 25 (1954).
(4) H. Svensson, *ibid.*, **1**, 90 (1954).
(5) H. Svensson, *ibid.*, **3**, 164 (1956).

VAN'T HOFF LABORATORY
STATE UNIVERSITY
UTRECHT, THE NETHERLANDS
H. J. VREEMAN
Y. WIERSEMA

RECEIVED DECEMBER 15, 1966